CRANFIELD UNIVERSITY

DAWID PIOTR HANAK

EVALUATION OF EFFICIENCY IMPROVEMENTS AND PERFORMANCE OF COAL-FIRED POWER PLANTS WITH POST-COMBUSTION CO_2 CAPTURE

SCHOOL OF ENERGY, ENVIRONMENT AND AGRIFOOD
PhD in Energy

PhD
Academic Year: 2015 – 2016

Principal supervisor: Prof. Vasilije Manović
Associate supervisor: Dr Chechet Biliyok

March 2016

CRANFIELD UNIVERSITY

SCHOOL OF ENERGY, ENVIRONMENT AND AGRIFOOD
PhD in Energy

PhD

Academic Year 2015 – 2016

DAWID PIOTR HANAK

EVALUATION OF EFFICIENCY IMPROVEMENTS AND PERFORMANCE OF COAL-FIRED POWER PLANTS WITH POST-COMBUSTION CO_2 CAPTURE

Principal supervisor: Prof. Vasilije Manović
Associate supervisor: Dr Chechet Biliyok

March 2016

This thesis is submitted in partial fulfilment of the requirements for the degree of PhD

ABSTRACT

The power sector needs to be decarbonised by 2050 to meet the global target for greenhouse gas emission reduction and prevent climate change. With fossil fuels expected to play a vital role in the future energy portfolio and high efficiency penalties related to mature CO_2 capture technologies, this research aimed at evaluating the efficiency improvements and alternate operating modes of the coal-fired power plants (CFPP) retrofitted with post-combustion CO_2 capture. To meet this aim, process models of the CFPPs, chilled ammonia process (CAP) and calcium looping (CaL) were developed in Aspen Plus® and benchmarked against data available in the literature. Also, the process model of chemical solvent scrubbing using monoethanolamine (MEA) was adapted from previous studies. Base-load analysis of the 580 MW_{el} CFPP retrofits revealed that if novel CAP retrofit configurations were employed, in which a new auxiliary steam turbine was coupled with the boiler feedwater pump for extracted steam pressure control, the net efficiency penalty was 8.7–8.8% points. This was close to the 9.5% points in the MEA retrofit scenario. Conversely, CaL retrofit resulted in a net efficiency penalty of 6.7–7.9% points, depending on the fuel used in the calciner. Importantly, when the optimised supercritical CO_2 cycle was used instead of the steam cycle for heat recovery, this figure was reduced to 5.8% points. Considering part-load operation of the 660 MW_{el} CFPP and uncertainty in the process model inputs, the most probable net efficiency penalties of the CaL and MEA retrofits were 9.5% and 11.5% points, respectively. Importantly, in the CaL retrofit scenarios, the net power output was found to be around 40% higher than that of the CFPP without CO_2 capture and double than that for the MEA retrofit scenario. Such performance of the CaL retrofit scenario led to higher profit than that of the 660 MW_{el} CFPP without CO_2 capture, especially if its inherent energy storage capability was utilised. Hence, this study revealed that CaL has the potential to significantly reduce the efficiency and economic penalties associated with mature CO_2 capture technologies.

Keywords: Energy storage, probabilistic performance analysis, CO_2 capture technologies, efficiency improvement, process modelling and simulation

This page intentionally left blank.

To my beloved wife Magdalena.

"*You have to learn the rules of the game.*
And then you have to play better than anyone else."

Albert Einstein

Nobel prize in Physics, 1921

"*Ever tried. Ever failed. No matter.*
Try Again.
Fail again.
Fail better."

Samuel Beckett

Nobel prize in Literature, 1969

This page intentionally left blank.

ACKNOWLEDGEMENTS

There are no proper words to express my heartfelt gratitude to my beloved wife Magdalena who provided me with her continuous support and encouragement throughout this physically and emotionally challenging time. I would love to thank you for your unlimited love and patience, and finally for your enormous understanding during the time I was away, working on this thesis. You know that I would not have been able to accomplish as much as I have, if it were not for you. Therefore, I dedicate this PhD thesis to you, my beloved wife, because your love and the prosperity of our family are the top priority to me.

I would not have gone so far if it were not for the support of my parents, Lucyna and Piotr, who have always provided me with love and guidance, and taught me to aim high and work hard. Thank you for your unconditional dedication, many years of support from the beginning of my education, even after my decision to move to the United Kingdom, and your faith in me throughout this time. I would love to give my honest appreciation to my parents-in-law, Małgorzata and Andrzej, who provided enormous encouragement and believed in me all this time. I hope I made you all proud.

This PhD thesis would have probably looked different if it were not for the guidance and support I obtained from my primary supervisor, Vasilije Manović, from the very beginning of the project. I would like to thank you for inspiring me to explore new ideas and encouraging me to publish in high-quality journals. I cannot find words that would express my appreciation for your always being there to discuss and for that you always supported my case. Your unlimited confidence in me helped me to grow as a researcher and taught me how to give my best. I am grateful that you shared with me countless insights on working in academia, which made me decide to pursue an academic career. I trust that the relation we have developed over this time will last, regardless of where life takes us.

Completing this work would have been more difficult if it were not for the support of my associate supervisor, Chechet Biliyok. Although you left

academia at the beginning of my PhD, you always found time to comment on my work, discuss the modelling challenges I encountered, and provided me with undeniable support for which I am grateful. I trust that there will be more opportunities to work together in future.

I would like to express my gratitude to my subject advisor, Ben Anthony, who supported my development during my PhD and preparation for viva via seminars in the fields of energy and power generation, and asking challenging questions during my progress review meetings. Also, I am innumerably grateful to Athanasios Kolios, who three years ago encouraged me to do a PhD and who supported me even before I started my PhD. Also, I would like to thank them for their contribution to my research that resulted in four co-authored journal papers.

Last, but not least, I would like to recognise the support from all the staff at the Energy theme and the Combustion and Carbon Capture and Storage Centre. My deep appreciation goes especially to Sam Skears and Melissa Lucas who promptly answered countless questions and provided me with enormous administrative support during the course of my research.

LIST OF PUBLICATIONS

Hanak, D.P., Kolios, A.J., and Manovic, V. (2016), "Comparison of probabilistic performance of calcium looping and chemical solvent scrubbing retrofits for CO_2 capture from coal-fired power plant", *Applied Energy*, 172, 323–336.

Hanak, D.P. and Manovic, V. (2016), “Calcium looping with supercritical CO_2 cycle for decarbonisation of coal-fired power plant”, *Energy*, 102, 343–353.

Hanak, D.P., Biliyok, C., and Manovic, V. (2016), “Calcium looping with inherent energy storage for decarbonisation of coal-fired power plant”, *Energy and Environmental Science*, 9, 971–983.

Hanak, D.P., Biliyok, C., Anthony, E.J., and Manovic, V. (2015), “Modelling and comparison of calcium looping and chemical solvent scrubbing retrofits for CO_2 capture from coal-fired power plant”, *International Journal of Greenhouse Gas Control*, 42, 226–236.

Hanak, D.P., Anthony, E.J., and Manovic, V. (2015), “A review of developments in pilot-plant testing and modelling of calcium looping process for CO_2 capture from power generation systems”, *Energy and Environmental Science*, 8, 2199–2249.

Hanak, D.P., Biliyok, C., and Manovic, V. (2015), “Evaluation and modelling of part-load performance of coal-fired power plant with post-combustion CO_2 capture”, *Energy and Fuels*, 29 (6), 3833–3844.

Hanak, D.P., Biliyok, C., and Manovic, V. (2015), “Efficiency improvements for the coal-fired power plant retrofit with CO_2 capture plant using chilled ammonia process”, *Applied Energy*, 151, 258–272.

Hanak, D.P., Biliyok, C., and Manovic, V. (2015), "Rate-based model development, validation and analysis of chilled ammonia process as an alternative CO_2 capture technology for coal-fired power plants", *International Journal of Greenhouse Gas Control*, 34, 52–62.

Hanak, D.P., Kolios, A.J., Biliyok, C., and Manovic, V. (2015), "Probabilistic performance assessment of a coal-fired power plant", *Applied Energy*, 139, 350–364.

This page intentionally left blank.

DECLARATION

I declare that no part of the work presented in this PhD thesis has been submitted for any other degree or other academic or professional distinction. Nine papers published between 2015 and 2016 in high-impact-factor journals are contained in this submission. These contributions to knowledge are co-authored with Vasilije Manovic (Principal supervisor, all papers), Chechet Biliyok (Associate supervisor, six papers), Edward J. Anthony (Subject advisor, two papers), and Athanasios J. Kolios (Senior lecturer in Risk and Reliability Engineering, two papers), who contributed through proof-reading and providing critical comments on the manuscripts prior to their submission to the journals. The nine journal papers contained in this submission were published by Elsevier, Royal Society of Chemistry, and American Chemical Society that allow reusing and reproducing the entire published material in an unchanged form in the PhD Thesis.

Elsevier[a]

"*Theses and dissertations which contain embedded PJAs [Published Journal Article] as part of the formal submission can be posted publicly by the awarding institution with DOI links back to the formal publications on ScienceDirect*."

Royal Society of Chemistry[b]

"*You do not need to request permission to reuse your own figures, diagrams, etc, that were originally published in a Royal Society of Chemistry publication. However, permission should be requested for use of the whole article or chapter except if reusing it in a thesis.*"

"*When the author accepts the licence to publish for a journal article, he/she retains certain rights concerning the deposition of the whole article."* "*Republish*

[a] Elsevier (2016), *Article sharing*, Elsevier B.V., available online: www.elsevier.com/about/company-information/policies/sharing (last accessed:18/03/2016)
[b] RSC (2016), *Licences, copyright & permissions*, Royal Society of Chemistry, available online: http://www.rsc.org/journals-books-databases/journal-authors-reviewers/licences-copyright-permissions/#about-licence (last accessed: 18/03/2016)

the PDF of the version of record in theses of the author(s) in printed form and may make available this PDF in the theses of author(s) via any website(s) that the university(ies) of the author(s) may have for the deposition of theses. No embargo period applies."

American Chemical Society[c]

"*Reuse/Republication of the Entire Work in Theses or Collections: Authors may reuse all or part of the Submitted, Accepted or Published Work in a thesis or dissertation that the author writes and is required to submit to satisfy the criteria of degree-granting institutions. Such reuse is permitted subject to the ACS' "Ethical Guidelines to Publication of Chemical Research"; the author should secure written confirmation (via letter or email) from the respective ACS journal editor(s) to avoid potential conflicts with journal prior publication*/embargo policies. Appropriate citation of the Published Work must be made**. If the thesis or dissertation to be published is in electronic format, a direct link to the Published Work must also be included using the ACS Articles on Request author-directed link.*"

[c] ASC (2016), *Permissions/RightsLinks - Permission Requests and Credit Lines*, American Chemical Society Publications, available online: http://pubs.acs.org/page/copyright/permissions_otherpub.html (last accessed: 18/03/2016).

TABLE OF CONTENTS

LIST OF FIGURES

LIST OF TABLES

LIST OF ABBREVIATIONS

2DS	2°C scenario
AAP	Aqueous ammonia process
AMP	2-amino-2-methyl-1-propanol
CaL	Calcium looping
CAP	Chilled ammonia process
CCS	Carbon capture and storage
ESA	Electrical swing adsorption
IL	Ionic liquids
MDEA	Methyldiethanolamine
MEA	Monoethanolamine
OECD	Organisation for Economic Cooperation and Development
PSA	Pressure swing adsorption
PZ	Piperazine
s-CO_2	Supercritical CO_2 cycle
TSA	Temperature swing adsorption
VSA	Vacuum swing adsorption

1 INTRODUCTION

1.1 Background

A recent study by the Intergovernmental Panel on Climate Change (2013) has revealed that anthropogenic activities have contributed to climate change with a 95% probability. This is mainly attributed to the extensive utilisation of fossil fuels that led to an increase in the average CO_2 concentration in the atmosphere from 280 ppm_v in the pre-industrial period to more than 400 ppm_v in May 2013 (IEA, 2013a; Olivier et al., 2013) and to 401.6 ppm_v in December 2015 (Dlugokencky and Tans, 2016). The recent data by the National Oceanic and Atmospheric Administration (Dlugokencky and Tans, 2016; IEA, 2015a) suggest that the global mean CO_2 concentration has been increasing at a rate of 2.1 ppm_v per year over the past decade (Figure 1-1). If such trend continues and no mitigation measures are implemented, the global mean CO_2 concentration could increase to 540–685 ppm_v, depending on whether this trend would be of the first or second order.

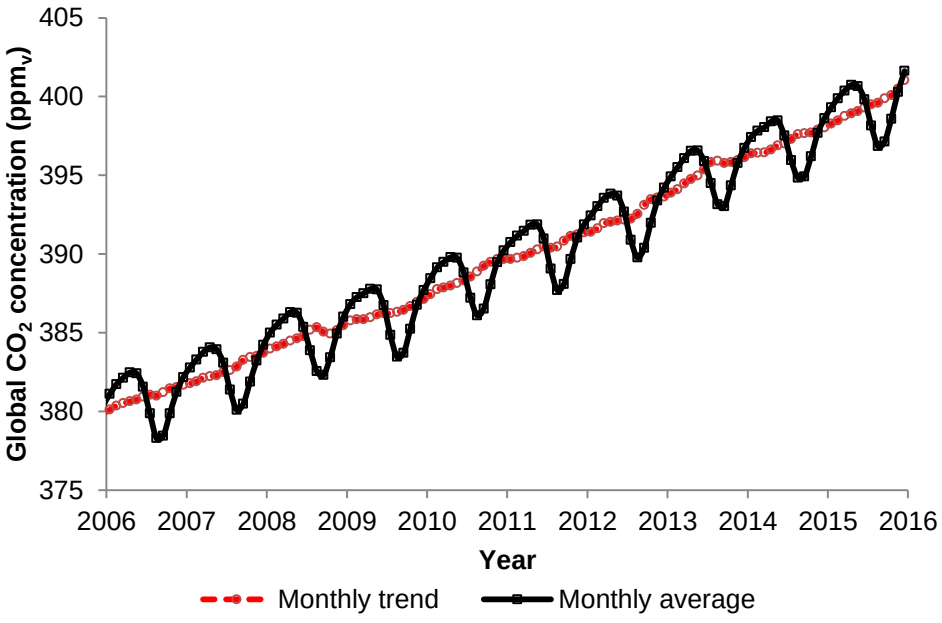

Figure 1-1: Variability of the global monthly mean CO_2 concentration over the past decade (Dlugokencky and Tans, 2016)

Because CO_2 is regarded as the most important species that contributes to the global warming effect, such a rise in its atmospheric concentration is blamed for fluctuations of the weather phenomena observed over the past five decades (GCCSI, 2012; IPCC, 2013; Maroto-Valer, 2010). Furthermore, it has been reported that anthropogenic greenhouse gas emissions have not only resulted in the increase of the mean Earth surface temperature by 0.74°C between 1906 and 2005, but also in the rise in the frequency of other weather phenomena, such as droughts, heavy precipitation, winds and cyclone activity. This has been found to result in melting of ice caps and snow covers, rise in the sea level and permanent flooding (IPCC, 2007a; Maroto-Valer, 2010). Therefore, if the current trend continues, there is a high confidence that further increase of the global mean temperature over the current level, even by 1–2°C, could greatly increase the frequency of extreme weather events, such as heat waves, heavy precipitation over most land areas, and coastal flooding due to unusually high sea levels (IPCC, 2014a, 2014b). These events could lead to disruption of existing ecosystems, fatalities due to heat waves and water shortages for elongated periods of time, drastic reduction of crop yields posing large risks to global food security, and even species extinction (IPCC, 2007a; King et al., 2015; Stangeland, 2007).

It has been suggested by the Intergovernmental Panel on Climate Change (2007b) that to limit the mean global temperature increase to 2–2.4°C above the pre-industrial level, which corresponds to a greenhouse gas stabilisation level of 450–550 $ppm_{v,CO2eq}$, the global CO_2 emissions have to be at least halved by 2050 compared to the emission levels in 1990. To preserve a 50% chance of keeping the mean global temperature increase below 2°C, it has been estimated that a maximum of 2900–3200 Gt of CO_2 can be emitted from anthropogenic sources, of which 1970 Gt of CO_2 have already been emitted before 2014 (IPCC, 2014c). To mitigate adverse climate change, it was agreed at the Copenhagen Conference held in 2009 to limit the atmospheric greenhouse gas concentration to 450 $ppm_{v,CO2eq}$ (European Commission, 2011a). To comply with this recommendation, the European Union has a commitment to reduce its greenhouse gas emissions by 30% by 2020

(European Commission, 2007), 40% by 2030 (European Commission, 2014; European Council, 2014) and even by 80–95% by 2050 (European Commission, 2011a). In the United Kingdom, the Climate Change Act (2008) has set up the legally binding target to reduce greenhouse gas emissions relative to 1990 levels by at least 80% by 2050. Yet, it has been recently suggested through the Paris Agreement reached at the 21st Conference of the Parties that to significantly reduce the risks and impacts of climate change, the mean temperature increase needs to be held well below 2°C and efforts to limit it to 1.5°C above pre-industrial levels need to be pursued (UN, 2015).

Being highly dependent upon fossil fuels, the power sector alone was responsible for more than a third of the total greenhouse gas emissions in 2010 (UNEP, 2012). Therefore, it is projected to become nearly completely decarbonised by 2050 to help meet the greenhouse gas emission reduction target (European Commission, 2011b). This implies that although contribution of all sectors of the European Union economy is required to reach the greenhouse gas emissions reduction target, a transition towards low-carbon power generation is crucial to mitigate adverse climate change. For this reason, a 2°C scenario (2DS) presented by the International Energy Agency (2010a, 2013b) assumes that decarbonisation of the power sector would solely account for 36% of the global greenhouse gas emission reduction in 2020. This scenario predicts also that although coal will be present in the energy portfolio, it needs to be utilised efficiently and in agreement with the environmental targets. At the same time, renewable energy technologies, gas-fired power plants and nuclear power plants should be widely implemented at the expense of coal-based power generation (IEA, 2010a, 2013c). Yet, recent reports published by the International Energy Agency (2013a, 2015b) have stated that the world is not on track to meet the 2DS objectives due to delay in implementation of low-carbon technologies. For this reason, the International Energy Agency has argued that the temperature increase is more likely to fall between 3.6°C and 5.3°C rather than below 2°C. Although meeting 2DS objectives is still achievable, it would be a challenging and demanding task requiring immediate action.

1.2 Motivation

A main reason behind the high carbon-intensity of the power sector is a large share (>40%) of coal in the global electricity production portfolio (Figure 1-2) (IEA, 2010b, 2015b, 2015c). Coal-fired power plants alone were responsible for over 70% of total CO_2 emissions from the power sector in 2010 (IEA, 2013b) and accounted for nearly 30% of the global primary energy consumption in 2012 (IEA, 2015b). Moreover, the recent emergence of shale gas in North America has resulted in an increase of American coal exports. This, in turn, has been reflected by the changes in the European Union energy market where the share of coal in electricity generation has increased considerably at the expense of the share of gas (IEA, 2013b). If the current market trend continues, coal would remain in use to meet an ample proportion of the power generation capacity, as predicted by the Energy Information Administration (2015). Consequently, decarbonisation of the power sector could become even more challenging in the future, especially in light of projected expansion of the energy demand by up to 37% by 2040 (EIA, 2015).

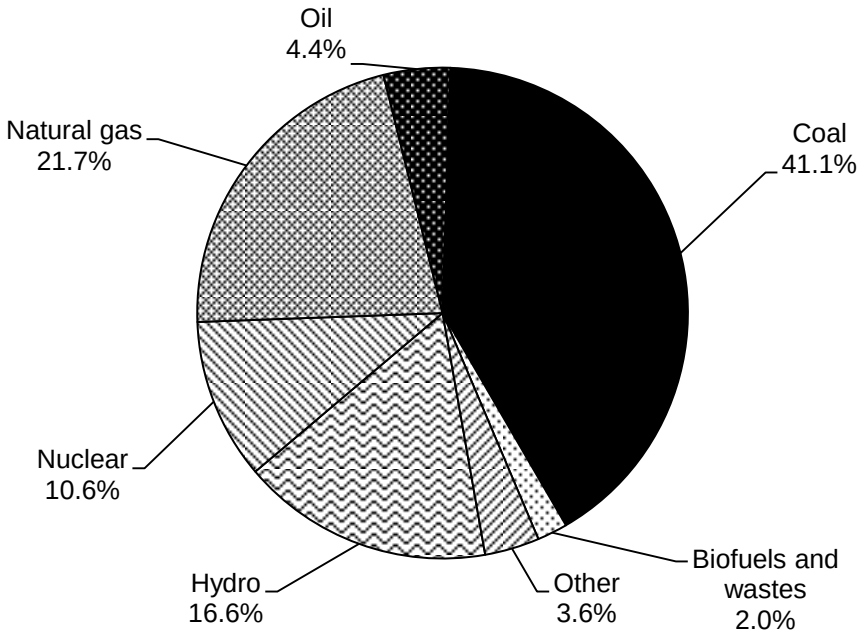

Figure 1-2: Energy sources share in global electricity supply in 2013 (IEA, 2015c)

Another reason for the high carbon-intensity of the power sector is the low average net efficiency of the global coal-based power plant fleet ($33\%_{LHV}$) that

is the result of a large share (75%) of inefficient subcritical units (IEA, 2013b). For this reason, implementation of coal-fired power plants that operate at supercritical steam parameters has been identified as an essential measure to meet the Copenhagen Accord goals (IEA, 2010a). The supercritical unit is characterised by higher thermal efficiency, and thus its specific CO_2 emissions can be lower by up to 15% compared to the subcritical unit of the same capacity (Beér, 2007). In the long term, however, implementation of the supercritical units would not suffice for a complete decarbonisation of the power sector as increase in the power generation efficiency and fuel switching are predicted to account only for 1% of the cumulative CO_2 emission reduction by 2050 (IEA, 2015d, 2015e). According to the International Energy Agency (2015d, 2015e), around 43% of the cumulative CO_2 emissions from the power sector between 2012 and 2050 could be mitigated through implementation of carbon capture and storage (CCS), and utilisation of renewable energy sources.

CCS is expected to play a pivotal role in the reduction of greenhouse gas emissions from the power sector and is expected to result in a 13% cumulative reduction of CO_2 emission between 2012 and 2050 (IEA, 2015d, 2015e). However, rapid development and demonstration of CCS technologies are required if they are to be deployed after 2020 to meet 2DS objectives (IEA, 2010a). Unfortunately, although appropriate devices for CCS deployment exist in other industries (Rodríguez et al., 2010), current CCS projects in the power sector meet only 25% of the 2DS 2020 objective (IEA, 2013b) and the first-of-a-kind large-scale demonstration plant retrofitted to a coal-fired power plant was only commissioned in 2014 (Stéphenne, 2014). A main challenge that keeps CCS from large-scale deployment in the power sector is considerable capital and operating cost that would affect the cost of electricity. Despite being currently claimed as an economically infeasible solution for coal-fired power plants, the state of CCS deployment can be compared with flue gas desulphurisation technology that was initially criticised for imposing energy penalties on power plant output (Markusson, 2012).

Although three main CO_2 capture approaches were identified as applicable in the power sector − post-combustion, pre-combustion and oxy-combustion carbon capture − the post-combustion approach is expected to make a significant contribution to CO_2 emission reduction from fossil fuel power plants (Oexmann et al., 2012; Pfaff et al., 2010; Strube and Manfrida, 2011). However, the relatively high capital cost of the post-combustion CO_2 capture plant, which stems from the size of equipment required to accommodate the flue gas volume, and high energy-intensity of the mature processes leading to considerable efficiency penalty, which can reach up to 12.5% points (Xu et al., 2010; Yang et al., 2010), are associated with a significant increase in the cost of electricity (Table 1-1) (Bhown and Freeman, 2011; CSIRO, 2012). Although no cost-effective technology for fossil fuel power plants has yet been developed and demonstrated on a commercial scale, it is estimated that the capital investment to achieve the CO_2 emission reduction target without CCS would be increased by 40% (IEA, 2013b). Regardless of the associated costs, large-scale deployment of these technologies has also been predicted to reduce wholesale electricity prices in the United Kingdom by up to 15% by 2030 compared to a no-CCS scenario (Orion Innovation, 2013). Therefore, not only would CCS help to protect the climate, it would be a benefit to the fossil-fuel power plant fleet in future. Despite the challenges that need to be solved, it is expected that 63% of coal-fired power plants will be equipped with CCS installations by 2050 (IEA, 2013b).

Table 1-1: Impact of post-combustion CO_2 capture plant on electricity generation cost (CSIRO, 2012)

Plant type	Cost of electricity generation* [€/MW_{el}h]	
	No capture	Full-load capture
Subcritical	41.2	92.8
Supercritical	40.7	88.1
Ultra-supercritical	40.6	86.7

*USD/EUR conversion rate = 0.89 (10/02/2016)

Although fossil fuels are bound to remain an important energy source, it is predicted that the share of renewable energy sources in the energy portfolio

could increase to above 50% by 2050 (IEA, 2012). The greatest challenge of the renewable energy sources is, however, their intermittence (Pardo et al., 2014; Twidell and Weir, 2006) that would affect operation of the existing energy network (Jiang et al., 2012; Singh et al., 2011). Namely, the remaining power generation assets, mostly fossil-fuel power systems, would need to flexibly balance energy supply and demand, so that neither energy produced from the renewable energy sources is wasted nor energy shortages occur. Such periods of variable load operation or no operation would impose efficiency and economic penalties on the fossil-fuel power systems, especially for plants linked with CCS that are better suited for base-load operation (Arias et al., 2014). Due to their capacity of decoupling the energy supply and demand (IEA, 2014), energy storage technologies can increase the efficiency of energy utilisation and thus should be widely deployed along with low-emission technologies. However, energy storage could contribute towards CO_2 emission reduction only for high level penetration of renewable energy sources (Tuohy and O'Malley, 2011; Ummels et al., 2008). Otherwise, energy storage could increase CO_2 emissions, the extent of which depends on carbon prices and share of coal-based generation in the energy portfolio (IEA, 2012; Ummels et al., 2008) and, therefore, a synergy between renewable energy sources, low-carbon fossil fuel power generation and energy storage needs to be pursued.

1.3 Aim and objectives

The aim of this research is identification, quantification and analysis of the efficiency improvements and alternate operating modes of the coal-fired power plant retrofitted with post-combustion CO_2 capture process. To meet this aim, the following objectives have been established for this research project:

1. Conduct a general review on the efficiency improvement methods applicable to post-combustion CO_2 capture plants.
2. Conduct a detailed review of developments in the pilot-plant testing and modelling of the calcium looping process.
3. Develop base- and part-load models of the coal-fired power plant and validate them against data available in the public domain.

4. Develop and validate models of calcium looping and chilled ammonia post-combustion CO_2 capture plants.
5. Investigate alternative CO_2 capture technologies and integration configurations for reduction of the net efficiency penalty resulting from the CO_2 capture plant retrofit to the coal-fired power plants.
6. Evaluate performance of the developed configurations under off-design and alternative operating modes.
7. Adapt a methodology for a probabilistic performance assessment to analyse the impact of the post-combustion CO_2 capture plant retrofit to the coal-fired power plant.

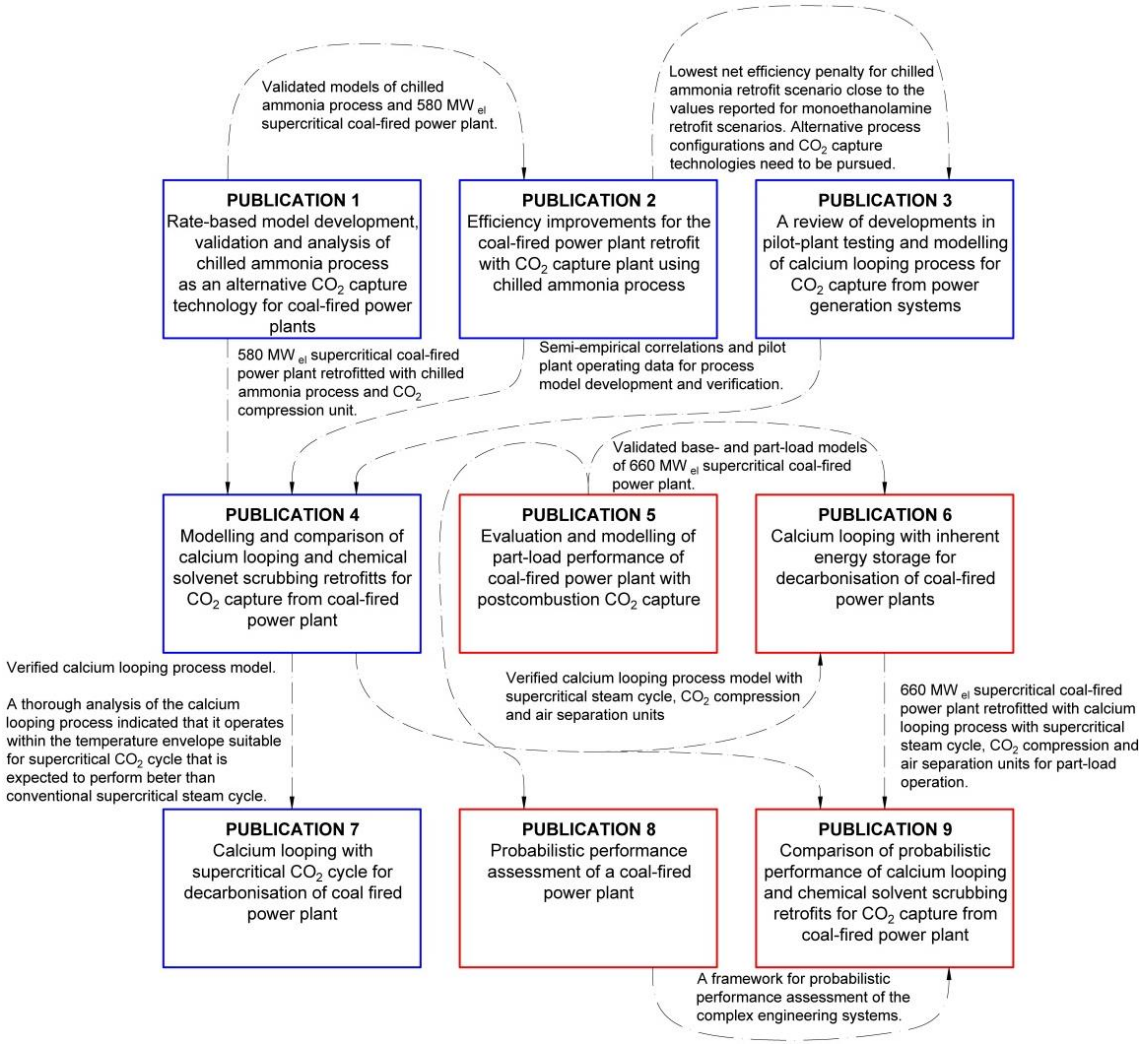

Figure 1-3: Coherence and interconnections of the project outputs (blue boxes refer to the base-load analysis and red boxes refer to the off-design and part-load analysis)

1.4 Novelty and linkage of project outputs

To achieve the objectives established for this research project, a number of contributions to the scientific body of knowledge have been made. These have been reported in nine peer-reviewed journal publications the linkage of which is presented in Figure 1-3.

Chemical solvent scrubbing using monoethanolamine (MEA) is regarded as the reference CO_2 capture technology that will probably be used in the early-stage commercial-scale post-combustion CO_2 capture plants (Blamey et al., 2010; Padurean et al., 2011; Pfaff et al., 2010). However, this technology is associated with solvent degradation and high energy requirement for solvent regeneration. Therefore, it has been found to impose a penalty on both the thermodynamic and economic performance of the retrofitted coal-fired power plant. For this reason, alternative chemical solvents have been investigated and NH_3 has been found to be a good candidate to replace MEA in post-combustion CO_2 capture plants. This is primarily due to lower energy requirement for solvent regeneration (Ciferno et al., 2005; Gal, 2006; Romeo et al., 2008b) and better resistance to solvent degradation due to the presence of SO_x and NO_x in the flue gas (Wang et al., 2011; Zhao et al., 2012). Although performance of the chilled ammonia process (CAP), which operates at low temperatures (<20°C) to limit NH_3 slip in the absorber (Linnenberg et al., 2012), has already been investigated through thermodynamic modelling and process simulations (Darde et al., 2010; Jilvero et al., 2011; Linnenberg et al., 2012; Versteeg and Rubin, 2011), most of the studies utilised the equilibrium-based approach. As the rate-based approach has been reported to be more accurate and reliable in modelling CO_2 capture plants based on chemical solvent scrubbing (Afkhamipour and Mofarahi, 2013), such approach has been employed to represent the CAP plant (Publication 1). Due to no pilot plant operating data available for the CAP process, the rate-based model for the aqueous ammonia process (AAP) was first developed. The prediction of this model was found to be in agreement with the operating data from the Munmorah pilot plant (Yu et al., 2011). The process model has been then tuned to operate under

CAP conditions (Objective 4) and scaled up for 90% CO_2 capture level from the commercial-scale 580 MW_{el} supercritical coal-fired power plant, which has been developed based on, and validated with, data provided in the revised NETL report (Black, 2013) (Objective 3). In addition, process analysis has also been performed to identify the optimum operating point. The equivalent work requirement for the CAP plant operated under optimised conditions was found to be up to 15.7% lower than for the reference MEA plant. Next, high-fidelity models of the commercial-scale CAP plant and the 580 MW_{el} supercritical coal-fired power plant developed in Publication 1 were integrated in a common simulation environment to evaluate the improvements in the net thermal efficiency of the retrofitted system through increasing the degree of heat and work integration (Publication 2, Objective 5). As opposed to the other studies evaluating CAP retrofits to coal-fired power plants, the rate-based approach was used to reliably estimate the energy requirement of the CAP plant and the Stodola ellipse law was employed to account for the pressure loss due to steam extraction from the steam cycle (Objective 6). Analysis of a basic integration scenario revealed that the efficiency penalty fell between 10.4–10.9% points depending on the stripper pressure (10.0–17.5 bar). In evaluating novel measures to improve performance of the retrofitted system, the efficiency penalty was reduced to 8.7–8.8% points through coupling a new single- or two-stage auxiliary steam turbine, respectively, with the boiler feedwater pump for extracted steam pressure control and attaching a back-pressure turbine for maintaining desired discharge pressure of the intermediate-pressure steam turbine. Nevertheless, the process analysis has indicated that the net impact on the performance of the reference coal-fired power plant is close to the lowest value reported in literature for post-combustion chemical solvent scrubbing using amines (Goto et al., 2013; Xu et al., 2010; Yang et al., 2010). Therefore, further measures, including heat integration, alternative process configurations and CO_2 capture technologies have been pursued.

A promising alternative to chemical solvent scrubbing is an emerging CO_2 capture technology called calcium looping (CaL) that uses a calcium-based

solid sorbent at high temperature to remove CO_2 from flue gas leaving the coal-fired power plant (Abanades et al., 2015). The state-of-the-art integration scenarios reported in the literature assume that the high-grade heat available in the CaL process is recovered to generate an additional amount of steam in the secondary steam cycle. Retrofit of the CaL plant to coal-fired power plants was found to not only reduce the net efficiency penalty to 3–8% points (Abanades et al., 2005; Martínez et al., 2011; Romeo et al., 2008a; Ströhle et al., 2009; Vorrias et al., 2013; Yang et al., 2010), but also to increase the net power output of the retrofitted system by 50–80% (Hanak et al., 2015a; Li et al., 2008; Romeo et al., 2009; Ströhle et al., 2009; Vorrias et al., 2013). In recent years, development of the CaL process for decarbonisation of fossil fuel power plants has advanced rapidly, especially after 2009, due to the introduction of new test facilities, novel correlations for process modelling, and novel process configurations for improved performance. Therefore, the developments emanating from the new test facilities worldwide, modelling approaches and integration scenarios have been reviewed to guide and drive the development of the CaL concept (Publication 3, Objective 2). Having reviewed the bench-scale and pilot-plant test facilities available worldwide, the characteristics and operating conditions of these facilities, as well as the key experimental findings have been extracted and summarised to provide information for development, and validation or verification of the CaL process models. Furthermore, the current literature was found to offer a vast range of models and semi-empirical correlations to represent the processes involved in CaL, which have been thoroughly reviewed and classified under five model complexity levels. In addition, the limitations of the particular model complexity level were assessed and the needs for modelling baselines for further process analyses were identified. Such information would assist researchers to select the appropriate model to represent CaL performance depending on the complexity and level of detail required. Finally, the focus was put on reviewing scenarios for CaL retrofitted to the fossil fuel power plants, including coal-fired power plants, natural gas combined cycle power plants and integrated gasification combined cycle power plants, as well as novel CaL process

configurations for improved process performance. This review aimed at evaluating the current state-of-the-art and providing a baseline for development of novel process configurations that would result in lower net efficiency penalties when retrofitted with fossil fuel power plants.

Using the findings from, and pilot-plant data gathered through, the detailed literature review (Publication 3), the CaL process model has been developed and its performance has been verified against the operating data from the 1.7 MW_{th} pilot facility at la Pereda power plant (Publication 4, Objective 4). As the model predictions were found to be in agreement with the pilot-plant data under different flue gas loads, it has been scaled up to process the flue gas from the 580 MW_{el} supercritical coal-fired power plant, the model of which has been developed in Publication 1. Using the same coal-fired power plant as a reference, the performance of the CaL plant have been directly compared for the first time against more mature MEA and CAP plants, the high-fidelity process models of which have been developed previously (Hanak et al., 2014, 2015b) and the integration strategy has been described in Publication 2. The results of the process analysis revealed that the efficiency penalty imposed in the CaL retrofit scenario was 6.7–7.9% points, depending on the kind of fuel used for oxy-combustion in the calciner. Such performance of CaL complies with the data reported in the literature and compares favourably to the MEA and CAP retrofit scenarios, which have resulted in net efficiency penalties of 9.5% and 9.0% points, respectively (Objective 5). Moreover, the retrofit of CaL to the considered coal-fired power plant was found to be less complex and, because CaL can be seen as a new boiler, to generate double net power output compared to the chemical solvent scrubbing scenarios. The process analysis also revealed that more than 70% of the total parasitic load in the CaL plant stems from the power requirement to run compressors in the CO_2 compression and air separation units. This implied that further reductions in the net efficiency penalty of the CaL retrofit scenario can be reached through alternative process integration configurations that would be characterised with reduced heat requirement for sorbent regeneration and alternative CaL process configurations, such as high-pressure calcination, combined calcium and

chemical looping process, and development of indirectly-fired calciner designs. Finally, it has been identified that if biomass is used as a fuel in the calciner, the CaL retrofit scenario can become a negative emitter of CO_2, contributing to decarbonisation of the power system to an even higher extent.

Having analysed the CaL retrofit scenario thoroughly (Publication 4), it has been noted that the CaL plant operates within a temperature range similar to the other technologies, such as nuclear or concentrating solar power plants, for which alternative thermodynamic cycles, such as the Brayton cycle using He or supercritical CO_2 (s-CO_2), have been successfully adapted (Floyd et al., 2013; Herranz et al., 2009; Linares et al., 2015; Moisseytsev and Sienicki, 2009; Padilla et al., 2015; Turchi et al., 2013; Yu et al., 2015). In contrast to the state-of-the-art CaL integration scenarios, which assume that high-grade heat from the CaL plant is used to generate steam for the conventional steam cycle based on the Rankine cycle, it has been proposed to link the CaL plant with the s-CO_2 cycle for high-grade heat recovery (Publication 7, Objective 5). The process analysis of the proposed concept revealed that the net efficiency penalty of such retrofit scenario would be 1%$_{HHV}$ point better compared to the CaL with the conventional reheated supercritical steam cycle operating with the same high-pressure turbine inlet conditions (242.2 bar/593°C/593°C) reported in Publication 4. A further reduction of the net efficiency penalty to 5.8%$_{HHV}$ points was achieved through considering a pump instead of a first CO_2 compression stage and increasing the turbine inlet temperature to 620°C and pressure to 300 bar, proving viability of the proposed concept for coal-fired power plant decarbonisation. Further improvements in the performance of CaL with the s-CO_2 retrofit scenario could be achieved through increasing the level of heat integration in the CaL plant, minimising the parasitic load associated with O_2 production and CO_2 compression, as well as increasing the efficiency of the secondary steam cycle through developing novel configurations that would allow increasing the turbine inlet temperature.

Fossil fuel power plants with CO_2 capture are expected play an essential role in the future energy portfolio because these systems will need to act as flexible

power generating capacity that will make up for the intermittency of renewable energy sources (IEA, 2012; Jiang et al., 2012; Singh et al., 2011). Therefore, it is essential to quantify the performance of CO_2 capture retrofit scenarios under part-load operation and to benchmark them with the performance under base-load operation. Although commercial software, such as EBSILON Professional, GateCycle, and Cycle Tempo, allows analysing the part-load performance of fossil fuel power plants, it does not support such analysis for the CO_2 retrofit scenarios. Therefore, it is a common practice to use separate software to model the CO_2 capture plant and the fossil-fuel power plant, and then to feed the results back from one simulation environment to another via automatic interface or manual iterations (Cau et al., 2014a, 2014b; Karmakar and Kolar, 2013; Pfaff et al., 2010; Tola and Pettinau, 2014). Although the power cycles were successfully modelled in process simulators (Han et al., 2014; Pei et al., 2013; Seltzer et al., 2006; Yan et al., 2013), which are commonly used to model CO_2 capture processes, model predictions have usually been limited to base-load cases, making them unsuitable for analysis of multiple off-design or part-load cases. Moreover, in modelling the off-design performance of chemical scrubbing CO_2 capture plants, it is a common practice to assume a fixed regeneration temperature and the specific heat requirement for solvent regeneration (Jordal et al., 2012; Stępczyńska-Drygas et al., 2013). Therefore, a framework for building power cycle models in Aspen Plus®, which are capable of providing a reliable prediction for the part-load performance of CO_2 capture retrofit scenarios, has been proposed (Publication 5, Objective 6). Using this framework, the process model of the 660 MW_{el} supercritical coal-fired power plant has been developed and validated with data available in the literature under different part-load conditions (Objective 3). The overall prediction of the model was in good agreement with the available data, proving the validity of the proposed modelling framework, although the live steam pressure was underestimated at part-load operation, up to a maximum of 5.3%. The process analysis of the 660 MW_{el} supercritical coal-fired power plant retrofitted with the MEA solvent scrubbing plant, the process model of which has been developed previously by Hanak et al. (2014), revealed that the net

efficiency penalty would vary between 10.5–14.7%$_{HHV}$ points, depending on the operating load and the extracted steam pressure. It has also been observed that the heat requirement for solvent regeneration has not changed linearly with reduction in the power plant load. This implies that the assumption of constant specific heat requirement for solvent regeneration is not valid, and will lead to underestimation of the amount of heat required by the CO_2 capture plant. Importantly, it has been shown that the net efficiency of the retrofitted system can be overestimated by up to 1.3%$_{HHV}$ point, if the off-design conditions due to steam extraction are not properly accounted for. Therefore, this study reinforces the need for using detailed high-fidelity process models in analysing the CO_2 capture retrofit scenarios in order to obtain a more profound insight into operation of the retrofitted system and assess the process performance in a more reliable fashion.

In contrast to the fossil-fuel power plants, however, the mature CO_2 capture systems have been shown to be better suited for base-load operation (Arias et al., 2014). This is mostly because they would impose higher efficiency penalties under part-load operation, as has been shown in Publication 5. Moreover, in the energy portfolio comprising a large share of renewables, it is expected that energy storage technologies would be widely deployed along with low-emission technologies in order to maintain the balance between electricity supply and demand. These technologies would also increase the degree of energy utilisation by storing the excess amount of energy from renewable energy sources that would have been otherwise wasted. Before being proposed as a viable CO_2 capture technology for coal-fired power plants, CaL had been proposed for energy storage from solar power plants (Baker, 1973; Ervin, 1977); however, challenges such as the requirement for temporary CO_2 storage and sorbent deactivation were identified and delayed the technology implementation (Ervin, 1977; Yan et al., 2015). By linking the energy storage and CO_2 capture capabilities of CaL, the novel concept for CaL with inherent energy storage has been proposed (Publication 6, Objective 6). Such process would resolve the issues related to the energy storage capacity as the coal-fired power plant would act as a permanent source of CO_2 and hydration could be

used as a mean for sorbent regeneration (Objective 5). The techno-economic assessment of the proposed concept, which was conducted using the process models presented in Publication 4 and Publication 5, revealed that integration of the CCS and energy storage capability of CaL can increase the degree of energy utilisation and, more importantly, can lead to higher profit than for current fossil fuel power plants without CO_2 capture. It is expected that other clean coal technologies, such as chemical looping combustion or oxy-combustion, would also benefit from utilising their inherent energy storage capacity.

Although analysis of the CO_2 capture retrofit scenarios under variable operating loads and modes provides a valuable insight into the process design, process equipment is usually sized using safety factors, which are retrieved from sizing guidelines based mainly on field experience, to avoid exceedance of material and operability limits. Such approach can lead to equipment oversizing, and thus lower equipment efficiency, and increased capital and operating costs (ABB, 2009; Drbal et al., 1996; Liptak, 2005). Therefore, it has been proposed to apply an alternative non-intrusive stochastic methodology to determine the probability of equipment failure under uncertain input (Publication 8, Objective 7). Such a probabilistic approach to assessment of coal-fired power plant performance utilises a set of deterministic outputs, which were generated using the 660 MW_{el} supercritical coal-fired power plant model described in Publication 5, to develop the robust approximation model that was used in the Monte Carlo simulation to evaluate the reliability indices and the probabilities for equipment failures. The probabilistic analysis revealed that the operating load of the coal-fired power plant and its uncertainty have the highest impact on the operating conditions, indicating the need for considering application of the probabilistic approach to process design. Therefore, the probabilistic approach presented in Publication 8 has been employed to compare the performance of the 660 MW_{el} supercritical coal-fired power plant retrofitted with the MEA plant and the CaL plant (Publication 9, Objective 7). The design matrix for the probabilistic analysis has been generated using the process models developed in Publication 4, Publication 5

and Publication 6. The probabilistic analysis revealed that the most probable values for the efficiency penalties are 9.5% and 11.5% points in the CaL and MEA retrofit scenarios, respectively. Also, the net power output in the CaL retrofit scenario was found to be 40% higher than that of the reference coal-fired power plant and two times higher than that in the case of the MEA retrofit scenario, even considering higher uncertainty in the operating conditions of the CaL process. Finally, the probabilistic approach generated valuable information on the equipment operating envelope that would help designers assessing the number of equipment trains and their operating limits.

In summary, via this research project the following definitive contributions to the scientific body of knowledge are made:

- A review of recent developments in the pilot-plant testing and modelling of the CaL process for power generation systems is performed in order to systematise the rapid advancements of this technology, especially after 2009, since the last major reviews by Blamey et al. (2010) and Dean et al. (2011).

- The large-sale CAP process for CO_2 capture from the coal-fired power plant is modelled using the rate-based approach, and a detailed description of the process model and its scale-up are presented, as opposed to other studies presented in the literature. Application of such approach to CAP process modelling is expected to provide a more reliable prediction of the actual process performance, and thus its energy requirement, compared to the commonly applied equilibrium approach. In addition, optimum thermodynamic and environmental performance is determined via a sensitivity study.

- Novel CAP retrofit scenarios are evaluated using a high-fidelity process model of the coal-fired power plant and the rate-based model of the CAP process to reduce the net efficiency penalty. Two novel configurations comprising a single- or two-stage auxiliary steam turbine coupled with the boiler feedwater pump and a back-pressure turbine for steam

pressure control in the retrofitted system are found to reduce the net efficiency penalty of the basic integration scenario by 2.1–2.2% points.

- Thermodynamic performance of CaL, CAP and MEA scrubbing retrofit scenarios is compared using the same reference coal-fired power plant for the first time, proving the superior performance of the CaL retrofit scenario at lower process complexity. The influence of key operating specifications of CaL and the fuel used in the calciner on the retrofitted system performance is also evaluated. The CaL retrofit scenario is found to impose a net efficiency penalty of 6.7–7.9% points, compared to 9% and 9.5% points for CAP and MEA retrofit scenarios, respectively.

- Application of the supercritical CO_2 cycle instead of the conventional steam cycle to recover heat from the CaL process retrofitted to the coal-fired power plant is proposed, as opposed to the state-of-the-art retrofit scenarios in the present literature. A sensitivity study on the supercritical CO_2 hardware and turbine operating conditions is performed. It has been shown that implementation of this cycle can reduce the net efficiency penalty by up to 2.1% points compared to the retrofit scenario in which the excess heat from CaL is utilised in the conventional steam cycle.

- A framework for building power cycle models in Aspen Plus® for evaluating the part-load and off-design performance of different CO_2 capture retrofit scenarios is proposed. Using this framework, the performance of the MEA retrofit scenario at different operating loads is thoroughly evaluated and the overestimation in the net thermal efficiency due to neglecting the off-design conditions is estimated.

- A novel concept for CaL with inherent energy storage for decarbonisation of the coal-fired power plant is proposed. Moreover, a techno-economic analysis is performed to show the benefits of the proposed concept over the reference system without energy storage and CO_2 capture.

- A probabilistic approach to assessment of coal-fired power plant performance is adapted for the first time. A similar approach has been successfully adapted in safety-critical applications in nuclear, aviation, manufacturing and offshore industries. The probabilistic approach considers the effect of uncertainty in the process model inputs on the performance prediction to estimate the probability that the specific system thresholds are exceeded. Such information will support equipment design and will indicate if conservative safety factors are required.

- Performance of the CaL and MEA retrofit scenarios is compared using the probabilistic approach. As such approach considers the effect of uncertainties on the performance prediction, it is expected that the estimation of net efficiency penalties and variation in the net power output would be more realistic. Additionally, the retrofit systems operating envelope is revealed, bringing a more profound insight into process operation, and thus its design. Furthermore, an implication of uncertainty and expected operating envelope on the CO_2 capture design is analysed through estimation of the probabilities that critical system thresholds are exceeded due to uncertainty in the system's operating conditions.

1.5 Outline of PhD thesis

The structure of this thesis has been organised around seven objectives established in Section 1.3 and comprises four main modules: literature review, model development, deterministic analysis and probabilistic analysis. Each module had input from several chapters and contributed towards dissemination of the research findings through publications in peer-reviewed journals, which were published due to rapid advancements in the field of low-carbon power generation and CCS (Figure 1-4). The content of each chapter is outlined below.

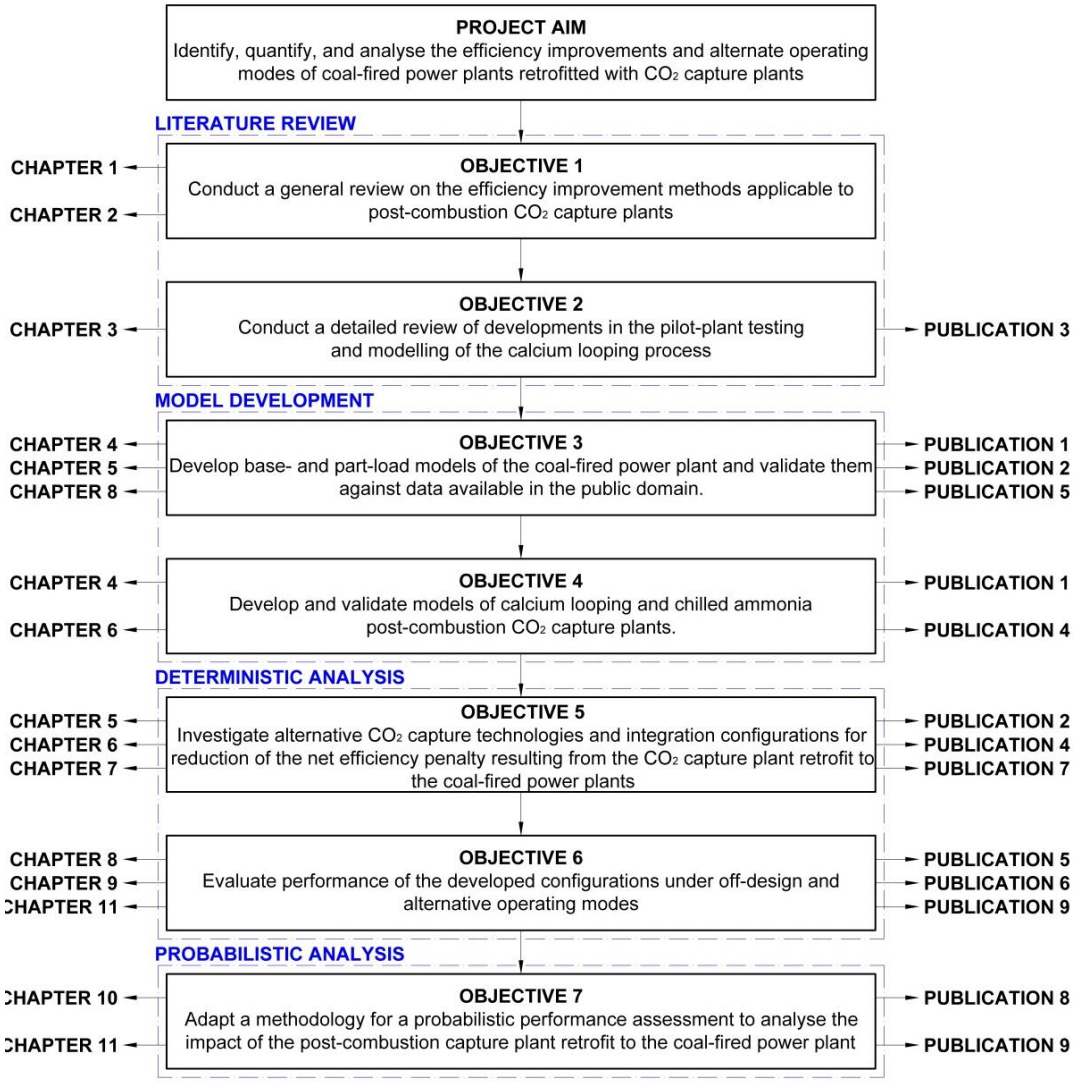

Figure 1-4: Structure of the PhD thesis and linkage of published papers to the project objectives

The background information and motivation for this PhD project that led to establishing the research aim and objectives were provided in Chapter 1. A general literature review presented in Chapter 2 provides a rationale for the power sector decarbonisation through outlining the information on climate change and greenhouse gas emissions. The decarbonisation measures for coal-fired power plants and the current stage of CCS deployment are also reviewed. The main part of this review provides an overview of the CCS chain, CO_2 capture and separation options viable for coal-fired power plants, and identification of efficiency improvements in post-combustion CO_2 capture. Since CaL has been identified as an emerging CO_2 capture technology for coal-fired

power plants, Chapter 3 presents a systematic review of the developments in pilot-plant testing, process modelling and integration of this technology with fossil fuel power plants, as well as identifies future research needs.

Use of alternative solvents, such as NH_3, has been identified as a viable option for reduction of the energy-intensity of chemical solvent scrubbing CO_2 capture technology. Chapter 4 provides a description of the rate-based model development, validation and analysis of CAP, as well as identifies its optimum operating conditions. The optimised model is then utilised to assess the efficiency improvements via alternative process configurations, work and heat integration, and reoptimisation of the operating conditions. Chapter 5, therefore, provides a description of the evaluated process configurations and benchmarks them against the reference MEA retrofit scenario. As no substantial improvement was obtained, Chapter 6 focuses on development and verification of the CaL process model, as well as performance comparison of CaL, CAP and reference MEA retrofit scenarios. Chapter 7 evaluates further improvement of the CaL retrofit scenario via investigating applicability of the s-CO_2 cycle to recover excess heat from the CaL process.

As coal-fired power plants often operate under part-load conditions to follow the market demand for electricity and such operation will become even more important at high penetration levels of renewable energy sources, Chapter 8 provides a framework for modelling of part-load or off-design operation of coal-fired power plants retrofitted with a post-combustion CO_2 capture plant. Additionally, the framework is used to benchmark different retrofit scenarios and to quantify the error made on neglecting off-design operation due to the CO_2 capture plant retrofit. Also, a techno-economic analysis of a new concept for CaL with inherent energy storage for decarbonisation of the coal-fired power plant is reported in Chapter 9. Furthermore, data generated using the part-load modelling framework are used in probabilistic analysis of the coal-fired power plant and comparison of the coal-fired power plant retrofit scenarios in Chapter 10 and Chapter 11, respectively. The general implications of the results obtained throughout this PhD project are discussed in Chapter 12. Finally,

Chapter 13 draws conclusions from this research project and provides recommendations for future research.

1.6 Dissemination from the PhD thesis

1.6.1 Peer-reviewed journal publications

Hanak, D.P., Kolios, A.J., and Manovic, V. (2016), "Comparison of probabilistic performance of calcium looping and chemical solvent scrubbing retrofits for CO_2 capture from coal-fired power plant", *Applied Energy*, 172, 323–336.

Hanak, D.P. and Manovic, V. (2016), “Calcium looping with supercritical CO_2 cycle for decarbonisation of coal-fired power plant”, *Energy*, 102, 343–353.

Hanak, D.P., Biliyok, C., and Manovic, V. (2016), “Calcium looping with inherent energy storage for decarbonisation of coal-fired power plant”, *Energy and Environmental Science*, 9, 971–983.

Hanak, D.P., Biliyok, C., Anthony, E.J., and Manovic, V. (2015), “Modelling and comparison of calcium looping and chemical solvent scrubbing retrofits for CO_2 capture from coal-fired power plant”, *International Journal of Greenhouse Gas Control*, 42, 226–236.

Hanak, D.P., Anthony, E.J., and Manovic, V. (2015), “A review of developments in pilot-plant testing and modelling of calcium looping process for CO_2 capture from power generation systems”, *Energy and Environmental Science*, 8, 2199–2249.

Hanak, D.P., Biliyok, C., and Manovic, V. (2015), “Evaluation and modelling of part-load performance of coal-fired power plant with post-combustion CO_2 capture”, *Energy and Fuels*, 29 (6), 3833–3844.

Hanak, D.P., Biliyok, C., and Manovic, V. (2015), “Efficiency improvements for the coal-fired power plant retrofit with CO_2 capture plant using chilled ammonia process”, *Applied Energy*, 151, 258–272.

Hanak, D.P., Biliyok, C., and Manovic, V. (2015), "Rate-based model development, validation and analysis of chilled ammonia process as an alternative CO_2 capture technology for coal-fired power plants", *International Journal of Greenhouse Gas Control*, 34, 52–62.

Hanak, D.P., Kolios, A.J., Biliyok, C., and Manovic, V. (2015), "Probabilistic performance assessment of a coal-fired power plant", *Applied Energy*, 139, 350–364.

1.6.2 Conference publications

Hanak, D.P., Biliyok, C., Anthony, E.J., and Manovic, V. (2015), “A study of integration of calcium looping CO_2 capture plant and coal-fired power plant”, *Proceedings of 7th International Conference on Clean Coal Technologies*, Cracow, Poland, available online: http://bit.ly/1Urn0pN (last accessed: 29/03/2016).

Hanak, D.P., Manovic, V., and Anthony, E.J. (2014), "The Future of Ca Looping - A review of developments", *Proceedings of Industrial Fluidization South Africa (IFSA 2014)*, Johannesburg, South Africa, 9–33.

Hanak, D.P., Biliyok, C., Yeung, H. and Manovic, V. (2014), “Rate-based modelling of chilled ammonia process (CAP) for CO_2 capture”, *Computer Aided Process Engineering*, 33, 181–186.

1.6.3 Conference and workshop presentations

Hanak, D.P., Biliyok, C., and Manovic, V. (2016), “Calcium looping for decarbonisation of coal-fired power plants”, *Science for the Green Economy Conference*, 13–14th January 2016, held at Cranfield University, Cranfield, UK.

Hanak, D.P., Biliyok, C., and Manovic, V. (2015), “Calcium looping for decarbonisation of coal-fired power plants”, *School of Energy, Environment and Agrifood Laboratory Opening Event*, 23rd November 2015, held at Cranfield University, Cranfield, UK.

Hanak, D.P., Biliyok, C., Anthony, E.J., and Manovic, V. (2015), “Evaluation of a calcium looping CO_2 capture plant retrofit to a coal-fired power plant”, *IEAGHG 6th High Temperature Solid Looping Cycles Network Meeting*, 1–2nd September 2015, held at Politecnico Di Milano, Milano, Italy.

Hanak, D.P., Biliyok, C., Anthony, E.J., and Manovic, V. (2015), “A study of integration of calcium looping CO_2 capture plant and coal-fired power

plant", *7th International Conference on Clean Coal Technologies*, 17–21st May 2015, held at Jagiellonian University, Cracow, Poland.

Hanak, D.P., Biliyok, C., and Manovic, V. (2015), "A calcium looping process as an efficient CO_2 capture technology for coal-fired power plants", *UKCCSRC Spring Biannual Meeting*, 19–21st April 2015, held at Cranfield University, Cranfield, UK.

Hanak, D.P., Biliyok, C., and Manovic, V. (2015), "A calcium looping process as an efficient CO_2 capture technology for coal-fired power plants", *Renewable Energy Marine Structures EPSRC Doctoral Training Centre Opening Event*, 4th March 2014, Cranfield University, Cranfield, UK.

Hanak, D.P., Biliyok, C., and Manovic, V. (2015), "A calcium looping process as an efficient CO_2 capture technology for coal-fired power plants", *UKCCSRC Network Early Career Researcher Winter School*, 16–19th February 2015, held at University of Nottingham, Nottingham, UK.

Hanak, D.P., Kolios, A.J., Biliyok, C., and Manovic, V. (2015), "Probabilistic performance assessment of a coal-fired power plant", 'Risk, resilience and adaptation' *A Cranfield seminar with Professor Sir Mark Walport, FRS FMed Sc*, 26th January 2015, held at Cranfield University, Shrivenham, UK.

Hanak, D.P., Biliyok, C., and Manovic, V., "Identification of heat integration opportunities in calcium looping CO_2 capture plant", *10th European Conference on Coal Research and its Applications*, 17–19th September 2014, held at University of Hull, Kingston upon Hull, UK.

Hanak, D.P., Biliyok, C., Yeung, H., and Manovic, V. (2014), "Rate-based Modelling of Chilled Ammonia Process (CAP) for CO_2 Capture", *24th European Symposium on Computer Aided Process Engineering*, 15–18th June 2014, held at Hungarian Academy of Sciences, Budapest, Hungary.

Hanak, D.P., Biliyok, C., and Manovic, V. (2014), "A calcium looping process as a cost-effective CO_2 capture technology for coal-fired power plants decarbonisation", *UKCCSRC Early Career Researcher Annual Networking Meeting*, 24–25th March 2014, held at University of York, York, UK.

References

Abanades, J.C., Anthony, E.J., Wang, J., and Oakey, J.E. (2005), “Fluidized bed combustion systems integrating CO_2 capture with CaO”, *Environmental Science and Technology*, 39, 2861–2866.

Abanades, J.C., Arias, B., Lyngfelt, A., Mattisson, T., Wiley, D.E., Li, H., Ho, M.T., Mangano, E., and Brandani, S. (2015), ”Emerging CO_2 capture systems”, *International Journal of Greenhouse Gas Control*, 40, 126–166.

ABB (2009), *Power Generation. Energy Efficient Design of Auxiliary Systems in Fossil-Fuel Power Plants*, ABB, Zurich, Switzerland and Wickliffe, OH, USA.

Afkhamipour, M. and Mofarahi, M. (2013), “Comparison of rate-based and equilibrium-stage models of a packed column for post-combustion CO_2 capture using 2-amino-2-methyl-1-propanol (AMP) solution”, *International Journal of Greenhouse Gas Control*, 15, 186–199.

Arias, B., Criado, Y.A., Sanchez-Biezma, A., and Abanades, J.C. (2014), ”Oxy-fired fluidized bed combustors with a flexible power output using circulating solids for thermal energy storage”, *Applied Energy*, 132, 127–136.

Baker, R. (1973), “The reversibility of the reaction $CaCO_3 \rightleftarrows CaO+CO_2$”, *Journal of Applied Chemistry and Biotechnology*, 23 (10), 733–742.

Beér, J.M. (2007), “High efficiency electric power generation: The environmental role”, *Progress in Energy and Combustion Science*, 33, 107–134.

Bhown, A.S. and Freeman, B.C. (2011), “Analysis and status of post-combustion carbon dioxide capture technologies”, *Environmental Science and Technology,* 45, 8624–8632.

Black, J. (2013), *Cost and performance baseline for fossil energy plants. Volume 1: Bituminous coal and natural gas to electricity*, Report no.: DOE20101397, Revision 2a, National Energy Technology Laboratory, Pittsburgh, PA, USA.

Blamey, J., Anthony, E.J., Wang, J., and Fennell, P.S. (2010), “The calcium looping cycle for large-scale CO_2 capture”, *Progress in Energy and Combustion Science*, 36, 260–279.

Cau, G., Tola, V., and Bassano, C. (2014a), “Performance evaluation of high-sulphur coal-fired USC plant integrated with SNO_X and CO_2 capture sections”, *Applied Thermal Engineering*, 74, 136–145.

Cau, G., Tola, V., and Deiana, P. (2014b), “Comparative performance assessment of USC and IGCC power plants integrated with CO_2 capture systems” *Fuel*, 116, 820–833.

Ciferno, J.P., DiPietro, P., and Tarka, T. (2005), *An economic scoping study for CO_2 capture using aqueous ammonia*, National Energy Technology Laboratory; National Energy Technology Laboratory; Advanced Resources International; Energetics Incorporated, Pittsburgh, PA, USA.

Climate Change Act 2008, Chapter 2 (2008), The Stationery Office, London, UK.

CSIRO (2012), *Assessing post-combustion capture for coal-fired power stations in Asia-Pacific partnership countries*, CSIRO Advanced Coal Technology, Newcastle, NSW, Australia.

Darde, V., Thomsen, K., van Well, W.J.M., and Stenby, E.H. (2010), “Chilled ammonia process for CO_2 capture”, *International Journal of Greenhouse Gas Control*, 4, 131–136.

Dean, C.C., Blamey, J., Florin, N.H., Al-Jeboori, M.J., and Fennell, P.S. (2011), “The calcium looping cycle for CO_2 capture from power generation, cement manufacture and hydrogen production”, *Chemical Engineering Research and Design*, 89 (6), 836–855.

Dlugokencky, E. and Tans, P. (2016), *Recent global CO_2*, NOAA Earth System Research Laboratory, available online: http://1.usa.gov/JN3NgG (last accessed 21/03/2016).

Drbal, L., Westra, K., and Boston, P. (1996), *Power Plant Engineering*, Springer, New York, NY, USA.

EIA (2015), *Annual energy outlook 2015 with projections to 2040*, U.S. Energy Information Administration, Washington, DC, USA.

Ervin, G. (1977), “Solar heat storage using chemical reactions”, *Journal of Solid State Chemistry,* 22 (1), 51–61.

European Commission (2014), *Communication from the Commission to the European Parliament, the Council, the European Economic and Social Committee and the Committee of the Regions, A policy framework for climate and energy in the period from 2020 to 2030*, European Commission, Brussels, Belgium.

European Commission (2011a), *Communication from the Commission to the European Parliament, the Council, the European Economic and Social Committee and the Committee of the Regions - A Roadmap for moving to a competitive low carbon economy in 2050*, European Commission, Brussels, Belgium.

European Commission (2011b), *Communication from the Commission to the European Parliament, the Council, the European Economic and Social Committee of the Regions - Energy Roadmap 2050*, European Commission, Brussels, Belgium.

European Commission (2007), *Communication from the Commission to the Council, the European Parliament, the European Economic and Social Committee and the Committee of the Regions, Limiting global climate change to 2 degrees Celsius: The way ahead for 2020 and beyond*, Commission of the European Communities, Brussels, Belgium.

European Council (2014), *European Council 23/24 October 2014 – Conclusions*, European Council, Brussels, Belgium.

Floyd, J., Alpy, N., Moisseytsev, A., Haubensack, D., Rodriguez, G., Sienicki, J., and Avakian, G. (2013), “A numerical investigation of the sCO_2 recompression cycle off-design behaviour, coupled to a sodium cooled fast reactor, for seasonal variation in the heat sink temperature”, *Nuclear Engineering and Design*, 260, 78–92.

Gal, E. (2006), *Chilled-ammonia post combustion CO_2 capture system – laboratory and economic evaluation results*, Electric Power Research Institute, Palo Alto, CA, USA.

GCCSI (2012), *The global status of CCS: 2012*, Global CCS Institute, Canberra, Australia.

Goto, K., Yogo, K., and Higashii, T. (2013), "A review of efficiency penalty in a coal-fired power plant with post-combustion CO_2 capture", *Applied Energy*, 111, 710–720.

Han, D., Duan, L., Duan, Y., Hu, H., and Pan, X. (2014), "Simulation and optimization of pressurized oxy-fuel combustion system", *Proceedings of the Chinese Society of Electrical Engineering*, 34, 756–762.

Hanak, D.P., Biliyok, C., Anthony, E.J., and Manovic, V. (2015a), "Modelling and comparison of calcium looping and chemical solvent scrubbing retrofits for CO_2 capture from coal-fired power plant", *International Journal of Greenhouse Gas Control*, 42, 226–236.

Hanak, D.P., Biliyok, C., and Manovic, V. (2015b), "Rate-based model development, validation and analysis of chilled ammonia process as an alternative CO_2 capture technology for coal-fired power plants", *International Journal of Greenhouse Gas Control*, 34, 52–62.

Hanak, D.P., Biliyok, C., Yeung, H., and Białecki, R., (2014), "Heat integration and exergy analysis for a supercritical high-ash coal-fired power plant integrated with a post-combustion carbon capture process", *Fuel* 134, 126–139.

Herranz, L.E., Linares, J.I., and Moratilla, B.Y. (2009), "Power cycle assessment of nuclear high temperature gas-cooled reactors", *Applied Thermal Engineering*, 29, 1759–1765.

IEA (2015a), *CO_2 emissions from fuel combustion – highlights*, IEA Publications, Paris, France.

IEA (2015b), *Tracking clean energy progress 2015. Energy technology perspectives 2015 excerpt. IEA Input to the Clean Energy Ministerial*, IEA Publications, Paris, France.

IEA (2015c), *Key electricity trends: Excerpt from Electricity Information* 2015, IEA Publications, Paris, France.

IEA (2015d), *Carbon capture and storage: The solution for deep emissions reductions*, IEA Publications, Paris, France.

IEA (2015e), *Energy technology perspectives 2015*, IEA Publications, Paris, France.

IEA (2014), *Technology roadmap: Energy storage*, IEA Publications, Paris, France.

IEA (2013a), *Redrawing the energy-climate map. World energy outlook special report*, IEA Publications, Paris, France.

IEA (2013b), *Tracking clean energy progress 2013. IEA Input to the clean energy ministerial*, IEA Publications, Paris, France.

IEA (2013c), *Technology roadmap: Carbon capture and storage,* IEA Publications, Paris, France.

IEA (2012), *Energy technology perspectives 2012: Pathways to a clean energy system*, IEA Publications, Paris, France.

IEA (2010a), *Energy technology perspectives 2010: Scenarios & strategies to 2050*, IEA Publications, Paris, France.

IEA (2010b), *Power generation from coal: Measuring and reporting efficiency performance and CO_2 emissions*, IEA Publications, Paris, France.

IPCC (2014a), *Climate change 2014: impacts, adaptation, and vulnerability. Contribution of working group II to the fifth assessment report of the Intergovernmental Panel on Climate Change*, Cambridge University Press, Cambridge, UK and New York, NY, USA.

IPCC (2014b), *Climate Change 2014: mitigation of climate change. Contribution of working group III to the fifth assessment report of the Intergovernmental Panel on Climate Change*, Cambridge University Press, Cambridge, UK and New York, NY, USA.

IPCC (2014c), *Climate change 2014: synthesis report. Contribution of working groups I, II and III to the fifth assessment report of the Intergovernmental*

Panel on Climate Change, Cambridge University Press, Cambridge, UK and New York, NY, USA.

IPCC (2013), *Climate change 2013: The physical science basis. Contribution of working group I to the fifth assessment report of the Intergovernmental Panel on Climate Change*. Cambridge Unviersity Press, Cambridge, UK and New York, NY, USA.

IPCC (2007a), *Climate change 2007: The physical science basis. Contribution of working group I to the fourth assessment report of the Intergovernmental Panel on Climate Change*. Cambridge University Press, Cambridge, UK and New York, NY, USA.

IPCC (2007b), *Climate change 2007: mitigation. Contribution of working group III to the fourth assessment report of the Intergovernmental Panel on Climate Change*, Cambridge University Press, Cambridge, United Kingdom and New York, NY, USA.

Jiang, R., Wang, J., and Guan, Y. (2012), "Robust unit commitment with wind power and pumped storage hydro", *IEEE Transactions on Power Systems*, 27, 800–810.

Jilvero, H., Normann, F., Andersson, K., and Johnsson, F. (2011), "Thermal integration and modelling of the chilled ammonia process", *Energy Procedia*, 4, 1713–1720.

Jordal, K., Ystad, P.A.M., Anantharaman, R., Chikukwa, A., and Bolland, O. (2012), "Design-point and part-load considerations for natural gas combined cycle plants with post combustion capture", *International Journal of Greenhouse Gas Control*, 11, 271–282.

Karmakar, S. and Kolar, A.K. (2013), "Thermodynamic analysis of high-ash coal-fired power plant with carbon dioxide capture", *International Journal of Energy Research*, 37, 522–534.

King, D., Schrag, D., Dadi, Z., Ye, Q., and Gosh, A. (2015), *Climate change: A risk assessment,* Centre for Science Policy, University of Cambridge, Cambridge, UK.

Li, Z.S., Cai, N.S., Croiset, E., Zhen-Shan, L., and Ning-Sheng, C. (2008), ”Process analysis of CO_2 capture from flue gas using carbonation/calcination cycles”, *AIChE Journal*, 54, 1912–1925.

Linares, J.I., Herranz, L.E., Fernández, I., Cantizano, A., and Moratilla, B.Y. (2015), “*Supercritical CO_2 Brayton power cycles for DEMO fusion reactor based on helium cooled lithium lead blanket*”, *Applied Thermal Engineering*, 76, 123–133.

Linnenberg, S., Darde, V., Oexmann, J., Kather, A., van Well, W.J.M., and Thomsen, K. (2012), “Evaluating the impact of an ammonia-based post-combustion CO_2 capture process on a steam power plant with different cooling water temperatures”, *International Journal of Greenhouse Gas Control*, 10, 1–14.

Liptak, B.G. (2005), *Instrument engineers’ handbook: process control and optimization*, CRC-Press, London, UK; New York, NY, USA; Washington, DC, USA.

Markusson, N. (2012), *The politics of FGD deployment in the UK (1980s-2009)*, UK Energy Research Centre, London, UK, available online: http://bit.ly/22rG8bK (last accessed: 21/03/2016).

Maroto-Valer, M.M., (2010), *Developments and innovation in carbon dioxide (CO_2) capture and storage technology. Volume 1: Carbon dioxide (CO_2) capture, transportation and industrial applications*, CRC press, London, UK; New York, NY, USA; Washington, DC, USA.

Martínez, I., Murillo, R., Grasa, G., and Abanades, J.C. (2011), “Integration of a Ca looping system for CO_2 capture in existing power plants”, *AIChE Journal*, 57, 2599–2607.

Moisseytsev, A. and Sienicki, J.J. (2009), “Investigation of alternative layouts for the supercritical carbon dioxide Brayton cycle for a sodium-cooled fast reactor”, *Nuclear Engineering and Design*, 239, 1362–1371.

Oexmann, J., Kather, A., Linnenberg, S., and Liebenthal, U. (2012), “Post-combustion CO_2 capture: chemical absorption processes in coal-fired

steam power plants", *Greenhouse Gases: Science and Technology*, 2, 80–98.

Olivier, J.G.J., Janssens-Maenhout, G., Muntean, M., and Peters, J.A.H.W. (2013), *Trends in global CO_2 emissions: 2013 Report*, PBL Netherlands Environmental Assessment Agency, The Hague, Netherlands.

Orion Innovations (2013), *A UK Vision for carbon capture and storage*, Orion Innovations Ltd., London, UK.

Padilla, R.V., Soo Too, Y.C., Benito, R., and Stein, W. (2015), "Exergetic analysis of supercritical CO_2 Brayton cycles integrated with solar central receivers", *Applied Energy*, 148, 348–365.

Padurean, A., Cormos, C.C., Cormos, A.M., and Agachi, P.S. (2011), "Multicriterial analysis of post-combustion carbon dioxide capture using alkanolamines", *International Journal of Greenhouse Gas Control*, 5, 676–685.

Pardo, P., Deydier, A., Anxionnaz-Minvielle, Z., Rougé, S., Cabassud, M., and Cognet, P. (2014), "A review on high temperature thermochemical heat energy storage", *Renewable and Sustainable Energy Reviews*, 32, 591–610.

Pei, X., He, B., Yan, L., Wang, C., Song, W., and Song, J. (2013), "Process simulation of oxy-fuel combustion for a 300 MW pulverized coal-fired power plant using Aspen Plus", *Energy Conversion and Management*, 76, 581–587.

Pfaff, I., Oexmann, J., and Kather, A. (2010), "Optimised integration of post-combustion CO_2 capture process in greenfield power plants", *Energy*, 35, 4030–4041.

Rodríguez, N., Alonso, M., and Abanades, J.C. (2010), "Average activity of CaO particles in a calcium looping system", *Chemical Engineering Journal*, 156, 388–394.

Romeo, L.M., Abanades, J.C., Escosa, J.M., Paño, J., Giménez, A., Sánchez-Biezma, A., and Ballesteros, J.C. (2008a), "Oxyfuel

carbonation/calcination cycle for low cost CO_2 capture in existing power plants", *Energy Conversion and Management*, 49, 2809–2814.

Romeo, L.M., Espatolero, S., and Bolea, I. (2008b), "Designing a supercritical steam cycle to integrate the energy requirements of CO_2 amine scrubbing", *International Journal of Greenhouse Gas Control*, 2, 563–570.

Romeo, L.M., Lara, Y., Lisbona, P., and Escosa, J.M. (2009), "Optimizing make-up flow in a CO_2 capture system using CaO", *Chemical Engineering Journal*, 147, 252–258.

Seltzer, A., Fan, Z., and Robertson, A. (2006), *Conceptual design of supercritical O_2-based PC boiler*, Foster Wheeler Power Group, Inc, Livingston, NJ, USA.

Singh, M., Khadkikar, V., Chandra, A., and Varma, R.K. (2011), "Grid interconnection of renewable energy sources at the distribution level with power-quality improvement features", *IEEE Transactions on Power Delivery*, 26, 307–315.

Stangeland, A. (2007), "A model for the CO_2 capture potential", *International Journal of Greenhouse Gas Control*, 1, 418–429.

Stępczyńska-Drygas, K., Łukowicz, H., and Dykas, S. (2013), "Calculation of an advanced ultra-supercritical power unit with CO_2 capture installation", *Energy Conversion and Management*, 74, 201–208.

Stéphenne, K. (2014), "Start-up of world's first commercial post-combustion coal fired CCS project: Contribution of Shell Cansolv to Saskpower Boundary Dam ICCS project", *Energy Procedia,* 63, 6106–6110.

Ströhle, J., Lasheras, A., Galloy, A., and Epple, B. (2009), "Simulation of the carbonate looping process for post-combustion CO_2 capture from a coal-fired power plant", *Chemical Engineering and Technology*, 32, 435–442.

Strube, R. and Manfrida, G. (2011), "CO_2 capture in coal-fired power plants - impact on plant performance", *International Journal of Greenhouse Gas Control*, 5, 710–726.

Tola, V. and Pettinau, A. (2014), “Power generation plants with carbon capture and storage: A techno-economic comparison between coal combustion and gasification technologies”, *Applied Energy*,113, 1461–1474.

Tuohy, A. and O’Malley, M. (2011), “Pumped storage in systems with very high wind penetration”, *Energy Policy*, 39, 1965–1974.

Turchi, C.S., Ma, Z., Neises, T.W., and Wagner, M.J. (2013), “Thermodynamic study of advanced supercritical carbon dioxide power cycles for concentrating solar power systems”, *Journal of Solar Energy Engineering*, 135, 041007.

Twidell, J. and Weir, A.D. (2006), *Renewable energy resources*, Second Edition, Taylor and Francis, London, UK and New York, USA.

Ummels, B.C., Pelgrum, E., and Kling, W.L. (2008), “Integration of large-scale wind power and use of energy storage in the Netherlands’ electricity supply”, *IET Renewable Power Generation*, 2, 34–46.

UN (2015), *Adoption of the Paris Agreement*, United Nations Framework Convention on Climate Change, Paris, France.

UNEP (2012), *The emissions gap report 2012*, United Nations Environment Programme (UNEP), Nairobi, Kenya.

Versteeg, P. and Rubin, E.S. (2011), “A technical and economic assessment of ammonia-based post-combustion CO_2 capture at coal-fired power plants”, *International Journal of Greenhouse Gas Control*, 5, 1596–1605.

Vorrias, I., Atsonios, K., Nikolopoulos, A., Nikolopoulos, N., Grammelis, P., and Kakaras, E. (2013), “Calcium looping for CO_2 capture from a lignite fired power plant”, *Fuel,* 113, 826–836.

Wang, M., Lawal, A., Stephenson, P., Sidders, J., and Ramshaw, C. (2011), “Post-combustion CO_2 capture with chemical absorption: A state-of-the-art review”, *Chemical Engineering Research and Design*, 89, 1609–1624.

Xu, G., Jin, H.G., Yang, Y.P., Xu, Y.J., Lin, H., and Duan, L. (2010), “A comprehensive techno-economic analysis method for power generation systems with CO_2 capture”, *International Journal of Energy Research*, 34, 321–332.

Yan, T., Wang, R.Z., Li, T.X., Wang, L.W., and Fred, I.T. (2015), “A review of promising candidate reactions for chemical heat storage”, *Renewable and Sustainable Energy Reviews*, 43, 13–31.

Yan, L., He, B., Pei, X., Li, X., and Wang, C. (2013), “Energy and exergy analyses of a zero emission coal system”, *Energy*, 55, 1094–1103.

Yang, Y., Zhai, R., Duan, L., Kavosh, M., Patchigolla, K., and Oakey, J. (2010), “Integration and evaluation of a power plant with a CaO-based CO_2 capture system”, *International Journal of Greenhouse Gas Control*, 4, 603–612.

Yu, S.C., Chen, L., Zhao, Y., Li, H.X., and Zhang, X.R. (2015), “A brief review study of various thermodynamic cycles for high temperature power generation systems”, *Energy Conversion and Management*, 94, 68–83.

Yu, H., Morgan, S., Allport, A., Cottrell, A., Do, T., McGregor, J., Wardhaugh, L., and Feron, P. (2011), “Results from trialling aqueous NH_3 based post-combustion capture in a pilot plant at Munmorah power station: Absorption”, *Chemical Engineering Research and Design*, 89, 1204–1215.

Zhao, B., Su, Y., Tao, W., Li, L., and Peng, Y. (2012), “Post-combustion CO_2 capture by aqueous ammonia: A state-of-the-art review”, *International Journal of Greenhouse Gas Control*, 9, 355–371.

This page intentionally left blank.

2 GENERAL LITERATURE REVIEW

2.1 Climate change and greenhouse gas emission

The Intergovernmental Panel on Climate Change (2007, 2012) has defined climate as an average weather usually described in terms of the variability and mean of temperature, precipitation and wind over a period of time, typically 30 years. Therefore, climate change is related to a long-term alternation of the climate state due to the fluctuations, and/or changes in the mean, of its properties (IPCC, 2012). The time-dependent evolution of the Earth's climate (Figure 2-1) is driven by both internal dynamics of the climate system and external factors the change of which affect the climate state.

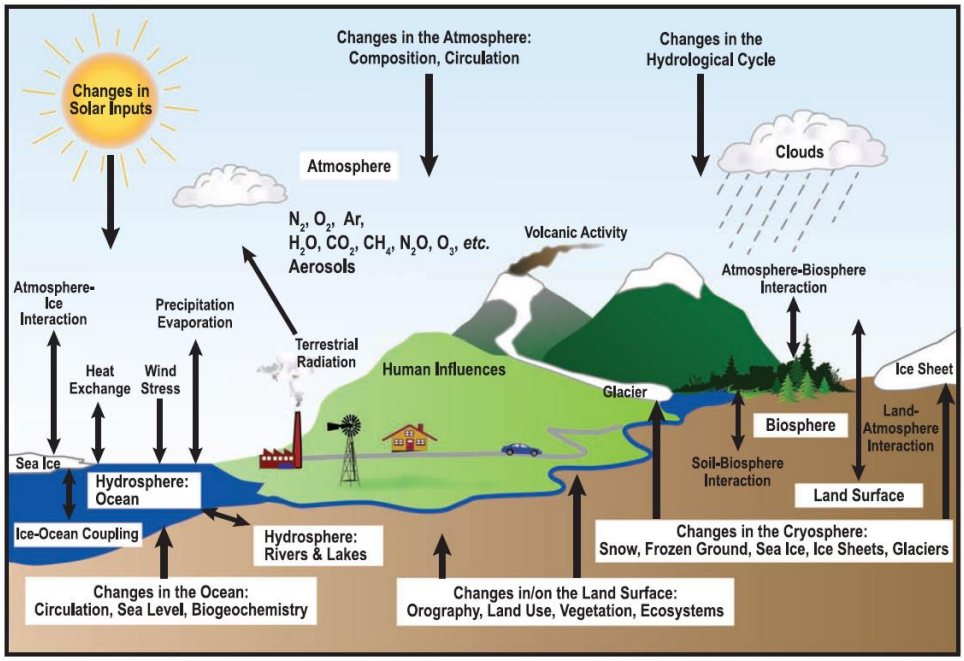

Figure 2-1: Schematic representation of the Earth's climate system interactions and external factors (IPCC, 2007)

Natural phenomena, such as volcanic eruptions and changes in solar radiation, as well as anthropogenic greenhouse gas emissions are claimed to be the main representatives of the external factors affecting climate change. It can also be generalised that if it had not been for the Sun's activity, none of the existing ecosystems would probably have developed on Earth since the solar radiation can be seen as a power source for the Earth's climate system. Therefore,

changes in solar radiation affect variations of the climate system that has been observed in weather variations (IPCC, 2007).

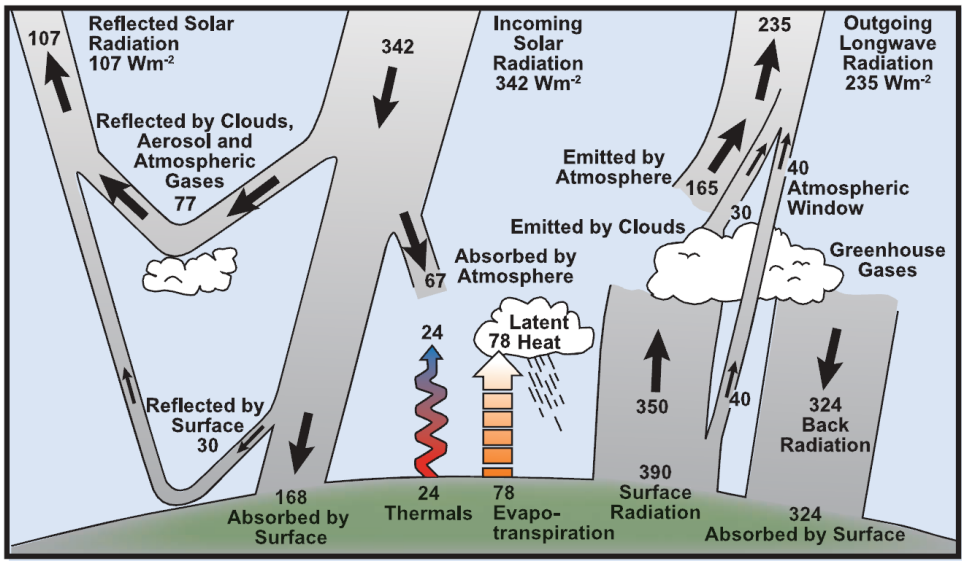

Figure 2-2: Estimate of the Earth's annual mean energy balance (IPCC, 2007)

The Earth's radiation balance can be altered via variation of its three main components (Figure 2-2). First, the amount of incoming solar radiation varies due to the change in Earth's distance from the Sun throughout the year. Second, the fraction of reflected solar radiation, so-called albedo, is affected due to possible variations in cloud cover and particulates content in the atmosphere. Third, the long wavelength radiation from the Earth back towards space is altered as a result of fluctuations of the atmospheric concentration of greenhouse gases (IPCC, 2007). The Earth's climate, in turn, responds accordingly to any change in the Earth's radiation balance, as the amount of incoming solar energy must be balanced by emitting, on average, the same amount of energy back towards space. If the amount of outgoing and incoming radiation were equal, the mean temperature at the Earth's surface would have reached -19°C. This, however, does not reflect the reality. The Earth's mean surface temperature reaches 14°C due to absorption of thermal radiation, which is emitted by the Earth's surface into the atmosphere as a result of the greenhouse effect (IPCC, 2007, 2012). The greenhouse effect results from the presence of greenhouse gases and clouds in the atmosphere that can absorb and reflect thermal radiation. Despite being the most abundant

gases in the atmosphere, the greenhouse effect exerted by nitrogen and oxygen is negligible. Conversely, water vapour and CO_2 are the most important among the other greenhouse gases, such as methane, nitrous oxide, fluorinated gases, and ozone. Therefore, any addition to the greenhouse gases from anthropogenic sources (external factors) will alter the climate by amplifying the greenhouse effect that, in turn, will result in global warming. In the worst-case scenario, the rise in the atmospheric concentration of CO_2 would result in a self-reinforcing effect as such increase could result in a temperature increase that, in turn, would be accompanied by enhanced evaporation of water, increasing the water vapour concentration in the atmosphere and thus leading to further intensification of the greenhouse effect. For this reason, any variation in concentration of greenhouse gases in the atmosphere is reflected by the Earth's surface temperature changes (IPCC, 2007; Maroto-Valer, 2010).

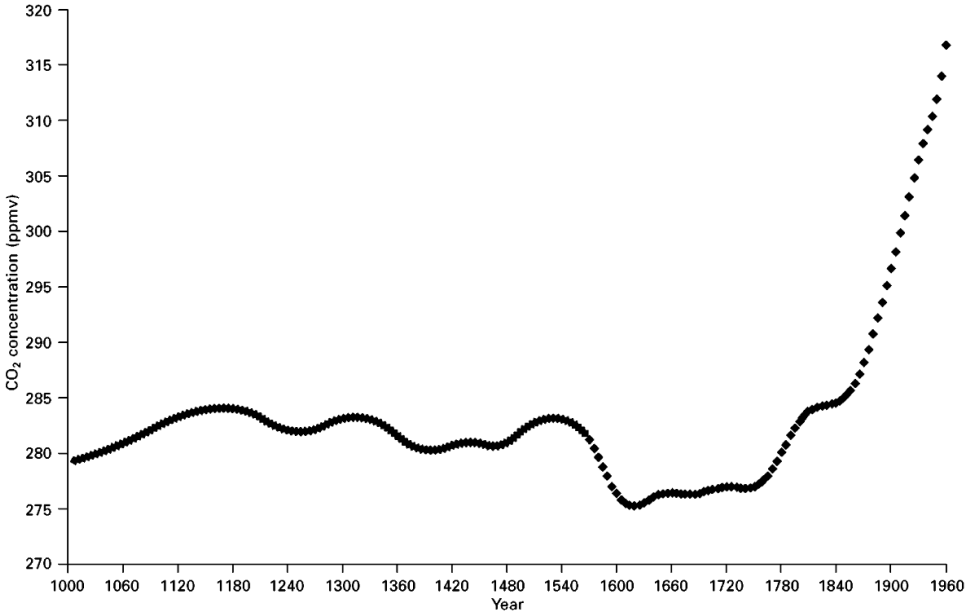

Figure 2-3: Annually averaged concentration of CO_2 in the atmosphere between 1010 and 1960 (Maroto-Valer, 2010)

Recently, scientists have determined that despite many external factors influencing the climate state, anthropogenic activities have become more intensive than natural phenomena in impacting the Earth's climate due to industrial development (IPCC, 2013, 2007; Maroto-Valer, 2010). Rapid industrial growth observed in the eighteenth century, which was accompanied

by development of fossil fuel combustion systems for industrial purposes, resulted in significant increase in the atmospheric CO_2 concentration (Figure 2-3) from the pre-industrial level of 280 ppm_v (Maroto-Valer, 2010). Now, due to continuous utilisation of fossil fuels as a main energy source, the average CO_2 concentration reached 401.6 ppm_v in December 2015 (Dlugokencky and Tans, 2016). Therefore, to avoid drastic climate change, further increase in anthropogenic greenhouse gas emissions, mostly CO_2, must be mitigated to limit the atmospheric concentration of greenhouse gases to 450 $ppm_{v,CO2eq}$. Considering the remaining estimated CO_2 emission budget of 930–1230 Gt and the fact that fossil fuels are expected to play an important role in the future energy portfolio, a rapid transition towards a green economy and wide deployment of low-carbon technologies need to be pursued.

2.2 Low-carbon technologies for CO_2 emission abatement

The global energy sector, comprising power, industry, transport and building sectors, was responsible for around two thirds of global CO_2 emissions in 2012, and thus its decarbonisation would be the largest contributor towards meeting 2DS objectives. However, no single technology exists that would be capable of decarbonising the entire energy sector. Therefore, it is expected that a portfolio of low-carbon technologies will be tailored and deployed to meet the CO_2 emission reduction target of each particular sector (IEA, 2015a, 2015b). As the power sector accounted for more than a third of total greenhouse gas emissions in 2010 (UNEP, 2012), its decarbonisation would significantly contribute towards meeting the 2DS emission reduction targets. Moreover, the power sector is often regarded as a precursor for deployment of clean technologies for other industries, and thus current research and development activities are highly focused on low-carbon technologies for this sector (Benton, 2015).

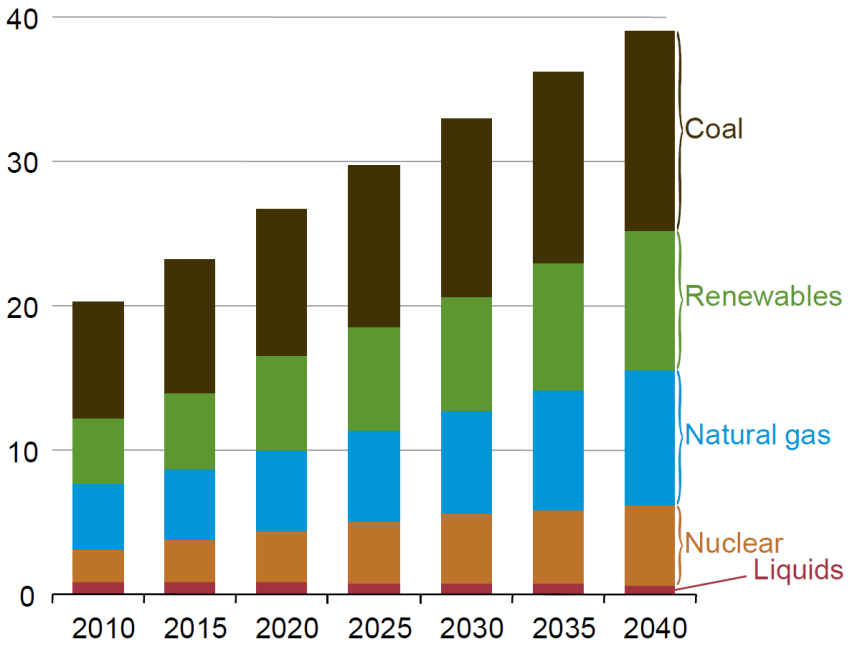

Figure 2-4: Projections of the fuel distribution in total electricity generation in trillion $kW_{el}h$ by 2040 (EIA, 2013)

The Environmental Information Agency (2013) predicted that the global electricity supply could increase from 20.2 to 39.0 trillion $kW_{el}h$ between 2010 and 2040, with an increase of about 15 trillion $kW_{el}h$ associated with countries that are not members of the Organisation for Economic Cooperation and Development (OECD), such as China and India. Although the new capacity added to meet the increasing electricity demand would mainly comprise renewable energy sources, natural gas combined cycle power plants and nuclear power plants (EIA, 2015), the projections indicate that coal-fired power plants will remain the predominant electricity source and will account for 36% of global electricity production in 2040. Regardless of the fact that renewable energy sources are the fastest growing sources of electricity generation in the global energy portfolio, electricity generating capacity utilising fossil fuels, such as coal, natural gas and oil, is predicted to account for about 62% of the electricity supply in 2040 (Figure 2-4) (EIA, 2013). Therefore, to meet the greenhouse gas emission reduction target and ensure the security of future electricity supply, while keeping the electricity price at an affordable level, low-carbon technologies that utilise fossil fuels in an environmentally-friendly and efficient manner need to be deployed.

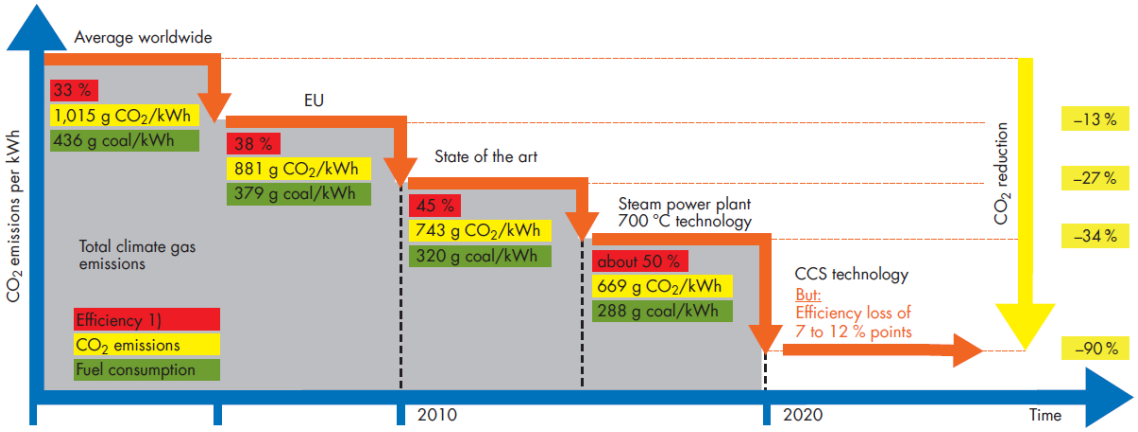

Figure 2-5: Decarbonisation measures for coal-fired power plants (VGB, 2013)

Until the concern regarding the environmental footprint of coal-fired power plants has been raised, the process economics, and thus revenue from electricity sales, has been the main driver for improvements in net thermal efficiency. Recently, reduction of CO_2 emissions has become another key driver for performance improvements (IEA, 2010, 2014). The global fleet of coal-fired power plants comprises a large share (75%) of subcritical units that can reach net thermal efficiency of 30–39%$_{LHV}$, depending on the unit size, coal quality and ambient conditions (IEA, 2014). For this reason, the average net thermal efficiency of the global coal-fired power plant fleet is as low as 33%$_{LHV}$ (Figure 2-5) (IEA, 2013a; VGB, 2013). If this figure is increased to 45–50%$_{LHV}$, a CO_2 emission reduction of up to 27–34% can be achieved.

Table 2-1: Characteristics of subcritical, supercritical and ultra-supercritical power plants fuelled with coal of lower heating value of 25 MJ/kg (Miller, 2011).

Unit type	Subcritical	Supercritical	Ultra-supercritical
Main steam pressure (bar)	221	221–250	>250
Main steam temperature (°C)	565	540–580	>580
Reheat steam temperature (°C)	565	540–580	>580
Efficiency (%$_{LHV}$)	33–39	38–42	>42
Specific coal consumption (g/kW$_{el}$h)	>380	340–380	320–340
CO_2 intensity factor (gCO_2/kW$_{el}$h)	>880	800–880	740–800

State-of-the-art coal-fired power plants, which operate under supercritical or ultra-supercritical steam parameters, are capable of reaching considerably higher net thermal efficiencies exceeding 42%$_{LHV}$ (Table 2-1). As the operating

steam conditions are limited by the material strength in some components of the boiler, steam turbines and piping, research and development efforts are being undertaken worldwide to develop new alloys, such as nickel-based super-alloys, that would support steam temperatures above 700°C and pressures above 300 bar (IEA, 2011). The net efficiency of the coal-fired power plant operating under such conditions would increase above $50\%_{LHV}$, bringing substantial improvements not only to the process economy, but also to its environmental performance (IEA, 2011, 2014). It has been estimated that the net thermal efficiency of the coal-fired power plant is mainly influenced by the steam temperature, as each increase of 20°C results in approximately 1% point increase in the net thermal efficiency (Miller, 2011). As 1% point increase in net efficiency would reduce CO_2 emissions by 2–3%, advanced ultra-supercritical coal-fired power plants would emit 40% less CO_2 than the subcritical unit of the same rated power output (IEA, 2014). However, even such considerable reduction in CO_2 emissions is not sufficient to decarbonise the power sector and thus integration of CCS technologies is required. Yet, mature CO_2 capture technologies are expected to reduce the net thermal efficiency of the coal-fired power plant by up to 12% points (VGB, 2013), which implies that the net thermal efficiency of the state-of-the-art coal-fired power plant will be downgraded on CCS retrofit to the level of inefficient subcritical units. For this reason, novel and less energy-intensive CO_2 capture processes need to be developed to ensure their commercialisation and large-scale deployment.

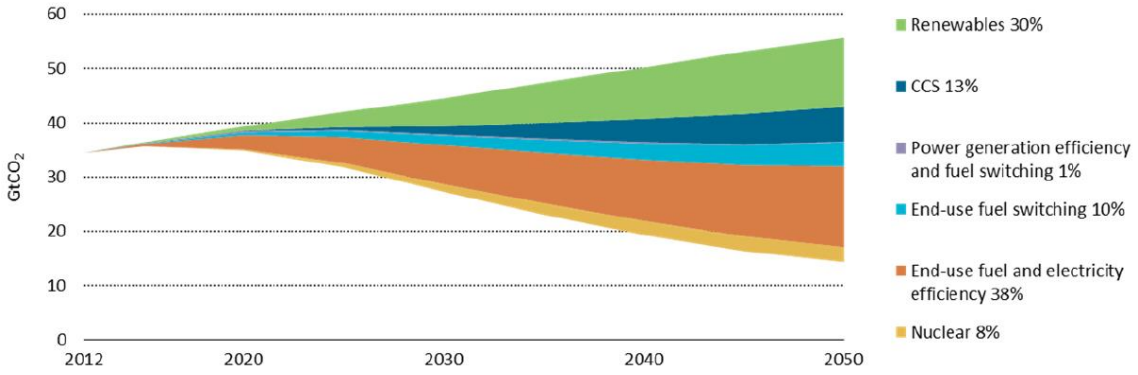

Figure 2-6: Contributions of the low-carbon technologies to global cumulative CO_2 reductions under 2DS scenario (IEA, 2015a, 2015b)

As indicated by the International Energy Agency (2015a, 2015b), a portfolio of low-carbon technologies needs to be deployed to decarbonise the power sector (Figure 2-6). It has been predicted that renewable energy sources, nuclear power plants and CCS would be the key contributors to global cumulative reductions in CO_2 emissions (IEA, 2015a, 2015b, 2015c). Considering the predicted high share of fossil fuels in the future energy portfolio, CCS is the key technology that will play a pivotal role in decarbonisation of the power sector. This is confirmed by the assessment made by the Intergovernmental Panel on Climate Change (2014) revealing that it is likely that 2DS objectives will not be met if deployment of CCS, bioenergy and their combinations is limited. Another incentive for large-scale deployment of CCS is the prediction that it would reduce wholesale electricity prices by up to 15% by 2030 and the cost of meeting the 2050 target for reduction of greenhouse gas emissions by 40% compared to a no-CCS scenario (IEA, 2013a; Orion Innovation, 2013).

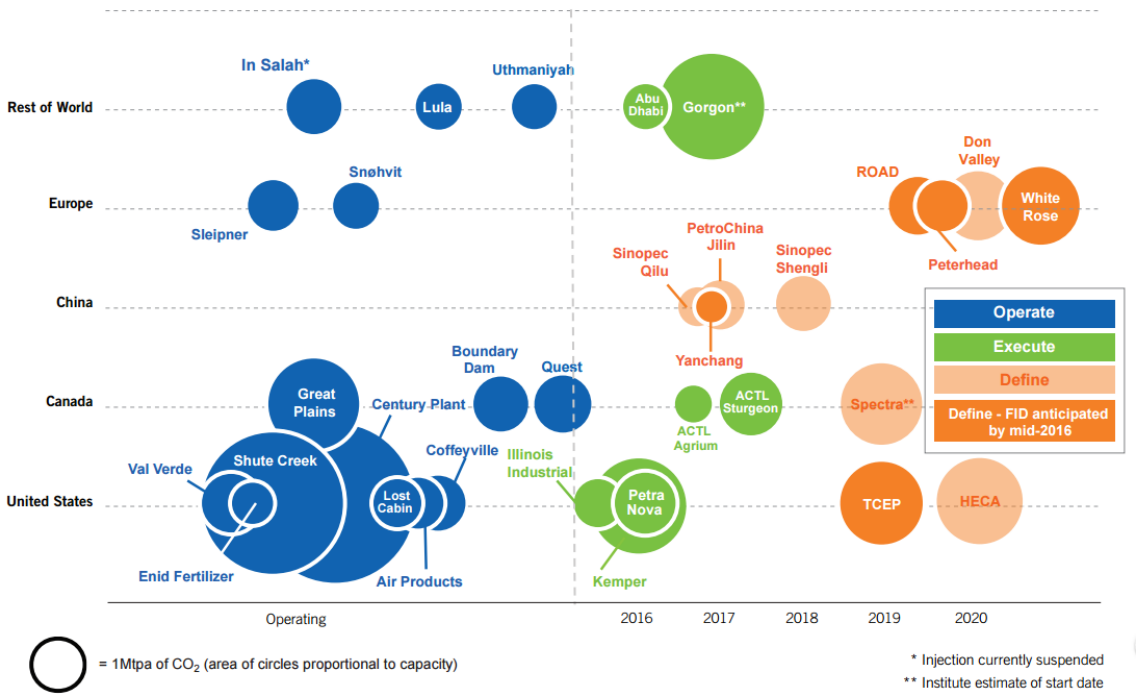

Figure 2-7: Overview of large-scale CCS projects at different project lifecycle stages (GCCSI, 2015)

Currently, there are fifteen large-scale projects in the operation stage, which capture 27 Mt of CO_2 per annum, and seven in the execute stage that will

become operational in 2016 and 2017. Further eleven projects are in advanced define stage and are expected to become operational beyond 2017 (Figure 2-7), while another twelve are in the early define stage. If successfully deployed, these forty-five projects would capture 80 Mt of CO_2 per annum after 2020 (GCCSI, 2015), which is only a fraction of the desired global CO_2 capture capacity of 4–6 Gt of CO_2 per annum by 2040 (GCCSI, 2015; IEA, 2009) and of around 10 Gt of CO_2 per annum by 2050 (IEA, 2009). Yet, early-stage deployment of the CCS projects is highly dependent on governmental incentives and the political climate. This is clearly seen in a recent suspension of funding at an advanced stage of the FutureGen project (Marshall and Quiñones, 2015; Sutton, 2015) and withdrawal of the government funding for the Peterhead and White Rose projects, making future progress on these projects unlikely (ECCC, 2016). Considering the International Energy Agency (2009) prediction of a hundred projects operating by 2020, which would capture 345 Gt of CO_2 per annum, and three-thousand-four-hundred projects operating by 2050, nearly half of which will be in the power sector, the deployment of CCS technologies is not on track to meet the 2DS objective. Although meeting the Paris Agreement objectives seems to be a challenging and demanding task in light of the progress in CCS deployment, these could be still achieved if immediate action is undertaken and relevant incentives are introduced.

2.3 Carbon capture and storage chain

CCS is a chain of processes aiming at reduction of the carbon footprint through mitigation of CO_2 emissions from fossil fuel combustion and industrial processes into the atmosphere. The processes included in this chain are CO_2 capture and separation, compression to supercritical pressure, transport, and safe long-term storage with monitoring in the geological formations (European Commission, 2009).

2.3.1 CO_2 capture

The first stage in the CCS chain aims at producing a high-purity CO_2 stream prior to its conditioning, transport and storage stages. Based on past experience gained in the fertiliser manufacturing, hydrogen production and natural gas

processing industries, three capture approaches were identified as applicable to the power sector (Figure 2-8) (Metz et al., 2005).

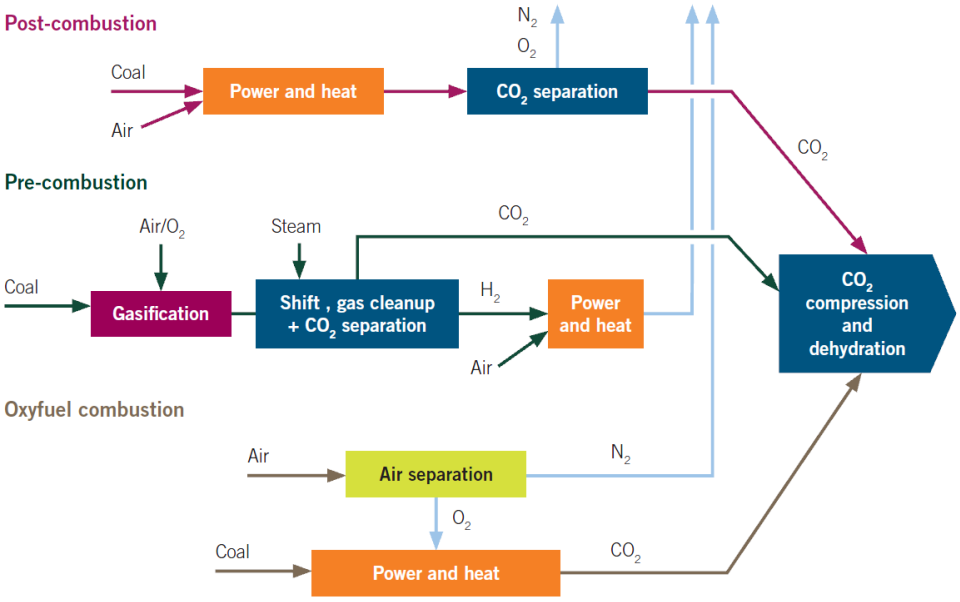

Figure 2-8: Main CO_2 capture approaches (GCCSI, 2012)

A post-combustion CO_2 capture approach includes technologies used to separate CO_2 from flue gas produced in fossil fuel combustion in an air-rich atmosphere. As no substantial changes are required to the power plant equipment, this CO_2 approach is preferred for retrofitting the existing fossil fuel power plant fleet where it can be retrofitted downstream of the conventional flue gas treatment train for NO_x, SO_x and particulate matter removal (Leung et al., 2014). It should be highlighted that these impurities need to be removed from flue gas prior to CO_2 capture, as their presence could degrade performance of the post-combustion CO_2 capture technologies (Kenarsari et al., 2013). Depending on the kind of fuel fed to the combustion process, the CO_2 concentration in flue gas varies between 3 to 15%$_{vol}$. Such low CO_2 concentration is associated with a large volume of flue gas to be processed, leading not only to high capital cost of the post-combustion CO_2 capture units, but mostly to high parasitic load associated with their integration (Olajire, 2010). A range of technologies utilising different principles, such as mature chemical or physical solvent absorption, membrane separation or sorbent adsorption can be applied to separate CO_2 from the flue gas stream produced in coal- or gas-fired

power plants. Regardless of the post-combustion technology used, an additional parasitic load is associated with the requirement for CO_2 compression prior to its transport and storage, as flue gas usually leaves the system at an atmospheric pressure (Metz et al., 2005; Spliethoff, 2010).

A pre-combustion CO_2 capture technology aims at partially oxidising the fuel to form synthetic gas (syngas) comprising mainly CO and H_2. This approach can be applied in both the integrated gasification combined cycle plants in which solid fuel, such as coal, is gasified under high temperature and pressure and the advanced gas combined cycle power plants in which natural gas is reformed in an oxygen-lean atmosphere. CO is then converted to CO_2 in reaction with steam in a catalytic water-gas shift reactor to produce a stream consisting solely of CO_2 and H_2. As CO_2 content in the syngas is within 15–60%$_{vol}$ (D'Alessandro et al., 2010), a physical solvent absorption process, such as the Rectisol or Selexol process, is economically favoured (Wang et al., 2011). At this stage, CO_2 is separated from H_2 that is then used to fuel the gas turbine cycle to produce electricity and/or heat (Herzog and Golomb, 2004; Metz et al., 2005). Alternatively, H_2 can be used in a fuel cell or as a feedstock for liquid fuel or chemicals production in the low-electricity-demand period (D'Alessandro et al., 2010; Florin and Fennell, 2010).

In an oxy-fuel combustion technology, fuel is combusted in an O_2-rich atmosphere and flue gas is composed mainly of CO_2 and water. Since fuel combustion in nearly pure O_2 results in a higher combustion temperature, flue gas is partially recycled (60%) to the combustion chamber to control the flame temperature (Kenarsari et al., 2013). Flue gas from fuel combustion under oxy-fuel conditions comprises mainly CO_2, $H_2O_{(g)}$, SO_x and particulate matter. Absence of N_2 in the oxidising medium not only reduces the NO_x emission, but also substantially reduces the size of the combustor (Kenarsari et al., 2013). Therefore, a pure CO_2 stream is obtained after removal of SO_x, NO_x and particulate matter in conventional flue gas desulphurisation, catalytic reduction system and electrostatic precipitator, respectively, and removal of $H_2O_{(g)}$ through condensation (Leung et al., 2014). An O_2 stream of high purity is

usually produced in a cryogenic air separation unit, taking place at a low temperature, by separating O_2 from other air constituents. As this process is highly energy-intensive (184–220 $kW_{el}h/tO_2$) (Romeo et al., 2008a; Ströhle et al., 2009), new technologies aiming at supplying O_2 to the combustion process, such as membranes and chemical looping combustion are being developed (Abanades et al., 2015).

2.3.2 CO_2 transport

Prior to being transported to the desired storage location, CO_2 needs to be conditioned to a state appropriate to the transport conditions (Figure 2-9), and thus desired mean of transport (Spliethoff, 2010). Depending on the volume and distance over which CO_2 needs to be transported, pipeline, ship or even trucks and rail transport can be used (Leung et al., 2014). Yet, onshore transportation via trucks and rail has a limited capacity and is characterised by high cost compared to pipelines. Therefore, CO_2 transport via pipeline, both onshore and offshore, and by ship is considered the most viable solution (Svensson et al., 2004).

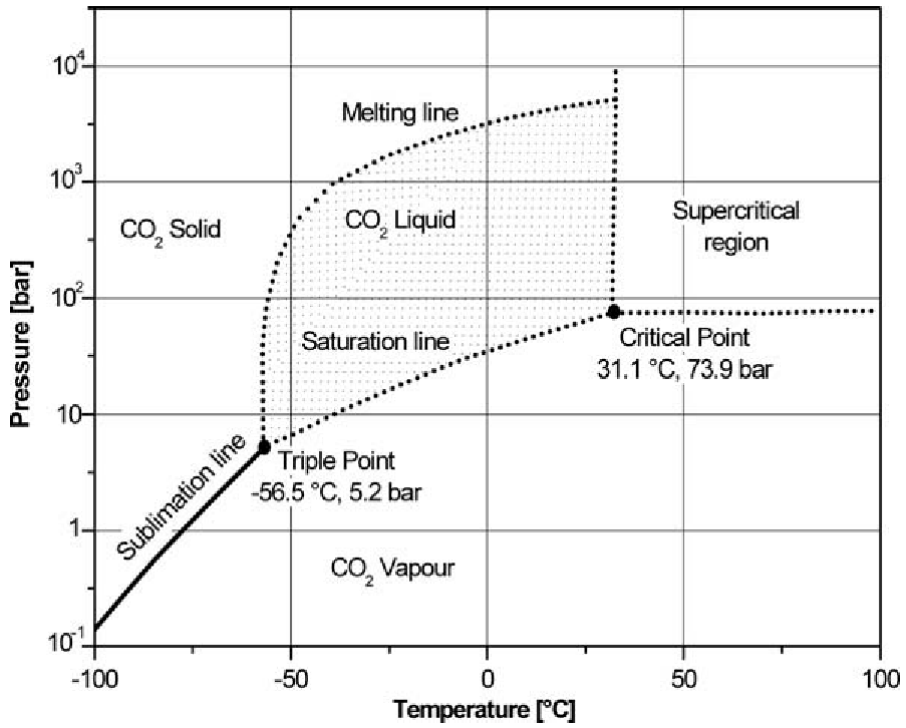

Figure 2-9: CO_2 phase diagram (Spliethoff, 2010)

Table 2-2: Energy consumption for CO_2 compression, liquefaction and solidification (Göttliche, 2004, 1999)

CO_2 transport conditioning method	Power requirement ($kW_{el}h/tCO_2$)	Power requirement related to coal chemical energy ($\%_{LHV}$)
Compression (110 bar)	110–130	3.5
Cryogenic liquefaction (25 bar, -15°C)	160	5.2
Dry ice production	260–420	8.4–13.5

Transport of CO_2 via pipeline is carried out at ambient temperature and in the liquid or supercritical phase, with the latter being regarded as the preferred option (Leung et al., 2014). It is well established that at ambient temperature, CO_2 pressure for pipeline transport in the dense phase should be about 110 bar (Metz et al., 2005), with values ranging between 85–150 bar (Leung et al., 2014). It has been estimated that for offshore transport distances exceeding 1000 km, CO_2 transport using ship, during which CO_2 is transported in the liquid or solid phase, becomes a more economically attractive option than offshore pipelines. For this reason, a techno-economic feasibility study should be conducted to select the most cost-efficient combination of CO_2 transport system, which could be achieved through maximising the CO_2 stream density while minimising the power requirement for its compression, liquefaction and solidification (Spliethoff, 2010). Göttliche (1999, 2004) has identified that among the CO_2 conditioning approaches, compression up to 110 bar results in the lowest energy requirement (Table 2-2). Therefore, a combination of CO_2 transport via pipeline, and ship is regarded as the most cost-effective option (Svensson et al., 2004).

2.3.3 CO_2 storage

Once CO_2 has been captured, conditioned and transported to the storage location, its long-term and safe storage must be assured to mitigate adverse effects or risks to the environment and human health (European Commission, 2009; Miller, 2011; Spliethoff, 2010). Geological storage is at present considered the most feasible option for CO_2 storage (Leung et al., 2014; Van

Der Zwaan and Smekens, 2009). Yet, other storage techniques, such as ocean storage, mineral carbonation and terrestrial carbonation could also contribute towards storing around 410–1670 $GtCO_2$ between 2000–2100, depending on the end-of-century CO_2 atmospheric concentration (Dooley, 2013; Maroto-Valer, 2010; Miller, 2011).

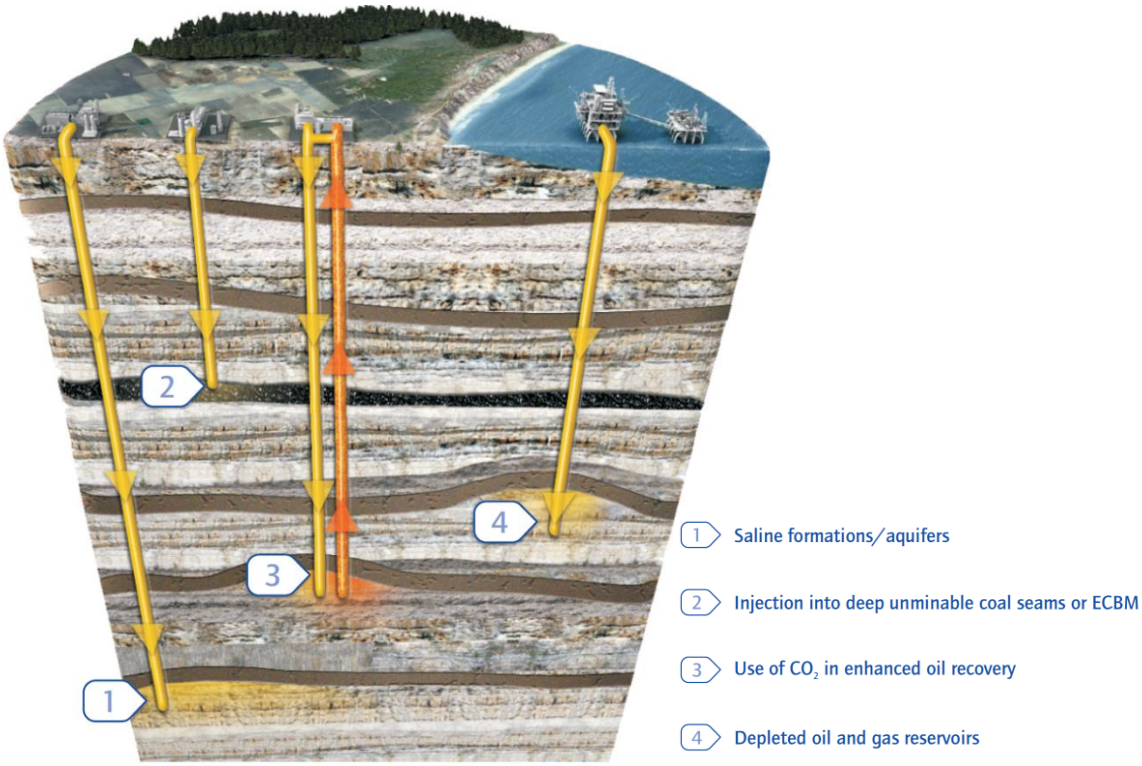

Figure 2-10: Overview of the suitable geological formations for CO_2 storage (IEA, 2013)

Having been already proven at commercial scale (Maroto-Valer, 2010), geological storage involves CO_2 injection into a wide range of geological formations such as underground oil, gas or water reservoirs, deep unminable coal seams having potential for enhanced coal-bed methane recovery, as well as deep saline geologic formations (Figure 2-10) for safe, long-term storage (IEA, 2013b; Miller, 2011). Identified formations are typically located one to three kilometres under the ground, which allows CO_2 to remain in the liquid or supercritical phase, and have the effective and practical capacity to globally store 13500 and 3900 Gt of CO_2, respectively (Dooley, 2013). The capacity of a geological formation to store CO_2 is determined by two trapping mechanisms.

The first trapping mechanism, physical trapping, corresponds to the physical characteristics of the geological formation that should include an impermeable shale or clay rock layer that prevents upward migration of CO_2 and, eventually, its leakage to the environment. The second trapping mechanism, geochemical trapping, involves a chemical reaction of CO_2 with the host rock to produce carbonates that minimises the probability of CO_2 leakage and allows for a long-term, safe storage. Importantly, when injected into oil and gas reservoirs, CO_2 can be simultaneously stored and utilised to enhance the production of oil and gas, bringing economic benefits to the oil and gas industry, as well as providing additional financial incentives for CCS in the power sector (Spliethoff, 2010). Such techniques for enhanced oil recovery have been practiced commercially since the early 1970s, especially in North America (IEA, 2013b). Also, enhanced gas recovery via injection of CO_2 into depleted gas reservoirs has been demonstrated (Miller, 2011).

Ocean storage is another potential storage option for storing CO_2, although it is perceived more negatively by the public compared to geological storage (Metz et al., 2005; Palmgren et al., 2004). Yet, it has been estimated that for atmospheric CO_2 concentrations of 350–1000 ppm_v, about 2300–10700 Gt of anthropogenic CO_2, respectively, will be eventually stored in the ocean due to the equilibrium between the atmosphere and the ocean (Metz et al., 2005). Ocean storage relies on limited mixing of the deep ocean and surface water at depths below 800–1000 m, resulting in the surface water layer acting as insulation from the atmosphere (Maroto-Valer, 2010; Miller, 2011; Spliethoff, 2010). Importantly, at depths below 2600 m, the water temperature drops to 2°C and CO_2 is denser than water (Spliethoff, 2010). As a result, the upward movement of CO_2 is restricted and a CO_2 lake is created. In addition, CO_2 interacts with water to form hydrates, and thus is stored for long periods of time (Miller, 2011).

Mineral carbonation is seen as a potential storage technique, in which CO_2 is fixed through carbonation of naturally abundant magnesium, iron and calcium oxides or silicates (Maroto-Valer, 2010; Miller, 2011), especially in locations

where geological storage capacity is limited or not viable (Sanna et al., 2014). It has been estimated that the mineral requirement of this process is 1.6–3.7 tonne per tonne of CO_2 to be fixed (Metz et al., 2005). Although this process is exothermic and has a theoretical potential for energy recovery, the kinetics of natural mineral carbonation is slow and thus an energy-intensive thermal pre-treatment is required to enhance the carbonation reaction rate (Metz et al., 2005). It has been estimated that the energy requirement for mineral carbonation would reduce the net power output of the power plant by 30–50% (Miller, 2011; Spliethoff, 2010), which makes this process economically infeasible at this time (Sanna et al., 2014).

Terrestrial ecosystems can be used to fix CO_2 emitted from anthropogenic sources, and thus they do not require CO_2 to be captured and transported. Such terrestrial carbon sequestration techniques involve tree planting, wetlands restoration, grass and grazing land management, forest preservation and fire management. This aims at removing CO_2 directly from the atmosphere through biological, chemical and geological processes taking place in the soil and plants, and/or preventing of the net CO_2 atmospheric emission from the terrestrial ecosystems (Maroto-Valer, 2010; Miller, 2011).

2.4 CO_2 separation and capture options for coal-fired power plants

Post-combustion CO_2 capture technologies are claimed to have the greatest potential for decarbonising the power sector as they can be both easily retrofitted to the existing power plant fleet and integrated to the new systems (Oexmann et al., 2012; Pfaff et al., 2010; Rackley, 2010; Strube and Manfrida, 2011). Although successfully implemented in other industries, physical solvent absorption, adsorption, membrane or cryogenic separation technologies have been thus far considered as not yet efficient options for coal-fired power plants due to high impurities content and low CO_2 concentration in, and atmospheric pressure of, flue gas (Oexmann et al., 2008; Pfaff et al., 2010; Strube and Manfrida, 2011). It has been claimed that due to low CO_2 concentration, and thus large volume of flue gas to be processed, membrane-, cryogenic- and

adsorbent-based systems would be characterised by higher energy demand compared to chemical solvent scrubbing and will only become cost-effective for higher CO_2 concentrations (Favre, 2007; Kanniche et al., 2010; Merkel et al., 2010). Therefore, chemical solvent scrubbing has been perceived as the technology of first choice for decarbonisation of coal-fired power plants (Blamey et al., 2010; Mac Dowell et al., 2010; Oexmann et al., 2008, 2012; Pfaff et al., 2010; Rackley, 2010; Strube and Manfrida, 2011). Yet, recent progress in the development of CCS indicates that other technologies could result in lower parasitic load on power plant performance, and thus may bring higher improvements to the economics of CCS.

2.4.1 Absorption process

Solvent-based absorption is a cyclic process in which CO_2 is scrubbed from flue gas on contact with the lean solvent that takes place in the packed absorber and is reclaimed from the rich solvent on heating in the regenerator (Figure 2-11). It has been identified that the most efficient manner to provide the heat requirement for solvent regeneration is to extract part of the low-pressure steam from the primary steam cycle (Lucquiaud and Gibbins, 2011).

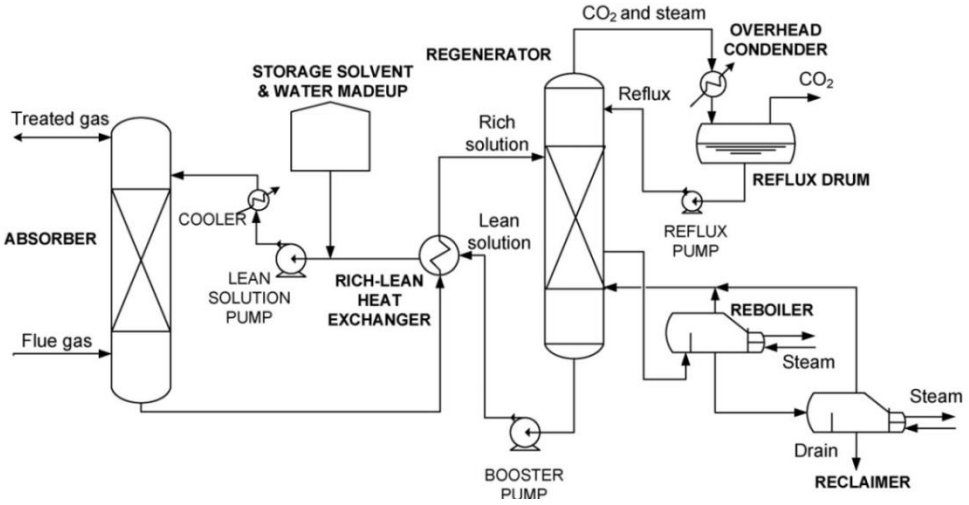

Figure 2-11: Typical configuration of solvent-based adsorption CO_2 capture process (Thitakamol et al., 2007)

To remove CO_2 from flue gas, solvent-based absorption technology can utilise either chemical or physical solvents. The former bond with CO_2 forming

intermediate compounds through a chemical reaction and can be regenerated on increasing the rich solvent temperature. The latter absorb CO_2 according to Henry's law at low temperature and high pressure, while regeneration is achieved using temperature or pressure change or the simultaneous change of both (D'Alessandro et al., 2010; Kenarsari et al., 2013; Rackley, 2010; Wang et al., 2011). The main difference between chemical and physical solvents is the dependence of solvent loading on the partial pressure of CO_2 in flue gas (Figure 2-12).

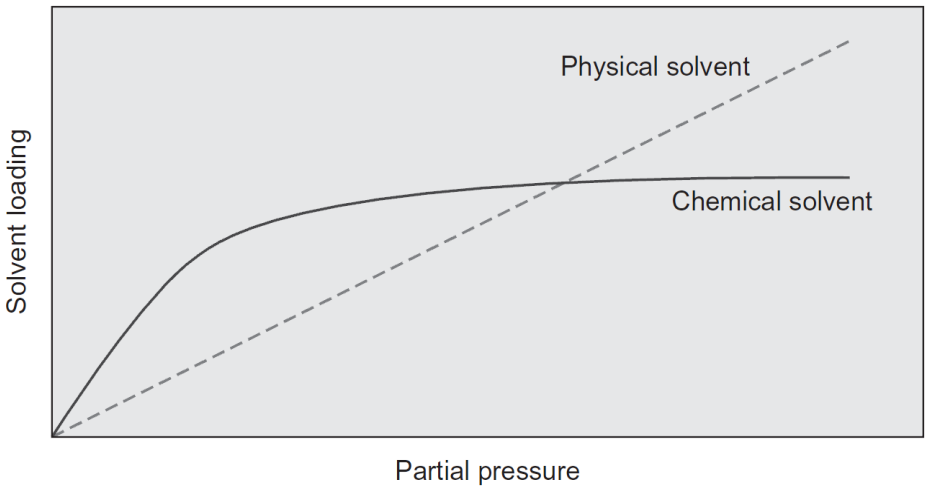

Figure 2-12: Effect of CO_2 partial pressure in flue gas on CO_2 loading of chemical and physical solvents (Rackley, 2010)

Chemical solvents provide a high CO_2 separation selectivity indicated by high loading at low CO_2 partial pressures, while physical solvents are preferred at high partial pressures (Kenarsari et al., 2013). It has been pointed out by Wang et al. (2011) that physical adsorption becomes unfeasible from the economic point of view for CO_2 partial pressures lower than $15\%_{vol,}$ and thus it would not be applicable for coal-fired power plants without substantial improvement in the absorption rate. Chemical solvent scrubbing using 25–$30\%_{wt}$ MEA solvent has been employed for CO_2 separation from flue gas for more than 50 years in other industries (Rochelle, 2009). Therefore, it is regarded as the technology of first choice for decarbonisation of coal-fired power plants. Yet, to avoid excessive solvent degradation, impurities from flue gas (NO_x, SO_x) must be

removed and the regeneration temperature kept below 125°C (Blamey et al., 2010; Boot-Handford et al., 2014; D'Alessandro et al., 2010; Kenarsari et al., 2013; Mac Dowell et al., 2010; Oexmann et al., 2008, 2012; Pfaff et al., 2010; Pires et al., 2011; Rackley, 2010; Strube and Manfrida, 2011). Considering the thermodynamic limitations, the realistic minimum net efficiency penalty associated with integration of the CO_2 capture plant using MEA solvent, which includes a CO_2 compression train, to the supercritical coal-fired power plant would be 6.8% points (Le Moullec, 2012). Yet, the actual efficiency penalty has been estimated to fall between 9.5–12.5% points (Goto et al., 2013; Hanak et al., 2014; Xu et al., 2010; Yang et al., 2010). This implies that although MEA solvent scrubbing is a mature technology, it will impose a significant thermodynamic and economic penalty on integration to coal-fired power plants.

2.4.2 Adsorption process

As opposed to the absorption process, in which CO_2 molecules dissolve in the bulk of the solvent, adsorption of CO_2 takes place at the surface of the solid sorbent. This is typically conducted in fixed bed or fluidised bed reactors using zeolites, activated carbon, metal oxides or alumina, as well as new materials, such as functionalised amine-based sorbents and metal-organic frameworks (Boot-Handford et al., 2014; D'Alessandro et al., 2010; Kenarsari et al., 2013; Leung et al., 2014). In the adsorption process the molecules of CO_2, so-called an adparticle, is bonded to the adsorbent via either a chemical bond in the chemisorption process or a combination of Van der Waals and electrostatic forces in the physisorption process (D'Alessandro et al., 2010). The adsorbent can then be regenerated via increasing the temperature in a temperature swing adsorption (TSA) process, reducing pressure in a pressure swing adsorption (PSA) process or both by increasing the temperature and reducing pressure in a pressure and temperature swing process (Figure 2-13). An alternative of the PSA process is a vacuum swing adsorption (VSA) process, in which the regeneration is conducted under vacuum conditions. As the gas-solid heat transfer is usually slow, the PSA process offers faster regeneration rate and lower energy requirement. Alternatively, the sorbent can be regenerated on

heating through applying low voltage in an electrical swing adsorption process (ESA), which would result in faster regeneration rate compared to the TSA process (Kenarsari et al., 2013).

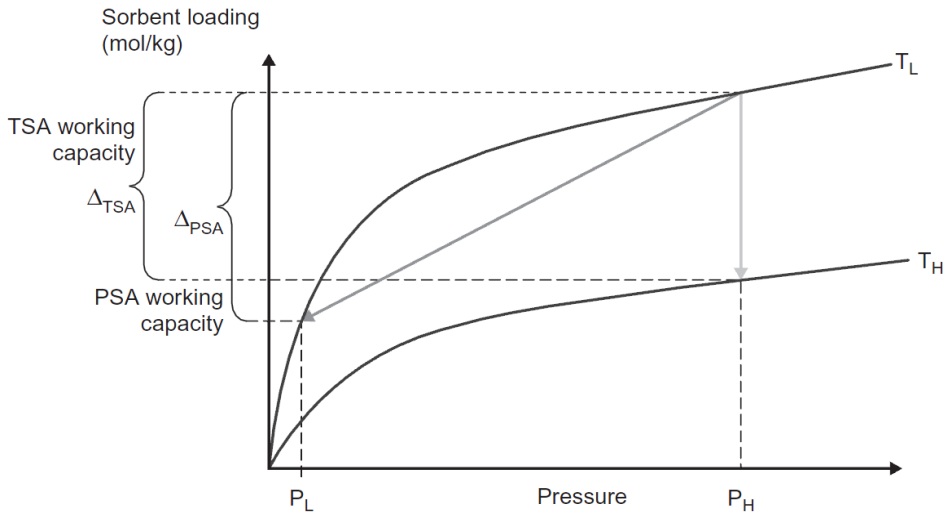

Figure 2-13: Sorbent loading for pressure swing and temperature swing adsorption process (Rackley, 2010)

The PSA process using zeolites has already been proposed for H_2 recovery from petroleum refineries and petrochemical processing (Cen and Yang, 1986; Yang et al., 1997). Integration of the VSA process (adsorption at 2 bar, regeneration at 0.1 bar) using Zeolite 13X, which is the most popular adsorbent (D'Alessandro et al., 2010), as the post-combustion CO_2 capture plant to the ultra-supercritical coal-fired power plant resulted in a net thermal efficiency penalty of 10.3% points. This was found to be 0.6% lower than for MEA solvent scrubbing retrofitted to the same reference coal-fired power plant (Riboldi and Bolland, 2015), proving that the VSA process has the potential to reduce the energy intensity associated with CO_2 capture from coal-fired power plants. A similar conclusion can be drawn when analysing performance of the TSA process using dry sodium carbonate, in which CO_2 was adsorbed at about 55°C and regenerated at about 140°C. Namely, the net efficiency penalty of such process on integration to the supercritical coal-fired power plant was found to be 7.1–9.9%, which was 1.9–4.5% lower compared to MEA solvent scrubbing (Nelson et al., 2009). Finally, use of metal oxides, such as CaO, in

high-temperature solid looping cycles, is regarded as an emerging CO_2 capture technology suitable for decarbonisation of coal-fired power plants (Abanades et al., 2015; D'Alessandro et al., 2010). In this TSA process using CaO, CO_2 is adsorbed by the sorbent at 600–650°C and reclaimed through sorbent regeneration at temperatures higher than 900°C. It has been reported that depending on the operating conditions and the steam conditions in the reference coal-fired power plant, the net efficiency penalty associated with this technology is expected to be between 3–8% points (Abanades et al., 2005; Martínez et al., 2011; Romeo et al., 2008a; Ströhle et al., 2009; Vorrias et al., 2013; Yang et al., 2010). Therefore, this technology has brought more attention than other adsorption processes, such as the PSA using zeolites and the TSA using dry carbonate sorbents, and is regarded as one of the three most important CO_2 capture technologies among chemical solvent scrubbing and oxy-fuel combustion (Mac Dowell et al., 2010). Yet, the cyclic performance of the adsorbent needs to be improved prior to a large-scale deployment of CaL (D'Alessandro et al., 2010; Dean et al., 2011).

2.4.3 Cryogenic process

Cryogenic separation of CO_2 from flue gas utilises differences in the boiling points of different species to produce a CO_2 stream of high purity. The phase diagram of CO_2 presented in Figure 2-9 indicates that the triple pressure of CO_2 is at 5.2 bar and -56.6°C (Rackley, 2010). As the cryogenic CO_2 separation (Figure 2-14) is conducted at significantly lower temperature than the triple point of water (0.006117 bar, 0.01°C), $H_2O_{(g)}$ needs to be removed from the flue gas to avoid ice formation and blockage of the evaporators in the system (Clodic et al., 2005). Dried and compressed flue gas is cooled down to sub-zero temperatures ranging between -135°C and -120°C which are lower than the temperature at which pure CO_2 desublimates (-78.5°C at atmospheric pressure) due to its low concentration in flue gas (Burt et al., 2009; Clodic et al., 2005; Le Moullec, 2012). Flue gas is further cooled on its expansion. As a result, CO_2 precipitates as a solid and is separated from the remaining flue gas. The CO_2 stream is then pressurised and along with the depleted flue gas

stream is heated in a cross-heat exchanger, simultaneously cooling the incoming flue gas stream, and leaves the CO_2 capture plant as a compressed liquid. Depending on the sub-cooling temperature, cryogenic CO_2 capture efficiency ranges between 90% at -120°C and 99% at -135°C (Burt et al., 2009).

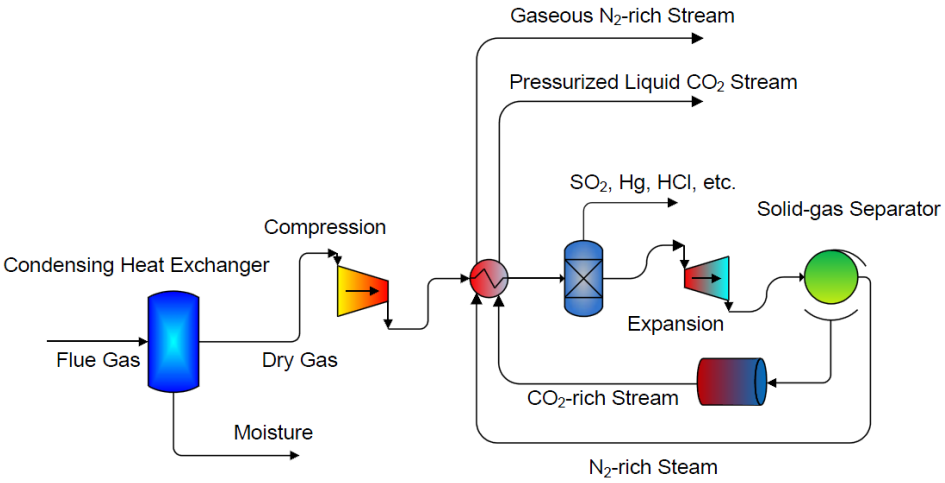

Figure 2-14: Schematic representation of cryogenic CO_2 capture process (Burt et al., 2009)

Considering the thermodynamic limitations, the realistic minimum efficiency penalty associated with utilising cryogenic CO_2 capture to decarbonise the supercritical coal-fired power plant would be 5.8% points. This is a 1% point improvement over the realistic minimum efficiency penalty of MEA solvent scrubbing (Le Moullec, 2012). The actual net efficiency penalty was estimated to vary between 7.3-10.7% points (Clodic et al., 2005; Schach et al., 2011) that is also lower compared to 9.5–12.5% points identified for MEA solvent scrubbing, revealing the potential of cryogenic CO_2 separation to reduce the efficiency penalties associated with mature CO_2 capture technologies.

2.4.4 Membrane process

Although gas separation using membranes has been successfully performed in other industries, such as air separation for technical grade nitrogen or O_2-enriched air production or H_2 separation in refineries and the petrochemical industry (Yampolskii, 2012), the development of this technology for CCS

application is still in its preliminary stages. Yet, membranes are regarded as a promising technology for post-combustion CO_2 capture and are expected to offer lower efficiency penalties compared to the mature chemical solvent scrubbing technologies (Kenarsari et al., 2013).

A membrane is a semi-permeable barrier that separates CO_2 from flue gas using various mechanisms driven by concentration and pressure gradients across the membrane (Olajire, 2010; Shekhawat et al., 2003; Wijmans and Baker, 2006):

- Knudsen diffusion that occurs in the membrane having pores with smaller diameter than the mean free path of the molecules in the gas phase, allowing utilising the difference in the mean free path of the gas molecules for separation (Figure 2-15a);
- surface diffusion that occurs when the diffusing molecules are adsorbed on the pore wall and then transported in the direction of the surface concentration gradient (Figure 2-15b);
- capillary condensation that occurs when multiple layers of the diffusing molecules are adsorbed on the pore wall, and condensation of the vapour species occurs at a pressure below the saturation point at given temperature, blocking transport of other molecules (Figure 2-15c);
- molecular sieving that utilises the differences in size of gas molecules in the gas mixture, allowing smaller particles to pass through the pores of the membrane, while excluding the larger particles from entering these pores (Figure 2-15d);
- solution-diffusion that occurs in dense membranes of small diameters (< 5 Å) and utilises the concentration gradient as a separation driving force (Figure 2-15e).

The main characteristics of the membrane's performance are selectivity, which determines the membrane's capability to remove particular species over the others, and permeability, which indicates the flux of a particular gas through the membrane. This means that the CO_2 separation rate is characterised by

CO_2 concentration in flue gas, the pressure difference across the membrane and CO_2 affinity for the membrane material (Olajire, 2010).

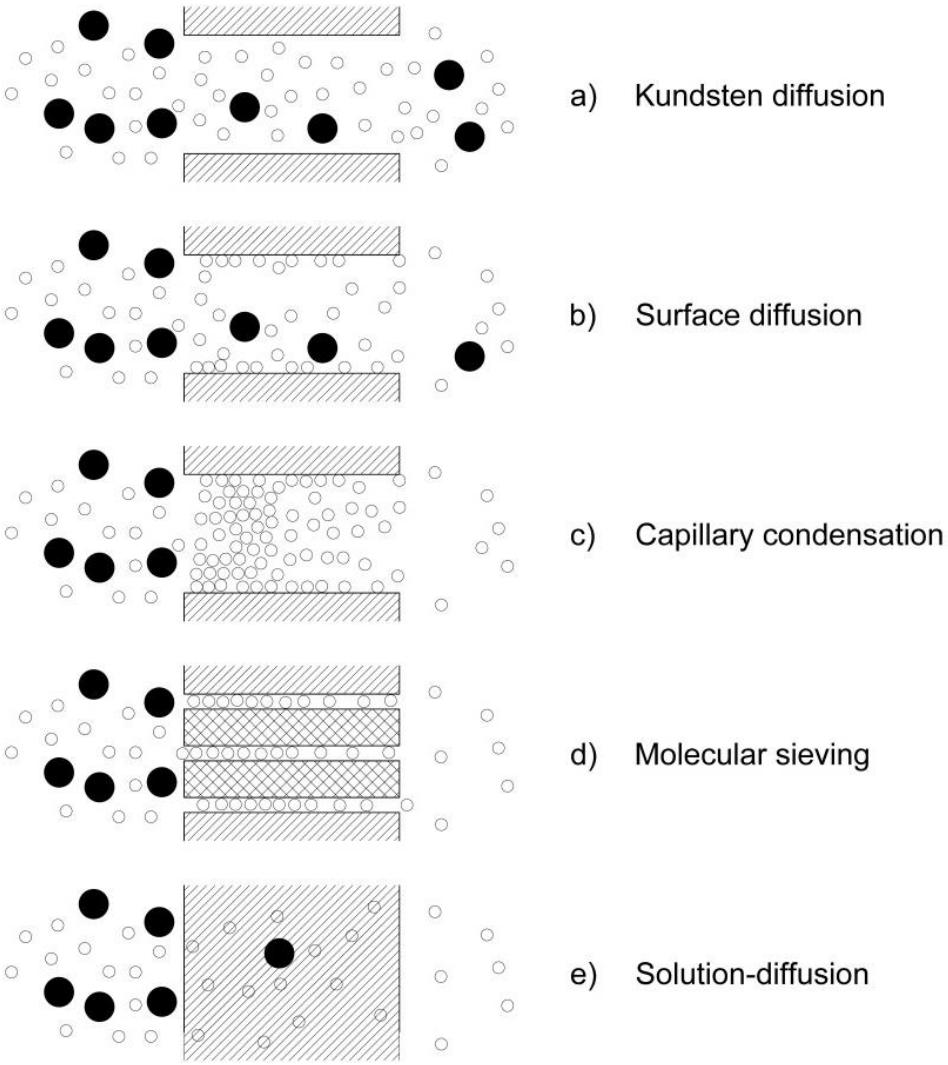

Figure 2-15: Schematic representation of main membrane gas separation mechanisms (Olajire, 2010; Shekhawat et al., 2003)

At the current stage of development, integration of membrane separation to the coal-fired power plant was found to impose net efficiency penalties ranging between 9.6–14.2% points (Maas et al., 2016; Zhai and Rubin, 2013). It has been stated that although membranes are capable of achieving CO_2 capture rates higher than 90% for CO_2 concentrations in flue gas of 10%$_{vol}$, such system would be highly energy-intensive (Favre, 2007). This is mainly associated with the need for flue gas compression to improve the separation driving force in the membrane (Favre, 2007; Kenarsari et al., 2013; Zhao et al., 2010).

Therefore, this CO_2 separation technology has the potential to provide better performance compared to the mature solvent adsorption processes for CO_2 concentrations higher than 20%$_{vol}$ (Favre, 2007).

2.5 Efficiency improvements in post-combustion CO_2 capture

Chemical solvent scrubbing using amine-based solvent and CaL, in addition to oxy-fuel combustion, are regarded as the most important CO_2 capture technologies for large-scale decarbonisation of fossil fuel power plants (Mac Dowell et al., 2010). Although CaL has been reported to impose lower net efficiency penalties on integration to the coal-fired power plant, there are further opportunities to improve performance of both technologies that include enhancements of the CO_2 capture material performance, heat integration, alternative process configurations for reduced parasitic load, and process intensification.

2.5.1 Material improvements

2.5.1.1 Chemical solvent scrubbing

A perfect chemical solvent for CO_2 capture would be characterised by fast reaction rate, high loading capacity, and low energy requirement for its regeneration (Rackley, 2010). It has been observed that there is a linear correlation between the amount of energy required for solvent regeneration and the net efficiency penalty imposed on integration of the chemical solvent scrubbing CO_2 capture plant (Dave et al., 2009; Goto et al., 2013; Romeo et al., 2008b). As a reduction in the regeneration energy of 1 GJ/tCO_2 is expected to reduce the net efficiency penalty by approximately 2% points, alternative solvents, such as amine- and carbonate-based solvents, have been widely investigated (Goto et al., 2013).

Considering alternative amine-based solvents, the tertiary and secondary amines have lower regeneration energy requirement and higher loading capacity over the primary amines, such as MEA, regarded as the reference solvent for chemical solvent scrubbing (Goto et al., 2013; Rackley, 2010). Yet, they are characterised with lower reaction rate, indicating the need for larger

equipment to achieve the desired CO_2 capture level. A viable option to overcome the drawbacks of a particular amine type and to combine the advantages of different amine types is the use of blended amine solvents (Rackley, 2010). Application of solvents, such as piperazine (PZ) and methyldiethanolamine (MDEA), as well as their blends was found to reduce the net efficiency penalty imposed on coal-fired power plant retrofits by 7% points (PZ) (Kvamsdal et al., 2014; Van Wagener et al., 2014) and 8.5% points (MDEA/PZ) (Kvamsdal et al., 2014). Moreover, integration of the amine scrubbing plant utilising MEA blended with the hindered amines, such as 2-amino-2-methyl-1-propanol (AMP), was found to reduce the net efficiency of the coal-fired power plant by 5.8% points, which does not account for the CO_2 compression parasitic load. This was found to be 1.3% lower than the figure obtained for the CO_2 capture plant using the reference MEA solvent that has been retrofitted to the same coal-fired power plant (Aroonwilas and Veawab, 2009).

Application of alternative solvents, such as NH_3, Na_2CO_3, K_2CO_3 and ionic liquids (IL), for CO_2 capture have also been investigated (Mirzaei et al., 2015). It has been shown that the lower heat of reaction between NH_3-based solvent and CO_2 results in less heat being required for solvent regeneration. Therefore, application of NH_3 for CO_2 capture from coal-fired power plants is expected to result in net efficiency penalties of 4.1 to 7% points (Ciferno et al., 2005; Gal, 2006; Romeo et al., 2008b). Yet, this has not been substantiated experimentally (Folger, 2013). Use of a carbonate-based solvent, such as K_2CO_3 with addition of PZ as a promoter, was found to require 29–33% less energy for solvent regeneration compared to the reference MEA solvent (Davidson, 2007; Oyenekan and Rochelle, 2005). Finally, IL can be used to tailor the aqueous solvent for CO_2 capture to reduce the regeneration energy by 13.5–50% compared to the reference MEA process (Gao et al., 2015; Jongpitisub et al., 2015; Khonkaen et al., 2014; Li et al., 2015; Simons et al., 2015). Yet, the capital investment for the IL-based CO_2 capture system would be at least double that for the MEA solvent scrubbing plant (Jongpitisub et al., 2015;

Khonkaen et al., 2014), and thus further techno-economic analysis is required to substantiate the additional capital cost.

2.5.1.2 Calcium looping

Although the calcium-based sorbent is characterised with considerably higher CO_2 capacity (393 gCO_2/kg at 50% conversion of CaO) compared to the reference MEA solvent (60 gCO_2/kg at 15.3%$_{wt}$ solubility) (Dasgupta et al., 2008), it decreases with the number of carbonation-calcination cycles due to sintering and sulphation (Borgwardt, 1989a, 1989b; Grasa et al., 2008). As the sorbent conversion is proportional to the active surface area of the sorbent particles (Grasa and Abanades, 2006), a number of sorbent enhancement measures have been proposed and proven to be successful at laboratory scale. These can be divided into chemical and physical sorbent enhancement measures (Ylätalo, 2013). The former group aims at improving the cyclic performance of calcium-based sorbent through altering the sorbent structure. This is achieved via doping the sorbent with any of a wide range of chemicals, such as organic and inorganic acids (HCl, CH_3COOH) (González et al., 2011; Li et al., 2009; Ridha et al., 2013), salts ($Mn(NO_3)_2$, $MnCO_3$, NaCl, Na_2CO_3) (Fennell et al., 2007; Sun et al., 2012), metal oxides (MgO, Al_2O_3, CeO_2) (Daud et al., 2016; Wang et al., 2015) as well as other metals and their compounds (K, Na, Li, Rb, Cs) (Reddy and Smirniotis, 2004). The latter group is based on physical measures to regenerate or prevent deterioration of the sorbent surface area. This includes sorbent pelletisation and biomass templating, steam reactivation, thermal treatment (Blamey et al., 2015, 2016; Coppola et al., 2015; Manovic and Anthony, 2010, 2008, 2007; Ridha et al., 2015; Sun et al., 2015), recarbonation (Valverde et al., 2014) and even acoustic fields (Valverde et al., 2013).

Although many studies have focused on improving the conversion of calcium-based sorbents, only a few identified the effect on the process energy requirement. Li et al. (2011) has estimated that doping of natural limestone with 50%$_{vol}$ acetic acid can reduce the calciner energy requirement by around 18%. Moreover, Dieter et al. (2014) has shown that 60% increase in the residual

activity of the calcium-based sorbent can reduce the net efficiency penalty of the integrated system by 0.2% points. Although sorbent modification methods can improve the performance of the integrated system, they add complexity to the process and thus the techno-economic evaluation of such systems needs to be conducted to prove their validity (Dean et al., 2011).

2.5.2 Heat integration

Enhancement of the heat integration degree between the CO_2 capture system and the power plant is regarded as a viable option for reduction of the parasitic load imposed on the power plant output on CO_2 capture plant integration (CSIRO, 2012). This can be achieved through utilisation of the waste heat available in the CO_2 capture plant and the CO_2 compression unit streams that otherwise would be cooled using the utility streams. The main sources of process performance improvement would stem from reduction of the steam extraction from steam turbines through feedwater heating using the waste heat (chemical solvent scrubbing) and reduction of additional fuel, and thus oxygen, requirement or increased generation of an additional amount of steam for an auxiliary steam cycle (calcium looping). A review of the studies on heat integration improvement revealed that the net efficiency could be improved by up to 3% points in chemical solvent scrubbing using amine-based solvent retrofitted to the coal-fired power plants (Hanak et al., 2014). Furthermore, appropriate design of the heat exchanger network in the CaL process would allow improving the process performance of the integrated system by about 1% point (Lara et al., 2013, 2014).

2.5.3 Alternative process configurations

2.5.3.1 Chemical solvent scrubbing

Optimisation of the CO_2 capture process flowsheet has been identified as an efficient but short-term approach leading to at least 20% reduction in energy consumption (Le Moullec and Kanniche, 2011). The most important modifications to the amine solvent scrubbing process available in the open and patent literature, which can be successfully applied to other chemical solvent

scrubbing systems, are inter-stage cooling, split-flow process, DMX^{TM} process, and vapour recompression (Cousins et al., 2011; Knudsen et al., 2009; Le Moullec and Kanniche, 2011; Raynal et al., 2011).

As CO_2 absorption is an exothermic process, reduction in the absorber operating temperature would enhance the adsorption process. Inter-stage cooling circuits have been identified as an effective way to control the absorber operating temperature. The main idea behind inter-stage cooling is the fact that the equilibrium partial pressure of CO_2 in the solvent is lowered on cooling and thus, the CO_2 absorption driving force is enhanced. As a result, the rich solvent loading is increased, leading to higher CO_2 carrying capacity of solvent. This, in turn, reduces the lean solvent flow rate required to achieve the same CO_2 capture efficiency (Chang and Shih, 2005; Freguia and Rochelle, 2003). Besides, more CO_2 flashes in the stripper which results in reduced reboiler duty (Aroonwilas and Veawab, 2007). The process with inter-stage temperature control was reported to result in reboiler duty reduced by 3.5% to 6.4%, depending on the number of intercooling stages (Cousins et al., 2011; Le Moullec and Kanniche, 2011).

The split-flow process (Figure 2-16) is a generic term that describes processes in which CO_2 absorption or solvent regeneration is conducted in multiple stages. The most commonly studied system comprises a partial solvent regeneration system and a staged feed to both absorber and stripper (Le Moullec and Kanniche, 2011). Introduction of the split-flow significantly reduces the CO_2 partial pressure in several stages of the absorber; hence, it increases the CO_2 driving force of the absorption process. This is mainly because the semi-lean solvent has a lower loading than the lean solvent at a feed stage and, in addition, is cooled down in the second cross-heat exchanger. Therefore, injection of semi-lean solvent at the middle stage of the absorber affects its temperature profile, resulting in higher rich loading. Although the split-flow configuration increases the process complexity, it is capable of reducing the reboiler duty by 11.6% (Cousins et al., 2011).

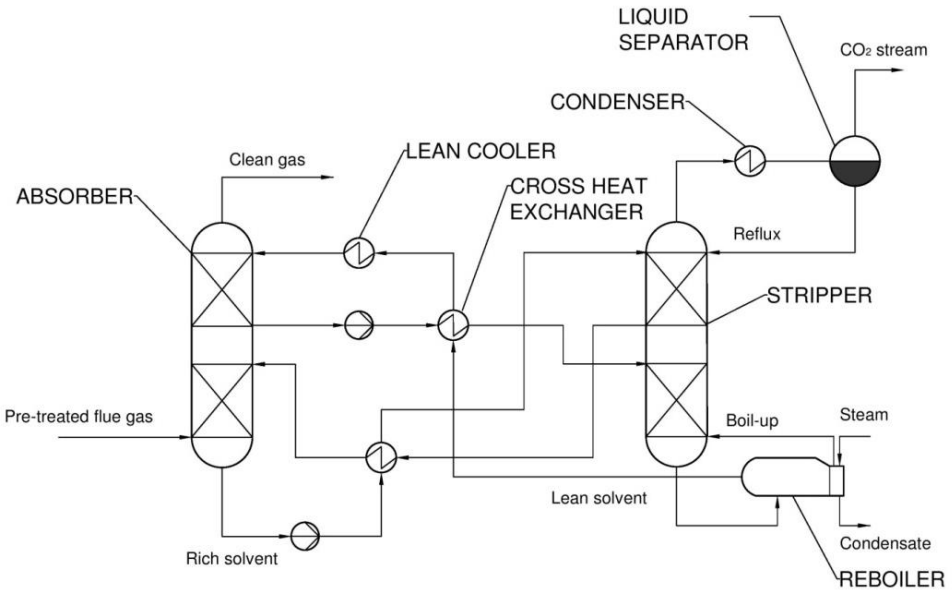

Figure 2-16: Process flow diagram of split-flow configuration (Cousins et al., 2011)

A rich-split process (Figure 2-17) is a simpler option of the split-flow process in which the rich stream is split in two streams before it reaches the cross-heat exchanger. The first stream is fed to the top stripper stage and remains unheated while the second stream is fed to the middle stripper stage and is heated in the cross-heat exchanger (Cousins et al., 2011, 2012). This allows the vapour released on heating in the cross-heat exchanger to pre-strip the cold rich solvent fed at the top stage of the stripper in comparison to the standard process where the vapour passes directly to the condenser having no benefit. Implementation of this configuration is reported to reduce the reboiler duty by 7–10% compared to the conventional process (Cousins et al., 2011, 2012).

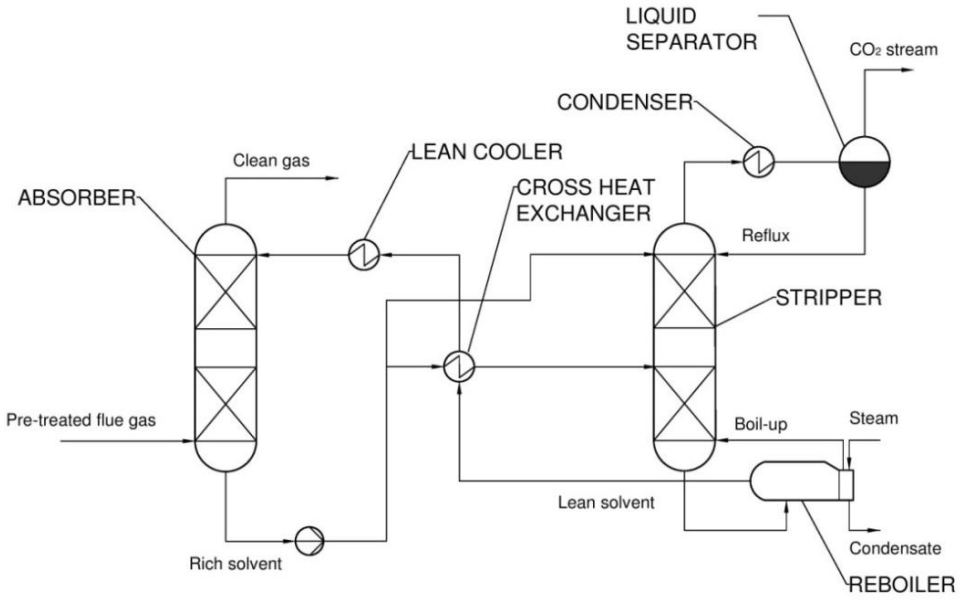

Figure 2-17: Process flow diagram of rich-split configuration

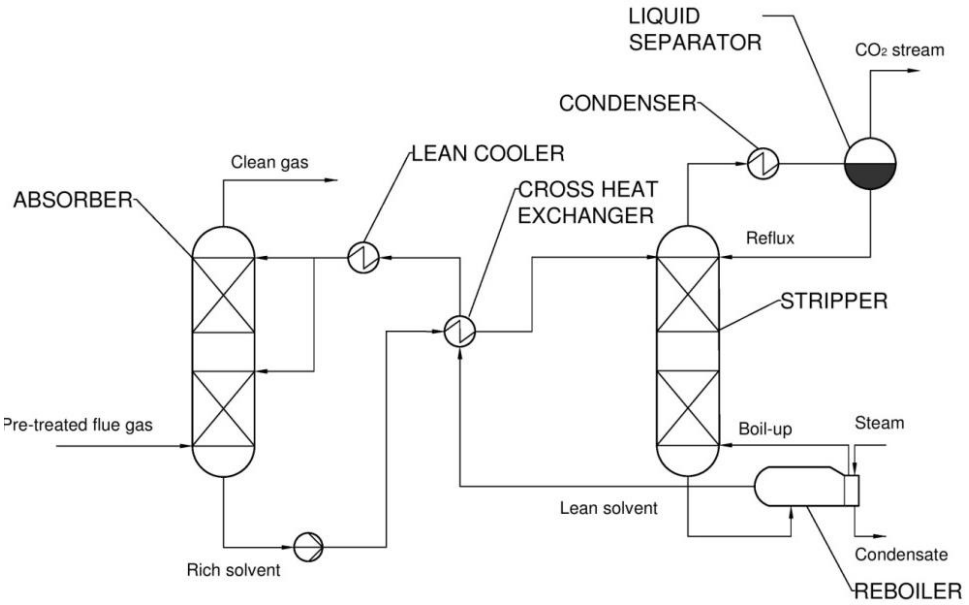

Figure 2-18: Process flow diagram of lean-split configuration

A lean-split configuration (Figure 2-18) that has been investigated by Knudsen et al. (2009) is another simplified approach to the split-flow process. In this case, the lean solution from the cross-heat exchanger is cooled down in the lean cooler, split and fed to the absorber at different locations. As the CO_2 absorption capacity of the solvent is higher for low lean loadings, the main principle behind the staged feed configuration is to minimise the loading and

equilibrate the driving force in the absorber (Le Moullec and Kanniche, 2011). Furthermore, as a portion of the lean solvent is fed at the middle stage of the absorber, it may be used as a mean of temperature control in the column. Such configuration is reported to reduce the process heat requirement by 11.9% (Knudsen et al., 2009).

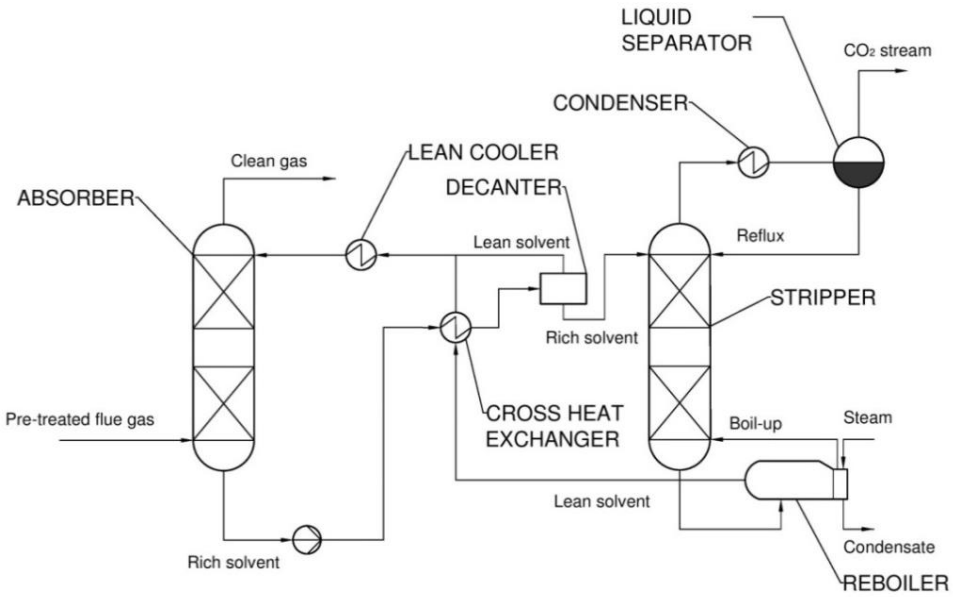

Figure 2-19: Simplified process flow diagram of the DMX™ process

The DMX™ process (Figure 2-19) utilises the property of demixing solvents to form two immiscible liquid phases at given solvent loading or temperature conditions. A liquid-liquid separation by decantation results in a lower amount of rich solution entering the stripper and thus, lower heat requirement for solvent regeneration. A light phase from the decanter is mixed with the lean solvent from the stripper bottoms and then fed to the absorber. The DMX™ process is characterised by 43.2% reduction in the heat requirement for solvent regeneration (Raynal et al., 2011).

Vapour recompression (Figure 2-20) is a process in which part of the reboiler vapour is extracted and recompressed. It can then be either condensed in the reboiler to partially satisfy the heat requirement for solvent regeneration, or reintroduced at the bottom of the stripper to provide an additional stripping stream. Although the former configuration results in the heat input to the reboiler

reduced by 19%, the electricity requirement of the system is increased and thus an economic analysis is required to assess its feasibility (Cousins et al., 2011).

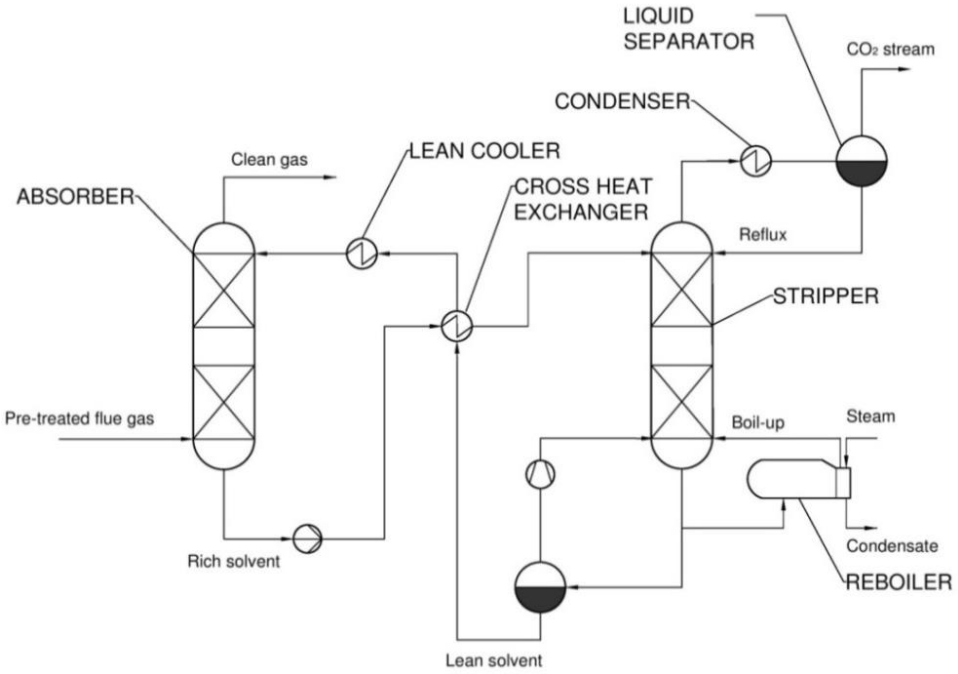

Figure 2-20: Process flow diagram of vapour recompression configuration

2.5.3.2 Calcium looping

Similarly to chemical solvent scrubbing, several process configurations for reduced parasitic load have been developed for CaL. This section reviews only the key configurations, while a detailed review is presented in Chapter 3 (Hanak et al., 2015).

Since the main source of the efficiency penalty in the CaL process stems from O_2 production for oxy-fuel combustion in the calciner, Abanades et al. (2005) have proposed an alternative calciner design in which the heat for sorbent regeneration is supplied through the metallic walls from an external source (Figure 2-21). Their study assumed that the heat source is a high-temperature fluidised bed combustor fuelled with an air and fuel mixture. Moreover, steam is used as a fluidising medium in the calciner. Although such configuration would be characterised by higher thermal efficiency and no requirement for O_2 production, it would require materials that have not yet been tested in practice. Yet, indirect heat transfer via heat pipes has been proposed as an alternative to

oxy-fuel combustion (Reitza et al., 2014). Nevertheless, this configuration was reported to be capable of increasing net thermal efficiency of the integrated power plant by 1.6% points (Abanades et al., 2005). Recently, this configuration has been shown to impose a net efficiency penalty of 0.6–0.7% points, if power required for CO_2 compression was not accounted for (Jayarathna et al., 2015).

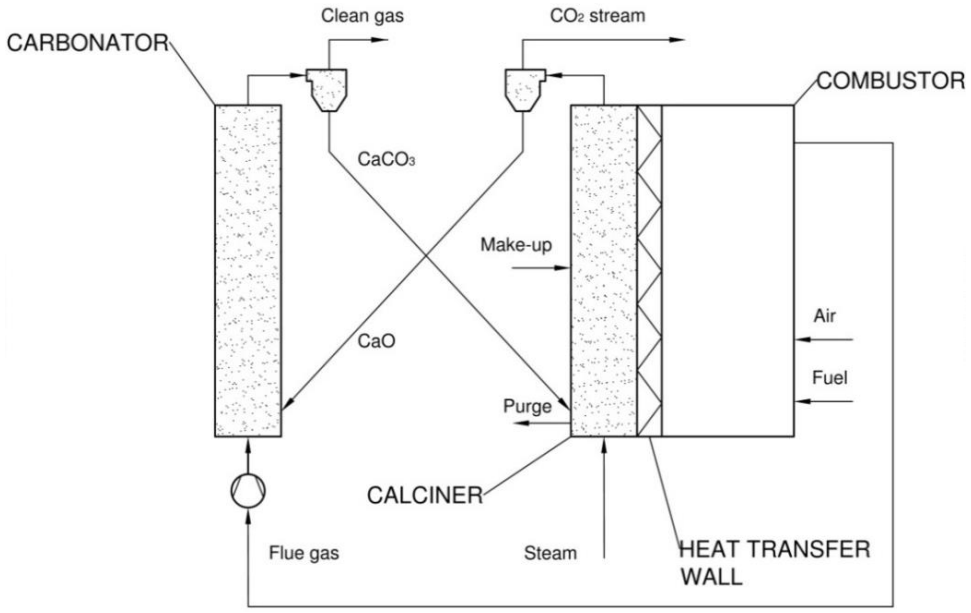

Figure 2-21: Heat transfer integrated calciner and combustor

In another configuration proposed by Abanades et al. (2005) the heat requirement of the calcination reaction is satisfied using a solid heat carrier (Figure 2-22). The process involves a common circulating fluidised bed combustor that is fired with an air and fuel mixture. The solid bed material, which is a dense material such as Al_2O_3 or deteriorated CaO, is heated up in the combustor, separated from the combustion gas stream and finally fed to the calciner. However, as this configuration assumes that the heat carrier particles would be mixed with the CO_2 sorbent in the calciner, it is still not clear whether continuous separation of these particles based on the difference in their density would be possible at the required scale. Nevertheless, an efficiency improvement of using this configuration is claimed to amount to 2.2% points.

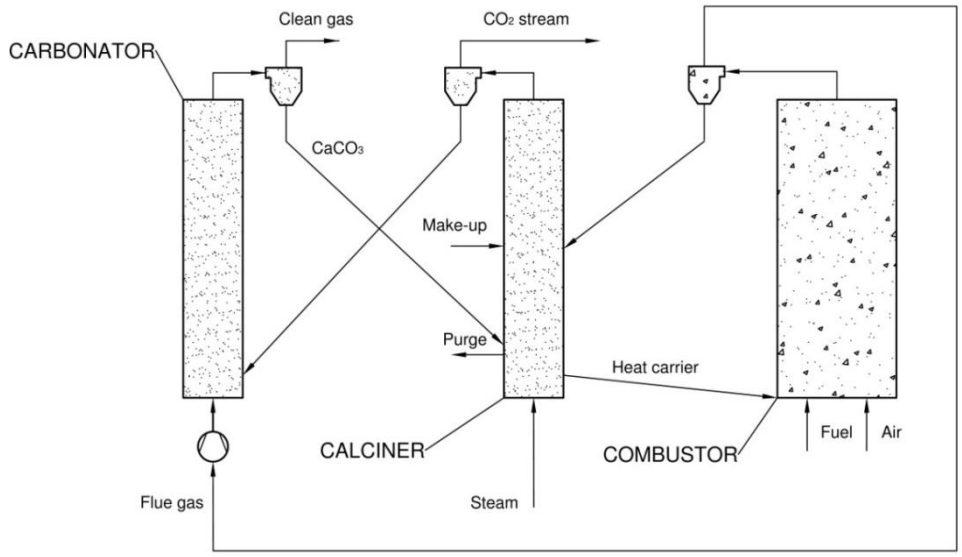

Figure 2-22: Indirect heat transfer from combustor to the calciner

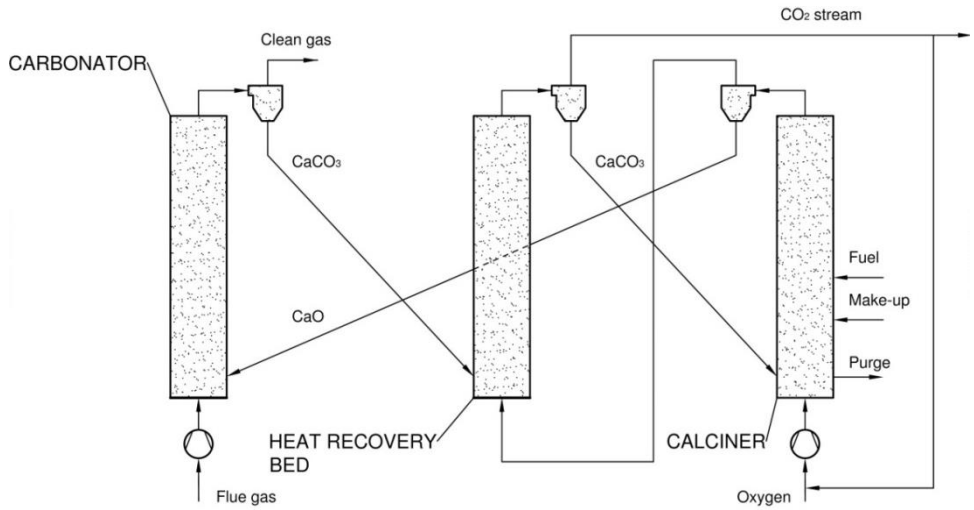

Figure 2-23: Three-bed configuration with an additional heat recovery bed

Martínez et al. (2012) have proposed another CaL process configuration that aims to preheat the $CaCO_3$ particles before they enter the calciner (Figure 2-23). In this configuration, the sensible heat of the CO_2 stream leaving the calciner is recovered to preheat the solid particles from the carbonator in an additional heat recovery fluidised bed. Although the flue gas acts as a fluidising medium and mixes with the partially carbonated sorbent particles, no carbonation reaction occurs in the heat recovery bed. This is because the fast carbonation reaction cannot take place as the active CaO remains in the core of each solid particle the surface of which has been covered with the $CaCO_3$ layer

formed in the carbonator (Arias et al., 2011). Although in this configuration the heat required by the calcination process is satisfied through oxy-fuel combustion, it is expected to increase the thermal efficiency of the CaL process by 1.4% points with a subsequent 9% reduction in fuel consumption.

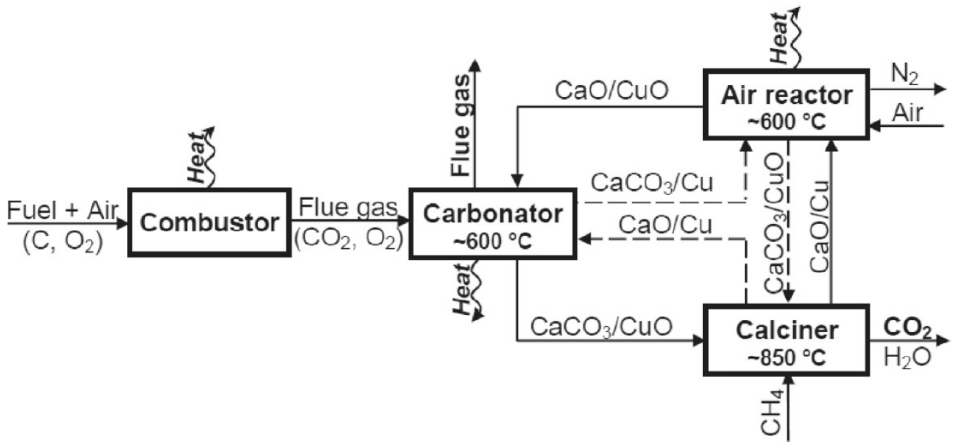

Figure 2-24: Conceptual design of CaO/CuO-looping cycle for CO_2 capture (Manovic and Anthony, 2011)

An experimental study conducted by Manovic and Anthony (2011) led to the conclusion that integration of CaL and chemical looping would be a practical solution for the post-combustion CO_2 capture plant. The superstructure (Figure 2-24) proposed by the authors comprises, in addition to the carbonator and calciner, an air reactor. In this configuration, heat for sorbent regeneration is provided through combustion of a gaseous fuel on contact with a metal oxide. The solid sorbent consists of both CaO and CuO, the latter being the oxygen carrier. Therefore, due to no requirement for cryogenic air separation, this technology was found to impose a net efficiency penalty of 3.5% points on integration to the coal-fired power plant (Ozcan et al., 2015). Yet, the authors claimed that further techno-economic studies are required to assess the validity of this technology.

2.5.4 Process intensification

Although implementation of advanced process configurations and enhanced heat integration in the system would result in energy savings, such configurations increase process complexity, and would be characterised by

higher capital investment and operating cost (Rochelle, 2009). Moreover, their implementation may limit power plant flexibility (Kvamsdal et al., 2009). These challenges can be addressed using process intensification principles. Using the conventional equipment, such as packed columns and fluidised beds, the process is limited by the mass transfer rate of CO_2 to the adsorbent/absorbent. This process can be improved by utilisation of enhanced acceleration.

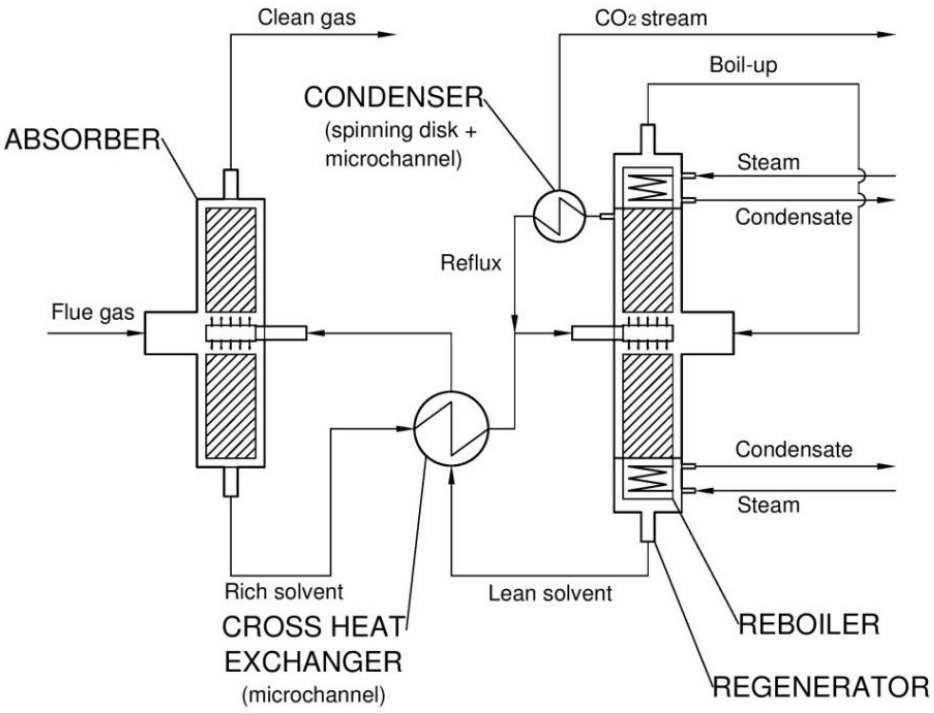

Figure 2-25: Conceptual design of intensified chemical solvent CO_2 capture plant

In gas-liquid systems, gravity enhancement, caused by centrifugal force due to high rotational speed of the rotating packed bed (Figure 2-25), results in greater interfacial area as the liquid is dispersed into droplets. This would result in reduction of the equipment volume by at least three orders of magnitude (Kang et al., 2014; Reay, 2008; Visscher et al., 2013). Although several models of the intensified amine scrubbing equipment have been recently published (Agarwal et al., 2010; Kang et al., 2014), neither the whole system nor impact of its integration to the power plant performance has been analysed.

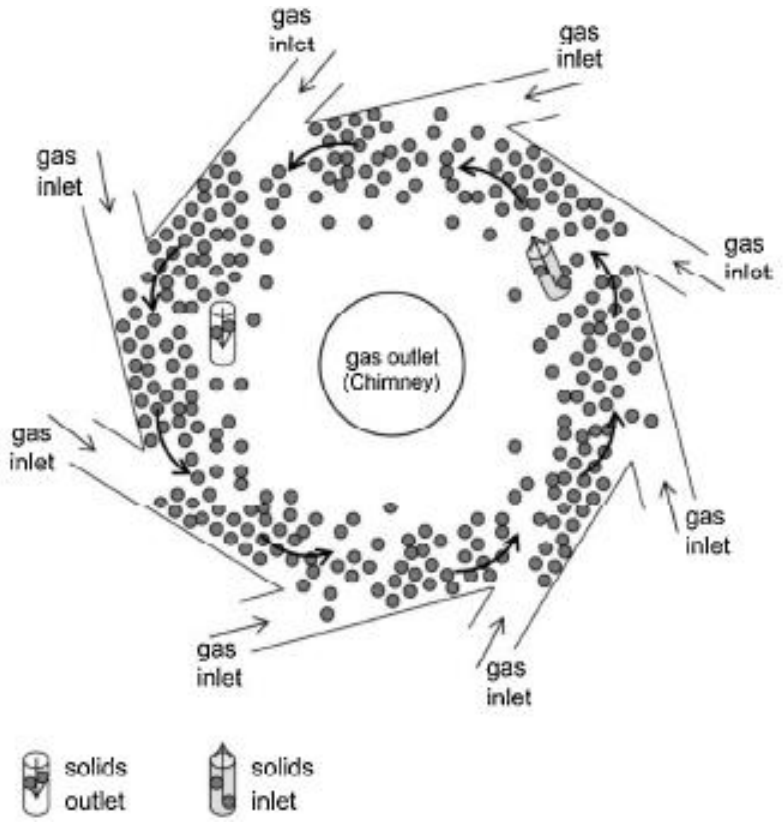

Figure 2-26: Conceptual design of intensified gas-solid reactor (Visscher et al., 2013)

Mass transfer in the solid-gas process can be intensified using a gas-solid vortex reactor in which the gas phase is injected tangentially into the reactor to generate centrifugal force acting on the solid particles (Figure 2-26). Application of such reactors was found to enhance the mass transfer rate ten times compared to the conventional fluidised bed during SO_2/NO_x adsorption (Ashcraft et al., 2013). In addition, heat transfer during fast biomass pyrolysis was found to be intensified by factor of 3–5 (Visscher et al., 2013). Nevertheless, no study has analysed application of the gas-solid vortex reactors for CO_2 absorption using solid sorbents.

Based on experience gained in other applications, use of the process intensification technologies instead of the conventional CO_2 capture equipment can yield not only reduced energy penalties, but also lower capital cost as intensified equipment would require smaller volumes to reach desired CO_2 capture level.

References

Abanades, J.C., Anthony, E.J., Wang, J., and Oakey, J.E. (2005), “Fluidized bed combustion systems integrating CO_2 capture with CaO”, *Environmental Science and Technology*, 39, 2861–2866.

Abanades, J.C., Arias, B., Lyngfelt, A., Mattisson, T., Wiley, D.E., Li, H., Ho, M.T., Mangano, E., and Brandani, S. (2015), “Emerging CO_2 capture systems”, *International Journal of Greenhouse Gas Control*, 40, 126–166.

Agarwal, L., Pavani, V., Rao, D.P., and Kaistha, N. (2010), “Process intensification in HiGee absorption and distillation: Design procedure and applications”, *Industrial and Engineering Chemistry Research*, 49, 10046–10058.

Arias, B., Abanades, J.C., and Grasa, G.S. (2011), “An analysis of the effect of carbonation conditions on CaO deactivation curves”, *Chemical Engineering Journal*, 167, 255–261.

Aroonwilas, A. and Veawab, A. (2009), “Integration of CO_2 capture unit using blended MEA-AMP solution into coal-fired power plants”, *Energy Procedia*, 1 (1) 4315–4321.

Aroonwilas, A. and Veawab, A. (2007), *Heat recovery gas absorption process*, WO Patent: WO2007107004 A1.

Ashcraft, R.W., Kovacevic, J., Heynderickx, G.J., and Marin, G.B. (2013), “Assessment of a gas-solid vortex reactor for SO_2/NO_x adsorption from flue gas”, *Industrial and Engineering Chemistry Research*, 52, 861–875.

Benton, D. (2015), *Decarbonising British industry*, Green Alliance, London, UK.

Blamey, J., Al-Jeboori, M.J., Manovic, V., Fennell, P.S., and Anthony, E.J. (2016), “CO_2 capture by calcium aluminate pellets in a small fluidized bed”, *Fuel Processing Technology*, 142, 100–106.

Blamey, J., Anthony, E.J., Wang, J., and Fennell, P.S. (2010), “The calcium looping cycle for large-scale CO_2 capture”, *Progress in Energy and Combustion Science*, 36, 260–279.

Blamey, J., Manovic, V., Anthony, E.J., Dugwell, D.R., and Fennell, P.S. (2015), "On steam hydration of CaO-based sorbent cycled for CO_2 capture", *Fuel*, 150, 269–277.

Boot-Handford, M.E., Abanades, J.C., Anthony, E.J., Blunt, M.J., Brandani, S., Mac Dowell, N., Fernandez, J.R., Ferrari, M.C., Gross, R., Hallett, J.P., Haszeldine, R.S., Heptonstall, P., Lyngfelt, A., Makuch, Z., Mangano, E., Porter, R.T.J., Pourkashanian, M., Rochelle, G.T., Shah, N., Yao, J.G., and Fennell, P.S. (2014), "Carbon capture and storage update", *Energy and Environmental Science*, 7, 130–189.

Borgwardt, R.H. (1989a), "Sintering of nascent calcium oxide", *Chemical Engineering Science*, 44, 53–60.

Borgwardt, R.H. (1989b), "Calcium oxide sintering in atmospheres containing water and carbon dioxide", *Industrial and Engineering Chemistry Research*, 28, 493–500.

Burt, S., Baxter, A., and Baxter, L. (2009), "Cryogenic CO_2 capture to control climate change emissions", *Proceedings of 34th International Technical Conference on Clean Coal and Fuel Systems,* Coal Technology Association, Clearwater, Florida, USA.

Cen, P. and Yang, R.T. (1986), "Bulk gas separation by pressure swing adsorption", *Industrial and Engineering Chemistry Fundamentals*, 25, 758–767.

Chang, H. and Shih, C.M. (2005), "Simulation and optimization for power plant flue gas CO_2 absorption-stripping systems", *Separation Science and Technology*, 40, 877–909.

Ciferno, J.P., DiPietro, P., and Tarka, T. (2005), *An economic scoping study for CO_2 capture using aqueous ammonia*, National Energy Technology Laboratory; Advanced Resources International; Energetics Incorporated, Pittsburgh, PA, USA.

Clodic, D., El Hitti, R., Younes, M., Bill, A., and Casier, F. (2005), "CO_2 capture by anti-sublimation—thermo-economic process evaluation", *Proceedings of*

4th Annual Conference on Carbon Capture and Sequestration, Alexandria, VA, USA.

Coppola, A., Palladino, L., Montagnaro, F., Scala, F., and Salatino, P. (2015), "Reactivation by steam hydration of sorbents for fluidized-bed calcium looping", *Energy and Fuels,* 29, 4436–4446.

Cousins, A., Cottrell, A., Lawson, A., Huang, S., and Feron, P.H.M. (2012), "Model verification and evaluation of the rich-split process modification at an Australian-based post combustion CO_2 capture pilot plant", *Greenhouse Gases: Science and Technology*, 2, 329–345.

Cousins, A., Wardhaugh, L.T., Feron, P.H.M. (2011), "Preliminary analysis of process flow sheet modifications for energy efficient CO_2 capture from flue gases using chemical absorption", *Chemical Engineering Research and Design*, 89, 1237–1251.

CSIRO (2012), *Assessing post-combustion capture for coal-fired power stations in Asia-Pacific partnership countries*, CSIRO Advanced Coal Technology, Newcastle, NSW, Australia.

D'Alessandro, D.M., Smit, B., and Long, J.R. (2010), "Carbon dioxide capture: prospects for new materials", *Angewandte Chemie International Edition*, 49, 6058–6082.

Dasgupta, D., Mondal, K., and Wiltowski, T. (2008), "Robust, high reactivity and enhanced capacity carbon dioxide removal agents for hydrogen production applications", *International Journal of Hydrogen Energy*, 33, 303–311.

Daud, F.D.M., Vignesh, K., Sreekantan, S., and Mohamed, A.R. (2016), "Improved CO_2 adsorption capacity and cyclic stability of CaO sorbents incorporated with MgO", *New Journal of Chemistry*, 40, 231–237.

Dave, N., Do, T., Puxty, G., Rowland, R., Feron, P.H.M., and Attalla, M.I. (2009), "CO_2 capture by aqueous amines and aqueous ammonia - A Comparison", *Energy Procedia*, 1 (1), 949–954.

Davidson, R. (2007), *Post-combustion carbon capture from coal fired plants - solvent scrubbing*, IEA Greenhouse Gas R&D Programme, Glos, UK.

Dean, C.C., Blamey, J., Florin, N.H., Al-Jeboori, M.J., and Fennell, P.S. (2011), "The calcium looping cycle for CO_2 capture from power generation, cement manufacture and hydrogen production", *Chemical Engineering Research and Design*, 89 (6), 836–855.

Dieter, H., Beirow, M., Schweitzer, D., Hawthorne, C., and Scheffknecht, G. (2014), "Efficiency and flexibility potential of calcium looping CO_2 capture", *Energy Procedia*, 63, 2129–2137.

Dlugokencky, E. and Tans, P. (2016), *Recent global CO_2*, NOAA Earth System Research Laboratory, available online: http://1.usa.gov/JN3NgG (last accessed 21/03/2016).

Dooley, J.J. (2013), "Estimating the supply and demand for deep geologic CO_2 storage capacity over the course of the 21st century: A meta-analysis of the literature", *Energy Procedia*, 37, 5141–5150.

ECCC (2016), *Future of carbon capture and storage in the UK*, The Stationery Office, London, UK.

EIA (2015), *Annual energy outlook 2015 with projections to 2040*, U.S. Energy Information Administration, Washington, DC, USA.

EIA (2013), *International Energy Outlook 2013*, U.S. Energy Information Administration, Washington, DC, USA.

European Commission (2009), *Directive 2009/31/EC of the European Parliament and of the Council of 23 April 2009 on the geological storage of carbon dioxide and amending Council Directive 85/337/EEC, European Parliament and Council Directives 2000/60/EC, 2001/80/EC, 2004/35/EC, 2006/12/EC, 2008/1/EC and Regulation (EC) No 1013/2006*, European Commission, Brussels, Belgium.

Favre, E. (2007), “Carbon dioxide recovery from post-combustion processes: Can gas permeation membranes compete with absorption?”, *Journal of Membrane Science*, 294, 50–59.

Fennell, P.S., Pacciani, R., Dennis, J.S., Davidson, J.F., and Hayhurst, A.N. (2007), “The effects of repeated cycles of calcination and carbonation on a variety of different limestones, as measured in a hot fluidized bed of sand”, *Energy and Fuels*, 21, 2072–2081.

Florin, N. amd Fennell, P.S. (2010), *Carbon capture technology: future fossil fuel use and mitigating climate change*, Grantham Research Institute on Climate Change, Imperial College London, London, UK, available online: http://bit.ly/1VuR9DG (last accessed: 21/03/2016)

Folger, P. (2013), *Carbon capture: A technology assessment*, Congressional Research Service, Washingtion, DC, USA, available online at: http://bit.ly/1esPfhA (last accessed: 23/03/2016).

Freguia, S. and Rochelle, G.T. (2003), “Modeling of CO_2 capture by aqueous monoethanolamine”, *AIChE Journal*, 49, 1676–1686.

Gal, E. (2006), *Chilled-ammonia post combustion CO_2 capture system – laboratory and economic evaluation results*, Electric Power Research Institute, Palo Alto, CA, USA.

Gao, J., Cao, L., Dong, H., Zhang, X., and Zhang, S. (2015), “Ionic liquids tailored amine aqueous solution for pre-combustion CO_2 capture: Role of imidazolium-based ionic liquids”, Applied Energy 154, 771–780.

GCCSI (2015), *The global status of CCS 2015: Summary report*, Global Carbon Capture and Storage Institute, Docklands, Australia.

GCCSI (2012), *The global status of CCS: 2012*, Global Carbon Capture and Storage Institute, Canberra, Australia.

González, B., Blamey, J., McBride-Wright, M., Carter, N., Dugwell, D., Fennell, P., and Abanades, J.C. (2011), “Calcium looping for CO_2 capture: Sorbent enhancement through doping”, *Energy Procedia*, 4, 402–409.

Goto, K., Yogo, K., and Higashii, T. (2013), “A review of efficiency penalty in a coal-fired power plant with post-combustion CO_2 capture”, *Applied Energy*, 111, 710–720.

Göttliche, G. (2004), *The energetics of carbon dioxide capture in power plants*, National Energy Technology Laboratory, Pittsburgh, PA, USA.

Göttliche, G. (1999), *Energetik der Kohlendioxidrückhaltung in Kraftwerken (The Energetics of Carbon Dioxide Capture in Power Plants)*, VDI-Verlag, Dusseldorf, Germany.

Grasa, G.S. and Abanades, J.C. (2006), “CO_2 capture capacity of CaO in long series of carbonation/calcination cycles”, *Industrial and Engineering Chemistry Research*, 45, 8846–8851.

Grasa, G.S., Alonso, M., and Abanades, J.C. (2008), “Sulfation of CaO particles in a carbonation/calcination loop to capture CO_2”, *Industrial and Engineering Chemistry Research*, 47, 1630–1635.

Hanak, D.P., Anthony, E.J., and Manovic, V. (2015), “A review of developments in pilot plant testing and modelling of calcium looping process for CO_2 capture from power generation systems”, *Energy and Environmental Science*, 8, 2199–2249.

Hanak, D.P., Biliyok, C., Yeung, H., and Białecki, R. (2014), “Heat integration and exergy analysis for a supercritical high-ash coal-fired power plant integrated with a post-combustion carbon capture process”, *Fuel*, 134, 126–139.

Herzog, H. and Golomb, D. (2004), “Carbon capture and storage from fossil fuel use”, *Encyclopedia of Energy*, 1, 1–11.

IEA (2015a), *Energy technology perspectives 2015: Executive summary*, IEA Publications, Paris, France.

IEA (2015b), *Carbon capture and storage: The solution for deep emissions reductions*, IEA Publications, Paris, France.

IEA (2015c), *Energy technology perspectives 2015*, IEA Publications, Paris, France.

IEA (2014), *Emission reduction through upgrade of coal-fired power plants: Learning from Chinese experience*, IEA Publications, Paris, France.

IEA (2013a), *Tracking clean energy progress 2013. IEA input to the clean energy ministerial*, IEA Publications, Paris, France.

IEA (2013b), *Technology roadmap: Carbon capture and storage*, IEA Publications, Paris, France.

IEA (2011), *Power generation from coal. Ongoing developments and outlook*, IEA Publications, Paris, France.

IEA (2010), *World Energy Outlook 2010*, IEA Publications, Paris, France.

IEA (2009), *Technology roadmap: Carbon capture and storage,* IEA Publications, Paris, France.

IPCC (2014), *Climate change 2014: synthesis report. Contribution of working groups I, II and III to the fifth assessment report of the Intergovernmental Panel on Climate Change*, Cambridge University Press, Cambridge, UK and New York, NY, USA.

IPCC (2013), *Climate change 2013: The physical science basis. Contribution of working group I to the fifth assessment report of the Intergovernmental Panel on Climate Change*, Cambridge Unviersity Press, Cambridge, UK and New York, NY, USA.

IPCC (2012), *Managing the risks of extreme events and disasters to advance climate change adaptation: special report of the Intergovernmental Panel on Climate Change*, Cambridge University Press, Cambridge, UK and New York, NY, USA.

IPCC (2007), *Climate change 2007: The physical science basis: contribution of working group I to the fourth assessment report of the Intergovernmental Panel on Climate Change*, Cambridge University Press, Cambridge, UK and New York, NY, USA.

Jayarathna, C.K., Mathisen, A., Øi, L.E., and Tokheim, L.A. (2015), “Process simulation of calcium looping with indirect calciner heat transfer”, *Proceedings of the 56th Conference on Simulation and Modelling*, Linköping, Sweden.

Jongpitisub, A., Siemanond, K., and Henni, A. (2015), “Process heat integration of 1-ethyl-3-metylimidazolium acetate for carbon-dioxide capture”, *Chemical Engineering Transactions*, 43, 1495–1500.

Kang, J.L., Sun, K., Wong, D.S.H., Jang, S.S., and Tan, C.S. (2014), “Modeling studies on absorption of CO_2 by monoethanolamine in rotating packed bed”, *International Journal of Greenhouse Gas Control*, 25, 141–150.

Kanniche, M., Gros-Bonnivard, R., Jaud, P., Valle-Marcos, J., Amann, J.M., and Bouallou, C, (2010), “Pre-combustion, post-combustion and oxy-combustion in thermal power plant for CO_2 capture”, *International Journal of Greenhouse Gas Control*, 30, 53–62.

Kenarsari, S.D., Yang, D., Jiang, G., Zhang, S., Wang, J., Russell, A.G., Wei, Q., and Fan, M. (2013), “Review of recent advances in carbon dioxide separation and capture”, *RSC Advances*, 3, 22739–22773.

Khonkaen, K., Siemanond, K., and Henni, A. (2014), “Simulation of carbon dioxide capture using ionic liquid 1-ethyl-3-methylimidazolium acetate”, *Computer Aided Chemical Engineering*, 33, 1045–1050.

Knudsen, J.N., Jensen, J.N., Vilhelmsen, P.J., and Biede, O. (2009), “Experience with CO_2 capture from coal flue gas in pilot-scale: Testing of different amine solvents”, *Energy Procedia*, 1 (1), 783–790.

Kvamsdal, H.M., Jakobsen, J.P., and Hoff, K.A. (2009), “Dynamic modeling and simulation of a CO_2 absorber column for post-combustion CO_2 capture”, *Chemical Engineering and Processing: Process Intensification*, 48 (1), 135–144.

Kvamsdal, H.M., Romano, M.C., van der Ham, L., Bonalumi, D., van Os, P., and Goetheer, E. (2014), “Energetic evaluation of a power plant integrated

with a piperazine-based CO_2 capture process", *International Journal of Greenhouse Gas Control*, 28, 343–355.

Lara, Y., Lisbona, P., Martínez, A., and Romeo, L.M. (2014), "A systematic approach for high temperature looping cycles integration", *Fuel*, 127, 4–12.

Lara, Y., Lisbona, P., Martínez, A., and Romeo, L.M. (2013), "Design and analysis of heat exchanger networks for integrated Ca-looping systems", *Applied Energy*, 111, 690–700.

Le Moullec, Y. (2012), "Assessment of carbon capture thermodynamic limitation on coal-fired power plant efficiency", *International Journal of Greenhouse Gas Control*, 7, 192–201.

Le Moullec, Y. and Kanniche, M. (2011), "Screening of flowsheet modifications for an efficient monoethanolamine (MEA) based post-combustion CO_2 capture", *International Journal of Greenhouse Gas Control*, 5, 727–740.

Leung, D.Y.C., Caramanna, G., and Maroto-Valer, M.M. (2014), "An overview of current status of carbon dioxide capture and storage technologies", *Renewable and Sustainable Energy Reviews*, 39, 426–443.

Li, W., Zhang, X., Lu, B., Sun, C., Li, S., and Zhang, S. (2015), "Performance of a hybrid solvent of amino acid and ionic liquid for CO_2 capture", *International Journal of Greenhouse Gas Control*, 42, 400–404.

Li, Y., Zhao, C., Chen, H., Ren, Q., and Duan, L. (2011), "CO_2 capture efficiency and energy requirement analysis of power plant using modified calcium-based sorbent looping cycle", *Energy*, 36, 1590–1598.

Li, Y., Zhao, C.S., Chen, H., and Liu, Y. (2009), "Enhancement of Ca-based sorbent multicyclic behavior in Ca looping process for CO_2 separation", *Chemical Engineering and Technology*, 32, 548–555.

Lucquiaud, M. and Gibbins, J. (2011), "On the integration of CO_2 capture with coal-fired power plants: A methodology to assess and optimise solvent-based post-combustion capture systems", *Chemical Engineering Research and Design*, 89, 1553–1571.

Maas, P., Nauels, N., Zhao, L., Markewitz, P., Scherer, V., Modigell, M., Stolten, D., and Hake, J.F. (2016), “Energetic and economic evaluation of membrane-based carbon capture routes for power plant processes”, *International Journal of Greenhouse Gas Control*, 44, 124–139.

Mac Dowell, N., Florin, N., Buchard, A., Hallett, J., Galindo, A., Jackson, G., Adjiman, C.S., Williams, C.K., Shah, N., and Fennell, P. (2010), “An overview of CO_2 capture technologies”, *Energy and Environmental Science*, 3, 1645–1669.

Manovic, V. and Anthony, E.J. (2011), “Integration of calcium and chemical looping combustion using composite CaO/CuO-based materials”, *Environmental Science and Technology*, 45, 10750–10756.

Manovic, V. and Anthony, E.J. (2010), “Lime-based sorbents for high-temperature CO_2 capture - a review of sorbent modification methods”, *International Journal of Environmental Research and Public Health*, 7, 3129–40.

Manovic, V. and Anthony, E.J. (2008), “Thermal activation of CaO-based sorbent and self-reactivation during CO_2 capture looping cycles”, *Environmental Science and Technology*, 42, 4170–4174.

Manovic, V. and Anthony, E.J. (2007), “Steam reactivation of spent CaO-based sorbent for multiple CO_2 capture cycles”, *Environmental Science and Technology*, 41, 1420–1425.

Maroto-Valer, M.M., (2010), *Developments and innovation in carbon dioxide (CO_2) capture and storage technology. Volume 1: Carbon dioxide (CO_2) capture*, *transportation and industrial applications*, CRC press, London, UK; New York, NY, USA; Washington, DC, USA.

Marshall, C. and Quiñones, M. (2015), “Clean coal power plant killed, again”, *Scientific American*, available online: http://bit.ly/1DAqa2i (last accessed 21/03/2016).

Martínez, A., Lara, Y., Lisbona, P., and Romeo, L.M. (2012), “Energy penalty reduction in the calcium looping cycle”, *International Journal of Greenhouse Gas Control*, 7, 74–81.

Martínez, I., Murillo, R., Grasa, G., and Abanades, J.C (2011), “Integration of a Ca looping system for CO_2 capture in existing power plants”, *AIChE Journal*, 57, 2599–2607.

Merkel, T.C., Lin, H., Wei, X., and Baker, R. (2010), “Power plant post-combustion carbon dioxide capture: An opportunity for membranes” *Journal of Membrane Science*, 359, 126–139.

Metz, B., Davidson, O., de Coninck, H., Loos, M., and Meyer, L. (2005), *IPCC Special Report on Carbon Dioxide Capture and Storage*, Cambridge University Press, Cambridge, United Kingdom and New York, NY, USA.

Miller, B.G. (2011), *Clean Coal Engineering Technology*, Butterworth-Heinemann, Burlington, MA, USA and Oxford, UK.

Mirzaei, S., Shamiri, A., and Aroua, M.K. (2015), “A review of different solvents, mass transfer, and hydrodynamics for postcombustion CO_2 capture”, *Reviews in Chemical Engineering*, 31 (6), 521–561.

Nelson, T.O., Green, D.A., Box, P., Gupta, R.P., Henningsen, G., and Turk, B.S. (2009), *Carbon dioxide capture from flue gas using dry regenerable sorbents*, RTI International, Durham, NC, USA.

Oexmann, J., Hensel, C., and Kather, A. (2008), “Post-combustion CO_2 capture from coal-fired power plants: Preliminary evaluation of an integrated chemical absorption process with piperazine-promoted potassium carbonate”, *International Journal of Greenhouse Gas Control*, 2, 539–552.

Oexmann, J., Kather, A., Linnenberg, S., and Liebenthal, U. (2012), “Post-combustion CO_2 capture: chemical absorption processes in coal-fired steam power plants”, *Greenhouse Gases: Science and Technology*, 2, 80–98.

Olajire, A.A. (2010), "CO_2 capture and separation technologies for end-of-pipe applications - A review", *Energy*, 35 (6), 2610–2628.

Orion Innovations (2013), *A UK Vision for carbon capture and storage*, Orion Innovations Ltd., London, UK.

Oyenekan, B.A. and Rochelle, G.T. (2005), "Stripper models for CO_2 capture by aqueous solvent", *Greenhouse Gas Control Technologies*, 7, 1861–1864.

Ozcan, D.C., Macchi, A., Lu, D.Y., Kierzkowska, A.M., Ahn, H., Müller, C.R., and Brandani, S. (2015), "Ca–Cu looping process for CO_2 capture from a power plant and its comparison with Ca-looping, oxy-combustion and amine-based CO_2 capture processes", *International Journal of Greenhouse Gas Control*, 43, 198–212.

Palmgren, C.R., Morgan, M.G., De Bruin, W.B., and Keith, D.W. (2004), "Initial public perceptions of deep geological and oceanic disposal of carbon dioxide", *Environmental Science and Technology*, 38, 6441–6450.

Pfaff, I., Oexmann, J., and Kather, A. (2010), "Optimised integration of post-combustion CO_2 capture process in greenfield power plants", *Energy*, 35, 4030–4041.

Pires, J.C.M., Martins, F.G., Alvim-Ferraz, M.C.M., and Simões, M. (2011), "Recent developments on carbon capture and storage: An overview", *Chemical Engineering Research and Design*, 89, 1446–1460.

Rackley, S.A. (2010), *Carbon Capture and Storage*, Elsevier, Burlington, USA.

Raynal, L., Alix, P., Bouillon, P.A., Gomez, A., de Nailly, M., Jacquin, M., Kittel, J., di Lella, A., Mougin, P., and Trapy, J. (2011), "The DMX^{TM} process: An original solution for lowering the cost of post-combustion carbon capture", *Energy Procedia*, 4, 779–786.

Reay, D. (2008), "The role of process intensification in cutting greenhouse gas emissions", *Applied Thermal Engineering*, 28, 2011–2019.

Reddy, E.P. and Smirniotis, P.G. (2004), “High-temperature sorbents for CO_2 made of alkali metals doped on CaO supports”, *Journal of Physical Chemistry B*, 108 (23), 7794–7800.

Reitza, M., Junka, M., Ströhle, J., and Epple, B. (2014), “Design and erection of a 300 kW_{th} indirectly heated carbonate looping test facility”, *Energy Procedia*, 63, 2170–2177.

Riboldi, L. and Bolland, O. (2015), “Evaluating pressure swing adsorption as a CO_2 separation technique in coal-fired power plants”, *International Journal of Greenhouse Gas Control*, 39, 1–16.

Ridha, F.N., Manovic, V., Macchi, A., Anthony, M.A., and Anthony, E.J. (2013), “Assessment of limestone treatment with organic acids for CO_2 capture in Ca-looping cycles”, *Fuel Processing Technology*, 116, 284–291.

Ridha, F.N., Wu, Y., Manovic, V., Macchi, A., and Anthony, E.J. (2015), “Enhanced CO_2 capture by biomass-templated $Ca(OH)_2$-based pellets”, *Chemical Engineering Journal*, 274, 69–75.

Rochelle, G.T. (2009), “Amine Scrubbing for CO_2 Capture”, *Science,* 325, 1652–1654.

Romeo, L.M., Abanades, J.C., Escosa, J.M., Paño, J., Giménez, A., Sánchez-Biezma, A., and Ballesteros, J.C. (2008a), “Oxyfuel carbonation/calcination cycle for low cost CO_2 capture in existing power plants”, *Energy Conversion and Management*, 49, 2809–2814.

Romeo, L.M., Espatolero, S., and Bolea, I. (2008b), “Designing a supercritical steam cycle to integrate the energy requirements of CO_2 amine scrubbing”, *International Journal of Greenhouse Gas Control*, 2, 563–570.

Sanna, A., Uibu, M., Caramanna, G., Kuusik, R., and Maroto-Valer, M.M. (2014), “A review of mineral carbonation technologies to sequester CO_2”, *Chemical Society Reviews*, 43, 8049–80.

Schach, M.O., Oyarzún, B., Schramm, H., Schneider, R., and Repke, J.U. (2011), “Feasibility study of CO_2 capture by anti-sublimation”, *Energy Procedia*, 4, 1403–1410.

Shekhawat, D., Luebke, D.R., and Pennline, H.W. (2003), *A review of carbon dioxide selective membranes*, National Energy Technology Laboratory, Pittsburgh, PA, USA.

Simons, T.J., Verheyen, T., Izgorodina, E.I., Vijayaraghavan, R., Young, S., Pearson, A.K., Pas, S.J., and MacFarlane, D.R. (2015), “Mechanisms of low temperature capture and regeneration of CO_2 using diamino protic ionic liquids”, *Physical Chemistry Chemical Physics*, 18, 1140–1149.

Spliethoff, H. (2010), *Power generation from solid fuels*, Springer, München, Germany.

Ströhle, J., Lasheras, A., Galloy, A., and Epple, B. (2009), “Simulation of the carbonate looping process for post-combustion CO_2 capture from a coal-fired power plant”, *Chemical Engineering and Technology*, 32, 435–442.

Strube, R. and Manfrida, G. (2011), “CO_2 capture in coal-fired power plants - Impact on plant performance”, *International Journal of Greenhouse Gas Control*, 5, 710–726.

Sun, J., Liu, W., Hu, Y., Li, M., Yang, X., Zhang, Y., and Xu, M. (2015), “Structurally improved, core-in-shell, CaO-based sorbent pellets for CO_2 capture”, *Energy and Fuels*, 29, 6636–6644.

Sun, R., Li, Y., Liu, H., Wu, S., and Lu, C. (2012), “CO_2 capture performance of calcium-based sorbent doped with manganese salts during calcium looping cycle”, *Applied Energy*, 89, 368–373.

Sutton, B. (2015), *Statement from Peabody Energy on the department of energy’s decision to suspend FutureGen*, Peabody Energy, available online: http://bit.ly/1VyC442 (last accessed: 22/03/2016).

Svensson, R., Odenberger, M., Johnsson, F., and Strömberg, L. (2004), "Transportation systems for CO_2 - Application to carbon capture and storage", *Energy Conversion and Managemenet*, 45, 2343–2353.

Thitakamol, B., Veawab, A., and Aroonwilas, A. (2007), "Environmental impacts of absorption-based CO_2 capture unit for post-combustion treatment of flue gas from coal-fired power plant", *International Journal of Greenhouse Gas Control*, 1, 318–342.

UNEP (2012), *The emissions gap report 2012*, United Nations Environment Programme (UNEP), Nairobi, Kenya.

Valverde, J.M., Raganati, F., Quintanilla, M.A.S., Ebri, J.M.P., Ammendola, P., and Chirone, R. (2013), "Enhancement of CO_2 capture at Ca-looping conditions by high-intensity acoustic fields", *Applied Energy*, 111, 538–549.

Valverde, J.M., Sanchez-Jimenez, P.E., Perez-Maqueda, L.A., Quintanilla, M.A.S., and Perez-Vaquero, J. (2014), "Role of crystal structure on CO_2 capture by limestone derived CaO subjected to carbonation/recarbonation/calcination cycles at Ca-looping conditions", *Applied Energy*, 125, 264–275.

Van Der Zwaan, B. and Smekens, K. (2009), "CO_2 capture and storage with leakage in an energy-climate model", *Environmental Modeling and Assessment*, 14, 135–148.

Van Wagener, D.H., Liebenthal, U., Plaza, J.M., Kather, A., and Rochelle, G.T. (2014), "Maximizing coal-fired power plant efficiency with integration of amine-based CO_2 capture in greenfield and retrofit scenarios", *Energy*, 72, 824–831.

VGB (2013), *Electricity generation: Facts and figures 2012/2013*, VGB PowerTech e.V., Essen, Germany, available online: http://bit.ly/1o3DjLb (last accessed: 22/03/2016).

Visscher, F., van der Schaaf, J., Nijhuis, T.A., and Schouten, J.C. (2013), "Rotating reactors – A review", *Chemical Engineering Research and Design*, 91, 1923–1940.

Vorrias, I., Atsonios, K., Nikolopoulos, A., Nikolopoulos, N., Grammelis, P., and Kakaras, E. (2013), “Calcium looping for CO_2 capture from a lignite fired power plant”, *Fuel* 113, 826–836.

Wang, M., Lawal, A., Stephenson, P., Sidders, J., and Ramshaw, C. (2011), “Post-combustion CO_2 capture with chemical absorption: A state-of-the-art review”, *Chemical Engineering Research and Design*, 89, 1609–1624.

Wang, S., Fan, S., Fan, L., Zhao, Y., and Ma, X. (2015), “Effect of cerium oxide doping on the performance of CaO-based sorbents during calcium looping cycles”, *Environmental Science and Technology*, 49, 5021–5027.

Wijmans, J.G. and Baker, R.W. (2006), “The solution–diffusion model: A unified approach to membrane permeation”, in: Yampolskii, Y., Pinnau, B., Freeman, B. (Eds.) (2006), *Materials Science of Membranes for Gas and Vapor Separation*, John Wiley and Sons, Chichester, UK, 158–189.

Xu, G., Jin, H.G., Yang, Y.P., Xu, Y.J., Lin, H., and Duan, L. (2010), “A comprehensive techno-economic analysis method for power generation systems with CO_2 capture”, *International Journal of Energy Research*, 34, 321–332.

Yampolskii, Y. (2012), “Polymeric gas separation membranes”, *Macromolecules*, 45 (8), 3298–3311.

Yang, J., Lee, C.H., and Chang, J.W. (1997), “Separation of hydrogen mixtures by a two-bed pressure swing adsorption process using zeolite 5A”, *Industrial and Engineering Chemistry Research*, 36, 2789–2798.

Yang, Y., Zhai, R., Duan, L., Kavosh, M., Patchigolla, K., and Oakey, J. (2010), “Integration and evaluation of a power plant with a CaO-based CO_2 capture system”, *International Journal of Greenhouse Gas Control*, 4, 603–612.

Ylätalo, J. (2013), *Model based analysis of the post-combustion calcium looping process for carbon dioxide capture* (PhD Thesis), Lappeenrata University of Technology, Lappeenrata, Finland, available online: http://bit.ly/21ER14b (last accessed: 22/03/2016).

Zhai, H. and Rubin, E.S. (2013), “The effects of membrane-based CO_2 capture system on pulverized coal power plant performance and cost” *Energy Procedia*, 37, 1117–1124.

Zhao, L., Riensche, E., Blum, L., and Stolten, D. (2010), “Multi-stage gas separation membrane processes used in post-combustion capture: Energetic and economic analyses”, *Journal of Membrane Science*, 359, 160–172.

This page intentionally left blank.

3 A REVIEW OF DEVELOPMENTS IN PILOT-PLANT TESTING AND MODELLING OF CALCIUM LOOPING PROCESS FOR CO_2 CAPTURE FROM POWER GENERATION SYSTEMS

Dawid P. Hanak, Edward J. Anthony and Vasilije Manovic

Published: Energy and Environmental Science, 2015, 8, 2199–2249[d]

Statement of contributions of joint authorship

Dawid P. Hanak conducted the systematic review and analysis of the literature, drafted and critically revised the manuscript, prepared tables and figures, as well as obtained permissions for reprinting or adapting the figures in the existing literature. Edward J. Anthony and Vasilije Manovic proof-read and critically commented on the manuscript prior to its submission to Energy and Environmental Science (Journal Impact Factor 2016: 20.523).

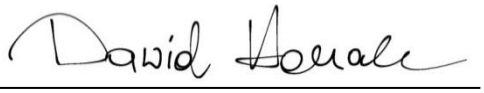

Dawid P. Hanak, PhD Candidate

Edward J. Anthony, Subject advisor

Vasilije Manovic, Principal supervisor

[d] Reprinted with permission from Hanak, D.P., Anthony, E.J., and Manovic, V. (2015), "A review of developments in pilot-plant testing and modelling of calcium looping process for CO_2 capture from power generation systems", *Energy and Environmental Science*, 8, 2199–2249, doi: 10.1039/c5ee01228g, Royal Society of Chemistry 2015.

Energy & Environmental Science

REVIEW

View Article Online
View Journal

Cite this: DOI: 10.1039/c5ee01228g

A review of developments in pilot-plant testing and modelling of calcium looping process for CO_2 capture from power generation systems

Dawid P. Hanak, Edward J. Anthony* and Vasilije Manovic

Received 20th April 2015,
Accepted 3rd June 2015

DOI: 10.1039/c5ee01228g

www.rsc.org/ees

A nearly complete decarbonisation of the power sector is essential to meet the European Union target for greenhouse gas emissions reduction. Carbon capture and storage technologies have been identified as a key measure in reducing the carbon-intensity of the power sector. However, no cost-effective technology has yet been developed on a commercial scale, which is mostly due to high capital cost. Moreover, the mature technologies, such as amine scrubbing or oxy-combustion technologies, impose a high projected efficiency penalty (8–12.5% points) upon integration to the power plant. The calcium looping process, which is currently being tested experimentally in bench- and pilot-scale plants worldwide, is regarded as a promising alternative to the chemical solvent scrubbing approach, as it leads to the projected efficiency penalty of 6–8% points. The calcium looping concept has been developing rapidly due to the introduction of new test facilities, new correlations for process modelling, and process configurations for improved performance. The first part of this review provides an overview of the bench- and pilot-plant test facilities available worldwide. The focus is put on summarising the characteristics and operating conditions of the test facilities, as well as extracting the key experimental findings. Additionally, the experimental data suitable for validation or verification of the process models are presented. In the second part, the approaches to the carbonator and the calciner reactor modelling are summarised and classified in five model complexity levels. Moreover, the model limitations are assessed and the needs for modelling baselines for further process analyses are identified. Finally, in the third part the approaches for the integration of calcium looping to the power generation systems and for the improvement of the process performance are identified and evaluated. This review indicates that calcium looping integration resulted in the projected efficiency penalty of 2.6–7.9% points for the coal-fired power plants and 9.1–11.4% points for the combined-cycle power plants. Also, it was found that the calcium looping process can be used to develop a novel high-efficiency (46.7%$_{LHV}$) coal-fired power generation system, making this technology even more promising compared to the other CO_2 capture technologies.

Broader context

Fossil fuels are expected to remain essential for the global power generation portfolio. As a result, carbon capture and storage technologies are expected to play a crucial role in greenhouse gas emissions reduction from the power generation sector. Mature technologies, such as amine scrubbing and oxy-combustion that are currently under demonstration at a commercial scale, are projected to reduce the net efficiency of electricity production by up to 12.5% points. For this reason, in order to minimise the efficiency penalty and the associated increase in the cost of electricity, novel CO_2 capture technologies are being developed. Calcium looping processes appears to be a promising technology that could reduce the efficiency penalty to 7% points. Development of this technology has advanced at a rapid rate over the past decade, especially since 2009. This review provides a comprehensive overview of bench- and pilot-plant testing, the available models to represent the process performance, alternative process configurations to reduce energy requirements and approaches for process integration for commercial-scale power generation systems. It is shown that further pilot-plant testing to generate data for process models validation could significantly minimise prediction uncertainty. Also, the requirement for baseline modelling assumptions and further development in sorbent performance are highlighted as key to future development.

1 Introduction

The European Union aims to reduce its greenhouse gas emissions relative to 1990 levels by 30% by 2020,[1] 40% by 2030,[2,3] and

Combustion and CCS Centre, Cranfield University, Bedford, Bedfordshire, MK43 0AL, UK. E-mail: b.j.anthony@cranfield.ac.uk

80–95% by 2050. To meet the 2050 target, a nearly complete decarbonisation of the power sector is required due to the high fossil fuel contribution in the energy mix.[4] Power generation accounted for more than one-third of the total greenhouse gas emissions in 2010.[5] For this reason, transformation of the power generation sector is key to limiting the average global temperature increase.[6]

One reason behind the high carbon intensity of the power generation sector is the major share (42%) of coal-fired power plants (CFPP) in the global supply of electricity,[7] the current average net thermal efficiency of which amounts to $33\%_{LHV}$ due to the high (75%) share of subcritical units in the global CFPP fleet.[6] Moreover, due to the recent emergence of shale gas in North America, American exports of coal have increased. As a result, the price of coal has fallen significantly in Europe and electricity generation from coal has increased at the expense of gas-based electricity generation.[6] If the current market trend continues, coal will continue to be used for power generation as predicted by the Energy Information Administration.[8] Hence, a complete decarbonisation of the power sector may be even more challenging in the future.

Carbon capture and storage (CCS) technologies are expected to play a crucial role in greenhouse gas emissions reduction from the power generation sector.[9] However, the first-of-a-kind large-scale CO_2 capture plant was only commissioned in 2014,[10] although the technology required for CCS deployment exists in other industries.[6,11] This is because no cost-effective technology for fossil fuel power plants has yet been fully demonstrated on a commercial scale. A relatively high capital cost, due to the size of equipment required to accommodate the flue gas volume, and the efficiency penalty associated with a significant increase in the cost of electricity,[12] make CCS infeasible at the moment. Nevertheless, the IEA 2 °C scenario predicts that 63% of the CFPPs will be equipped with CCS installations by 2050.[6] There are several mature CO_2 capture technologies that are close to market commercialisation in the power generation sector.[13,14]

The first full-scale capture project at Boundary Dam is based on a chemical absorption post-combustion capture plant using amine solvent,[10] with other post-combustion plants and oxy-combustion CFPPs under construction or in the planning stage.[9] Such technologies impose a significant projected efficiency penalty reaching up to 12.5% points, identified through analysis of the overall process performance using computational and modelling tools.[15–18] A reduction in the process efficiency, in turn, affects fuel economy and thus the cost of electricity. Moreover, these CO_2 capture technologies would require additional effort, and therefore cost, to mitigate the environmental, health and safety issues.[14] These are the main drivers for development of novel technologies that would affect electricity generation to a lesser degree, and would not be harmful to the environment or human health. A promising alternative to both oxy-combustion and chemical solvent absorption is a second generation CO_2 capture technology called calcium looping (CaL) that uses a calcium-based solid sorbent.

Development of the CaL process has advanced at a rapid rate over the past decade, especially since 2009. This is seen not only in the increased number of test facilities, but also in the

Table 1 A summary of the review studies related to calcium looping process

Source	Review scope
Stanmore and Gilot[19]	– Summary of the sintering, sulphation, particle fragmentation and attrition effect on the sorbent activity. – Detailed information on the correlations for mathematical modelling of carbonation, calcination, sulphation and sintering. – A brief overview of the models for prediction of the aerodynamics and trajectories of particles, as well as reaction rates in the circulating fluidised bed (CFB).
Harrison[20]	– Comparison of the standard steam-methane reforming process and the CaL process for H_2 production. Review of the thermodynamic analyses, sorbent durability and process configurations. – Review of the experimental studies on hydrogen production.
Florin and Harris[21]	– Review of process configurations for the enhanced hydrogen production from biomass gasification. – Summary of the sorbent regeneration measures. – A brief reference to the sorbent activity decay. – Review of the experimental trials on hydrogen production from carbonaceous fuels using calcium looping.
Blamey *et al.*[13]	– Detailed description of the carbonation, calcination, sintering and sorbent performance under repeated cycle operation. – Summary of sorbent deactivation and reactivation measures. – Review of the calcium looping process applications. – A brief summary of semi-empirical correlations allowing estimation of the sorbent conversion.
Dean *et al.*[14]	– Summary of the calcium looping cycle fundamentals, sorbent deactivation and sorbent performance. – Review of the calcium looping thermodynamic and economic performance, as well as its applicability in the cement industry and hydrogen production. – A brief reference to the sorbent activity decay. – Review of the pilot plant trials for calcium looping before 2011.
Anthony[22]	– Review of sorbents performance improvements and reactivation strategies for natural and synthetic sorbents. – Brief outline of calcium looping process applicability and experimental facilities.
Liu *et al.*[23]	– Review of sorbent performance enhancements. – Review of synthesis methods for sintering-resistant sorbents.
Kierzkowska *et al.*[24]	– Summary of the carbonation reaction fundamentals. – Review of recent developments in synthesis of CaO-based sorbents.
Romano *et al.*[25]	– Outline of CaL process simulations and notes on further modelling activities.
Boot-Handford *et al.*[15]	– Summary of the process performance, sorbent deactivation and regeneration. – A brief update on CaL pilot-plant trials.

increase in the development of process models. The CaL process has been widely investigated using thermodynamic and mathematical modelling, computational fluid dynamic (CFD) modelling and process modelling and integration into power generation systems. Analysis of mature technologies using process simulation and modelling tools has revealed that this approach allows a cost-effective investigation of concept feasibility and applicability, as well as development and optimisation of different process configurations. In addition, a whole process approach allows determination of the impact that integration of the CO_2 capture plant imposes on the power plant. However, a reliable assessment of the process performance requires the process models to be validated with experimental data.

Although pilot plant facilities and modelling approaches have been reviewed (Table 1), some critical aspects have not been analysed in detail. Moreover, the field of CaL has been developing rapidly due to the introduction of new test facilities, new correlations for process modelling, and CaL process configurations for improved performance. The aim of this paper is to review the available test facilities worldwide, the modelling approaches, and the integration studies that will guide the future development of the CaL process. The focus of the first part of this review will be on recent developments in CaL technology. The second part reviews the available approaches for prediction of the CaL process performance. Finally, the third part identifies and evaluates the approaches for CaL integration into power generation systems.

2 Calcium looping process for CO_2 capture

2.1 Process description

Use of calcium-based sorbents for CO_2 absorption was patented in 1933 and the research was primarily directed towards sorption-enhanced hydrogen production.[20,26] A configuration proposed by Hirama *et al.*[27] and Shimizu *et al.*,[28] which includes two interconnected CFBs operating under atmospheric pressure (Fig. 1), is the one most commonly referred to in the literature as appropriate for power generation systems. Application of such a configuration for the CaL process with appropriate design of the heat exchanger network (HEN) has been shown to have a thermal efficiency comparable to current combustion systems.[29]

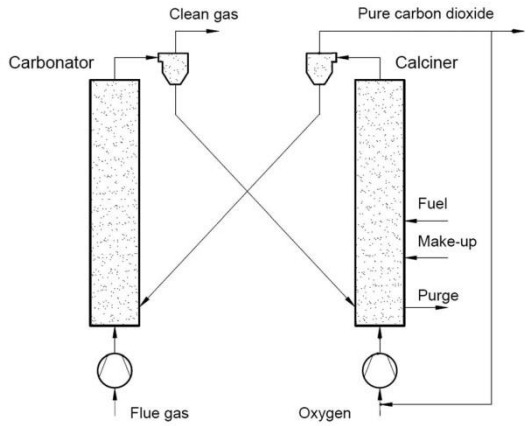

Fig. 1 Conceptual scheme of CaL process system for CO_2 capture.

In the CaL process the flue gas from fuel combustion in air, which usually contains between 4%$_{vol}$ and 15%$_{vol}$ CO_2 depending on the primary fuel used, is fed to the carbonator. In contrast to amine scrubbing, there is no requirement for flue gas precooling as absorption in the CaL process is conducted at a high temperature to assure high capture efficiency. Under such conditions, CO_2 reacts chemically with CaO through an exothermic solid-gas reaction.

CO_2 is removed from the flue gas in the form of solid $CaCO_3$ at a reasonably fast rate.[26,28,30,31] CO_2 removal efficiency decreases rapidly as the temperature increases and becomes zero at approximately 775 °C as the equilibrium partial pressure of CO_2 exceeds the partial pressure in flue gas containing 15%$_{vol}$ CO_2 above this temperature.[32] The optimal operating temperature of the carbonator ranges between 580 °C and 700 °C due to the trade-off between the reaction kinetics and the equilibrium driving forces.[33,34]

$CaCO_3$ is transferred to another fluidised-bed reactor, the so-called calciner, in which it is calcined and CO_2 is reclaimed.[26] Calcination is conducted at 850–950 °C to achieve rapid reaction without excessive sintering.[14,28,35] It needs to be highlighted that at 900 °C, the equilibrium CO_2 partial pressure is about 1 bar,[36] and hence a pure CO_2 stream can be theoretically achieved in the calciner operated at that temperature under atmospheric conditions. However, the higher calciner temperature is favourable and required in terms of reaction kinetics. On the other hand, a practical conversion rate can be achieved at temperatures below 900 °C if the gas atmosphere in calciner is diluted by steam, which can be easily separated by condensation from the CO_2 steam. Furthermore, since high-grade heat is available in the CaL process, which can be recovered to produce additional amounts of steam for the steam cycle, the higher carbonator and calciner temperatures are preferred in order to allow reaching desired steam parameters. Therefore, selection of the CaL operating temperatures can be seen as a design trilemma, in which the CO_2 capture level is restricted and process performance must be maximised, while the unit size minimised. As calcination is endothermic, additional fuel in the calciner is required. To produce a CO_2 stream of high purity, which can be directly transported for safe storage or use after the purification and compression stages, combustion takes place in an O_2/CO_2 environment.[28,37,38] Although this configuration has been demonstrated at the pilot-plant scale,[14] other configurations that use indirect heat sources may become available in future.[30,39] It is estimated that the calcination step consumes 35% to 50% of the overall heat input to the system.[40]

If it were not for sorbent sintering, attrition, and sulphation, the cyclic operation of carbonation and calcination would be performed without sorbent purge and make-up, and these processes would only be limited by thermodynamic equilibrium and the chemical reaction and diffusion rates. Manovic and Anthony[41] noted that the carbonator and the calciner should be operated within a particular temperature range in which the

minimum temperature is determined by the desired reaction rate while the maximum temperature is related to the desired CO_2 concentration. In general, the lower temperature limit is related to the desired partial pressure of CO_2, hence purity of the CO_2 stream, while the upper temperature is limited by the sorbent structural properties. Unfortunately, the conversion of the sorbent decreases with the number of carbonation and calcination cycles due to changes in particle structure,[42] especially due to enhanced sintering of CaO, which has been shown to be enhanced above 900 °C.[43] Regardless of having a negative impact on the sorbent performance, sulphur oxides would be efficiently captured due to the high Ca/S ratio in the calciner and the carbonator,[44] through indirect (1) and direct sulphation (2).[45]

$$CaO + SO_2 + 0.5O_2 \rightarrow CaSO_4 \quad (1)$$

$$CaCO_3 + SO_2 + 0.5O_2 \rightarrow CaSO_4 + CO_2 \quad (2)$$

2.2 Calcium looping as a novel CO_2 capture technology

CO_2 capture technologies commonly referred to in literature are: absorption-based separation using physical or chemical solvents; adsorption-based separation using solid sorbents; membrane separation; cryogenic separation techniques and oxy-fuel combustion; and biological systems using microbes or algae (Fig. 2).[46–49] However, due to the relatively low concentration of CO_2 in the flue gas (4–15%$_{vol}$), large volumes of flue gas need to be processed, and such technologies still have not been commercially deployed in the power industry due to a considerable drop in the net thermal efficiency of the integrated system, and also due to high equipment capital cost. As a result, the cost of electricity in the CFPPs and natural gas-fired combined cycle power plants retrofitted with CCS is expected to increase by 60–125% and 30–55%, respectively.[50–52] Although this is the key reason why development of new technologies needs to be pursued, there are also other issues which must be considered, such as environmental impact and operational safety.

Application of amines for CO_2 separation, such as monoethanolamine (MEA), has been first proposed for fuel gas or combustion gas by Bottoms in 1930.[54] This technology has been widely applied for sour gas sweetening and is used to remove CO_2 from natural gas or other industrial gases for ammonia and methanol production, as well as to produce CO_2 for enhanced oil recovery.[53,55,56] Using MEA or different amine-based solvents, such as piperazine (PZ) or methyldiethanolamine (MDEA), is currently the most likely technology to be applied to reduce the environmental impact of fossil fuel power plants.[13,15,57] Although several amine scrubbing processes have been operated in other industries,[58,59] the first full-scale demonstration plant using

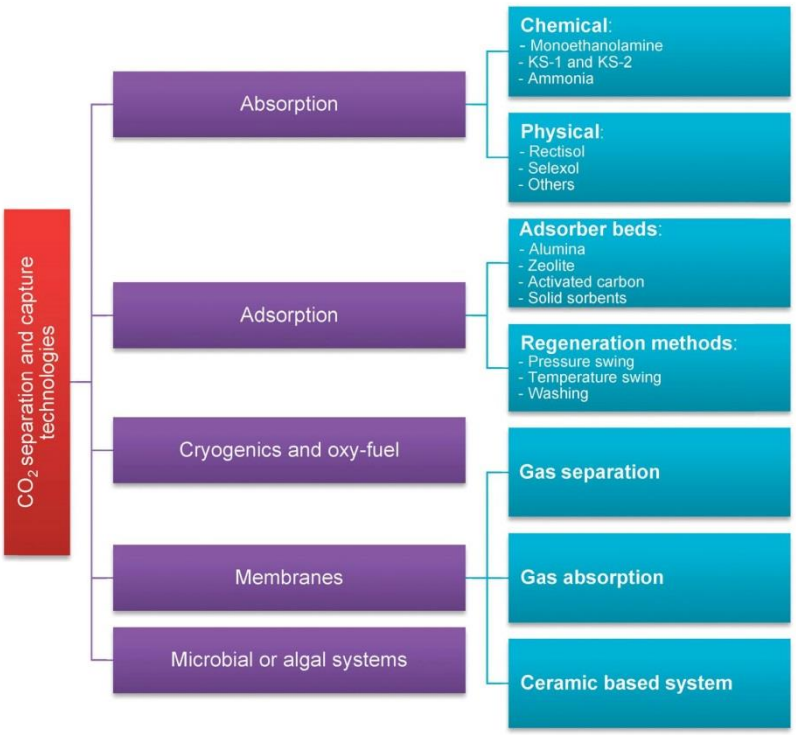

Fig. 2 Classification of the CO_2 separation and capture technologies (adapted with permission from Rao and Rubin.[53] Copyright 2015 American Chemical Society).

amine scrubbing technology from the power sector, which is Cansolv's integrated SO_2/CO_2 process fitted to Unit 3 of the Boundary Dam CFPP, and was only commissioned in 2014.[10] The following problems need to be resolved before amine scrubbing can be widely deployed in power generation:

- Solvent regeneration uses steam from the power plant steam cycle creating a projected efficiency penalty of 9.5–12.5% points when reference MEA solvent is employed.[16–18,60] Yet, recent studies identify that the projected efficiency penalty can be reduced to 8.5% points using amine-blends, such as MDEA/PZ,[61] or to 7.0% points using PZ solvent.[61,62]
- Amine solvents are prone to degradation due to reaction with O_2 and O_2-containing components in the flue gas, such as NO_x and SO_x, resulting in heat stable salts.[63]
- Solvent concentration is limited to 30% (MEA) to prevent plant equipment corrosion.[64]
- Inappropriate handling and disposal of degradation products may cause environmental and health issues.[14,64–66]

Using ammonia for CO_2 capture, which imposes a lower efficiency penalty, is proposed as an alternative to amine scrubbing.[67] Development of ammonia-based CO_2 capture processes reached the pilot-plant stage in a relatively short period of time. However, some projects were cancelled due to cost and schedule overruns.[68–70] The main advantages of ammonia over amine-based solvents are:

- It is commercially available at a lower price than MEA.
- It has higher CO_2 absorption capacity compared to an MEA solution of the same concentration.
- There is lower heat of reaction resulting in lower heat requirement for solvent regeneration. This is reflected in a projected efficiency penalty of 4.1 to 7% points[71–73] although this has not been substantiated experimentally.[59]
- There is no solvent degradation on contact with the flue gas components.
- The stripper can be operated at elevated pressure, hence temperature, leading to reduced compression work.
- Ammonia is not as corrosive as amines and can be used as a multicomponent (CO_2, SO_2, NO_x, HCl and HF) capture solvent.[74–76]

Unfortunately, although substitution of amines with ammonia may bring some reduction in the energy intensity of the capture process, it does not improve the process safety as ammonia is both a toxic substance and highly flammable. Moreover, a major drawback of ammonia is its high volatility leading to ammonia slip during the CO_2 absorption process.[63] To comply with environmental requirements, the ammonia slip can be controlled either by adding an additional ammonia water wash or by operating the absorber below 20 °C. Unfortunately, in both cases the resulting capital and operating costs increase and thus, as was expected,[59,74,77] only a slight reduction of the average cost of CO_2 avoided from \$61/t-CO_2 to \$53/t-CO_2 was reported.[78]

Another technology that is relatively close to market commercialisation is oxy-fuel combustion, in which the fuel is combusted in an O_2-rich atmosphere. Although there are neither commercial nor full-scale demonstration plants operating at the moment,[59] some projects are in the planning stage.[97] However, a recent suspension of funding at an advanced stage of the FutureGen project[79,80] shows that completion of such projects is highly dependent upon financial incentives and political climate. The primary advantage of oxy-combustion technology is that it produces a nearly pure CO_2 stream after the flue gas has been through SO_x and NO_x emission control systems and ash separation units. This CO_2 then only needs to be conditioned and dehydrated prior to compression and transport. The main challenges of this technology, which are likely to slow its wide implementation, are:

- The net efficiency of the oxy-fuel power plant is reduced by 8–12% points[15] because of the cryogenic air separation unit (ASU) for O_2 production.[13]
- High safety standards are required to prevent oxygen leakage.[13]
- The combustion temperature must be controlled to avoid hot spots in the combustion zone that would enhance NO_x production in the boiler.[15]
- Air leakage into the boiler must be minimised to maintain desired purity of the CO_2 stream and to minimise the power requirement of the CO_2 compression and purification unit.[81,82]

If the direct combustion of fuel is considered as a means for satisfying the heat requirement in the calciner, the CaL process can be seen as a merging of the post-combustion CO_2 capture and the oxy-combustion technologies, where only some portion of fuel is burned in an O_2-rich environment. Currently, CaL concepts are being tested experimentally at bench- and pilot-scale plants worldwide. The main advantages of the CaL system over the solvent-based CO_2 capture technologies are:

- Heat can be recovered and used to generate an additional amount of high-pressure steam through the exothermic carbonation of lime at 650–700 °C and utilisation of heat available in the process streams.[83]
- The predicted efficiency penalty is 7% to 8% points,[84] with the CO_2 capture stage accounting for 2% to 3%, which is mainly due to the oxygen requirement.[39] This is comparable to the efficiency penalty of a flue gas desulphurisation unit (FGD) (0.5–4%).[85]
- The technology uses fluidised bed reactors, which have been commercially proven for coal combustion systems.
- Compared to an oxy-fuel power plant, 30–50% less O_2 is required for oxy-combustion of fuel in the calciner, leading to smaller ASU size.[28,39]
- Natural limestone or dolomite, the source for CaO, is globally available and inexpensive[31] and CaO is characterised by high CO_2 absorption capacity.
- The average cost of CO_2 avoided is estimated to be \$29–50/t-CO_2 which is more than 50% less than for amine scrubbing.[78,86–89]
- Compared to solvents, $CaCO_3$ and CaO are much less hazardous to the operators' health and the environment.[14]

Reduction in the sorbent CO_2 carrying activity on cycling operation as a result of sintering, attrition and sulphation appears to be the major challenge of this technology. Although this results in a considerable amount of spent sorbent to be replaced, some part of the sorbent can be reused for cement production, increasing the profitability of both the power and cement industries.[14]

3 Review of calcium looping bench- and pilot-scale testing

Insight into system behaviour under various operating conditions is required to optimise process parameters and to assess feasibility, before commercial-scale installations are designed and built. Although the CaL process has only been considered for CO_2 capture from fossil-fuel power systems since 1999, a number of test facilities have already been built (Table 2), with rapid progress after 2009. The review by Dean *et al.*[14] devoted to the CaL process has described bench-scale tests using the 10 kW_{th} unit at IFK (University of Stuggart), 30 kW_{th} unit at the INCAR-CSIC, 75 kW_{th} unit at CANMET Energy and 120 kW_{th} unit at the Ohio State University. However, this review mostly focused on the attrition and material performance during the bench-scale tests. Moreover, the developments in the pilot-plant testing by 2010 and 2013 have been outlined by Anthony[22] and Boot-Handford *et al.*,[15] respectively. This section focuses on the progress in CaL process testing at a bench- and pilot-scale from 2010, with the aim of gathering the valuable design and operational data for development and validation of process models.

3.1 Industrial Technology Research Institute

3.1.1 Experimental facility description

3.1.1.1 Bench-scale unit. The Industrial Technology Research Institute (ITRI) in Taiwan has developed a 1 kW_{th} bench-scale unit, which can be operated in either batch or continuous mode. The unit comprises a bubbling fluidised bed (BFB) carbonator (gas velocity of 0.2–0.4 m s^{-1}), with a gas distributor located at the entrance, and a moving bed (MB) calciner. The solids are transported between the carbonator and the calciner through a 2.5-cm solid circulation pipe of 0.5 m length.[90]

The unit was modified by substituting the MB calciner with an air-fired rotary kiln calciner (RK) (Fig. 3). This increased the capacity to 3 kW_{th}. The calciner was designed to have a length-to-diameter ratio of 18.5 and an inclination angle of 5°, based on operating experience from the cement industry. Such design corresponds to a residence time of approximately 30 min at a speed of 1 rpm. Furthermore, liquefied petroleum gas is directly fired in the calciner using the 58 kW_{th} burner. The gas enters the BFB carbonator through the perforated plate distributor composed of 96 holes of 1.5 mm in diameter. Although the carbonation reaction is exothermic, the carbonator was heated using an external heating system to balance the heat losses to the environment.[91]

3.1.1.2 Pilot-scale facility. Design of the 1.9 MW_{th} pilot plant, which removes a tonne of CO_2 per hour from the Hualien cement plant flue gas containing 20–25% of CO_2,[92] was based on experience with the 3 kW_{th} unit. The perforated plate gas distributor was selected due to higher attainable velocities, based on cold model tests. The design consists of a double-layered perforated plate with 6 mm holes and an open-area ratio of 1.56%. As a means of temperature control thirty-six 2 m water-cooled double steel jackets were suspended at the top of the carbonator. The system is designed to operate with an

Table 2 Review of design and operating conditions of bench- and pilot-scale calcium looping facilities

		Carbonator				Calciner						
Research institute	Size (kW_{th})	Type[a]	Diameter (m)	Height (m)	Temperature (°C)	Type[a]	Diameter (m)	Height (m)	Temperature (°C)	Inlet CO_2 content ($\%_{vol}$)	Max. CO_2 capture level (%)	CO_2 purity ($\%_{vol}$)
Industrial Technology Research Institute	1	BFB	0.1	2.5	600–700	MB	0.05	0.9	800–900	12.5	99	N/A
	3	BFB	0.1	2.5	600–700	RK	0.27	5	500–1000	12.5	99	N/A
	1900	BFB	3.3	4.2	650	RK	0.9	5	500–1000	12.1–14.5	N/A	N/A
Consejo Superior de Investigaciones Cientificas	30	CFB	0.1	6.5	568–722	CFB	0.1	6	800–1000	15–16	90	27
	1700	CFB	0.65	15	600–715	CFB	0.75	15	820–950	12.5	90	85
Darmstadt University of Technology	1000	CFB	0.59	8.66	650–670	CFB	0.4	11.35	<1000	12–12.6	92	N/A
IFK at University of Stuttgart	10	BFB	0.114	3.5	630–700	CFB	0.071	12.4	850–900	15	97	20–55
	200	CFB	0.023	10	650	CFB	0.021	10	875–930	15	N/A	N/A
	200	CFB	0.033	6	600–680	CFB	0.021	10	875–930	15–16	93	N/A
Ohio State University	120	EB	N/A	N/A	450–650	RK	N/A	N/A	850–1300	3–25	>90	N/A
Vienna University of Technology	100	BFB	0.28[b]	2	650	CFB	0.08[b]	5	850	N/A	N/A	N/A
CANMET Energy	75	BFB/MB	0.1	2–5	580–720	CFB	0.1	4.5–5	850–950	8	97	N/A
Cranfield University	25	EB	0.1	4.3	600–650	BFB	0.165	1.2	900–950	15	80	N/A
Tsinghua University	10	BFB	0.149	1	630	BFB	0.117	1	850	15	95	22.5

[a] BFB – bubbling fluidized bed; CFB – circulating fluidised bed; MB – moving bed; EB – entrained bed; RK – rotary kiln. [b] Equivalent diameter based on cross-section area.

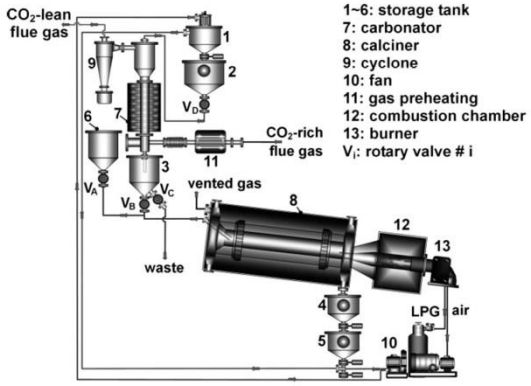

Fig. 3 3 kW_{th} bench-scale unit at ITRI (reprinted with permission from Chang *et al.*[91] Copyright 2015 Wiley).

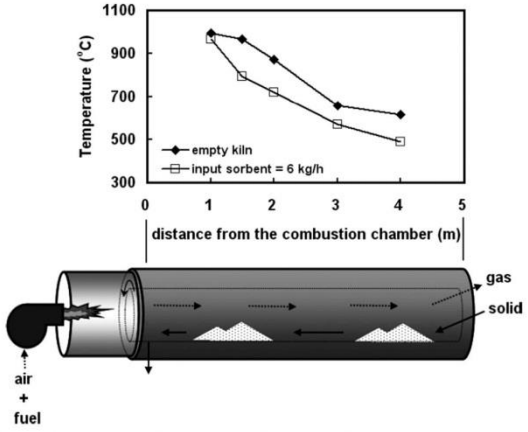

Fig. 4 Temperature distribution in the rotary kiln calciner in the first test (reprinted with permission from Chang *et al.*[91] Copyright 2015 Wiley).

average conversion of 20–40% and CO_2 capture levels of 80–95%. Heat for calcination is provided through direct oxy-combustion of diesel in the RK calciner which requires flue gas recirculation for temperature control. A key benefit of this configuration is more uniform temperature distribution in the calciner and thus, increased usable length for calcination.

3.1.2 Test campaign using 1 kW_{th} bench-scale unit. Tests were performed to assess CO_2 capture efficiency using a fluidising medium in the carbonator composed of 85%$_{vol}$ air and 15%$_{vol}$ CO_2. Prior to performing the experiments, the industrial grade limestone was calcined at a temperature of 850 °C.[90]

During 57 h of continuous operation 0.1 kg h^{-1} of fresh limestone was supplied to the calciner. The experiment revealed that the CO_2 capture level in the carbonator was maintained at above 99% over the entire time. Although preliminary results indicated the practicability of such a configuration, the MB carbonator was difficult to operate.[91]

3.1.3 Test campaign using 3 kW_{th} bench-scale unit. As in the previous case, the flue gas entering the carbonator contained approximately 15%$_{vol}$ CO_2, representative of values found in CFPPs. The flue gas was first preheated to 230 °C and then fed from the feed tank to the carbonator at a controlled rate of 47 dm^3 min^{-1}. To account for the sorbent deactivation, fresh limestone was fed to the calciner, while some of the solids circulating in the system, which comprises both inactive and active sorbent, was purged from the system.

The first test performed using the modified 3 kW_{th} unit was a batch test to evaluate operation of the RK calciner. It demonstrated that if the calciner is fed with fresh limestone at the rate of 6 kg h^{-1}, the useable length for the calcination reaction is approximately 1.5 m, corresponding to a sorbent residence time of 9 minutes. This arises because a temperature of 1000 °C was observed 1 m from the combustion chamber and thus excessive sintering would occur in this region (Fig. 4). On the other hand, a temperature of 721 °C was observed 2 m from the combustion chamber causing operating conditions downstream of the calciner to be unsuitable for the endothermic calcination reaction. Nevertheless, the calcination efficiency was found to be higher than 96%, while the carbonation conversion was 63.7%, proving low sorbent sintering rates.[91]

The 3 kW_{th} pilot plant was then used to run a 100 h campaign, the main objective of which was to keep the CO_2 capture level above 85%. This campaign showed that selection of the appropriate fresh sorbent make-up rate and spent sorbent purge rate is not only critical for reaching the desired CO_2 capture level, but also for ensuring stable and efficient operation of the system; if the make-up rate was lower than the purge rate, the total solid inventory in the system was reduced and excessive degradation of the sorbent activity was observed. On the other hand, increasing the solid inventory through an increased make-up rate improved the CO_2 capture level to above 99%. However, this would increase the operating cost of the process as it would require more heat input to the calciner. It needs to be highlighted that such a high level of inventory in the calciner had not been expected at the design stage, and thus, its efficiency dropped to 39% because insufficient heat was supplied through liquid petroleum gas combustion to sustain the endothermic calcination reaction.

When the inventory in the carbonator, which was operated at approximately 650 °C, fluctuated around the desired value the CO_2 capture level varied between 80% and 100%. The average residence time of solids in the carbonator was 2 h, with an average conversion of solids in the carbonator of 30% and a calcination efficiency of 75%. This campaign also revealed that particle attrition is an important phenomenon in the CaL system as the mean particle size decreased from 248 μm to 188 μm over this period.[91]

3.1.4 Data for process modelling. An unconventional process configuration developed at the ITRI, which includes the RK calciner, is beneficial in investigating integration opportunities between the power and cement industries. Since the equipment sizes and the key operating conditions have been disclosed,[90,91] the data available should be sufficient to, at least, verify the model behaviour in terms of solids inventory or operating temperatures

under varying operating conditions. Moreover, a simple verification could be performed for the carbonator and calciner performance. It will be of benefit to benchmark the model with the performance of the 1.9 MW_{th} pilot plant, provided that detailed experimental data become available.

3.2 Consejo Superior de Investigaciones Científicas

3.2.1 Experimental facility description

3.2.1.1 Bench-scale unit. The Instituto Nacional del Carbón – Consejo Superior de Investigaciones Científicas (INCAR-CSIC) has developed a 30 kW_{th} unit which consists of two interconnected CFB reactors. The carbonator is 6 m high and 0.1 m in internal diameter. It is fluidised using a synthetic flue gas containing 3–25%$_{vol}$ of CO_2 and is operated at 568–722 °C.[93] The heating system in the carbonator is only used during system start-up. Coal is combusted in 2–6% excess air to maintain the desired temperature in the calciner.[93] The calciner is 6.5 m high and the same internal diameter and is operated at 800–900 °C. Each reactor is equipped with a high-efficiency cyclone, from which the solids are directed through a vertical standpipe to the BFB loop seal.[94]

3.2.1.2 Pilot-scale facility. By combining the experience gained through running the 30 kW_{th} unit and the industrial experience for large-scale CFB combustors, INCAR-CSIC in agreement with ENDESA, Foster Wheeler and HUNOSA, with substantial R&D support from University of Stuttgart (IFK), Lappeenranta University, Imperial College and the University of Ottawa and CanmetENERGY, developed a 1.7 MW_{th} pilot plant designed to process approximately 1% of the flue gas produced in the 50 MW_{el} La Pereda CFPP in Asturias, Spain (Table 4). This project, called CaOling, was part-funded by the European Union 7th Framework Programme. The pilot plant comprises two interconnected CFB reactors 15 m in height with an internal diameter of 0.75 m in the calciner and 0.65 m in the carbonator (Fig. 5) operating with gas velocities of 3–5 m s^{-1} which are similar to those encountered in industrial CFBs.[95]

The typical operating temperatures for the carbonator and calciner are 600–715 °C and 820–950 °C, respectively. The temperature in the carbonator can be controlled through removable bayonet tubes. The calciner is directly fired with coal, either in an oxy-combustion or air-combustion environment. Fresh limestone is continuously fed to the calciner to maintain the desired average conversion of sorbent of 0.1–0.7 (Table 3). In both CFB reactors the solids leaving the risers are separated from the gas stream in the high-efficiency cyclones, and then directed to the double BFB loop seals by gravity. This design allows control of the solid looping rates between, and thus the solid inventories in, the CFB reactors.[96]

3.2.2 Test campaign using 30 kW_{th} bench-scale unit. The preliminary experiments conducted by Alonso *et al.*[94] revealed operating issues with the unit. A main concern was insufficiently high separation efficiency of the cyclones (92–97%) that led to loss of solids inventory. This resulted in unstable operation of the system as the solid looping rates and the solids inventory could only be kept constant for a short time. Nevertheless, this study showed that the carbonator was operated in nearly isothermal conditions (±20 °C) and that the actual CO_2 capture levels were close to equilibrium values at a particular carbonator temperature, provided that the amount of solid bed inventory and the solid looping rate were satisfactory.

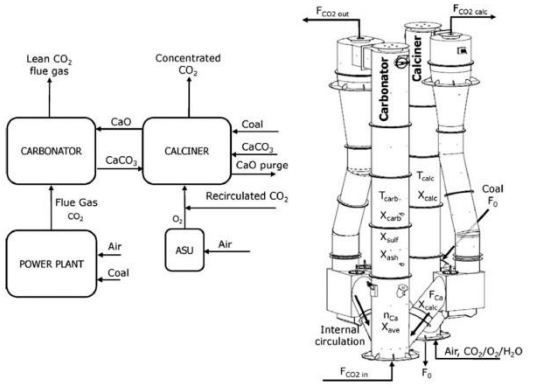

Fig. 5 Design of the 1.7 MW_{th} pilot plant at INCAR-CSIC (adapted with permission from Arias *et al.*[96] Copyright 2015 Elsevier).

On extension of the risers' heights and reconstruction of the high-efficiency cyclones, the system stability was improved. The modified system operated with CO_2 capture levels of 70–90%, which were close to the equilibrium value at 650 °C, depending on the gas velocity (2.0–2.1 m s^{-1}) and the solids circulation rates (0.8–2.3 kg m^{-2} s^{-1}). However, for the highly cycled particles, which can attain an average conversion close to the residual conversion of 0.07–0.12, the CO_2 capture level dropped to 65–75% for a solids circulation rate of 1.0–1.8 kg m^{-2} s^{-1}.[94]

In tests carried out by Rodríguez *et al.*,[93] the 30 kW_{th} unit was used to treat flue gas containing 20%$_{vol}$ CO_2. Initially 20 kg of limestone was loaded into the system that was operated at 800–850 °C for the calciner and 630–700 °C for the carbonator, with gas velocities of 3 m s^{-1}. The analysis revealed that the purity of the CO_2 stream released from the calciner was approximately 27%$_{vol}$ and the concentration of CO_2 in the clean gas was approximately 7%$_{vol}$. This corresponded to an actual CO_2 capture level of approximately 70%, which was lower than the equilibrium CO_2 capture level within this temperature range. It was found that under realistic operating conditions an actual CO_2 capture level of 70–90% was achievable for bed inventories of 400 kg m^{-2} for solid looping rates of 0.5–2.2 kg m^{-2} s^{-1}.

3.2.3 Test campaign using 1.7 MW_{th} pilot plant. Arias *et al.*[96] reports that the 1.7 MW_{th} pilot plant was operated for more than 1800 h, with 380 h in CO_2 capture mode with a CO_2 capture level of 40–95%. Stable operation under oxy-combustion in the calciner (excess O_2 of more than 5%$_{vol}$) has been maintained for 170 h.

Representative results from the experimental trials were reported for the first time by Sánchez-Biezma *et al.*[97] (Fig. 6). These results confirm the findings from previous studies that if the process is operated with proper solid inventory and sorbent activity, the actual CO_2 capture in the carbonator is close to the equilibrium value at given temperature (above 90% at 660 °C). Moreover, a SO_2 capture level of more than 95% was achieved.

Table 3 Operating conditions of the 1.7 MW_{th} pilot plant at INCAR-CSIC[a] [95,96]

Input from power plant	Value	Pilot plant operating conditions	Value
Flue gas flow rate (kg h^{-1})	680–2300	Maximum coal flow (kg h^{-1})	325
CO_2 concentration ($\%_{vol}$)	12.6	Maximum fresh sorbent flow (kg h^{-1})	300
O_2 concentration ($\%_{vol}$)	5.5	O_2 flow to calciner (kg h^{-1})	300–600
H_2O concentration ($\%_{vol}$)	7.0	CO_2 flow to calciner (kg h^{-1})	700–2250
SO_2 concentration ($\%_{vol}$)	0.07	Air flow to calciner (kg h^{-1})	600–2500
N_2 concentration* ($\%_{vol}$)	74.83	Inventory in carbonator (kg m^{-2})	100–1000

[a] Nitrogen concentration calculated to balance the remaining constituents.

Table 4 Operating conditions of the 75 kW_{th} CanmetENERGY pilot plant

Parameter	Minimum	Maximum
CFB calciner		
Initial sorbent inventory (kg)	4.5	5.0
Sorbent make-up batch (kg)	0.3	0.5
Biomass consumption rate (kg h^{-1})	4.0	7.6
Coal consumption rate (kg h^{-1})	2.6	5.8
Air flow rate (air-firing mode) (kg h^{-1})	8.0	14.4
O_2 flow rate (oxy-firing mode) (kg h^{-1})	5.2	7.7
Moving or bubbling FB carbonator		
Air flow rate (slpm)	40	100
CO_2 flow rate (slpm)	7.5	19.0
CO_2 concentration at inlet ($\%_{vol}$)	15.0	16.5
Air flow for solid conveying (slpm)	35	55

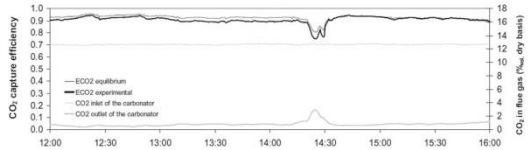

Fig. 6 Representative steady state results captured during testing of the 1.7 MW_{th} pilot plant at INCAR-CSIC (reprinted with permission from Sánchez-Biezma *et al.*[97] Copyright 2015 Elsevier).

As no fresh limestone was added to the system, the conversion of the CaO to $CaCO_3$ decreased towards the residual value of 0.1. Also, there were several issues with maintaining proper solid inventories when the oxy-firing mode was tested. Although CO_2 purity in the gas leaving the calciner reached 85% when the calciner temperature was 950 °C, low solid inventory and sorbent activity caused the CO_2 capture level to drop below the equilibrium level, to around 75%. Nevertheless, the authors claim that high CO_2 capture levels can be achieved even if highly deactivated sorbent is used with high sulphate conversions, provided the system is operated with the proper solid inventory.

Arias *et al.*[96] reported and thoroughly investigated the steady state operation of the 1.7 MW_{th} pilot plant at INCAR-CSIC. In the initial phase of the experimental trials, a CO_2 capture level of less than 40% was reached due to the high content of non-calcined limestone in the solid inventory because the calciner was operated below 920 °C. Moreover, the conversion dropped to 0.067 after more than 5 h of continuous operation without fresh limestone make-up. The same conclusion was drawn as in the study by Sánchez-Biezma *et al.*[97] that a CO_2 capture level of more than 80% can be reached, even when the sorbent has reached its residual conversion and there is a high SO_2 capture level (95%), provided enough solid inventory is available. These results confirm trends determined using the 30 kW_{th} unit and prove that the solid inventory and the sorbent conversion are the most relevant operating parameters in the carbonator reactor.

3.2.4 Data for process modelling. Information available in the literature, which includes detailed descriptions of the bench- and the pilot-scale facilities, provides essential input into model development. Most of the operating conditions, such as temperatures, solid looping rates, oxygen consumption rates and CO_2 contents in off-gases from the calciner and the carbonator have been disclosed. This allows for a local validation of model predictions. Moreover, global performance of the carbonator and the calciner can be validated.

Tests conducted using both facilities revealed that the carbonator operates at nearly isothermal conditions, which allows the assumption of isothermal conditions in modelling the FB reactors. Moreover, the actual CO_2 capture level was found to be close to that determined by equilibrium at a given temperature. Such assumption is, however, only valid for relatively active sorbent, as the experimental trials showed a reduction in CO_2 capture level for highly cycled particles.

3.3 Institute of Energy Systems and Technology at Darmstadt University of Technology

3.3.1 Experimental facility description. The 1 MW_{th} pilot plant erected and commissioned at Darmstadt University of Technology comprises two interconnected CFB reactors that are refractory lined to minimise heat loss (Fig. 7). The carbonator, which is 8.66 m high and 0.59 m in internal diameter, is equipped with internal cooling tubes to control the temperature. Moreover, in contrast to other pilot plants, fresh limestone is fed to the carbonator, where it is heated to 650 °C utilising the exothermal carbonation reaction. Such configuration is claimed to reduce fuel and O_2 consumption in the calciner.[98] In addition, synthetic flue gas, which can be heated up to 350 °C using auxiliary electric heaters, is used as a fluidising medium in the carbonator. O_2-enriched air preheated up to 450 °C is used to fluidise the calciner that is 11.35 m high and 0.4 m in internal diameter. To maintain the calcination reaction, the pilot plant is designed to combust either gaseous fuel, using a gas burner or a bed lance, or solid fuel, which is introduced by a gravimetric dosing system.

Unlike other pilot plants, the solids between the loop seals of the CFBs are transferred by screw conveyors. These can be equipped with heat transfer jackets, allowing for accurate control

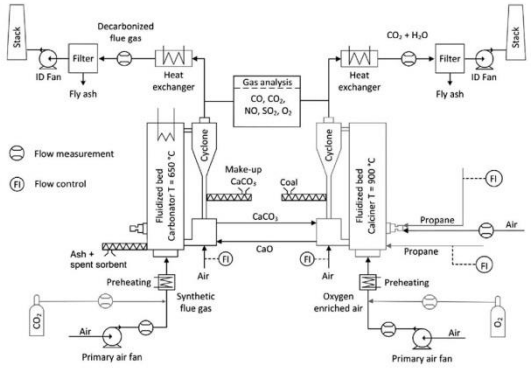

Fig. 7 Process flow diagram of the 1 MW_{th} pilot plant at Darmstadt University of Technology (reprinted with permission from Ströhle *et al.*[98] Copyright 2015 Elsevier).

of solids circulation rate and are capable of flexible operation under various loads. However, in a commercial-scale unit, large volumes of solids will be transferred between the reactors and the solid loads will vary due to changes in the power plant load, making the screw conveyors mechanically inefficient.[99] The flue gas and the CO_2 stream are subsequently cooled down in the heat exchangers, and then cleaned from fly ash in the fabric filters.

3.3.2 Test campaign. The first tests using the 1 MW_{th} pilot plant were conducted in July 2011. Since then, the facility has been operated for around 400 h to analyse CO_2 capture using the CaL process. In the first campaign, lasting 72 h, a continuous separation of CO_2 from the 1300 N m^3 h^{-1} synthetic gas comprising 10–12%$_{vol}$ CO_2 was analysed.[98] Throughout the campaign, the make-up flow was maintained at 70–150 kg h^{-1} and the solid looping rate between 1500 and 3000 kg h^{-1}. The study revealed that lower CO_2 capture levels are obtained if CaO, which has been calcined at 1000 °C before the test, is fed to the carbonator rather than fresh limestone. This is because a large fraction of older sorbent was present in the bed and caused a drop in the fraction of active sorbent. An increase in CO_2 capture level was observed when fresh limestone was fed to the carbonator. Despite the poor performance of the calciner cyclone and the low CO_2 concentration in the CO_2 stream caused by limited firing power in the calciner, the total CO_2 capture level was greater than 90%.

After increasing the power of the burners and the lances and improving the cyclone performance, a second test campaign using propane firing in the calciner was carried out. These changes led to a significant reduction in the make-up rate. Moreover, the fluidisation air was enriched with 50% O_2 to maintain a desirable gas velocity in the calciner and to ensure nearly complete combustion of propane. Again, the carbonator was operated at 660 °C and was fed with synthetic flue gas containing 12%$_{vol}$ CO_2. To maintain a desired average CO_2 capture level in the carbonator, the solid looping rate was kept at 2000 kg h^{-1}, which corresponded to an average Ca : C molar ratio of 11.6. The maximum CO_2 capture level in the carbonator was found to be 85%, increasing to 92% when oxy-combustion of propane in the calciner is considered.

In the third campaign, the calciner was fired with pulverised coal and the fluidisation air was enriched by 45–50% O_2. The temperature in the carbonator reached 670 °C. The same amount of synthetic flue gas was used as in the second campaign. To reach the same CO_2 capture level in the carbonator (85%), the solid looping ratio needed to be increased to approximately 2800 kg h^{-1} (Ca : C = 17.2). The CO_2 concentration in the clean gas was close to the equilibrium CO_2 concentration at that operating temperature. Therefore, the reaction was limited by chemical equilibrium leading to stable operating conditions. The CO_2 capture level dropped to approximately 60% when the temperature in the carbonator dropped to 610 °C.[98]

3.3.3 Data for process modelling. The description of the facility by Ströhle *et al.*[98] provides the information on equipment dimensions required for detailed process modelling. The data gathered from the three campaigns allow validation of the performance of a model overall and in respect of the carbonator CO_2 capture level. Some information on local parameters, such as fluidising air temperature, CO_2 flow rate at the inlet to the carbonator and the solid looping rates is available and would increase the quality of model validation. In addition, an operating range for some parameters, such as the fresh sorbent make-up rate and solid looping rate, was disclosed and would allow validation of a model at different operating points.

3.4 Institute of Combustion and Power Plant Technology at University of Stuttgart

3.4.1 Experimental facility description

3.4.1.1 10 kW_{th} bench-scale dual fluidised bed unit. The Institute of Combustion and Power Plant Technology (Institut für Feuerungs-und Kraftwerkstechnik, IFK) at the University of Stuttgart has developed a CaL bench-scale unit based on a 10 kW_{th} dual fluidised bed (DFB) that can be operated in continuous mode.[100] The practicability and stability of the DFB system was first analysed using a down-scaled cold model.[101,102]

In the 10 kW_{th} IFK unit, the CFB (gas velocity of 4–6 m s^{-1}) and the BFB (gas velocity less than 1.2 m s^{-1}) can each be operated either as the carbonator or calciner. A benefit of operating the BFB as the carbonator and the CFB as the calciner is ease in process control. The novel configuration of this DFB system results in control of the calcium circulation rate between the beds by varying the cone valve opening and the BFB absolute pressure. Due to heat losses to the environment, the CFB, the BFB and the solid circulation system are electrically heated.[103] The temperature in the calciner can be raised by direct natural gas combustion in O_2-enriched air (40%$_{vol}$ O_2), if the electric heating system capacity is insufficient.[100]

3.4.1.2 200 kW_{th} pilot-scale dual fluidised bed facility. To investigate the long-term performance of the process under real combustion conditions, a 200 kW_{th} pilot plant was built at the IFK. The pilot plant design includes a CFB calciner operating in a fast-fluidisation regime and a reconfigurable CFB carbonator that can operate either under a turbulent or fast-fluidised fluidisation

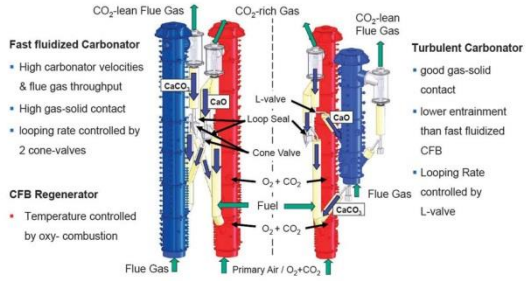

Fig. 8 Comparison of 200 kW_{th} DFB pilot plant configurations at IFK.[106]

regime (Fig. 8).[104,105] A design involving two symmetric CFBs, which operate in a fast-fluidised regime, required redesign of the solid circulation system and implementation of two cone valves for controlling the looping ratios in both CFBs independently.[105] Conversely, for the configuration with the carbonator operating in the turbulent regime, the solid circulation rate is controlled through the L-valve which is directly fed from the CFB calciner.[104]

The fast-fluidised CFB calciner, 10 m in height and 0.021 m in internal diameter, is equipped with a staged oxidant supply for oxy-combustion of solid fuel (coal, wood pellets, wood chips). Although the firing system is designed to handle up to 70%$_{vol}$ O_2 to meet the energy demand in the calciner, flue gas recirculation is implemented to achieve realistic operating conditions. In the turbulent fluidised bed carbonator (6 m in height and 0.033 m in internal diameter), the heat is removed using the FB heat exchanger. It is also designed to operate under lower fluidisation velocities and with lower residence time than the CFB carbonator.[104] The fast-fluidised CFB carbonator, 10 m high and 0.023 m in internal diameter,[102] is fluidised with the flue gas, and the heat released due to the exothermal reaction is removed *via* a water-cooled heat exchanger in the dense bed region and bayonet cooler in the lean bed region. The facility has a 400 kW_{th} gas burner to generate hot gas and heat up the system during start-up. To minimise the heat loss in the system, the reactors are lined with insulating concrete and refractory material resistant to abrasion.[105]

3.4.2 Test campaign using a 10 kW_{th} DFB unit. The tests were conducted using German limestone from Swabian Alb that was used to clean synthetic flue gas having 15%$_{vol}$ CO_2 to simulate CFPP conditions. It was relatively straightforward to achieve steady state operation with a minor make-up of fresh sorbent to account for attrition losses. When the carbonator was operated at 660 °C, the achievable CO_2 capture level exceeded 90%. The maximum level of 97% was observed in the periods when fresh sorbent was added to the carbonator, causing its temperature to drop to around 625 °C.

The effect of the carbonator operating temperature and the CO_2 capture level was then analysed and compared with the equilibrium data. The CO_2 capture level was reported to be close to that determined by chemical equilibrium at the given temperature, which was assured by maintaining a Ca : C ratio higher than 14.[103] A recent study by Varela *et al.*[107] identified that the CO_2 capture level of 90% is achievable at Ca : C ratio of 8, provided that steam is present in the carbonator and the calciner. Such behaviour is explained by likely enhancement of sorbent morphology in the presence of steam, favouring sorption and desorption of CO_2. Moreover, the increase of the CO_2 concentration in the calciner, which can be associated with CO_2 recycle to lower O_2 concentration in the fluidising gas, was found to significantly affect the reactor efficiency.

3.4.3 Test campaign using the 200 kW_{th} DFB facility. Dieter *et al.*[104] reported that more than 600 h of successful operation has been recorded and the facility was found to be hydrodynamically stable. The tests performed mainly aimed at reaching steady state conditions under variable temperature with synthetic flue gas containing 14%$_{vol}$ CO_2.

Although O_2 concentrations reached 50%$_{vol}$ during wood pellet combustion, no hot spots were observed and the temperature profile in the calciner was uniform (875–930 °C). This indicates the key benefit of staged oxidant supply. However, the desired temperature of 650 °C was observed only in the dense region of the turbulent FB carbonator, while the temperature was reduced in the upper region. Nevertheless, the CO_2 capture level was maintained above 90% indicating that most of the reaction takes place in the dense region. Fluctuations in the carbonator temperature (620–650 °C) have a minor effect on the carbonator efficiency. Furthermore, higher CO_2 capture levels are obtained if wet flue gas, such as from the desulphurisation unit, is fed to the carbonator. These results were found to closely follow the trend determined by the equilibrium calculations revealing good gas-solid contact in the carbonator (Fig. 9). This means that lower looping ratios would be required to reach the desired CO_2 capture level, leading to energy saving in the regenerator.[104]

3.4.4 Data for process modelling. The literature provides a detailed description of the equipment sizes and configurations, allowing for development of a model. Nevertheless, the limited information available on the equipment operating conditions and efficiencies and the lack of detailed stream data will restrict model validation, especially in terms of the conversion rates

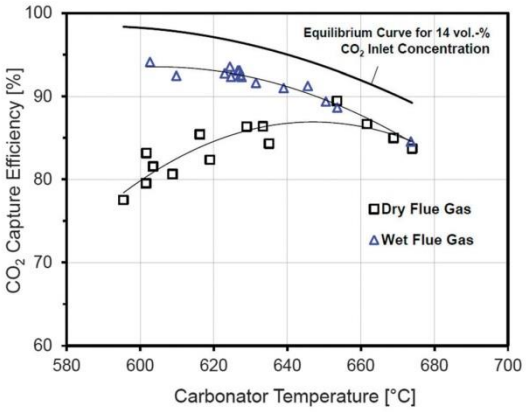

Fig. 9 Effect of the carbonator temperature on the CO_2 capture level data from the 200 kW_{th} DFB at IFK.[106]

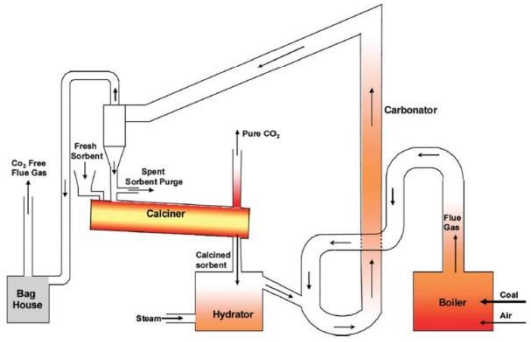

Fig. 10 Process flow diagram of the Ohio State University sub-pilot plant (reprinted with permission from Wang *et al.*[112] Copyright 2015 American Chemical Society).

and the solid looping rates. However, the results from both campaigns clearly indicate that the carbonator performance can be reasonably well represented using equilibrium models, provided an appropriate solid inventory, sorbent conversion and looping rate of Ca : C > 14 are assumed.

3.5 Ohio State University

3.5.1 Experimental facility description. The researchers at Ohio State University have pioneered the concept of simultaneous CO_2 and SO_2 capture using the Carbonation-Calcination Reaction process (CCR). The process was proposed as a merger of the Ohio State Carbonation Ash Reactivation (OSCAR) process[108–110] and the Calcium-based Reaction Separation for CO_2 (CaRS-CO_2) process,[111] two processes developed and patented by Ohio State University.

In the 120 kW_{th} sub-pilot plant (Fig. 10) the CaO or $Ca(OH)_2$ can be fed to the carbonator, which is the entrained bed (EB) reactor operated at 450–650 °C to allow for CO_2 and SO_2 capture. Sorbent regeneration is conducted in the electrically-heated RK calciner. Calcined sorbent is then hydrated using steam to improve the sorbent conversion over multiple cycles.[112] Some of the deactivated sorbent (2–10%) is purged and the fresh sorbent is fed directly to the calciner.

3.5.2 Test campaign. The CCR sub-pilot plant was used to purify flue gas produced in air-combustion of coal and natural gas in the stoker and containing 12.5%$_{vol}$ CO_2 and 1450 ppm$_v$ of SO_2. Prior to being fed to the carbonator the flue gas temperature was maintained at 650 °C using natural gas.

In the once-through test, Wang *et al.*[112] showed that the presence of fly ash in the carbonator does not affect the CO_2 and SO_2 capture levels. In addition, the amount of fly ash entering the carbonator needs to be considered when deciding on the purge fraction to maintain the proper amount of active sorbent in the system.

The study clearly indicated that application of $Ca(OH)_2$ with the mass median diameter (D_{50}) of 3 μm results in CO_2 capture levels between 40 and 100% for Ca : C ratios between 0.5 and 1.7. This performance was superior to traditional lime, as CO_2 capture levels of 9% were found for ground lime (D_{50} = 600 μm) and pulverised ground lime (D_{50} = 18 μm) at the same Ca : C ratio. Nevertheless, as pointed out by Dean *et al.*,[14] separation and fluidisation of such small particles from the gas stream in industrial-scale reactors would be extremely challenging and, therefore, the process feasibility and practicability is somewhat questionable.

3.5.3 Data for process modelling. Information on design characteristics of the CCR process available in the papers and patents is limited and does not reveal the equipment sizes. This would not allow for detailed model development. Nevertheless, simplified models, which consider only thermodynamic performance, could be developed.

The results of the test campaign are detailed enough to validate the global performance of a model. Unfortunately, no detailed information is provided on the local data, such as the solid looping rates or limestone make-up.

3.6 CANMET Energy Technology Centre

3.6.1 Experimental facility description. CanmetENERGY has developed a 75 kW_{th} pilot-scale DFB system which operates in semi-continuous mode to demonstrate the process feasibility. The system was first designed and analysed using process simulation by Hughes *et al.*[29] The pilot plant comprises a CFB calciner and a carbonator operated under either moving or bubbling bed conditions (Fig. 11).

Depending on the application the calciner is 4.5–5 m in height and 0.1 m in internal diameter and can be operated under air, O_2-enriched air or oxy-firing with flue gas recycle. The carbonator was divided into two stages to distinguish the combustion/sulphation and carbonation processes. Therefore, depending on the test performed it is 2–5 m in height and 0.1 m in internal diameter. Such configuration allows air or a mixture of air and superheated steam to fluidise both stages. To minimise the heat losses in the system, the reactors are lined with refractory and insulation materials. Moreover, each reactor is equipped with three 4.5–5 kW_{el} electric heaters that are used during start-up and sometimes to control the reactor temperature.[33,113] The CANMET Energy pilot plant has a novel

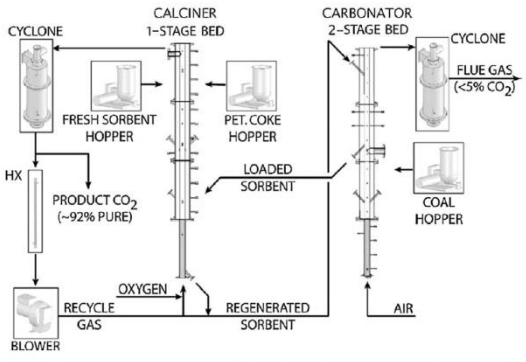

Fig. 11 Schematic of the 75 kW_{th} pilot plant developed at CANMET Energy (reprinted with permission from Hughes *et al.*[29] Copyright 2015 Elsevier).

solid transport system for sorbent looping that includes a 45° "T" that collects solids from the calciner-pierced distributor. The solids rate through the conveying line to the carbonator is controlled using a solenoid valve. The calcined sorbent enters the carbonator through the L-valve. Similarly, the 45° "T" line allows the carbonated sorbent to be directed to the calciner or to the second stage of the carbonator for SO_2 capture.

3.6.2 Test campaign using a 75 kW_{th} pilot plant. The 75 kW_{th} pilot plant has been operated under continuous mode for more than 50 hours (Table 4). During the tests, the carbonator was fed with a synthesised mixture of air and CO_2, to achieve CO_2 concentrations of 15–16%$_{vol}$. The fluidising air was preheated to 250 °C prior to being fed to the carbonator. The calciner was operated under three heating modes: electric heating, biomass combustion in air, and oxy-combustion of biomass and bituminous coal with flue gas recycle.

The tests performed by Lu *et al.*[33] confirmed that the CaL system can operate with a CO_2 capture level of 97% within the first several cycles. As the superficial gas velocity was increased, the CO_2 capture level decreased, which can be associated with lower residence time of gas in the carbonator. A considerable drop in the CO_2 capture level to approximately 72% was observed after 25 cycles. This confirms the impact of sorbent deactivation on process performance and implies the need for fresh sorbent make-up. The highest CO_2 capture level (98%) was reached within the temperature window of 580–600 °C for fresh sorbent and approximately 700 °C after 20 cycles. When the temperature dropped below 500 °C, the reaction rate slowed significantly. This was reflected in the off-gas CO_2 concentration of approximately 9–10%$_{vol}$ CO_2, hence in a drop of CO_2 capture level.

Finally, testing oxy-combustion of fuel in the calciner has proven this approach to be appropriate for providing heat for sorbent regeneration. There were no hot spots in the calciner, in spite of the high O_2 concentration in the primary gas of 40–50%$_{vol}$ balanced with the recycled flue gas. The maximum concentration of CO_2 was 85%$_{vol}$.

3.6.3 Data for process modelling. Information available in papers by Lu *et al.*[33] and Symonds *et al.*[113] include detailed descriptions of the process configuration and equipment dimensions which can be used to set up a model. Analysis of the CO_2 capture level under various operating conditions allows validation of the global performance of a model. Again, their study confirmed that the actual CO_2 capture levels could be close to the equilibrium values in practice. Their study also revealed that the carbonator temperature can be used as a means to maintain the desired CO_2 capture level, even with highly cycled sorbent. Although no information on the solid looping ratios and rates was provided, several operating limits were included in the paper by Lu *et al.*[33] that can form a basis for local validation of a model.

3.7 Cranfield University

3.7.1 Experimental facility description. A 25 kW_{th} bench-scale CaL rig developed at Cranfield University consists of an EB carbonator, 4.3 m high and 0.1 m in internal diameter, and a BFB calciner, 1.2 m high and 0.165 m in internal diameter.

Table 5 Optimal gas composition in 25 kW_{th} Cranfield University pilot plant[114]

Fluidising gas	Carbonator	Calciner
CO_2 volumetric flow rate (L min^{-1})	—	40
O_2 volumetric flow rate (L min^{-1})	—	16
Air volumetric flow rate (L min^{-1})	150	—
CH_4 volumetric flow rate (L min^{-1})	22.5	11

The desired operating temperature in the carbonator (600 °C) and the calciner (900–950 °C) is maintained using electric heating elements.[114]

The calciner is directly heated through oxy-combustion of natural gas. The resulting flue gas is used as the fluidising medium. The flue gas generated in the air-combustion of natural gas, which contains 8%$_{vol}$ CO_2, is used as the fluidising medium in the carbonator. The optimal operating gas input rates are presented in Table 5. Solid input to the calciner is achieved using a screw feeder with a maximum feeding rate of 1.6 kg h^{-1}. This proves the practical applicability of the screw conveyors for solid fuel and sorbent handling in the CaL units, as explained in Section 3.3.1. The solid looping rates are controlled *via* two fluidised loop seals, at the top and bottom of the calciner.[115] The unit has two cyclones at the top of the carbonator to ensure that the sorbent lost with the flue gas is kept to a minimum.[114]

3.7.2 Test campaign. A primary objective of the test campaign was maximisation of CO_2 capture level through modification of the process configuration and the operating conditions. CO_2 capture levels of 50% and 70% were reached with carbonator temperature windows of 650–700 °C and 600–650 °C, respectively. This improvement in efficiency at lower temperatures is attributed to its effects on chemical equilibrium, as reducing the temperature reduces the equilibrium CO_2 content and in turn increases the equilibrium CO_2 capture level.

Moreover, in batch runs the optimum CO_2 capture level, which was close to 90%, occurred for particle sizes between 125–250 μm. This was in agreement with results from another study carried out in the same group by Kavosh.[116] This behaviour was explained by an increase in the surface-to-volume ratio as the particle size was reduced. However, it was found that below 125 μm, the CO_2 capture level dropped below 50%. It appears that such small particles were Geldart's group C, and thus were difficult to fluidise leading to bed agglomeration.[117]

The maximum CO_2 capture level of 80% in the carbonator was reached after rig modifications resulting from the cold model, temperature and particle size distribution optimisation, and implementation of air shakers and heating elements to the loop seals to enhance solids transfer and temperature.[115]

3.7.3 Data for process modelling. The 25 kW_{th} unit has been described in detail in the analysed sources. As the description includes information on the equipment characteristics and operating conditions, it can be used for model development. The reliability of the CO_2 capture level prediction can be validated for various carbonator temperatures and particle size distributions. Unfortunately, the local level validation will be limited to flue gas and fuel oxy-firing in the calciner as no data on the solid circulating rates and solid inventory were disclosed.

3.8 Tsinghua University

3.8.1 Experimental facility description. The DFB system developed at Tsinghua University consists of two interconnected BFBs. The internal diameters of the carbonator and the calciner are 0.149 m and 0.117 m, respectively, and the height of each bed is 1 m. In this system, solids are transferred between the beds through the cyclones and the downcomers. In addition, solid injection nozzles are used to transport solids from the bed to the riser in each BFB. To compensate for the heat losses and to maintain the desired temperature in the carbonator and the calciner, each reactor was equipped with four 2.5 kW_{th} electric heaters. Additional electric heaters are used for heating the flue gas, the risers, the cyclones and the downcomers.[118]

3.8.2 Test campaign. In the test campaign, dolomite (D_{50} = 0.5 mm) was used as a source of natural sorbent to clean synthetic flue gas containing 12.1–14.5%$_{vol}$ CO_2. The solid looping rate was maintained at 30–36 kg h^{-1} which corresponded to an inventory height of 0.3 m in the two BFBs. When the desired temperatures in the carbonator (630 °C) and the calciner (850 °C) were achieved, the CO_2 fraction in the clean gas was 1.2%$_{vol}$, which corresponds to a CO_2 capture level of 89.2% in the carbonator. When the operating temperature of the carbonator was increased to 680 °C, the CO_2 fraction increased to 10%$_{vol}$ due to chemical equilibrium limitations.

In continuous CO_2 capture from synthetic flue gas, the calciner was operated at 810 °C, which led to maximum purity of 22.5%$_{vol}$ CO_2. On the other hand, the carbonator was operated at 640 °C reducing the CO_2 fraction in the clean gas to 0.7%$_{vol}$, which corresponds to a CO_2 capture level of 95%. Under such operating conditions the average conversion in the carbonator reached 70.4%. Due to incomplete calcination, the average conversion of particles leaving the carbonator was 16.2%. Finally, Fang *et al.*[118] have noted that after 7 h of continuous operation, the mean size of the particles was reduced to 0.16 mm and 0.42 mm in the calciner and the carbonator, respectively.

3.8.3 Data for process modelling. The bench-scale unit can serve as a basis for model development as its equipment sizes and operating conditions are or can be determined from other data provided by Fang *et al.*[118] A model can be validated at a global level as data are available for the carbonator CO_2 capture level under different operating conditions. Also, as the inlet gas flow rates to BFBs, the solid looping rates, and the CO_2 fraction in the gas streams from the carbonator and the calciner are available, local validation of the process streams can be conducted.

3.9 Vienna University of Technology

3.9.1 Experimental facility description. Researchers at the Vienna University of Technology have been testing a sorption-enhanced reforming (SER) process for biomass gasification in the 100 kW_{th} DFB gasifier facility (Fig. 12), another possible application of the CaL process.[119,120] Such process has a potential of improving the performance and reliability of the integrated-gasification combined cycle (IGCC) power plants. Other processes that utilise the sorption-enhanced reactions, such as a sorption-enhanced steam methane reforming (SE-SME), can yield high-purity H_2 (>95%$_{vol}$).[121,122] However, this process is more likely to be applied to meet increasing demands for H_2 in industrial processes, such as ammonia synthesis and fossil fuels processing,[123] rather than for large-scale power generation.

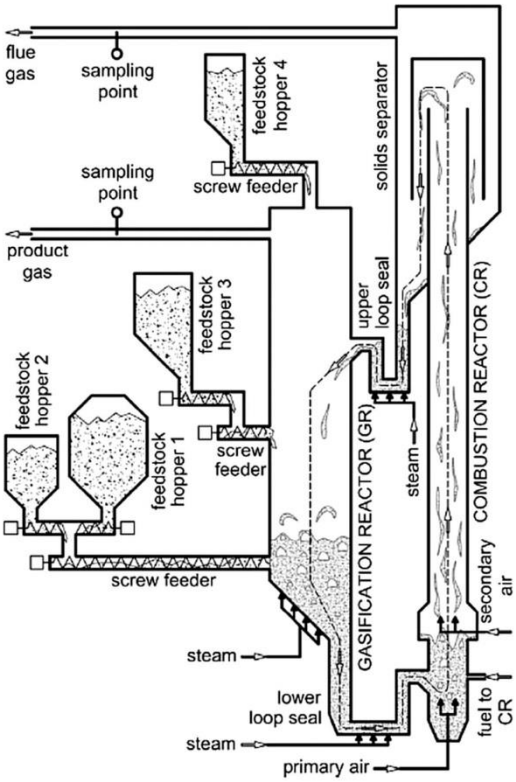

Fig. 12 Process flow diagram of the 100 kW_{th} bench-scale plant at Vienna University of Technology (reprinted with permission from Kirnbauer *et al.*[126] Copyright 2015 Elsevier).

In the conventional solid feedstock gasification process the BFB gasifier reactor operates at 850–900 °C, while air-combustion of fuel in the CFB combustor takes place at 920 °C. For this system, olivine was a suitable bed material with satisfactory resistance to attrition and moderate tar cracking activity.[120] The solids are transported between the reactors *via* two loop seals which are fluidised with steam. The concept was then successfully used for development of the biomass-fired 8 MW_{th} combined heat and power plant in Guessing, Austria that delivers 1.8 MW_{el} of electricity and 4.5 MW_{th} of heat to the local community.[124]

3.9.2 Test campaigns. The 100 kW_{th} unit has been modified to operate under SER process conditions with *in situ* CO_2 capture using limestone (Fig. 13). To assure proper conditions for the carbonation reaction, the BFB reactor temperature was reduced to approximately 700 °C[120] by reducing the solid looping rates between the reactors.[125]

The analysis by Pfeifer *et al.*[120] has revealed that compared to the conventional process, up to 70%$_{vol}$ higher H_2 yields are achievable.

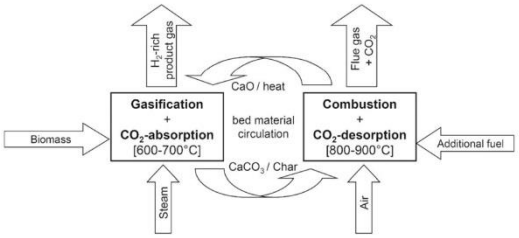

Fig. 13 Schematic representation of the sorption-enhanced reforming process with *in situ* CO_2 capture using calcium looping process (reprinted with permission from Koppatz *et al.*[125] Copyright 2015 Elsevier).

This is largely the result of an equilibrium shift in the water-gas shift reaction caused by CO_2 removal from the gasifier (Fig. 14). Moreover, a simultaneous reduction of the tar content from 4–8 g N^{-1} m^{-3} to 0.3–0.9 g N^{-1} m^{-3} was observed.

A first test campaign using the 8 MW_{el} Guessing CHP operating in SER mode was reported by Koppatz *et al.*[125] A temperature difference was required between the BFB gasifier and the CFB combustors to allow for efficient carbonation–calcination reactions. Therefore, the gasification temperature was reduced from 850–900 °C to 650–750 °C, while the combustion temperature was reduced from 950 °C to 850 °C. This was achieved through low solid looping rates. Moreover, olivine was substituted with limestone as the bed material. The content of H_2 and CH_4 in the syngas, hence its quality, decreases with increase of the gasification temperature. This could be explained by reduction of the driving force for the carbonation reaction, as the equilibrium partial pressure of CO_2 increases with temperature. The quality of the syngas produced in SER operating mode was higher than in the conventional process.

3.9.3 Data for process modelling. A detailed description of the experimental facility, which includes both the equipment dimensions and operating conditions, gives an opportunity for comprehensive equipment modelling. However, as the key objective of the test campaign was to improve syngas quality, no information was provided on the CO_2 capture level. Nevertheless, the available results allow validation of the syngas composition and comparison with the one reached in the conventional process. Although this kind of information does not provide a clear indicator of the CaL process performance in terms of the CO_2 capture level, it can still be used to validate the process performance.

3.10 Summary

In most of the studies, the key parameter describing performance of the CaL process is the CO_2 capture level. If a system is operated with appropriate solid inventory and sorbent conversion, the actual CO_2 capture level is close to the value determined by chemical equilibrium. This allows validation of the global performance of a model, which could be either equilibrium- or kinetics-based. Furthermore, unconventional configurations developed at ITRI and Ohio State University, which include the RK calciner, would be beneficial for validating a model when the power and cement integration is investigated.

The testing campaigns provide valuable insight in understanding process performance under varying operating conditions. Some information on local parameters, such as fluidising air temperature, flue gas composition and flow rate, CO_2 concentration in the gases leaving the CaL system, solid inventories or looping rates were disclosed. However, no complete data were available for any of the reviewed experimental campaigns. Further tests and more detailed data are required

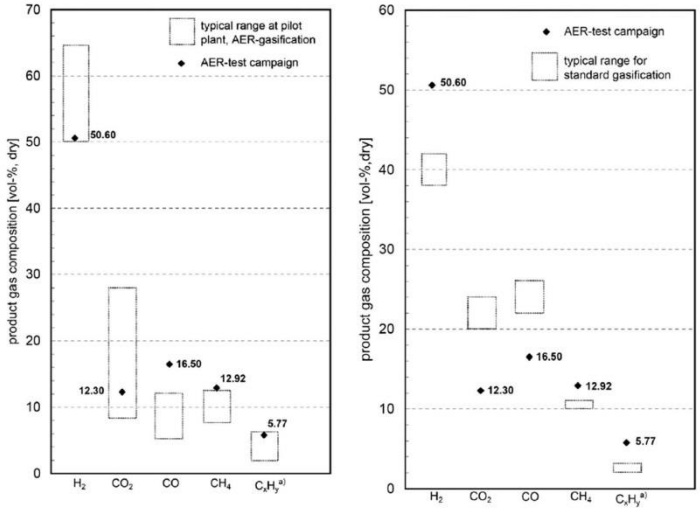

Fig. 14 Comparison of the syngas composition in conventional and SER gasification processes and the typical range at the pilot plant (adapted with permission from Koppatz *et al.*[125] Copyright 2015 Elsevier).

to allow validation of a model at the local level, and thus increase the quality of its prediction.

4 Models for the calcium looping processes

Development of novel power generation technologies needs to employ a range of analysis tools to evaluate various technology aspects. Therefore, experimental trials using bench- and pilot-scale facilities should be supported with analyses utilising mathematical and computational models that can be treated as a complementary source of information on process performance. Moreover, such models allow analysing the process scaling-up, and thus, expected net efficiency penalties, as well as operating and capital costs. Since the models vary in complexity and hence in computational requirements they can be applied at different stages of concept development to optimise the operating parameters of a process, to evaluate its performance under different operating conditions, or even to reliably size the equipment in the most time-efficient manner.

The current literature offers a selection of models for the key units, the carbonator and the calciner. They range from models based purely on thermodynamic equilibrium, usually defined by Gibbs' free energy minimisation,[26,32,127–131] through models considering sorbent degradation using semi-empirical correlations derived to fit experimental results,[11,16,34,39,42,84,86,132–146] to semi-predictive[28,30,31,37,93,135,147–149] and predictive models[150] that account for FB hydrodynamics and reaction kinetics. As the complexity of the models increases, the accuracy of their predictions increases as well. It needs to be stressed, however, that models of different complexity are suitable at different stages of process development; for example, thermodynamic or semi-empirical models would be more suitable for conceptual design studies, while predictive models would be appropriate at an advanced project stage, such as front-end engineering design. The CaL models available in the literature are reviewed in this section and their limitations are identified.

4.1 Modelling of the sorbent average conversion

The greatest challenge of using solid sorbents to capture CO_2 is the loss of their conversion with the number of carbonation–calcination cycles.[145] Thus far, the decay in sorbent maximum conversion, which is defined as the ratio of the actual and the theoretical mass of CaO that could have been converted to $CaCO_3$ for fully carbonated sorbent, has been represented using semi-empirical correlations. Since such representation includes fitting parameters, it would predict the activity decay well only for sorbent for which the values of fitting parameters were determined experimentally.

Dean *et al.*[14] have noted that the primary cause for sorbent deactivation is sintering of CaO during calcination at temperatures higher than 900 °C,[151] and high CO_2 and steam partial pressures.[43] High affinity of sorbent to SO_2 and H_2S, which are often present in the flue gas generated in a power plant, especially in units without FGD plants, would further affect the process performance due to increase in the solid looping rate. Although the once-through test performed by Sun *et al.*[152] in presence of SO_2 revealed no difference in the CO_2 capture in the chemically-controlled region of the carbonation, the calcination rate, and thus the sorbent conversion deteriorated as a result of $CaSO_4$ accumulation. Such observation was also made by Grasa *et al.*[153] The experimental trials showed that due to high Ca:S ratios in the system, the SO_2 and H_2S capture efficiencies could reach 100%.[112] As the regeneration process of sulphated sorbent is possible only at very high temperatures or in reducing conditions,[154,155] this would enhance sorbent sintering causing a further reduction in the activity. Moreover, attrition leading to excessive elutriation of sorbent and ash fouling could occur under such conditions.[13,14]

Sorbent performance is usually represented as a drop in the maximum sorbent particle conversion with the number of carbonation–calcination cycles (N). Since 2002, many semi-empirical correlations were developed to characterise the drop in the sorbent performance, for which the fitting parameters are often determined from the thermogravimetric analysis (TGA).[28,156–160] Such correlations were developed for non-pretreated sorbents,[42,139–145] and thermally pretreated sorbents[34,138] that experience self-reactivation.[34,161] Most of the semi-empirical correlations have been reviewed by Dean *et al.*,[14] and only the most important ones, required to understand the more complex models, are presented here.

A first semi-empirical model for the maximum sorbent conversion was developed by Abanades[145] based on the assumption that decay in the maximum carbonation conversion in the chemically-controlled stage depends only on the number of calcination–carbonation cycles.

$$X_N = k^{N+1} + X_r \tag{3}$$

There was a high degree of correlation between the maximum sorbent conversion predicted by the model and the experimental data (98.2%)[28,156,158–160] for a deactivation constant (k) and a residual carbonation conversion (X_r) of 0.782 and 0.174, respectively.

A study by Grasa and Abanades[143] has confirmed that the sorbent conversion decreases asymptotically to residual conversion that amounts to 0.075–0.08 and is constant when the number of calcination–carbonation cycles is higher than 50. Based on the proportionality between conversion and the surface area of highly cycled particles through the product layer thickness ($X = S/S_0$), Grasa and Abanades[143] have proposed a semi-empirical correlation for decay of the sorbent maximum conversion which is formulated similarly to typical catalyst deactivation correlations.

$$X_N = \frac{1}{\frac{1}{1 - X_r} + kN} + X_r \tag{4}$$

With a deactivation constant (k) of 0.52 and residual conversion (X_r) of 0.075, the prediction of the semi-empirical model presented in eqn (4) was accurate for a wide range of limestones, particle sizes and CO_2 partial pressures.

Li and Cai[139] have adopted a five-parameter correlation, with a similar structure to the one proposed by Abanades.[145]

$$X_N = a_1 f_1^{N+1} + a_2 f_2^{N+1} + X_r \quad (5)$$

Although the constants in eqn (5) were determined for a particular sorbent, no particular reference to their physical meaning was made. This semi-empirical model was found to successfully predict the decay in conversion of different sorbents (limestone, dolomite, $CaO/Ca_{12}Al_{14}O_{33}$), provided the fitting parameters were known.

4.1.1 Maximum average conversion of non-pretreated sorbent. The aforementioned semi-empirical models allow determination of the maximum carbonation conversion of sorbent particles that have undergone a given number of carbonation–calcination cycles. In real systems, however, the population of particles would comprise particles that have undergone different numbers of carbonation and calcination cycles. Based on the assumption that the solids are well mixed in the reactor, Abanades[145] proposed calculating the maximum average conversion in the carbonator as:

$$X_{ave,max} = \sum_{N=1}^{N=\infty} r_N X_N \quad (6)$$

The mass fraction of the particles that has undergone N carbonation–calcination cycles (r_N) is directly related to the solid looping rate (F_R) and fresh limestone makeup rate (F_0) as shown in eqn (7).

$$r_N = \frac{F_0 F_R^{N-1}}{(F_0 + F_R)^N} \quad (7)$$

Using the definition of the maximum carbonation conversion presented in eqn (3), Abanades *et al.*[39] have indicated that for a FB calciner (perfectly stirred reactor), the average conversion of sorbent entering the carbonator can be expressed using eqn (8) as a function of the process parameters: solid looping rate and fresh limestone make-up rate.

$$X_{ave,max} = \frac{k(1-X_r)F_0}{F_0 + F_R(1-X_r)} + X_r \quad (8)$$

Assuming that all sulphur present in the fuel reacts with the active sorbent to form $CaSO_4$, eqn (8) can be modified to account for sorbent deactivation caused by $CaSO_4$ formation.

$$X_{ave,max} = \frac{k(1-X_r)F_0}{F_0 + F_R(1-X_r)} + X_r - \frac{F_{CO_2}}{F_0 r_{C/S} y_{comb}} \quad (9)$$

As eqn (3) does not account for the residual conversion of sorbent, eqn (4) proposed by Grasa and Abanades[143] appears to be the most commonly applied in the literature. However, Li and Cai[139] have claimed that it is difficult to determine an explicit solution for an infinite sum in eqn (6) when the maximum conversion of the sorbent is formulated similarly to eqn (4). Therefore, they have derived a correlation for the average conversion by incorporating eqn (5) into eqn (6) and calculating the limit of the infinite sum of the geometric series. For $f_2 = 0$ the proposed correlation reduces to eqn (8) derived by Abanades *et al.*[39]

$$X_{ave,max} = \frac{a_1 f_1 F_0}{F_0 + F_R(1-f_1)} + \frac{a_2 f_2 F_0}{F_0 + F_R(1-f_2)} + X_r \quad (10)$$

Rodríguez *et al.*[11] have considered the impact of the reactor performance indicators, which define the extent of calcination (f_{calc}) or carbonation (f_{carb}) in each reactor, as well as the impact of the uncalcined sorbent (r_0) on the maximum average conversion.

$$f_{calc} = \frac{X_{carb} - X_{calc}}{X_{carb}} \quad (11)$$

$$f_{carb} = \frac{X_{carb} - X_{calc}}{X_{ave,max} - X_{calc}} \quad (12)$$

$$r_0 = \frac{F_0(1-f_{calc})}{F_0 + F_R f_{calc}} \quad (13)$$

Having incorporated eqn (11)–(13) into eqn (6), and utilising the maximum conversion model proposed by Li and Cai,[139] Rodríguez *et al.*[11] derived a semi-empirical correlation for maximum average conversion.

$$X_{ave,max} = (F_0 + F_R r_0) f_{calc} \times \left[\frac{a_1 {f_1}^2}{F_0 + F_R f_{carb} f_{calc}(1-f_1)} + \frac{a_2 {f_2}^2}{F_0 + F_R f_{carb} f_{calc}(1-f_2)} + \frac{X_r}{F_0} \right] \quad (14)$$

Eqn (14) reduces to an equation similar to the one derived by Li and Cai[139] for $f_{calc} = 1$ and $f_{carb} = 1$, with the only difference being the squared f_1 and f_2 fitting parameters. However, it allows estimation of the maximum average sorbent conversion that can be reached in the carbonator. Mantripragada and Rubin[162] stated that the actual conversion depends on the carbonation and calcination degree; hence the actual conversion in the carbonator and the calciner, which can be seen as equivalent to rich- and lean-loading in the solvent scrubbing technologies, are corrected based on the carbonator and the calciner performance, using the following expressions:

$$X_{carb} = \frac{f_{carb}}{1 - (1-f_{carb})(1-f_{calc})} X_{ave,max} \quad (15)$$

$$X_{calc} = (1 - f_{calc}) X_{carb} \quad (16)$$

4.1.2 Maximum average conversion of hydrated sorbent. Partial hydration is an option for sorbent reactivation that yields higher average sorbent conversions compared to unhydrated sorbent.[163–167] Hence, the system can operate at lower solid looping and make-up rates leading to a reduced heat requirement for the calciner.[40] In this concept (Fig. 15) some of the solids leaving the calciner (F_H) are diverted to the hydrator, while the remaining ($F_R - F_H$) circulate to the carbonator as usual. Therefore, the average conversion models reviewed in Section 4.1.1 are not applicable.

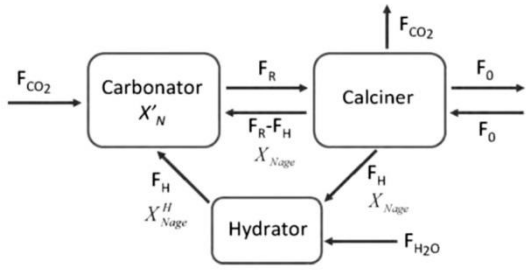

Fig. 15 Calcium looping process with sorbent reactivation through hydration (reprinted with permission from Arias *et al.*[137] Copyright 2015 Elsevier).

Arias *et al.*[137] have proposed a conversion model that can be used to predict the performance of a CaL plant with a hydrator operating in a continuous mode. As such a configuration does not produce any change in the number of carbonation–calcination cycles that each particle has undergone, the fraction of particles that has undergone N carbonation–calcination cycles can be still estimated using eqn (7). Moreover, since different fractions of sorbent having different maximum conversions are fed to the carbonator, the maximum conversion for a given calcination–carbonation cycle number N can be represented as:

$$X_N{}' = X_{N_{\mathrm{age}}}\frac{F_{\mathrm{R}} - F_{\mathrm{H}}}{F_{\mathrm{R}}} + X^{\mathrm{H}}_{N_{\mathrm{age}}}\frac{F_{\mathrm{H}}}{F_{\mathrm{R}}} \tag{17}$$

To estimate the maximum conversion $X_N{}'$, the particle age N_{age}, with conversion capacity in the previous cycle $N-1$, needs to be determined. For known value of $X_{N-1}{}'$, which was taken by Arias *et al.*[137] as approximately 0.7, the particle age before its Nth calcination is estimated using eqn (4) in reverse.

$$N_{\mathrm{age}-1} = \left(\frac{1}{k}\right)\left(\frac{1}{X_{N-1}{}' - X_{\mathrm{r}}} - \frac{1}{1 - X_{\mathrm{r}}}\right) \tag{18}$$

The corresponding maximum conversions for the hydrated ($X^{\mathrm{H}}_{N_{\mathrm{age}}}$) or non-pretreated ($X_{N_{\mathrm{age}}}$) sorbent can then be estimated using eqn (4). The decay constant (k^{H}) and the residual conversion ($X^{\mathrm{H}}_{\mathrm{r}}$) for the regenerated sorbent depend on the degree of hydration, and were estimated to be 0.63 and 0.15, respectively for 20% hydration, and 1.39 and 0.36, respectively for 60% hydration based on experimental data from Grasa *et al.*[166] (Fig. 16).

Stable maximum conversions were reached for a relatively small number of cycles. This is a result of a balance between the increase in sorbent conversion due to hydration and the loss in each carbonation–calcination cycle due to sintering.[137] Finally, the maximum average conversion of the sorbent can be determined as:

$$X_{\mathrm{ave,max}} = \sum_{N=1}^{N=\infty} r_N X_N{}' \tag{19}$$

4.2 Modelling of carbonation and calcination kinetic rates

4.2.1 Apparent kinetics model for carbonation. Lee[168] has developed a kinetic model for CaO carbonation conversion that is reportedly simple to implement during process design and

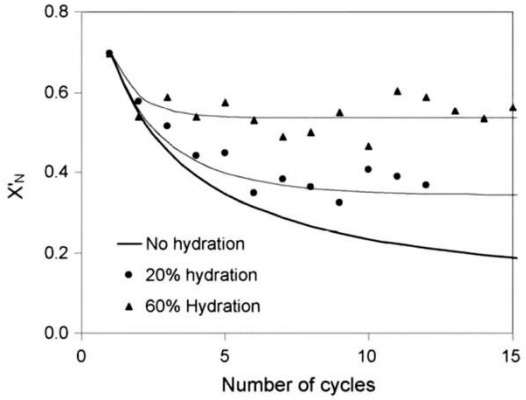

Fig. 16 Comparison of the experimental data in Grasa *et al.*[166] and the model prediction with $F_{\mathrm{H}}/F_{\mathrm{R}}$ = 1 (reprinted with permission from Arias *et al.*[137] Copyright 2015 Elsevier).

modelling. In this model, the CaO conversion rate is expressed as a function of the kinetic rate constant (k_{r}) and the actual and maximum conversion.

$$\frac{\mathrm{d}X}{\mathrm{d}t} = k_{\mathrm{r}}\left(1 - \frac{X}{X_{\mathrm{max}}}\right)^n \tag{20}$$

When n = 2, the model prediction is close to the experimental data presented by Bhatia and Perlmutter,[169] as well as Gupta and Fan.[170] This was reflected in a lowest correlation coefficient of 95%.

Eqn (20) was formulated in such a way that it could be used to describe both chemical- and diffusion-controlled regions of the carbonation reaction. Having estimated the values for activation energies and pre-exponential factors using data from both sources, Lee[168] identified that the type of limestone does not have a great impact on the chemical-controlled regime parameters, while it does for the diffusion-controlled ones (Table 6). This was explained by the strong impact of the CaO morphology on the reaction rate in the diffusion-controlled region.

4.2.2 Carbonation kinetic model for highly cycled particles. Grasa *et al.*[171] have proposed a model for sorbent conversion that utilises a rate expression consistent with a grain model for the carbonation reaction. The expression is similar to the one determined by Abanades *et al.*[136]

$$\frac{\mathrm{d}X}{\mathrm{d}t} = k_{\mathrm{s}} S_N (1 - X)^{\frac{2}{3}}\left(C_{\mathrm{CO_2}} - C_{\mathrm{CO_2,eq}}\right) \tag{21}$$

The model assumes that the active surface area of the particle that has undergone N calcination–carbonation cycles decreases proportionally with the maximum conversion of the particles at the end of the fast carbonation period. It also assumes that the $CaCO_3$ layer thickness (h) reaches a maximum of 50 nm in this period.

$$S_N = \frac{V_{\mathrm{MCaCO_3}}\rho_{\mathrm{CaO}}}{M_{\mathrm{CaO}}h} X_N \tag{22}$$

Table 6 Characteristic parameters for the rate constant k[168]

	Bhatia and Perlmutter[169]		Gupta and Fan[170]	
Controlling mechanism	Activation energy (kJ mol^{-1})	Pre-exponential factor (s^{-1})	Activation energy (kJ mol^{-1})	Pre-exponential factor (s^{-1})
Chemical reaction	72.2	171.67	72.7	193.33
Mass transfer	189.3	2.62×10^{8}	102.5	3.88×10^{3}

Using eqn (4) to determine the maximum conversion at given cycle N, the active surfaces were determined to be between 1×10^{6} and 2×10^{6} m^2 m^{-3} for highly cycled particles, while the rate constant k_s was estimated to be 3.2×10^{-10} to 8.9×10^{-10} m^4 mol^{-1} s^{-1}. Similar values were yielded (3.1×10^{-10} to 8.7×10^{-10} m^4 mol^{-1} s^{-1}) when the pore model described in eqn (23) was applied with the pore structural parameter defined as $\Psi_N = 4\pi L_N/S_N^2$.

$$\frac{dX}{dt} = k_s S_N \left(C_{CO_2} - C_{CO_2,eq}\right)(1-X)\sqrt{1 - \Psi \ln(1-X)} \quad (23)$$

Moreover, Grasa *et al.*[171] have pointed out that the central value of the estimated rate constant is remarkably close to the value of 6.05×10^{-10} m^4 mol^{-1} s^{-1} estimated using the pore model by Bhatia and Perlmutter.[169]

4.2.3 Changing grain size carbonation and calcination models. Recently, Yu *et al.*[172] have developed a kinetic model to represent the carbonation process through modification of the existing changing grain size model that was previously used to represent the reaction between CaO and SO_2.[173] This model assumes that carbonation is an unsteady-state process with the CO_2 concentration inside the particle represented in the radial coordinate system as the sum of the diffusion and chemical reaction terms.

$$\frac{dC_{CO_2}}{dt} = r_{CO_2} + \frac{1}{R^2}\frac{\partial}{\partial R}\left(D_e R^2 \frac{\partial C_{CO_2}}{\partial R}\right) \quad (24)$$

The first term in eqn (24) accounts for the reversible carbonation reaction for which the reaction rate per unit volume of the particle includes both carbonation and calcination reaction rates.

$$r_{CO_2} = -\left[k_{carb} S_0 \left(\frac{r_i}{r_0}\right)^2 V_R C_{CO_2} - k_{calc} S_0 \left(\frac{r_i}{r_0}\right)^2\right] \quad (25)$$

In the model, the carbonation rate constant is represented using eqn (26) proposed by Sun *et al.*,[174] while eqn (27) used for the calcination rate constant is taken from Borgwardt.[175]

$$k_{carb} = \begin{cases} 1.67 \times 10^{-4} \exp\left(-\dfrac{24\,000}{R_g T}\right)\left(P_{CO_2} - P_{CO_2,eq}\right) & \text{if } P_{CO_2} - P_{CO_2,eq} < 10 \text{ kPa} \\ 1.67 \times 10^{-3} \exp\left(-\dfrac{24\,000}{R_g T}\right) & \text{if } P_{CO_2} - P_{CO_2,eq} > 10 \text{ kPa} \end{cases} \quad (26)$$

$$k_{calc} = 3 \times 10^{-2} \exp\left(-\frac{205\,000}{R_g T}\right) \quad (27)$$

The equilibrium partial pressure ($P_{CO_2,eq}$) was calculated as a function of the reactor temperature,[36] and the initial surface area of CaO was determined based on the initial particle porosity (ε_0), initial grain radius (r_0) and molar volume of CaO and $CaCO_3$.

$$P_{CO_2,eq} = 10^{\left(7.079 - \frac{8808}{T}\right)} \quad (28)$$

$$S_0 = \frac{3(1-\varepsilon_0)}{r_0}\frac{V_{m,CaO}}{V_{m,CaCO_3}} \quad (29)$$

According to the changing grain size model, the change in the un-reacted radius of the CaO grain is dependent on the carbonation and calcination rate constants.

$$\frac{dr_i}{dt} = -\left(k_{carb} V_R V_R C_{CO_2} - k_{calc} V_R\right) \quad (30)$$

The local and average conversions of CaO were expressed as:

$$X = 1 - \left(\frac{r_i}{r_0}\right)^3 \quad (31)$$

$$X(t) = \frac{1}{\frac{4}{3}\pi {R_0}^3}\int_0^{R_0} 4\pi R^2 X \, dR \quad (32)$$

The second term in eqn (24) accounts for the effective diffusivity of CO_2 through the sorbent particle. It accounts for the product layer diffusivity (D_p), molecular diffusivity of CO_2 in N_2 (D_{m,CO_2}), the Knudsen diffusivity (D_K) and the porosity changes inside the particle during the reaction (ε).

$$D_e = \left[(1-X)\left(\frac{1}{D_{m,CO_2}} + \frac{1}{D_K}\right)^{-1} + XD_p\right]\varepsilon^2 \quad (33)$$

Yu *et al.*[172] have validated the model with the experimental result for the CGMG75 sorbent, which was composed of 75%$_{wt}$ CaO and 25%$_{wt}$ MgO, and 15%$_{vol}$ CO_2 in the synthetic flue gas. As shown in Fig. 17, the model prediction accurately reproduces the experimental data in both chemical-controlled and diffusion-controlled regions of the carbonation process.

García-Labiano *et al.*[176] proposed incorporating the Langmuir–Hinshelwood mechanism into the changing grain size model to describe the calcination process. The model is based on the similar mass balance to the one presented in eqn (24), but with the negative sign for the CO_2 source term, and accounts for both the diffusion and the reaction of the gas

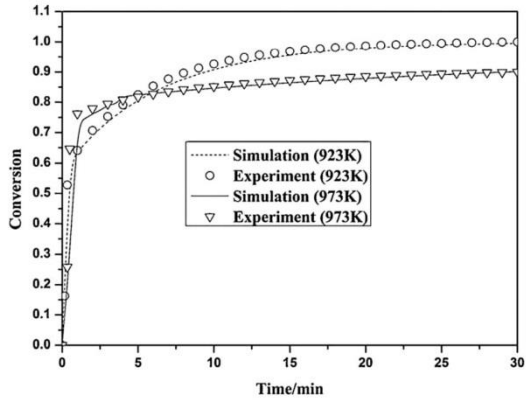

Fig. 17 Validation of the Yu *et al.*[172] model with the experimental data (reprinted with permisson from Yu *et al.*[172] Copyright 2015 Elsevier).

in a differential volume of the particle.

$$\frac{\partial C_{CO_2}}{\partial t} = -r_{CO_2} + \frac{1}{R^2}\frac{\partial}{\partial R}\left(D_e R^2 \frac{\partial C_{CO_2}}{\partial R}\right) \quad (34)$$

However, in contrast to the model by Yu *et al.*,[172] the calcination reaction is described using the two-stage Langmuir–Hinshelwood mechanism. In the first stage, considering that one CO_2 molecule can be chemisorbed on n out of L active sites, $CaCO_3$ is decomposed to CaO and adsorbed CO_2. CO_2 is then desorbed from the active site in the second step.

$$CaCO_3 + nL \underset{k_1}{\overset{k_2}{\rightleftharpoons}} CaO + nL(CO_2) \qquad K_1 = \frac{k_1}{k_2} \quad (35)$$

$$nL(CO_2) \underset{k_D}{\overset{k_A}{\rightleftharpoons}} CO_2 + nL \qquad K_A = \frac{k_A}{k_D} \quad (36)$$

The kinetic rate of calcination per unit of particle volume was then described as:

$$r_{CO_2} = k_{calc} S_e (1-\theta)\left(1 - \frac{P_{CO_2}}{P_{CO_2,eq}}\right) \quad (37)$$

The fraction of the active sites (θ) was found to be well represented by the Freundlich isotherm, for which the adsorption constant was represented using the Arrhenius expression.

$$\theta = c_0 \exp\left(-\frac{E}{R_g T}\right) P_{CO_2}^{\frac{1}{2}} \quad (38)$$

According to the changing grain size model, the reaction surface is dependent on the particle radius that, in turn, changes as the reaction proceeds.

$$S_e = S_0 \left(\frac{r_1}{r_0}\right)^2 \quad (39)$$

$$r_0 = \frac{3(1-\varepsilon_0)}{S_0} \quad (40)$$

$$r_1 = k_{calc} V_{M,CaCO_3}\left(1 - \frac{P_{CO_2}}{P_{CO_2,eq}}\right) \quad (41)$$

The effective diffusion was represented as a combination of the molecular and Knudsen diffusions, as well as the particle porosity.

$$D_e = \left(\frac{1}{D_{m,CO_2}} + \frac{1}{D_K}\right)^{-1} \varepsilon^2 \quad (42)$$

$$\varepsilon = \varepsilon_0 - \frac{\rho_{CaCO_3}\left(V_{M,CaO} - V_{M,CaCO_3}\right)}{M_{CaCO_3}}(1-\varepsilon_0)X(R,t) \quad (43)$$

The variation in the porosity inside the particle was determined from the initial porosity, the stoichiometric volume ratio of solid product to reactant product, and the local conversion of $CaCO_3$ given by eqn (43). The average conversion at a given time is represented using the same form as in eqn (32).

García-Labiano *et al.*[176] have validated the prediction of the model at different CO_2 partial and equilibrium pressures using different limestone compositions and found good agreement between the model prediction and the experimental data (Fig. 18). The changing grain size models, which were adapted to the carbonation and calcination processes, were found to closely represent the particle conversion at given temperature. Although these did not account for sorbent sulphation and ash accumulation, such models would provide a valuable tool in calciner modelling, provided they are coupled with reactor hydrodynamics.

4.3 Carbonator reactor modelling

4.3.1 Semi-predictive model with simple hydrodynamics. Alonso *et al.*[30] have developed a model for the carbonator that combines simple hydrodynamics correlations with the average conversion of the sorbent and residence time distribution functions. They have introduced a definition of the active fraction (f_a) of the particles that is dependent only on the actual residence time (t^*) and the average residence time (τ) in the carbonator.

$$f_a = 1 - \exp\left(-\frac{t^*}{\tau}\right) \quad (44)$$

$$\tau = \frac{N_{Ca}}{F_R} = \frac{W_{CaO}}{M_{CaO} F_R} \quad (45)$$

This definition of the active fraction of the particles in the carbonator, along with the definition for the average maximum conversion given by eqn (6), led to the following expression for the actual average sorbent conversion at the exit of the carbonator (46) and the CO_2 capture level in the carbonator (47).

$$X = X_{ave,max}\frac{\tau}{t^*}\left[1 - \exp\left(-\frac{t^*}{\tau}\right)\right] = X_{ave,max}\frac{f_a}{\ln\left[\frac{1}{1-f_a}\right]} \quad (46)$$

$$E_{carb} = \frac{F_R}{F_{CO_2}} X_{ave,max}\frac{f_a}{\ln\left[\frac{1}{1-f_a}\right]} \quad (47)$$

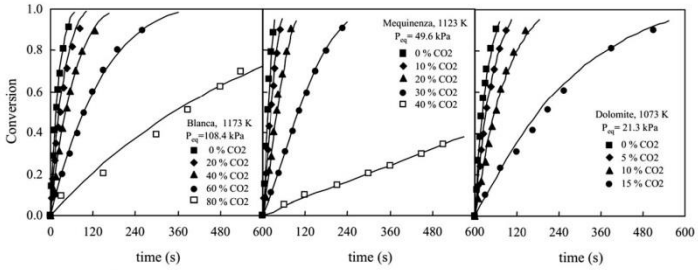

Fig. 18 Validation of the García-Labiano *et al.*[176] model with the experimental data (reprinted with permission from García-Labiano *et al.*[176] Copyright 2015 Elsevier).

Based on the carbon balance in the carbonator reactor, the same amount of CO_2 disappears from the gas phase and reacts with CaO to form $CaCO_3$.

$$F_{CO_2}E_{carb} = F_R X = N_{Ca} f_a \frac{dX_{ave,max}}{dt} \quad (48)$$

Only one value for the active fraction exists for a given operating point of the system that is characterised by the sorbent looping rate (F_R), fresh sorbent make-up rate (F_0), CO_2 rate to the carbonator (F_{CO_2}) and solids inventory (W_{CaO}). Therefore, the value for the active fraction at which the system is in balance is calculated iteratively.

The average reaction rate expression shown in eqn (49) proposed by Alonso *et al.*[30] does not consider the characteristic term for the grain models $(1 - X)^{2/3}$. Although this change makes it slightly different from the expressions proposed by Abanades *et al.*[136] and Grasa *et al.*,[171] the authors claim that this will not have a significant effect on prediction accuracy, as the conversion is low despite the relatively fresh sorbent and thus this term would be close to unity.

$$\frac{dX_{ave,max}}{dt} = k_s S_{ave,max}\left(C_{CO_2} - C_{CO_2,eq}\right) \quad (49)$$

Alonso *et al.*[30] assumed a conservative value for the carbonation rate constant of 4×10^{-10} m^4 mol^{-1} s^{-1} that falls within the lower part of the range 3.2×10^{-10}–8.9×10^{-10} m^4 mol^{-1} s^{-1} identified by Grasa *et al.*[171] In contrast to the previous study by Abanades *et al.*,[136] the average surface available for the carbonation reaction is calculated as a function of the average conversion, using an expression proposed by Grasa *et al.*[171]

$$S_{ave,max} = \frac{\frac{\rho_{CaO}}{M_{CaO}}}{h\frac{\rho_{CaCO_3}}{M_{CaCO_3}}} X_{ave,max} \quad (50)$$

Finally, the CO_2 capture level in the carbonator can be estimated from the carbon balance in the gas phase which can be formulated as a differential equation assuming a plug flow of the gas phase and perfect mixing of the solids.

$$F_{CO_2}\frac{dE_{carb}}{dz} = Af_a\frac{\rho_{CaO}}{M_{CaO}}r_{ave} = Af_a\frac{\rho_{CaO}}{M_{CaO}}k_s S_{ave,max}\rho_{M,g} \times \left[\frac{\left(f_{CO_2,0} - f_{CO_2,eq}\right) + \left(f_{CO_2,0}f_{CO_2,eq} - f_{CO_2,0}\right)E_{carb}}{1 - f_{CO_2,0}E_{carb}}\right] \quad (51)$$

Rodríguez *et al.*[93] and Charitos *et al.*[149] have developed a kinetic expression for the carbonation process based on the experimental studies using the 30 kW_{th} unit at INCAR-CSIC and the 10 kW_{th} unit at IFK. Their model is based on a CO_2 mass balance for a system operating at steady state, which is similar to the one formulated by Alonso *et al.*,[30] and is related to the amount of CO_2 captured in the bed.

$$F_{CO_2}E_{carb} = \frac{W_{CaO}}{M_{CaO}}\frac{dX}{dt} \quad (52)$$

Assuming that only a fraction of the CaO reacts with the CO_2 in the carbonator (X_{ave}), the first-order expression for the carbonation kinetic rate is:

$$\frac{dX}{dt} = \varphi_e k_{carb} X_{ave,max}\left(\overline{v_{CO_2}} - v_{CO_2,eq}\right) \quad (53)$$

Rodríguez *et al.*[93] found that for two limestones investigated at the INCAR-CSIC unit the carbonation rate constant (k_{carb}) was 0.37 s^{-1}. The investigation revealed that the reaction rate constant depends on the test unit as it was equal to 0.26 s^{-1} for the IFK unit and 0.33 s^{-1} for the INCAR-CSIC unit. The authors claim that this is in agreement with previous publications[169,177] reporting that temperature has little effect on carbonation rates. Moreover, the proposed model includes an effectivity factor (φ_e) that accounts for all physical resistances to the carbonation process and ideally it should be equal to unity for a stationary system. In reality, analysis of the experimental data revealed that the carbonator effectivity factor varies between 0.8 and 1.3. Such a high deviation from unity was probably a result of measurement uncertainty, as estimation of the solid circulation rates and average carbonation conversion is associated with an error reaching ±20%.[93,149]

Finally, using the definition for the active fraction of sorbent (f_a) proposed by Alonso *et al.*,[30] an expression for the CO_2 capture level, which links the average conversion of sorbent and the residence time distribution in the bed, was proposed.

$$E_{carb} = \varphi_e k_{carb} X_{ave,max} f_a \tau\left(\overline{v_{CO_2}} - v_{CO_2,eq}\right) \quad (54)$$

In the carbonator models proposed by Alonso *et al.*,[30] Rodríguez *et al.*[93] and Charitos *et al.*[149] only simple hydrodynamics and the average sorbent conversion were considered in estimating the carbonator CO_2 capture level. In the model by Alonso *et al.*,[30] the effect of the decay in sorbent conversion on the kinetic reaction rate is considered through estimation of the average surface area

that is available for the carbonation reaction. Conversely, the model by Rodríguez *et al.*[93] and Charitos *et al.*[149] assumes a fixed value for the carbonation rate constant, which was found to be similar for different limestones. Nevertheless, these models do not consider either sorbent sulphation or ash accumulation. However, the average sorbent conversion correlation used in each model can be easily adapted to account for sorbent sulphation, leading to more accurate prediction of the solid looping rates, and thus the heat requirement in the calciner.

4.3.2 Semi-predictive model with two-zone K–L hydrodynamics. Shimizu *et al.*[28] have carried out a study using a quartz fixed bed reactor with an inner diameter of 20 mm, and identified that the change in CO_2 concentration did not affect the kinetic constant (k_r = 0.025 m^3 mol^{-1} s^{-1}) and the maximum conversion at which the reaction rate approaches zero (X_{max} = 0.3). As the reaction was found to be first order with respect to the CO_2 concentration, the following kinetic expression was proposed:

$$\frac{dX}{dt} = k_r C_{CO_2}(X_{max} - X) = k_r C_{CO_2} X_{max} \exp(-kC_{CO_2} t) \quad (55)$$

Assuming perfect mixing of solids and determining their average solid residence time in the reactor, Shimizu *et al.*[28] determined the average reaction rate as:

$$\tau = \frac{AH_D(1-\varepsilon_f)}{F_R} \quad (56)$$

$$\overline{\frac{dX}{dt}} = \int_0^\infty k_r C_{CO_2} X_{max} \exp(-k_r C_{CO_2} t)\frac{1}{\tau}\exp\left(-\frac{t}{\tau}\right)dt = \frac{k_r C_{CO_2} X_{max}}{k_r C_{CO_2}\tau + 1} \quad (57)$$

To account for BFB reactor hydrodynamics in estimating the CO_2 capture level, a two-zone model for an intermediate-sized particle by Kunii and Levenspiel (K–L)[178] was employed. The model assumes that the fluidised bed consists of bubble and emulsion regions in which the CO_2 concentration changes with height.

$$-\delta u_b{}^* \frac{dC_{CO_2,b}}{dz} = \delta K_{be}(C_{CO_2,b} - C_{CO_2,e}) + \frac{\gamma_b k_r C_{CO_2,b} X_{max}\rho_s}{M(k_r C_{CO_2,b}\tau + 1)} \quad (58)$$

$$-(1-\delta)u_{mf}\frac{dC_{CO_2,e}}{dz} = -\delta K_{be}(C_{CO_2,b} - C_{CO_2,e}) + \frac{(1-\delta)(1-\varepsilon_{mf})k_r C_{CO_2,e} X_{max}\rho_s}{M(k_r C_{CO_2}\tau + 1)} \quad (59)$$

Eqn (58) and (59) can be solved with the initial condition that $C_b = C_e = C_{in}$ at $z = 0$. The superficial gas velocity at the minimum fluidising conditions (u_{mf}) can be expressed as:

$$u_{mf} = \frac{d_p{}^2(\rho_s - \rho_g)g\varepsilon_{mf}{}^3\Phi_s{}^2}{150\mu(1-\varepsilon_{mf})} \quad (60)$$

Assuming a bubble diameter (d_b), the bubble and emulsion interchange coefficient (K_{be}) is defined as:

$$K_{be} = 4.5\left(\frac{u_{mf}}{d_b}\right) \quad (61)$$

Furthermore, the velocity of the rising bubble gas (u_b*) is determined from the bubble rise velocity (u_b), the minimum fluidisation velocity (u_{mf}) and the superficial gas velocity (u_0).

$$u_b{}^* = u_b + 3u_{mf} \quad (62)$$

$$u_b = u_0 - u_{mf} + 0.711(gd_b)^{0.5} \quad (63)$$

The last parameter required to compute CO_2 concentrations is the volume of bubbles per unit bed volume (δ) defined as:

$$\delta = \frac{u_0 - u_{mf}}{u_b + 2u_{mf}} \quad (64)$$

Finally, the average CO_2 concentration at a given bed height is represented by considering both the emulsion and the bubble zones:

$$C_{CO_2,ave,z} = \frac{\delta u_b{}^* C_{CO_2,b} + (1-\delta)u_{mf}C_{CO_2,e}}{u_0} \quad (65)$$

Using a similar approach to Shimizu *et al.*,[28] Abanades *et al.*[136] have proposed a carbonator model based on the two-zone K–L formulations for CO_2 mass balance in the emulsion and the bubble phases. However, in their model the bubble fraction is estimated as proportional to the extremes for fine and large particles defined by Kunii and Levenspiel.[179]

$$\delta = \frac{u_0 - u_{mf}}{u_b + \frac{5u_{mf} - u_b\varepsilon_{mf}}{4}} \quad (66)$$

Furthermore, the velocity of the rising bubble gas was defined based on the gas balance in the bed cross-section as:

$$u_b{}^* = \frac{u_0 - (1-\delta)u_{mf}}{\delta} \quad (67)$$

Having assumed that there were no solids in the bubble phase (γ_b = 0), and that only an active fraction of CaO (f_a), defined as the difference between the maximum carbonation conversion (X_N) and the actual conversion of CaO to $CaCO_3$ (X), reacted in the fast reaction regime, the following K–L formulations for the CO_2 mass balance in the bubble and emulsion phases were derived:

$$-\delta u_b{}^* \frac{dC_{CO_2,b}}{dz} = \delta K_{be}(C_{CO_2,b} - C_{CO_2,e}) \quad (68)$$

$$-(1-\delta)u_{mf}\frac{dC_{CO_2,e}}{dz} = -\delta K_{be}(C_{CO_2,b} - C_{CO_2,e}) + (1-\delta)(1-\varepsilon_{mf})f_a k_r C_{CO_2,e} \quad (69)$$

Similarly to Shimizu *et al.*,[28] Abanades *et al.*[136] have used eqn (61) to estimate the gas-interchange coefficient (K_{be}). Conversely, the overall reaction rate constant (k_r) was determined by considering both the kinetic- and diffusion-controlled regions of the carbonation reaction.

$$k_r = \frac{1}{\frac{d_p}{6k_g} + \frac{1}{K_{ri}}} \quad (70)$$

The mass transfer coefficient (k_g) is estimated using the Turnbull and Davidson[180] correlation for the Sherwood number (Sh)

that considers the effective CO_2 diffusivity in air, Reynolds number at minimum fluidisation conditions (Re_{mf}) and Schmidt number (Sc).

$$Sh = \frac{D_{CO_2}}{d_p k_g} = 2\varepsilon_{mf} + 0.95 Re_{mf}^{0.5} Sc^{0.3} \quad (71)$$

The carbonation rate is considered to be first order with respect to CO_2 and the mass transfer of CO_2 toward the CaO particle. It is expressed using semi-empirical eqn (72) similar to the one proposed by Bhatia and Perlmutter[169] with correction for decreasing conversion of the sorbent with number of cycles, which is calculated using eqn (4). In addition, the kinetic rate constant is a function of the conversion and is rewritten to have suitable units for the K–L model as presented in eqn (73).

$$\frac{dX}{dt} = \frac{k_s S_0}{1 - e_0} X_N (1 - X)^{\frac{2}{3}} \left(C_{CO_2} - C_{CO_2,eq}\right) \quad (72)$$

$$K_{ri} = k_s \frac{X_N S_0 \rho_{CaO}}{M_{CaO}} (1 - X)^{\frac{2}{3}} \quad (73)$$

In eqn (72) and (73), the intrinsic reaction rate constant (k_s) of 5.95×10^{-10} m^4 mol^{-1} s^{-1} was found to be independent of temperature between 400 °C and 725 °C for the CO_2 volume fraction range of 0.1–0.42. The initial surface area of fresh CaO (S_0) was 40×10^6 m^2 m^{-3} with initial porosity (e_0) of 0.5. Additionally, it was assumed that if the maximum carbonation conversion is reached, the chemical reaction rate becomes zero.

Using TGA, Li *et al.*[181] have identified that the carbonation rate was independent of temperature between 600 °C and 700 °C. Moreover, the maximum conversion of the sorbent was found to be independent of the CO_2 concentration and increased with temperature. Based on these findings, Fang *et al.*[135] proposed the following semi-empirical equation for the carbonation rate. It accounts for the effect of the total pressure on the rate of sorbent carbonation.

$$\frac{dX_N}{dt} = k_r \left(1 - \frac{X_N}{X_{max,N}}\right)^m \left(C_{CO_2} - C_{CO_2,eq}\right)^{0.083\frac{P}{P_0}} \quad (74)$$

In this model, the exponent m was equal to 2/3 for the kinetic-controlled region and 4/3 for the diffusion-controlled region of the carbonation reaction. The corresponding kinetic rate constants (k_r) were found to be 0.0025 m^3 mol^{-1} s^{-1} and 0.0021 m^3 mol^{-1} s^{-1} for kinetic- and diffusion-controlled regions, respectively.

Again, Fang *et al.*[135] proposed using the two-zone K–L model[179] to represent carbonator hydrodynamics. The model is similar to the one adapted by Abanades *et al.*,[136] with a minor change to account for the solids present in the bubbles. Assuming the volume fraction of solids dispersed in the bubbles (y_b) to be between 10^{-2} and 10^{-3}, the mass balance for the bubble phase is:

$$-\delta u_b^* \frac{dC_{CO_2,b}}{dz} = \delta K_{be}\left(C_{CO_2,b} - C_{CO_2,e}\right) + \delta y_b f_a K_r \left(C_{CO_2,b} - C_{CO_2,eq}\right) \quad (75)$$

The carbonation rate constant in the units suitable for the K–L model and the active fraction of CaO in the carbonation process were expressed as:

$$K_r = k_c \left(1 - \frac{X_N}{X_{max,N}}\right)^m \frac{\rho_{CaO}}{M_{CaO}} \quad (76)$$

$$f_a = X_{max,N} - X_N \quad (77)$$

Finally, the overall conversion of CO_2 in the reactor was estimated as the average concentration in the emulsion and the bubble phase.

$$X_{CO_2,exit} = 1 - \frac{\delta u_b^* C_{CO_2,b,exit} + (1 - \delta) u_{mf} C_{CO_2,e,exit}}{u_0 C_{CO_2,in}} \quad (78)$$

Although the model by Shimizu *et al.*[28] provided a good representation of the CO_2 capture level in the carbonator, several improvements could be made to enhance prediction accuracy. In the model developed by Abanades *et al.*,[136] a semi-empirical correlation was used to determine sorbent deactivation with the number of carbonation–calcination cycles, which substituted the fixed conversion value after four cycles used by Shimizu *et al.*[28] Moreover, the overall kinetic rate constant defined by the model by Abanades *et al.*[136] accounted for both the chemical reaction rate and the mass transfer rate, resulting in a further improvement in prediction accuracy. A further improvement in the semi-predictive carbonator model was achieved by Fang *et al.*[135] whose model is capable of predicting process performance separately in the chemically- and diffusion-controlled regions of the carbonation reaction. Unfortunately, these semi-predictive models do not account for sorbent sulphation and ash accumulation in the system and this may cause under-estimation of the solids looping rates and, thus the heat requirement in the calciner.

4.3.3 Semi-predictive model with three-zone K–L hydrodynamics. Romano[84] has developed a model for a CFB carbonator by combining the improved three-zone K–L model[182,183] with the maximum conversion expression proposed by Grasa and Abanades[143] and the carbonation kinetics developed by Grasa *et al.*[171] The model developed by Romano[84] is the first one that accounts for the impact of sulphation on average sorbent conversion. This is achieved through estimation of the decay constant and the residual sorbent conversion by fitting eqn (4) to the experimental data from Grasa *et al.*[153]

In the carbonator model, the uniform riser temperature, particle size distribution and superficial velocity were assumed, along with no gas-side mass transfer resistance and perfect solid mixing. The model considered two statistical distributions. The first determines the carbonation–calcination cycle number that a given particle has already experienced using the correlations provided by Abanades[145] and Rodríguez *et al.*[11] These, in combination of the maximum sorbent conversion correlation by Grasa and Abanades[143] with fitting parameters adjusted to consider sulphation, allow determining the maximum average sorbent conversion. The second characterises the fraction of particles of a given residence time in the carbonator, for which the average residence time is defined as in the model by Alonso *et al.*[30] The active solid inventory is

defined in eqn (80) to account for sulphation and ash accumulation effects.

$$f_t = \frac{1}{\tau}\exp\left(-\frac{t}{\tau}\right) \quad (79)$$

$$N_{Ca} = \frac{W_s}{M_s}\left(1 - x_{ash} - x_{CaSO_4}\right) \quad (80)$$

The actual average conversion of the sorbent for a given CO_2 concentration (C_{CO_2}*) and the average carbonation level are determined as:

$$X_{ave} = \sum_{N_{age}=1}^{\infty} r_{N_{age}} \int_0^{\infty} f_t X\left(t, N, C_{CO_2}{}^*\right) dt \quad (81)$$

$$f_{carb} = \frac{X_{ave}}{X_{max,ave}} \quad (82)$$

Using the same approach, the average kinetic constant in suitable units for the K–L model is computed as:

$$K_{ri,ave} = \frac{\rho_s}{M_s} \sum_{N_{age}=1}^{\infty} r_{N_{age}} \int_0^{\infty} f_t k_s S_N \left[1 - X\left(t, N, C_{CO_2}{}^*\right)\right]^{\frac{2}{3}} dt \quad (83)$$

The CO_2 capture level in the carbonator model is then separately calculated from the carbonator mass balance and the K–L model:

$$E_{carb} = \frac{F_R X_{ave}}{F_{CO_2}} = \frac{F_{CO_2} - V_{g,out} C_{CO_2,out}}{F_{CO_2}} \quad (84)$$

Since both the actual average conversion determined using eqn (81) and the outlet CO_2 concentration computed using the K–L model with the average kinetic constant estimated in eqn (83) depend on C_{CO_2}*, the model is solved in an iterative process by varying C_{CO_2}* until eqn (84) is satisfied. This approach was found to reliably predict the performance of the carbonator reactor for the INCAR-CSIC and IFK test units.

The model developed recently by Romano[84] is the most advanced carbonator semi-predictive model available currently as it considers the effect of reactor hydrodynamics on the CO_2 capture level, reaction kinetics, the influence of sulphation on sorbent conversion and ash accumulation. Although it does not consider the diffusion region of the carbonation process, this region is usually neglected in industrial applications, to allow for a compact design of the CFB reactor.[84,145]

4.4 Calciner reactor modelling

4.4.1 Semi-predictive model with simple hydrodynamics. Martínez *et al.*[134] have proposed a model to predict the performance of the calcination process that is based on the steady-state overall mass balance of the calciner.

$$F_{CO_2,calc} = N_{Ca} \cdot r_{calc} = (F_{Ca} + F_0)(X_{carb,ave} - X_{calc}) \quad (85)$$

The average $CaCO_3$ content in the total flow entering the calciner ($X_{carb,ave}$) is determined based on solid flow from the carbonator (F_{ca}) and fresh limestone make-up (F_0). The kinetic rate of the calcination reaction was developed in the earlier work by Martínez *et al.*[184] It was based on the grain model and is similar to the calciner model by Fang *et al.*[135]

$$\frac{d(X_{carb} - X_{calc})}{dt} = k_{calc}\left(1 - \frac{X_{carb} - X_{calc}}{X_{carb}}\right)^{\frac{2}{3}} \left(C_{CO_2,eq} - C_{CO_2}\right) \quad (86)$$

The time required for complete calcination can be determined by integrating eqn (86).

$$t_{calc}{}^* = \frac{3 \cdot X_{carb}}{k_{calc}\left(C_{CO_2,eq} - C_{CO_2}\right)} \quad (87)$$

Martínez *et al.*[184] determined that the calcination rate is constant and independent of the $CaCO_3$ content in the particle. Therefore, the average calcination rate was expressed as:

$$r_{calc} = \begin{cases} \dfrac{X_{carb,ave}}{t_{calc}{}^*} = \dfrac{k_{calc}\left(C_{CO_2,eq} - C_{CO_2}\right)}{3} & \text{for } t < t_{calc}{}^* \\ 0 & \text{for } t \geq t_{calc}{}^* \end{cases} \quad (88)$$

Based on the assumption that the solid phase in the calciner is perfectly mixed and considering the average particle residence time in the calciner, the fraction of particles that has a residence time lower than the time required for complete calcination can be estimated as:

$$f_a = 1 - \exp\left(-\frac{t_{calc}{}^*}{\tau}\right) \quad (89)$$

$$\tau = \frac{N_{Ca}}{F_{Ca} + F_0} \quad (90)$$

Using these definitions, the amount of $CaCO_3$ that disappeared from the solid phase and the amount of CO_2 released in the calciner are given as:

$$(F_{Ca} + F_0)\left(X_{carb,ave} - X_{calc}\right) = (F_{Ca} + F_0) X_{carb,ave} \frac{f_a}{\ln\left[\frac{1}{1 - f_a}\right]} \quad (91)$$

$$N_{Ca} \cdot r_{calc} = N_{Ca} \cdot f_a \cdot \frac{k_{calc}\left(C_{CO_2,eq} - C_{CO_2}\right)}{3} \quad (92)$$

Finally, the efficiency of the calciner (E_{calc}) can be estimated as:

$$E_{calc} = \frac{X_{carb} - X_{calc}}{X_{carb}} = \frac{f_a}{\ln\left[\frac{1}{1 - f_a}\right]} \quad (93)$$

To solve the model an approach similar to the one proposed by Romano[84] needs to be applied. Namely, the value of the C_{CO_2} concentration for which eqn (85) will be satisfied needs to be found in an iterative process.

The calciner semi-predictive model proposed by Martínez *et al.*,[134] has the same level of complexity as the carbonator semi-predictive model by Alonso *et al.*[30] Therefore, these models should be used together to represent CaL performance. The model has the same disadvantages that it does not consider sorbent sulphation and ash accumulation in the system.

4.4.2 Semi-predictive model with two-zone K–L hydrodynamics. As for the carbonator model, Fang *et al.*[135] used experimental data generated by Li *et al.*[181] to develop an apparent kinetic model for the calcination reaction.

$$\frac{dX_{calc}}{dt} = k_{calc}(1 - X_{calc})^{\frac{2}{3}}\left(C_{CO_2,eq} - C_{CO_2}\right) \quad (94)$$

The TGA conducted under 90% CO_2 revealed that conversion during the calcination process is inhibited by both temperature and CO_2 concentration. Therefore, the calcination rate constant (k_{calc}) was given in the Arrhenius equation form with the pre-exponential factor ($k_{0,calc}$) of 23 797 and the activation energy (E_a) of 150 kJ mol^{-1}.

Unlike other calciner models, the model proposed by Fang *et al.*[135] accounted for the reactor hydrodynamics using the same K–L model[179] as presented for the carbonator model. In this model, the calcination rate constant and the fraction of $CaCO_3$ that was not regenerated in the calcination stage are represented as:

$$k_r = k_{calc}(1 - X_{calc})^{\frac{2}{3}}\frac{\rho_{CaCO_3}}{M_{CaCO_3}} \quad (95)$$

$$f_a = (1 - X_{calc})X_{max} \quad (96)$$

The semi-predictive model for the calciner proposed by Fang *et al.*[135] provides an enhanced prediction of process performance over the model by Martínez *et al.*,[134] as it considers the detailed hydrodynamics of the reactor. Moreover, the model takes both the chemically- and diffusion-controlled regions into account. However, no correlation was made with sorbent sulphation and ash accumulation in the system, which appears to be the common issue in the process models reviewed here.

4.4.3 Predictive model with CFD hydrodynamics. Ylätalo *et al.*[150] have adapted the CFB3D model code developed by Myöhänen *et al.*[185] to model a three-dimensional oxy-fired calciner reactor (Fig. 19). The calcination reaction rate is expressed using the kinetic constant provided by Silcox *et al.*[186] and the CO_2 equilibrium pressure by Barin.[187]

$$r_{calc} = 1.22 \cdot \exp\left(-\frac{4026}{T}\right) S_m M_{CaCO_3}\left(p_{CO_2,eq} - p_{CO_2}\right) \quad (97)$$

The model included detailed modelling of sulphation in the calciner using the correlations developed by Myöhänen *et al.*[185] that account for the specific reaction surface area ($S_{m,i}$) of component i.

$$r_{sulf} = 0.001\exp\left(-\frac{2400}{T}\right)\exp\left(-8X_{CaSO_4}\right)C_{SO_2}C_{O_2}S_{m,CaO}M_{CaO} \quad (98)$$

$$r_{dir,sulf} = 0.01\exp\left(-\frac{3031}{T}\right)C_{SO_2}^{0.9}C_{CO_2}^{-0.75}C_{SO_2}^{0.001}S_{m,CaCO_3}M_{CaCO_3} \quad (99)$$

$$r_{de\text{-}sulf} = 0.005\exp\left(-\frac{10\,000}{T}\right)C_{CO}S_{m,CaSO_4}M_{CaSO_4} \quad (100)$$

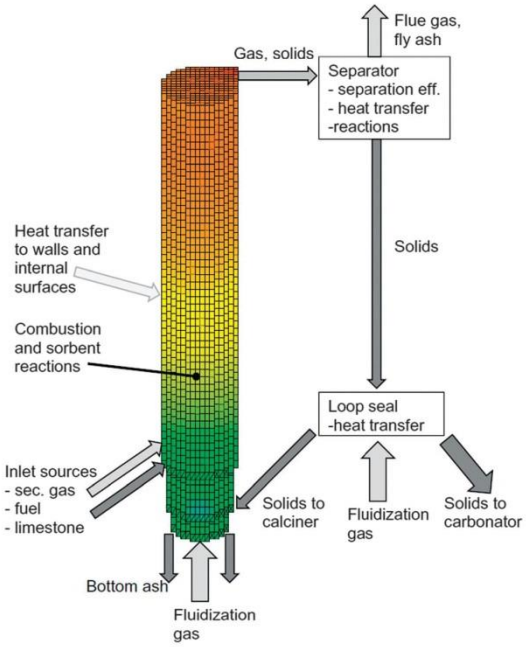

Fig. 19 Three-dimensional CFB calciner model frame (reprinted with permission from Ylätalo *et al.*[150] Copyright 2015 Elsevier).

In contrast to the calciner models presented previously, the CFD model proposed by Ylätalo *et al.*[150] provides detailed information on how sulphation and sorbent properties could affect the calciner performance. Although more demanding computationally, such models will deliver more reliable predictions of calciner operating conditions as they are capable of predicting the temperature and the solids distribution across the reactor. Not only could the CFD models be used to reliably predict and/or optimise performance of the CFB reactor, they can be integrated into the process-wide simulation. Recently, Atsonios *et al.*[188] have proposed to use the CFD model to generate information on CFB hydrodynamics (carbonator and calciner) and CO_2 distribution in the bed (calciner), which is then fed to the carbonator and the calciner kinetic models in the process simulation.

4.5 Summary

The review of the carbonator reactor models undertaken in this section revealed that there are several approaches available in the open literature. However, some of the assumptions or formulations behind these models impose important limitations that may affect the accuracy of their predictions.

The review findings show that five main complexity levels can be distinguished (Fig. 20). Models in the first level are based on first principles, energy and material conservation laws. At an early stage of concept development, which could include uncertainties related to process operating conditions

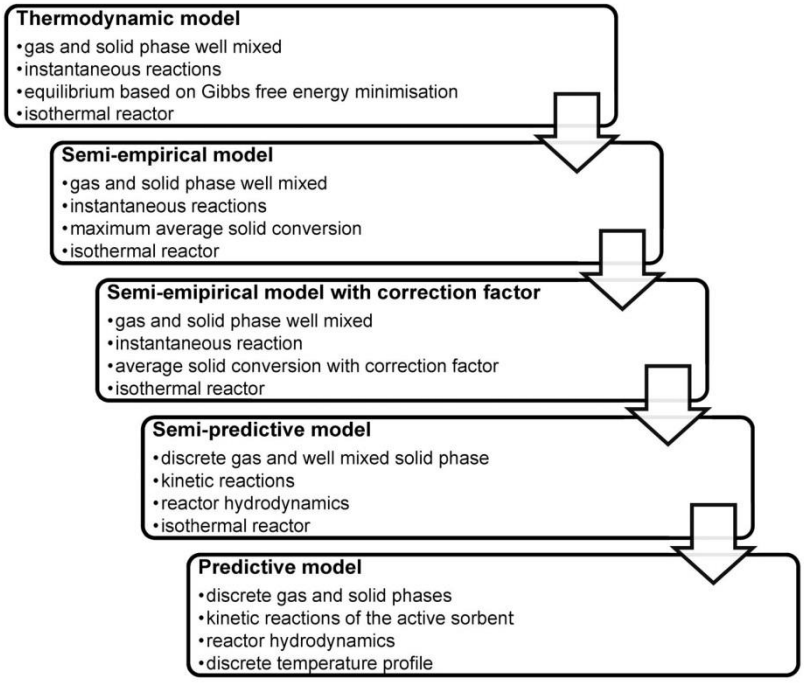

Fig. 20 Different levels of calcium looping model complexity.

and/or sorbent properties, thermodynamic models would perform well and could be used to estimate performance limited by equilibrium. The greatest limitation of such models is lack of correlation to the physical size of the reactor and the assumption of instantaneous reactions. Additionally, in most cases the equilibrium composition in the reactor, hence the sorbent conversion, is based on minimisation of Gibbs' free energy at specified operating conditions and does not depend on what happens upstream of the unit.

The last limitation of the thermodynamic models is partially eliminated in the semi-empirical models, which allow determination of the maximum average sorbent conversion depending on the solid looping rate and fresh sorbent make-up rate, as well as carbonator and calciner performance.[11,39,139] These models, however, assume that the sorbent achieves its maximum average conversion under certain operating conditions, predicting actual reactor performance close to equilibrium performance. Although the results from experimental trials using the 1.7 MW_{th} pilot plant at INCAR-CSIC showed that this assumption is valid for systems operating with high sorbent conversions, which require high fresh sorbent make-up rates, systems operating with low average conversions achieve around 60–90% of equilibrium performance (Fig. 21).

To improve model accuracy, actual average sorbent conversion is determined by applying a correction factor to the maximum average sorbent conversion in the third level models. This factor can be either assumed,[133,146] as presented in Section 5, or calculated based on the actual and average residence times of the sorbent in the reactor.[30,134] The latter approach greatly enhances model prediction as the determined correction factor accounts for the solid inventory and the reaction kinetics in the reactor.

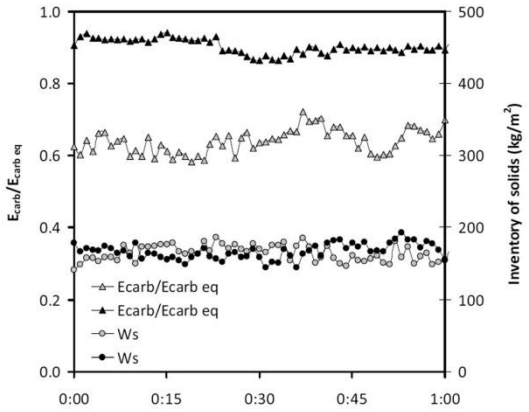

Fig. 21 Comparison of the actual and the equilibrium performance of 1.7 MW_{th} pilot plant at INCAR-CSIC operating at carbonator temperature of 660–690 °C with X_{ave} = 0.11 (grey) and X_{ave} = 0.21 (black) (reprinted with permission from Arias *et al.*[96] Copyright 2015 Elsevier).

The fourth level is achieved through a detailed consideration of reaction kinetics and hydrodynamics in determining the

performance of the reactor. Most of the semi-predictive models developed to predict the performance of the calciner[135] and the carbonator[28,84,135,136] used the hydrodynamic formulations developed by Kunii and Levenspiel,[178,179,182,183] which offer an analytical solution. This approach improves the prediction as the gas concentration depends on the operating conditions and location in the reactor, as well as the sorbent properties. A number of parameters in the K–L model need to be specified, but their values have not been substantiated experimentally and could affect the accuracy of the model.

This, and other assumptions such as isothermal operation and well-mixed solid phase, can be eliminated by applying the predictive models that combine industrial CFD codes with experimentally-determined reaction kinetics to evaluate the reactor[150,189] or the whole CaL plant[188] performance. Such models are the most complex and, therefore, computationally demanding. Although predictive models give the closest representation of the CaL process, they are not applicable at the early stage of concept design because any change in the process design would be followed by a long simulation period required to assess the impact of that change.

In addition to presenting the current approaches for modelling of the CaL processes and identifying their limitations, this review has identified that neither sorbent sulphation nor ash accumulation are widely considered in the models currently developed. The only models accounting for sorbent sulphation were the carbonator model by Romano[84] and the calciner model by Ylätalo *et al.*[150] described in Sections 4.3.3 and 4.4.3, respectively. Although it was claimed by Abanades *et al.*[136] that sorbent sulphation will have a minor effect on carbonation, the experimental analysis by Grasa *et al.*[153] suggests that even a change in the sulphation level of 0.5% in each cycle affects the sorbent decay curve (Fig. 22).

Despite the fact that ash presence in the system would increase the inert solid looping rate and the bed inventory required to achieve a given CO_2 capture efficiency, the effect of ash accumulation in the system was only included in the model by Romano.[84] Moreover, none of the reviewed models account for sorbent attrition and fragmentation, which was identified as another challenge of the CaL process.[13] Therefore, in addition to the sulphation effect on sorbent performance and ash accumulation, loss of sorbent due to attrition and fragmentation should also be considered in the future modelling attempts. This can be done, for example, by implementing the semi-empirical model for sorbent attrition developed by Fennell *et al.*[190] or by adapting the semi-detailed model developed for coal fragmentation by Senneca *et al.*[191]

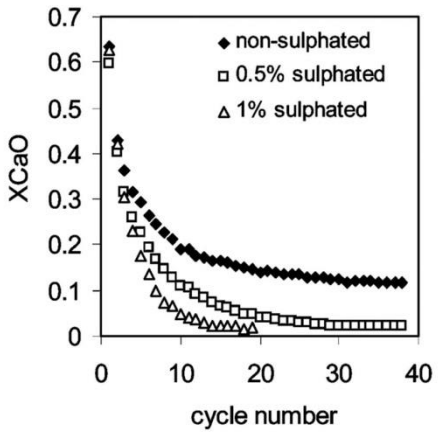

Fig. 22 Decay in the carbonation conversion with the number of carbonation–calcination cycles under different sulphation conversions (reprinted with permission from Grasa *et al.*[153] Copyright 2015 American Chemical Society).

5 Integration of calcium looping to power plants

A key reason for development of computational models for CO_2 capture processes is the ease with which they can be used to analyse retrofit scenarios of existing power plants, or to develop novel concepts for cleaner power generation systems. Models can be a cost-efficient complement to experimental trials of a particular system design under various operating conditions. The greatest advantage of using computational models is the ease of conducting a process-wide analysis for determining optimal overall process performance by indicating the possible integration points.

Since 1999, when the CaL integration was proposed as a viable option for CO_2 capture from CFPPs,[28] a number of studies have investigated different aspects of process integration aiming at improvement of the overall process performance. These included enhancement of process integration through heat exchange network analyses and reduction of CaL process energy requirements through implementation of alternative configurations. The applicability of the CaL process for CO_2 capture from combined cycle power plants was also investigated.

The greatest disadvantage of conventional CO_2 capture systems is a relatively high projected efficiency penalty leading to increased fuel consumption and cost. This section reviews process integration and conceptual studies to quantify efficiency penalties in CFPPs and combined cycle power plants. In addition, the modelling approach for both the power cycle and the CaL process are identified and limitations are analysed to provide a guide for further modelling attempts.

5.1 Conventional coal-fired power plants

5.1.1 Feasibility study for calcium looping for conventional power generation systems. A conceptual study by Shimizu *et al.*[28] analysed the impact of CaL plant integration on a supercritical CFPP. High-pressure steam generated in air-combustion of bituminous coal was used to generate electricity in the primary steam cycle, which operates with gross thermal efficiency of 46.6%$_{HHV}$. Flue gas was treated in the CaL plant with the carbonator operating at 650 °C and the calciner operating at 950 °C with 100% efficiency. The performance of the carbonation process was predicted using the carbonator model described in Section 4.3.2.

With a Ca : C ratio of 8.29, which is slightly smaller than values reported in the pilot-plant tests, and average conversion of 11%, CO_2 capture of 83% was reached in the carbonator, leading to an overall CO_2 capture level of 90.4%. The waste heat in the CaL plant was recovered to produce superheated and reheated steam at subcritical conditions of 172.25 bar/566 °C and 30.4 bar/538 °C, respectively. The gross thermal efficiency of the secondary steam cycle was assumed to be 42.6%$_{HHV}$. With the gross and net power outputs of the integrated system of 1000 MW_{el} and 817 MW_{el}, respectively, the net efficiency was estimated to be 33.4%$_{HHV}$. This was 1.4% points higher than for an oxy-fired combustor with a primary steam cycle of the same gross power output and thus indicated feasibility of the CaL process for reducing CO_2 emissions from the CFPPs.

Unfortunately, Shimizu *et al.*[28] provided no benchmark to the reference CFPP without CO_2 capture plant, which would provide insight into how the retrofit affected the overall performance of the system. Also, sorbent decay was ignored as only four carbonation–calcination cycles were considered in determining sorbent conversion. Furthermore, the performance of both steam cycles was assumed rather than estimated using thermodynamic calculation or process simulation. Although this assumption could be valid for a CFPP operating at a fixed load, it does not allow prediction of part-load operation without knowledge of the gross efficiency correlation. Additionally, by assuming the gross thermal efficiency, the analysis did not account for the power consumption of the CFPP auxiliary equipment, with only ASU and CO_2 compression unit (CCU) considered in estimation of the net thermal efficiency. The power requirements for the CFPP and the CaL plant auxiliary equipment need to be considered to improve the prediction reliability and avoid over-estimating the net thermal efficiency of the integrated system.

5.1.2 Heat integration with the primary and secondary steam cycle. High-temperature operation of the CaL process allows recovering high-grade heat to produce an additional amount of steam. Therefore, there are two options for integrating the CaL process with the existing CFPPs: steam can be utilised either in the primary steam cycle with the assumption that the steam generation rate in the boiler is reduced and the gross power output of the integrated system kept constant, or in the secondary steam cycle leading to higher gross power output. Yang *et al.*[16] investigated both integration options. In the first case, the CaL plant was integrated with the primary steam cycle of an existing 600 MW_{el} CFPP operating with net thermal efficiency of 40.6%$_{LHV}$. Performance of a carbonator operated at 650 °C was represented using the correlation by Abanades *et al.*,[145] with a maximum conversion of 20% to reach 85% CO_2 capture level at Ca : C ratio of 5. It needs to be highlighted that compared to the Ca : C values reported in the pilot-plant tests reviewed in Section 3, the assumed Ca : C ratio is 1.5–3 times lower. This would cause underestimation of the solid looping rate and thus, heat requirement in the calciner. In this study, the calciner was operated at 900 °C and heat for sorbent regeneration was provided through oxy-combustion of coal. The parasitic load stemmed only from the ASU power requirement as no CCU was considered.

Yang *et al.*[16] first proposed using heat in the CaL system to substitute the feedwater heating train in the primary steam cycle. Although this is a valid approach for integrated systems, which has been often proposed for integration of amine-based CO_2 capture plants,[60,73,192–194] its applicability to existing CFPPs could be limited by the swallowing capacity of the steam turbines and/or the electric generator. Moreover, the suggestion by Yang *et al.*[16] that these extractions reduce the thermal efficiency of CFPPs is invalid from the thermodynamic point of view, as they increase the average temperature of heat addition in the boiler leading to an increase in thermal efficiency.[195] Yet, the indicated power output increase of 148.8 MW_{el} and increase in the net thermal efficiency from 19.4%$_{LHV}$ to 25.3%$_{LHV}$, which stems from a higher degree of waste heat utilisation in the integrated system leading to minimisation of steam extractions, could not be achievable in reality due to operational limitations of the existing system. In another integration option, part of the boiler heat load was replaced by heat load from the CaL plant. The boiler in the CaL plant can provide 43.1% of the heat required by the system to operate with gross power output of 600 MW_{el} and net thermal efficiency of 34.1%$_{LHV}$. However, a further study on how such off-design operation conditions would affect the boiler performance needs to be conducted. Furthermore, in evaluating other integration options, the highest net thermal efficiency of 36.8%$_{LHV}$ and gross power output of 1000 MW_{el} were reached when the waste heat from the CaL plant was utilised to generate high-pressure steam to drive the secondary steam cycle. This result revealed that implementation of a secondary steam cycle and its integration with the CaL plant provides superior performance compared to the other CFPP integration options. This is also beneficial in terms of long-term revenue and meeting market demand. However, the estimated minimum net efficiency penalty of 3.8% points (excluding power requirement for CO_2 compression) may not be a representative result, due to low Ca : C ratio assumed in the carbonator.

In addition to evaluating different integration options, the effect of CaL integration to CFPPs operating with different steam conditions was investigated. Martínez *et al.*[83] analysed integration of a CaL plant to an existing 350 MW_{el} subcritical CFPP with net efficiency of 36%$_{LHV}$. The flue gas leaving the boiler, which contained 14.5%$_{vol}$ CO_2, was desulphurised and then entered the CaL plant at typical stack conditions (1.16 bar/180 °C). Performance of the carbonator, which was operated at 650 °C, was represented using the model proposed by Alonso *et al.*[30] described in Section 4.3.1 with the kinetic expression proposed by Grasa *et al.*[196] The sorbent was regenerated in the calciner operating at 950 °C and complete calcination was assumed. The temperature in the calciner was maintained through oxy-combustion of South African coal. Even though this coal contains a relatively small amount of sulphur and the flue gas was desulphurised, an additional amount of $CaCO_3$ (F_{Ca}/F_S = 3) was provided with the make-up stream to account for sorbent sulphation losses. Moreover, part of the captured CO_2 was recycled to maintain the O_2 concentration in the oxidizing gas at 25%$_{mol}$.

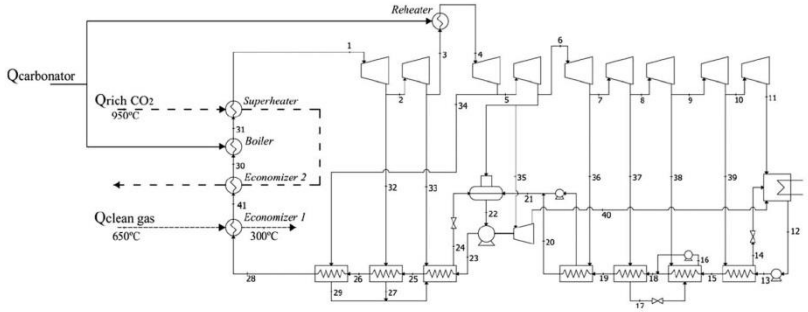

Fig. 23 Reference integration configuration for the CaL plant and supercritical steam cycle (reprinted with permission from Martínez *et al.*[83] Copyright 2015 John Wiley and Sons).

Heat in the carbonator, the clean gas stream and the CO_2 stream was used to generate steam to run the secondary steam cycle (Fig. 23), the gross thermal efficiency of which was assumed to be $45\%_{LHV}$. After deducting the auxiliary power consumption of the plant, the net thermal efficiency was $36\%_{LHV}$. By adjusting the solid circulation rate, the CO_2 capture level in the carbonator was maintained at 70–90%, leading to maximum net thermal efficiency of $33.1\%_{LHV}$–$33.4\%_{LHV}$. Although an increase in the CO_2 capture level required higher solid circulation rates, the increase in steam generation exceeded the increased heat requirement in the calciner leading to a rise in net thermal efficiency. The make-up rate was found to be a critical parameter as its increase led to reduction in net thermal efficiency, since more heat was required for fresh sorbent preheating. However, operation at low make-up rates would result in low conversion of the sorbent and thus high circulation rates requiring a larger reactor. Nevertheless, the viability of a CaL plant for subcritical CFPPs, for which the projected efficiency penalties ranged between 8.3% and 10.3% points, has been confirmed. Interestingly, if part of the spent sorbent was utilised in the cement plant as raw material, the amount of energy required for sorbent calcination was not accounted for in the net thermal efficiency calculation, leading to efficiency penalties between 7.5% and 9% points. The study clearly showed that this retrofit would be beneficial for the existing fleet of subcritical power plants, increasing their life span and environmental performance without a drastic net thermal efficiency drop, as is the case for conventional CO_2 capture plants. Nevertheless, performance of the steam cycle, ASU and CCU is determined based on assumed performance indicators that may not be valid for part-load operation. Also, Martínez *et al.*[37] benchmarked the performance of the integrated system against a hypothetical system rather than an existing power plant, which results in misleading conclusions regarding the projected efficiency penalty imposed on the retrofitted system. The performance of an integrated system should be benchmarked against the performance of an existing system to identify the net effect of the CaL plant integration.

Romeo *et al.*[86] have investigated the integration of a secondary supercritical steam cycle (280 bar/600 °C/600 °C) with a CaL plant retrofitted to an existing 450 MW_{el} supercritical CFPP. In the CaL plant design, the temperatures in the carbonator and the calciner were kept at 650 °C and 875 °C, respectively. The performance of the system was represented by assuming 5% purge leading to average sorbent conversion of about 20%. Heat for sorbent recovery was added through combustion of low-sulphur high-rank coal in pure O_2-stream produced in the ASU with specific power of 220 kW h per t-O_2. Romeo *et al.*[86] claimed that no CO_2 recirculation was needed to control the temperature in the calciner because of the large solid inflow at 650 °C and the endothermic character of the calcination reaction. Despite the fact that the pure O_2 stream will be diluted by CO_2 liberated in the calcination reaction, the local temperature of coal particles can be higher than the average bed temperature due to their combustion in a high-O_2-concentration environment.[197,198] Such high temperatures can lead to local hot spots in the calciner on contact of the coal and sorbent particles and cause enhanced sintering and, thus deactivation of the sorbent.[199]

Analysing the CaL process, Romeo *et al.*[86] have proposed an integration configuration comprising five heat integration zones, in which waste heat from the carbonator, CO_2 stream, clean gas stream and purge stream were utilised to generate live and reheated steam, as well as to preheat the feedwater. The secondary supercritical steam cycle driven by heat recovered in the CaL plant generated an additional 193.6 MW_{el} of net power output with net efficiency of $26.7\%_{LHV}$. Although this increased the net power output of the integrated system by 45.3%, the net thermal efficiency dropped by 7.9% points, from $44.9\%_{LHV}$ for the reference CFPP to $37.0\%_{LHV}$ for the integrated system.

Further improvement of the integrated system efficiency can be reached through development of integration schemes characterised with higher heat utilisation levels using a systematic HEN analysis, which is commonly applied in different industries. Such analysis has been used by Lara *et al.*[200,201] to design the heat recovery system for waste heat recovery from the CaL plant, which captures CO_2 from a 500 MW_{el} CFPP with net thermal efficiency of $38.2\%_{LHV}$, to generate steam to drive the secondary steam cycle (290 bar/600 °C/620 °C). Unfortunately, no information was provided on the assumptions made to assess the performance of the carbonator and the calciner.

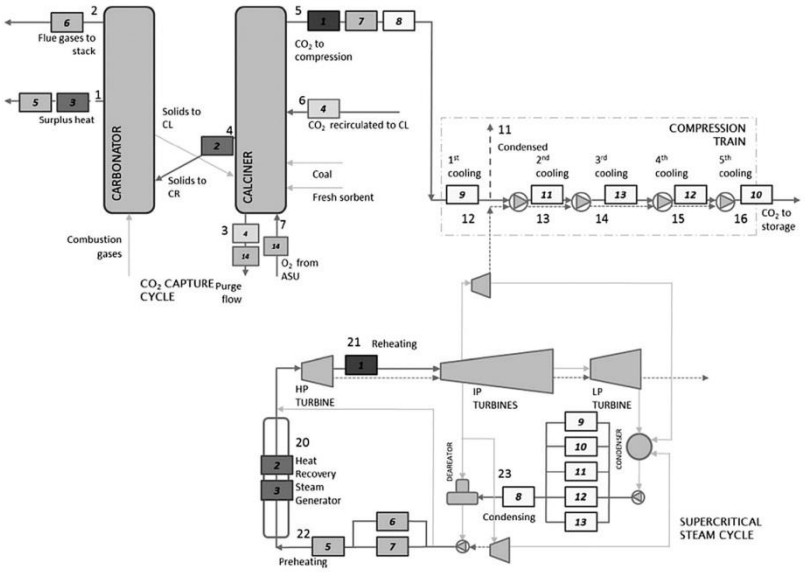

Fig. 24 Economically favourable heat exchanger network design for CaL integration (reprinted with permission from Lara *et al.*[200] Copyright 2015 Elsevier).

Among different HEN configurations proposed, the economically favoured configuration was reached when the streams were matched in such a way that they were exhausted in a single heat exchanger (Fig. 24). This configuration resulted in a net thermal efficiency increase of 0.2% points[201] and 1.2% points.[200]

In contrast to most previous studies, Vorrias *et al.*[132] have investigated integration of a CaL plant to a lignite-fired power plant (235.4 bar/540 °C/540 °C) that delivers 330 MW_{el} of gross power output with net thermal efficiency of 39.1%$_{LHV}$. In this study the conventional CaL plant configuration, which comprises the carbonator and the calciner reactors interconnected with solid lines and operating at 650 °C and 900 °C, respectively, was used. Having assumed that the carbonation reaction reached chemical equilibrium, sorbent conversion in the carbonator was represented using the maximum average conversion model by Abanades *et al.*[39] without the correction factor. The performance of the calciner was represented using the chemical and phase equilibrium through the Gibbs' free energy minimization at a given temperature. Also, the heat for sorbent regeneration is provided through oxy-combustion of lignite in an oxidizing medium containing 80%$_{vol}$ O_2. Although Vorrias *et al.*[132] claimed that this concentration was sufficient to avoid hot spots in the calciner that would increase the sorbent sintering rate, experimental and other modelling trials[33,98,100,104,133] suggested that the O_2 concentration should be below 50%$_{vol}$ to avoid hot-spots in the reactor and thus excessive degradation of the sorbent performance.

Further, to utilise high-grade heat to generate additional steam to run the secondary supercritical steam cycle (235.4 bar/540 °C/540 °C), Vorrias *et al.*[132] proposed to integrate two systems for increased heat utilisation in the CaL plant. The first is a solid recirculation heat exchanger which is proposed to be a set of concentric L-valves as illustrated in Fig. 25a. It is assumed that the system performs as a co-current heat exchanger with a temperature approach of 10 °C. However, the performance of such a system at a large scale has not yet been demonstrated. Moreover, as lignite consists of a considerable amount of moisture (36.8%$_{wt}$), oxy-combustion performance would be affected. Therefore, the second system, a BFB lignite dryer (Fig. 25b) which uses recompressed water vapour as a fluidising medium, was proposed to reduce the moisture content in lignite to 12%$_{wt}$, comparable to the average moisture content of hard coal.[202]

Analysis of the overall process performance revealed that the net thermal efficiency of the integrated system reached 34.1%$_{LHV}$ if both the solid–solid heat exchanger and the BFB lignite dryer were implemented. This falls to 34.0%$_{LHV}$ and 32.5%$_{LHV}$, respectively, if only the first or second system is implemented. Nevertheless, the net projected efficiency penalty imposed on integration of the CaL plant reached the lowest value of 5.0% points, which is considerably lower than in previous studies. It is not known if such improvement results from implementing the proposed systems or using no correction factor to determine the actual average sorbent conversion and high O_2 concentration in the oxidising medium. The net projected efficiency penalty due to CaL plant integration was found to be 2.9% points lower than for a corresponding MEA plant, but only 0.9% points lower for an oxy-fuel lignite-fired power plant.

5.1.3 Alternative configurations for efficiency improvement. Although most studies of the CaL process focus on the conventional process configuration proposed by Shimizu,[28] other configurations, which aim to improve the overall process efficiency mainly through reduction of the O_2 requirement, were proposed by Abanades *et al.*[39] and Martínez *et al.*[133]

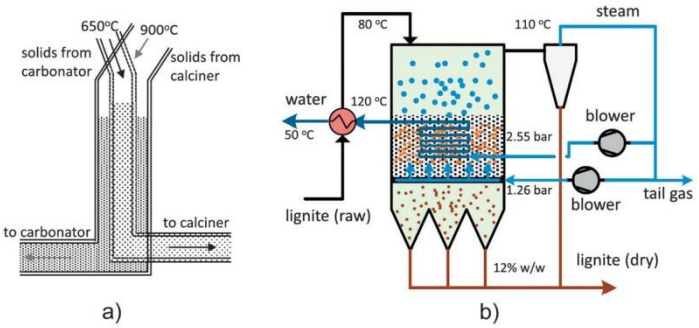

Fig. 25 Design of (a) solid–solid heat exchanger and (b) lignite bubbling fluidised bed dryer (reprinted with permission from Vorrias *et al.*[132] Copyright 2015 Elsevier).

In the first study proposing alternative configurations for efficiency improvement, Abanades *et al.*[39] investigated integration of a 100 MW_{el} supercritical CFPP with an assumed net thermal efficiency of $46\%_{LHV}$. In the basic configuration, the flue gas was treated in the carbonator operated at 650 °C, the performance of which is modelled using eqn (8) and (9). A complete sorbent regeneration was conducted at 950 °C using oxy-combustion of coal. In addition, the overall CO_2 capture level was assumed to be 90% and the captured CO_2 was compressed to 100 bar prior to being transported. Considering the power requirement to run the CCU and the ASU, the efficiency of the integrated system dropped by 7.2% points, to 38.8%.

As the efficiency penalty in the CaL process stems mainly from the O_2 production for oxy-fuel combustion in the calciner, Abanades *et al.*[39] have proposed an alternative calciner design in which the heat for the sorbent regeneration is supplied through the metallic walls from an external source (Fig. 26). Their study assumed that the heat source is a fluidised bed combustor fuelled with an air and fuel mixture that operates at 1050 °C. Steam is used as a fluidising medium in the calciner operated at 850 °C, leading to a CO_2 partial pressure of 0.4 bar. Although this configuration would be characterised by higher thermal efficiency and no requirement for O_2 production, it would require materials that have not yet been tested in practice. Also, a close integration of the combustor and the calciner is required, as a considerable heat transfer area of 800 m^2 is required. Despite the engineering challenges, this configuration was reported to have a net thermal efficiency of 39.4%, resulting in a projected efficiency penalty of 6.6% points. This is 1.6% points less than for the basic configuration.

To avoid application of untested materials, Abanades *et al.*[39] proposed that the heat requirement of the calcination reaction could be satisfied using a solid heat carrier (Fig. 27). In this configuration, CO_2 partial pressure of 0.4 bar, which is required to lower the calcination temperature to 850 °C, is achieved through utilisation of a vacuum. The process involves a common

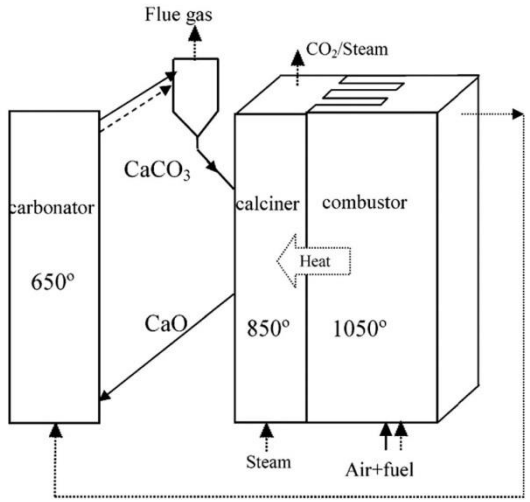

Fig. 26 Heat transfer-integrated calciner and combustor (reprinted with permission from Abanades *et al.*[39] Copyright 2015 American Chemical Society).

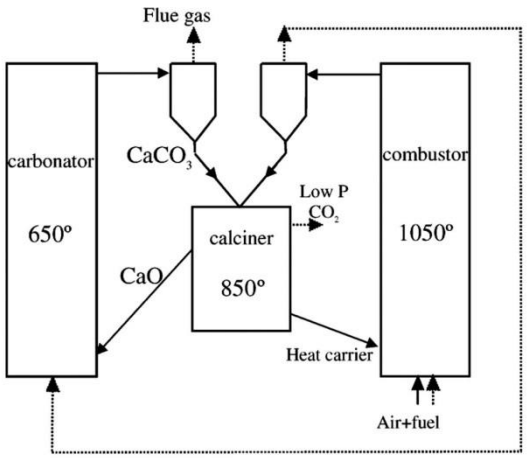

Fig. 27 Indirect heat transfer from combustor to the calciner (reprinted with permission from Abanades *et al.*[39] Copyright 2015 American Chemical Society).

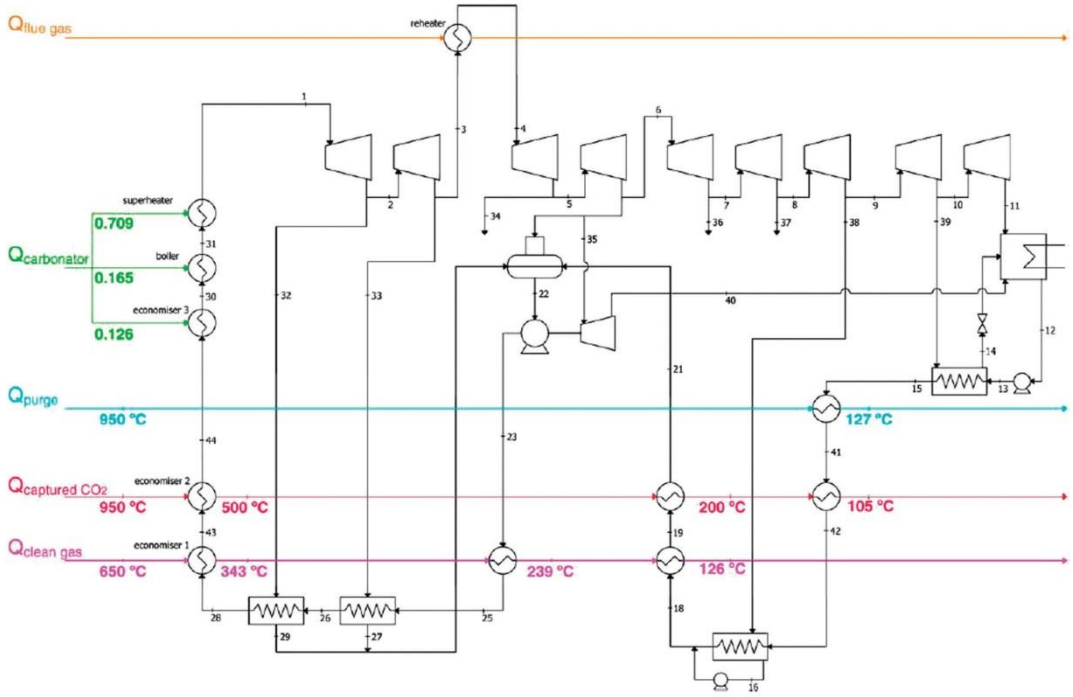

Fig. 28 Heat integration of the three-fluidised-bed combustion system with CaL CO_2 capture with the supercritical steam cycle (reprinted with permission from Martínez *et al.*[148] Copyright 2015 Elsevier).

CFB combustor that is fired with an air and fuel mixture. The solid bed material, which is a dense material, such as Al_2O_3 or deteriorated CaO, is heated in the combustor, separated from the combustion gas stream and finally fed to the calciner. However, as this configuration assumes that the heat carrier particles would be mixed with the CO_2 sorbent in the calciner, it is still not clear whether a continuous separation of these particles based on differences in their densities would be possible at the required scale. Nevertheless, this configuration offers net thermal efficiency of 40.0%$_{LHV}$, which is 2.2% points over the basic CaL configuration.

This configuration was also investigated by Martínez *et al.*[148] who studied its integration with the supercritical steam cycle (600 °C/280 bar). The coal combustion took place at 1030 °C, with 15%$_{vol}$ of excess air that entered the combustor at 400 °C. The energy input to the system through the coal combustion was assumed to be 1 GW_{th}. The flue gas, which contained 15.7%$_{vol}$ CO_2, was used to reheat the steam in the steam cycle and to preheat the combustion air, and eventually entered the carbonator at 380 °C. The carbonator, which operated at 650 °C, was modelled using the carbonator model developed by Alonso *et al.*[30] with the kinetic model for the multiple reaction cycles by Grasa *et al.*[196] Under given operating conditions, the CO_2 capture efficiency in the carbonator was estimated to be 89%. Again, a complete calcination process took place in the calciner operated at 950 °C, which corresponds to partial pressure of 1.93 bar. Heat for the sorbent regeneration came from the solid stream heated in the combustor. The pressure of the separated CO_2 was increased to 150 bar in the CCU comprising the five-stage compressor and the pump, and then it was cooled to 40 °C.

Martínez *et al.*[148] have identified five possible heat sources in the analysed CaL plant, which were heat released in the carbonator and heat carried with the clean gas, purge, flue gas and CO_2 process streams. Having integrated these sources as illustrated in Fig. 28 and considering the power requirement for CO_2 compression, the net power output of 378 MW_{el}, corresponding to net thermal efficiency of 37.8%, was obtained. This was 4.3% points higher than a comparable oxy-fired CFPP.

More recently, Martínez *et al.*[133] have proposed several process configurations that aim to reduce the efficiency penalty in a CaL plant integrated to a 500 MW_{el} CFPP of gross thermal efficiency of 44.4%$_{LHV}$. The temperature in the carbonator and calciner were set at 650 °C and 930 °C. The performance of the carbonator was represented by the maximum average conversion of the sorbent determined using the expression proposed by Abanades[145] and Grasa *et al.*,[171] and a correction factor of 0.8 to estimate the actual average conversion. Complete calcination was assumed in the calciner. As heat for sorbent regeneration was provided through oxy-combustion of coal, O_2 was produced in the ASU, which was characterised with specific power consumption of 220 kW h per t-O_2. Recirculated CO_2 amounted to 40% of the inlet gas to control the temperature in the calciner.

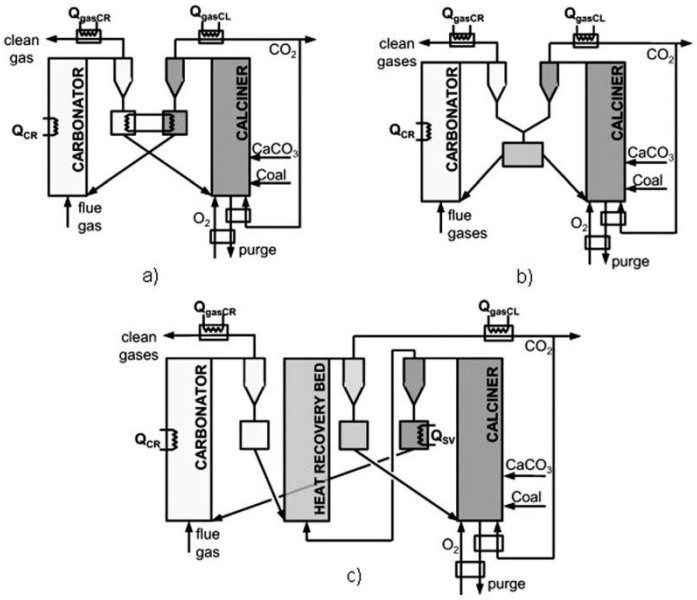

Fig. 29 Alternative calcium looping process configurations including: (a) seal valve indirect heat exchanger, (b) mixing seal valve and (c) heat recovery fluidised bed (adapted with permission from Martinez *et al.*[133] Copyright 2015 Elsevier).

The first configuration (Fig. 29a) assumes that heat is transferred from the solids leaving the calciner to the solids leaving the carbonator by means of an indirect heat exchanger integrated with the seal valves of the reactors. It is assumed that the solids leave both seal valves at the same temperature. However, this is not achievable in practice as there is no developed technology to carry out this process. To overcome this engineering challenge, Martínez *et al.*[133] proposed using a single mixing seal valve for both reactors (Fig. 29b). Although in this configuration solids can directly exchange heat, the fraction of the active CaO entering the carbonator is reduced due to solid mixing. In the last configuration, the sensible heat of the CO_2 stream leaving the calciner is recovered to preheat the solid particles from the carbonator in an additional heat recovery fluidised bed (Fig. 29c). Although the flue gas acts as a fluidising medium and mixes with the partially carbonated sorbent particles, no carbonation reaction could occur in the heat recovery bed. This is because the fast carbonation reaction cannot proceed, as the active CaO was trapped in the core of each solid particle, the surface of which has been covered with the $CaCO_3$ layer formed in the carbonator.[203] Although in this configuration the heat required by the calcination process is satisfied through oxy-fuel combustion, it is expected to increase the thermal efficiency of the CaL process by 1.4% points with a subsequent reduction in fuel consumption of 9%.

Another configuration proposed by Martínez *et al.*[204] utilises a multi-step cyclonic preheater, which is similar to the ones used in the cement industry (Fig. 30). In this additional piece of equipment heat available in the CO_2 stream leaving the calciner is utilised to preheat solids leaving the carbonator to around 725 °C prior to entering the calciner. The temperature in the carbonator and calciner were set at 650 °C and 950 °C. The performance of the carbonator and the calciner were represented by the Charitos *et al.*[149] (Section 4.3.1) and Martínez *et al.*[134] (Section 4.4.1) models, respectively. Although implementation of the cyclonic preheater has not changed the energetic efficiency of the integrated system, it reduced the energy requirement of the calciner. This was shown in reduction of the coal consumption by up to 13.3% and the oxygen consumption by 13.6%.

Finally, following the successful demonstration of the sub-pilot facility described in Section 3.5, Wang *et al.*[26,32] have investigated a CFPP retrofit with the CaL plant involving a sorbent regeneration stage through hydration (Fig. 31). Compared to the conventional CaL process, the proposed CCR process comprises an additional reactor which aims to improve conversion of the sorbent.

The performance of the calciner and hydrator reactors was computed based on the assumption that the systems reach equilibrium state at 1000 °C and 500 °C, respectively. In the conventional CaL process, a high calcination temperature would cause an excessive sintering of the sorbent leading to a reduction in the sorbent carrying capacity.[13] This is not the case in the CCR process as the sorbent is reactivated on contact with steam in the hydrator. Probably the lack of CO_2 recirculation to control the O_2 concentration in the calciner was also due to the sorbent regeneration potential of the CCR process. Furthermore, in the experimental campaign using the sub-pilot CCR plant the CO_2 capture level of 90% in the carbonator was achieved at a Ca : C of 1.3. In the carbonator model used by Wang *et al.*,[26,32] a Ca : C ratio of 1.4 was used to determine the

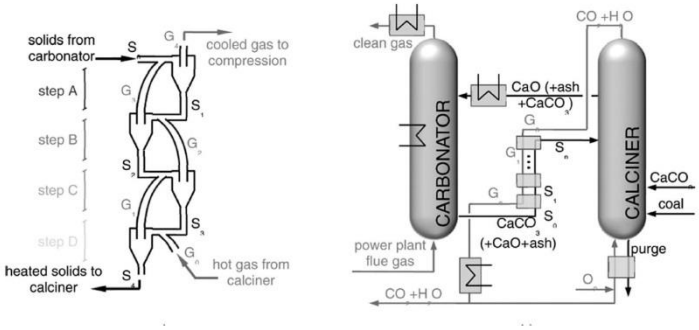

Fig. 30 Improvement of the calcium looping process performance through implementation of the cyclonic preheater (reprinted with permission from Martínez *et al.*[204] Copyright 2015 American Chemical Society).

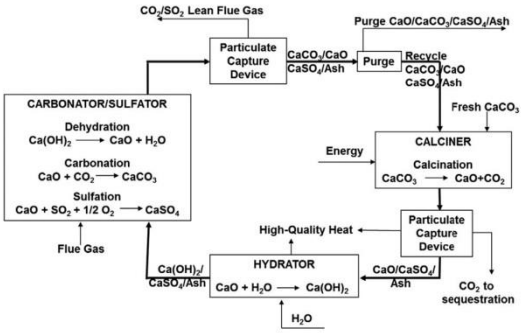

Fig. 31 Conceptual design of hydrated calcium looping process (reprinted with permission from Wang *et al.*[32] Copyright 2015 Elsevier).

solid looping rate required to capture 90% of CO_2 and 100% of SO_2 at 625 °C.

Wang *et al.*[32] have analysed integration of the CCR process into the 561 MW_{el} subcritical CFPP operating with an assumed net thermal efficiency of 33.5%$_{HHV}$. As mentioned above, although this approach works relatively well at full-load operation, any deviation from this point would reduce the prediction accuracy. Waste heat from the CCR process was used to generate high-quality steam that is sent to the primary cycles and replaced part of the steam generated in the power boiler. This means that the existing boiler would need to operate in part-load mode. Analysing the integration impact on the overall process efficiency, they have found that a maximum net efficiency of 26.9%$_{HHV}$ was reached if the calciner was indirectly heated using the flue gas from the combustion process. On the other hand, when the calciner was directly heated through oxy-combustion of coal or natural gas, the net efficiency decreased to 26.5%$_{HHV}$ and 26.1%$_{HHV}$, respectively. Such values for net thermal efficiency are considerably lower than in previous integration analyses reviewed. The main reason behind this is low net thermal efficiency of the reference power plant. The maximum projected efficiency penalty was estimated to be 7.4% points, which is considerably less than the 9–12% points estimated for amine-based or oxy-combustion systems. Furthermore, Wang *et al.*[26] have shown that the projected efficiency penalty for the CCR process is 22.2% lower than for a traditional CaL process. As the latter process operates on higher average conversions, this reduction can be associated with reduction of the solid looping rates between the reactors, which leads to a decrease in the heat requirement in the calciner.

5.1.4 Comparison between the average conversion and semi-predictive calcium looping model. A review of the integration and process improvement studies revealed that different models have been used to represent the carbonator performance, with the average conversion and semi-predictive models being most commonly applied. On the other hand the calciner performance has been represented using an equilibrium-based model in all studies reviewed. Therefore, it is important to highlight the impact of the carbonator model selection on the prediction of the integrated process performance.

Ströhle *et al.*[147] and Lasheras *et al.*[31] have analysed integration of a CaL plant to a 1000 MW_{el} ultra-supercritical CFPP (285 bar/600 °C/620 °C), which had a net thermal efficiency of 45.6%, with the aim of optimising overall process performance They assumed that a conventional CaL plant configuration was retrofitted to the existing FGD plant, thus the sulphation effect was kept to a minimum. Waste heat from the CaL plant was used to generate additional steam for the secondary steam cycle with an assumed net thermal efficiency of 49.98%. The performance of the calciner, operated at 900 °C, was determined using a Gibbs reactor and the heat for sorbent regeneration was provided through oxy-combustion of coal (w_{ASU} = 184 kW h per t-O_2). The carbonator was operated at 650 °C with an assumed pressure drop of 100–200 mbar and SO_2 conversion of 99% due to the large Ca/S ratio.

Ströhle *et al.*[147] have compared two commonly applied approaches for carbonator modelling, the maximum average conversion of sorbent model by Abanades *et al.*[39] and the 1D carbonator model by Abanades *et al.*[136] and evaluated the differences between these approaches in terms of overall process performance. Assuming a CO_2 capture level in the carbonator of 80%, application of the maximum average conversion model led to underestimation of the O_2 input to the calciner,

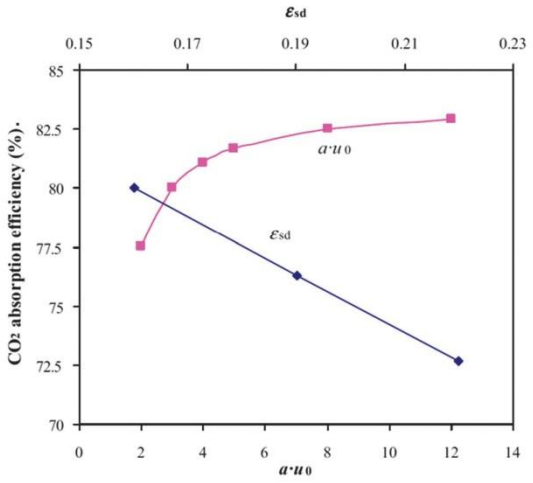

Fig. 32 Effect of KL CFB model uncertainty on the CO_2 capture level in the carbonator (reprinted with permission from Lasheras *et al.*[31] Copyright 2015 Elsevier).

solid looping rates and heat available for steam generation. However, in contrast to studies by Martínez *et al.*[133] and Berstad *et al.*,[146] no correction was made to the maximum average conversion to determine the actual average conversion of the sorbent. Nevertheless, net thermal efficiencies were estimated to be 42.9% and 42.4% for the maximum average conversion and the predictive 1D carbonator model, respectively. It can be concluded, therefore, that application of the maximum average conversion model with a reasonable correction factor would give a reasonable prediction of the overall process performance.

In a study by Lasheras *et al.*,[31] the effect of the uncertainty in the K–L CFB model, which requires specification of the decay constant (a) and the solid fraction in the dense region (ε_d), on the overall process performance was assessed. The analysis revealed that variation in the key input parameters led to 10% variation of the CO_2 capture level in the carbonator (Fig. 32). This indicates that further experimental studies are required to identify the K–L model parameters.

5.2 Combined cycle power plants

5.2.1 Feasibility of calcium looping process for natural gas-fired power plants. Conversely to previous studies that analysed integration of a CaL plant to a CFPP, Berstad *et al.*[146] have analysed the applicability of this CO_2 capture technology to decarbonise a natural gas combined-cycle power plant (NGCC). The reference NGCC delivers 416.4 MW_{el} with net thermal efficiency of 52.6%$_{HHV}$. To account for the gas pressure losses in the carbonator, the gas turbine discharge pressure was increased by 0.02 bar, resulting in a discharge temperature of 611 °C. Such a temperature makes it more feasible to retrofit the CaL plant right after the gas turbine island (Fig. 33).

CO_2 capture from NGCCs is more difficult than from CFPPs, as the CO_2 concentration in the flue gas is approximately 4%$_{vol}$. Therefore, to achieve a CO_2 capture level between 85% and 86% in the carbonator, its operating temperature needs to be 600 °C. To represent the performance of the carbonator, the maximum average conversion model proposed by Rodríguez *et al.*[11,40] was used. As the actual carbonation conversion (X_{carb}) is usually lower than the maximum value, a correction factor of 0.75, expressed as the X_{carb}/X_{ave} ratio, was adapted to enhance the accuracy of the model prediction. Such a conservative assumption is in agreement with the experimental results as presented in Section 3. To reach the actual carbonation conversion of 0.2, a F_0/F_{CaO} ratio of 0.06 was used. The sorbent is regenerated in the calciner, which is modelled as an equilibrium reactor with a calcination efficiency of 100%. A temperature of 950 °C is maintained in the calciner by means of oxy-combustion of

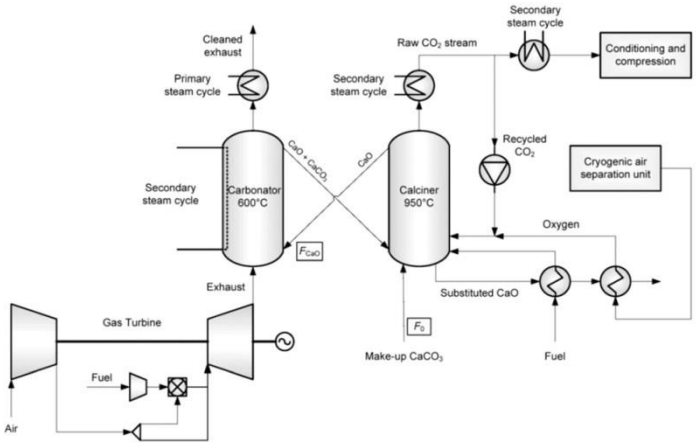

Fig. 33 Conceptual design of integration of calcium looping plant to natural gas combined cycle power plant (reprinted with permission from Berstad *et al.*[146] Copyright 2015 Elsevier).

natural gas. The $95\%_{mol}$-purity O_2 stream is produced in the cryogenic ASU and mixed with the recycled CO_2 to maintain $25\%_{mol}$ O_2 concentration in the oxidising gas. The pressure drop in the calciner is accounted for through an increase of the recycled CO_2 pressure of 0.03 bar. The remaining CO_2 is directed to the CCU, which is modelled as four compression stages and one pumping stage with intercooling to 28 °C, where it is compressed to 150 bar before being transported.

The waste heat from the CaL plant was utilised to generate an additional amount of steam that was then used to drive the secondary steam cycle. As the solids transported from the calciner to the carbonator carry a considerable amount of energy, the effect of the heat recuperation between the solid streams on the energy requirement in the calciner was investigated. Overall, three options for steam conditions (120 bar/560 °C/560 °C, 120 bar/610 °C/610 °C and 202 bar/610 °C/610 °C) were analysed for two CaL process configurations (with and without solid–solid heat recuperation). The study revealed that in the best case scenario, where solid–solid heat recuperation was implemented and the HP steam was generated at 610 °C and 202 bar, the projected efficiency penalty amounted to 9.1% points. This was found to be 1.3% points higher than for the reference NGCC with a conventional MEA CO_2 capture plant. Therefore, a CaL plant may not be a preferable option for NGCCs, which can be attributed to low CO_2 concentration in flue gas that results in lower driving force for the carbonation reaction. In turn, to reach the desired CO_2 capture level, the carbonator operating temperature needed to be lowered to 600 °C. The primary steam cycle location upstream of the CaL plant contributed to the efficiency penalty as less flue gas was fed to the primary waste heat steam generator. A possible solution for both issues was presented by Biliyok and Yeung[205] who showed that exhaust gas recirculation and/or supplementary firing could increase the flue gas temperature, flow rate and CO_2 concentration. However, feasibility of this solution is doubtful as it would further increase the capital cost by 20%, while reducing the levelised cost of electricity by only 6%.

5.2.2 High-reliability and high-efficiency coal-gasification power generation systems. The need for high-efficiency and environmentally friendly fossil-fuel power generation systems led to development of IGCC as an alternative to CFPPs. Kunze *et al.*[131] considered the reference 510 MW_{el} IGCC plant having net thermal efficiency of $39.4\%_{LHV}$, in which coal is gasified in the O_2-rich environment. Produced syngas is then cleaned to remove impurities, such as metals, sulphur and nitrogen compounds, and CO is converted to CO_2 in the water–gas shift reaction, which is then removed through a pre-combustion system using acid gas removal (AGR) based on an amine (MDEA) process. Finally, the purified syngas, which at this stage consists mostly of H_2, is combusted in a gas turbine coupled with an electric generator. The waste heat from the discharge gas is used to generate high-pressure steam at 170 bar, which then generates electricity in the bottoming steam cycle.

Kunze *et al.*[131] have proposed substituting a pre-combustion AGR system with a post-combustion CaL plant (Fig. 34). The carbonator was modelled as a stoichiometric reactor with conversion of 20% and operating temperature of 650 °C. The

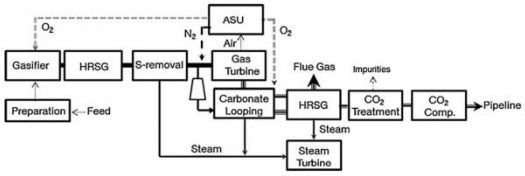

Fig. 34 Conceptual design of integration of calcium looping plant to IGCC (reprinted with permission from Kunze *et al.*[131] Copyright 2015 Elsevier).

desired CO_2 capture level in the carbonator of 90% was assured through adjusting the solids looping rate in the system. In contrast to the other studies, the calciner, which operated at 950 °C, was modelled as a stoichiometric reactor with conversion of 95% to account for sorbent sintering. The heat requirement for sorbent regeneration was met through direct oxy-combustion of syngas in the calciner. It was proposed that O_2 was produced using the oxygen transfer membrane, which separates O_2 from the high-pressure air diverted from the gas turbine compressor at temperatures of 850–900 °C, and then mixed with recycled CO_2 to control the calcination temperature. The remaining CO_2 was sent to purification and compression to 110 bar.

The waste heat available in the CaL plant was utilised to generate high-pressure steam (250 bar/630 °C/650 °C) that was fed to a bottoming dual-pressure supercritical steam cycle. This substitution of a subcritical bottoming steam cycle in the conventional IGCC plant led to improvement in net thermal efficiency of 3.8% points, to $43.2\%_{LHV}$ and a 9.5% increase in the net thermal power, to 462 MW_{el}. Such performance is in the range for the supercritical CFPPs without a CO_2 capture plant.[206,207] For this reason, the IGCC plants with CaL could be a feasible option for production of clean power from coal, with an increased reliability due to the lack of complicated chemical plant as in the conventional systems.

Alternative process configuration for a H_2-fuelled IGCC power plant that comprises a DFB system has been proposed by Wang *et al.*[130] (Fig. 35). The performance of each reactor in the system was based on the assumption that chemical and phase equilibrium is reached. The gasifier reactor is composed of the BFB gasifier, in which allothermal steam gasification of coal takes place at 700 °C, integrated with a carbonator riser operated at 600 °C. As the gasifier is assumed to operate with 50% conversion of coal, the unreacted char and sorbent are fed to the calciner, which operates at 900 °C. The heat required to sustain the calcination reaction stems from the oxy-combustion of char. The H_2-rich gas is used to fuel an F-class gas turbine, in which the compressor operates at a pressure ratio of 17 and expander temperature of 1350 °C.

The waste heat available in the integrated system is utilised to sustain the gasification reaction by diverting part of the regenerated sorbent to the gasifier and to generate the steam for the bottoming subcritical steam cycle (125 bar/565 °C/565 °C). The net thermal efficiency of the proposed process was $42.7\%_{LHV}$, while a CO_2 capture level of 95% was reached.

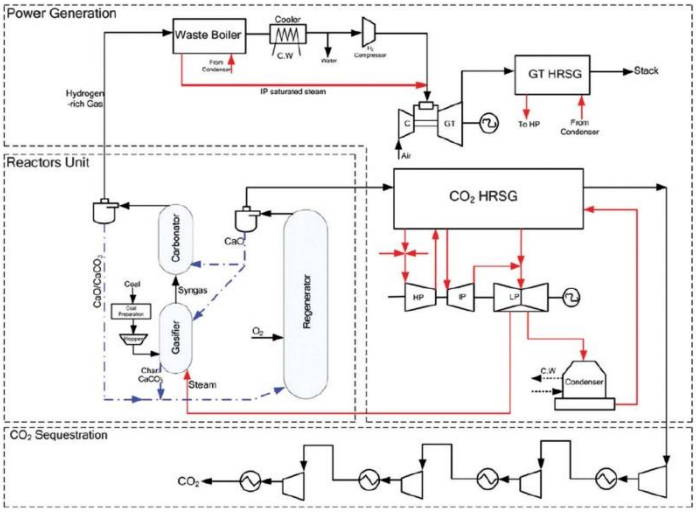

Fig. 35 Conceptual design of integration of calcium looping plant to IGCC (reprinted with permission from Wang *et al.*[130] Copyright 2015 Elsevier).

The efficiency was considerably higher than for a supercritical CFPP retrofitted with an ammonia-based CO_2 capture plant (net thermal efficiency of 27.9%$_{HHV}$).[208] This is also 5.7% points higher than for a CFPP retrofitted with the CaL plant analysed by Romeo *et al.*[86] (Section 5.1.2).

It is also important to benchmark the process performance improvements through substitution of the dual-stage Selexol process, which is commonly considered in the IGCC power plants, with the CaL plant. Connell *et al.*[129] have evaluated such performance improvement in an IGCC power plant, which comprises two F-class gas turbines (Case 2 in Black *et al.*[209]). In the considered CaL configuration, which was based on the double-looping CCR process developed and successfully demonstrated by Wang *et al.*,[26,32] each reactor was assumed to reach chemical and phase equilibrium at a given operating temperature. In contrast to previous studies, the carbonator was operated at 33 bar, which required a temperature of 700 °C to allow $Ca(OH)_2$ dissociation and hence the water/gas shift reaction. To increase the average sorbent conversion, and hence operate the system at Ca : C ratio of 1.3 that was identified in the pilot-plant testing to allow reaching more than 90% CO_2 capture, the sorbent is hydrated at 2 bar and 493 °C. The reason for the hydrator being operated at an elevated pressure was to increase its operating temperature and allow for more waste heat recovery in the system. An operating temperature of more than 875 °C in the calciner is maintained through oxy-combustion of coal. The conceptual IGCC design assumes that the heat from the CaL plant is utilised to generate steam for the bottoming steam cycle (Fig. 36).

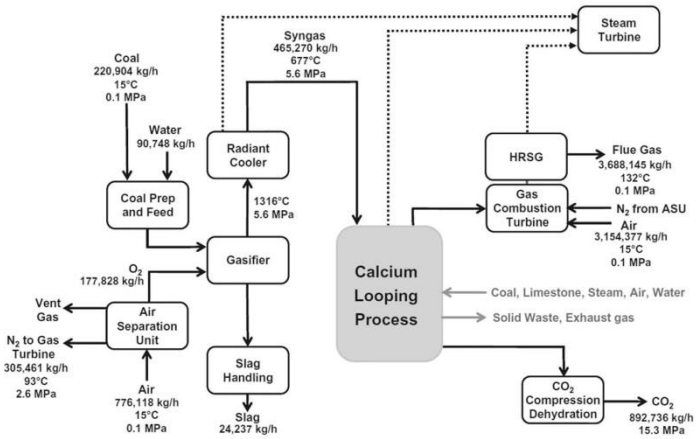

Fig. 36 Conceptual design of integration of calcium looping plant to IGCC (reprinted with permission from Connell *et al.*[129] Copyright 2015 Elsevier).

Having compared the performance of the IGCC with the CCR process and the conventional IGCC with dual stage Selexol process, Connell *et al.*[129] have found that net thermal efficiency increased by 0.4% points, from 32.7%$_{HHV}$ to 33.1%$_{HHV}$, with the coal oxy-combustion accounting for 41% of the total heat input to the process. This performance was 6.5% points higher than for a comparable subcritical CFPP retrofitted with an MEA scrubbing system.[209] More importantly, the net power output of the system increased by 71.7%, from 543.2 MW_{el} to 932.9 MW_{el}.

In the IGCC power plant, the CaL process can be used as either post-combustion, with the standard AGR process used for syngas treatment, or pre-combustion technology. Cormos and Cormos[128] have investigated the difference between these approaches for a 561.15 MW_{el} IGCC power plant of 44.36%$_{LHV}$ net thermal efficiency. The performance of all reactors in the system was determined based on thermodynamic equilibrium, as no significant differences were found when the kinetics of the calcination and carbonation processes were considered. In the investigated CaL plant, the carbonator and the calciner were operated at 650–700 °C and 900–950 °C, respectively. The temperature in the calciner was maintained through oxy-combustion of coal. It was also assumed that the CaL plant was fully heat-integrated with the rest of the plant.

In the first configuration, the CaL plant was proposed to be retrofitted after the power block (Fig. 37a), which would provide a flexible integrated system. Conversely, the second configuration assumes that the carbonator was located after the AGR plant (Fig. 37b). Steam is supplied directly to the calciner to facilitate the water/gas shift reaction allowing the H_2-rich stream to be fed to the power block.

Analysis of the overall plant performance indicators revealed that on integration of the CaL plant the net thermal efficiency dropped by 10.1% points for the post-combustion configuration and by 7.3% points for the pre-combustion configuration. With utilisation of the waste heat to produce high-pressure steam, which was then used to produce power in the bottoming steam cycle, the net power output increased by 14.6% and 19.4% for the post-combustion and pre-combustion configurations, respectively. Although such results show that the former configuration is more promising in terms of overall process performance, its higher integration degree would affect plant flexibility. Moreover, Cormos and Cormos[128] have concluded that the net efficiency penalty of the post-combustion configuration is comparable with the one associated with conventional post-combustion scrubbing technologies. Hence application of CaL as a post-combustion CO_2 capture plant will not bring any benefit in terms of process performance. However, the pre-combustion configuration was found to result in a net efficiency penalty 1–2% points lower than conventional pre-combustion scrubbing technologies.

5.2.3 Zero-emissions coal-based power generation systems. Due to high-temperature operation of the CaL process, it can serve as a base for development of novel highly-efficient and low-emission power generation systems. Two alternative coal-gasification combined cycle power plants, which utilise the CaL process as both a pre-combustion CO_2 capture technology and heat source, have been investigated by Romano and Lozza.[127,210] Both zero-emissions coal mixed technology (ZECOMIX) (Fig. 38) and zero-emissions coal mixed technology with air gas turbine (ZECOMAG) (Fig. 39) can be divided into four sections – chemical island, oxygen island, CO_2 island and power island – and they only differ in the power island configuration.

In the chemical island, where each reactor was assumed to operate under equilibrium conditions, coal slurry is gasified under an H_2 atmosphere in a hydrogasifier producing syngas that is then shifted to the H_2-rich stream in the carbonator. A small amount of O_2 is utilised to sustain the operating temperature at 700–1000 °C, depending on the operating pressure ranging between 30 bar and 70 bar. The overall chemical

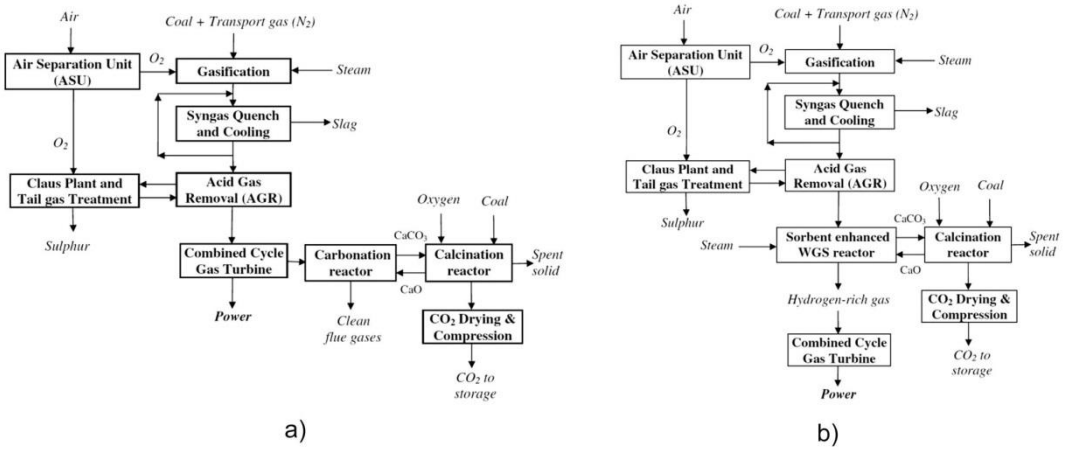

Fig. 37 Conceptual design of integration of (a) post-combustion and (b) pre-combustion calcium looping plant to IGCC (adapted with permission from Cormos and Comros.[128] Copyright 2015 Elsevier).

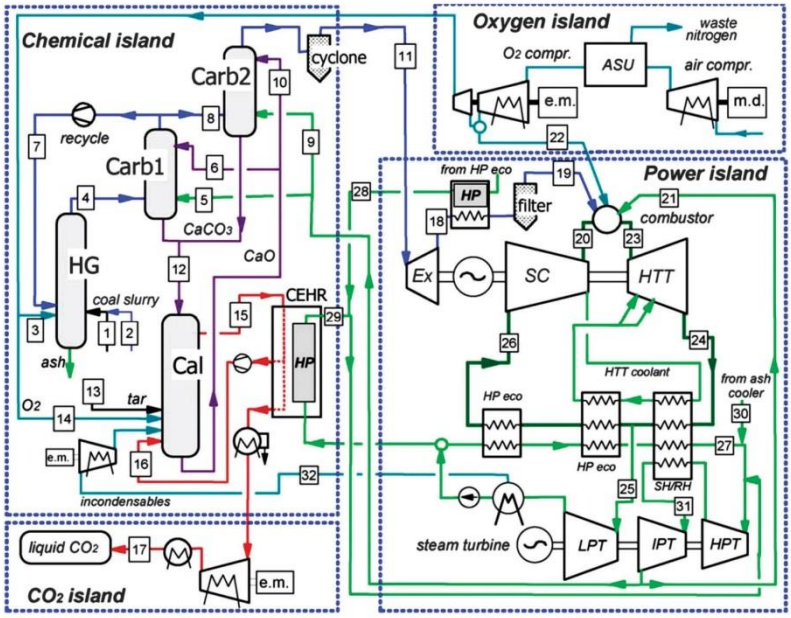

Fig. 38 Conceptual design of Zero-Emissions COal MIXed technology (reprinted with permission from Romano and Lozza.[210] Copyright 2015 Elsevier).

reaction taking place in the hydrogasifier and the carbonator is presented in eqn (101). This reaction was found to be exothermal, as the heat released on the exothermal CO_2 removal from the syngas was enough to sustain the steam

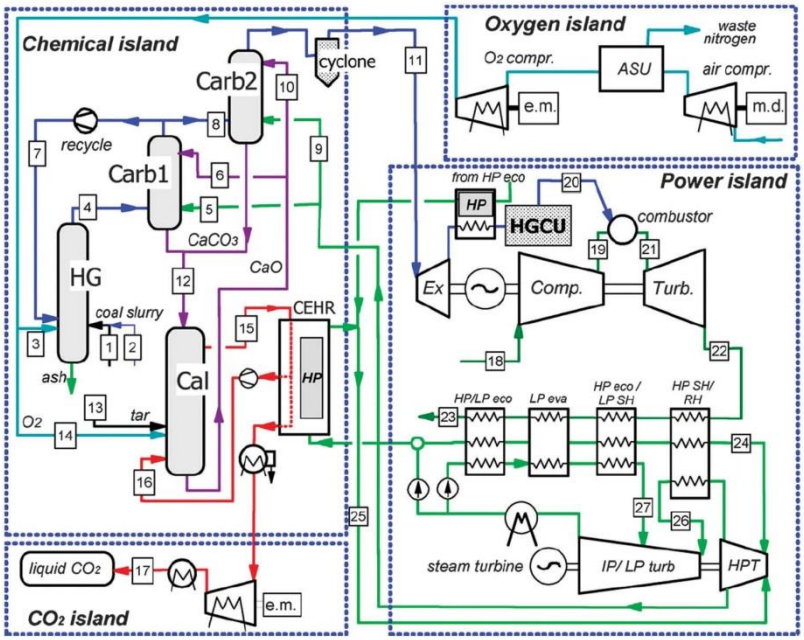

Fig. 39 Conceptual design of Zero-Emissions COal Mixed technology with Air Gas turbine (reprinted with permission from Romano and Lozza.[127] Copyright 2015 Elsevier).

reforming reaction. Part of the H_2-rich stream is recycled from the carbonator to the hydrogasifier.

$$CH_4 + 2H_2O + CaO \rightarrow 4H_2 + CaCO_3 \qquad \Delta H_r^\circ = -14.5 \text{ kJ mol}^{-1} \qquad (101)$$

It was assumed that the carbonator operates with an average conversion of 50% that was substantiated with the expected progress in sorbent treatment, production and reactivation.[210] Sorbent regeneration was assumed to be conducted at an elevated pressure and temperatures ranging between 920 °C and 1250 °C, regardless of sorbent sintering and degradation. Such high temperatures were achieved through oxy-combustion of the refinery residuals with 90% oxygen excess, as usage of the produced syngas would reduce the net thermal efficiency of the process, while usage of coal at such a high temperature would result in ash melting.

The power island of ZECOMIX technology comprises a semi-closed Joule cycle, in which heat from the syngas oxy-combustion and the combustion gases are mixed with compressed steam to control the combustor outlet temperature. Such a mixture is expanded in a high-temperature steam turbine and then used for supercritical steam generation in the bottoming steam cycle. The incondensable species, such as CO_2 and O_2, are removed from the condenser and from the deaerator with part of the steam sent to the calciner. This approach allows the ASU load to be minimised as unreacted O_2 is recycled to the calciner. Conversely, ZECOMAG technology has a more conventional power island, in which the syngas is burned with air in an open gas turbine cycle, and the discharged flue gas is used to generate supercritical steam in the dual-pressure heat recovery steam generator for the steam cycle.[127] Despite its more conventional configuration, ZECOMAG cannot be considered as a zero-emissions technology as the gas turbine flue gas, which consists of CO_2, NO_x and SO_x, is exhausted to the environment.

Analysis of the overall process performance revealed that ZECOMIX and ZECOMAG yield similar maximum net thermal efficiencies of 46.69%$_{LHV}$ and 46.74%$_{LHV}$, respectively. The analysis also revealed that the net efficiency of ZECOMIX was degraded by 0.59% points on increase of the steam compressor pressure from 25 bar to 48.5 bar, and by 2.32% points on reduction of the calciner temperature to 920 °C. In addition, reduction of the average sorbent conversion in the carbonator from 66.7% to 20.0% was found to reduce the net thermal efficiency of ZECOMIX by 3% points and of ZECOMAG by 2.5%. This indicates that sorbent performance is critical in terms of the overall process efficiency. Finally, the net power output of 667.5 MW_{el} for ZECOMIX when the steam compressor is operated with a pressure ratio of 25, was found to be 25.2% higher than for ZECOMAG with the gas turbine compressor operated with a pressure ratio of 20. The maximum net power output achievable by ZECOMIX was found to be 1242.2 MW_{el} if the steam compressor inlet pressure was increased from 1.02 bar to 1.9 bar.

5.3 Summary

5.3.1 Integration impact on the overall process performance. Depending on the power plant type, the net projected efficiency penalty imposed by post-combustion CaL plant integration was 2.6[37]–7.9%[86] points for a CFPP and 9.1–11.4%[146] points for a combined cycle power plant.

A very low net projected efficiency penalty of 2.6% points was estimated by Martínez *et al.*[37] in investigating a subcritical CFPP retrofit with a CaL plant and supercritical secondary steam cycle. This shows that implementation of CaL plants into subcritical units, the majority of the current CFPP fleet, would result in a minor net efficiency penalty compared to conventional CO_2 capture technologies. Nevertheless, the mean net projected efficiency penalty for a CFPP was 6–7% points with 2.5–3% points associated with the CaL plant itself and the remainder caused by the CCU. Yang *et al.*[16] have estimated an extremely low net thermal efficiency of 21.2% for a CaL plant integrated into a CFPP without any heat recovery system. This implies that as high-grade heat is available in the CaL plant, it needs to be recovered efficiently to reach high overall performance.

The studies by Berstad *et al.*[146] and Cormos and Cormos[128] revealed that integration of a CaL plant as a post-combustion technology into the NGCC and the IGCC power plant would result in a net efficiency penalty comparable to conventional CO_2 capture systems. This could be associated with low partial pressure of CO_2 in the flue gas, and thus lower driving force for the carbonation reaction. However, in studies where a CaL plant was used as a substitute for a complex gas processing plant integrated as a pre-combustion CO_2 capture technology into an IGCC system, the net thermal efficiency increased by 0.4[129]–3.8%[131] points, and reached 43.2%$_{LHV}$.[131] The study by Romano and Lozza[127,210] revealed that development of new coal-based power generation systems based on the CaL process, which are characterised by net thermal efficiencies of 46.69%$_{LHV}$ for CO_2 capture higher than 95%, is feasible. Such values for net thermal efficiency, which are in the range of supercritical and ultra-supercritical CFPPs without CO_2 capture plants, and increased process reliability due to the lack of complicated chemical plant indicate that gasification-based power plants with pre-combustion CaL could become a cost-efficient and environmentally-friendly technology for coal-based power generation, and could allow further coal utilisation.

It is important to highlight that all of the reviewed studies use different initial sets of assumptions regarding the reference power plant. Moreover, the reference net thermal efficiencies of the CFPPs gathered in Table 7 vary between 32.7–44.6%$_{HHV}$ (studies using higher heating value basis), and 36.0–46.0%$_{LHV}$ (studies using lower heating value basis). However, as mentioned in the introduction, the average net thermal efficiency of the existing global fleet has been identified to be 33%$_{LHV}$, which corresponds to 30–31%$_{HHV}$ depending on fuel composition.[211] As the sub-critical units, which operate with low net thermal efficiencies and yet account for around 75% of the global CFPP capacity,[6] can be expected to be still in operation in the near future, the further analyses of the CaL process integration should focus on a portfolio of steam conditions to assure prediction accuracy and realism. This implies that baseline reference models for CaL process integration need to be established, which can be done, for example, by replicating

Table 7 Summary of the process integration studies

Reference	Power plant type	Gross power output (MW_{el})	Reference net thermal efficiency ($\%_{LHV}$)	Net thermal efficiency of integrated system ($\%_{LHV}$)	Efficiency penalty (% points)
Shimizu *et al.*[28]	SC-CFPP[a]	1000	N/A	33.4[d]	N/A
Yang *et al.*[16]	SC-CFPP[a]	600	40.6	25.3–36.8	3.8–15.3
Abanades *et al.*[39]	USC-CFPP[a]	100	46	38.8–40.0	6–7.2
Martínez *et al.*[83]	SubC-CFPP[a]	350	36	30.3–33.4	2.6–5.7
Martínez *et al.*[148]	SC-CFPP[a]	433.7	N/A	37.8	N/A
Martínez *et al.*[133]	CFPP[b]	500	44.35		N/A
Romeo *et al.*[86]	SC-CFPP[a]	450	44.93	37.0	7.93
Lara *et al.*[200]	SC-CFPP[a]	500	38.2	33.0	5.2
Lara *et al.*[201]	SC-CFPP[a]	500	38.2	34.0	6.2
Ströhle *et al.*[147]	USC-CFPP[a]	1100	45.6	42.4–42.8	2.8–3.2
Lasheras[31]	USC-CFPP[a]	1000	45.6	42.7	2.9
Wang *et al.*[32]	USC-CFPP[a]	561	44.6[d]	37.2–38.0[d]	6.6–7.4
Wang *et al.*[26]	SubC-CFPP[a]	500[e]	35.8[d]	N/A	N/A
Wang *et al.*[26]	SC-CFPP[a]	500[e]	39.0[d]	N/A	N/A
Vorrias *et al.*[132]	SC-LFPP[c]	330	42.5	37.5	5.0
Berstad *et al.*[146]	NGCC	418.8	52.6[d]	41.2–43.5[d]	9.1–11.4
Kunze *et al.*[131]	IGCC	510	39.4	43.2	−3.8
Wang *et al.*[130]	IGCC	N/A	N/A	42.7	N/A
Connel *et al.*[129]	IGCC	734	32.7[d]	33.1[d]	−0.4
Cormos and Cormos[128]	IGCC	561.2	44.4	34.2–37.0	7.4–10.2
Romano and Lozza[210]	ZECOMIX	N/A	N/A	44.4–46.7	N/A
Romano and Lozza[127]	ZECOMAG	N/A	N/A	46.7	N/A

[a] SC – supercritical; USC – ultra-supercritical; SubC – Subcritical. [b] Steam conditions not specified. [c] Supercritical lignite-fired power plant. [d] HHV basis. [e] Net power output.

CFPP (subcritical and supercritical), NGCC and IGCC models from the revised NETL report[209] and developing ultra-supercritical CFPP model based on the European Benchmarking Task Force documents.[212,213] Table 7 reveals that not only are the reference CFPPs based on different steam conditions, from sub-critical to ultra-supercritical, but also their gross power outputs and net thermal efficiencies vary considerably. The performance of the reference IGCC plants vary significantly as well. As this makes a comparison of results across different analyses impossible, a set of baseline reference models, which should include models for CFPP, NGCC and IGCC plants with consideration of different steam conditions, needs to be established. Such baseline reference models would allow for a reliable comparison of further process developments using process simulations.

5.3.2 Modelling approaches, assumptions and limitations. This review identified limitations in the approaches for modelling CaL plants and their integration into the power plants (Table 8). Firstly, it was found that in several studies the net or gross thermal efficiency of the secondary steam cycle,[26,28,31,32,37,39,83,147] as well as specific power consumptions of ASU[26,28,31,32,83,86,128,130,133,146,147,200,201] and CCU[26,28,32,83] were assumed rather than estimated using thermodynamic or process models. Although this approach could be valid for a particular system operating at a fixed load, any deviation from the operating point, such as part-load operation, would reduce the accuracy of the prediction. Moreover, such approach applied to represent the performance of the secondary steam cycle, ASU and CCU, restricts applicability of a detailed design of the HEN of the entire process.

Secondly, the studies reviewed assumed that total calcination is achieved in the calciner, with the exception of the study by Kunze *et al.*[131] who assumed 95% conversion in the calciner to account for less favourable calcination conditions. Thirdly, all the studies utilised thermodynamic models to represent the calcination process, mostly achieving chemical equilibrium through Gibbs' free energy minimisation. Most of the studies analysing the combined cycle power plants used thermodynamic models also for the carbonator, with the exception of Berstad *et al.*,[146] while more complex models, such as average conversion models[16,39,132,133,147] and 1D carbonator models based on K–L hydrodynamics[28,31,147] were used in analysing the CFPPs. Interestingly, the study by Ströhe *et al.*,[147] in which both models have been compared, revealed that, although application of the maximum average conversion model without the correction factor resulted in underestimation of several process parameters, the overall process performance of a CFPP with a CaL process was the same for both models. Furthermore, the sensitivity study performed by Lasheras *et al.*[31] revealed that the uncertainty in the K–L model can affect CaL plant performance by up to 10%. As this can have a significant effect on estimation of overall process performance, further experimental tests are necessary to identify the required parameters.

It is worth pointing out that the lower operating temperature (600 °C) of the carbonator in the CaL linked with the NGCC compared to studies reviewed in Section 5.1 (650 °C), which assessed integration of the CFPP and the CaL process, results in slower carbonation reaction, hence larger units are required. Moreover, low CO_2 partial pressure in the NGCC flue gas makes the carbonation process more difficult, and thus the maximum CO_2 capture level of only 86% in the carbonator was achieved. Although the carbonator temperature could be further lowered, favouring chemical equilibrium at the expense of reaction kinetics, the desired high-pressure steam temperature of 550–560 °C[146] would not be achievable.

Table 8 Summary of modelling approaches and assumptions in investigating calcium looping integration to power plants

	Carbonator assumptions		Calciner assumptions		Modelling approach for other system components		
Reference	Model	Operating conditions	Model	Operating conditions	ASU	CCU	Secondary steam cycle
Shimizu *et al.*[28]	Semi-predictive model with KL hydrodynamics	T = 650 °C Ca : C = 8.29 E_{carb} = 83%	Equilibrium	T = 950 °C X_{calc} = 100%	Assumed w_{ASU} = 25.9 MJ per kmol-O_2	Assumed w_{CCU} = 24.5 MJ kmol^{-1}-CO_2	Assumed η_g = 42.6%$_{HHV}$
Yang *et al.*[16]	Average conversion w/o correction	T = 650 °C Ca : C = 5 E_{carb} = 85%	Equilibrium	T = 900 °C	Assumed w_{ASU} = 220 kW h per t-O_2	Not considered	Thermodynamic model
Abanades *et al.*[39]	Average conversion w/o correction	T = 650 °C E_{carb} = 75.2%	Equilibrium	T = 950 °C X_{calc} = 100%	Estimated using process model	Estimated using process model	N/A
Martínez *et al.*[83]	Semi-predictive model with simple hydrodynamics	T = 650 °C E_{carb} = 70–90% u_0 = 6 m s^{-1}	Equilibrium	T = 950 °C λ_{O_2} = 1.05 X_{calc} = 100% $y_{O_2,fluidising\ gas}$ = 25%$_{vol}$	Assumed w_{ASU} = 160 kW h per t-O_2	Assumed w_{CCU} = 100 kW h/t-CO_2	Assumed η_g = 45%
Martínez *et al.*[148]	Semi-predictive model with simple hydrodynamics	T = 650 °C E_{carb} = 89%	Equilibrium	T = 950 °C E_{calc} = 100%	Not specified	Estimated using adiabatic compression model with η_a = 75%	Thermodynamic model
Martínez *et al.*[133]	Average conversion with correction	T = 650 °C X_{carb}/X_{ave} = 0.8 E_{carb} = 90%	Equilibrium	T = 930 °C X_{calc} = 100%	Assumed w_{ASU} = 220 kW h per t-O_2	N/A	N/A
Romeo *et al.*[86]	Average conversion w/o correction	T = 650 °C X_{carb} = 20% E_{carb} = 85%	Equilibrium	T = 875–950 °C X_{calc} = 100% $y_{O_2,fluidising\ gas}$ = 95%$_{vol}$	Assumed w_{ASU} = 220 kW h per t-O_2	N/A	Thermodynamic model
Lara *et al.*[200,201]	Average conversion w/o correction	T = 650 °C Ca : C = 5	Equilibrium	T = 950 °C F_0/F_R = 0.025	Assumed w_{ASU} = 220 kW h per t-O_2	Estimated using isentropic compression model with η_i = 80%	Thermodynamic model
Ströhle *et al.*,[147] Lasheras *et al.*[31]	Average conversion w/o correction and Semi-predictive mode with K–L hydrodynamics	T = 650 °C E_{carb} = 80% E_{SO_2} = 99%	Equilibrium	T = 900 °C λ_{O_2} = 1.10 X_{coal} = 0.995	Assumed w_{ASU} = 184.8 kW h per t-O_2	N/A	Assumed η_g = 50.3%$_{LHV}$
Wang *et al.*[26,32]	Equilibrium	T = 625 °C Ca : C = 1.4 E_{carb} = 90% E_{SO_2} = 100%	Equilibrium	T = 1000 °C $y_{O_2,fluidising\ gas}$ = 95%$_{vol}$	Assumed w_{ASU} = 200 kW h per t-O_2	Assumed w_{ASU} = 119 kW h/t-CO_2	Assumed η_g = 42%$_{HHV}$
Vorrias *et al.*[132]	Average conversion w/o correction	T = 650 °C Ca : C = 7 E_{carb} = 90%	Equilibrium	T = 950 °C F_0/F_{CO_2} = 0.1 $y_{O_2,fluidising\ gas}$ = 80%$_{vol}$	Estimated using process model	Estimated using process model	Thermodynamic model
Berstad *et al.*[146]	Average conversion with correction	T = 600 °C X_{carb}/X_{ave} = 0.75 E_{carb} = 85–86%	Equilibrium	T = 950 °C F_0/F_R = 0.06 λ_{O_2} = 1.03 X_{calc} = 100% $y_{O2,fluidising\ gas}$ = 25%$_{vol}$	Assumed w_{ASU} = 200 kW h per t-O_2	Estimated using polytrophic compression model with η_p = 75–80%	Thermodynamic model
Kunze *et al.*[131]	Average conversion w/o correction	T = 650 °C X_{carb} = 0.2 E_{carb} = 90%	Equilibrium	T = 950 °C X_{calc} = 95%	Assumed w_{ASU} = 28 kW h per t-O_2	Assumed w_{ASU} = 83 kW h/t-CO_2	N/A
Wang *et al.*[130]	Equilibrium	T = 600 °C	Equilibrium	T = 900 °C	Assumed w_{ASU} = 245 kW h per t-O_2	Estimated using isentropic compression model with η_i = 75%	Thermodynamic model
Connel *et al.*[129]	Equilibrium	T = 700 °C E_{carb} > 90%	Equilibrium	T > 875 °C	N/A	N/A	N/A
Cormos and Cormos[128]	Equilibrium	T = 650–700 °C	Equilibrium	T = 900–950 °C	Assumed w_{ASU} = 225 kW h per t-O_2	Estimated using process model	Thermodynamic model
Romano and Lozza[127,210]	Equilibrium	T = 875–882 °C X_{carb} = 0.5	Equilibrium	T = 1250	Estimated	Estimated using isentropic compression model with η_i = 89.5%	Thermodynamic model

Finally, although the operating temperatures of the carbonator and the calciner were found to be similar in all studies reviewed, selection of several important parameters seem to be inconsistent (Table 8). Namely, some studies assume that the O_2 in the calciner fluidising gas is diluted with recycled CO_2, and its concentration varies from $25\%_{vol}$[83,146] to $80\%_{vol}$.[132] In addition, several studies claimed that no CO_2 recycle is required and $95\%_{vol}$-purity O_2 can be directly fed to the calciner.[26,32,86] Current pilot-plant testing activities were conducted with the O_2 concentration below $50\%_{vol}$.[33,98,100,104] Therefore, to limit the sorbent deterioration, further integration studies should include the CO_2 recycle to control the temperature in the calciner. Another important parameter is Ca : C ratio that has been assumed to be between 5–8.29 to reach the CO_2 capture levels in the carbonator up to 90% using non-pretreated sorbent. It needs to be highlighted that the pilot-plant tests reviewed in Section 3 claimed that to reach such reduction in the CO_2 emissions in the carbonator, the Ca : C ratio should be higher than 8–11.6.[98,103,107] For this reason, in the studies where low Ca : C ratios were used to reach high CO_2 capture level in the carbonator, prediction of the process performance may be overly optimistic due to under-estimated solids looping rate, and thus heat requirement in the calciner. Moreover, the excess O_2 and the relative limestone make-up rate, which is represented using F_0/F_R ratio, were found to vary between 1.03–1.10 and 0.025–0.06, respectively. This implies the need for establishing baseline design parameters for the CaL process that would allow comparing process performance across analyses.

6 The future of calcium looping in power generation systems

In light of increasing environmental concerns, the power sector seems to be the first in line to be completely decarbonised by 2050. High reliance on coal, however, makes this a challenging task requiring implementation of CO_2 capture technologies in the existing coal-based power generation fleet. Unfortunately, conventional technologies, which utilise chemical sorbents and oxy-fuel combustion, result in a considerable drop in system efficiency, leading to an increase in the cost of electricity. The CaL process is regarded as a feasible alternative to conventional technologies because not only is it characterised by lower loss in power plant efficiency, but it is also capable of increasing the power output of the system.

CaL process viability and performance have been widely investigated in bench- and pilot-scale facilities the size of which varies between 1 kW_{th} and 1.7 MW_{th}. The test campaigns reported in the open literature provide valuable insight into the process operation that can be used for process model development. Nevertheless, this review has shown that the available data were not detailed enough for any test facility to be useful for detailed process model validation. This is caused by, for example, the uncertainty associated with the solid looping rate measurements. To allow detailed process model validation, however, more detailed data should be reported for future tests.

The CaL experimental trials have revealed that the actual CO_2 capture level can be close to that determined by equilibrium provided sufficient solids inventory of moderate conversion and looping rate are maintained. However, deterioration of the sorbent performance, triggered mainly by sintering and sulphation, requires relatively high make-up rates to reach the desired level of average sorbent conversion, which affects the economic performance of the system. Therefore, the further developments of the sorbent performance enhancement measures and/or novel sorbents experiencing lower performance deterioration need to be pursued in the near to mid-term timescale.

To date, the predictions of process performance have been modelled with different levels of complexity. Five levels can be distinguished, which differ in application of the kinetic or equilibrium reactions, considering the concentration changes in the gas and solid phases and implementation of FB hydrodynamics. Importantly, the effect of sulphation on the sorbent activity and inert solids accumulation in the system were rarely included in the models available in the literature. Therefore, to improve the accuracy and reliability of the overall process performance prediction, future models should account for sorbent sulphation and ash accumulation.

Application of the CaL plant to typical coal-based power generation systems was found to impose lower efficiency penalties (6–7% points), compared to conventional CO_2 capture systems, proving the technology viability. Moreover, novel power generation systems that are based on the CaL process have been proposed, and reach net thermal efficiencies close to those of ultrasupercritical CFPPs without CO_2 capture. This implies that the CaL plant can serve as a base system for development of state-of-the-art power generation systems that could be implemented on a large scale in place of current technologies. Nevertheless, it is highlighted that the analyses performed to date used not only different CaL modelling approaches, but more importantly they employed different reference power plants and sets of CaL operating conditions. As this restricts the accuracy of process performance comparison across these analyses, the baseline reference models for the power plant and CaL plant need to be developed. In the near term, such baseline models would allow a reliable comparison of the process performances of the further analyses of the CaL process improvements.

List of abbreviations

AGR	Acid gas removal
ASU	Air separation unit
BFB	Bubbling fluidised bed
CaL	Calcium looping
CaRS-CO_2	Calcium-based reaction separation for CO_2
CCR	Carbonation–calcination reaction process
CCS	Carbon capture and storage
CCU	CO_2 compression unit
CFB	Circulating fluidised bed
CFD	Computational fluid dynamics

CFPP	Coal-fired power plant
DFB	Dual fluidised bed
EB	Entrained bed
FGD	Flue gas desulphurisation unit
HEN	Heat exchanger networks
IFK	The Institute of Combustion and Power Plant Technology (Institut für Feuerungs-und Kraftwerkstechnik)
IGCC	Integrated-gasification combined cycle power plant
INCAR-CSIC	The Instituto Nacional del Carbón – Consejo Superior de Investigaciones Científicas
ITRI	The Industrial Technology Research Institute
K–L	Kunii and Levenspiel model
MB	Moving bed
MDEA	Methyldiethanolamine
MEA	Monoethanolamine
NGCC	Natural gas combined cycle power plant
OSCAR	The Ohio State carbonation ash reactivation process
PZ	Piperazine
RK	Rotary kiln
SER	Sorption-enhanced reforming process
SME	Sorption-enhanced methane steam reforming
TGA	Thermo-gravimetric analyser
ZECOMAG	Zero-emissions coal mixed technology with air gas turbine
ZECOMIX	Zero-emissions coal mixed technology

Nomenclature

Latin symbols

A	Bed cross-section area, m^2
a_1	Fitting parameter in Li and Cai[133] correlation, —
a_2	Fitting parameter in Li and Cai[133] correlation, —
c_0	Freundlich isotherm characteristic, —
C_i	Concentration of species i, kmol m^{-3}
D	Diffusivity coefficient, m^2 s^{-1}
d_b	Bubble diameter, m s^{-1}
E	Activation energy, J $kmol^{-1}$
E_{carb}	CO_2 capture level in the carbonator, —
E_{calc}	Efficiency of the calciner, —
f	Extent of calcination or carbonation, —
F_0	$CaCO_3$ makeup rate, kmol s^{-1}
f_1	Fitting parameter in Li and Cai[133] correlation, —
f_2	Fitting parameter in Li and Cai[133] correlation, —
f_a	Active fraction of particles, —
F_{CO_2}	CO_2 flow rate in the flue gas, kmol s^{-1}
F_H	Sorbent rate diverted to the hydrator, kmol s^{-1}
F_R	CaO looping rate, kmol s^{-1}
h	$CaCO_3$ layer thickness, nm
H_D	Height of the dense phase, m
k	Kinetic rate constant or sorbent deactivation constant or proportionality constant, 1 s^{-1}, m^3 mol^{-1} s^{-1}, m^4 mol^{-1} s^{-1}, —
K_{be}	Bubble and emulsion interchange coefficient, —
k_g	Mass transfer coefficient, m s^{-1}
N	Number of calcination–carbonation cycle, —
n	Sorbent sintering exponent or number of active sites in Langmuir–Hinshelwood mechanism, —
N_{Ca}	Mole inventory of CaO in the bed, kmol
M_i	Molar mass of species i, kg $kmol^{-1}$
P_{CO_2}	Partial pressure of CO_2, atm
r	Reaction rate, kmol m^{-3} s^{-1}, 1 s^{-1}
R	Particle radius, m
r_0	Mole fraction of particles that has never been calcined or initial grain radius, — or m
$r_{C/S}$	Molar ratio of carbon and sulphur in the fuel, —
Re	Reynolds number, —
R_g	Gas constant, J $kmol^{-1}$ K^{-1}
r_N	Mass fraction of particles that has undergone N carbonation–calcination cycles, —
r_i	Un-reacted radius of CaO grain, M
S	Particle surface area, m^2 m^{-3}
Sc	Schmidt number, —
Sh	Sherwood number, —
T	Temperature, K
t^*	Actual residence time, s
u_0	Superficial gas velocity, m s^{-1}
u_b	Bubble rise velocity, m s^{-1}
u_b^*	Rising bubble gas velocity, m s^{-1}
v_{CO_2}	Volume fraction of CO_2 in the gas phase, —
$V_{M,i}$	Molar volume of species i, m^3 $kmol^{-1}$
W_{CaO}	Mass inventory of CaO in the bed, kg
X	Sorbent conversion, —
y_{comb}	mass ratio between fuel going to the main combustor and total fuel into the plant, —

Greek symbols

δ	Volume of bubbles per unit bed volume, —
ε	Porosity of sorbent particle or solid fraction in the reactor, —
θ	Fraction of the active sites, —
ρ_i	Mass density of species i, kg m^{-3}
τ	Average residence time, s
φ_e	Effectivity factor, —
Φ_s	Particle sphericity, —
Ψ	Sorbent pore structural parameter, —

Superscripts

H	Hydrated sorbent

Subscripts

0	Initial conditions
ave,max	Refer to maximum average sorbent conversion
b	Refer to bubble zone
calc	Variable related to calciner operating conditions or stream leaving calciner
carb	Variable related to carbonator operating conditions or stream leaving carbonator
e	Refer to emulsion zone

eq	Equilibrium conditions
mf	Refer to minimum fluidising conditions
max	Refer to maximum sorbent conversion
r	Refer to residual sorbent conversion
s	Refer to intrinsic kinetic constant

References

1 European Commission, *Communication from the Commission to the European Parliament, the Council, the European Economic and Social Committee and the Committee of the Regions, International climate policy post-Copenhagen: Acting now to reinvigorate global action on climate change*, COM(2010) 86, Commission of the European Communities, Brussels, Belgium, 2010.

2 European Commission, *Communication from the Commission to the European Parliament, the Council, the European Economic and Social Committee and the Committee of the Regions, A policy framework for climate and energy in the period from 2020 to 2030*, European Commission, COM(2014) 15, Brussels, Belgium, 2014.

3 European Council, *European Council 23/24 October 2014 – Conclusions, EUCO gv 169/14 CO EUR 13 CONCL 5*, European Commission, Brussels, Belgium, 2014.

4 European Commission, *Communication from the Commission to the European Parliament, the Council, the European Economic and Social Committee of the Regions - Energy Roadmap 2050*, COM(2011) 885/2, European Commission, Brussels, Belgium, 2011.

5 UNEP, *The Emissions Gap Report 2012*, United Nations Environment Programme (UNEP), Nairobi, Kenya, 2012.

6 IEA, *Tracking Clean Energy Progress 2013. IEA Input to the Clean Energy Ministerial*, IEA Publications, Paris, France, 2013.

7 IEA, *Power generation from coal: Measuring and reporting efficiency performance and CO_2 emissions*, IEA Publications, Paris, France, 2010.

8 EIA, *International Energy Outlook 2011, DOE/EIA-0484(2011)*, U.S. Energy Information Administration, Washington, USA, 2011.

9 IEA, *Technology Roadmap: Carbon capture and storage*, IEA Publications, Paris, France, 2013.

10 K. Stéphenne, Start-up of world's first commercial post-combustion coal fired ccs project: Contribution of Shell CANSOLV to Saskpower Boundary Dam ICCS project, in *12thInternational Conference on Greenhouse Gas Control Technologies*, ed. T. Dixon, S. Twinning and H. Herzog, GHGT, Austin, TX, USA, 2014, vol. 63, p. 6106.

11 N. Rodríguez, M. Alonso and J. C. Abanades, Average activity of CaO particles in a calcium looping system, *Chem. Eng. J.*, 2010, **156**(2), 388–394.

12 A. S. Bhown and B. C. Freeman, Analysis and status of post-combustion carbon dioxide capture technologies, *Environ. Sci. Technol.*, 2011, **45**(20), 8624–8632.

13 J. Blamey, E. Anthony, J. Wang and P. Fennell, The calcium looping cycle for large-scale CO_2 capture, *Prog. Energy Combust. Sci.*, 2010, **36**(2), 260–279.

14 C. C. Dean, J. Blamey, N. H. Florin, M. J. Al-Jeboori and P. S. Fennell, The calcium looping cycle for CO_2 capture from power generation, cement manufacture and hydrogen production, *Chem. Eng. Res. Des.*, 2011, **89**, 836–855.

15 M. E. Boot-Handford, J. C. Abanades, E. J. Anthony, M. J. Blunt, S. Brandani, N. Mac Dowell, J. R. Fernandez, M. C. Ferrari, R. Gross, J. P. Hallett, R. S. Haszeldine, P. Heptonstall, A. Lyngfelt, Z. Makuch, E. Mangano, R. T. J. Porter, M. Pourkashanian, G. T. Rochelle, N. Shah, J. G. Yao and P. S. Fennell, Carbon capture and storage update, *Energy Environ. Sci.*, 2014, **7**, 130–189.

16 Y. Yang, R. Zhai, L. Duan, M. Kavosh, K. Patchigolla and J. Oakey, Integration and evaluation of a power plant with a CaO-based CO_2 capture system, *Int. J. Greenhouse Gas Control*, 2010, **4**(4), 603–612.

17 G. Xu, H. G. Jin, Y. P. Yang, Y. J. Xu, H. Lin and L. Duan, A comprehensive techno-economic analysis method for power generation systems with CO2 capture, *Int. J. Energy Res.*, 2010, **34**(4), 321–332.

18 K. Goto, K. Yogo and T. Higashii, A review of efficiency penalty in a coal-fired power plant with post-combustion CO_2 capture, *Appl. Energy*, 2013, **111**, 710–720.

19 B. R. Stanmore and P. Gilot, Review—calcination and carbonation of limestone during thermal cycling for CO_2 sequestration, *Fuel Process. Technol.*, 2005, **86**(16), 1707–1743.

20 D. P. Harrison, Sorption-Enhanced Hydrogen Production: A Review, *Ind. Eng. Chem. Res.*, 2008, **47**(17), 6486–6501.

21 N. H. Florin and A. T. Harris, Enhanced hydrogen production from biomass with in situ carbon dioxide capture using calcium oxide sorbents, *Chem. Eng. Sci.*, 2008, **63**(2), 287–316.

22 E. J. Anthony, Ca looping technology: Current status, developments and future directions, *Greenhouse Gases: Sci. Technol.*, 2011, **1**(1), 36–47.

23 W. Liu, H. An, C. Qin, J. Yin, G. Wang, B. Feng and M. Xu, Performance enhancement of calcium oxide sorbents for cyclic CO_2 capture-a review, *Energy Fuels*, 2012, **26**(5), 2751–2767.

24 A. M. Kierzkowska, R. Pacciani and C. R. Müller, CaO-based CO_2 sorbents: From fundamentals to the development of new, highly effective materials, *ChemSusChem*, 2013, **6**(7), 1130–1148.

25 M.C. Romano, I. Martínez, R. Muroillo, B. Arstad, R. Blom, D.C. Ozcan, H. Ahn and S. Brandani, Process simulation of Ca-looping processes: Review and guidelines, 2013, 11th International Conference on Greenhouse Gas Control Technologies, GHGT 2012, 37, 18-22 November 2012, Kyoto, Japan, 142.

26 W. Wang, S. Ramkumar and L. Fan, Energy penalty of CO_2 capture for the Carbonation–Calcination Reaction (CCR) Process: Parametric effects and comparisons with alternative processes, *Fuel*, 2013, **104**, 561–574.

27 T. Hirama, H. Hosoda, K. Kitano and T. Shimizu, *Method of separating carbon dioxide from carbon dioxide containing gas and combustion apparatus having function to separate carbon dioxide from the combustion gas*, *UK Pat.*, 2291051A, 1996.

28 T. Shimizu, T. Hirama, H. Hosoda, K. Kitano, M. Inagaki and K. Tejima, A Twin Fluid-Bed Reactor for Removal of CO_2 from Combustion Processes, *Chem. Eng. Res. Des.*, 1999, **77**(1), 62–68.
29 R. W. Hughes, D. Y. Lu, E. J. Anthony and A. Macchi, Design, process simulation and construction of an atmospheric dual fluidized bed combustion system for in situ CO2 capture using high-temperature sorbents, *Fuel Process. Technol.*, 2005, **86**(14–15), 1523–1531.
30 M. Alonso, N. Rodríguez, G. Grasa and J. C. Abanades, Modelling of a fluidized bed carbonator reactor to capture CO_2 from a combustion flue gas, *Chem. Eng. Sci.*, 2009, **64**(5), 883–891.
31 A. Lasheras, J. Ströhle, A. Galloy and B. Epple, Carbonate looping process simulation using a 1D fluidized bed model for the carbonator, *Int. J. Greenhouse Gas Control*, 2011, **5**(4), 686–693.
32 W. Wang, S. Ramkumar, D. Wong and L. Fan, Simulations and process analysis of the carbonation–calcination reaction process with intermediate hydration, *Fuel*, 2012, **92**(1), 94–106.
33 D. Y. Lu, R. W. Hughes and E. J. Anthony, Ca-based sorbent looping combustion for CO2 capture in pilot-scale dual fluidized beds, *Fuel Process. Technol.*, 2008, **89**(12), 1386–1395.
34 J. M. Valverde, A model on the CaO multicyclic conversion in the Ca-looping process, *Chem. Eng. J.*, 2013, **228**, 1195–1206.
35 J. Yin, C. Qui, B. Feng, L. Ge, C. Luo, W. Liu and H. An, Calcium Looping for CO_2 Capture at a Constant High Temperature, *Energy Fuels*, 2014, **28**(1), 307–318.
36 E. H. Baker, The calcium oxide-carbon dioxide system in the pressure range 1-300 atmospheres, *J. Chem. Soc.*, 1962, 464–470.
37 I. Martínez, R. Murillo, G. Grasa and J. C. Abanades, Integration of a Ca-looping system for CO_2 capture in an existing power plant, *Energy Procedia*, 2011, **4**, 1699–1706.
38 J. Valverde, P. E. Sanchez-Jimenez, A. Perejon and L. A. Perez-Maqueda, CO_2 multicyclic capture of pretreated/doped CaO in the Ca-looping process. Theory and experiments, *Phys. Chem. Chem. Phys.*, 2013, **15**, 11775–11793.
39 J. C. Abanades, E. J. Anthony, J. Wang and J. E. Oakey, Fluidized Bed Combustion Systems Integrating CO_2 Capture with CaO, *Environ. Sci. Technol.*, 2005, **39**(8), 2861–2866.
40 N. Rodriguez, M. Alonso, G. Grasa and J. C. Abanades, Heat requirements in a calciner of $CaCO_3$ integrated in a CO_2 capture system using CaO, *Chem. Eng. J.*, 2008, **138**(1–3), 148–154.
41 V. Manovic and E. J. Anthony, Improvement of CaO-based sorbent performance for CO_2 looping cycles, *J. Therm. Sci.*, 2009, **13**(1), 89–104.
42 C. J. Abanades and D. Alvarez, Conversion limits in the reaction of CO_2 with lime, *Energy Fuels*, 2003, **17**, 308–315.
43 R. H. Borgwardt, Calcium oxide sintering in atmospheres containing water and carbon dioxide, *Ind. Eng. Chem. Res.*, 1989, **28**(4), 493–500.
44 L. Zhen-Shan and C. Ning-Sheng, Process analysis of CO_2 capture from flue gas using carbonation–calcination cycles, *Environmental and Energy Engineering*, 2008, **54**(7), 1912–1925.
45 F. García-Labiano, A. Rufas, L. F. De Diego, M. D. L. Obras-Loscertales, P. Gayán, A. Abad and J. Adánez, Calcium-based sorbents behaviour during sulphation at oxy-fuel fluidised bed combustion conditions, *Fuel*, 2011, **90**(10), 3100–3108.
46 M. C. Duke, B. Ladewig, S. Smart, V. Rudolph and J. C. D. Da Costa, Assessment of post-combustion carbon capture technologies for power generation, *Front. Chem. Eng. China*, 2010, **4**(2), 184–195.
47 M. Maroto-Valer, *Developments and Innovation in Carbon Dioxide (CO_2) Capture and Storage Technology, Volume 1 - Carbon Dioxide (CO_2) Capture, Transport and Industrial Applications,* Woodhead Publishing, Cambridge, UK, 2010.
48 S. A. Rackley, *Carbon Capture and Storage*, Elsevier, Burlington, USA, 2010.
49 B. Zhao and Y. Su, Process effect of microalgal-carbon dioxide fixation and biomass production: A review, *Renewable Sustainable Energy Rev.*, 2014, **31**, 121–132.
50 H. S. Kheshgi, H. Thomann, N. A. Bhore, R. B. Hirsch, M. E. Parker and G. F. Teletzke, Perspectives on CCS cost and economics, *SPE Economics and Management*, 2012, **4**(1), 24–31.
51 M. Renner, Carbon prices and CCS investment: A comparative study between the European Union and China, *Energy Policy*, 2014, **75**, 327–340.
52 CSIRO, *Assessing Post-Combustion Capture for Coal-fired Power Stations in Asia-Pacific Partnership Countries, EP116217*, CSIRO Advanced Coal Technology, Newcastle, NW, USA, 2012.
53 A. B. Rao and E. S. Rubin, A Technical, Economic and Environmental Assessment of Amine-Based CO_2 Capture Technology for Power Plant Greenhouse Gas Control, *Environ. Sci. Technol.*, 2002, **36**(20), 4467–4475.
54 R. R. Bottoms, *Process for separating acidic gases*, *U.S. Pat.*, 1783901, 1930, available online at: http://bit.ly/1GIWnoS, accessed 30/05/2015.
55 L. Kohl and R. B. Nielsen, *Gas purification*, 5th edn, Gulf Publishing Company, Huston, Texas, USA, 1997.
56 L. E. Öi, CO_2 removal by absorption: Challenges in modelling, *Math. Comp. Model. Dyn.*, 2010, **16**(6), 511–533.
57 J. C. M. Pires, F. G. Martins, M. C. M. Alvim-Ferraz and M. Simões, Recent developments on carbon capture and storage: an overview, *Chem. Eng. Res. Des.*, 2011, **89**(9), 1446–1460.
58 E. S. Rubin, H. Mantripragada, A. Marks, P. Versteeg and J. Kitchin, The outlook for improved carbon capture technology, *Prog. Energy Combust. Sci.*, 2012, **38**(5), 630–671.
59 P. Folger, *Carbon Capture: A Technology Assessment, R41325*, Congressional Research Service, 2013available online at: http://bit.ly/1esPfhA, accessed 30/05/2015.
60 D. P. Hanak, C. Biliyok, H. Yeung and R. Białecki, Heat integration and exergy analysis for a high ash supercritical coal-fired power plant integrated with a post-combustion carbon capture process, *Fuel*, 2014, **134**, 126–139.
61 H. M. Kvamsdal, M. C. Romano, L. van der Ham, D. Bonalumi, P. van Os and E. Goetheer, Energetic evaluation of a power plant integrated with a piperazine-based

CO_2 capture process, *Int. J. Greenhouse Gas Control*, 2014, **28**(1), 343–355.

62 D. H. Van Wagener, U. Liebenthal, J. M. Plaza, A. Kather and G. T. Rochelle, Maximizing coal-fired power plant efficiency with integration of amine-based CO_2 capture in greenfield and retrofit scenarios, *Energy*, 2014, **72**, 824–831.

63 R. Strube and G. Manfrida, CO_2 capture in coal-fired power plants - impact on plant performance, *Int. J. Greenhouse Gas Control*, 2011, **5**(4), 710–726.

64 R. Shao and A. Stangeland, *Amines Used in CO_2 Capture - Health and Environmental Impacts*, The Bellona Foundation, 2009, available at: http://bit.ly/1fpznvO, accessed 30/05/2015.

65 B. Thitakamol, A. Veawab and A. Aroonwilas, Environmental impacts of absorption-based CO_2 capture unit for post-combustion treatment of flue gas from coal-fired power plant, *Int. J. Greenhouse Gas Control*, 2007, **1**(3), 318–342.

66 K. Veltman, B. Singh and E. G. Hertwich, Human and Environmental Impact Assessment of Postcombustion CO_2 Capture Focusing on Emissions from Amine-Based Scrubbing Solvents to Air, *Environ. Sci. Technol.*, 2010, **44**(4), 1496–1502.

67 H. Bai and A. C. Yeh, Removal of CO_2 Greenhouse Gas by Ammonia Scrubbing, *Ind. Eng. Chem. Res.*, 1997, **36**(6), 2490–2493.

68 T. Brown, C. C. Perry and B. Manthey, *Pleasant Prairie carbon capture demonstration project, Progress report*, Alstom, Wisconsin, 2009.

69 V. Telikapalli, F. Kozak, J. Francois, B. Sherrick, J. Black, D. Muraskin, M. Cage, M. Hammond and G. Spitznogle, CCS with the Alstom chilled ammonia process development program–Field pilot results, *Energy Procedia*, 2011, **4**, 273–281.

70 H. Yu, S. Morgan, A. Allport, A. Cottrell, T. Do, J. McGregor, L. Wardhaugh and P. Feron, Results from trialling aqueous NH_3 based post-combustion capture in a pilot plant at Munmorah power station: Absorption, *Chem. Eng. Res. Des.*, 2011, **89**(8), 1204–1215.

71 J. P. Ciferno, P. DiPietro and T. Tarka, *An economic scoping study for CO_2 capture using aqueous ammonia*, National Energy Technology Laboratory, Advanced Resources International, Energetics Incorporated, 2005.

72 E. Gal, *Chilled-ammonia Post Combustion CO_2 Capture System–Laboratory and Economic Evaluation Results, 1012797*, EPRI, Palo Alto, CA, USA, 2006.

73 L. M. Romeo, S. Espatolero and I. Bolea, Designing a supercritical steam cycle to integrate the energy requirements of CO_2 amine scrubbing, *Int. J. Greenhouse Gas Control*, 2008, **2**(4), 563–570.

74 M. Wang, A. Lawal, P. Stephenson, J. Sidders and C. Ramshaw, Post-combustion CO_2 capture with chemical absorption: A state-of-the-art review, *Chem. Eng. Res. Des.*, 2011, **89**(9), 1609–1624.

75 K. P. Resnik, J. T. Yeh and H. W. Pennline, Aqua ammonia process for simultaneous removal of CO_2, SO_2 and NO_x, *Int. J. Environ. Technol. Manage.*, 2004, **4**(1–2), 89–104.

76 F. Shakerian, K. Kim, J. E. Szulejko and J. Park, A comparative review between amines and ammonia as sorptive media for post-combustion CO_2 capture, *Appl. Energy*, 2015, **148**, 10–22.

77 B. Zhao, Y. Su, W. Tao, L. i. Li and Y. Peng, Post-combustion CO_2 capture by aqueous ammonia: A state-of-the-art review, *Int. J. Greenhouse Gas Control*, 2012, **9**, 355–371.

78 M. Zhao, A. I. Minett and A. T. Harris, A review of techno-economic models for the retrofitting of conventional pulverised-coal power plants for post-combustion capture (PCC) of CO_2, *Energy Environ. Sci.*, 2013, **6**(1), 25–40.

79 B. Sutton, Statement from Peabody Energy on the Department Of Energy's decision to suspend FutureGen, *Peabody Energy*, 2015, available online at http://bit.ly/1LsNh3d, 18/03/2015.

80 C. Marshall and M. Quiñones, Clean Coal Power Plant Killed, Again, *Sci. Am.*, 2015, available online at: http://bit.ly/1DAqa2i, 18/03/2015.

81 R. Soundararajan and T. Gundersen, Coal based power plants using oxy-combustion for CO_2 capture: Pressurized coal combustion to reduce capture penalty, *Appl. Therm. Eng.*, 2013, **61**(1), 115–122.

82 R. Soundararajan, T. Gundersen and M. Ditaranto, *Oxy-combustion coal based power plants: Study of operating pressure, oxygen purity and downstream purification parameters*, Italian Association of Chemical Engineering – AIDIC, 2014.

83 I. Martínez, R. Murillo, G. Grasa and J. Carlos Abanades, Integration of a Ca looping system for CO_2 capture in existing power plants, *AIChE J.*, 2011, **57**(9), 2599–2607.

84 M. C. Romano, Modeling the carbonator of a Ca-looping process for CO_2 capture from power plant flue gas, *Chem. Eng. Sci.*, 2012, **69**(1), 257–269.

85 N. Markusson, The politics of FGD deployment in the UK (1980s-2009), *Case study for the project CCS: Realising the potential*, University of Edinburgh, Edinburgh, Scotland, 2012.

86 L. M. Romeo, J. C. Abanades, J. M. Escosa, J. Paño, A. Giménez, A. Sánchez-Biezma and J. C. Ballesteros, Oxyfuel carbonation–calcination cycle for low cost CO_2 capture in existing power plants, *Energy Convers. Manage.*, 2008, **49**(10), 2809–2814.

87 J. C. Abanades, G. Grasa, M. Alonso, N. Rodriguez, E. J. Anthony and L. M. Romeo, Cost structure of a postcombustion CO_2 capture system using CaO, *Environ. Sci. Technol.*, 2007, **41**(15), 5523–5527.

88 C. C. Cormos, Economic evaluations of coal-based combustion and gasification power plants with post-combustion CO_2 capture using calcium looping cycle, *Energy*, 2014, **78**, 665–673.

89 C. C. Cormos, Assessment of chemical absorption/adsorption for post-combustion CO_2 capture from Natural Gas Combined Cycle (NGCC) power plants, *Appl. Therm. Eng.*, 2015, **82**, 120–128.

90 C. Huang, H. Hsu, W. Liu, J. Cheng, W. Chen, T. Wen and W. Chen, Development of post-combustion CO_2 capture with $CaO/CaCO_3$ looping in a bench scale plant, *Energy Procedia*, 2011, **4**, 1268–1275.

91 M. H. Chang, C. M. Huang, W. H. Liu, W. C. Chen, J. Y. Cheng, W. Chen, T. W. Wen, S. Ouyang, C. H. Shen and

H. W. Hsu, Design and Experimental Investigation of Calcium Looping Process for 3-kW_{th} and 1.9-MW_{th} Facilities, *Chem. Eng. Technol.*, 2013, **36**(9), 1525–1532.

92 X. CCSA, Taiwan inaugurates advanced carbon capture plant, *CCSA Weekly Newsletter*, 2013, **212**(2), 4.

93 N. Rodríguez, M. Alonso and J. C. Abanades, Experimental investigation of a circulating fluidized-bed reactor to capture CO_2 with CaO, *AIChE J.*, 2011, **57**(5), 1356–1366.

94 M. Alonso, N. Rodríguez, B. González, G. Grasa, R. Murillo and J. C. Abanades, Carbon dioxide capture from combustion flue gases with a calcium oxide chemical loop. Experimental results and process development, *Int. J. Greenhouse Gas Control*, 2010, **4**(2), 167–173.

95 A. Sánchez-Biezma, J. C. Ballesteros, L. Diaz, E. de Zárraga, F. J. Álvarez, J. López, B. Arias, G. Grasa and J. C. Abanades, Postcombustion CO_2 capture with CaO. Status of the technology and next steps towards large scale demonstration, *Energy Procedia*, 2011, **4**, 852–859.

96 B. Arias, M. E. Diego, J. C. Abanades, M. Lorenzo, L. Diaz, D. Martínez, J. Alvarez and A. Sánchez-Biezma, Demonstration of steady state CO_2 capture in a 1.7MW_{th} calcium looping pilot, *Int. J. Greenhouse Gas Control*, 2013, **18**, 237–245.

97 A. Sánchez-Biezma, J. Paniagua, L. Diaz, M. Lorenzo, J. Alvarez, D. Martínez, B. Arias, M. E. Diego and J. C. Abanades, Testing postcombustion CO_2 capture with CaO in a 1.7 MW_t pilot facility, *Energy Procedia*, 2013, **37**, 1–8.

98 J. Ströhle, M. Junk, J. Kremer, A. Galloy and B. Epple, Carbonate looping experiments in a 1 MWth pilot plant and model validation, *Fuel*, 2014, **127**, 13–22.

99 L. Bates, Screw conveyors, in *Bulk solids handling: equipment selection and operation*, ed. D. McGlinchey, Blackwell Publishing Ltd, UK, 2008, 1st edn, pp. 197–220.

100 N. Rodríguez, M. Alonso, J. C. Abanades, A. Charitos, C. Hawthorne, G. Scheffknecht, D. Y. Lu and E. J. Anthony, Comparison of experimental results from three dual fluidized bed test facilities capturing CO_2 with CaO, *Energy Procedia*, 2011, **4**, 393–401.

101 A. Charitos, C. Hawthorne, A. R. Bidwe, L. Korovesis, A. Schuster and G. Scheffknecht, Hydrodynamic analysis of a 10 kW_{th} Calcium Looping Dual Fluidized Bed for post-combustion CO_2 capture, *Powder Technol.*, 2010, **200**(3), 117–127.

102 H. Dieter, A. R. Bidwe, G. Varela-Duelli, A. Charitos, C. Hawthorne and G. Scheffknecht, Development of the calcium looping CO_2 capture technology from lab to pilot scale at IFK, University of Stuttgart, *Fuel*, 2014, **127**, 23–37.

103 A. Charitos, C. Hawthorne, A. R. Bidwe, S. Sivalingam, A. Schuster, H. Spliethoff and G. Scheffknecht, Parametric investigation of the calcium looping process for CO_2 capture in a 10 kW_{th} dual fluidized bed, *Int. J. Greenhouse Gas Control*, 2010, **4**(5), 776–784.

104 H. Dieter, C. Hawthorne, M. Zieba and G. Scheffknecht, Progress in Calcium Looping Post Combustion CO_2 Capture: Successful Pilot Scale Demonstration, *Energy Procedia*, 2013, **37**, 48–56.

105 C. Hawthorne, H. Dieter, A. Bidwe, A. Schuster, G. Scheffknecht, S. Unterberger and M. Käß, CO_2 capture with CaO in a 200 kW_{th} dual fluidized bed pilot plant, *Energy Procedia*, 2011, **4**, 441–448.

106 H. Dieter, Design concepts, operating experiences and experimental results of the 200 kW_{th} calcium-looping pilot plant, *2nd International Workshop on Oxy-FBC Technology*, 28-29 June, Stuttgart, 2012, available at: http://bit.ly/1aqVqok, 30/05/2015.

107 G. Varela, A. Charitos, M. E. Diego, E. Stavroulakis, H. Dieter and G. Scheffknecht, Investigations at a 10 kW_{th} calcium looping dual fluidized bed facility: Limestone calcination and CO_2 capture under high CO_2 and water vapor atmosphere, *Int. J. Greenhouse Gas Control*, 2015, **33**, 103–112.

108 A. Ghosh-Dastidar and S. Mahuli, *Calcium carbonate sorbent and methods of making and using same*, *US Pat.*, 5779464, 1998.

109 S. Mahuli and R. Agnihotri, *Suspension carbonation process of reaction of partially utilized sorbent*, *US Pat.*, 6309996 B1, 2001.

110 H. Gupta, T. J. Thomas, A. A. Park, M. V. Iyer, P. Gupta, R. Agnihotri, R. A. Jadhav, H. W. Walker, L. K. Weavers, T. Butalia and L. Fan, Pilot-scale demonstration of the OSCAR process for high-temperature multipollutant control of coal combustion flue gas, using carbonated fly ash and mesoporous calcium carbonate, *Ind. Eng. Chem. Res.*, 2007, **46**(14), 5051–5060.

111 L. Fan, H. Gupta and M. V. Iyer, *Separation of carbon dioxide (CO_2) from gas mixtures by calcium based reaction reparation (CaRS-CO_2) process, US Pat., 0233029, 2008.*

112 W. Wang, S. Ramkumar, S. Li, D. Wong, M. Iyer, B. B. Sakadjian, R. M. Statnick and L. Fan, Subpilot demonstration of the carbonation-calcination reaction (CCR) process: High-temperature CO_2 and sulfur capture from coal-fired power plants, *Ind. Eng. Chem. Res.*, 2010, **49**(11), 5094–5101.

113 R. T. Symonds, D. Y. Lu, R. W. Hughes, E. J. Anthony and A. Macchi, CO_2 capture from simulated syngas via cyclic carbonation–calcination for a naturally occurring limestone: Pilot-plant testing, *Ind. Eng. Chem. Res.*, 2009, **48**(18), 8431–8440.

114 A. Cotton, K. N. Finney, K. Patchigolla, R. E. A. Eatwell-Hall, J. E. Oakey, J. Swithenbank and V. Sharifi, Quantification of trace element emissions from low-carbon emission energy sources: (I) Ca-looping cycle for post-combustion CO2 capture and (II) fixed bed, air blown down-draft gasifier, *Chem. Eng. Sci.*, 2014, **107**, 13–29.

115 A. M. Cotton, *Engineering scale-up and environmental effects of the calcium looping cycle for post-combustion CO_2 capture, PhD thesis,* Cranfield University, Cranfield, UK, 2013.

116 M. Kavosh, *Process engineering and development of post-combustion CO_2 separation from fuels using limestone in CaO-looping cycle, PhD thesis,* Cranfield University, Cranfield, 2011.

117 D. Geldart, Types of gas fluidization, *Powder Technol.*, 1973, **7**(5), 285–292.

118 F. Fang, Z. S. Li and N. S. Cai, Continuous CO_2 capture from flue gases using a dual fluidized bed reactor with

calcium-based sorbent, *Ind. Eng. Chem. Res.*, 2009, **48**(24), 11140–11147.

119 I. Aigner, C. Pfeifer and H. Hofbauer, Co-gasification of coal and wood in a dual fluidized bed gasifier, *Fuel*, 2011, **90**(7), 2404–2412.

120 C. Pfeifer, J.C. Schmid, T. Pröll and H. Hofbauer, Next generation biomass gasifier, Proceedings of the 19th European Biomass Conference and Exhibition, June 6-10 2010, Berlin, Germany, 2010.

121 M. Broda, V. Manovic, Q. Imtiaz, A. M. Kierzkowska, E. J. Anthony and C. R. Müller, High-purity hydrogen via the sorption-enhanced steam methane reforming reaction over a synthetic CaO-based sorbent and a Ni catalyst, *Environ. Sci. Technol.*, 2013, **47**(11), 6007–6014.

122 J. R. Hufton, S. Mayorga and S. Sircar, Sorption-enhanced reaction process for hydrogen production, *AIChE J.*, 1999, **45**(2), 248–256.

123 S. Rawadieh and V. G. Gomes, Steam reforming for hydrogen generation with in situ adsorptive separation, *Int. J. Hydrogen Energy*, 2009, **34**(1), 343–355.

124 H. Hofbauer, R. Rauch, K. Bosch, R. Koch and C. Aichernig, Biomass CHP Plant Güssing – A Success Story, in *Pyrolysis and Gasification of Biomass and Waste*, ed. A. V. Bridgwater, CPL Press, Newsbury, UK, 2003, pp. 371–383.

125 S. Koppatz, C. Pfeifer, R. Rauch, H. Hofbauer, T. Marquard-Moellenstedt and M. Specht, H_2 rich product gas by steam gasification of biomass with in situ CO_2 absorption in a dual fluidized bed system of 8 MW fuel input, *Fuel Process. Technol.*, 2009, **90**(7–8), 914–921.

126 F. Kirnbauer, V. Wilk and H. Hofbauer, Performance improvement of dual fluidized bed gasifiers by temperature reduction: The behavior of tar species in the product gas, *Fuel*, 2013, **108**, 534–542.

127 M. C. Romano and G. G. Lozza, Long-term coal gasification-based power with near-zero emissions. Part B: Zecomag and oxy-fuel IGCC cycles, *Int. J. Greenhouse Gas Control*, 2010, **4**(3), 469–477.

128 C. C. Cormos and A. M. Cormos, Assessment of calcium-based chemical looping options for gasification power plants, *Int. J. Hydrogen Energy*, 2013, **38**(5), 2306–2317.

129 D. P. Connell, D. A. Lewandowski, S. Ramkumar, N. Phalak, R. M. Statnick and L. Fan, Process simulation and economic analysis of the Calcium Looping Process (CLP) for hydrogen and electricity production from coal and natural gas, *Fuel*, 2013, **105**, 383–396.

130 D. Wang, S. Chen, C. Xu and W. Xiang, Energy and exergy analysis of a new hydrogen-fueled power plant based on calcium looping process, *Int. J. Hydrogen Energy*, 2013, **38**(13), 5389–5400.

131 C. Kunze, S. De and H. Spliethoff, A novel IGCC plant with membrane oxygen separation and carbon capture by carbonation-calcinations loop, *Int. J. Greenhouse Gas Control*, 2011, **5**(5), 1176–1183.

132 I. Vorrias, K. Atsonios, A. Nikolopoulos, N. Nikolopoulos, P. Grammelis and E. Kakaras, Calcium looping for CO_2 capture from a lignite fired power plant, *Fuel*, 2013, **113**, 826–836.

133 A. Martínez, Y. Lara, P. Lisbona and L. M. Romeo, Energy penalty reduction in the calcium looping cycle, *Int. J. Greenhouse Gas Control*, 2012, **7**, 74–81.

134 I. Martínez, G. Grasa, R. Murillo, B. Arias and J. C. Abanades, Modelling the continuous calcination of $CaCO_3$ in a Ca-looping system, *Chem. Eng. J.*, 2013, **215–216**, 174–181.

135 F. Fang, Z. Li and N. Cai, Experiment and modeling of CO_2 capture from flue gases at high temperature in a fluidized bed reactor with Ca-based sorbents, *Energy Fuels*, 2009, **23**(1), 207–216.

136 C. J. Abanades, E. J. Anthony, D. Y. Lu, C. Salvador and D. Alvarez, Capture of CO_2 from combustion gases in a fluidized bed of CaO, *Environmental and Energy Engineering*, 2004, **50**(7), 1614–1622.

137 B. Arias, G. S. Grasa and J. C. Abanades, Effect of sorbent hydration on the average activity of CaO in a Ca-looping system, *Chem. Eng. J.*, 2010, **163**(3), 324–330.

138 P. Lisbona, A. Martínez, Y. Lara and L. M. Romeo, Integration of carbonate CO_2 capture cycle and coal-fired power plants. A comparative study for different sorbents, *Energy Fuels*, 2010, **24**(1), 728–736.

139 Z. Li, N. Cai and E. Croiset, Process analysis of CO_2 capture from flue gas using carbonation–calcination cycles, *AIChE J.*, 2008, **54**(7), 1912–1925.

140 J. M. Valverde, P. E. Sanchez-Jimenez and L. A. Perez-Maqueda, Ca-looping for postcombustion CO_2 capture: a comparative analysis on the performances of dolomite and limestone, *Appl. Energy*, 2015, **138**, 202–215.

141 J. Wang and E. J. Anthony, A common decay behavior in cyclic processes, *Chem. Eng. Commun.*, 2007, **194**(11), 1409–1420.

142 J. Wang and E. J. Anthony, On the decay behavior of the CO_2 absorption capacity of CaO-based sorbents, *Ind. Eng. Chem. Res.*, 2005, **44**(3), 627–629.

143 G. S. Grasa and J. C. Abanades, CO_2 capture capacity of CaO in long series of carbonation–calcination cycles, *Ind. Eng. Chem. Res.*, 2006, **45**(26), 8846–8851.

144 A. I. Lysikov, A. N. Salanov and A. G. Okunev, Change of CO_2 carrying capacity of CaO in isothermal recarbonation-decomposition cycles, *Ind. Eng. Chem. Res.*, 2007, **46**(13), 4633–4638.

145 J. C. Abanades, The maximum capture efficiency of CO_2 using a carbonation–calcination cycle of $CaO/CaCO_3$, *Chem. Eng. J.*, 2002, **90**(3), 303–306.

146 D. Berstad, R. Anantharaman and K. Jordal, Post-combustion CO_2 capture from a natural gas combined cycle by $CaO/CaCO_3$ looping, *Int. J. Greenhouse Gas Control*, 2012, **11**, 25–33.

147 J. Ströhle, A. Lasheras, A. Galloy and B. Epple, Simulation of the carbonate looping process for post-combustion CO_2 capture from a coal-fired power plant, *Chem. Eng. Technol.*, 2009, **32**(3), 435–442.

148 I. Martínez, R. Murillo, G. Grasa, N. Rodríguez and J. C. Abanades, Conceptual design of a three fluidised beds combustion system capturing CO_2 with CaO, *Int. J. Greenhouse Gas Control*, 2011, **5**(3), 498–504.

149 A. Charitos, N. Rodríguez, C. Hawthorne, M. Alonso, M. Zieba, B. Arias, G. Kopanakis, G. Scheffknecht and J. C. Abanades, Experimental Validation of the Calcium Looping CO_2 Capture Process with Two Circulating Fluidized Bed Carbonator Reactors, *Ind. Eng. Chem. Res.*, 2011, **50**(16), 9685–9695.

150 J. Ylätalo, J. Parkkinen, J. Ritvanen, T. Tynjälä and T. Hyppänen, Modeling of the oxy-combustion calciner in the post-combustion calcium looping process, *Fuel*, 2013, **113**, 770–779.

151 R. H. Borgwardt, Sintering of nascent calcium oxide, *Chem. Eng. Sci.*, 1989, **44**(1), 53–60.

152 P. Sun, J. R. Grace, C. J. Lim and E. J. Anthony, Removal of CO_2 by calcium-based sorbents in the presence of SO2, *Energy Fuels*, 2007, **21**(1), 163–170.

153 G. S. Grasa, M. Alonso and J. C. Abanades, Sulfation of CaO particles in a carbonation–calcination loop to capture CO_2, *Ind. Eng. Chem. Res.*, 2008, **47**(5), 1630–1635.

154 E. J. Anthony and D. L. Granatstein, Sulfation phenomena in fluidized bed combustion systems, *Prog. Energy Combust. Sci.*, 2001, **27**(2), 215–236.

155 A. Lyngfelt and B. Leckner, Sulphur capture in fluidized bed boilers: The effect of reductive decomposition of CaSO4, *Chem. Eng. J.*, 1989, **40**(2), 59–69.

156 R. Baker, The reversibility of the reaction $CaCO_3 \leftarrow CaO + CO_2$, *J. Appl. Chem. Biotechnol.*, 1973, **23**(10), 733–742.

157 C. Salvador, D. Lu, E. J. Anthony and J. C. Abanades, Enhancement of CaO for CO_2 capture in an FBC environment, *Chem. Eng. J.*, 2003, **96**(1–3), 187–195.

158 G. P. Curran, C. E. Fink and E. Gorin, Carbon dioxide-acceptor gasification process: studies of acceptor properties, *Advanced Chemistry Services*, 1967, **69**, 141–165.

159 A. Silaban, M. Narcida and D. P. Harrison, Characteristics of the reversible reaction between $CO_{2(g)}$ and calcined dolomite, *Chem. Eng. Commun.*, 1996, **146**(1), 149–162.

160 M. Aihara, T. Nagai, J. Matsushita, Y. Negishi and H. Ohya, Development of porous solid reactant for thermal-energy storage and temperature upgrade using carbonation/decarbonation reaction, *Appl. Energy*, 2001, **69**(3), 225–238.

161 V. Manovic, E. J. Anthony, G. Grasa and J. C. Abanades, CO_2 looping cycle performance of a high-purity limestone after thermal activation/doping, *Energy Fuels*, 2008, **22**(5), 3258–3264.

162 H. C. Mantripragada and E. S. Rubin, Calcium looping cycle for CO_2 capture - Performance, cost and feasibility analysis, *Energy Procedia*, 2013, **63**, 2199–2206.

163 V. Manovic and E. J. Anthony, Steam reactivation of spent CaO-based sorbent for multiple CO_2 capture cycles, *Environ. Sci. Technol.*, 2007, **41**(4), 1420–1425.

164 P. S. Fennell, J. F. Davidson, J. S. Dennis and A. N. Hayhurst, Regeneration of sintered limestone sorbents for the sequestration of CO_2 from combustion and other systems, *J. Energy Inst.*, 2007, **80**(2), 116–119.

165 R. W. Hughes, D. Lu, E. J. Anthony and Y. Wu, Improved long-term conversion of limestone-derived sorbents for in situ capture of CO_2 in a fluidized bed combustor, *Ind. Eng. Chem. Res.*, 2004, **43**(18), 5529–5539.

166 G. Grasa, R. Murillo, M. Alonso, B. González, N. Rodríguez and J.C. Abanades, Steam reactivation of CaO-based natural sorbents applied to a carbonation–calcination loop for CO2 capture, 4th International Conference on Clean Coal Technologies, Dresden, Germany, 2009. Cited in; B. Arias, G. S. Grasa and J. C. Abanades, Effect of sorbent hydration on the average activity of CaO in a Ca-looping system, *Chem. Eng. J.*, 2010, **163**, 324–330.

167 J. Blamey, V. Manovic, E. J. Anthony, D. R. Dugwell and P. S. Fennell, On steam hydration of CaO-based sorbent cycled for CO_2 capture, *Fuel*, 2015, **150**, 269–277.

168 D. K. Lee, An apparent kinetic model for the carbonation of calcium oxide by carbon dioxide, *Chem. Eng. J.*, 2004, **100**(1–3), 71–77.

169 S. Bhatia and D. Perlmutter, Effect of the product layer on the kinetics of the CO_2-lime reaction, *AIChE J.*, 1983, **29**(1), 79–86.

170 G. Gupta and L. S. Fan, Carbonation-calcination cycle using high reactivity calcium oxide for carbon dioxide separation from flue gas, *Ind. Eng. Chem. Res.*, 2002, **41**, 4035–4042.

171 G. S. Grasa, J. C. Abanades, M. Alonso and B. González, Reactivity of highly cycled particles of CaO in a carbonation–calcination loop, *Chem. Eng. J.*, 2008, **137**(3), 561–567.

172 Y. S. Yu, W. Q. Liu, H. An, F. S. Yang, G. X. Wang, B. Feng, Z. X. Zhang and V. Rudolph, Modeling of the carbonation behavior of a calcium based sorbent for CO_2 capture, *Int. J. Greenhouse Gas Control*, 2012, **10**, 510–519.

173 S. K. Mahuli, R. Agnihotri, R. Jadhav, S. Chauk and L. Fan, Combined calcination, sintering and sulfation model for $CaCO_3$-SO_2 reaction, *AIChE J.*, 1999, **45**(2), 367–381.

174 P. Sun, J. R. Grace, C. J. Lim and E. J. Anthony, Determination of intrinsic rate constants of the CaO-CO_2 reaction, *Chem. Eng. Sci.*, 2008, **63**(1), 47–56.

175 R. H. Borgwardt, Calcination kinetics and surface area of dispersed limestone particles, *AIChE J.*, 1985, **31**(1), 103–111.

176 F. García-Labiano, A. Abad, L. F. de Diego, P. Gayán and J. Adánez, Calcination of calcium-based sorbents at pressure in a broad range of CO_2 concentrations, *Chem. Eng. Sci.*, 2002, **57**(13), 2381–2393.

177 J. S. Dennis and A. N. Hayhurst, The effect of CO_2 on the kinetics and extent of calcination of limestone and dolomite particles in fluidised beds, *Chem. Eng. Sci.*, 1987, **42**(10), 2361–2372.

178 D. Kunii and O. Levenspiel, *Fluidization engineering*, Butterworth-Heinemann, Stoneham, MA, USA, 2nd edn, 1991.

179 D. Kunii and O. Levenspiel, Fluidized reactor models. 1. For bubbling beds of fine, intermediate and large particles. 2. For the lean phase. Freeboard and fast fluidization, *Ind. Eng. Chem. Res.*, 1990, **29**(7), 1226–1234.

180 E. Turnbull and J. F. Davidson, Fluidized combustion of char and volatiles from coal, *AIChE J.*, 1984, **30**(6), 881–889.

181 Z. Li and N. Cai, Modeling of multiple cycles for sorption-enhanced steam methane reforming and sorbent regeneration in fixed bed reactor, *Energy Fuels*, 2007, **21**(5), 2909–2918.

182 D. Kunii and O. Levenspiel, Circulating fluidized-bed reactors, *Chem. Eng. Sci.*, 1997, **52**(15), 2471–2482.

183 D. Kunii and O. Levenspiel, The K-L reactor model for circulating fluidized beds, *Chem. Eng. Sci.*, 2000, **55**(20), 4563–4570.
184 I. Martínez, G. Grasa, R. Murillo, B. Arias and J. C. Abanades, Kinetics of calcination of partially carbonated particles in a Ca-looping system for CO_2 capture, *Energy Fuels*, 2012, **26**(2), 1432–1440.
185 K. Myöhänen and T. Hyppänen, A three-dimensional model frame for modelling combustion and gasification in circulating fluidized bed furnaces, *Int. J. Chem. React. Eng.*, 2011, **9**, A25.
186 G. D. Silcox, J. C. Kramlich and D. W. Pershing, Mathematical model for the flash calcination of dispersed $CaCO_3$ and $Ca(OH)_2$ particles, *Ind. Eng. Chem. Res.*, 1989, **28**(2), 155–160.
187 *Thermochemical data of pure substances, VCH Verlagsgesellshaft mbH*, ed. I. Barin, Federal Republic of Germany, Weumheim, 1989.
188 K. Atsonios, M. Zeneli, A. Nikolopoulos, N. Nikolopoulos, P. Grammelis and E. Kakaras, Calcium looping process simulation based on an advanced thermodynamic model combined with CFD analysis, *Fuel*, 2015, **153**, 371–381.
189 J. Ylätalo, J. Ritvanen, B. Arias, T. Tynjälä and T. Hyppänen, 1-Dimensional modelling and simulation of the calcium looping process, *Int. J. Greenhouse Gas Control*, 2012, **9**, 130–135.
190 P. S. Fennell, R. Pacciani, J. S. Dennis, J. F. Davidson and A. N. Hayhurst, The effects of repeated cycles of calcination and carbonation on a variety of different limestones, as measured in a hot fluidized bed of sand, *Energy Fuels*, 2007, **21**(4), 2072–2081.
191 O. Senneca, M. Urciuolo and R. Chirone, A semidetailed model of primary fragmentation of coal, *Fuel*, 2013, **104**, 253–261.
192 J. R. Gibbins and R. I. Crane, Scope for reductions in the cost of CO_2 capture using flue gas scrubbing with amine solvents, *Proc. Inst. Mech. Eng., Part A*, 2004, **218**(4), 231–239.
193 R. Khalilpour and A. Abbas, HEN optimization for efficient retrofitting of coal-fired power plants with post-combustion carbon capture, *Int. J. Greenhouse Gas Control*, 2011, **5**(2), 189–199.
194 S. Kishimoto, T. Hirata, M. Iijima, T. Ohishi, K. Higaki and R. Mitchell, Current status of MHI's CO_2 recovery technology and optimization of CO_2 recovery plant with a PC fired power plant, *Energy Procedia*, 2009, **1**(1), 1091–1098.
195 Y. A. Cengel and M. A. Boles, *Thermodynamics: an engineering approach*, McGraw-Hill, New York, NY, USA, 6th in SI units edn, 2007.
196 G. Grasa, R. Murillo, M. Alonso and J. C. Abanades, Application of the random pore model to the carbonation cyclic reaction, *AIChE J.*, 2009, **55**(5), 1246–1255.
197 T. Joutsenoja, P. Heino, R. Hernberg and B. Bonn, Pyrometric temperature and size measurements of burning coal particles in a fluidized bed combustion reactor, *Combust. Flame*, 1999, **118**(4), 707–717.
198 V. Manovic, M. Komatina and S. Oka, Modeling the temperature in coal char particle during fluidized bed combustion, *Fuel*, 2008, **87**(6), 905–914.
199 R. T. Symonds, D. Y. Lu, V. Manovic and E. J. Anthony, Pilot-scale study of CO_2 capture by CaO-based sorbents in the presence of steam and SO_2, *Ind. Eng. Chem. Res.*, 2012, **51**(21), 7177–7184.
200 Y. Lara, P. Lisbona, A. Martínez and L. M. Romeo, A systematic approach for high temperature looping cycles integration, *Fuel*, 2014, **127**, 4–12.
201 Y. Lara, P. Lisbona, A. Martínez and L. M. Romeo, Design and analysis of heat exchanger networks for integrated Ca-looping systems, *Appl. Energy*, 2013, **111**, 690–700.
202 ECN, ECN Phyllis classification, 2012, available at: http://bit.ly/1hrh1cu, accessed 30/05/2015.
203 B. Arias, J. C. Abanades and G. S. Grasa, An analysis of the effect of carbonation conditions on CaO deactivation curves, *Chem. Eng. J.*, 2011, **167**(1), 255–261.
204 A. Martínez, Y. Lara, P. Lisbona and L. M. Romeo, Operation of a cyclonic preheater in the ca-looping for CO_2 capture, *Environ. Sci. Technol.*, 2013, **47**(19), 11335–11341.
205 C. Biliyok and H. Yeung, Evaluation of natural gas combined cycle power plant for post-combustion CO_2 capture integration, *Int. J. Greenhouse Gas Control*, 2013, **19**, 396–405.
206 B. G. Miller, *Clean Coal Engineering Technology*, Butterworth-Heinemann, Boston, USA, 2011.
207 IEA, *CO2 Emissions from Fuel Combustion - Highlights*, OECD/IEA, Paris, France, 2012 edn, 2012.
208 P. Versteeg and E. S. Rubin, A technical and economic assessment of ammonia-based post-combustion CO_2 capture at coal-fired power plants, *Int. J. Greenhouse Gas Control*, 2011, **5**(6), 1596–1605.
209 J. Black, *Cost and Performance Baseline for Fossil Energy Plants Volume 1: Bituminous Coal and Natural Gas to Electricity, DOE/2010/1397 Revision 2a*, National Energy Technology Laboratory, 2013.
210 M. C. Romano and G. G. Lozza, Long-term coal gasification-based power plants with near-zero emissions. Part A: Zecomix cycle, *Int. J. Greenhouse Gas Control*, 2010, **4**(3), 459–468.
211 IEA, *Technology Roadmap: High-Efficiency, Low-Emissions Coal-Fired Power Generation*, OECD/IEA, Paris, France, 2012.
212 R. Anantharaman, O. Bolland, N. Booth, E. van Dorst, C. Ekstrom, E. Sanchez Fernandes, F. Franco, E. Macchi, G. Manzolini, D. Nikolic, A. Pfeffer, M. Prins, S. Rezvani and L. Robinson, *CArbon-free Electricity by SEWGS: Advanced materials, Reactor- and process design. D 4.9 European best practice guidelines for assessment of CO_2 capture technologies, 213206 FP7 - ENERGY.2007.5.1.1,* Politecnico di Milano, Alstom UK, 2011.
213 O. Bollard, N. Booth, F. Franco, E. Macchi, G. Manzolini, R. Naqvi, A. Pfeffer, S. Rezvani and M. Abu Zara, *Enabling advanced pre-combustion capture techniques and plants. D 1.4.1 Common Framework Definition Document, 211971 FP7 - ENERGY.2007.5.1.1*, Alstom UK, 2009.

4 RATE-BASED MODEL DEVELOPMENT, VALIDATION AND ANALYSIS OF CHILLED AMMONIA PROCESS AS AN ALTERNATIVE CO_2 CAPTURE TECHNOLOGY FOR COAL-FIRED POWER PLANTS

Dawid P. Hanak, Chechet Biliyok and Vasilije Manovic

Published: International Journal of Greenhouse Gas Control, 2015, 34, 52–62[e]

Statement of contributions of joint authorship

Dawid P. Hanak conducted the literature review, developed, validated and scaled-up relevant process models, performed simulations and data analysis, drafted and critically revised the manuscript, as well as prepared tables and figures. Chechet Biliyok and Vasilije Manovic proof-read and critically commented on the manuscript prior to its submission to International Journal of Greenhouse Gas Control (Journal Impact Factor 2016: 3.946).

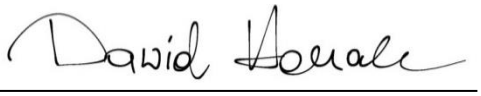

Dawid P. Hanak, PhD Candidate

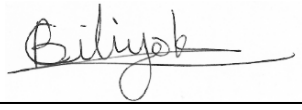

Chechet Biliyok, Associate supervisor

Vasilije Manovic, Principal supervisor

[e] Reprinted with permission from Hanak, D.P., Biliyok, C., and Manovic, V. (2015), "Rate-based model development, validation and analysis of chilled ammonia process as an alternative CO_2 capture technology for coal-fired power plants", *International Journal of Greenhouse Gas Control*, 34, 52–62, doi: 10.1016/j.ijggc.2014.12.013, Elsevier 2015.

International Journal of Greenhouse Gas Control 34 (2015) 52–62

Contents lists available at ScienceDirect

International Journal of Greenhouse Gas Control

journal homepage: www.elsevier.com/locate/ijggc

Rate-based model development, validation and analysis of chilled ammonia process as an alternative CO_2 capture technology for coal-fired power plants

Dawid P. Hanak*, Chechet Biliyok, Vasilije Manovic

Combustion and CCS Centre, Cranfield University, Bedford, Bedfordshire MK43 0AL, UK

ARTICLE INFO

Article history:
Received 10 October 2014
Received in revised form
22 December 2014
Accepted 22 December 2014

Keywords:
Chilled ammonia process
Coal-fired power plant
Carbon capture
Rate-based modelling

ABSTRACT

Due to recent concerns about climate change, which has been triggered by greenhouse gas emissions, the European Union has recommended the decarbonisation of the power sector by 2050 in order to meet its emission reduction target. As a large share of the power generation is currently based on fossil fuels, mainly coal, with this trend expected to continue, clean coal technologies need to be developed. Carbon capture and storage using chemical solvents has been identified to be the most suitable option for coal-fired power plants. The technology which is closest to market commercialisation uses amines, such as monoethanolamine, as a solvent. However, high degradation rates due to impurities present in the flue gas and a considerable heat requirement for solvent regeneration make the application of alternative solvents necessary. In this study, a rate-based aqueous ammonia process model was developed, validated and then modified to a chilled ammonia process model. The model was then scaled up to process flue gas from a 580 MW_{el} supercritical coal-fired power plant. A sensitivity study revealed that the lowest parasitic load occurs for the lean solvent characterised by 12.5%$_{wt}$ NH_3 concentration and 0.29 loading, with the stripper operated between 12.5 and 17.5 bar. The equivalent work requirement for a CAP plant operated at such conditions was found to be up to 15.7% lower than the reference amine scrubbing plant.

1. Introduction

To mitigate the adverse effects of climate change, the European Union committed to reduce its greenhouse gas emissions by at least 80% compared to 1990 levels by the year 2050 (European Commission, 2011). Although the power sector, which is currently dependent on fossil fuel combustion, is a major contributor to global CO_2 emissions, the 2 °C scenario presented by the IEA (2011) assumes that coal-based power generation will still play an essential role in the future energy portfolio. Carbon capture and storage technologies are expected to contribute towards the power sector decarbonisation efforts (Qi et al., 2013), yet only one commercial-scale full cycle facility has been recently commissioned (Fountain, 2014). Post-combustion capture (PCC) plants based upon chemical absorption are a recognised means of reducing CO_2 emissions from coal-fired power plants (CFPP) (Wang et al., 2011; CO2CRC, 2011; Linnenberg et al., 2012). A key advantage of PCC plants is the ease with which they can be retrofitted to the existing fleet of the CFPPs and integrated to new installations (Rackley, 2010). Substantial changes to the CFPP equipment are avoided with a PCC plant retrofit, and a high operating flexibility would be maintained due to relatively independent operation of the CFPP and PCC plant (Wang et al., 2011; CO2CRC, 2011).

Monoethanolamine (MEA) is regarded as the reference chemical solvent, as it will probably be used in the early stage commercial-scale PCC plants integrated to the CFPPs (Padurean et al., 2011; Pfaff et al., 2010). The drawback of using MEA as a solvent is a high penalty imposed on the power plant efficiency. This is mainly caused by a large amount of heat required for solvent regeneration. For the systems without a high degree of heat integration, a reported reduction of the net efficiency reaches up to 14.5% (Bozzuto et al., 2001) with the mean efficiency penalty of 9–11% points (Buchanan et al., 2000; Ciferno et al., 2005; Gerdes et al.,

Abbreviations: AAP, aqueous ammonia process; CAP, chilled ammonia process; CCU, CO_2 compression unit; CFPP, coal-fired power plant; DCC, direct contact cooler; ELECNRTL, electrolyte non-random two-liquid thermodynamic method; GHG, greenhouse gas; HP, high pressure; IP, intermediate pressure; LP, low pressure; MEA, monoethanolamine; PCC, post-combustion capture; PR–BM, Peng–Robinson–Boston–Mathias equation of state.

* Corresponding author. Tel.: +44 01234 750111x5235.
E-mail address: d.p.hanak@cranfield.ac.uk (D.P. Hanak).

http://dx.doi.org/10.1016/j.ijggc.2014.12.013
1750-5836/

Notation

Latin parameters

α_{ij}	reaction order of component i in reaction j (–)
C	concentration (kmol/m^3)
COP	coefficient of performance (–)
E_j	activation energy of reaction j (J/kmol)
K_{eq}	equilibrium constant (–)
k^o	pre-exponential factor (kmol/m^3 s)
Q	thermal duty (MW_{th})
R	gas constant (J/kmol K)
r_j	reaction rate of reaction j (1/s)
T	temperature (K)
W	electric power requirement (MW_{el})

Greek parameters

γ_{NH_3}	solvent loading (mol/mol)

Subscripts

reb	reboiler
chill	chillller
sink	heat sink
pump	rich solvent pump

2010; IEAGHG, 2004; Parsons et al., 2002; Romeo et al., 2008). Moreover, the stripper operating pressure is limited by the thermal degradation limit of amines (Pfaff et al., 2010). Also, amine solvents are sensitive to impurities contained in the CFPP flue gas, such as SO_x and NO_x, with which they form heat-stable salts, and O_2 with which they undergo oxidation (Qi et al., 2013; Ciferno et al., 2005). Therefore, measures aimed at reducing the capture process energy intensity and solvent degradation need to be investigated.

In spite of its toxicity and flammability, NH_3 appears to be a good candidate to replace MEA as a solvent in the PCC plants with reported efficiency penalty ranging between 4.1 and 7% (Ciferno et al., 2005; Romeo et al., 2008; Gal, 2006). This, however, has not been substantiated experimentally yet (Folger, 2013). Key features of NH_3 as a solvent include its relatively low price, commercial availability and a comparatively high CO_2 absorption capacity. In addition, CO_2 absorption by NH_3 is characterised by a lower heat of reaction compared to MEA and thus, less heat is required to regenerate the solvent. Also, NH_3 is not as corrosive as MEA and can be used as a multicomponent capture solvent as it does not degrade on contact with flue gas impurities (Wang et al., 2011; Zhao et al., 2012). However, the drawbacks of using NH_3 in place of MEA include its relatively slow kinetics of CO_2 absorption, which results in larger equipment required, and NH_3 slip in the absorber (Bandyopadhyay, 2011; Strube and Manfrida, 2011).

Other promising PCC technologies currently under development, such as membrane separation and high-temperature solid sorbent looping technologies, which would impose lower energy penalties, are far from being commercialised. Application of membranes is expected to reduce the PCC energy demand by up to 90% compared to direct flue gas scrubbers (Duke et al., 2010); however, the operational issues that result from flue gas impurities, atmospheric pressure and relatively low CO_2 partial pressure need to be resolved. In addition, high-temperature processes using solid sorbents have been estimated to impose an efficiency penalty of only 7–8% (Romano, 2012), and though the well-established fluidised bed technology is utilised, the challenges of sorbent deactivation and regeneration must be resolved before large-scale deployment (Abanades and Alvarez, 2003).

1.1. Ammonia as an alternative to amine solvents

A concept of using NH_3 as an alternative solvent to MEA was first proposed by Bai and Yeh (1997), who experimentally analysed the chemical absorption of CO_2 into NH_3 solution, and found that a capture level of 95% is achievable. Two options for NH_3-based PCC are commonly reported (Linnenberg et al., 2012): aqueous ammonia process (AAP) with CO_2 absorption taking place at ambient temperature (>20 °C) and chilled ammonia process (CAP) in which the CO_2 is absorbed at a low temperature (<20 °C). As NH_3 is characterised by high volatility, which increases with temperature, low-temperature operation of the CAP absorber results in a significant reduction in NH_3 evaporation and thus, NH_3 slip in the absorber (Darde et al., 2010). Not only does it ensure that fugitive NH_3 emissions to the environment are avoided, but it also reduces the capacity or even the requirement of washing sections. This probably makes the CAP process a more feasible option for integration into power plants.

Compared to the MEA-based system, the CAP plant operates efficiently at low temperatures. For this reason, the flue gas temperature needs to be maintained between 0 and 20 °C, preferably between 0 and 10 °C. This is achieved using a system of direct contact coolers (DCC), in which flue gas is first cooled to around 25 °C on direct contact with cooling water, and then chilled to 0–10 °C using a chiller (Gal, 2006; Kothandaraman, 2010; Darde et al., 2009). Chilled flue gas enters the bottom of the absorber while the chilled lean ammonia solvent, which is characterised by lean loading between 0.25 and 0.67, is fed at the top. The solvent loading (γ_{NH_3}) is defined by Eq. (1) (Niu et al., 2012).

$$\gamma_{NH_3} = \frac{[CO_2] + [HCO_3^-] + [CO_3^{2-}] + [NH_2COO^-]}{[NH_3] + [NH_4^+] + [NH_2COO^-]} \quad (1)$$

In the absorber column packing, CO_2 from flue gas is absorbed into the lean solvent at atmospheric pressure. The resulting rich solution leaves the bottom of the absorber with loading between 0.5 and 1. The rich loading could be increased by partial recycling of the rich solution back to the absorber. This also helps in keeping the absorber operating temperature below 20 °C (Gal, 2006; Darde et al., 2009).

The lower the lean solvent loading, the higher is the CO_2 absorption capacity of the solvent. This, however, results in increased partial pressure of NH_3, and hence higher NH_3 slip from the absorber. For this reason, it is advisable to use the CAP absorber equipped with the NH_3 water wash section that utilises large amounts of cold water to remove NH_3 from the treated flue gas. Furthermore, lower concentrations of NH_3, compared to MEA, are utilised in the solvent solution. This causes an increased energy requirement due to highly diluted NH_3 solution (Kothandaraman, 2010).

The rich stream leaving the absorber bottom is pressurised up to 138 bar by a high-pressure pump on its way to the cross heat exchanger, where it is heated up by the lean solution leaving the stripper bottoms, prior to being fed to the stripper. At this pressure, the stripper temperature ranges between 50 and 200 °C. Such operating conditions minimise the evaporation of NH_3 and water, allowing a pure, high-pressure CO_2 stream to be collected from the solution at the top of the stripper (Gal, 2006; Darde et al., 2009). The lean solution, from the stripper bottom, is cooled in the cross heat exchanger and the lean chiller down to a temperature below 10 °C (Kothandaraman, 2010).

1.2. Process modelling of ammonia-based post-combustion CO_2 capture

Although amine scrubbing is the capture technology that is closest to commercialisation (Blamey et al., 2010; Berstad et al., 2012), the benefits of NH_3-based solvent performance require rigorous investigation, especially to quantify the parasitic load that integration of the capture plant would impose on the power plant output. This can be done via modelling and simulations.

Two approaches for modelling of chemical absorption in packed columns are commonly encountered in literature: equilibrium-based and rate-based modelling. In the equilibrium-based approach, it is assumed that vapour and liquid phases exist in equilibrium on a number of theoretical stages. The performance of each stage is characterised by the height equivalent to a theoretical stage and Murphee efficiencies. The rate-based approach involves multi-component mass and heat transfer, as well as chemical reactions, which can be represented by a chemical equilibrium or reaction kinetics (Kothandaraman, 2010). As a result, application of a rate-based modelling approach to model CO_2 absorption and desorption processes is reported to be more accurate and reliable than the equilibrium modelling approach (Afkhamipour and Mofarahi, 2013).

Although the CAP process has been investigated in literature through thermodynamic modelling (Darde et al., 2010) and process simulation (Linnenberg et al., 2012; Jilvero et al., 2011; Versteeg and Rubin, 2011), most of the studies performed were equilibrium based. In particular, Linnenberg et al. (2012) and Darde et al. (2011) used the extended UNIQUAC thermodynamic method to model the complex CO_2–NH_3–H_2O systems. Strube and Manfrida (2011) were the first to apply a rate-based modelling approach to the CAP capture plant. In their work, however, the lean solvent temperature was only reduced to 20 °C, with no intercooling of solvent in the absorbers. As a result, absorption most likely took place at AAP conditions (>20 °C). Nevertheless, a comparison of the rate-based and equilibrium models revealed that the equilibrium approach resulted in an overestimation of rich loading and in the underestimation of the solvent circulation rate and NH_3 slip. This conforms to the conclusions presented by Asprion (2006) who claimed that the application of equilibrium modelling for reactive separation processes results in large deviations from reality. Therefore, rigorous rate-based modelling must be applied to the CAP model development to achieve reliable predictions of the capture plant performance.

Niu et al. (2012) developed a rate-based model of the absorber while Yu et al. (2014) and Zhang and Guo (2014) developed a rate-based model of the stripper in an AAP plant, which were validated with experimental data, and found the model performance to be in good agreement with the data. Additionally, the effectiveness of the rate-based approach was confirmed by Qi et al. (2013) and Zhang and Guo (2013a) who validated their AAP models against the experimental data recorded from the Munmorah pilot plant. However, the large-scale model developed by Zhang and Guo (2013a) for a 500 MW_{el} CFPP achieved the capture level of only 50%.

All of these studies have focused on models for the AAP, with few considering the solvent regenerator, and only one attempting to model a large-scale capture process. However, no study on the development of rate-based modelling of the large-scale CAP process has been presented in the literature. As such models are proven to provide a more reliable prediction of the actual process performance and thus, its integration impact on the power plant performance, a detailed description of the rate-based process modelling of the CAP capture plant and its scale-up are undertaken in this paper. Furthermore, a process analysis is conducted to identify the optimum energy and environmental performance.

Table 1
Validation of the Aspen Plus model performance.

Parameter	Source (Black, 2013)	Aspen Plus model	Deviation (%)
Plant gross output (MW_{el})	580.4	580.4	0.0
Net plant efficiency ($\%_{HHV}$)	39.2	38.5	5.0
Coal consumption rate (kg/s)	51.6	53.8	5.8
Combustion air rate (kg/s)	507.3	526.5	3.8
Steam generation rate (kg/s)	462.3	462.3	0.0

2. Model development

2.1. Supercritical coal-fired power plant

A supercritical CFPP model used as a benchmark in this study, which is developed based on the revised NETL report (Black, 2013), is presented schematically in Fig. 1. The model comprises three sub-models: a supercritical boiler model, a flue gas treatment train, both modelled using Peng–Robinson–Boston–Mathias (PR–BM) equation of state, and a steam cycle in which the unit operations are represented by STEAMNBS correlation.

In addition to the combustion air preheater, the supercritical boiler consists of two main sections: coal combustion and steam generator. The coal rate is adjusted to meet the gross power output of 580 MW_{el}. The combustion process is modelled using the Aspen Plus solid modelling features as recommended by AspenTech (2013). Such approach can be expected to provide a better prediction of the flue gas composition, which, in turn, assures a more reliable prediction of the PCC plant performance. The steam generator consists of the heat exchange sections, which are the primary, secondary, and reheat superheaters, as well as the economiser, modelled as a set of heat exchangers. Both the live (242 bar) and reheat steam generated in these sections are leaving the boiler at the temperature of 593 °C (Black, 2013). Moreover, the model is equipped with flue gas cleaning equipment that includes selective catalytic reduction for NO_x emission control, the electrostatic precipitator for fly ash removal and the flue gas desulphurisation plant.

The steam generated in the supercritical boiler is fed to the turbine section of the CFPP that consists of high- (HP), intermediate- (IP) and low-pressure (LP) extraction condensing steam turbines, the design isentropic efficiencies of which were determined to match the steam discharge conditions (Black, 2013). Moreover, part of the steam from the turbine sections is drawn to feed the main feedwater heating train. This consists of five LP feedwater heaters (LPFWH), the last one of which is called deaerator and is a mixed feedwater heater, and three HP feedwater heaters (HPFWH). Performance of the feedwater heaters is characterised by the minimal temperature difference, which is the difference between the subcooled condensate and inlet feedwater temperature, equal to 5.56 °C (Black, 2013). The steam from the last turbine section is fully condensed in the condenser operating at 0.069 bar.

The overall system performance of the model developed in Aspen Plus complies with values reported in the revised NETL report (Black, 2013), as shown in Table 1. A difference in the net efficiency of the CFPP results from the fact that the moisture content and heat of coal decomposition in the fuel is accounted for in the developed model, hence a slight increase in the fuel consumption is required to reach the rated gross power output.

2.2. Chilled ammonia process plant

2.2.1. Model development and validation

Since no pilot-plant operational data are available for the CAP, a rate-based AAP model is first developed in Aspen Plus V8.4 and

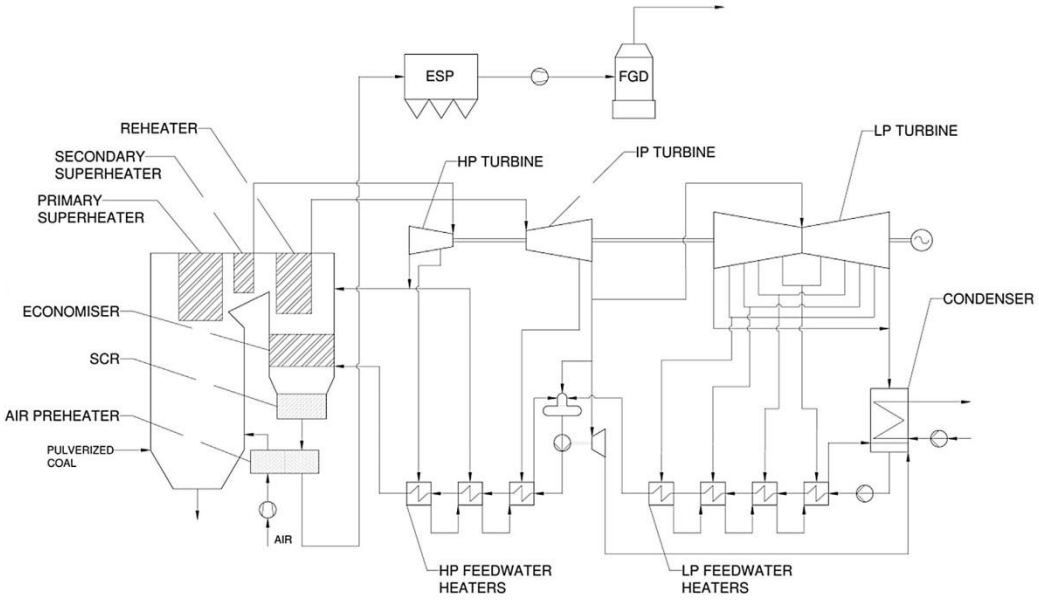

Fig. 1. Process flow diagram of reference 580 MW_{el} supercritical CFPP.

validated with the data available from the Munmorah pilot plant (Table 2).

The pilot-plant consists of two absorbers that were operated in series during the experiments reported by Yu et al. (2011). A developed AAP model was validated in simulations consisting of a single absorber of doubled height. The absorber and stripper are modelled using rate-based capability in RadFrac units, with a closed recycle to achieve a more reliable prediction of the process performance (Biliyok et al., 2012).

The electrolyte non-random two-liquid (ELECNRTL) thermodynamic method is applied for the liquid phase and Redlich–Kwong equation of state is used for the vapour phase properties. The CO_2–NH_3–H_2O chemistry is defined by equilibrium (Eqs. (2)–(4)), salt precipitation (Eq. (5)) and kinetic reactions (Eqs. (6)–(9)) (AspenTech, 2008).

$$NH_3 + H_2O \leftrightarrow NH_4^+ + OH^- \quad (2)$$

$$2H_2O \leftrightarrow H_3O^+ + OH^- \quad (3)$$

$$HCO_3^- + H_2O \leftrightarrow CO_3^{2-} + H_3O^+ \quad (4)$$

$$NH_4HCO_{3(s)} \leftrightarrow NH_4^+ + HCO_3^- \quad (5)$$

$$CO_2 + OH^- \rightarrow HCO_3^- \quad (6)$$

$$HCO_3^- \rightarrow CO_2 + OH^- \quad (7)$$

$$NH_3 + CO_2 + H_2O \rightarrow H_2NCOO^- + H_3O^+ \quad (8)$$

$$H_2NCOO^- + H_3O^+ \rightarrow NH_3 + CO_2 + H_2O \quad (9)$$

The equilibrium constants (K_{eq}) for the reactions presented in Eqs. (2)–(5), given on a molar concentration basis, are temperature dependent and are defined as:

$$\ln K_{eq} = A + \frac{B}{T} + C \cdot \ln T + D \cdot T \quad (10)$$

The values of A, B, C and D for Eqs. (2)–(4) were taken from Edwards et al. (1978), while for Eq. (5) from the solubility data presented by Trypuc and Kielkowska (1996) (Table 3).

The reaction rates (r) of the reactions (j) presented in Eqs. (6)–(9) are determined by the power law:

$$r_j = k_j^o \exp\left(-\frac{E_j}{RT}\right) \prod_{i=1}^{N} C_i^{a_{ij}} \quad (11)$$

where k^o is the pre-exponential factor of reaction j, T is the temperature, E is its activation energy, R is the gas constant, C is the concentration (molar basis) of component i, and α is the reaction order of component i in reaction j.

Power law parameters for the reactions presented in Eqs. (8) and (9) are available from experiments conducted by Pinsent et al. (1956a,b), Puxty et al. (2010) and Jilvero et al. (2014) (Table 4). Therefore, each set of kinetic parameters is applied to the rate-based model and the one that provides the closest match with the Munmorah pilot-plant data is selected for further analysis.

Table 2
Design and operating data of the Munmorah pilot plant (Zhang and Guo, 2013a; Yu et al., 2011).

Parameter	Absorber	Regenerator
Number of columns	2	1
Diameter (m)	0.6	0.6
Packing height (m)	3.9	3.4
Packing type	25 mm Pall Ring	25 mm Pall Ring
Bottom temperature (°C)	26	120
Top pressure (bar)	1.013	6

Table 3
Coefficients of equilibrium constants.

Reaction	A	B	C	D
Eq. (2)	−1.2566	−3335.7	1.4971	−0.0370566
Eq. (3)	132.899	−13445.9	−22.4773	0
Eq. (4)	216.049	−12431.7	−35.4819	0
Eq. (5)	8.06447535	−5013.7598	0	0

Table 4
Power law expression constants.

Reaction	Source	Pre-exponential factor k^o_j (kmol/m^3 s)	Activation energy E_j (J/kmol)
Eq. (6)	Pinsent et al. (1956a)	4.32×10^{13}	55470913.2
Eq. (7)	Pinsent et al. (1956a)	2.38×10^{17}	123305447.0
Eq. (8)	Pinsent et al. (1956b)	1.35×10^{11}	48504078.0
	Puxty et al. (2010)	1.66×10^{14}	60990168.0
	Jilvero et al. (2014)	6.51×10^{13}	60090608.0
Eq. (9)	Pinsent et al. (1956b)	4.75×10^{20}	69203617.2
	Puxty et al. (2010)	1.27×10^{22}	80215648.0
	Jilvero et al. (2014)	4.97×10^{21}	79316088.0

Implementation of the power law parameters estimated by Pinsent et al. (1956b) data provided close prediction of the Munmorah pilot plant for the test case under consideration. When the Puxty et al. (2010) and Jilvero et al. (2014) power law parameters were implemented, the CO_2 absorption rate was over-estimated by 23.8% and 22.9%, respectively (Table 5). This, in turn, resulted in the reboiler duty higher by 27.6% and 27.4%, respectively, that would have a considerable impact on the prediction accuracy of the overall process performance. Therefore, it is concluded that the power law parameters for the reactions presented in Eqs. (8) and (9) determined from Pinsent et al. (1956b) data provide a better representation of the absorption and desorption processes.

The parameters given by Pinsent et al. (1956b) were obtained from data for NH_3 concentrations of 0.19 kmol/m^3 and 0.027 kmol/m^3, while higher concentrations are used in this study. Therefore, it is important to understand the influence of NH_3 concentration on the reaction rate, in order to justify the use of kinetic parameters provided by Pinsent et al. (1956b). Derks and Versteeg (2009) experimentally revealed that the reaction rate is linearly dependent on NH_3 concentration for values higher than 0.1 kmol/m^3 (Fig. 2). Moreover, their results can be seen as a linear extension of data from Pinsent et al. (1956b) . Therefore, the power law parameters for reactions presented in Eqs. (8) and (9) based on the Pinsent et al. (1956b) can be used to extrapolate the reaction rates at higher NH_3 concentrations. In fact, these parameters have been previously applied with success in modelling of the AAP process (Qi et al., 2013; Niu et al., 2012; Yu et al., 2011; Brettschneider et al., 2004).

The rate-based model performance is further compared with two more pilot plant test cases in Table 6 to confirm its validity. It is concluded that the prediction of the process performance provided by the rate-based model is in good agreement with the pilot-plant performance. Small deviations of the key parameters received from the model are within experimental uncertainty resulting from the measurement equipment accuracy.

2.2.2. Chilled ammonia process modelling and scale up

The operating conditions in the model are modified to match CAP process, using process information provided in Gal (2006). As illustrated in Fig. 3, the flue gas and lean solvent are chilled to 7 and 10 °C, respectively, before being fed to the absorber. Although the rich solution can be regenerated at pressures reaching up to 138 bar, the stripper is initially operated at the pressure of 10 bar due to the structural and material limitations (Strube and Manfrida, 2011), but most importantly due to reboiler steam pressure considerations. The stripper condenser operates at 20 °C and stripper reboiler at approximately 150–160 °C, preventing NH_3 and water from evaporating to ensure that a pure, high-pressure CO_2 stream is collected at the top of the stripper.

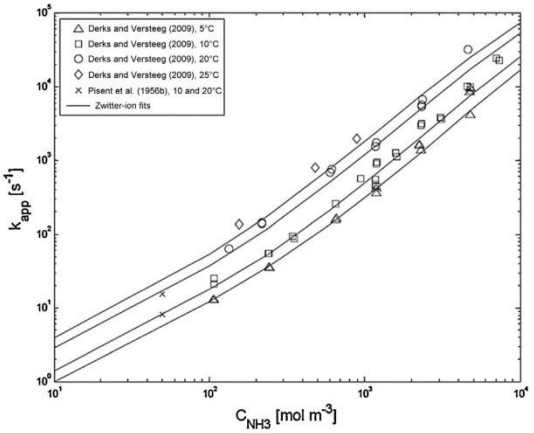

Fig. 2. Apparent kinetic rates for CO_2 absorption by aqueous solution of NH_3 (Reprinted from Derks and Versteeg (2009) with permission from Elsevier).

Although Gal (2006) has stated that NH_3 concentration in the lean solvent may reach up to 28%$_{wt}$, this results in a high NH_3 slip and requires additional water wash for the flue gas to meet the emission standards. This, in turn, requires an additional amount of energy and increases the efficiency penalty. Therefore, the NH_3

Table 5
Effect of the rate constants on process performance prediction.

Parameter	Test ID 31			
	Experiment (Yu et al., 2011)	Pinsent et al. (1956b)	Puxty et al. (2010)	Jilvero et al. (2014)
Inlet flue gas flow rate (kg/h)	646	646	646	646
Inlet CO_2 flow rate (kg/h)	99.3	99.3	99.3	99.3
CO_2 lean loading (mol/mol)	0.24 ± 0.01	0.24	0.24	0.24
CO_2 rich loading (mol/mol)	0.32 ± 0.03	0.34	0.37	0.36
CO_2 absorption rate (kg/h)	80 ± 2	79.8	99.0	98.3
CO_2 capture level (%)	80.2	80.4	99.7	98.9
Stripper bottoms temperature (°C)	131.6	133.8	146.2	146.2
Reboiler duty (kW)	111.0	109.0	141.6	141.4
Lean solvent flow rate (L/min)	134.0	134.0	134.0	134.0
Lean solvent NH_3 concentration (%$_{wt}$)	4.08 ± 0.1	4.08	4.08	4.08

Table 6
Validation of the rate-based AAP model against the Munmorah pilot-plant data.

Parameter	Test ID 31			Test ID 32			Test ID 32B		
	Experiment	Simulation	Difference	Experiment	Simulation	Difference	Experiment	Simulation	Difference
Inlet flue gas flow rate (kg/h)	646	646	0	780	780	0.00	821	821	0.00
Inlet CO_2 flow rate (kg/h)	99.3	99.3	0	123	123	0.00	112.7	112.7	0.00
CO_2 lean loading (mol/mol)	0.24 ± 0.01	0.24	0	0.24 ± 0.03	0.27	−0.03	0.22 ± 0.02	0.22	0.00
CO_2 rich loading (mol/mol)	0.32 ± 0.03	0.34	−0.02	0.37 ± 0.03	0.40	−0.03	0.32 ± 0.03	0.35	0.03
CO_2 absorption rate (kg/h)	80 ± 2	79.8	0.20	76 ± 5	80.2	−4.20	80 ± 4	81.33	−1.33
CO_2 capture level (%)	80.2	80.4	−0.20	61.7	65.2	−3.50	71.4	72.17	−0.77
Stripper bottom liquid temperature (°C)	131.6	133.8	−2.2	129.7	133	−3.30	131.6	138.4	−6.80
Reboiler duty (kW)	111.0	109.0	−2	111.0	105.1	5.90	111.0	114.8	−3.80
Lean solvent flow rate (L/min)	134.0	134.0	0	134.0	134.0	0.00	134.0	134.1	−0.10
Lean solvent NH_3 concentration (%$_{wt}$)	4.08 ± 0.1	4.08	0	3.6 ± 0.4	3.2	0.40	3.9 ± 0.2	3.7	0.20

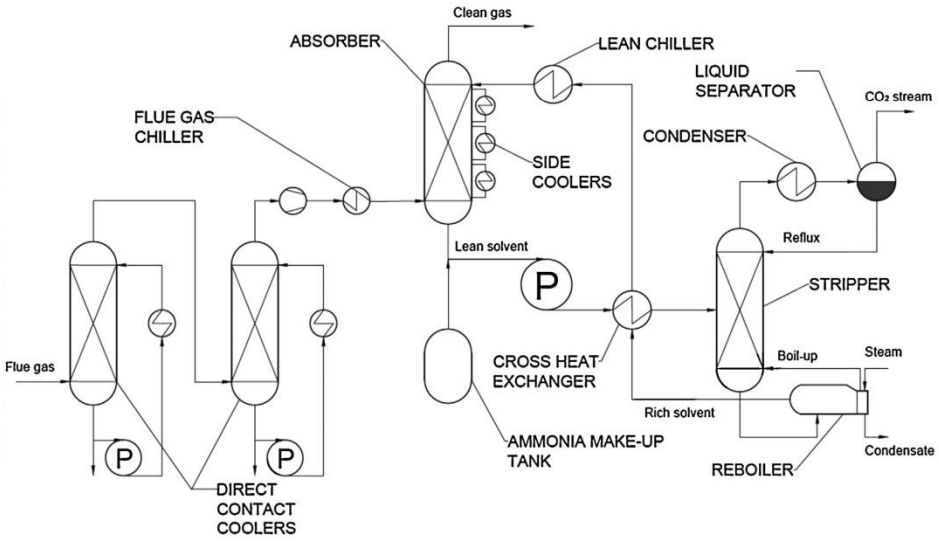

Fig. 3. Simplified process flow diagram of full-scale CAP capture plant.

concentration is set at 15%$_{wt}$, as Zhao et al. (2012) have shown that such a moderate NH_3 concentration results in improved CO_2 absorption capacity. A lean solvent loading of 0.25 is used in the preliminary CAP model development. Additionally, very low temperatures may result in salt precipitation in both the absorber and the stripper, which can clog the packing. Therefore, the absorber is operated below 20 °C and cooled with cooling water of ambient temperature to minimise the chilling duty required. Although a detailed design to address the temperature bulge in the absorber is beyond this study scope, the coolers are located between 7.5 and 18.0 m from the absorber bottom to control the temperature distribution in the absorber. Such an approach is similar to the one proposed by Kothandaraman (2010).

Finally, the model is scaled up to meet the requirement of 90% CO_2 capture level from the 580 MW_{el} CFPP. Using the generalised pressure drop correlation, along with physical properties available in the simulation, the cross-sectional areas of the absorber and stripper columns are determined. As Sinnott and Towler (2013) have recommended the design pressure drop values for absorbers and strippers to be between 15 and 50 mmH_2O/m of packing, a pressure drop of 42 mmH_2O/m is selected. Process stream information and initial design parameters are given in Table 7.

A MELLAPAK 350X packing, which has been recognised to provide excellent performance with columns of up to 15 m in diameter (Sulzer, 2012), is used in sizing the columns. To determine the required number of units, a sensitivity study is conducted (Fig. 4). It reveals that using one absorber would require a diameter of 18.4 m. Such a solution is not viable in terms of structural limitations and operational reliability. Therefore, with consideration of the part-load operation of the power plant, two absorbers of 13 m diameter, and one stripper of 10 m diameter are selected. The main parameters characterising the developed full-scale CAP model are presented in Table 8.

Table 7
CAP–PCC preliminary design.

Parameter	Value
Flue gas flow rate (kg/s)	562.0
Flue gas CO_2 content (%$_{wt}$)	21.64
Captured CO_2 flow rate (kg/s)	109.5
Required lean solvent flow rate (kg/s)	2014.0
Absorber cross sectional area requirement (m^2)	264.8
Stripper cross sectional area requirement (m^2)	78.4
Absorber and stripper packing height (m)	30
Absorber and stripper packing type	Mellapak 350X

2.3. CO_2 compression unit

Metz and Davidson (2007) state that sufficient CO_2 stream conditions for the pipeline transport are ambient temperature and

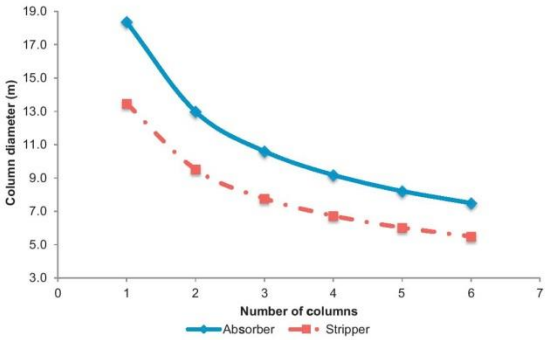

Fig. 4. Determination of a column number for the large-scale chilled ammonia process.

Table 8
Full-scale CAP plant operating conditions.

Stream parameter	Value	Equipment parameter	Value
Liquid-gas ratio (mass basis)	3.647	Reboiler temperature (°C)	164.9
Lean loading (mol/mol)	0.250	Specific reboiler duty ($MW_{th}/kgCO_2$)	3.4
Rich loading (mol/mol)	0.415	Condenser temperature (°C)	20.0
CO_2 stream purity (mass basis)	0.938	Stripper pressure (bar)	10.0
CO_2 capture level (mass basis)	0.900	Reflux ratio (mass basis)	0.233

pressure of 110 bar. To minimise the compression work required, it is assumed that CO_2 is first compressed to the critical pressure of 74 bar and then pumped to 110 bar prior to transport (Table 9). Although the energy requirement of the capture section imposes the highest energy penalty on the CFPP, a CO_2 conditioning energy requirement prior to transport is of significant magnitude and must be considered in the analysis.

Each compression stage of the CO_2 compression unit (CCU) consists of a centrifugal compressor, stage intercoolers and scrubbers. Such configuration brings two-fold benefits to the system performance: firstly, the volumetric flow rate of the gas through the compressor is reduced on cooling, hence required compression power is reduced; secondly, the moisture and impurities content in the gas stream is reduced, preventing erosion of the compressor components. The CO_2 compression is modelled using the polytrophic compression model with constant stage polytrophic efficiency (78–79%) (Pfaff et al., 2010; Posch and Haider, 2012). A number of compression stages for a particular case is determined based on the assumption that the pressure ratio and the polytrophic head should not exceed 3 and 3050 m, respectively, due to equipment limitations (Sanpasertparnich et al., 2010).

Table 9
CO_2 compression unit specification and preliminary performance.

Unit	Discharge pressure (bar)	Discharge temperature (°C)	Net power consumption (MW_{el})
1st compressor	16.793	72.85	4.52
2nd compressor	27.790	93.27	4.46
3rd compressor	47.745	96.65	4.27
4th compressor	74.000	83.45	2.56
Pump	110.000	31.57	0.31

3. Parametric study

3.1. Considerations

In general, the chilling duty of the system depends on the lean solvent flow rate and temperature. More importantly, the reboiler duty determines the steam requirement. Therefore, to achieve an optimal operating condition in the CAP plant, while maintaining a 90% capture level, both the solvent flow rate and the reboiler duty must be minimised. Therefore, parametric studies are conducted on parameters that influence both variables:

- lean solvent NH_3 concentration between 7.5 and 17.5%$_{wt}$;
- lean loading between 0.25 and 0.31;
- stripper pressure between 10 and 40 bar.

Although the CAP plant can be operated with a higher lean solvent NH_3 concentration and lean loadings, this would result in solid precipitation. This, in turn, would result in clogging of the packed columns and thus, a reduction in the capture performance due to decrease in the liquid–gas mass transfer area.

When the CAP plant is integrated to a power plant, there are four main units that require energy input from the power plant – electricity is required to drive pumps (W_{pump}), compressors (W_{comp}) and chillers (W_{chill}), which is calculated based on the chilling duty (Q_{chill}) using Eq. (12) with the coefficient of performance assumed to be 7.8 (MHI, 2012), and heat is required in the reboiler (Q_{reb}) for solvent regeneration, usually by extracting steam from the power plant steam cycle. To determine the total parasitic load, a summation of the electricity and heat requirements would be thermodynamically inaccurate as they differ in the energy quality. Therefore, an equivalent work is determined to evaluate the overall energy requirement (W_{eq}) of the CAP using Eq. (13) (Van Wagener and Rochelle, 2011). The electricity generated by the generator coupled with the steam turbines before CAP plant integration is a function of Carnot efficiency, which accounts for non-ideal expansion in the turbine. Moreover, the equivalent work also depends on the reboiler temperature (T_{reb}) and the sink temperature (T_{sink}), which is about 15 °C in the temperate regions of Europe.

$$COP = \frac{Q_{chill}}{W_{chill}} \tag{12}$$

$$W_{eq} = 0.75 \cdot Q_{reb} \cdot \left(\frac{T_{reb} + 10 - T_{sink}}{T_{reb} + 10}\right) + W_{pump} + W_{chill} + W_{comp} \tag{13}$$

3.2. Effect on reboiler duty

An increase in the solvent NH_3 concentration results in a reduction in the required circulation flow rate (Fig. 5). This, in turn, impacts the reboiler duty, as more solvent entering the reboiler requires more energy for its heating. However, as lean solvent of high loading is characterised by diminished solvent absorption capacity, it is observed in Fig. 5 that operating at lean loadings higher than 0.30 for NH_3 concentrations higher than 15%$_{wt}$ would require an increase in the solvent circulation rate to achieve a 90% capture level. Therefore, a combination of higher solvent concentrations and lower lean loadings may be recommended, as this leads to lower solvent circulation rates as predicted in the analysis, and hence less chilling duty and pumping power are targeted. Unfortunately, operating the CAP plant under such conditions results in greater NH_3 slip in the absorber, which increases with increasing solvent concentration and decreasing lean loading (Fig. 6).

More importantly, the analysis reveals a complex impact on the reboiler duty (Fig. 7). For the lean loading of 0.25, increasing

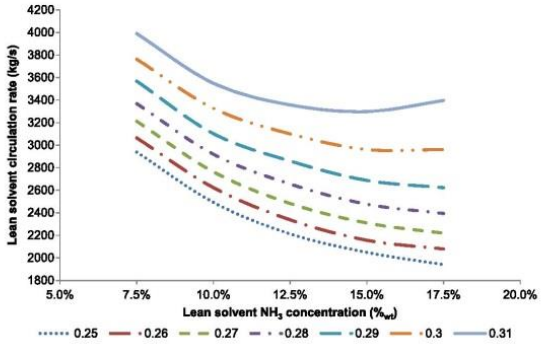

Fig. 5. Impact of the solvent concentration and loading on the solvent circulation rate.

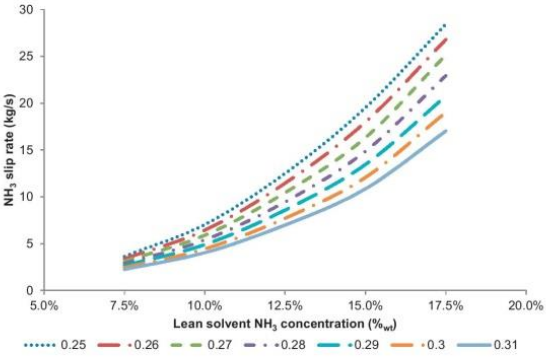

Fig. 6. Impact of the solvent concentration and loading on the NH_3 slip rate in the absorber.

the solvent NH_3 concentration causes a uniform reduction of the reboiler duty. This is due to the reduced solvent circulation rate, which is a consequence of the higher NH_3 concentration, when a 90% capture level is maintained. The impact of the reduced solvent circulation rate on the reboiler duty diminishes at higher lean loadings, where any increase in the NH_3 concentration in the solvent results only in a slight reduction of the reboiler duty (lean loading of 0.26) and even in a significant increase in the reboiler duty (above 0.26) at solvent concentrations higher than 12.5%$_{wt}$. This complex behaviour can be attributed to the changing energy demand of the

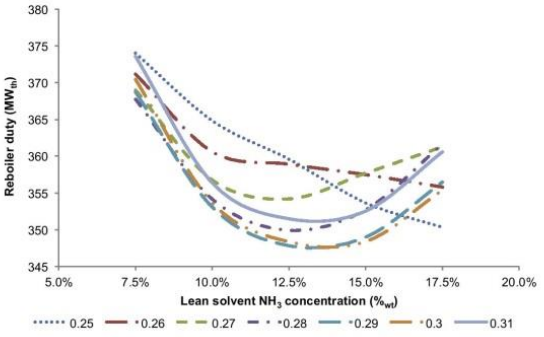

Fig. 7. Impact of the solvent concentration and loading on the reboiler duty.

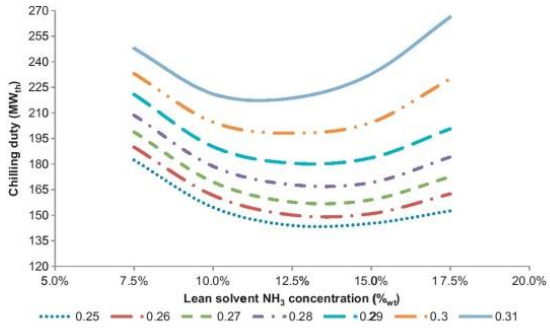

Fig. 8. Impact of the solvent concentration and lean loading on the chilling duty.

components that contribute to make up the reboiler duty. Biliyok and Yeung (2013) surmised that the energy supplied to the reboiler for solvent regeneration in the stripper is used to:

- increase the rich solvent to the reboiler temperature (sensible heat);
- evaporate the solvent (latent heat), which then acts as a stripping agent in the stripper;
- reverse the chemical reaction that has taken place in the absorber (heat of reaction);
- liberate CO_2 dissolved in the solvent (heat of dissolution).

As a rate-based model, with chemical reactions implemented, is used in this work, such complex interactions can be explored. The summation of the heat of reaction and dissolution is the heat of absorption, and in general, a higher solvent concentration means more solvent available for chemical reaction. Therefore, a higher heat of absorption is expected, as more heat is liberated per unit volume of the solvent in the absorber. Therefore, although higher NH_3 concentrations lead to lower lean solvent flow rates and thus reduced sensible heat requirement to increase the rich solvent temperature, they result in more energy required to reverse the exothermic reaction that has taken place in the absorber.

Moreover, although operation of the CAP plant with the solvent NH_3 concentration of 17.5%$_{wt}$ and low lean loadings improves process performance, it leads to high NH_3 slip. Consequently, the optimum operating point for the CAP plant falls within the range of NH_3 concentration of 10–15%$_{wt}$ and a lean loading of 0.28–0.31.

3.3. Effect on chilling duty

The CAP CO_2 capture plant comprises two chillers – the flue gas chiller, whose duty is unchanged as the flue gas load is fixed, and the lean chiller, whose duty is dependent upon the solvent NH_3 concentration and lean loading, both of which affect the solvent circulation rate (Fig. 5), as well as the lean solvent temperature. From Fig. 8, it is clear that the CAP plant chilling requirement increases with the lean solvent loading at constant solvent NH_3 concentration, due to a corresponding increase in the solvent circulation rate.

However, for the considered range of lean loading values, the chilling duty requirement falls to a minimum value at approximately 12.5%$_{wt}$, and then begins to increase as solvent NH_3 concentration is increased. This is explained by the reduction in the solvent circulation rate as NH_3 concentration increases, which results in a reduction of the chilling duty for solvents. As NH_3 concentration exceeds 12.5%$_{wt}$, the chiller duty requirement increases as the solvent circulating flow rate decreases. This is due to the

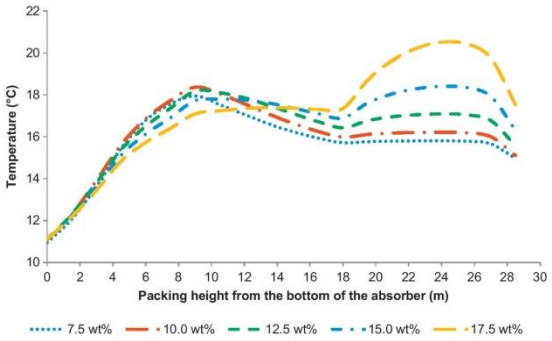

Fig. 9. Impact of the solvent concentration on the absorber temperature profile at lean loading of 0.29.

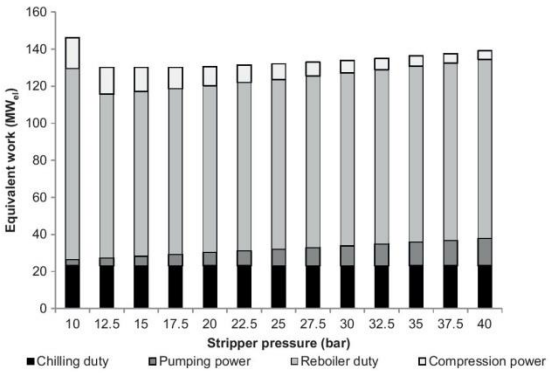

Fig. 11. Impact of the stripper on the equivalent work requirement.

temperature profile in the absorber, which reveals that temperature increases with higher NH_3 concentration in the solvent (Fig. 9).

This temperature increase is brought about by a higher rate of chemical reaction in the absorber, which releases more heat due to its exothermic nature. In addition, due to the lower circulation rate at constant flue gas rate, and hence lower liquid-gas ratio, at higher solvent NH_3 concentration the temperature bulge is located at the top of the absorber, above the cooling section (Fig. 9). As the rich solution leaves the absorber at higher temperature, less heat is transferred in the cross heat exchanger. Therefore, the lean solution enters the lean chiller at higher temperature, which is why a greater chiller duty is required to maintain CAP conditions. Therefore, to minimise the chilling duty the CAP plant should be operated between 10 and 15%$_{wt}$ for NH_3 solvent concentrations and between 0.25 and 0.30 for lean loading.

3.4. Optimum operating point

3.4.1. Optimum lean solvent NH_3 concentration and loading

To identify the operating conditions resulting in the minimal parasitic load imposed on the power plant by the CAP process, an equivalent work is determined for the range of lean solvent NH_3 concentrations and lean loadings.

Fig. 10 reveals that the energy requirement of the CAP plant is greatest at low solvent NH_3 concentration. This is due to high electricity demand for both chillers and pumps, as well as a high heat requirement for solvent regeneration. An increase in the solvent NH_3 concentration reduces the overall energy requirement up to a clear minimum value that can be identified for the lean solvent NH_3 concentration of about 12.5%$_{wt}$. Above this value the overall energy requirement increases, as expected from the trends observed in the reboiler and chilling duty.

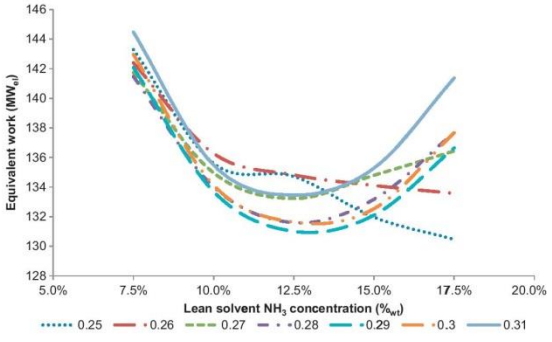

Fig. 10. Impact of the solvent concentration and lean loading on the equivalent work requirement.

The parametric study revealed that the minimal equivalent work requirement of the CAP plant is achieved at a solvent NH_3 concentration of about 12.5%$_{wt}$ and a lean loading of 0.29. Compared to different operating points presented in Fig. 6, operation of the CAP plant under such conditions is characterised by moderate NH_3 slip rate in the clean gas of 8.6 kg/s, as a result of relatively high lean loading, even though absorber temperatures remain below 20 °C. This corresponds to the NH_3 slip of 30,900 ppmv, which is 19.2% less compared to 38,200 ppmv estimated by Zhang and Guo (2013a) for the large-scale AAP plant. Moreover, based on the models for the CO_2 capture plant using 30%$_{wt}$ MEA developed by Hanak et al. (2014), in which the CO_2 absorption is conducted at temperatures close to the AAP conditions, the MEA slip in the absorber is two orders of magnitude lower and amounts to 181 ppmv.

Such NH_3 emission rate is unacceptable as high NH_3 concentration can cause severe harm to the plant operators' health and adverse environmental effects (APM, 2013). Therefore, the regulations regarding the allowable human exposure NH_3 concentrations have been implemented worldwide that vary between 20 ppmv (Manning et al., 2007; Barrasa et al., 2012) and 50 ppmv (Han et al., 2013). It needs to be pointed out that the maximum allowable NH_3 slip in the selective catalytic reduction system for NO_x emission mitigation is usually set as 5 ppmv (DiFrancesco et al., 1997; Schallert, 1993; Zhou et al., 2013; Jensen-Holm et al., 2007), with the average of 2 ppmv for 90% NO_x removal in ideal uniform conditions (Rogers and Nolan, 2001). Based on the study by Zhang and Guo (2013b), who identified that the average NH_3 slip of 1–2 ppmv in the AAP plant corresponds to the NH_3 slip rate of 0.0006 kg/s, an additional water wash section is required. However, this is not included in the scope of this study.

3.4.2. Optimum stripper pressure

All scenarios presented above were conducted with the assumption that the stripper is operated at 10 bar. However, as it is claimed that the CAP plant would perform better at elevated pressures, the impact of the stripper pressure on the equivalent work requirement is analysed (Fig. 11).

This analysis revealed that variation in the stripper pressure has a minor effect on the chilling duty. Conversely, it has a considerable impact on the rich pump energy requirement. Yet, an increase in the pumping power resulted in the CO_2 stream taken from the top of the stripper at a higher pressure. This considerably reduces

the compression work requirement. This also lowers the reboiler duty required; however, the operating temperature of the reboiler increases with pressure; hence steam of higher quality would be required. A reduction of the reboiler duty caused by the increase in the CO_2 and H_2O equilibrium partial pressures ratio at higher temperatures was found to be typical for solvents of high heat of CO_2 absorption (Darde et al., 2012). Finally, to operate the stripper at higher pressures, thicker column walls or materials of higher strength would be employed, which would directly increase the capital cost.

Overall, the minimal equivalent work of 130 MW_{el} was observed at stripper pressures between 12.5 bar and 17.5 bar. Within this range, an increase in the equivalent work related to the reboiler duty and the pumping power requirement is balanced by a decrease in the compression power requirement. For higher stripper pressures, however, the compressor power requirement reduction is outweighed by the increase of the remaining constituents, resulting in the equivalent work increase. Comparing performance of the CAP plant and the conventional MEA process, it is found that the equivalent work estimated in this study for the CAP plant (323 kWh/tCO_2) is 4.7–15.7% lower (339–383 kWh/tCO_2) (Hanak et al., 2014; Ahn et al., 2013).

4. Conclusions

This study was undertaken to develop a large-scale rate-based model of CAP and to explore its expected advantages over MEA and AAP processes. First, a pilot-plant scale AAP rate-based model was developed and validated with the Munmorah pilot-plant data to prove the efficacy of the proposed modelling approach. As the model was found to be in agreement with the plant data, it was then tuned to operate under CAP conditions, before it was scaled up to handle the flue gas from a 580 MW_{el} coal-fired power plant. A parametric study identified the dimensions and number of columns required at this scale. It was identified that two absorbers and a single stripper are required to accommodate this volume of flue gas. Such configuration is expected to be beneficial under part-load operation.

The impact of the lean solvent NH_3 concentration and loading are analysed, and an optimum operational point was found, which results in the lowest parasitic load on the CFPP, for the conditions under consideration, at NH_3 concentration of about 12.5%$_{wt}$, loading of about 0.29 and stripper pressure between 12.5 bar and 17.5 bar. At this point, the CAP plant performance resulted in a 4.7–15.7% reduction in the equivalent work required by the PCC plant with CCU compared to the MEA process, although a significant chilling duty is also imposed.

References

Abanades, C.J., Alvarez, D., 2003. Conversion limits in the reaction of CO_2 with lime. Energy Fuels 17, 308–315.

Afkhamipour, M., Mofarahi, M., 2013. Comparison of rate-based and equilibrium-stage models of a packed column for post-combustion CO_2 capture using 2-amino-2-methyl-1-propanol (AMP) solution. Int. J. Greenh. Gas Control 15, 186–199.

Ahn, H., Luberti, M., Liu, Z., Brandani, S., 2013. Process configuration studies of the amine capture process for coal-fired power plants. Int. J. Greenh. Gas Control 16, 29–40.

Avantor Performance Materials, 2013. Safety Data Sheet – Ammonia Solution, Strong; Ammonium Hydroxide, Available at: http://bit.ly/1D97y9L (accessed 10.12.14).

AspenTech, 2008. Rate-Based Model of the CO_2 Capture Process by NH_3 using Aspen Plus. Aspen Technology, Inc., Cambridge, MA, USA.

AspenTech, 2013. Aspen Plus: Getting Started Modeling Processes with Solids. Aspen Technology, Inc., Burlington, MA, USA.

Asprion, N., 2006. Nonequilibrium rate-based simulation of reactive systems: simulation model, heat transfer, and influence of film discretization. Ind. Eng. Chem. Res. 45 (6), 2054–2069.

Bai, H., Yeh, A.C., 1997. Removal of CO_2 greenhouse gas by ammonia scrubbing. Ind. Eng. Chem. Res. 36 (6), 2490–2493.

Bandyopadhyay, A., 2011. Amine versus ammonia absorption of CO_2 as a measure of reducing GHG emission: a critical analysis. Clean Technol. Environ. Policy 13 (2), 269–294.

Barrasa, M., Lamosa, S., Fernandez, M.D., Fernandez, E., 2012. Occupational exposure to carbon dioxide, ammonia and hydrogen sulphide on livestock farms in north-west Spain. Ann. Agric. Environ. Med. 19 (1), 17–24.

Berstad, D., Anantharaman, R., Jordal, K., 2012. Post-combustion CO_2 capture from a natural gas combined cycle by $CaO/CaCO_3$ looping. Int. J. Greenh. Gas Control 11, 25–33.

Biliyok, C., Yeung, H., 2013. Evaluation of natural gas combined cycle power plant for post-combustion CO_2 capture integration. Int. J. Greenh. Gas Control 19, 396–405.

Biliyok, C., Lawal, A., Wang, M., Seibert, F., 2012. Dynamic modelling, validation and analysis of post-combustion chemical absorption CO_2 capture plant. Int. J. Greenh. Gas Control 9, 428–445.

Black, J., 2013. Cost and Performance Baseline for Fossil Energy Plants Volume 1: Bituminous Coal and Natural Gas to Electricity, DOE/2010/1397 Revision 2a. National Energy Technology Laboratory.

Blamey, J., Anthony, E., Wang, J., Fennell, P., 2010. The calcium looping cycle for large-scale CO_2 capture. Prog. Energy Combust. Sci. 36 (2), 260–279.

Bozzuto, C.R., Nsakala, N., Liljedahl, G.N., Palkes, M., Marion, J.L., Vogel, D., 2001. Engineering Feasibility and Economics of CO_2 Capture on an Existing US Coal-Fired Power Plant. ALSTOM Power Inc. Power Plant Laboratories, Windsor, CT, USA.

Brettschneider, O., Thiele, R., Faber, R., Thielert, H., Wozny, G., 2004. Experimental investigation and simulation of the chemical absorption in a packed column for the system NH_3–CO_2–H_2S–NaOH–H_2O. Sep. Purif. Technol. 39 (3), 139–159.

Buchanan, T., DeLallo, M., Schoff, R., White, J., 2000. Evaluation of Innovative Fossil Fuel Power Plants with CO_2 Removal, 1000316. Electric Power Research Institute, Palo Alto, CA, USA.

Ciferno, J.P., DiPietro, P., Tarka, T., 2005. An Economic Scoping Study for CO_2 Capture Using Aqueous Ammonia. National Energy Technology Laboratory; Advanced Resources International; Energetics Incorporated.

CO2CRC, 2011. Why Post-Combustion Capture?, Available at: http://bit.ly/1khfk5Y (accessed 20.06.13).

Darde, V., Thomsen, K., van Well, W.J.M., Stenby, E.H., 2009. Chilled ammonia process for CO_2 capture. Energy Procedia 1 (1), 1035–1042.

Darde, V., Thomsen, K., van Well, W.J.M., Stenby, E.H., 2010. Chilled ammonia process for CO_2 capture. Int. J. Greenh. Gas Control 4 (2), 131–136.

Darde, V., van Well, W.J.M., Stenby, E.H., Thomsen, K., 2011. CO_2 capture using aqueous ammonia: kinetic study and process simulation. Energy Procedia 4, 1443–1450.

Darde, V., Maribo-Mogensen, B., van Well, W.J.M., Stenby, E.H., Thomsen, K., 2012. Process simulation of CO_2 capture with aqueous ammonia using the Extended UNIQUAC model. Int. J. Greenh. Gas Control 10, 74–87.

Derks, P.W.J., Versteeg, G.F., 2009. Kinetics of absorption of carbon dioxide in aqueous ammonia solutions. In: 9th International Conference on Greenhouse Gas Control Technologies, GHGT-9, vol. 1, 16th–20th November 2008, Washington, DC, p. 1139.

DiFrancesco, C.E., Pritchard, S.G., Hinton, W.S., 1997. Successful implementation of cormetechcatalystin high sulfur coal-fired SCR demonstration project. In: NETL Conference on Selective Catalytic and Non-Catalytic Reduction for NO_x Control, NETL.

Duke, M.C., Ladewig, B., Smart, S., Rudolph, V., Da Costa, J.C.D., 2010. Assessment of post-combustion carbon capture technologies for power generation. Front. Chem. Eng. China 4 (2), 184–195.

Edwards, T.J., Maurer, G., Newman, J., Prausnitz, J.M., 1978. Vapor–liquid equilibria in multicomponent aqueous solutions of volatile weak electrolytes. J. Am. Inst. Chem. Eng. 24 (6), 966–976.

European Commission, 2011. Communication from the Commission to the European Parliament, the Council, the European Economic and Social Committee of the Regions – Energy Roadmap 2050, COM (2011) 885/2. European Commission, Brussels, Belgium.

Folger, P., 2013. Carbon Capture: A Technology Assessment, R41325. Congressional Research Service, Available at: http://bit.ly/1esPfhA (accessed 20.12.14).

Fountain, H., 2014. First carbon capture plant opens in Canada. N. Y. Times, B2, Available at: http://nyti.ms/1xx7lXc (accessed 19.12.14).

Gal, E., 2006. Chilled-Ammonia Post Combustion CO_2 Capture System – Laboratory and Economic Evaluation Results, 1012797. EPRI, Palo Alto, CA, USA.

Gerdes, K., Haslbeck, J.L., Kuehn, N.J., Lewis, E.G., Pinkerton, L.L., Simpson, J., Turner, M.J., Varghese, E., Woods, M.C., 2010. Cost and performance baseline for fossil energy plants. Bituminous Coal and Natural Gas to Electricity, 2010/1397, vol. 1. DOE/NETL, Pittsburgh, PA, USA.

Han, K., Ahn, C.K., Lee, M.S., Rhee, C.H., Kim, J.Y., Chun, H.D., 2013. Current status and challenges of the ammonia-based CO_2 capture technologies toward commercialization. Int. J. Greenh. Gas Control 14, 270–281.

Hanak, D.P., Biliyok, C., Yeung, H., Białecki, R., 2014. Heat integration and exergy analysis for a high ash supercritical coal-fired power plant integrated with a post-combustion carbon capture process. Fuel 134, 126–139.

IEA, 2011. World Energy Outlook 2011. OECD/IEA, Paris, France.

IEAGHG, 2004. Improvements in Power Generation with Post-Combustion Capture of CO_2, PH4/33. IEA Greenhouse Gas R&D Programme, UK.

Jensen-Holm, H., Lindenhoff, P., Safronov, S., 2007. SCR Design Issues in Reduction of NOx Emissions from Thermal Power Plants. Haldor Topsoe, Available at: http://bit.ly/1DGza6j (accessed 16.12.14).
Jilvero, H., Normann, F., Andersson, K., Johnsson, F., 2011. Thermal integration and modelling of the chilled ammonia process. Energy Procedia 4, 1713–1720.
Jilvero, H., Normann, F., Andersson, K., Johnsson, F., 2014. The rate of CO_2 absorption in ammonia-implications on absorber design. Ind. Eng. Chem. Res. 53 (16), 6750–6758.
Kothandaraman, A., (PhD thesis) 2010. Carbon Dioxide Capture by Chemical Absorption: A Solvent Comparison Study. Massachusetts Institute of Technology, Cambridge, MA, USA.
Linnenberg, S., Darde, V., Oexmann, J., Kather, A., van Well, W.J.M., Thomsen, K., 2012. Evaluating the impact of an ammonia-based post-combustion CO_2 capture process on a steam power plant with different cooling water temperatures. Int. J. Greenh. Gas Control 10, 1–14.
Manning, L., Chadd, S.A., Baines, R.N., 2007. Key health and welfare indicators for broiler production. World's Poult. Sci. J. 63 (1), 46–62.
Metz, B., Davidson, O.R., 2007. Climate Change 2007: Mitigation: Contribution of Working Group III to the Fourth Assessment Report of the Intergovernmental Panel on Climate Change. Intergovernmental Panel on Climate Change.
MHI, 2012. AART Chillers, Available at: http://bit.ly/1juJfsK (accessed 27.07.13).
Niu, Z., Guo, Y., Zeng, Q., Lin, W., 2012. Experimental studies and rate-based process simulations of CO_2 absorption with aqueous ammonia solutions. Ind. Eng. Chem. Res. 51 (14), 5309–5319.
Padurean, A., Cormos, C.C., Cormos, A.M., Agachi, P.S., 2011. Multicriterial analysis of post-combustion carbon dioxide capture using alkanolamines. Int. J. Greenh. Gas Control 5 (4), 676–685.
Parsons, E.L., Shelton, W.W., Lyons, J.L., 2002. Advanced Fossil Power Systems Comparison Study. National Energy Technology Laboratory, Morgantown, WV, USA.
Pfaff, I., Oexmann, J., Kather, A., 2010. Optimised integration of post-combustion CO_2 capture process in greenfield power plants. Energy 35 (10), 4030–4041.
Pinsent, B.R.W., Pearson, L., Roughton, F.J.W., 1956a. The kinetics of combination of carbon dioxide with hydroxide ions. Trans. Faraday Soc. 52, 1512–1520.
Pinsent, B.R.W., Pearson, L., Roughton, F.J.W., 1956b. The kinetics of combination of carbon dioxide with ammonia. Trans. Faraday Soc. 52, 1594–1598.
Posch, S., Haider, M., 2012. Optimization of CO_2 compression and purification units (CO2CPU) for CCS power plants. Fuel 101, 254–263.
Puxty, G., Rowland, R., Attalla, M., 2010. Comparison of the rate of CO_2 absorption into aqueous ammonia and monoethanolamine. Chem. Eng. Sci. 65 (2), 915–922.
Qi, G., Wang, S., Yu, H., Wardhaugh, L., Feron, P., Chen, C., 2013. Development of a rate-based model for CO_2 absorption using aqueous NH_3 in a packed column. Int. J. Greenh. Gas Control 17, 450–461.
Rackley, S.A., 2010. Carbon Capture and Storage. Elsevier, Burlington, USA.
Rogers, K.J., Nolan, P.S., 2001. SCR Reactor Performance Profiling and Results Analysis, BR-1717. The Babcock and Wilcox Company, Barberton, OH.
Romano, M.C., 2012. Modeling the carbonator of a Ca-looping process for CO_2 capture from power plant flue gas. Chem. Eng. Sci. 69 (1), 257–269.
Romeo, L.M., Espatolero, S., Bolea, I., 2008. Designing a supercritical steam cycle to integrate the energy requirements of CO_2 amine scrubbing. Int. J. Greenh. Gas Control 2 (4), 563–570.
Sanpasertparnich, T., Idem, R., Bolea, I., de Montigny, D., Tontiwachwuthikul, P., 2010. Integration of post-combustion capture and storage into a pulverized coal-fired power plant. Int. J. Greenh. Gas Control 4 (3), 499–510.
Schallert, B., 1993. Selective catalytic reduction of NOx from coal fired power plants. Catal. Today 16 (2), 207–236.
Sinnott, R.K., Towler, G., 2013. Chemical Engineering Design – Principles, Practice and Economics of Plant and Process Design, 2nd ed. Elsevier, Oxford, UK.
Strube, R., Manfrida, G., 2011. CO_2 capture in coal-fired power plants – impact on plant performance. Int. J. Greenh. Gas Control 5 (4), 710–726.
Sulzer, 2012. Structured Packings for Distillation, Absorption and Reactive Distillation. Sulzer Chemtech Ltd., Winterthur, Switzerland.
Trypuc, M., Kielkowska, U., 1996. Solubility in the $NH_4HCO_3 + NH_4VO_3 + H_2O$ system. J. Chem. Eng. Data 41 (5), 1005–1007.
Van Wagener, D.H., Rochelle, G.T., 2011. Stripper configurations for CO_2 capture by aqueous monoethanolamine. Chem. Eng. Res. Des. 89 (9), 1639–1646.
Versteeg, P., Rubin, E.S., 2011. Technical and economic assessment of ammonia-based post-combustion CO_2 capture. Energy Procedia 4, 1957–1964.
Wang, M., Lawal, A., Stephenson, P., Sidders, J., Ramshaw, C., 2011. Post-combustion CO_2 capture with chemical absorption: a state-of-the-art review. Chem. Eng. Res. Des. 89 (9), 1609–1624.
Yu, H., Morgan, S., Allport, A., Cottrell, A., Do, T., McGregor, J., Wardhaugh, L., Feron, P., 2011. Results from trialling aqueous NH_3 based post-combustion capture in a pilot plant at Munmorah power station: absorption. Chem. Eng. Res. Des. 89 (8), 1204–1215.
Yu, J., Wang, S., Yu, H., Wardhaugh, L., Feron, P., 2014. Rate-based modelling of CO_2 regeneration in ammonia based CO_2 capture process. Int. J. Greenh. Gas Control 28, 203–215.
Zhang, M., Guo, Y., 2013a. Process simulations of large-scale CO_2 capture in coal-fired power plants using aqueous ammonia solution. Int. J. Greenh. Gas Control 16, 61–71.
Zhang, M., Guo, Y., 2013b. Process simulations of NH_3 abatement system for large-scale CO_2 capture using aqueous ammonia solution. Int. J. Greenh. Gas Control 18, 114–127.
Zhang, M., Guo, Y., 2014. A comprehensive model for regeneration process of CO_2 capture using aqueous ammonia solution. Int. J. Greenh. Gas Control 29, 22–34.
Zhao, B., Su, Y., Tao, W., Li, L.i., Peng, Y., 2012. Post-combustion CO_2 capture by aqueous ammonia: a state-of-the-art review. Int. J. Greenh. Gas Control 9, 355–371.
Zhou, H., Hu, S., Mo, G., Tang, Q., Cen, K., 2013. Highly efficient and economical nitrogen oxides controlled by an in-furnace urea solution pyrolysis coupled with SCR system for a coal-fired utility boiler. Asia Pac. J. Chem. Eng. 8 (4), 593–606.

5 EFFICIENCY IMPROVEMENTS FOR THE COAL-FIRED POWER PLANT RETROFIT WITH CO_2 CAPTURE PLANT USING CHILLED AMMONIA PROCESS

Dawid P. Hanak, Chechet Biliyok and Vasilije Manovic

Published: Applied Energy, 2015, 151, 258–272[f]

Statement of contributions of joint authorship

Dawid P. Hanak conducted the literature review, performed process analysis via process modelling and simulation, drafted and critically revised the manuscript, as well as prepared tables and figures. Chechet Biliyok and Vasilije Manovic proof-read and critically commented on the manuscript prior to its submission to Applied Energy (Journal Impact Factor 2016: 5.613).

Dawid P. Hanak, PhD Candidate

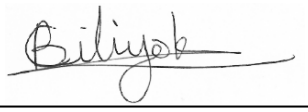

Chechet Biliyok, Associate supervisor

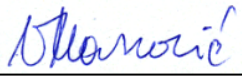

Vasilije Manovic, Principal supervisor

[f] Reprinted with permission from Hanak, D.P., Biliyok, C., and Manovic, V. (2015), "Efficiency improvements for the coal-fired power plant retrofit with CO_2 capture plant using chilled ammonia process", *Applied Energy*, 151, 258–272, doi: 10.1016/j.apenergy.2015.04.059, Elsevier 2015.

Applied Energy 151 (2015) 258–272

Contents lists available at ScienceDirect

Applied Energy

journal homepage: www.elsevier.com/locate/apenergy

Efficiency improvements for the coal-fired power plant retrofit with CO_2 capture plant using chilled ammonia process

Dawid P. Hanak *, Chechet Biliyok, Vasilije Manovic

Combustion and CCS Centre, Cranfield University, Bedford, Bedfordshire MK43 0AL, UK

HIGHLIGHTS

- NH_3 has been proposed as a viable solvent to reduce the efficiency penalty.
- Retrofit of a coal-fired power plant with a chilled ammonia process was analysed.
- A base case scenario showed that efficiency penalty fell between 10.4% and 10.9%.
- Alternative process configurations for the efficiency improvement were investigated.
- The efficiency penalty was reduced to 8.7%.

GRAPHICAL ABSTRACT

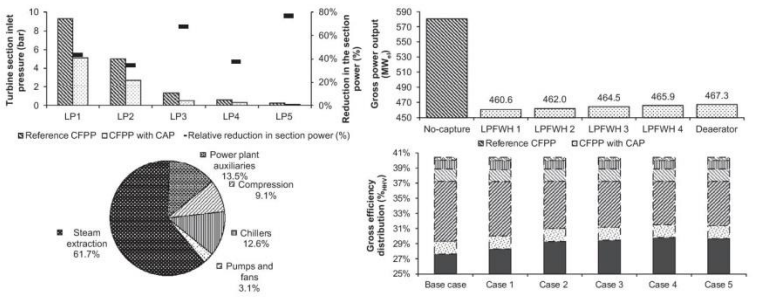

ARTICLE INFO

Article history:
Received 1 December 2014
Received in revised form 13 April 2015
Accepted 15 April 2015

Keywords:
Chilled ammonia process
Coal-fired power plant
Carbon capture
Rate-based modelling
Efficiency penalty reduction

ABSTRACT

Development of clean coal technologies for power generation is crucial in meeting the European Union 2050 target to reduce greenhouse gas emissions. CO_2 capture technology using chemical solvents currently has the highest potential to decarbonise coal-based power generation. Substitution of amine solvent with NH_3 has been proposed as a viable option to reduce the efficiency penalty. In this study, the scenario of a supercritical coal-fired power plant retrofitted with a chilled ammonia process capture plant and CO_2 compression unit was modelled in a common simulation environment. To fully assess the integration impact on power plant performance, the pressure loss due to steam extraction has been taken into account by using the Stodola ellipse law. Analysis of a basic integration scenario revealed that the efficiency penalty fell between 10.4% and 10.9% points depending on the stripper pressure. The quality of extracted steam became insufficient to meet the reboiler heat requirement above a stripper pressure of 21.8 bar, and the lowest efficiency penalty was obtained when reboiler condensate was returned to the deaerator in the power plant. In evaluating measures to improve integration, the efficiency penalty was reduced to 8.7–8.8% points through the integration of a single-stage or two-stage auxiliary steam turbine, respectively, and a back-pressure turbine. Nevertheless, the analysis has indicated that the net impact on power plant performance is similar to that of an amine-based post-combustion CO_2 capture plant.

1. Introduction

Mitigation of the adverse effects of climate change requires limiting the global CO_2 concentration to 450 ppm_v by 2050 [1]. To achieve this, greenhouse gas emissions need to fall by 80% by the year 2050, compared to 1990 levels. In 2011, coal-based power generation accounted for 29% of the global energy demand, simultaneously resulting in 44% of CO_2 emission from energy-related sources [2]. As a result, post-combustion capture (PCC) using chemical solvents is considered as a viable approach to reduce the environmental impact of coal-fired power plants, due to the

* Corresponding author. Tel.: +44 (0) 1234 750111x8254.
E-mail address: d.p.hanak@cranfield.ac.uk (D.P. Hanak).

http://dx.doi.org/10.1016/j.apenergy.2015.04.059
0306-2619/

Nomenclature

Parameters

a	turbine design parameter (–)
$\dot{m}$	mass flow rate (kg/s)
n	adiabatic index (–)
p	steam pressure (bar)
v	velocity (m/s)
ρ	density (kg/m^3)
η_i	isentropic efficiency (–)

Superscripts

0	parameter at design conditions

Subscripts

in	stream parameter at inlet to the unit operation
out	stream parameter at outlet from the unit operation

Abbreviations

AAP	aqueous ammonia process
CAP	chilled ammonia process
CCU	CO_2 compression unit
CFPP	coal-fired power plant
HI	heat integration
HP	high-pressure
IP	intermediate-pressure
LP	low-pressure
HPFWH	high-pressure feedwater heater
LPFWH	low-pressure feedwater heater
MEA	monoethanolamine
PCC	post-combustion capture

ease of integration, high flexibility and independent operation [3–5].

Currently, amines, such as monoethanolamine (MEA), are the default solvents for PCC. These introduce substantial parasitic loads on the power plant due to the amount of energy required for solvent regeneration, resulting in efficiency losses of 9.5–12.5% points in coal-fired power plants (CFPP) [6–8]. These efficiency penalties can be mitigated through application of rotating packed beds that enhance the mass and heat transfer, which results in reductions in the size of the reactors and decreased energy requirements [9–11]. Although several models of the intensified amine scrubbing equipment have been recently published [11–13], neither the whole system nor impact of its integration on power plant performance has been analysed. Furthermore, solvent substitution has been identified as a viable measure to reduce the energy intensity of the PCC plants [14,15]. Goto et al. [8] reviewed the impact of integration of the PCC plant for a number of alternative chemical solvents, and revealed that the efficiency penalty can be reduced to 8.0–8.5% points with NH_3 [16,17] and to 8.5% points with amine-blends, such as methyldiethanolamine/piperazine [18]. Moreover, studies by Kvamsdal et al. [19] and Van Wagener et al. [20] showed that the use of piperazine as a solvent can reduce the efficiency penalty to 7.0–7.2% points. An alternative to chemical solvent absorption is application of novel CO_2 membranes, which has the potential to reduce the efficiency penalty to 6.4–8.5% at a low cost [21]. However, the issues related to flue gas impurities, low gas pressure and CO_2 partial pressure still need to be resolved [22]. Another alternative is to use solid sorbents in high-temperature processes that would impose an efficiency penalty of 7–8% points [23]. Regardless of the fact that the well-established fluidised bed technology is utilised, the challenges of sorbent deactivation and reactivation need to be resolved before large-scale deployment [24].

Development of NH_3-based PCC processes has reached the pilot plant stage in a relatively short period of time and it was projected that these processes would become commercially available by 2015 [25]. Different options for the NH_3-based PCC plant have been tested at the pilot-plant scale – the aqueous ammonia process (AAP) at Munmorah pilot plant [26] and the chilled ammonia process (CAP) at Pleasant Prairie and Mountaineer CFPPs – but the CAP campaigns were cancelled due to cost and schedule overruns [27,28].

The main advantages of NH_3 over amine-based solvents have been recently reviewed by Shakerian et al. [29] and are:

- commercial availability at lower price;
- higher CO_2 absorption capacity compared to the MEA solution of the same concentration;
- lower heat of reaction resulting in lower heat requirement for solvent regeneration;
- projected efficiency penalty as low as 4.1–7.0% points [30–32], which is yet to be substantiated experimentally [33], though efficiency penalty has been determined to be between 8.5% and 11.6% points [5];
- no solvent degradation on contact with the flue gas components;
- stripper can be operated at elevated pressure/temperature, leading to less compression work required;
- NH_3 is not as corrosive as amines and can be used as a multi-component capture solvent [4].

A major drawback of using NH_3 is its high volatility leading to NH_3 slip in the absorber [34]. To comply with environmental requirements, the NH_3 slip can be controlled either by adding an additional acid water wash or by operating the absorber below 20 °C in the so-called CAP process. Unfortunately, both cases would lead to increased capital and operating costs and to only slight improvement of the overall process performance over amine-based systems [4,33,35].

Until recently, the CAP process has been evaluated through thermodynamic modelling [36] and process simulation [5,37–39] using only an equilibrium approach. Versteeg and Rubin [38] used a thermodynamic Electrolyte NRTL model available in Aspen Plus to perform a basic analysis of the CAP plant integration to the CFPP, and revealed that implementation of the CAP process provides no improvement over the conventional amine-based PCC as the net efficiency penalty amounted to 11.2% points. This has been confirmed by Linnenberg et al. [5], who modelled the CAP process in Aspen Plus using the Extended UNIQUAC equilibrium model and the supercritical coal-fired power plant in EBSILON Professional. In their study, the efficiency for the base case ranged between 10.4% and 11.6% points, depending on the cooling water temperature. However, they showed that optimisation of the process parameters can reduce the net efficiency penalty to between 8.5% and 9.5% points, depending on the CAP configuration used. A similar integration impact was also obtained by Valenti et al. [40] (8.6% points); however, the CAP model in their study was composed of flash drums connected in series and, thus they have not accounted for the mass and heat transfer in the packing.

Since neither of these studies involved the rate-based modelling approach for the absorption and regeneration processes in the CAP plant, nor analysed the enhancements for process integration, the aim of this paper is to evaluate the alternative CFPP retrofit scenarios using a high-fidelity process model of a CFPP and a rate-based CAP plant. Retrofit scenarios considered are based on the integration configurations developed for the amine-based PCC, conducted in a common simulation environment, with the Stodola ellipse law implemented to fully assess the integration impact resulting from pressure losses. Finally, process performance improvement, through heat and work integration, is also explored.

2. Model development

2.1. Supercritical coal-fired power plant

A high-fidelity supercritical CFPP model was developed in Aspen Plus V8.4 and compared with data from a revised NETL report [41]. A maximum error of 5.8% in coal consumption rate was observed. The verified power plant model is used as a benchmark scenario in this study. The CFPP (Fig. 1) comprises a supercritical power boiler with NO_x and SO_x emission control equipment and the electrostatic precipitator, which has all been modelled thermodynamically using the Peng-Robinson–Boston-Mathias (PR-BM) equation of state, as well as a steam cycle that has been thermodynamically described with steam tables (STEAMNBS). The performance of the CFPP is characterised by gross power output of 580.4 MW_{el}, net thermal efficiency of 38.5%$_{HHV}$ and other key performance parameters as presented in Table 1.

Steam turbines are modelled as individual turbine sections, hence the high- (HP), intermediate- (IP) and low-pressure (LP) cylinders are further divided into the required steam turbine sections. For each section, the isentropic efficiency was estimated to match the desired discharge temperature in the revised NETL report [41]. In all scenarios investigated, the condenser is assumed to operate at a fixed pressure of 0.069 bar, which corresponds to a condensation temperature of 38.7 °C. A condenser area is estimated to ensure a cooling water temperature increase of 11 °C under design conditions. Under off-design conditions, only a minor change in the overall heat coefficient is expected, hence a fixed UA value is imposed while the cooling water temperature difference is increased to meet the duty requirement. The feedwater heating train comprises five LP feedwater heaters (LPFWH) including the deaerator, and three surface HP feedwater heaters (HPFWH). At design conditions, the feedwater heaters are characterised by the terminal temperature difference of 2.78 °C and the minimal temperature difference between subcooled condensate and inlet feedwater of 5.56 °C. As the UA value cannot be estimated in a reliable and accurate way for the heat transfer during the phase change, a method used in Cycle Tempo software by TUDelft [42], which relates the aforementioned temperature differences with the ratio of the off-design and design feedwater flow rate, is adapted to determine the off-design performance of the feedwater heaters.

Integrating the CO_2 capture plant using chemical solvents requires a large amount of heat for solvent regeneration in the reboiler. Condensing steam extracted from the IP/LP crossover pipe

Table 1
Supercritical CFPP key performance parameters.

Parameter	Value
Flue gas stream (kg/s)	617.2
CO_2 content in flue gas (%$_{vol}$)	15.2
Higher heating value of coal (MJ/kg)	26.1
Coal consumption rate (kg/s)	53.8
Air consumption rate (kg/s)	526.5
Live steam generation rate (kg/s)	462.3
Excess air ratio (%$_{vol}$)	20.0
Live steam pressure (bar)	242.3
Reheated steam pressure (bar)	45.2
IP/LP crossover pressure (bar)	9.3
Condenser pressure (bar)	0.069
Live and reheated steam temperature (°C)	593.3
Mechanical efficiency of the rotational machinery (%)	99.0

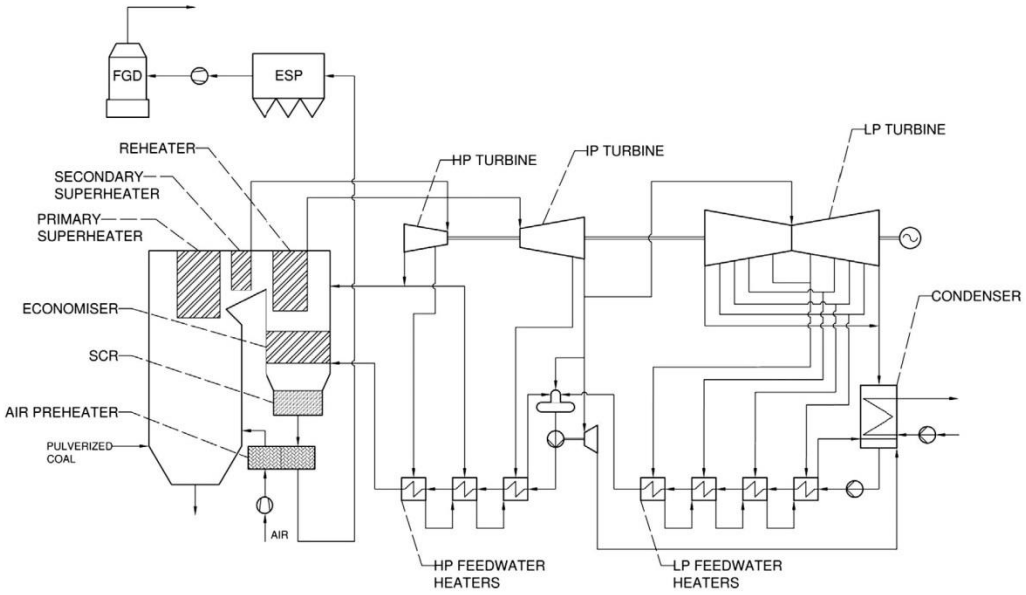

Fig. 1. Process flow diagram of reference supercritical CFPP.

of the existing power plant has been found to be the most efficient option for meeting this heat requirement [43], though at the expense of highly off-design operating conditions in the LP turbine. Therefore, the power output of this section drops not only as a result of reduced LP turbine throughput, but also due to inlet pressure loss resulting from steam expansion downstream the extraction point. As the condenser pressure is assumed to be fixed, pressure gradients across turbine sections are determined using Stodola's ellipse law presented in Eq. (1) [44–46] to determine the inlet pressure in a back-to-front manner. This is implemented using the Aspen Simulation Workbook in MS Excel.

$$\frac{\dot{m}_{in}}{\dot{m}^0_{in}} = \frac{p_{in}}{p^0_{in}} \cdot \sqrt{\frac{p^0_{in} \cdot \rho_{in}}{p_{in} \cdot \rho^0_{in}}} \cdot \sqrt{\frac{1 - \left(\frac{p_{out}}{p_{in}}\right)^{\frac{n+1}{n}}}{1 - \left(\frac{p^0_{out}}{p^0_{in}}\right)^{\frac{n+1}{n}}}} \tag{1}$$

Furthermore, reduction in the steam pressure downstream of the extraction point results in an increase in velocity, and hence kinetic energy at the inlet to the LP turbine. Kinetic energy of steam increases further on expansion in the LP turbine stages, and thus the turbine discharge loss would be higher than under design conditions. This, in turn, would affect the isentropic efficiency of the LP turbine and could cause operational issues, such as vibration of the last stage moving blades [47]. Therefore, the isentropic efficiency is updated using Eq. (2), which is based on the approach used by Salisbury [48] and Knopf [45] assuming that each turbine section reaches its optimal performance at design conditions and comprises 50% reaction blading ($a = 0.7071$).

$$\frac{\eta_i}{\eta^0_i} \cong 2\frac{a}{\frac{V^0_{in}}{V_{in}}} \cdot \left[\left(a - \frac{a}{\frac{V^0_{in}}{V_{in}}}\right) + \sqrt{\left(a - \frac{a}{\frac{V^0_{in}}{V_{in}}}\right)^2 + 1 - a^2}\right] \tag{2}$$

2.2. CO_2 capture system using chilled ammonia process

A high-fidelity rate-based model of the CAP plant (Fig. 2), used to evaluate the impact of integration to the CFPP, has been developed and described in detail by Hanak et al. [49]. The model predictions were found to be in close agreement with the pilot plant data, with the errors within the experimental uncertainty. The electrolyte non-random two-liquid (ELECNRTL) thermodynamic method for liquid phase is combined with the Redlich-Kwong equation of state for the vapour phase for prediction of the vapour-liquid equilibrium. The kinetic parameters determined by Pinsent et al. [50] were used to describe the chemical reactions in the system. Although these parameters were determined in a dilute system, Derks and Versteeg [51] showed that the apparent rate of CO_2 absorption by aqueous solution of NH_3 increases linearly with NH_3 concentration. Hence, the kinetic parameters provided by Pinsent et al. [50] remain valid at higher NH_3 concentrations.

The model was then scaled up using the generalised pressure drop correlation. The parametric studies revealed that the parasitic load imposed on the CFPP performance, which is expressed in terms of equivalent work accounting for power output loss due to steam extraction, capture plant auxiliaries, chillers and CO_2 compression power requirement is minimal at a lean solvent concentration of 12.5%$_{wt}$ NH_3 and lean loading of 0.29. Moreover, salt precipitation in the column does not occur under these operating conditions, thus some related potential operational problems can be avoided. The design and performance data of the CAP plant are presented in Table 2.

A CO_2 compression unit (CCU) is also sized to assess the energy requirements for compression. Each compression stage of the CCU consists of a centrifugal compressor, stage intercooler and scrubber. To minimise the compression work required, it is assumed that CO_2 is first compressed to the critical pressure of 74 bar and cooled to 30 °C, before being pumped to 110 bar, an appropriate pressure for CO_2 transport [52]. Although the energy requirement of the CO_2 capture section imposes the highest energy penalty on the CFPP, a significant amount of energy is required for CO_2 conditioning prior to transport and must be considered in the analysis. The CCU is modelled using constant compression stage polytrophic efficiencies of 78–79%, and the pump isentropic efficiency of 80% [53,54]. The number of compression stages for each particular case is determined based on the assumptions that the pressure ratio

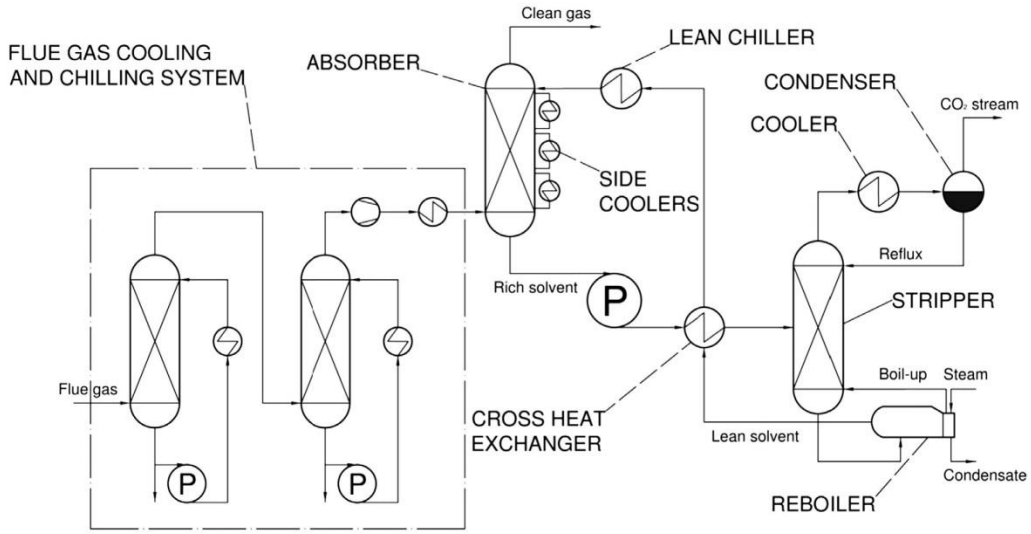

Fig. 2. Process flow diagram of chilled ammonia CO_2 capture plant.

Table 2
CAP plant equipment design and operating conditions.

Design parameters	Value	Operating parameters	Value
Columns height (m)	30	CO_2 capture efficiency (%)	90.0
Absorber diameter (m)	13	Reboiler temperature (°C)	151.1
Number of absorbers	2	Equivalent work (kW h/tCO_2)	324.9
Stripper diameter (m)	10	Flue gas inlet temperature (°C)	7.0
Number of strippers	1	Stripper pressure (bar)	10.0
Packing type	Mellapack 350X	Absorber pressure (bar)	1.0

and the polytrophic head should not exceed 3 and 3050 m, respectively, due to equipment limitations [55].

3. Process integration

3.1. Considerations

Retrofit of the CFPP with the CAP plant (Fig. 3) includes several interface points: connecting ducts to send the flue gas to the CAP plant (I); electrical connections for solvent pump (II); chiller (III); CO_2 compressors (IV); and tie-ins for steam extraction (V) to the CAP plant reboiler and condensate return (VI) to the power plant steam cycle.

The location of steam extraction in the steam cycle is highly dependent upon the conditions in the stripper reboiler. Unlike amines, NH_3 does not undergo thermal degradation at high temperatures, but vaporises and condenses back to liquid on cooling. Therefore, the stripper of the CAP plant can be operated at higher pressures, and hence higher temperatures. This, in turn, results in

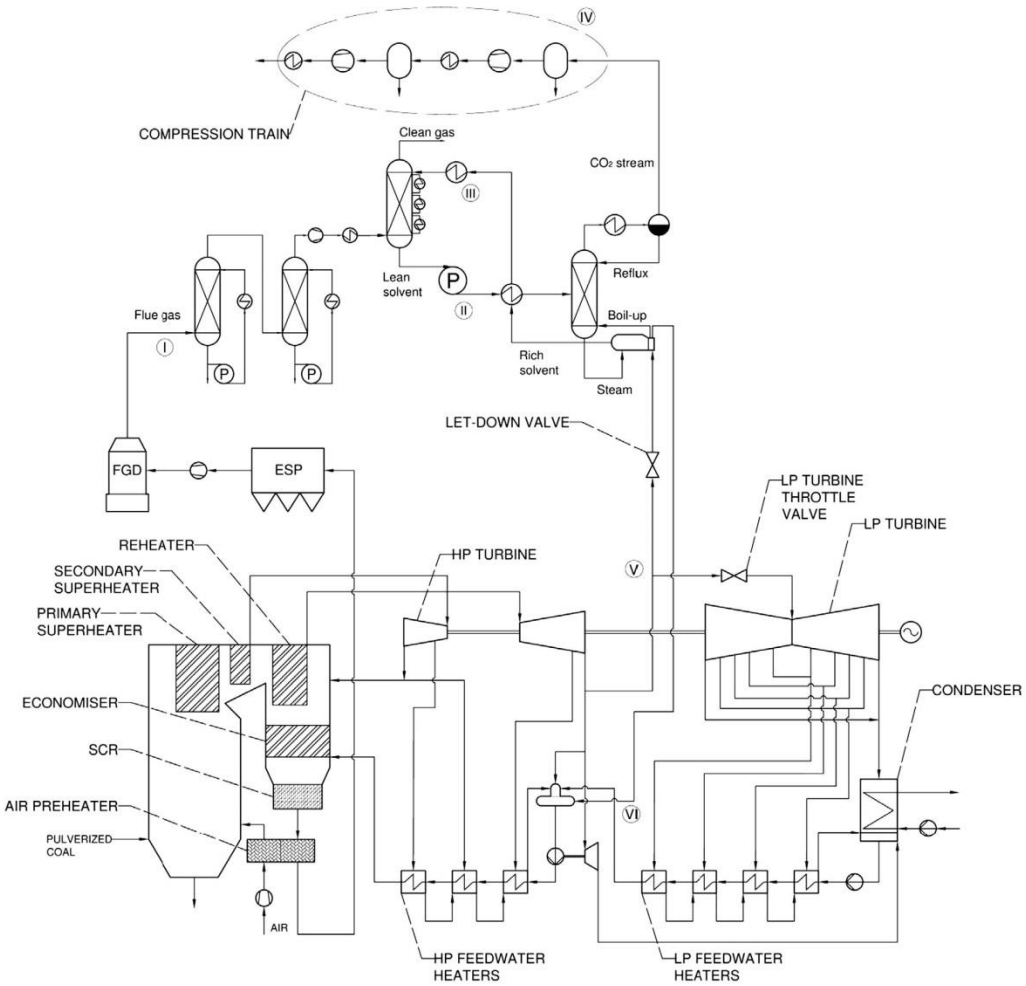

Fig. 3. Process flow diagram of the PCC and CCU integrated into the reference supercritical CFPP.

less compression work required to deliver the desired pipeline pressure, and potentially a reduction in the amount of heat required for solvent regeneration. However, such high pressures would require steam of higher quality and thus, may not always result in improvement in the net thermal efficiency. Therefore, the feasibility of operating the stripper at higher pressures in the integrated system needs to be analysed.

Several options for the PCC plant integration to the steam cycle have already been proposed by IEA [56], where different turbine configurations were investigated. Although these intermediate-/low-pressure (IP/LP) turbine configurations would allow steam extraction at the pressure desirable for the CO_2 capture process, they are mainly applicable in the new-built scenarios. It must be stressed, however, that the IP turbine discharge pressure in the existing fleet of the CFPPs varies and is usually much higher than required for solvent regeneration. If this is the case and, as extraction of steam from the IP/LP crossover pipe would cause upstream pressure drop, the LP turbine needs to be throttled to maintain the IP turbine discharge pressure so that steam of appropriate quality can be extracted while keeping the energy losses to a minimum.

As the CAP plant can be operated at higher pressures, the stripper pressure is varied between 10 bar and 40 bar to identify the viable operating range for the considered CFPP. In the evaluation of PCC integration, it is assumed that steam can be extracted from the IP/LP crossover pipe and its pressure reduced so that 10 °C temperature gradient is maintained between the steam saturation temperature and the desired reboiler temperature. As the heat duty of the reboiler is of a significant magnitude, it can be expected that a large fraction of the IP/LP crossover steam will be extracted. Such reduction in the existing LP turbine throughput will cause it to operate in off-design mode due to pressure drop upstream of the extraction point [57]. To account for the pressure loss in the turbine, new extraction pressures for feedwater heating are approximated using the Stodola ellipse law. Furthermore, to minimise the steam extraction impact on the overall system performance, the LP turbine is throttled so that the IP turbine design discharge pressure is maintained.

Finally, as the condensate is expected to exit the reboiler at a considerable temperature, the location of its return to the steam cycle would affect the power output of the CFPP. For this reason, different scenarios are evaluated to identify the optimal return location for which the energy penalty resulting from the capture plant integration is minimised.

3.2. Process integration analysis

3.2.1. Steam requirement for solvent regeneration

The requirements of the CAP plant on the reference CFPP, with a stripper operating pressure of 10 bar, are presented in Table 3. To meet the temperature pinch in the reboiler, IP/LP steam needs to condense at 161.1 °C and thus, its pressure needs to be reduced to 6.35 bar. Having assumed complete steam condensation in the reboiler, the required steam extraction flow rate was estimated to be 138.9 kg/s, corresponding to 43.9% of the CFPP IP/LP steam flow rate. Moreover, although the absorbers were cooled with cooling water instead of a refrigerant, a considerable amount of chilling was still required to keep the lean solvent and flue gas temperatures at the desired levels. Using a refrigerant would have resulted in an increased parasitic load on the CFPP output, as the chiller compressors require electricity to keep the refrigerant at a sufficiently low temperature.

Table 3
Key parameters characterising the capture plant integration.

Parameter	Value
Reboiler duty (MW_{th})	347.8
IP steam requirement (kg/s)	138.9
Required steam pressure (bar)	6.35
Condensate temperature (°C)	161.1
PCC auxiliary power requirement (MW_{el})	3.40
Chilling power requirement (MW_{el})	23.14
CCU power requirement (MW_{el})	16.67

Steam extraction for the solvent regeneration resulted in a considerable change in the pressure distribution in the CFPP LP turbine (Fig. 4). As the Stodola ellipse law has been implemented, it is estimated that extraction of 43.9% of the LP steam results in approximately 50.0% reduction in the inlet pressure of the subsequent turbine stages and in 48.8% drop in the LP turbine power output. This indicates that if one of the interface points of the PCC plant is steam extraction from the steam cycle, the effect on the pressure profile across the turbine sections upstream of the extraction point needs to be accounted for to reliably assess the PCC integration impact.

3.2.2. Available steam quality

Analysis of steam quality (Fig. 5) was conducted by varying the stripper operating pressure from 10 to 40 bar, keeping the lean loading constant and adjusting the solvent circulation rate to maintain the CO_2 capture level of 90%. The analysis revealed that the IP/LP steam pressure requirement increases gradually along with the stripper operating pressure. Such behaviour corresponds to a shift in the boiling point with pressure increase that leads to a subsequent increase in the reboiler temperature. As the design IP/LP crossover pressure is 9.3 bar, the analysis revealed that the stripper can be operated at the maximum pressure of 21.8 bar. Above this pressure, the saturation pressure of extracted steam, which corresponds to the steam dew temperature required to meet the temperature pinch in the reboiler, was found to exceed the IP/LP pressure and thus the steam quality became insufficient to meet the CAP reboiler requirements.

This challenge can be resolved through investigation of the alternative integration options in which either HP steam is extracted, for example, from the HP turbine discharge, or the LP turbine is further throttled to increase the IP turbine discharge pressure. These solutions, however, would cause higher efficiency penalties as either less HP steam would be utilised in the steam turbine or the LP turbine power output would be further reduced on throttling.

3.2.3. Optimal condensate return location

In terms of the energy efficiency, it can be expected that the optimum performance will be reached if the condensate is returned to the feedwater train at a point of similar temperature. This is because further preheating of the reboiler condensate will be avoided in a scenario where the condensate is returned at a point where the feedwater temperature is higher.

Having analysed the retrofitted CFPP process flow diagram, returning the condensate to the condenser is a possible option. However, it would result in dissipation of a large amount of energy and the whole feedwater stream would need to be preheated in the low-pressure feedwater heaters (LPFWH). This would result in higher IP and LP steam extraction rates leading to less steam being used to generate power in the steam turbines. Therefore, returning the reboiler condensate to the condenser was judged to be not a feasible option and was not considered in this study.

Analysis of the viable return locations (Fig. 6) revealed that returning the reboiler condensate before LPFWH 1 provided the worst performance, as the condensate temperature was much larger than that of the feedwater. Returning the condensate before the next LPFWHs (2–4) was found to result in a gradual increase of the gross power output. This was caused by less steam being

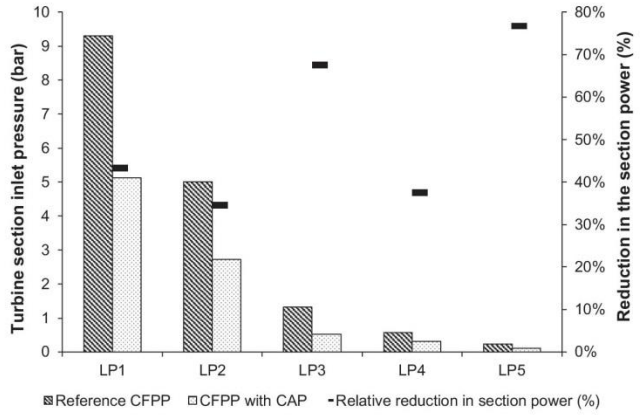

Fig. 4. Effect of steam extraction on pressure distribution in the LP turbine.

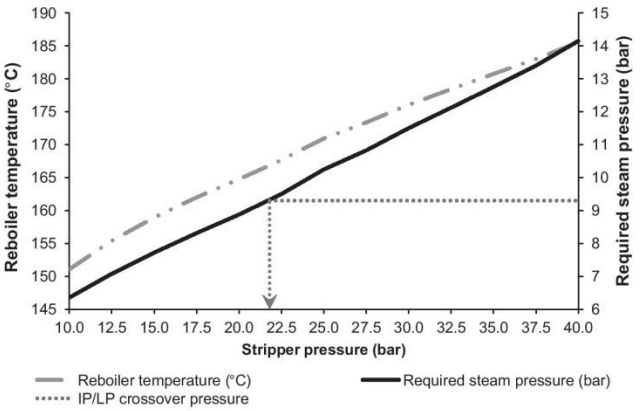

Fig. 5. Effect of the stripper pressure on the reboiler temperature and required steam pressure.

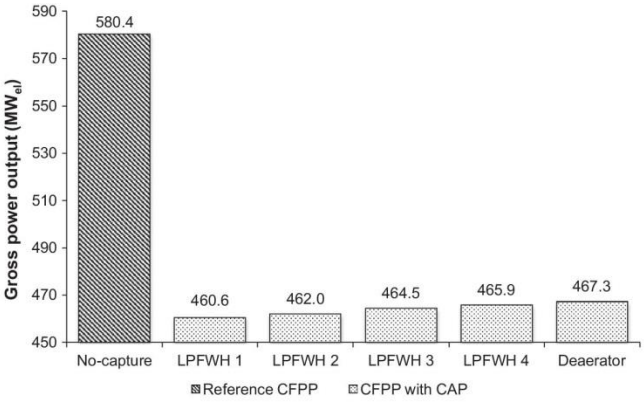

Fig. 6. Effect of reboiler condensate return location on CFPP gross power output.

extracted for the feedwater heating, and by smaller differences between the feedwater and the condensate temperatures. Nevertheless, deterioration of the LP turbine inlet pressure due to steam extraction triggered subsequent reduction in the pressure, and hence the steam saturation temperature, resulting in a decrease of feedwater temperature leaving the LPFWHs from 147.2 °C to 125.0 °C. As the reboiler condensate temperature (161.1 °C) is higher than the reference feedwater temperature at the discharge from LPFWH 4 (147.2 °C), it implies that the deaerator is the optimal location for the reboiler condensate return. This was confirmed by analysis of the integrated system that has delivered the highest gross power output when the reboiler condensate was returned directly to the deaerator. A benefit of such return location was reduced LP steam consumption for feedwater heating, as less feedwater needed to be preheated downstream of the return location. Therefore, the net reduction of steam extraction in the LP turbine sections for feedwater heating resulted in more steam being available for power generation in the steam turbines, causing an increase in the gross power output of the CFPP.

3.3. Process performance analysis

A comparison of the power generation performance of the CFPP with and without the CAP plant (Table 4) revealed that the net efficiency of the CFPP dropped by 10.9% points on PCC plant integration. This value is comparable to values reported in the literature and is of the same magnitude as that of the reference amine-based PCC plant [5].

The parasitic load imposed on the net power plant output amounted to 155.7 MW_{el} and was higher than the theoretical equivalent work requirement of approximately 131.0 MW_{el} identified in Hanak et al. [49]. This revealed a limitation of most of the previous attempts based on thermodynamic estimates, as these did not account for the pressure drop across the LP steam turbine and for subsequent changes in steam extractions and thus LP feedwater temperatures. The differences between the actual and expected level of the parasitic load stemmed from a change in steam pressure distribution across and drop in the isentropic efficiency of the LP turbine due to steam throttling and extraction. This indicates that to accurately account for the PCC plant integration to the CFPP, the change in the pressure distribution must be included in the analysis.

Fig. 7 reveals that the most important driver causing a reduction in net power output was the LP steam extraction for solvent regeneration (61.7%). However, unlike the amine scrubbing plant, in which the efficiency penalty stems nearly completely from steam extraction, solvent pumps and CO_2 compression, the requirement for lean solvent and flue gas chilling in the CAP plant introduces a considerable parasitic load, which accounted for 12.6% of the net efficiency penalty.

Importantly, due to the efficiency penalty caused by the CAP plant integration, 39.2% more chemical energy, hence coal, would need to be provided in the boiler to maintain the net power output of 552.7 MW_{el}. In reality, such a rated net power output may not be achievable as the coal handling equipment is not designed to process that amount of coal. Therefore, the large reduction in the net amount of electricity generated would substantially affect the unit cost of electricity and thus, the plant profitability.

Table 4
System performance, environmental and integration impact indicators for supercritical CFPP with and without CAP plant.

Parameter	Reference CFPP	Basic CAP integration
System performance indicators		
Gross electricity production (MW_{el})	580.4	467.2
Total auxiliary electricity consumption (MW_{el})	27.7	70.2
Net electricity production (MW_{el})	552.7	397.0
Gross thermal efficiency ($\%_{HHV}$)	40.4	32.5
Net thermal efficiency ($\%_{HHV}$)	38.5	27.6
Net specific chemical energy consumption (kW_{ch}/kW_{el})	2.6	3.6
Specific coal consumption (g/kW h_{el})	350.3	487.7
CO_2 intensity factor (g/kW h_{el})	792.3	110.3
Integration impact indicators		
Net energy penalty (%)	–	28.2
Net efficiency penalty (%)	–	10.8
Increase in net specific chemical energy consumption (%)	–	39.2

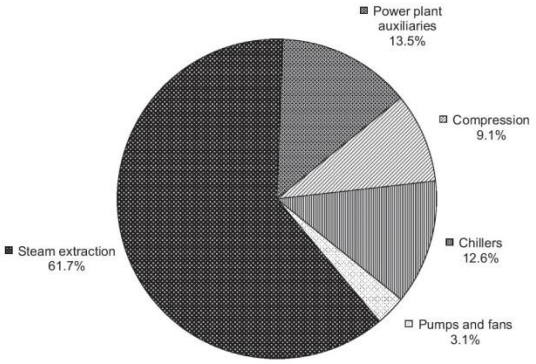

Fig. 7. A parasitic load distribution for the CFPP integrated with the CAP plant.

4. Improvement of the overall process performance

4.1. Advanced process integration configurations

In the investigated system, the IP/LP crossover steam has a higher operating pressure than is required for solvent regeneration at 10 bar and thus, steam pressure is reduced in the let-down valve. This pressure drop, in addition to the steam pressure loss due to steam extraction, results in the loss of a considerable amount of useful energy and is a major contributor to the efficiency penalty. One solution to minimise this negative effect could be a retrofit of the existing IP turbine with a new one characterised by a discharge pressure designed for the PCC plant operation. However, the CFPP retrofitted in this way is unlikely to reach its rated performance when the PCC is shut down, for example, during peak load operation [56]. Another solution is the implementation of enhanced process integration configurations that were developed for the amine-based system, as well as improvement through heat integration and development of new configurations. Although such solutions would require additional capital investment, it is expected that their implementation would result in increased net thermal efficiency. However, a higher degree of integration results in diminishing of flexibility and reliability of the plant.

4.1.1. Single IP/LP crossover pressure system (Case 1)

The first process configuration analysed in this study is the single crossover pressure system (Fig. 8) [58], where the pressure of steam extracted for solvent regeneration is reduced to the desired pressure via a let-down turbine instead of the let-down valve. This introduces flexibility, as the discharge pressure of the turbine can be adjusted to what is required for solvent regeneration. Hence, the solvent can be upgraded without the requirement of major

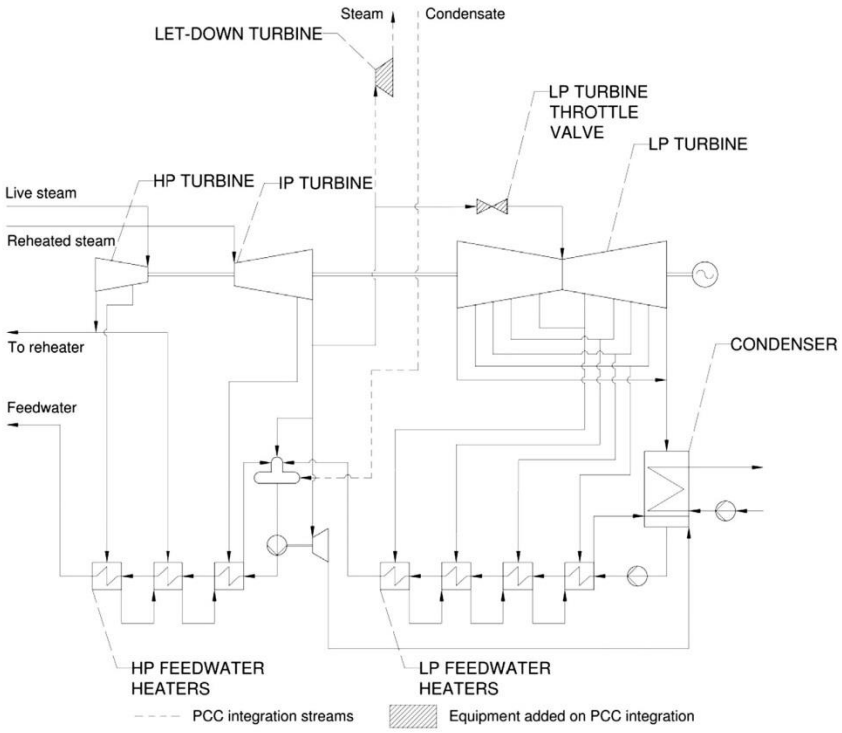

Fig. 8. Additional let-down turbine in the single crossover pressure system.

changes to the existing system. In this study, the isentropic efficiency of the let-down turbine is assumed to be the same as that of the LP turbine.

4.1.2. Dual IP/LP crossover pressure system (Case 2)

In a dual crossover pressure configuration (Fig. 9) [58], a back-pressure turbine is used to maintain IP turbine discharge pressure, as opposed to a throttling valve. In the investigated scenario, the same isentropic efficiency attained in the LP turbine is used for both the let-down and back-pressure turbines and the discharge pressure of the back-pressure turbine is determined using the Stodola ellipse law, which is dependent on steam flow rate.

4.1.3. Dual IP/LP crossover pressure system with heat integration (Case 3)

In the configurations described above, steam would leave the let-down turbine at the desirable pressure for solvent regeneration; however, its temperature would still be significantly higher than the reboiler temperature. Such temperature gradients would result in exergy losses in the system [59]. Therefore, steam needs to be de-superheated prior to being condensed in the reboiler. This is achieved by using the steam to preheat the HP feedwater leaving the boiler feedwater pump (Fig. 10). The advantage of such configuration would be reduction of the IP steam extraction rates to the HPFWHs, and thus an increase in the net thermal efficiency.

4.1.4. Auxiliary steam turbine retrofit (Cases 4 and 5)

Lastly, the supercritical CFPP under investigation is equipped with an auxiliary steam turbine to drive the boiler feedwater pump, which is fed with the IP/LP crossover steam. A novel process integration proposed in this study is the retrofit of the auxiliary steam turbine for use as the let-down turbine so that its discharge pressure matches the reboiler requirements. It is expected that more steam would be extracted to deliver the same amount of mechanical energy as by the conventional auxiliary turbine to achieve the desired boiler feedwater pump discharge pressure. As the pressure ratio of the auxiliary turbine would be lower, it is possible that more steam would be extracted than required for solvent regeneration. The steam that is discharged from the new auxiliary turbine at 6.35 bar, which corresponds to the reboiler steam pressure requirement when the stripper is at an operational pressure of 10 bar (Fig. 5), is first de-superheated, then part of it is used to meet the heat required for the solvent regeneration in the reboiler. The rest is mixed with the steam extracted from the LP turbine to the fourth LPFWH (Fig. 11). Alternatively, IP/LP steam can be expanded in a two-stage auxiliary steam turbine, where most of it is extracted after the first stage to meet the reboiler heat requirement, while the rest is expanded in the second stage and returned to the condenser using the existing connection (Fig. 12). It is expected that such designs of auxiliary steam turbine would require more steam than the one determined by the reboiler requirement.

4.2. Performance evaluation of the process configurations

Analysis of the process configurations (Fig. 13) revealed that in the CAP plant with the stripper operating at 10 bar, substitution of the let-down valve with the let-down turbine (Case 1) results in a rise in the net plant efficiency by 0.7% points, in spite of an increased extraction rate from 138.9 kg/s to 144.35 kg/s having a

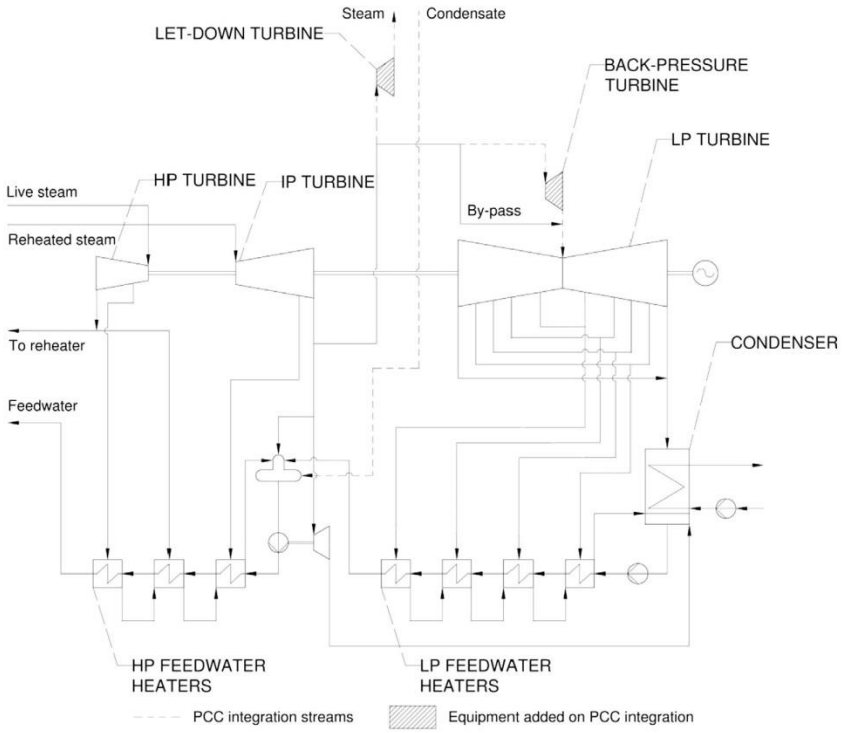

Fig. 9. Additional let-down and back-pressure turbines in the dual crossover pressure system.

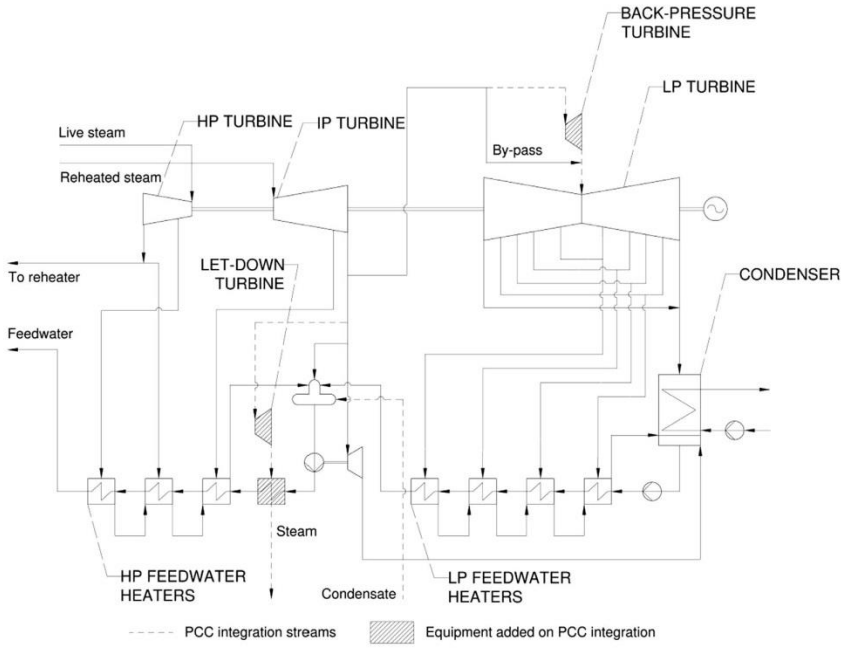

Fig. 10. Additional let-down and back-pressure turbines in the dual crossover pressure system with high-pressure heat integration.

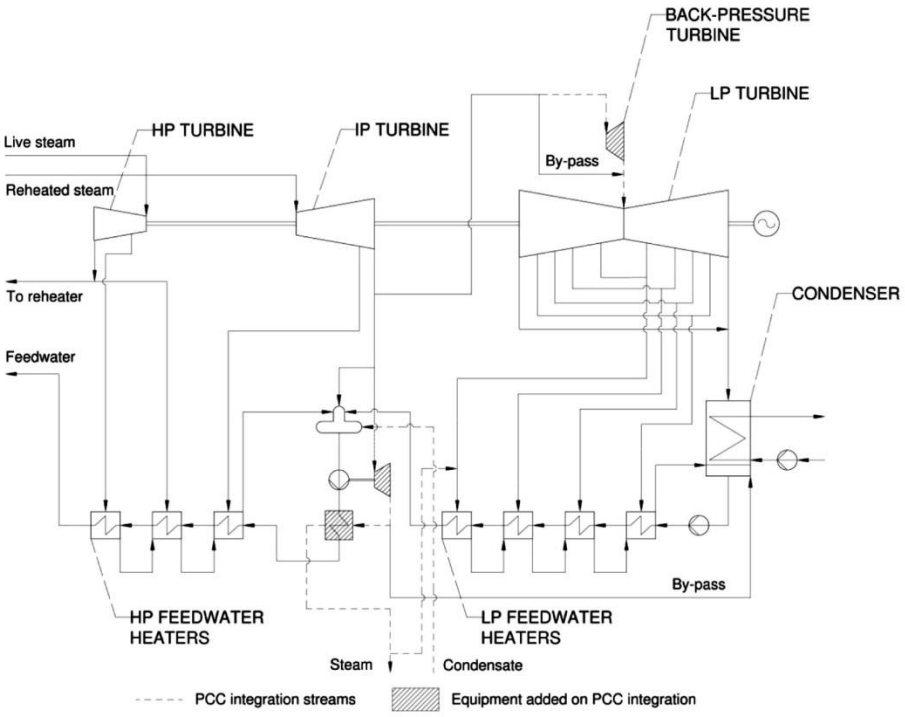

Fig. 11. Single-stage auxiliary steam turbine retrofit with high- and low-pressure heat integration.

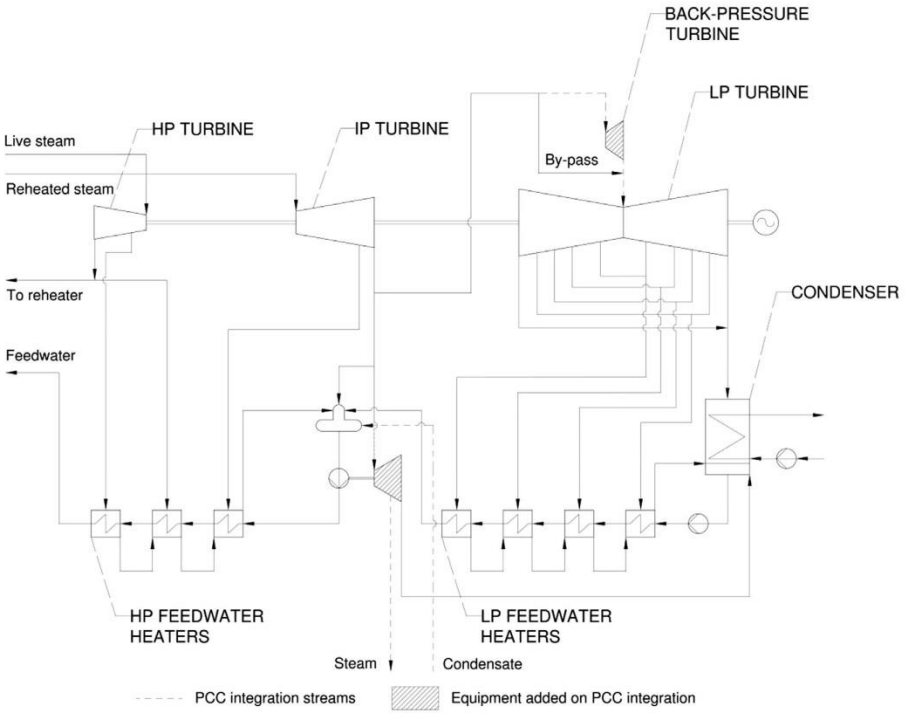

Fig. 12. Two-stage auxiliary steam turbine retrofit.

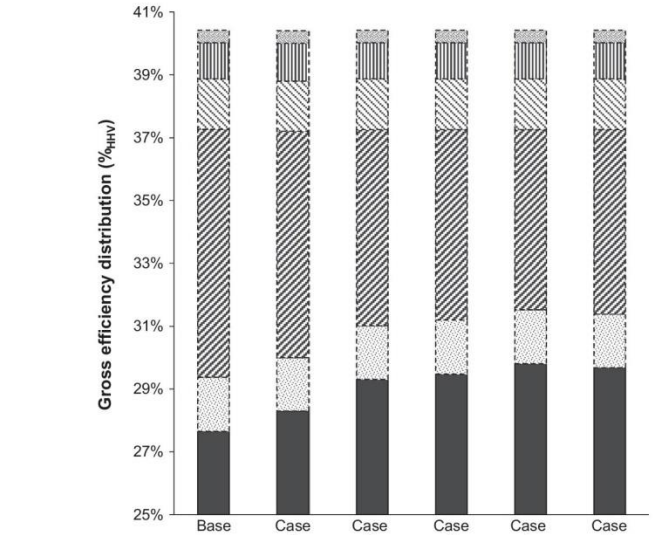

	Base case	Case 1	Case 2	Case 3	Case 4	Case 5
Pumps and fans	0.4%	0.4%	0.4%	0.4%	0.4%	0.4%
CO2 compressors	1.2%	1.2%	1.2%	1.2%	1.2%	1.2%
Chillers	1.6%	1.6%	1.6%	1.6%	1.6%	1.6%
Steam extraction	7.9%	7.2%	6.2%	6.1%	5.7%	5.9%
Power plant auxiliaries	1.7%	1.7%	1.7%	1.7%	1.7%	1.7%
Net thermal efficiency	27.7%	28.3%	29.3%	29.5%	29.8%	29.7%

Fig. 13. Process performance improvement measures for the CAP with stripper operated at 10 bar.

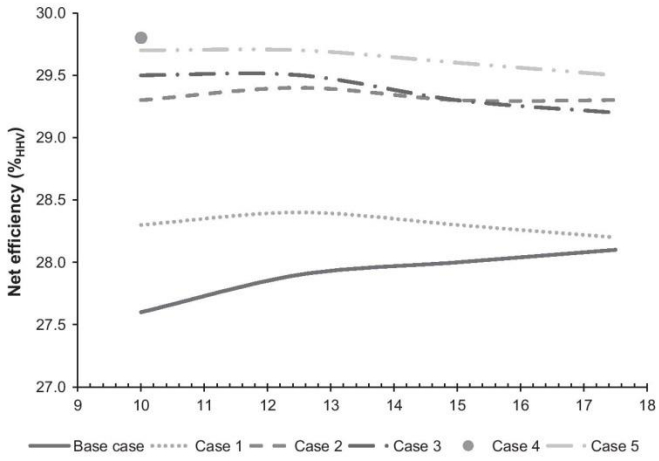

Fig. 14. Impact of the stripper pressure on the net thermal efficiency.

minor impact on the pressure distribution upstream of the steam extraction tie-in. A further increase of 1.0% points was observed when the back-pressure turbine was implemented to maintain the IP turbine discharge pressure (Case 2), leading to an overall gain of 1.7% points. This improvement in net thermal efficiency was the result of more efficient steam utilisation, which was previously wasted in the basic integration case due to the pressure reduction in the valves. Therefore, the impact of steam extraction on gross efficiency was reduced from 7.9% points in the basic integration to 6.2% points in Case 2. In addition, Cases 1 and 2 were characterised by the specific coal consumption of 476.4 g/kW h_{el} and 460.1 g/kW h_{el}, which is lower than in the basic integration scenario by 2.4% and 5.6%, respectively, enhancing the process economics and fuel safety.

Additionally, it was found that the net thermal efficiency was higher if extracted steam was used to preheat the HP feedwater

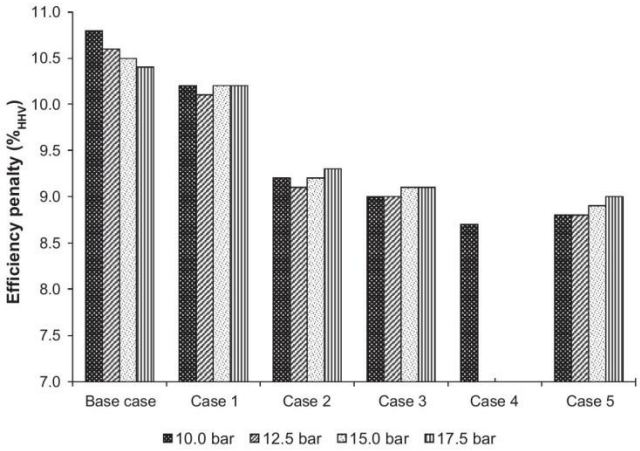

Fig. 15. Process performance improvements for the CAP.

prior to being fed to the reboiler (Case 3). Although such a configuration resulted in an extraction rate of 162.15 kg/s, which is considerably higher than in the basic integration scenario, the net thermal efficiency is further increased by 0.2% points to 29.5%$_{HHV}$, leading to 6.6% reduction in the specific fuel consumption. Such process performance improvement was the result of a reduced temperature difference between steam entering the reboiler, which was cooled from 316.1 °C to 191.6 °C, and the solvent in the reboiler (151.1 °C), as well as reduction in the IP steam extraction for the HPFWHs.

The results from the enhanced process configurations also reveal that it is feasible to retrofit the existing auxiliary turbine so that it is used to adjust the steam pressure to the reboiler requirement. Compared to the basic integration scenario, the retrofit of the single-stage auxiliary turbine (Case 4) and the two-stage auxiliary turbine (Case 5) resulted in rises in the net thermal efficiency of 2.2% and 2.1% points, respectively. Such improvement was also reflected in 7.8% and 7.3% reduction in the specific coal consumption, respectively. The major difference between these cases is the amount of IP steam extracted, amounting to 191.5 kg/s for Case 4 and 149.83 kg/s for Case 5, which is considerably higher than 28.3 kg/s in the reference CFPP. As the reboiler heat requirement was met with 161.9 kg/s (Case 4) and 144.35 kg/s (Case 5) of the expanded and de-superheated steam, it is clear that part of the steam at the de-superheater discharge must be diverted and utilised elsewhere. In Case 4, 15.5% of the steam was found to be more than enough to substitute the LP steam extraction to LPFWH 4, leading to an increase of the final LP feedwater temperature from 125.0 °C to 164.4 °C, which is even higher than 147.2 °C in the reference CFPP. This leads to less IP steam required to meet the desired operating temperature in the deaerator, increasing the useful amount of steam. In Case 5, in turn, only 3.7% of the steam was diverted to the second stage of the auxiliary turbine, in which it was expanded to the condenser pressure. Although no heat integration was made with the LP feedwater train as in Case 4, an additional amount of power generated resulted from a considerable drop in the IP steam extraction rate, leading to higher gross power output. As this configuration (i) provides the second highest net thermal efficiency, (ii) can utilise the existing piping to return the expanded steam to the condenser and (iii) requires a smaller auxiliary steam turbine to be retrofitted, it can be seen as a cost-efficient option for integration of the CAP CO_2 capture plant in the CFPP.

4.3. Evaluation of stripper operating pressure effect

The impact of stripper operating pressures on the net thermal efficiency of the different process configurations was evaluated (Fig. 14). Although a maximum pressure of 21.8 bar can be achieved in the stripper of the integrated plant, stripper pressure is limited to 17.5 bar in this analysis, as Hanak et al. [49] have shown that the CAP plant can be operated more efficiently at stripper pressures of 12.5–17.5 bar. And as expected, increase in the stripper operating pressure reduced the net efficiency penalty from 10.9% points at 10 bar to 10.4% points at 17.5 bar for the basic integration case. Although Hanak et al. [49] have estimated the same equivalent work for stripper pressures of 12.5–17.5 bar, the steam extraction rate decreased with pressure increase and thus, more steam was available for power generation in the LP turbine leading to the increase in net efficiency.

As already stated, a higher stripper operating pressure implies that steam of higher quality, and thus pressure, is required for solvent regeneration. Therefore, the discharge pressure of the let-down turbine for the advanced configurations increases with the operating pressure of the stripper, which in addition to the reduced steam extraction rate, results in less power being generated in the let-down turbine. As shown in Fig. 14, this effect was balanced by reduction of the parasitic load of the CAP plant when the stripper operates at 12.5 bar, resulting in a net efficiency similar to that at 10 bar stripper pressure. However, further increase in the stripper pressure results in higher efficiency penalty as further reduction in let-down turbine power output is greater than the reduction in the CAP plant parasitic load (Fig. 15). Additionally, the analysis revealed that Case 4 can be implemented only for a stripper pressure of 10 bar, as beyond this point, the amount of steam diverted to the LP feedwater train become too high to be utilised without major modifications to the system, and leads to partial evaporation of the LP feedwater before it enters the deaerator. Conversely, Case 5 allows the stripper pressure to be flexibly adjusted and its implementation led to the lowest efficiency penalties for all stripper pressures.

Among all integration scenarios analysed, the highest net efficiency of 29.8%$_{HHV}$ is observed under Case 4. Compared to the basic integration scenario, Case 4 would result in 7.8% reduction in the specific coal consumption. However, as Case 5 at 10.0 and 12.5 bar has the second highest net efficiency (29.7%$_{HHV}$) and as this configuration is expected to require minimal changes to the

existing steam cycle design, it would provide a feasible and cost-effective measure in reducing the efficiency penalty imposed on CO_2 capture plant integration. Although the net efficiency penalty of 8.7% points estimated in the best case is less by 0.8% points compared to the lowest efficiency penalty reported for amine scrubbing (9.5%), integration of the CO_2 capture plant using CAP process has still a considerable effect on the integrated system performance. Therefore, further measures, including heat integration, alternative process configurations and CO_2 capture technologies need to be pursued.

5. Conclusions

This study aimed to evaluate the integration of the CFPP with the CAP plant using the high-fidelity process models. To reliably assess the impact of PCC integration, the effect of steam extraction on the pressure profile across the turbine sections upstream of the extraction point was accounted for using the Stodola ellipse law. In the CAP plant, it was found that solvent regeneration can be conducted at elevated pressures up to 21.8 bar, at which the IP/LP steam quality becomes insufficient to meet the reboiler heat requirement.

Under a basic process integration scenario, net efficiency fell by 10.9% points from 38.5%$_{HHV}$ for CFPP without CAP to 27.6%$_{HHV}$ for the integrated plant, which corresponds to the efficiency penalties reported in the literature. Therefore, advanced integration configurations, which include substitution of the let-down and throttle valves with the let-down and back-pressure steam turbines, heat integration for steam de-superheating and auxiliary turbine integration, were investigated in this study. It was observed that the overall process performance would be enhanced by 1.7% efficiency points if the steam pressure is controlled using a combination of a let-down turbine and a back-pressure turbine. Additionally, if steam extracted from the steam cycle is also de-superheated using the HP feedwater before it is sent to the PCC, the net efficiency is improved by 1.7% points compared to the base case. The efficiency improvement of 2.1–2.2% points was reached when the novel configuration proposed in this study (which involves coupling of a new two-stage or a single-stage auxiliary steam turbine with the boiler feedwater pump) was implemented. Nevertheless, the efficiency penalty of the integrated system is still close to the amine scrubbing systems.

References

[1] IPCC (2007), Climate change 2007: mitigation: contribution of working group III to the fourth assessment report of the intergovernmental panel on climate change, Cambridge University Press, Cambridge, United Kingdom and New York, NY, USA.

[2] IEA (2014), Tracking Clean Energy Progress 2014. Energy Technology Perspectives 2014 Excerpt. IEA Input to the Clean Energy Ministerial, IEA Publications, Paris, France.

[3] Rackley SA. Carbon capture and storage. Burlington, USA: Elsevier; 2010.

[4] Wang M, Lawal A, Stephenson P, Sidders J, Ramshaw C. Post-combustion CO_2 capture with chemical absorption: a state-of-the-art review. Chem Eng Res Des 2011;89(9):1609–24.

[5] Linnenberg S, Darde V, Oexmann J, Kather A, van Well WJM, Thomsen K. Evaluating the impact of an ammonia-based post-combustion CO_2 capture process on a steam power plant with different cooling water temperatures. Int J Greenhouse Gas Control 2012;10:1–14.

[6] Yang Y, Zhai R, Duan L, Kavosh M, Patchigolla K, Oakey J. Integration and evaluation of a power plant with a CaO-based CO_2 capture system. Int J Greenhouse Gas Control 2010;4(4):603–12.

[7] Xu G, Jin HG, Yang YP, Xu YJ, Lin H, Duan L. A comprehensive techno-economic analysis method for power generation systems with CO_2 capture. Int J Energy Res 2010;34(4):321–32.

[8] Goto K, Yogo K, Higashii T. A review of efficiency penalty in a coal-fired power plant with post-combustion CO_2 capture. Appl Energy 2013;111:710–20.

[9] Reay D. The role of process intensification in cutting greenhouse gas emissions. Appl Therm Eng 2008;28(16):2011–9.

[10] Visscher F, van der Schaaf J, Nijhuis TA, Schouten JC. Rotating reactors – a review. Chem Eng Res Des 2013;91(10):1923–40.

[11] Kang J, Sun K, Wong DS, Jang S, Tan C. Modeling studies on absorption of CO_2 by monoethanolamine in rotating packed bed. Int J Greenhouse Gas Control 2014;25:141–50.

[12] Agarwal L, Pavani V, Rao DP, Kaistha N. Process intensification in HiGee absorption and distillation: Design procedure and applications. Ind Eng Chem Res 2010;49(20):10046–58.

[13] Zhao B, Su Y, Tao W. Mass transfer performance of CO_2 capture in rotating packed bed: dimensionless modeling and intelligent prediction. Appl Energy 2014;136:132–42.

[14] Aroonwilas A, Veawab A. Integration of CO_2 capture unit using single- and blended-amines into supercritical coal-fired power plants: Implications for emission and energy management. Int J Greenhouse Gas Control 2007;1(2):143–50.

[15] Manzolini G, Sanchez Fernandez E, Rezvani S, Macchi E, Goetheer ELV, Vlugt TJH. Economic assessment of novel amine based CO_2 capture technologies integrated in power plants based on European Benchmarking Task Force methodology. Appl Energy 2015;138:546–58.

[16] Versteeg P, Rubin ES. A technical and economic assessment of ammonia-based post-combustion CO_2 capture at coal-fired power plants. Int J Greenhouse Gas Control 2011;5(6):1596–605.

[17] Valenti G, Bonalumi D, Macchi E. Modeling of ultra super critical power plants integrated with the chilled ammonia process. In: 10th International Conference on Greenhouse Gas Control Technologies, vol. 4, 19 September 2010 through 23 September 2010, Amsterdam, 2011. p. 1721.

[18] Oexmann J, Hasenbein C, Kather A. Semi-empirical model for the direct simulation of power plant with integrated post-combustion CO2 capture processes by wet chemical absorption. In: 10th International Conference on Greenhouse Gas Control Technologies, vol. 4, 19 September 2010 through 23 September 2010, Amsterdam, 2011. p. 1276.

[19] Kvamsdal HM, Romano MC, van der Ham L, Bonalumi D, van Os P, Goetheer E. Energetic evaluation of a power plant integrated with a piperazine-based CO_2 capture process. Int J Greenhouse Gas Control 2014;28(1):343–55.

[20] Van Wagener DH, Liebenthal U, Plaza JM, Kather A, Rochelle GT. Maximizing coal-fired power plant efficiency with integration of amine-based CO_2 capture in greenfield and retrofit scenarios. Energy 2014;72:824–31.

[21] Zhao L, Riensche E, Blum L, Stolten D. Multi-stage gas separation membrane processes used in post-combustion capture: energetic and economic analyses. J Membr Sci 2010;359(1–2):160–72.

[22] Duke MC, Ladewig B, Smart S, Rudolph V, Da Costa JCD. Assessment of post-combustion carbon capture technologies for power generation. Front Chem Eng China 2010;4(2):184–95.

[23] Romano MC. Modeling the carbonator of a Ca-looping process for CO_2 capture from power plant flue gas. Chem Eng Sci 2012;69(1):257–69.

[24] Abanades CJ, Alvarez D. Conversion limits in the reaction of CO_2 with lime. Energy Fuels 2003;17:308–15.

[25] Tobiesen A, Falck da Silva E, Kvamsdal HM, Hoff KA, Knuutila H, Mejdell T. Evaluation of post-combustion CO2 capture solvent concepts, SINTEF F9109. Trondheim, Norway: SINTEF Materials and Chemistry; 2009.

[26] Yu H, Morgan S, Allport A, Cottrell A, Do T, McGregor J, et al. Results from trialling aqueous NH_3 based post-combustion capture in a pilot plant at Munmorah power station: Absorption. Chem Eng Res Des 2011;89(8):1204–15.

[27] Brown T, Perry CC, Manthey B. Pleasant Prairie carbon capture demonstration project, Progress report Oct. 8, 2009, Alstom, Wisconsin, 2009.

[28] Telikapalli V, Kozak F, Francois J, Sherrick B, Black J, Muraskin D, et al. CCS with the Alstom chilled ammonia process development program–Field pilot results. Energy Procedia 2011;4:273–81.

[29] Shakerian F, Kim K, Szulejko JE, Park J. A comparative review between amines and ammonia as sorptive media for post-combustion CO_2 capture. Appl Energy 2015;148:10–22.

[30] Ciferno JP, DiPietro P, Tarka T. An economic scoping study for CO2 capture using aqueous ammonia, National Energy Technology Laboratory; Advanced Resources International; Energetics Incorporated, 2005.

[31] Gal E. Chilled-ammonia Post Combustion CO2 Capture System–Laboratory and Economic Evaluation Results, 1012797, EPRI, Palo Alto, CA, USA, 2006.

[32] Romeo LM, Espatolero S, Bolea I. Designing a supercritical steam cycle to integrate the energy requirements of CO_2 amine scrubbing. Int J Greenhouse Gas Control 2008;2(4):563–70.

[33] Folger P. *Carbon Capture: A Technology Assessment*, R41325, Congressional Research Service, 2013. <http://bit.ly/1esPfhA>.

[34] Strube R, Manfrida G. CO_2 capture in coal-fired power plants – impact on plant performance. Int J Greenhouse Gas Control 2011;5(4):710–26.

[35] Zhao B, Su Y, Tao W, Li Li, Peng Y. Post-combustion CO2 capture by aqueous ammonia: a state-of-the-art review. Int J Greenhouse Gas Control 2012;9:355–71.

[36] Darde V, Thomsen K, van Well WJM, Stenby EH. Chilled ammonia process for CO_2 capture. Int J Greenhouse Gas Control 2010;4(2):131–6.

[37] Jilvero H, Normann F, Andersson K, Johnsson F. Thermal integration and modelling of the chilled ammonia process. Energy Procedia 2011;4:1713–20.

[38] Versteeg P, Rubin ES. Technical and economic assessment of ammonia-based post-combustion CO2 capture. Energy Procedia 2011;4:1957–64.

[39] Mathias PM, Reddy S, O'Connell JP. Quantitative evaluation of the chilled-ammonia process for CO_2 capture using thermodynamic analysis and process simulation. Int J Greenhouse Gas Control 2010;4(2):174–9.

[40] Valenti G, Bonalumi D, Macchi E. A parametric investigation of the Chilled Ammonia Process from energy and economic perspectives. Fuel 2012;101:74–83.

[41] Black J. Cost and Performance Baseline for Fossil Energy Plants Volume 1: Bituminous Coal and Natural Gas to Electricity, DOE/2010/1397 Revision 2a, National Energy Technology Laboratory, 2013.
[42] TUDelft, *Cycle Tempo: Reference Guide*, TUDelft, 2004. <http://www.cycle-tempo.nl/>.
[43] Lucquiaud M, Gibbins J. On the integration of CO_2 capture with coal-fired power plants: A methodology to assess and optimise solvent-based post-combustion capture systems. Chem Eng Res Des 2011;89(9):1553–71.
[44] Cooke DH. Modelling of off-design multistage turbine pressures by Stodola's ellipse. Houston, TX, USA: Bechtel Power Corporation; 1983.
[45] Knopf FC. Modeling, analysis and optimization of process and energy systems. Hoboken, NJ, USA: Wiley; 2012.
[46] Rusinowski H. Diagnostyka cieplna eksploatacji w energetyce (Thermal identification in power engineering). Katowice, Poland (in Polish): Polska Akademia Nauk; 2010.
[47] Megerle B, Stephen Rice T, McBean I, Ott P. Numerical and experimental investigation of the aerodynamic excitation of a model low-pressure steam turbine stage operating under low volume flow. J Eng Gas Turbines Power 2013;135(1).
[48] Salisbury JK. Steam turbines and their cycles, Robert E. Krieger Publishing, Huntington, NY, USA, 1950.
[49] Hanak DP, Biliyok C, Manovic V. Rate-based model development, validation and analysis of chilled ammonia process as an alternative CO_2 capture technology for coal-fired power plants. Int J Greenhouse Gas Control 2015;34:52–62.
[50] Pinsent BRW, Pearson L, Roughton FJW. The kinetics of combination of carbon dioxide with ammonia. Trans Faraday Soc 1956;52:1594–8.
[51] Derks PWJ, Versteeg GF. Kinetics of absorption of carbon dioxide in aqueous ammonia solutions. In: 9th International Conference on Greenhouse Gas Control Technologies, GHGT-9, vol. 1, 16 November 2008 through 20 November 2008, Washington DC, 2009. p. 1139.
[52] IPCC (2007), Climate change 2007: mitigation: contribution of working group III to the fourth assessment report of the intergovernmental panel on climate change [B Metz, OR Davidson, PR Bosch, R Dave, LA Meyer, editors], Cambridge University Press, Cambridge, United Kingdom and New York, NY, USA.
[53] Pfaff I, Oexmann J, Kather A. Optimised integration of post-combustion CO_2 capture process in greenfield power plants. Energy 2010;35(10):4030–41.
[54] Posch S, Haider M. Optimization of CO_2 compression and purification units (CO2CPU) for CCS power plants. Fuel 2012;101:254–63.
[55] Sanpasertparnich T, Idem R, Bolea I, de Montigny D, Tontiwachwuthikul P. Integration of post-combustion capture and storage into a pulverized coal-fired power plant. Int J Greenhouse Gas Control 2010;4(3):499–510.
[56] IEA (2007), CO2 Capture ready plants, 2007/4, OECD/IEA, Glos, UK.
[57] Xu G, Yang YP, Ding J, Li S, Liu W, Zhang K. Analysis and optimization of CO_2 capture in an existing coal-fired power plant in China. Energy 2013;58:117–27.
[58] Lucquiaud M, Gibbins J. Effective retrofitting of post-combustion CO_2 capture to coal-fired power plants and insensitivity of CO_2 abatement costs to base plant efficiency. Int J Greenhouse Gas Control 2011;5(3):427–38.
[59] Szargut J. Exergy method: technical and ecological applications. Southampton, UK: WIT; 2005.

6 MODELLING AND COMPARISON OF CALCIUM LOOPING AND CHEMICAL SOLVENT SCRUBBING RETROFITS FOR CO_2 CAPTURE FROM COAL-FIRED POWER PLANT

Dawid P. Hanak, Chechet Biliyok, Edward J. Anthony and Vasilije Manovic

Published: International Journal of Greenhouse Gas Control, 2015, 42, 226–236[g]

Statement of contributions of joint authorship

Dawid P. Hanak conducted the literature review, performed process analysis via process modelling and simulation, drafted and critically revised the manuscript, as well as prepared tables and figures. Chechet Biliyok, Edward J. Anthony, and Vasilije Manovic proof-read and critically commented on the manuscript prior to its submission to International Journal of Greenhouse Gas Control (Journal Impact Factor 2016: 3.946).

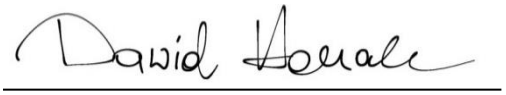

Dawid P. Hanak, PhD Candidate

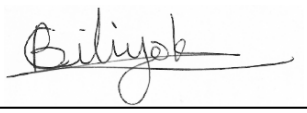

Chechet Biliyok, Associate supervisor

Edward J. Anthony, Subject advisor

Vasilije Manovic, Principal supervisor

[g] Reprinted with permission from Hanak, D.P., Biliyok, C., Anthony, E.J., and Manovic, V. (2015), "Modelling and comparison of calcium looping and chemical solvent scrubbing retrofits for CO_2 capture from coal-fired power plant", *International Journal of Greenhouse Gas Control*, 42, 226–236, doi: 10.1016/j.ijggc.2015.08.003, Elsevier 2015.

International Journal of Greenhouse Gas Control 42 (2015) 226–236

Contents lists available at ScienceDirect

International Journal of Greenhouse Gas Control

journal homepage: www.elsevier.com/locate/ijggc

Modelling and comparison of calcium looping and chemical solvent scrubbing retrofits for CO_2 capture from coal-fired power plant

Dawid P. Hanak, Chechet Biliyok, Edward J. Anthony, Vasilije Manovic*

Combustion and CCS Centre, Cranfield University, Bedford MK43 0AL, Bedfordshire, UK

ARTICLE INFO

Article history:
Received 21 May 2015
Received in revised form 3 August 2015
Accepted 4 August 2015

Keywords:
Calcium looping
Coal-fired power plant
Carbon capture
Efficiency penalty reduction

ABSTRACT

Carbon capture and storage (CCS) is expected to provide a cost-effective means of CO_2 emission reduction from the power sector. Amine scrubbing, which is the closest CCS technology to the market, is a suitable option for coal-fired power plants in retrofit scenarios. However, the energy requirement for solvent regeneration in chemical absorption CO_2 capture processes causes a substantial reduction in the power plant efficiency and power output. Therefore, novel technologies with lower efficiency penalties need to be developed. One promising option is calcium looping (CaL) which is based on the reversible carbonation/calcination reaction of calcium-based sorbent that takes place at high temperature. For the purpose of this study, the CaL process was model was developed and then linked to a high-fidelity model of a reference 580 MW_{el} supercritical coal-fired power plant. A secondary steam cycle was also modelled for recovery of high-grade heat from the CaL process. The results of the process analysis revealed that the efficiency penalty imposed in the CaL plant retrofit scenario was 6.7–7.9% points. Such performance compares favourably to the monoethanolamine and chilled ammonia scrubbing retrofit scenarios, which have efficiency penalties of 9.5% and 9.0%, respectively. Moreover, the retrofit of the CaL process was found to be less complex, and would result in two times higher net power output compared to the chemical solvent scrubbing scenarios. This is an important advantage of the CaL plant over the more mature CO_2 capture technologies, especially for the power plant operators who are looking to increase the system capacity to meet the increasing electricity demand and, at the same time, to reduce the CO_2 emissions.

1. Introduction

Carbon capture and storage (CCS) technologies are expected to be essential for reducing the environmental impact of the power sector (IEA, 2013a). However, the first large-scale CO_2 capture plant integrated to a power plant was only commissioned in late-2014 (Stéphenne, 2014), although the devices required for CCS deployment have been available in other industries (Rodríguez et al., 2010; IEA, 2013b). This is because CO_2 capture technologies for fossil fuel power plants struggle to be cost-effective at commercial scale. The reasons for this include relatively high capital cost, due to the size of units required to accommodate the flue gas volume, and the efficiency penalty, which varies between 9.5 and 12.5% points for amine scrubbing (Xu et al., 2010), 8.5–11% points for ammonia scrubbing (Linnenberg et al., 2012) and 8–12% points for oxy-fuel combustion (Boot-Handford et al., 2014). The result is a significant increase in the cost of electricity (Bhown and Freeman, 2011), which makes CCS less economically attractive at the moment. Therefore, novel CO_2 capture processes which introduce lower efficiency penalties need to be developed. One promising option proposed by Shimizu et al. (1999) for coal-fired power plants (CFPP) is the calcium looping (CaL) process, which is based on the reversible reaction between lime and CO_2 at high temperature.

With several evaluations of CFPP retrofit with the CaL process published in open literature to date, the CaL technology has been shown to offer superior performance to the other CO_2 capture technologies, as the efficiency penalty can be reduced to 3–8% points (Romeo et al., 2008; Martínez et al., 2011; Abanades et al., 2005; Vorrias et al., 2013; Yang et al., 2010; Ströhle et al., 2009). However, recent reviews of the CaL integration studies (Hanak et al., 2015a; Romano et al., 2013) have also shown that application of CaL as a post-combustion technology in the natural gas combined cycle power plants (Berstad et al., 2012) and integrated gasification

Abbreviations: ASU, air separation unit; CaL, calcium looping; CAP, chilled ammonia process; CCS, carbon capture and storage; CCU, CO_2 compression unit; CFPP, coal-fired power plant; HRSG, heat-recovery steam generator; MEA, monoethanolamine.

* Corresponding author. Tel.: +44 1234 75 4649.
E-mail address: v.manovic@cranfield.ac.uk (V. Manovic).

http://dx.doi.org/10.1016/j.ijggc.2015.08.003
1750-5836/

Nomenclature

a_1	Li et al. (Grasa and Abanades, 2006) model fitting parameter (–)
a_2	Li et al. (Grasa and Abanades, 2006) model fitting parameter (–)
b	Li et al. (Grasa and Abanades, 2006) model fitting parameter (–)
F_0	fresh-limestone make up rate (kmol/s)
f_1	Li et al. (Grasa and Abanades, 2006) model fitting parameter (–)
f_2	Li et al. (Grasa and Abanades, 2006) model fitting parameter (–)
E_{CO_2}	CO_2 capture level in the carbonator (–)
F_{CO_2}	CO_2 flow rate entering the carbonator (kmol/s)
F_R	CaO looping rate (kmol/s)
f_{calc}	calcination reaction extent (–)
f_{carb}	carbonation reaction extent (–)
r_0	fraction of never calcined limestone in the system (–)
X_{ave}	average sorbent conversion (–)
X_{calc}	sorbent conversion in the calciner (–)
X_{carb}	sorbent conversion in the carbonator (–)
ΔX_{carb}	carbonation conversion (–)

combined cycle power plant (Cormos and Cormos, 2013) would result in the comparable net efficiency penalty to the more mature CO_2 capture technologies (7.4–11.4% points).

Analysis of these studies revealed that that the fresh limestone make-up rate, which is often represented by the F_0/F_R ratio, appears to be the key parameter affecting the process performance, as it determines the average conversion of the sorbent in the system. The F_0/F_R value was reported to be between 0.025 (Mantripragada and Rubin, 2013) and 0.06 (Berstad et al., 2012) with values up to 0.1 being considered as economically feasible (Rodriguez et al., 2008). However, only few studies (Martínez et al., 2011; Vorrias et al., 2013; Lasheras et al., 2011) have investigated the effect of the F_0/F_R ratio on the process performance and attempted its optimisation. Nonetheless, it is clear that the sorbent make-up rate should be optimised based the trade-off between the process thermodynamic performance and economics. Moreover, there seems to be a large discrepancy in selection of the O_2 content in the fluidising gas in the calciner as the values between 25%$_{vol}$ (Martínez et al., 2011) and 95%$_{vol}$ (Romeo et al., 2008) have been used. Despite the endothermic calcination reaction taking place in the calciner, high O_2 contents can lead to local hot-spots in the calciner and to enhanced sintering of the sorbent (Symonds et al., 2012). However, operation with a 95%$_{vol}$ O_2 content would reduce the system size and complexity of the calciner as no CO_2 recycle would be needed.

Although performance of the CaL process has been compared with more mature technologies by Zhao et al. (2013) and Vorrias et al. (2013), there are some issues that need to be addressed. In the former study technologies were benchmarked using results from different literature sources; hence they were based on different sets of assumptions regarding the CO_2 capture plant and the reference power plant. This issue has been raised in a recent review of the CaL process integration, which has identified the need for using reference power plants in comparison of different technologies and retrofit scenarios (Hanak et al., 2015a). Also, in the study by Vorrias et al. (2013), the estimated efficiency penalties of the monoethanolamine (MEA) scrubbing (7.8% points) and the oxy-combustion (5.9% points) appear to be overly optimistic, and fall in the CaL range identified in the other studies (Romeo et al., 2008; Martínez et al., 2011; Abanades et al., 2005; Romeo et al., 2009).

Table 1
Supercritical coal-fired power plant key performance parameters.

Parameter	Value
Gross power output (MW_{el})	580.4
Net power output (MW_{el})	552.7
Net thermal efficiency(%$_{HHV}$)	38.5
Flue gas stream (kg/s)	617.2
CO_2 content in flue gas (%$_{vol}$)	15.2
Coal consumption rate (kg/s)	53.8
Air consumption rate (kg/s)	526.5
Live steam generation rate (kg/s)	462.3
Excess air ratio (%$_{vol}$)	20.0
Live steam pressure (bar)	242.3
Reheated steam pressure (bar)	45.2
Intermediate-/low-pressure crossover pipe pressure (bar)	9.3
Condenser pressure (bar)	0.069
Live and reheated steam temperature (°C)	593.3
Mechanical efficiency of the rotational machinery (%)	99.0

Therefore, the primary aim of this study is to compare the CaL process against more mature technologies using the same reference CFPP, and high-fidelity models of amine scrubbing (Hanak et al., 2014) and chilled ammonia scrubbing (Hanak et al., 2015b). Additionally, the impact of key operating specifications, such as F_0/F_R and O_2 content in the calciner fluidising gas, on the process performance of the CFPP retrofitted with the CaL system is investigated.

2. Model development

2.1. Supercritical coal-fired power plant

A reference model of the 580 MW_{el} supercritical CFPP, comprising supercritical boiler, flue gas treatment train, and steam cycle submodels, has previously been developed (Hanak et al., 2015b) and validated with the data available in the NETL report (Black, 2013). The key performance parameters of the model are provided in Table 1.

2.2. Calcium looping plant

2.2.1. Process model description

The flue gas from the power plant enters the carbonator, which is modelled using a stoichiometric reactor. The exothermic carbonation reaction occurs between CO_2 in flue gas and CaO in the sorbent. The temperature in the reactor needs to be controlled and maintained within the range of 580–700 °C to ensure an appropriate balance between the reaction kinetics and the equilibrium driving forces (Lu et al., 2008; Valverde, 2013). The sorbent is regenerated in the calciner (>900 °C), which is modelled as a Gibbs reactor and in which an additional amount of fuel is combusted in an O_2/CO_2 environment to drive the endothermic calcination reaction (Shimizu et al., 1999; Martínez et al., 2011). If biomass and/or coal are used as fuel, decomposition of the solid fuel is modelled using the yield reactor. Although the conversion of the regenerated sorbent decreases with the number of carbonation/calcination cycles (Abanades, 2002), it is reused in the carbonator, with some part replaced by fresh sorbent.

Several semi-empirical models have been proposed in the open literature to describe how the maximum sorbent conversion deteriorates with the number of cycles (Valverde, 2013; Li et al., 2008; Grasa and Abanades, 2006; Wang and Anthony, 2007; Abanades and Alvarez, 2003). However, such models cannot be directly applied to represent conversion in real system, as particles will have undergone different numbers of carbonation/calcination cycles are present in such a system (Abanades, 2002), and complete carbonation and calcination reactions will not be achieved. Therefore, in this study, the maximum average conversion of the sorbent is

Table 2
Evaluation of the calcium looping process model prediction.

	Flue gas flow to carbonator (kg/h)	Maximum coal flow to the calciner (kg/h)	Maximum limestone make-up (kg/h)	Oxygen flow to calciner (kg/h)	Carbon dioxide flow to calciner (kg/h)	Average conversion (–)*
Pilot plant	680–2300	325	300	300–600	700–2250	0.1–0.7
Curve 1	680	94	94	151	426	0.318 (0.212)
	1400	194	194	311	880	0.318 (0.212)
	2300	317	317	509	1432	0.318 (0.212)
Curve 2	680	118	118	190	530	0.167 (0.111)
	1400	244	244	390	1092	0.167 (0.111)
	2300	401	401	642	1803	0.167 (0.111)
Curve 3	680	92	92	148	419	0.342 (0.227)
	1400	190	190	305	863	0.342 (0.227)
	2300	312	312	501	1418	0.342 (0.227)
Curve 4	680	95	95	152	427	0.308 (0.205)
	1400	195	195	313	879	0.308 (0.205)
	2300	320	320	514	1443	0.308 (0.205)

* Values in the bracket refer to the carbonation conversion.

determined using the model derived by Rodríguez et al. (2010), which utilises the semi-empirical correlation proposed by Li et al. (2008). As shown in Eq. (1), the maximum average conversion in this model is a function of the carbonation (f_{carb}) and calcination extent (f_{calc}), sorbent characteristics (a_1, a_2, f_1, f_2, b), fresh limestone make-up (F_0) and solid looping rate (F_R). In addition, the carbonation conversion and the CO_2 capture level, which are used to determine the solids looping rate, are calculated using Eqs. (2) and (3), respectively. Finally, the equilibrium partial pressure of CO_2 in the gas streams leaving the carbonator and the calciner is determined using correlation by Baker (1962), to account for the equilibrium limitations.

$$X_{ave} = (F_0 + F_R r_0) f_{calc} \times \left[\frac{a_1 f_1^2}{F_0 + F_R f_{carb} f_{calc} (1 - f_1)} + \frac{a_2 f_2^2}{F_0 + F_R f_{carb} f_{calc} (1 - f_2)} + \frac{b}{F_0} \right] \quad (1)$$

$$\Delta X_{carb} = f_{calc} f_{carb} X_{ave} \quad (2)$$

$$E_{CO_2} = \frac{F_R}{F_{CO_2}} \Delta X_{carb} \quad (3)$$

The values of the five fitting parameters in Eq. (1) are determined for the four different deactivation curves presented in the literature: (i) no sulphation and (ii) 1% sulphation during each cycle (Grasa et al., 2008), (iii) 1.7 MW_{th} la Pereda pilot plant (Sánchez-Biezma et al., 2013), and (iv) the semi-empirical model proposed by Grasa and Abanades (2006). Fig. 1 reveals that application of the semi-empirical correlation proposed by Li et al. (2008) results in a good correlation with the thermogravimetric data (Curves 1 and 2), with $R^2 > 0.99$, and it provides the same prediction as the model proposed by Grasa and Abanades (2006) (Curve 3, $R^2 = 1$). Interestingly, the highest R^2 value achieved for the fit of the INCAR pilot plant data (Curve 4) is 0.86, which is due to higher measurement errors in the pilot plant compared to thermogravimetric analysis, for which the operating conditions are well-controlled. Although this curve starts only on the 5th cycle, extrapolation of Curve 4 gives the conversion of 0.714 for the 1st cycle that is close to 0.700 predicted by the model proposed by Grasa and Abanades (2006).

2.2.2. Evaluation of model prediction

Some operating data from the bench- and the pilot-scale plants at INCAR-CSIC and IFK at Stuttgart have been published (Sánchez-Biezma et al., 2011, 2013; Arias et al., 2013; Charitos et al., 2011), however they are not suitable for validation of process models predictions. In addition, Romano (2012) has pointed out that detailed operational data for particular test runs from bench-scale and pilot-plant testing are not yet available in the open literature. However, some comparison of model prediction with experimental data can provide valuable information on credibility of the model and help determine whether the model prediction satisfies the desired intent under comparable operating conditions (Romano, 2012; Roy, 2005; Pace, 2004).

The predictions of the process model have been compared with the operating data (Table 2) for three different flue gas flow rates (680, 1400 and 2300 kg/h), representing the minimum, average and maximum operating values reported by Sánchez-Biezma et al. (2013). In general, the model prediction showed a good agreement with the experimental data in terms of coal and limestone flow rates for all curves except for Curve 2. A large difference in prediction of the CO_2 flow rate to the calciner stems from the assumption of a 30%$_{vol,wet}$ O_2 content in the calciner fluidising gas, while this value was varied between 21 and 35%$_{vol}$ in the experimental tests (Arias et al., 2013). Moreover, the difference between the O_2 flow rate to the calciner may result from the fact that a partial recycle of the CO_2 stream, containing 2.5%$_{vol,dry}$ O_2, was considered in the model, as opposed to the situation for the pilot plant trials (Sánchez-Biezma et al., 2011) in which the CO_2 recycle was not considered.

2.2.3. Assumptions for a commercial-scale calcium looping process

The model developed is adapted to the commercial-scale CaL plant by implementing the operating conditions based on the open literature and summarised in Table 3. The deactivation Curve 4 is chosen, as it represents the performance of the sorbent that could be observed in commercial-scale facilities, and it is assumed that

Table 3
Initial operating conditions of the commercial-scale calcium looping plant.

Parameter	Value
Carbonator temperature (°C)	650
Calciner temperature (°C)	900
Carbonated sorbent fraction (–)	0.70
Calcined sorbent fraction (–)	0.95
Fluidising fan pressure increase (mbar)	150
Excess oxygen (%$_{vol,dry}$)	2.5
Relative fresh limestone make-up rate* (–)	0.05

* Relative fresh limestone make-up rate is defined as ratio of fresh limestone make-up and sorbent looping rates on a molar basis.

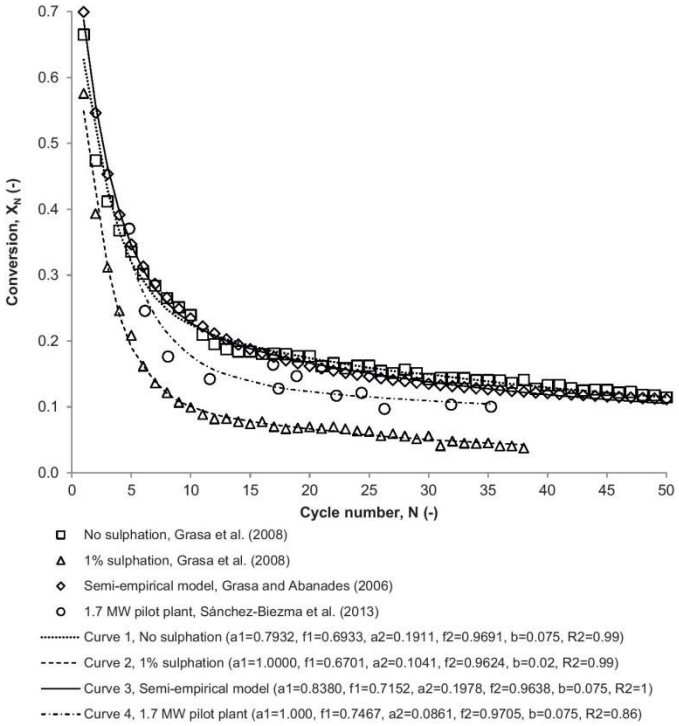

Fig. 1. Determination of the deactivation curve fitting parameters.

the calciner is fed with La Blanca limestone (Manovic et al., 2008). In addition, it is assumed that the fluidising fans increase the pressure of the flue gas and the fluidising gas by 150 mbar (Ströhle et al., 2009). Also, the carbonation and the calcination fraction are 0.7 and 0.95, respectively (Berstad et al., 2012). Finally, part of the CO_2 stream from the calciner is recycled to maintain the O_2 content in the fluidising gas at a level of 30%$_{vol}$ and the air flow rate to the ASU is adjusted to ensure nearly complete combustion of fuel in the calciner and to maintain 2.5%$_{vol,dry}$ excess O_2 in the CO_2 stream. Such specifications are within typical ranges for oxy-fired furnaces (Yan et al., 2015).

2.3. Air separation and CO_2 compression units

A cryogenic ASU is used to produce O_2 for the oxy-combustion in the calciner. A model of the standard double-column ASU has been developed in Aspen Plus (AspenTech, 2011), based on the operating conditions of the Polk integrated gasification combined cycle power plant by Tampa Electric (Hornick and McDaniel, 2002). This model is adapted to reflect the Linde process by a slight reduction in the high-pressure column pressure, from 6.1 bar to 5.6 bar, and substitution of the column trays with the 350Y structured packing in both low- and high-pressure columns (AG L, 2013). To enable part-load operation, two ASU trains are considered that are sized to operate with 75% flooding when processing 600 kg/s of air, each delivering 95%$_{vol}$ O_2 stream at 17 °C. The air compressors are modelled using the polytrophic compression model with constant stage polytrophic efficiency (79–80%). The specific power requirement was found to be 229.3 kW h/tO_2, which is slightly higher than that of 184–220 kW h/tO_2 usually assumed in the literature (Romeo et al., 2008; Ströhle et al., 2009).

It is well established that the CO_2 stream pressure at ambient temperature for the pipeline transport is 110 bar (Metz et al., 2005). To minimise the power requirement of the CCU, it is assumed that CO_2 produced in the CaL plant is first compressed to 80 bar, which is just over the critical pressure due to impurities content, cooled down to 25 °C and then pumped to 110 bar prior to transport. The CCU is modelled as a set of nine compression stages, so that the pressure ratio and the polytrophic head do not exceed 3 and 3050 m, respectively, due to equipment limitations (Sanpasertparnich et al., 2010). Each compression stage consists of a centrifugal compressor, stage intercoolers and scrubbers. The CO_2 compression is modelled using the polytrophic compression model with constant stage polytrophic efficiency (78–80%) (Pfaff et al., 2010; Posch and Haider, 2012) and the pump characterised with an isentropic efficiency of 80%.

3. Process integration

3.1. Considerations

Due to the large amount of high-grade recoverable heat available in the CaL plant, there are different options for integrating this system with the CFPP. In the first configuration, the gross power output of the integrated system would be kept at the reference CFPP level, as the steam generated at a desired temperature and pressure in a heat recovery steam generator (HRSG) can be sent to the existing steam cycle, while the steam generated in the existing boiler would be reduced. Alternatively, in the case of large systems comprising more than one power boiler, the steam generated from one of the existing boilers can be replaced with the steam generated in the HRSG, while keeping the gross power output at

Table 4
Design basis for the heat recovery steam generator and the steam cycle.

Parameter	Value
Isentropic efficiency of high-pressure steam turbine (%)	92.0
Isentropic efficiency of intermediate-pressure steam turbine (%)	94.0
Isentropic efficiency of low-pressure steam turbine (%)	88.0
Electric generator efficiency (%)	97.5
Mechanical efficiency of the rotational machinery (%)	99.6
Reheater and superheater minimum temperature approach (°C)	25.0
Economiser minimum temperature approach (°C)	10.0
Gas-gas heat exchangers minimum temperature approach (°C)	10.0
Feedwater heaters minimum temperature approach (°C)	10.0

the reference level. In a third configuration, steam generated in the HRSG is sent off to the secondary steam cycle, leading to an increase of the gross power output of the integrated system with respect to the reference CFPP. The heat exchanger network in all configurations can be designed to reach two different goals: either to maximise the steam generation rate through recovering most of the heat in the HRSG, or to minimise the fuel consumption in the calciner through maximising the heat transfer to the CaL process streams.

Comparing these configurations it is clear that the first and second configuration would require smaller capital investment as the CaL unit (first configuration only) would be smaller, which is a result of less flue gas to be pre-treated due to reduction of the exiting boiler load, and no need for the secondary steam cycle. However, utilising the steam generated in the HRSG in the primary steam cycle denies the greatest benefit of the CaL process, which is its capability of increasing the net power output of the integrated system.

The integration configuration considered in this study (Fig. 2) comprises the HRSG that generates steam, which has the same parameters as the boiler (593.3 °C/593.3 °C/242.3 bar) and is designed to maximise the steam generation rate, and the secondary steam cycle of characteristic similar to the primary steam cycle. The only difference between the primary and the secondary steam cycle is that in the latter the feedwater is heated using heat available in the CO_2 and the clean gas from the CaL plant and steam is extracted only to meet the requirements of the deaerator. As there are no steam bleedings from the steam turbines for feedwater heating (despite the steam extraction to a deaerator), the proposed configuration would not only allow for higher gross power output and higher degree of heat recovery from the process streams, but also it is less complex compared to the conventional steam cycle. The isentropic efficiencies for the steam turbines, the mechanical efficiency of the rotary equipment and the minimum temperature approaches of the heat exchangers are adapted from Anantharaman et al. (2011), and are summarised in Table 4. It is also assumed that there is no heat exchange between the solid streams including fuel, sorbent, limestone make-up and purge streams.

It is common for studies on retrofit of the CFPP with the CaL process that the process performance is evaluated only for an initial set of parameters, which are selected based on the information available in the open literature, and no further process-wise parametric analysis to determine the optimum operating parameters is applied. Such analysis, however, should be performed for each novel process configuration, so that the techno-economic performance of the integrated system is maximised. Here, the parametric studies are conducted by varying:

- fresh limestone make-up rate between 0.02 and 0.10;
- O_2 content in the calciner fluidising gas between 20 and 95%$_{vol,wet}$;
- O_2 excess between 1.5 and 4.5%$_{vol,dry}$;
- CO_2 capture level in the carbonator between 70 and 90%.

Table 5
System performance and retrofit impact indicators for supercritical coal-fired power plant with and without calcium looping process.

Parameter	Reference CFPP	CaL retrofit
System performance indicators		
Gross electricity production (MW_{el})	580.4	1137.3
Total auxiliary electricity consumption (MW_{el})	27.7	268.3
Net electricity production (MW_{el})	552.7	869.0
Gross thermal efficiency (%$_{HHV}$)	40.4	39.1
Net thermal efficiency (%$_{HHV}$)	38.5	29.9
Net specific chemical energy consumption (kW_{ch}/kW_{el})	2.6	3.3
Specific coal consumption (g/kWh_{el})	350.3	448.6
Integration impact indicators		
Increase in the net power output (%)	–	57.2
Net efficiency penalty (% points)	–	8.6
Increase in net specific chemical energy consumption (%)	–	28.7

In pilot-plant tests of the CaL concept, coal was used as fuel in the calciner (Arias et al., 2013; Ströhle et al., 2014). However, this would lead to ash accumulation and thus larger solid looping rates (Romano, 2012). As a result, a larger units and more heat would be required for sorbent pre-heating in the calciner. Therefore, low ash or no-ash-containing alternative fuels should be also investigated. Other fuels, such as propane (Ströhle et al., 2014) and biomass (Lu et al., 2008; Dieter et al., 2014), have also been utilised during the pilot-plant tests. Utilisation of natural gas in the calciner has been considered for natural gas combined cycle power plants (Berstad et al., 2012) and in novel application of CaL for production of heat and CO_2 enrichment of greenhouses (Ramezani et al., 2015). As biomass is considered as CO_2-neutral fuel, the development of a biomass combustion process based on CaL with in-situ CO_2 capture, in which biomass is fired in both carbonator (air combustion) and calciner (oxy-combustion), has recently received some attention. Such a process has been proven technically and economically viable during the pilot-plant tests (Charitos et al., 2011; Alonso et al., 2014) and from process analysis (Ozcan et al., 2014). It needs to be highlighted, however, that one of the largest operating biomass-fired fluidised bed system, located in Polaniec, Poland, delivers only 205 MW_{el} (447 MW_{th}), and there are plans to extend the capacity to 400–600 MW_{el} (Natunen et al., 2013). Based on guidance from the experimental studies, the impact of using different fuels[1] is analysed in this study for four cases: coal, coal/biomass mixture (80%$_{wt}$/20%$_{wt}$), biomass and natural gas.

3.2. Performance analysis

Analysis of the retrofit of the CFPP with the CaL plant (Table 5), in which coal was used as the fuel in the calciner, revealed that if 90% of CO_2 is removed from the power plant flue gas, which corresponds to the total CO_2 capture level of 95.7%, the net thermal efficiency of the integrated system was reduced by 8.6% points, while the net power output increased by 57.2%. Such an increase agrees with the values reported in the literature (Vorrias et al., 2013; Ströhle et al., 2009; Romeo et al., 2009; Li et al., 2008). In addition, the net efficiency penalty estimated for the initial set of operating specifications is

[1] Information regarding the fuels composition is provided in the Supplementary information.

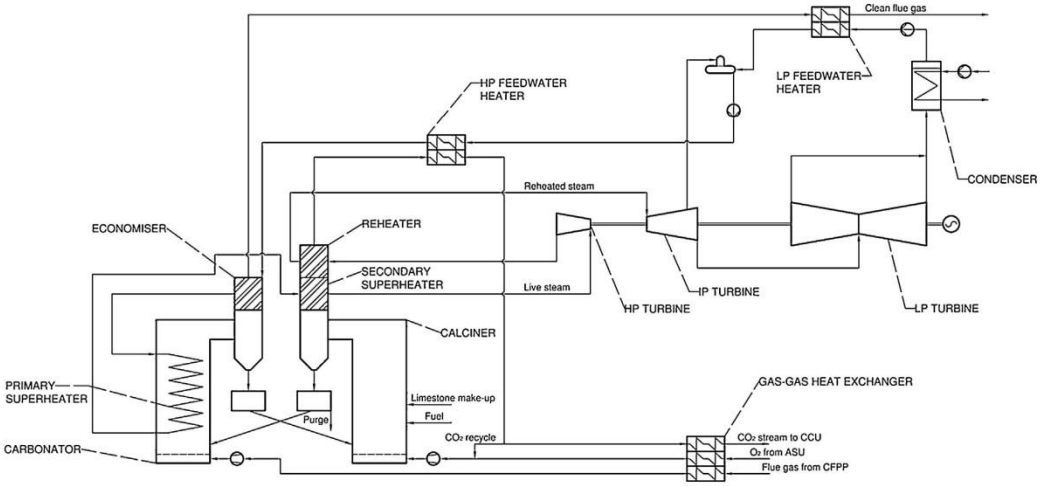

Fig. 2. Heat integration of the calcium looping process, the heat recovery steam generator and the secondary steam cycle.

comparable to the oxy-combustion (8.0% points) (Boot-Handford et al., 2014) and chilled ammonia process (8.7% points) (Hanak et al., 2015c) technologies. Therefore, the parametric analysis is required to minimise the net efficiency penalty imposed by the CaL plant retrofit.

It can be clearly observed in Fig. 3 that depending on key operating parameters specified and the fuel used in the calciner, the net power output of the integrated system increases by 37–87%. For this reason, the system of dual interconnected fluidised beds can be seen as a new power boiler, in which the heat input from fuel combustion is used primarily for sorbent regeneration in the calciner, while the high-grade heat available in the carbonator and the process streams is utilised for generation of an additional amount of high-pressure steam. Interestingly, the increase in the net power output was found to be higher for the high-ash fuels (coal and coal/biomass) for F_0/F_R values lower than 0.05 and for O_2 contents in the calciner fluidising gas higher than $30\%_{vol,wet}$. Otherwise, the low-ash fuels (biomass and natural gas) offered higher net power outputs. However, under such conditions large amounts of fuel and fluidising gas are fed to the calciner, and large amount of total solids are circulated between reactors due to ash accumulation. This directly translates to an increase in the capital and operating costs, as large fluidised beds and ASU columns would be required to accommodate such volumes of solids and air, making such design unattractive.

Importantly, Fig. 4 reveals that the net thermal efficiency of the integrated system is most affected by the sorbent make-up rate, CO_2 capture efficiency, and O_2 content in the calciner fluidising gas, and varies from $27.2\%_{HHV}$ to $31.4\%_{HHV}$. These values correspond to efficiency penalties of 11.3% points for the biomass-fired calciner at F_0/F_R of 0.10, and 7.1% points for the natural gas fired calciner at F_0/F_R of 0.02, with values of the other operating specifications kept at the initial level for both cases. This shows that selection of the fuel would not only affect the size of the CaL process units, but will also have a considerable impact on the net thermal efficiency of the integrated system. It needs to be highlighted, however, that for the retrofit scenario it could be more beneficial to sacrifice process efficiency to some extent, and to use the same fuel (coal or coal/biomass in most cases), instead of investing in a new natural gas connection to the local gas grid.

4. Comparison with chemical solvent scrubbing

4.1. Considerations

As CaL is considered as an emerging CO_2 capture technology, it is worth comparing its performance with the more established technologies. To provide a benchmark cases for the CaL plant, high-fidelity models for the monoethanolamine (MEA) and chilled ammonia scrubbing (CAP), which have been developed previously (Hanak et al., 2014, 2015b), are integrated to the 580 MW_{el} CFPP for the total 90% capture level. The key operating and performance parameters are summarised in Table 6.

The operating specifications for the CaL plant are presented in Table 7 and have been selected based on the parametric study performed above. The reason for choosing the F_0/F_R value of 0.02 for a biomass- or natural gas-fired calciner, and 0.04 for the remaining cases is the fact that such make-up rates would result in similar total solid looping rates, and would ensure reasonable sizes for the reactors. Furthermore, to maximise the efficiency, the O_2 content in the calciner fluidising gas is increased to $40\%_{vol}$ compared to the initial operating specifications. Although this would reduce the net power output, the net efficiency of the integrated system would increase. Finally, the total CO_2 capture level of 90% is imposed for all investigated cases, except for the biomass-fired calciner case, in which the CO_2 capture level in the carbonator is fixed at the same level as for the coal/biomass-fired calciner case.

4.2. Retrofit configuration analysis

Process analysis revealed important differences between the CaL and the chemical solvent scrubbing retrofits, arising mainly

Table 6
Parameters characterising the chemical solvent CO_2 capture plant operation.

Parameter	Amine scrubbing	Chilled ammonia scrubbing
Stripper pressure (bar)	1.7	12.5
Required steam pressure (bar)	2.9	7.1
Lean loading (mole basis)	0.29	0.29
Reboiler duty (MW_{th})	513.6	343.2
IP/LP steam requirement (kg/s)	224.7	131.3
Condensate temperature (°C)	132.4	165.4

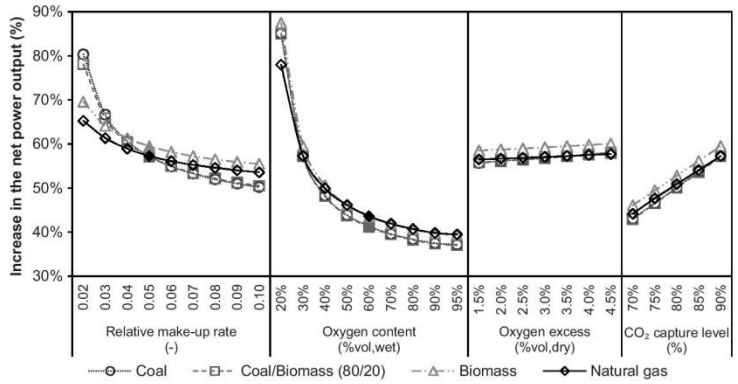

Fig. 3. Impact of calcium looping operating parameters on the increase in the net power output of the integrated system. Filled markers identify the initial operating conditions presented in Table 3.

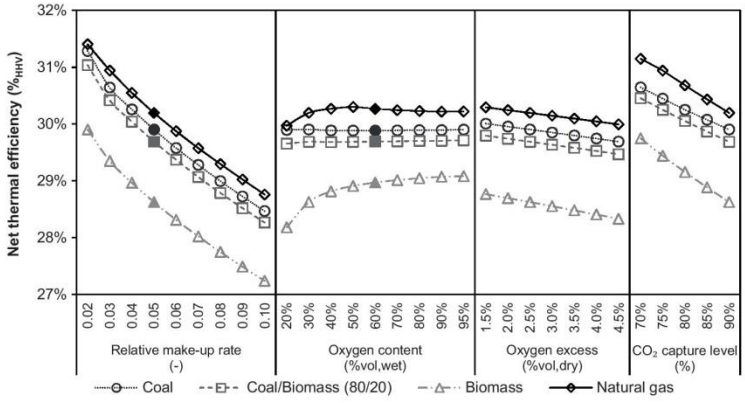

Fig. 4. Impact of calcium looping operating parameters on the net thermal efficiency of the integrated system. Filled markers identify the initial operating conditions presented in Table 3. Net thermal efficiency of the reference coal-fired power plant without calcium looping CO_2 capture plant is 38.5%$_{HHV}$.

from the degree of integration with the existing CFPP. Namely, integration of the chemical solvent scrubbing plant requires intermediate-/low-pressure (IP/LP) steam extraction from the existing steam cycle. As the steam pressure in the IP/LP crossover pipe is usually at much higher pressure than required for solvent regeneration, steam pressure needs to be adjusted to the reboiler requirement and then desuperheated with the high-pressure feedwater. To minimise the energy losses, this is achieved using a let-down turbine. Moreover, the steam pressure downstream the extraction point decreases and thus, a back-pressure turbine is needed to maintain the desired IP/LP crossover pressure (Fig. 5) (Lucquiaud and Gibbins, 2011).

Conversely, as discussed in Section 3.1, the CaL retrofit configuration considered in this study, in which the high-grade heat from the CaL plant is utilised to generate power in the secondary steam cycle, does not require any changes to the layout and the operation of the existing CFPP. Therefore, it can be considered to be less complex. Using such a configuration, the operators would not only benefit from increased net power output, but also from flexibility standpoint. The latter is because as opposed to the chemical solvent scrubbing technologies, the CaL plant would follow the CFPP operation without feedback in the form of the steam requirement.

4.3. Process performance analysis

A comparison of the key performance indicators for the CFPP retrofitted with amine scrubbing, chilled ammonia scrubbing and CaL CO_2 capture plants is presented in Table 8. It is clear that CaL offers superior performance over technologies using chemical solvents, by achieving an efficiency penalty of 6.7–7.9% points

Table 7
Operating specifications for the calcium looping process.

Parameter	Coal	Coal and Biomass	Biomass	Natural gas
Limestone make-up rate (F_0/F_R) (–)	0.04	0.04	0.02	0.02
Carbonator temperature (°C)	650	650	650	650
Calciner temperature (°C)	900	900	900	900
Oxygen content ($\%_{vol,wet}$)	40	40	40	40
Excess oxygen ($\%_{vol,dry}$)	2.5	2.5	2.5	2.5

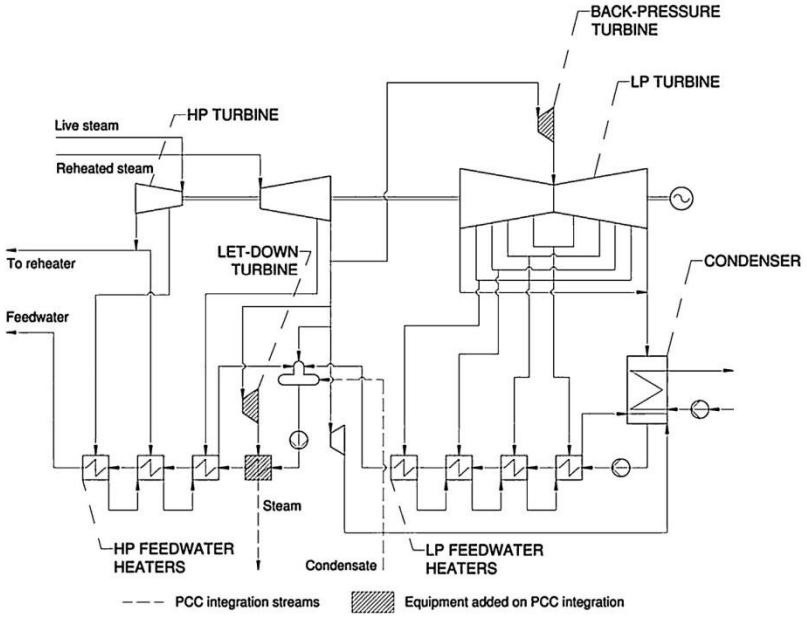

Fig. 5. Integration of the chemical solvent scrubbing CO_2 capture to CFPP.

depending on the fuel and operating specifications used. Such improvement in the performance has a positive effect on the increase in chemical energy consumption, which can be reduced from 32.8% for amine scrubbing to 25.6% for the coal-fired calciner or to 21.0% for the natural gas-fired calciner. This implies that even in the worst case scenario of the CaL retrofit (coal-fired scenario), the efficiency penalty is reduced by 1.6% points and the increase in chemical energy consumption is reduced by 7.2% points compared to the reference amine scrubbing system (MEA).

Table 8
Comparison of the key performance technologies for chemical solvent and calcium looping CO_2 capture plant.

Parameter	Reference CFPP	Amine scrubbing	Chilled ammonia scrubbing	Calcium looping			
				Coal	Coal and biomass	Biomass	Natural gas
System performance indicators							
Gross electricity production (MW_{el})	580.4	475.2	492.0	1023.3	973.4	1037.4	1061.5
Total auxiliary electricity consumption (MW_{el})	27.7	59.0	67.9	223.5	205.0	222.4	212.1
Net electricity production (MW_{el})	552.7	416.2	424.1	799.9	768.4	815.0	849.4
Gross thermal efficiency ($\%_{HHV}$)	40.4	33.1	34.3	39.2	39.0	39.6	39.8
Net thermal efficiency ($\%_{HHV}$)	38.5	29.0	29.5	30.6	30.8	31.1	31.8
Net specific chemical energy consumption (kW_{ch}/kW_{el})	2.6	3.5	3.4	3.3	3.2	3.2	3.1
Specific coal consumption (g/kWh_{el})	350.3	465.1	456.4	438.2	452.2	560.7	327.8
Integration impact indicators							
Ratio of total CO_2 captured and generated in the integrated system (–)	–	0.900	0.900	0.900	0.900	1.545	0.900
Ratio of CO_2 captured in absorber/carbonator and generated in the coal-fired power plant (–)		0.900	0.900	0.796	0.711	0.711	0.834
Change in the net power output (MW_{el})	–	−136.5	−128.6	247.2	215.7	262.4	296.8
Net efficiency penalty (% points)	–	9.5	9.0	7.9	7.7	7.4	6.7
Increase in net specific chemical energy consumption (%)	–	32.8	30.3	25.6	25.1	23.8	21.0

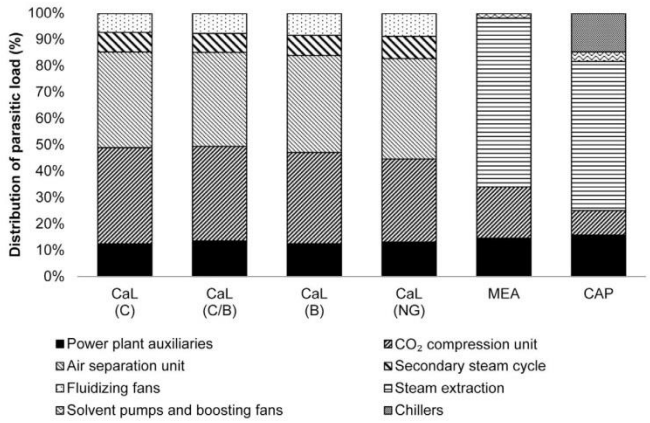

Fig. 6. Comparison of a parasitic load distribution for the coal-fired power plant retrofitted with investigated CO_2 capture technologies.

The performance analysis also revealed that more than 70% of the total parasitic load in the CaL plant stem from the power requirement to run compressors in the CCU and the ASU. Therefore, the efficiency penalty imposed by the retrofit of the CaL plant can become be even further reduced by investigating alternative process integration configurations, which would reduce heat requirement for sorbent regeneration, and alternative CaL processes including high-pressure calcination, combined calcium looping and chemical looping process, as well as development of in-direct fired calciner designs. Conversely, in the MEA and the CAP plants the main source of the efficiency penalty is the steam extraction (Fig. 6). Although the solvent regeneration in the CAP plant was conducted at elevated pressure (12.5 bar) compared do the MEA plant (1.7 bar), leading to reduction in the CCU power (54.5%) and reboiler heat (16.0%) requirements, the steam extraction accounted for more than 55% of the total parasitic load. Although the use of other solvents, such as piperazine, the efficiency penalty can be reduced to 7% points (Kvamsdal et al., 2014), the parasitic load of the amine scrubbing system is still estimated to reduce the power plant output by 20–30% (Boot-Handford et al., 2014). Therefore, the efficiency penalty imposed by the CaL plant retrofit is not only lower than the chemical solvent scrubbing technologies, it is also most likely to be reduced further since the progress in development of less energy intensive ASU, which is the most important contributor to the efficiency penalty, is also being made for other technologies (Perrin et al., 2014).

Moreover, it is important to highlight that in each CaL case except the biomass-fired calciner, the removal rate of CO_2 from the power plant flue gas is lower than in both solvent scrubbing technologies. This because all additional amount of CO_2 produced from fuel combustion and fresh limestone calcination in the calciner is captured, leading to the total CO_2 capture level[2] of 90%. When pure biomass was used in the calciner, the integrated system become a negative emitter of CO_2, as the ratio of the CO_2 captured in the system and the CO_2 generated in the system was 1.545. This means that due to the CO_2-neutral character of biomass the integrated system has a potential to operate as a CO_2-negative system, regardless of the CO_2 capture level of 71.1% in the carbonator.

[2] Total CO_2 capture rate considers the amount of CO_2 captured from the flue gas in the carbonator, and the amount of CO_2 captured from additional fuel combustion and fresh limestone calcination in the calciner.

Although the initial capital investment for the CaL plant integration would be higher, mostly because of the need for the secondary steam cycle and the ASU, the net power output of the integrated system would be higher by a factor of 2 compared to the chemical solvent scrubbing technologies, improving the revenue from electricity production. This is an important advantage of the CaL plant over the more mature CO_2 capture technologies, especially for the power plant operators who are looking to increase the system capacity to meet the increasing electricity demand and, at the same time, to reduce the CO_2 emissions. It is also important to highlight that different operating specifications used in the CaL plant resulted in different gross thermal efficiencies of the secondary steam cycle (39.2–39.8%$_{HHV}$) and thus, a process-wide approach to system analysis should be used to improve the process performance.

5. Conclusions

The CaL process, an emerging CO_2 capture technology, has been identified as a promising option for decarbonising the power industry with a reduced efficiency penalty compared to the first generation technologies. For the purpose of this study, a CaL process model has been developed and its prediction has been compared with operational data from the 1.7 MW_{th} pilot plant at la Pereda power plant. The model predictions were found to be in agreement with the pilot-plant data under different flue gas loads.

Furthermore, retrofit of a CaL plant to a 580 MW_{el} supercritical CFPP was analysed. The study revealed that when 90% of CO_2 is removed from the power plant flue gas, which corresponds to a total CO_2 capture level of 95.7%, the net thermal efficiency of the integrated system was reduced by 8.6% points, while the net power output increased by 57.2%. The performance of the integrated system was then analysed under different operating specifications. This revealed that the net thermal efficiency of the integrated system and the net power output are most affected by the sorbent make-up rate, CO_2 capture efficiency, and O_2 content in the calciner fluidising gas.

Finally, the performance of the CaL plant is benchmarked against more mature technologies – the MEA and the CAP chemical scrubbing processes – using the same reference CFPP. The process analysis revealed that compared to the chemical solvent scrubbing technologies, the retrofit of the CaL process is not only less complex (no changes required in the existing CFPP), but would also impose a smaller efficiency penalty. Considering different fuels used in the

calciner, retrofit of this emerging technology was found to reduce the net efficiency of the integrated system by 6.7–7.9% points, which is considerably lower than 9.5% points for MEA and 9.0% points for CAP CO_2 capture plant. Moreover, when biomass is used in the calciner, the plant can potentially operate as a CO_2-negative technology. Finally, if the CaL plant is employed for CO_2 capture and integrated with the secondary steam cycle, the net power output of the retrofitted system can be increased (39.0–53.7% for the scenarios explored in this study), which is an important benefit of CaL taking into account the increasing demand for electricity with reduced CO_2 emissions.

Appendix A. Supplementary data

Supplementary data associated with this article can be found, in the online version, at doi:10.1016/j.ijggc.2015.08.003.

References

Abanades, C.J., Alvarez, D., 2003. Conversion limits in the reaction of CO_2 with lime. Energy Fuels 17, 308–315.

Abanades, J.C., Anthony, E.J., Wang, J., Oakey, J.E., 2005. Fluidized bed combustion systems integrating CO_2 capture with CaO. Environ. Sci. Technol. 39, 2861–2866.

Abanades, J.C., 2002. The maximum capture efficiency of CO_2 using a carbonation/calcination cycle of CaO/$CaCO_3$. Chem. Eng. J. 90, 303–306, http://dx.doi.org/10.1016/S1385-8947(02)00126-2.

AG L, 2013. History and Technological Progress. Cryogenic Air Separation. Linde AG, Engineering Division, Pullach, Germany.

Alonso, M., Diego, M.E., Pérez, C., Chamberlain, J.R., Abanades, J.C., 2014. Biomass combustion with in situ CO_2 capture by CaO in a 300 kWth circulating fluidized bed facility. Int. J. Greenhouse Gas Control 29, 142–152, http://dx.doi.org/10.1016/j.ijggc.2014.08.002.

Anantharaman, R., Bolland, O., Booth, N., van Dorst, E., Ekstrom, C., Sanchez Fernandes, E., et al., 2011. CArbon-free Electricity by SEWGS: Advanced Materials, Reactor-, and Process Design. D 4.9 European Best Practice Guidelines for Assessment of CO_2 Capture Technologies, vol. 213206 FP7. Politecnico di Milano–Alstom, UK.

Arias, B., Diego, M.E., Abanades, J.C., Lorenzo, M., Diaz, L., Martínez, D., et al., 2013. Demonstration of steady state CO_2 capture in a 1.7 MWth calcium looping pilot. Int. J. Greenhouse Gas Control 18, 237–245, http://dx.doi.org/10.1016/j.ijggc.2013.07.014.

AspenTech, 2011. Aspen Plus IGCC Model. Aspen Technology, Inc, Burlington, MA, USA.

Baker, E.H., 1962. The calcium oxide-carbon dioxide system in the pressure range 1–300 atmospheres. J. Chem. Soc., 464–470, http://dx.doi.org/10.1039/JR9620000464.

Berstad, D., Anantharaman, R., Jordal, K., 2012. Post-combustion CO_2 capture from a natural gas combined cycle by CaO/$CaCO_3$ looping. Int. J. Greenhouse Gas Control 11, 25–33, http://dx.doi.org/10.1016/j.ijggc.2012.07.021.

Bhown, A.S., Freeman, B.C., 2011. Analysis and status of post-combustion carbon dioxide capture technologies. Environ. Sci. Technol. 45, 8624–8632.

Black, J., 2013. Cost and Performance Baseline for Fossil Energy Plants Volume 1: Bituminous Coal and Natural Gas to Electricity, vol. DOE/2010/1. National Energy Technology Laboratory, http://www.netl.doe.gov/File%20Library/Research/Energy%20Analysis/OE/BitBase_FinRep_Rev2a-3_20130919_1.pdf.

Boot-Handford, M.E., Abanades, J.C., Anthony, E.J., Blunt, M.J., Brandani, S., Mac Dowell, N., et al., 2014. Carbon capture and storage update. Energy Environ. Sci., 130–189, http://dx.doi.org/10.1039/C3EE42350F.

Charitos, A., Rodrííguez, N., Hawthorne, C., Alonso, M., Zieba, M., Arias, B., et al., 2011. Experimental validation of the calcium looping CO_2 capture process with two circulating fluidized bed carbonator reactors. Ind. Eng. Chem. Res. 50, 9685–9695, http://dx.doi.org/10.1021/ie200579f.

Cormos, C.-C., Cormos, A.-M., 2013. Assessment of calcium-based chemical looping options for gasification power plants. Int. J. Hydrogen Energy 38, 2306–2317, http://dx.doi.org/10.1016/j.ijhydene.2012.11.128.

Dieter, H., Bidwe, A.R., Varela-Duelli, G., Charitos, A., Hawthorne, C., Scheffknecht, G., 2014. Development of the calcium looping CO_2 capture technology from lab to pilot scale at IFK, University of Stuttgart. Fuel 127, 23–37, http://dx.doi.org/10.1016/j.fuel.2014.01.063.

Grasa, G.S., Abanades, J.C., 2006. CO_2 capture capacity of CaO in long series of carbonation/calcination cycles. Ind. Eng. Chem. Res. 45, 8846–8851, http://dx.doi.org/10.1021/ie0606946.

Grasa, G.S., Alonso, M., Abanades, J.C., 2008. Sulfation of CaO particles in a carbonation/calcination loop to capture CO_2. Ind. Eng. Chem. Res. 47, 1630–1635, http://dx.doi.org/10.1021/ie070937+.

Hanak, D.P., Biliyok, C., Yeung, H., Białecki, R., 2014. Heat integration and exergy analysis for a high ash supercritical coal-fired power plant integrated with a post-combustion carbon capture process. Fuel 134, 126–139.

Hanak, D.P., Anthony, E.J., Manovic, V., 2015a. A review of developments in pilot plant testing and modelling of calcium looping process for CO_2 capture from power generation systems. Energy Environ. Sci. 8, 2199–2249, http://dx.doi.org/10.1039/C5EE01228G.

Hanak, D.P., Biliyok, C., Manovic, V., 2015b. Rate-based model development, validation and analysis of chilled ammonia process as an alternative CO_2 capture technology for coal-fired power plants. Int. J. Greenhouse Gas Control 34, 52–62.

Hanak, D.P., Biliyok, C., Manovic, V., 2015c. Efficiency improvements for the coal-fired power plant retrofit with CO_2 capture plant using chilled ammonia process. Appl. Energy 151, 258–272, http://dx.doi.org/10.1016/j.apenergy.2015.04.059.

Hornick, M.J., McDaniel, J.E., 2002. Tampa Electric Polk Power Station Integrated Gasification Combined Cycle Project—Final Technical Report, vol. DE-FC-21-9. The U.S. Department of Energy, Office of Fossil Energy, National Energy Technology Laboratory, Morgantown, West Virginia, USA.

IEA, 2013a. Technology Roadmap: Carbon Capture and Storage. International Energy Agency, Paris, France.

IEA, 2013b. Tracking Clean Energy Progress 2013. IEA Input to the Clean Energy Ministerial. IEA Publications, Paris, France.

Kvamsdal, H.M., Romano, M.C., van der Ham, L., Bonalumi, D., van Os, P., Goetheer, E., 2014. Energetic evaluation of a power plant integrated with apiperazine-based CO2capture process. Int. J. Greenhouse Gas Control 28, 343–355, http://dx.doi.org/10.1016/j.ijggc.2014.07.004.

Lasheras, A., Ströhle, J., Galloy, A., Epple, B., 2011. Carbonate looping process simulation using a 1D fluidized bed model for the carbonator. Int. J. Greenhouse Gas Control 5, 686–693, http://dx.doi.org/10.1016/j.ijggc.2011.01.005.

Li, Z.-S., Cai, N.-S., Croiset, E., 2008. Process analysis of CO_2 capture from flue gas using carbonation/calcination cycles. AIChE J. 54, 1912–1925, http://dx.doi.org/10.1002/aic.11486.

Linnenberg, S., Darde, V., Oexmann, J., Kather, A., van Well, W.J.M., Thomsen, K., 2012. Evaluating the impact of an ammonia-based post-combustion CO_2 capture process on a steam power plant with different cooling water temperatures. Int. J. Greenhouse Gas Control 10, 1–14, http://dx.doi.org/10.1016/j.ijggc.2012.05.003.

Lu, D.Y., Hughes, R.W., Anthony, E.J., 2008. Ca-based sorbent looping combustion for CO_2 capture in pilot-scale dual fluidized beds. Fuel Process. Technol. 89, 1386–1395, http://dx.doi.org/10.1016/j.fuproc.2008.06.011.

Lucquiaud, M., Gibbins, J., 2011. Effective retrofitting of post-combustion CO_2 capture to coal-fired power plants and insensitivity of CO_2 abatement costs to base plant efficiency. Int. J. Greenhouse Gas Control 5, 427–438, http://dx.doi.org/10.1016/j.ijggc.2010.09.003.

Manovic, V., Anthony, E.J., Grasa, G., Abanades, J.C., 2008. CO_2 looping cycle performance of a high-purity limestone after thermal activation/doping. Energy Fuels 22, 3258–3264, http://dx.doi.org/10.1021/ef800316 h.

Mantripragada, H.C., Rubin, E.S., 2013. Calcium looping cycle for CO_2 capture—performance, cost and feasibility analysis. Energy Procedia 63, 2199–2206.

Martínez, I., Murillo, R., Grasa, G., Carlos Abanades, J., 2011. Integration of a Ca looping system for CO2 capture in existing power plants. AIChE J. 57, 2599–2607, http://dx.doi.org/10.1002/aic.12461.

Metz, B., Davidson, O., de Coninck, H., Loos, M., Meyer, L., 2005. IPCC Special Report on Carbon Dioxide Capture and Storage. Cambridge University Press, Cambridge, United Kingdom and New York, NY, USA.

Natunen, M., Jäntti, T., Goral, D., Nuortimo, K., 2013. First Operating Experiences of 55 MWe Konin and 205 MWe Polaniec CFB Boilers Firing 100% Biomass (Foster Wheeler Energia Oy). PowerGen Eur, Vienna, Austria.

Ozcan, D.C., Alonso, M., Ahn, H., Abanades, J.C., Brandani, S., 2014. Process and cost analysis of a biomass power plant with in situ calcium loopingCO_2 capture process. Ind. Eng. Chem. Res. 53, 10721–10733, http://dx.doi.org/10.1021/ie500606 v.

Pace, D.K., 2004. Modeling and simulation verification and validation challenges. Johns Hopkins APL Tech. Dig. 25, 163–172.

Perrin, N., Dubettier, R., Lockwood, F., Tranier, J.-P., Bourhy-Weber, C., Terrien, P., 2014. Oxycombustion for coal power plants: advantages, solutions and projects. Appl. Therm. Eng. 74, 75–82, http://dx.doi.org/10.1016/j.applthermaleng.2014.03.074.

Pfaff, I., Oexmann, J., Kather, A., 2010. Optimised integration of post-combustion CO_2 capture process in greenfield power plants. Energy 35, 4030–4041.

Posch, S., Haider, M., 2012. Optimization of CO_2 compression and purification units (CO_2CPU) for CCS power plants. Fuel 101, 254–263, http://dx.doi.org/10.1016/j.fuel.2011.07.039.

Ramezani, M., Shah, K., Doroodchi, E., Moghtaderi, B., 2015. Application of a novel calcium looping process for production of heat and carbon dioxide enrichment of greenhouses. Energy Convers. Manage. 103, 129–138, http://dx.doi.org/10.1016/j.enconman.2015.06.044.

Rodriguez, N., Alonso, M., Grasa, G., Abanades, J.C., 2008. Heat requirements in a calciner of $CaCO_3$ integrated in a CO_2 capture system using CaO. Chem. Eng. J. 138, 148–154, http://dx.doi.org/10.1016/j.cej.2007.06.005.

Rodríguez, N., Alonso, M., Abanades, J.C., 2010. Average activity of CaO particles in a calcium looping system. Chem. Eng. J. 156, 388–394, http://dx.doi.org/10.1016/j.cej.2009.10.055.

Romano, M.C., Martínez, I., Murillo, R., Arstad, B., Blom, R., Ozcan, D.C., Ahn, H., Brandani, S., 2013. Process simulation of Ca-looping processes: review and guidelines. Energy Procedia 37, 142–150, http://dx.doi.org/10.1016/j.egypro.2013.05.095.

Romano, M.C., 2012. Modeling the carbonator of a Ca-looping process for CO_2 capture from power plant flue gas. Chem. Eng. Sci. 69, 257–269, http://dx.doi.org/10.1016/j.ces.2011.10.041.

Romeo, L.M., Abanades, J.C., Escosa, J.M., Paño, J., Giménez, A., Sánchez-Biezma, A., et al., 2008. Oxyfuel carbonation/calcination cycle for low cost CO_2 capture in existing power plants. Energy Convers. Manage. 49, 2809–2814, http://dx.doi.org/10.1016/j.enconman.2008.03.022.

Romeo, L.M., Lara, Y., Lisbona, P., Escosa, J.M., 2009. Optimizing make-up flow in a CO_2 capture system using CaO. Chem. Eng. J. 147, 252–258, http://dx.doi.org/10.1016/j.cej.2008.07.010.

Roy, C.J., 2005. Review of code and solution verification procedures for computational simulation. J. Comput. Phys. 205, 131–156, http://dx.doi.org/10.1016/j.jcp.2004.10.036.

Sánchez-Biezma, A., Ballesteros, J.C., Diaz, L., de Zárraga, E., Álvarez, F.J., López, J., Arias, B., Grasa, G., Abanades, J.C., 2011. Postcombustion CO_2 capture with CaO, Status of the technology and next steps towards large scale demonstration. Energy Procedia 4, 852–859, http://dx.doi.org/10.1016/j.egypro.2011.01.129.

Sánchez-Biezma, A., Paniagua, J., Diaz, L., Lorenzo, M., Alvarez, J., Martínez, D., Arias, B., Diego, M.E., Abanades, J.C., 2013. Testing postcombustion CO_2 capture with CaO in a 1.7 MWt pilot facility. Energy Procedia 37, 1–8, http://dx.doi.org/10.1016/j.egypro.2013.05.078.

Sanpasertparnich, T., Idem, R., Bolea, I., de Montigny, D., Tontiwachwuthikul, P., 2010. Integration of post-combustion capture and storage into a pulverized coal-fired power plant. Int. J. Greenhouse Gas Control 4, 499–510.

Shimizu, T., Hirama, T., Hosoda, H., Kitano, K., Inagaki, M., Tejima, K., 1999. A Twin Fluid-Bed Reactor for Removal of CO_2 from Combustion Processes. Chem. Eng. Res. Des. 77, 62–68, http://dx.doi.org/10.1205/026387699525882.

Stéphenne, K., 2014. In: T. D, S. T, H. H. (Ed.), Start-up of World's First Commercial Post-Combustion Coal Fired CCS Project: Contribution of Shell Cansolv to Saskpower Boundary Dam ICCS Project. 12th Int. Conf. Greenh. Gas Control Technol., vol. 63, pp. 6106–6110, http://dx.doi.org/10.1016/j.egypro.2014.11.642.

Ströhle, J., Lasheras, A., Galloy, A., Epple, B., 2009. Simulation of the carbonate looping process for post-combustion CO_2 capture from a coal-fired power plant. Chem. Eng. Technol. 32, 435–442, http://dx.doi.org/10.1002/ceat.200800569.

Ströhle, J., Junk, M., Kremer, J., Galloy, A., Epple, B., 2014. Carbonate looping experiments in a 1 MWth pilot plant and model validation. Fuel 127, 13–22, http://dx.doi.org/10.1016/j.fuel.2013.12.043.

Symonds, R.T., Lu, D.Y., Manovic, V., Anthony, E.J., 2012. Pilot-scale study of CO_2 capture by CaO-based sorbents in the presence of steam and SO_2. Ind. Eng. Chem. Res. 51, 7177–7184, http://dx.doi.org/10.1021/ie2030129.

Valverde, J.M., 2013. A model on the CaO multicyclic conversion in the Ca-looping process. Chem. Eng. J. 228, 1195–1206.

Vorrias, I., Atsonios, K., Nikolopoulos, A., Nikolopoulos, N., Grammelis, P., Kakaras, E., 2013. Calcium looping for CO_2 capture from a lignite fired power plant. Fuel 113, 826–836, http://dx.doi.org/10.1016/j.fuel.2012.12.087.

Wang, J., Anthony, E.J., 2007. A common decay behavior in cyclic processes. Chem. Eng. Commun. 194, 1409–1420, http://dx.doi.org/10.1080/00986440701401594.

Xu, G., Jin, H.G., Yang, Y.P., Xu, Y.J., Lin, H., Duan, L., 2010. A comprehensive techno-economic analysis method for power generation systems with CO_2 capture. Int. J. Energy Res. 34, 321–332, http://dx.doi.org/10.1002/er.1559.

Yan, K., Wu, X., Hoadley, A., Xu, X., Zhang, J., Zhang, L., 2015. Sensitivity analysis of oxy-fuel power plant system. Energy Convers. Manage. 98, 138–150, http://dx.doi.org/10.1016/j.enconman.2015.03.088.

Yang, Y., Zhai, R., Duan, L., Kavosh, M., Patchigolla, K., Oakey, J., 2010. Integration and evaluation of a power plant with a CaO-based CO_2 capture system. Int. J. Greenhouse Gas Control 4, 603–612, http://dx.doi.org/10.1016/j.ijggc.2010.01.004.

Zhao, M., Minett, A.I., Harris, A.T., 2013. A review of techno-economic models for the retrofitting of conventional pulverised-coal power plants for post-combustion capture (PCC) of CO_2. Energy Environ. Sci. 6, 25–40, http://dx.doi.org/10.1039/c2ee22890.

7 CALCIUM LOOPING WITH SUPERCRITICAL CO_2 CYCLE FOR DECARBONISATION OF COAL-FIRED POWER PLANT

Dawid P. Hanak and Vasilije Manovic

Published: Energy, 2016, 102, 343–353[h]

Statement of contributions of joint authorship

Dawid P. Hanak conducted the literature review, performed process analysis via process modelling and simulation, drafted and critically revised the manuscript, as well as prepared tables and figures. Vasilije Manovic proof-read and critically commented on the manuscript prior to its submission to Energy (Journal Impact Factor 2016: 4.844).

Dawid P. Hanak, PhD Candidate

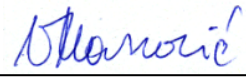

Vasilije Manovic, Principal supervisor

[h] Reprinted with permission from Hanak, D.P. and Manovic, V. (2016), "Calcium looping with supercritical CO_2 cycle for decarbonisation of coal-fired power plant", *Energy*, 102, 343–353, doi: 10.1016/j.energy.2016.02.079, Elsevier 2016.

Energy 102 (2016) 343–353

Contents lists available at ScienceDirect

Energy

journal homepage: www.elsevier.com/locate/energy

Calcium looping with supercritical CO_2 cycle for decarbonisation of coal-fired power plant

Dawid P. Hanak*, Vasilije Manovic

Combustion and CCS Centre, Cranfield University, Bedford, Bedfordshire, MK43 0AL, UK

ARTICLE INFO

Article history:
Received 16 October 2015
Received in revised form
28 January 2016
Accepted 14 February 2016
Available online xxx

Keywords:
Calcium looping
Carbon capture
Coal-fired power plant
Supercritical CO_2 cycle
Recompression Brayton cycle
Efficiency penalty reduction

ABSTRACT

State-of-the-art integration scenarios of calcium looping (CaL), which is an emerging CO_2 capture technology, assume that excess heat is used to raise steam for the steam cycle and result in a net efficiency penalty of 6.0–8.0% points. In this study, a concept using the supercritical CO_2 cycle (s-CO_2) instead of the conventional steam cycle is proposed. Retrofit of CaL with recompression s-CO_2 cycle to the 580 MW_{el} coal-fired power plant was found to result in a net efficiency penalty of 6.9%$_{HHV}$ points. This is 1%$_{HHV}$ point lower than that for the same system linked with the steam cycle having the same turbine inlet conditions (593.3 °C/242.3 bar). A further reduction of the net efficiency penalty to 5.8%$_{HHV}$ points was achieved through considering a pump instead of a first CO_2 compression stage and increasing the turbine inlet temperature to 620 °C and pressure to 300 bar. As the s-CO_2 cycle's specific capital cost is up to 27% lower than that of the equivalent steam cycle, CaL with s-CO_2 cycle is a viable option for the coal-fired power plant decarbonisation. Moreover, it can be expected that this cycle can be successfully implemented in other high-temperature looping cycles, such as chemical looping combustion.

1. Introduction

The power generation sector is one of the key sectors that need to be decarbonised by 2050 to meet the greenhouse gas emission reduction target and to mitigate drastic climate change [1–4]. It has been predicted that its near-complete decarbonisation would account for approximately 28% of the total CO_2 emission reduction in 2025 [5]. Regardless of that, coal-fired power plants are currently responsible for more than 70% of the total CO_2 emissions from the power sector and their share in the energy portfolio is predicted to decrease only by around 6%, for example, from around 40% [5,6] in 2013 to 34% in 2040 [6]. On the other hand, a 5% increase in the renewable energy sources share is predicted within this time frame [6]. Yet, large-scale deployment of renewables requires more backup capacity to make up for their intermittency, introducing additional costs. As a result, coal-based power generation remains more attractive for investors and is expected to remain the key power source in the future energy portfolio [7]. Therefore, carbon capture and storage (CCS) is expected to act, at least, as a bridge to the clean power generation future [8].

Regardless of the recent progress in oxy-combustion and chemical solvent scrubbing post-combustion CO_2 capture technologies [9,10], the efficiency penalty associated with integration of these systems to coal-fired power plants is predicted to be 7.0–12.5% points [11–16], which would increase the cost of electricity by at least 60% [17–20]. Therefore, emerging technologies, which offer more competitive performance of the retrofitted system, are being developed [21]. Calcium looping (CaL), which is based on the reversible carbonation reaction of lime, has been proposed as a viable and efficient process for decarbonisation of coal-fired power plants [22]. A recent review [23] revealed that the efficiency penalty associated with CaL is projected to be within 6.0–8.0% points, depending on the level of heat integration. The main reason behind the superior performance of CaL compared to the more mature CO_2 capture technologies, is its high-temperature operation and high-grade heat availability [22,24,25].

The state-of-the-art CaL integration scenarios assume that high-grade heat is recovered to generate steam at a high pressure, which is then used to generate power in the conventional steam cycle based on the Rankine cycle. Yet, it is worth highlighting that CaL operates within the temperature range of 600–950 °C [23], which is similar to the operating temperatures of the natural gas turbine bottoming cycle (600 °C) [26], high-temperature gas-cooled nuclear reactors (850–1000 °C) [27], sodium-cooled fast nuclear

* Corresponding author.
E-mail address: d.p.hanak@cranfield.ac.uk (D.P. Hanak).

http://dx.doi.org/10.1016/j.energy.2016.02.079
0360-5442/

reactors (500–550 °C) [28,29], helium-cooled fusion nuclear reactors (500 °C) [30] and concentrating solar power plants (800–900 °C) [31,32] – technologies for which alternative thermodynamic cycles, such as the Brayton cycle using He or supercritical CO_2 (s-CO_2), have been investigated.

Compared to the conventional supercritical steam cycle based on the Rankine cycle, the He and s-CO_2 cycles can achieve higher cycle efficiencies that can be as high as 50–60%, depending on the turbine inlet conditions and the cycle architecture [31–34]. Dostal et al. [34] have shown that the s-CO_2 cycle outperforms the equivalent He cycle at the same turbine inlet temperature. This is mostly because of near-critical-point operation of the CO_2 compressors resulting in the compression power requirement being only around 30% of the turbine power output. Also, due to the high density and low heat capacity of supercritical CO_2, the size of the turbomachinery is considerably smaller than that for the steam cycle and the He cycle. In addition, the layout of the system based on the Brayton cycle is simpler than that for the steam cycle [34–37]. All of these features of the s-CO_2 cycle are reflected in the specific capital cost ($/$MW_{el}$), which for this cycle has been estimated to be up to 27% lower than for the superheated steam cycle and 11% lower than the equivalent He cycle [34], making the s-CO_2 cycle a technically and economically viable option for future power generation systems. This is also reflected in a wide spectrum of investigated applications of the s-CO_2 cycle that vary from low-grade waste heat recovery systems [38], fuel cell hybrid systems [39] and liquefied natural gas power and refrigeration systems [40,41], through to solar [31,32,42], nuclear [27–30,34,38,43] and even coal-fired power plants [44]. The aforementioned qualities make the s-CO_2 cycle worth considering as an alternative to the conventional Rankine steam cycle [35].

Reduction of the efficiency and economic penalties associated with CO_2 capture is required for the industrial deployment of these technologies. CaL, as an emerging CO_2 capture technology, has already been proven as a viable alternative to mature technologies for decarbonisation of coal-fired power plants. Yet, the state-of-the-art integration scenarios suggest that the excess high-grade heat from the CaL plant can be utilised in the primary or the secondary steam cycle for power generation [23]. Due to higher cycle efficiency and lower specific capital cost associated with the s-CO_2 cycle compared to the steam cycle, the concept of the CaL plant with s-CO_2 cycle for decarbonisation of a coal-fired power plant is proposed in this study. For the purpose of this study, the s-CO_2 process model was developed and then adapted to the existing CaL process model [45]. The performance of the proposed retrofit scenario is first compared with the CaL plant with the supercritical reheated steam cycle reported by Hanak et al. [45]. Then, the impact of variations of the s-CO_2 hardware and the turbine inlet conditions on the net thermal efficiency of the retrofitted system are investigated. Finally, the optimum design is proposed based on sensitivity studies and further improvements in the retrofitted system performance are identified.

2. Process model development

2.1. Process description

This study analyses a scenario in which the CaL plant, which comprises two interconnected fluidised bed reactors operating at atmospheric pressure, is retrofitted to a 580 MW_{el} coal-fired power plant to achieve a total CO_2 capture level of 90%. In this system, CO_2 from the flue gas is removed in the carbonator, which operates at 650 °C, through the exothermic reaction with CaO. The saturated sorbent ($CaCO_3$) is then regenerated at a high temperature (900 °C) in the calciner, which is ensured through oxy-combustion of coal. The high-temperature operation of the CaL plant allows for high-grade heat recovery from the carbonator and the process streams. The high-grade heat is utilised to generate an additional amount of power in the s-CO_2 cycle, which is evaluated in this study as an alternative to the supercritical steam cycle considered thus far in the literature [22–24,46–53].

The s-CO_2 cycle, which was introduced by Feher [36], is a closed-loop Brayton cycle that is highly recuperative and operates entirely above CO_2 critical pressure [28,36,38]. The heat capacity of supercritical CO_2 varies substantially with pressure [29], and thus the simple s-CO_2 cycle suffers from large irreversibility in the recuperator caused by the heat capacity imbalance between its hot and cold sides [35]. This causes a pinch point problem in the recuperator [31,35] that is reflected in the minimum temperature approach occurring inside the heat exchanger [34]. In the recompression s-CO_2 cycle (Fig. 1), which is considered in this study, this issue is resolved through recompressing part of the CO_2 stream without heat rejection to compensate the heat capacity difference in a low-temperature recuperator (LTR) [29]. As a result of increased LTR effectiveness, the hot stream enters a high-temperature recuperator (HTR) at a higher temperature. This, in turn, increases the temperature of the hot stream leaving the HTR and thus the average temperature of heat addition, leading to higher cycle efficiency [28].

2.2. Supercritical coal-fired power plant

A process model of a 580 MW_{el} supercritical coal-fired power plant, which is considered as a benchmark in this study, was developed in Aspen Plus and described in detail by Hanak et al. [25,54]. The prediction of this model was found to be in close agreement with data provided in the revised NETL report [55], confirming the efficacy of the modelling approach and high fidelity of the model.

The coal-fired power plant model comprises three sub-models: supercritical boiler and flue gas treatment train (NO_x, SO_x and fly ash) models, both modelled using Peng–Robinson–Boston–Mathias (PR–BM) equation of state, as well as a steam cycle model that has been thermodynamically described with steam tables (STEAMNBS). Coal combustion is modelled using solid modelling features recommended by AspenTech [56]. The boiler heat exchange sections, which include the primary, secondary, and reheat superheaters, as well as the economiser, are modelled using *HEATX* block with pressure drops and temperature levels set based on the revised NETL report [55]. Steam turbines are modelled as individual turbine sections using *COMPR* block, hence the high-, intermediate- and low-pressure cylinders are further divided into the required steam turbine sections. The isentropic efficiency was estimated to match the desired discharge temperature of each section, which was provided in the revised NETL report [55]. The condenser is modelled as *HEATX* block and is assumed to operate at a fixed pressure of 0.069 bar, which corresponds to a condensation temperature of 38.7 °C. The performance of the modelled coal-fired power plant is characterised by gross power output of 580.4 MW_{el}, net thermal efficiency of 38.5%$_{HHV}$ and other key performance parameters estimated by Hanak et al. [25] and presented in Table 1.

2.3. Calcium looping plant with supercritical steam cycle

The process model of the CaL plant, which is modelled using SOLIDS property method, with a supercritical steam cycle was developed in Aspen Plus and described in detail in Hanak et al. [45]. The prediction of the CaL model showed good agreement with data available in the literature [57–60].

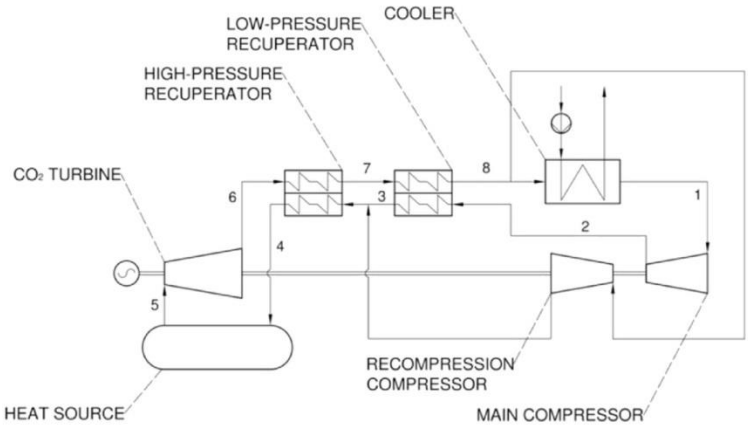

Fig. 1. Scheme of the recompression supercritical CO_2 (s-CO_2) cycle.

Table 1
Reference coal-fired power plant and CaL retrofit (supercritical steam cycle) operating specification.

Parameter	Reference coal-fired power plant [25]	CaL retrofit (supercritical steam cycle) [45]
System performance indicators		
Gross power output (MW_{el})	580.4	1023.3
Net power output (MW_{el})	552.7	799.9
Net thermal efficiency($\%_{HHV}$)	38.5	30.6
Specific coal consumption ($g/kW_{el}h$)	350.3	438.2
Calcium looping specification		
Limestone make-up rate (F_0/F_R) (−)	–	0.04
Carbonator temperature (°C)	–	650
Calciner temperature (°C)	–	900
Oxygen content in calciner fluidising gas ($\%_{vol,wet}$)	–	40
Excess oxygen ($\%_{vol,dry}$)	–	2.5
Primary and secondary steam cycle specification		
Live steam pressure (bar)	242.3	
Reheated steam pressure (bar)	45.2	
Intermediate-/low-pressure crossover pressure (bar)	9.3	
Condenser pressure (bar)	0.069	
Live and reheated steam temperature (°C)	593.3	

In the CaL model, the carbonation process is modelled using the *RSTOIC* block in conjunction with the maximum average sorbent conversion model derived by Rodríguez et al. [61] and presented in Eq. (1). The maximum average conversion in this model is a function of the carbonation (f_{carb}) and calcination extent (f_{calc}), sorbent characteristics (a_1, a_2, f_1, f_2, b), which were estimated based on experimental data from the 1.7 MW_{th} INCAR-CSIC pilot plant [57], fresh limestone make-up (F_0) and solids looping rate (F_R). The carbonation conversion and the CO_2 capture level, which are used to determine the solids looping rate, are estimated using Eq. (2) and Eq. (3), respectively.

$$X_{ave} = \left(F_0 + F_R\frac{F_0(1-f_{calc})}{F_0 + F_R f_{calc}}\right) f_{calc}\left[\frac{a_1 f_1^2}{F_0 + F_R f_{carb} f_{calc}(1-f_1)} + \frac{a_2 f_2^2}{F_0 + F_R f_{carb} f_{calc}(1-f_2)} + \frac{b}{F}\right] \quad (1)$$

$$\Delta X_{carb} = f_{calc} f_{carb} X_{ave} \quad (2)$$

$$E_{CO_2} = \frac{F_R}{F_{CO_2}} \Delta X_{carb} \quad (3)$$

The calcination process, which aims at regeneration of the saturated sorbent, is modelled using *RGibbs* block that determines the chemical and phase equilibrium through the Gibbs' free energy minimisation at a given temperature. The equilibrium limits of the carbonation and calcination processes are accounted for using the correlation derived by Baker [62] to estimate the equilibrium partial pressure of CO_2 in the gas streams leaving the reactors. Finally, the CaL plant model comprises the auxiliary units, such as conventional air separation unit (ASU) and CO2 compression unit (CCU), for which a detailed modelling approach is widely described in the literature [45,54,63–66].

In the retrofitted system operating with the characteristics presented in Table 1, which were identified in Hanak et al. [45], the high-grade heat from the CaL plant was utilised to generate high-pressure steam, which has the same parameters as the supercritical boiler (593.3 °C/593.3 °C/242.3 bar), for the secondary steam cycle of similar operating conditions to the primary steam cycle. Both the HRSG (heat recovery steam generator) and the secondary steam cycle were modelled using the same approach as adapted for the coal-fired power plant model. The analysis performed by Hanak et al. [45] revealed that retrofit of the CaL plant with supercritical steam cycle to the reference coal-fired power plant increased the net power output of the retrofitted system by 44.7% and resulted in 7.9%$_{HHV}$ points drop in its net efficiency (Table 1). The performance

of the CaL plant with the supercritical steam cycle will be used to assess if application of the s-CO_2 cycle to recover the high-grade heat from the CaL plant will bring performance benefits.

2.4. Supercritical CO_2 cycle

2.4.1. Model description and verification

A process model of the recompression s-CO_2 cycle has been developed in Aspen Plus based on data from Moisseytsev and Sienicki [29], who analysed the integration of the s-CO_2 cycle with the reference 96 MW_{el} sodium-cooled fast reactor. One of the main technical challenges of the s-CO_2 cycle is estimation accuracy of the turbomachinery efficiencies [44], as these units are still under development and only a few have been tested at bench- and pilot-scale [42,67]. In the open literature, the performance of the CO_2 turbine is usually represented using its isentropic efficiency, the typical value of which is between 87.0% and 93.4% [28,31,34,43,68,69]. Similarly, the performance of the main and the recompression compressors is represented by isentropic efficiency of 85.0–95.5% [28,31,34,43,44].

Using the parameters presented in Table 2, which were taken from Moisseytsev and Sienicki [29] and Le Moullec [44], the Lee-Kesler-Plocker equation of state [44], the *HEATX* blocks to represent performance of the LTR, HTR and cooler, and the *COMPR* blocks to represent performance of the CO_2 turbines and compressors, the net efficiency of the cycle presented in Fig. 1 is estimated to be 39.6%, which is 0.8% points lower than that of the reference study [29]. The main reason for such deviation is the fact that the isentropic efficiencies for the CO_2 turbine and compressors were not provided in the reference study [29] and thus were taken from Le Moullec [44], who used the same reference system in his study. This is reflected in small deviations in prediction of the temperatures for the steams leaving the main compressor and the CO_2 turbine (Table 3). Nevertheless, the model prediction was found to be in good agreement with the literature data as the highest relative error was 2.8%.

2.4.2. Adaptation of supercritical CO_2 cycle to calcium looping

A large fraction of the high-grade heat needs to be recovered from the flue gas and pure CO_2 streams leaving the CaL plant. The recompression s-CO_2 cycle shown in Fig. 1 cannot, therefore, be directly integrated with CaL because the sensible heat of the process streams below 500 °C would not be utilised in the system, leading to high energy losses. The same issue was encountered by Le Moullec [44], who analysed the implementation of the recompression s-CO_2 cycle in place of the steam cycle in the coal-fired power plant with an amine scrubbing CO_2 capture plant. This study showed that the low-grade heat can be recovered from the process streams by extracting part of the CO_2 stream leaving the main CO_2 compressor at low temperature and returning it after the HTR. The same approach is applied in this study (Fig. 2) and the low-grade heat from the clean flue gas stream is recovered by cooling it to 60.0 °C using around 15–17% of the CO_2 flow leaving the main compressor at 44.4 °C. Moreover, heat carried with the CO_2 stream at 900 °C is first used to superheat the CO_2 stream to the desired high-pressure turbine inlet temperature, and then to preheat the flue gas and the O_2 streams entering the CaL plant.

To maximise the CaL excess heat utilisation and the efficiency of the recompression s-CO_2 cycle, a single reheat and a single intercooling stage are considered in the base configuration. In this configuration, the high-pressure and the intermediate-pressure turbine inlet temperature is 593.3 °C. In addition, the high-pressure turbine inlet pressure is set as 242.3 bar and both turbine stages operate with constant pressure ratio. Such assumptions for the base configuration allow its direct comparison with the reference configuration, in which the excess heat from CaL is utilised in the supercritical reheated steam cycle. Design of the heat exchanger network is based on the assumption that the minimum temperature approach of the heat exchangers is 10 °C [70], with exception of recuperators and superheaters/reheaters for which the minimum temperature approach of 5 °C [31,32], and 25 °C [70], respectively, is used. Finally, the reported values for the mechanical efficiency of the turbomachinery and the electric efficiency of the generator vary between 99.6–100.0% [28,70] and 97.5%–98.5% [29,55,70], respectively. In this study the mechanical efficiencies of 99.8% and 99.6% are selected for CO_2 turbines and compressors, respectively, while the electric efficiency of 98.0% is chosen for the generator. The key design parameters for the recompression s-CO_2 cycle adapted to the CaL plant are summarised in Table 4.

Table 2
Reference recompression supercritical CO_2 cycle operating parameters.

Parameter	Value
Main compressor discharge pressure (bar)	200.0
Recompression compressor discharge pressure (bar)	199.6
Turbine discharge pressure (bar)	77.3
Cycle lowest pressure (bar)	74.0
Cooler outlet temperature (°C)	31.3
Fraction of CO_2 to recompression (%)	29.0
Turbine isentropic efficiency (%)	93.0
Compressor isentropic efficiency (%)	90.0
Mechanical efficiency of the rotational machinery (%)	99.0
Generator efficiency (%)	98.5

3. Process analysis

3.1. Considerations

Having adapted the recompression s-CO_2 cycle to recover the excess heat from the CaL plant, the retrofitted system needs to be benchmarked with the systems currently considered as state of the art. Therefore, the performance of the base configuration is compared with the CaL plant integrated with the supercritical reheated steam cycle. The comparison is made to the best configuration from Hanak et al. [45] in which oxy-combustion of coal is used to provide heat for sorbent regeneration in the calciner. Moreover, in both configurations, the CaL plant is retrofitted to the 580 MW_{el} supercritical coal-fired power plant to achieve the total CO_2 capture level of 90%.

A common feature of each Brayton cycle is the fact that the cycle efficiency can be further improved by introducing more reheat and intercooling stages, which would increase the average temperature of heat addition and decrease the average temperature of heat rejection, respectively. Despite additional cost associated with the additional equipment, such designs would allow

Table 3
Benchmark of the supercritical recompression CO_2 cycle stream data with Moisseytsev and Sienicki [29].

Stream	Temperature (°C)		Pressure (bar)	
	Literature	Model	Literature	Model
1	31.3	31.3	74.0	74.0
2	84.4	82.8	200.0	200.0
3	171.8	171.8	199.6	199.6
4	323.3	323.3	199.1	199.1
5	471.8	471.5	198.4	198.4
6	362.3	361.8	77.3	77.3
7	190.7	189.0	76.9	76.9
8	90.2	87.7	76.3	76.3

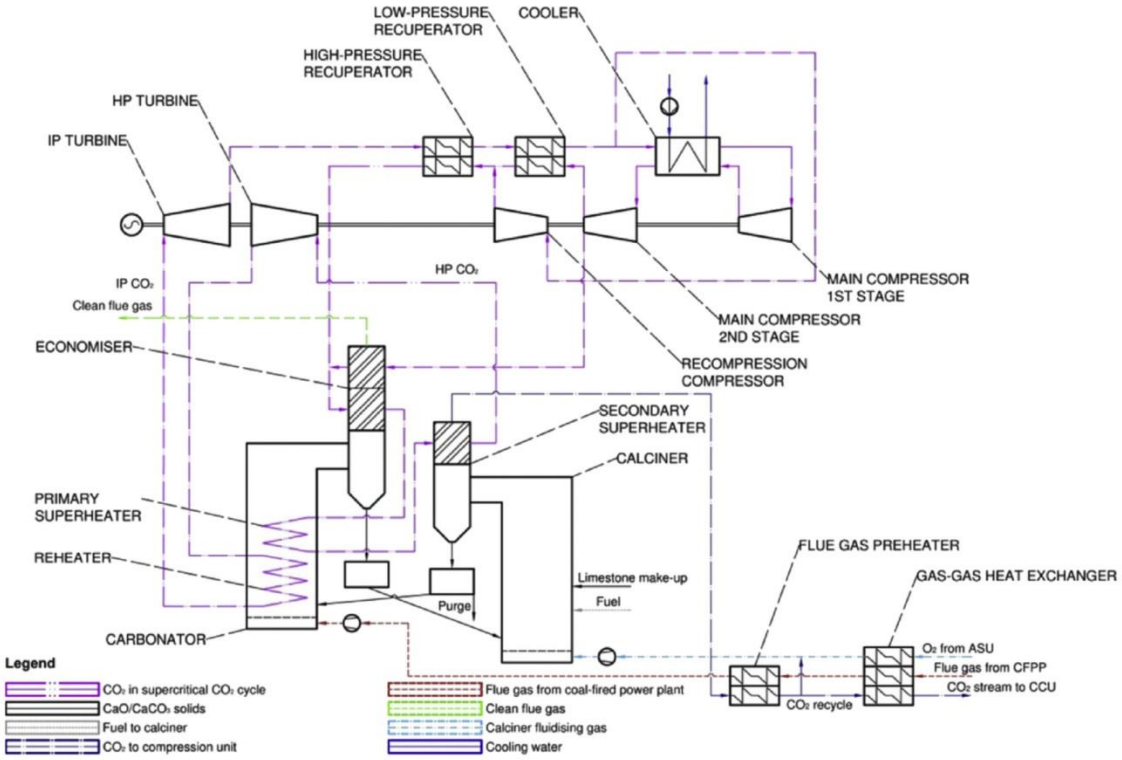

Fig. 2. Scheme of the calcium looping process integrated with the recompression supercritical CO_2 cycle.

Table 4
Design basis for the recompression supercritical CO_2 cycle.

Parameter	Value
Isentropic efficiency of CO_2 turbines (%)	93.0
Isentropic efficiency of main compressors (%)	90.0
Isentropic efficiency of recompression compressor (%)	90.0
Mechanical efficiency of CO_2 turbines (%)	99.8
Mechanical efficiency of compressors (%)	99.6
Electric generator efficiency (%)	98.0
Reheater and superheater minimum temperature approach (°C)	25.0
Heat exchangers minimum temperature approach (°C)	10.0
Recuperators minimum temperature approach (°C)	5.0
Heat exchanger pressure drop (%)	2.0

for more compact design of reheaters and intercoolers [44]. Dostal et al. [34] have estimated that the first reheat stage results in about 1.2% points improvement in the s-CO_2 cycle efficiency, while the second reheat stage adds only about 0.5% points to the efficiency. Their study also revealed that intercooling can increase the s-CO_2 cycle efficiency by up to 0.8% points. Although introducing more than one reheat and intercooling stage may not be an economically attractive option [34], it is worth exploring their effect on the net efficiency of the retrofitted system. Moreover, the fact that CO_2 is above its supercritical pressure (74 bar) throughout the cycle allows turning it to the dense phase by cooling it below the critical temperature (31.3 °C). As a result, a pump can be used in place of the main compressor to increase the CO_2 pressure. Therefore, the following cases are considered in the configuration sensitivity study:

- Effect of reheat considering up to three expansion stages.
- Effect of intercooling by considering up to three compression stages.
- Effect of using a pump instead of the main compressor.

The performance of each thermodynamic cycle can be improved by increasing the operating temperature and pressure at the turbine inlet. Therefore, another sensitivity analysis is conducted to assess the effect of the high-pressure turbine inlet pressure and temperature on the net efficiency of the retrofitted system by varying the pressure between 200 and 300 bar and the temperature between 540 and 640 °C. Finally, by combining both sensitivity studies the performance of the optimum design is estimated.

3.2. Performance evaluation

Analysis of the retrofit of the 580 MW_{el} coal-fired power plant with CaL plant using either the recompression s-CO_2 cycle or the supercritical steam cycle for excess heat recovery (Table 5) revealed that the gross and the net power output in both configurations were comparable and only slightly higher for the former cycle. Nevertheless, the net efficiency of the CaL integrated with the recompression s-CO_2 cycle was found to be 1%$_{HHV}$ point higher for the same high-pressure turbine inlet conditions. This is not only the result of a higher degree of high-grade heat utilisation in the recompression s-CO_2 cycle, but also due to more heat recovered to preheat the flue gas and the O_2 streams entering the CaL plant, which resulted in 2.9% reduction in the specific coal consumption of the retrofitted system

(4.7% reduction of the coal consumption in the calciner). As the specific capital cost ($/MW$_{el}$) of the s-$CO_2$ cycle has been estimated to be up to 27% lower than that of the supercritical steam cycle operating in the same envelope [34], the recompression s-CO_2 cycle can be considered as a technically and economically viable option for decarbonisation of coal-fired power plants using CaL.

Analysing the distribution of the parasitic load (Fig. 3), which again was estimated to be only slightly lower for the recompression s-CO_2 cycle, it is worth pointing out that the power requirement to run the ASU and the CCU compressors accounted for around 72.5% of the total system power requirement for both investigated configurations. As the remaining part of the parasitic load can be considered as unavoidable, further improvement of the retrofitted system's performance can be achieved through a more efficient secondary cycle, higher level of heat integration in the CaL plant, alternative O_2 sources, such as chemical looping combustion [71] or membranes [72,73] for oxy-combustion of fuel or heat sources to sustain sorbent regeneration and alternative CO_2 compression options.

3.3. Recompression supercritical CO_2 cycle sensitivity study

3.3.1. Hardware analysis

The impact of the number of reheating and intercooling stages, as well as the kind of pressure-change equipment (compressors or pumps) is presented in Fig. 4. It can be clearly seen that change in the hardware has a small effect on the parasitic load distribution, as the reduction in the gross efficiency associated with the power requirements of the particular components of the retrofitted system varies by up to 0.1%$_{HHV}$ points. Hence, improvement of the retrofitted system's performance is mostly associated with a higher cycle efficiency of the recompression s-CO_2 cycle.

The analysis revealed also that the net efficiency of the retrofitted system is more sensitive to the number of intercooling stages rather than to the number of reheating stages. Implementation of the first (T2C2) and the second (T3C2) reheat stage results in the net efficiency of the retrofitted system higher by 0.3%$_{HHV}$ points and 0.4%$_{HHV}$ points, respectively, with respect to the configuration without reheat (T1C2). Conversely, the net efficiency increase over the configuration without intercooling (T2C1) of 0.5%$_{HHV}$ points and 0.7%$_{HHV}$ points is reached on implementation of one (T2C2) and two (T2C3) intercooling stages, respectively. Hence, the base configuration with the single reheat and one intercooling stage appears to be an optimum one, as the addition of the second reheat and second intercooling stage results in net efficiency improvement of only 0.1%$_{HHV}$ points and 0.2%$_{HHV}$ points, respectively, and may not be economically viable. Importantly, the addition of intercooling allows reducing the clean flue gas temperature to 60 °C, which is only slightly above the flue gas discharge temperature in the reference coal-fired power plant (57.2 °C), from 108.9 °C. As a result, more low-grade heat is recovered from the CaL plant and used for power generation.

Additionally, implementation of one pump in place of the first compression stage in the base configuration (T2C1P1) resulted in a 0.4%$_{HHV}$ point increase, while substitution of both compression stages with pumps (T2P2) resulted in only 0.1%$_{HHV}$ point increase in the net thermal efficiency. This is because CO_2 is in the dense phase at the pump discharge, and thus enters the LTR at a lower temperature. The former configuration results in the highest net thermal efficiency of the retrofitted system, which is 32.0%$_{HHV}$ corresponding to an efficiency penalty of 6.4%$_{HHV}$ points.

3.3.2. Turbine inlet conditions analysis

As shown in Fig. 5, increase in the net thermal efficiency of the retrofitted system is directly proportional to the increases in both the turbine inlet temperature and pressure. Yet, the maximum turbine inlet temperature (640 °C) was limited by the assumption that the reheater outlet temperature is equal to the high-pressure turbine inlet temperature and the minimum temperature approach in the reheater of 10 °C. Nevertheless, Dostal et al. [34] claimed that the recompression s-CO_2 cycle operating at the maximum temperature of 650 °C and pressure higher than 200 bar is the most promising layout for the s-CO_2 cycle. Although increasing the turbine inlet temperature to 640 °C was found to increase the net thermal efficiency to 32.1%$_{HHV}$, which corresponds to 6.4%$_{HHV}$ points drop from the reference value, it would require a large heat exchange area to reach the desired minimum temperature approach. Hence, a turbine inlet temperature of 620 °C, which resulted in net thermal efficiency of 31.9%$_{HHV}$ and is the maximum temperature for the most advanced supercritical steam cycles [44], would be more suitable for short- to mid-term applications. Moreover, a maximum turbine inlet pressure of 300 bar was selected, because such pressures are allowed by a very-high-grade steel, which is required to allow for high-temperature operation and to prevent the system from corrosion induced by the flue gas components [44]. It was estimated that the retrofitted system with the recompression s-CO_2 cycle operating with such turbine inlet pressure had the net thermal efficiency of 31.9%$_{HHV}$.

Finally, it can be observed that the correlation with the temperature (Fig. 5a) is nearly linear, while it is of second order for the pressure (Fig. 5b). Such correlation for the latter parameter can be associated with the extent of the pressure drop in the heat exchangers, which increases with the cycle operating pressure. Analysis of the net thermal efficiency trends in Fig. 5 indicated that further increase in the turbine inlet temperature, which would require a more complex heat exchanger network and a multiple shaft turbine design, could result in an improvement of the process

Table 5
Comparison of the key performance indicators.

Parameter	Reference coal-fired power plant [25]	CaL retrofit (supercritical steam cycle) [45]	CaL retrofit (s-CO_2 cycle)
System performance indicators			
Gross power output (MW$_{el}$)	580.4	1023.3	1024.3
Total auxiliary electricity consumption (MW$_{el}$)	27.7	223.5	217.9
Net power output (MW$_{el}$)	552.7	799.9	806.4
Gross thermal efficiency (%$_{HHV}$)	40.4	39.2	40.1
Net thermal efficiency (%$_{HHV}$)	38.5	30.6	31.6
Net specific chemical energy consumption (kW$_{ch}$/kW$_{el}$)	2.6	3.3	3.2
Specific coal consumption (g/kW$_{el}$h)	350.3	438.2	425.4
Integration impact indicators			
Increase in the net power output (%)	–	44.7	45.9
Net efficiency penalty (%$_{HHV}$ points)	–	7.9	6.9
Increase in net specific chemical energy consumption (%)	–	26.9	23.1
Carbonator CO_2 capture level (%)	–	79.6	80.0
Total CO_2 capture level (%)	0.0	90.0	90.0
CO_2 intensity factor (g/kW$_{el}$h)	792.3	111.6	108.7

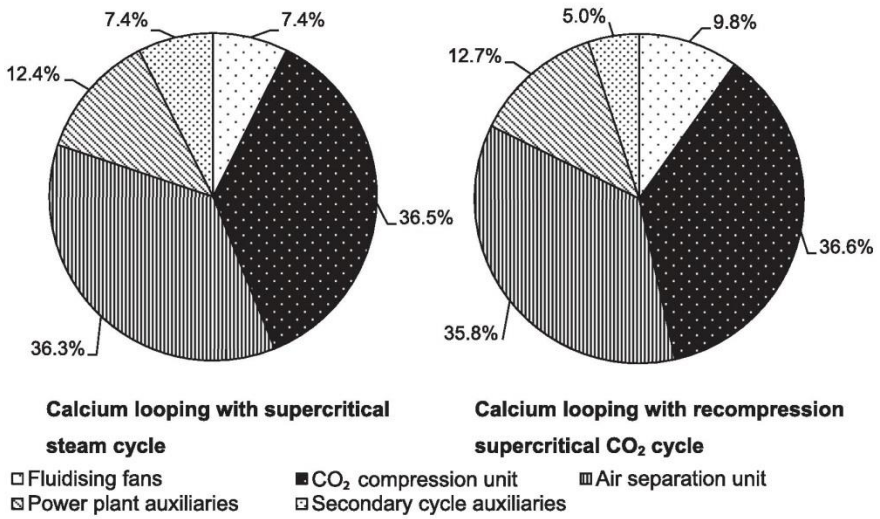

Fig. 3. Effect of the calcium looping secondary thermodynamic cycle selection on a parasitic load distribution for the 580 MW_{el} coal-fired power plant retrofit scenario.

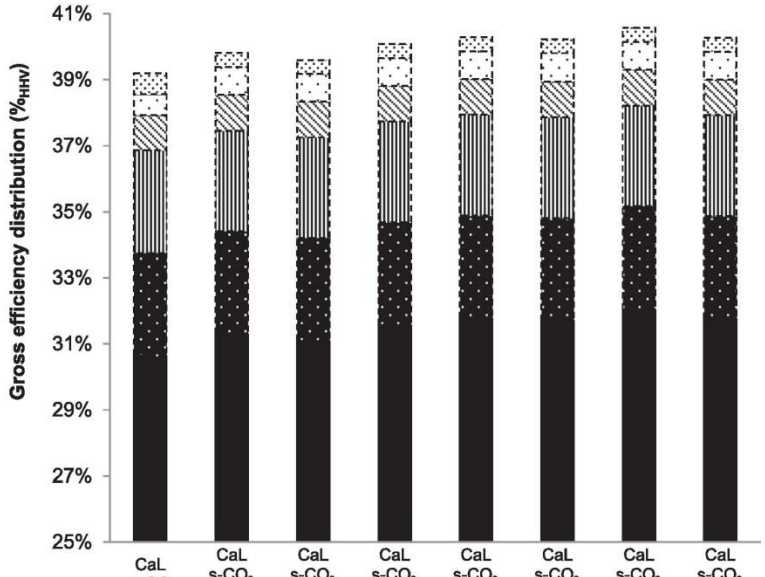

	CaL s-SC	CaL s-CO_2 (T1C2)	CaL s-CO_2 (T2C1)	CaL s-CO_2 (T2C2)	CaL s-CO_2 (T2C3)	CaL s-CO_2 (T3C2)	CaL s-CO_2 (T2C1P1)	CaL s-CO_2 (T2P2)
Secondary cycle auxilares	0.6%	0.4%	0.4%	0.4%	0.4%	0.4%	0.4%	0.4%
Fluidising fans	0.6%	0.8%	0.8%	0.8%	0.8%	0.9%	0.8%	0.8%
Power plant auxiliaries	1.1%	1.1%	1.1%	1.1%	1.1%	1.1%	1.1%	1.1%
Air separation unit	3.1%	3.1%	3.0%	3.1%	3.1%	3.0%	3.1%	3.1%
CO_2 compression unit	3.1%	3.1%	3.1%	3.1%	3.1%	3.1%	3.1%	3.1%
Net efficiency	30.6%	31.3%	31.1%	31.6%	31.8%	31.7%	32.0%	31.7%

Fig. 4. Effect of recompression supercritical CO_2 cycle configuration on integrated process performance. TxCyPz indicates number of turbine stages *x*, compression stages *y*, and pumping stages *z* in the configuration considered. CaL s-SC refers to the reference configuration in which the excess high-grade heat from CaL is recovered in the supercritical steam cycle, while CaL s-CO_2 refers to the configurations in which the excess high-grade heat from CaL is recovered in the recompression s-CO_2 cycle.

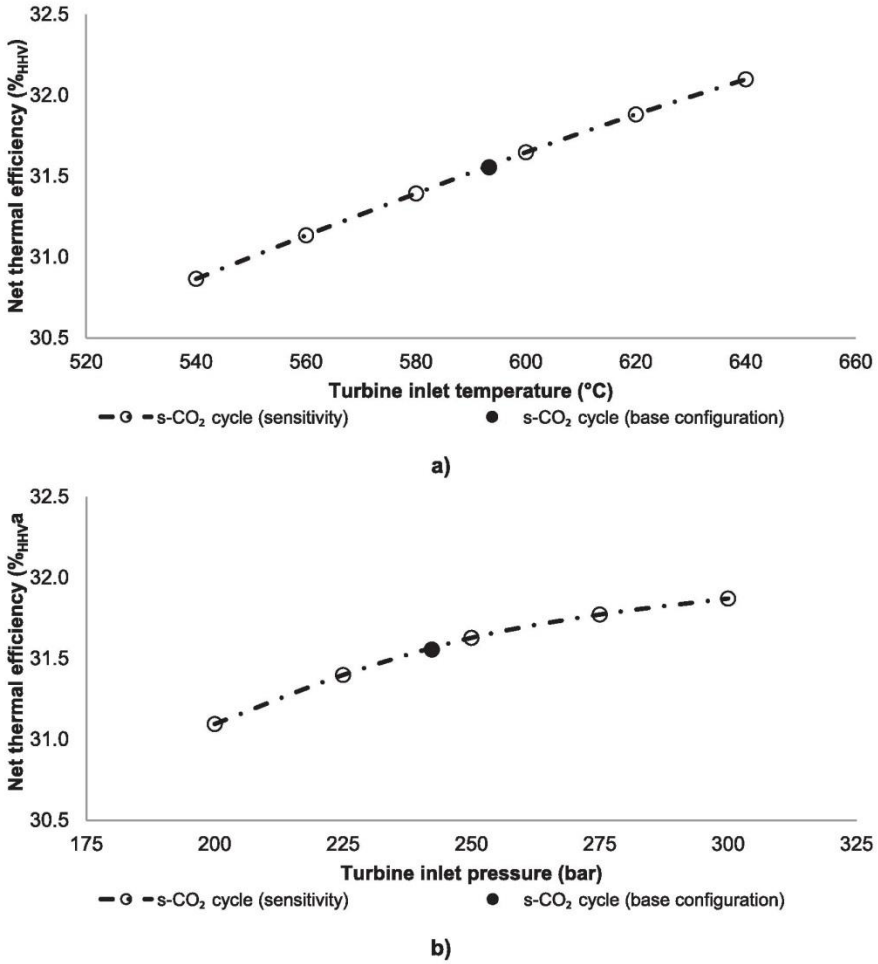

Fig. 5. Effect of turbine inlet a) temperature and b) pressure on the net thermal efficiency of the retrofitted system.

performance of about 0.1% per each 10 °C increase in the turbine inlet temperature. On the contrary, an increase in the turbine inlet pressure can be expected not to improve the net thermal efficiency of the retrofitted system much, mostly due to the associated increase in the pressure drop in the system.

3.3.3. Optimum recompression supercritical CO_2 cycle design

Having investigated how the performance of the retrofitted system varies with the recompression s-CO_2 cycle hardware and the turbine inlet conditions, the optimum configurations have been proposed and benchmarked against the base configuration in Table 6.

It has been demonstrated in Section 3.3.2 that by increasing the turbine inlet temperature to 620 °C, or increasing the pressure to 300 bar, the net thermal efficiency can increase by 0.3%$_{HHV}$ points. Unfortunately, no synergy effect occurred when both parameters were increased at the same time (Case 1), as the net thermal efficiency identified in Table 6 increased by 0.6%$_{HHV}$ points over the base configuration, which is equal to the sum of increments incurred by a separate increase in the turbine inlet temperature and pressure. Moreover, allowing for higher capital cost, addition of the second intercooling stage (Case 2) improves the performance by another 0.2%$_{HHV}$ points, lowering the net efficiency penalty to 6.1%$_{HHV}$ points. Alternatively, by considering the pump in place of the first stage of the main compressor (Case 3), the retrofitted system performance can be improved by 0.5%$_{HHV}$ points, resulting in the net efficiency penalty of 5.8%$_{HHV}$ points. This corresponds to 1.1%$_{HHV}$ points improvement over the base configuration and 2.1%$_{HHV}$ points improvement over the best configuration for CaL with the supercritical steam cycle for coal-fired calciner reported by Hanak et al. [45].

4. Conclusions

This study proposed to use the recompression s-CO_2 cycle in place of the conventional steam cycle to recover high-grade heat from the CaL plant, which was retrofitted to the 580 MW_{el} supercritical coal-fired power plant. The recompression s-CO_2 was adapted to allow for a high degree of heat integration and to utilise the low-grade heat. The net efficiency of the base configuration, which was characterised

Table 6
Comparison of the key performance indicators for the optimised configurations.

Parameter	Base case (T2C2)	Case 1 (T2C2)	Case 2 (T2C3)	Case 3 (T2C1P1)
Turbine inlet conditions				
Temperature (°C)	593.3	620.0	620.0	620.0
Pressure (bar)	242.3	300.0	300.0	300.0
System performance indicators				
Gross power output (MW_{el})	1024.3	1039.6	1045.7	1053.3
Net power output (MW_{el})	806.4	821.5	827.5	835.0
Gross thermal efficiency ($\%_{HHV}$)	40.1	40.8	41.0	41.3
Net thermal efficiency ($\%_{HHV}$)	31.6	32.2	32.4	32.7
Specific coal consumption ($g/kW_{el}h$)	425.4	416.9	413.9	410.1
Integration impact indicators				
Net efficiency penalty ($\%_{HHV}$ points)	6.9	6.3	6.1	5.8
CO_2 intensity factor ($g/kW_{el}h$)	108.7	106.5	105.7	104.7

by single reheat and intercooling stages (T2C2), was estimated to be 1.0%$_{HHV}$ points higher compared to the reference supercritical steam cycle under the same turbine inlet conditions.

Further improvements in the net efficiency of the retrofitted system were achieved by varying the hardware and the turbine inlet conditions. It was found that adding the second reheat (T3C2) and second intercooling (T2C3) resulted in 0.1%$_{HHV}$ and 0.2%$_{HHV}$ points increase in the net efficiency of the retrofitted system, respectively. Also, replacing the first stage of the main compressor (T2C1P1) with the pump was found to increase the net efficiency by 0.4%$_{HHV}$ points. Furthermore, it was found that increase of the turbine inlet temperature and pressure to 640 °C and 300 bar would increase the net efficiency of the retrofitted system to 32.1%$_{HHV}$ and 31.9%$_{HHV}$, respectively. However, considering the material availability and the short- to mid-term application of the proposed concept, the temperature of 620 °C and pressure of 300 bar were selected for the optimal configurations. Depending on the hardware configuration, the net efficiency of the system can be increased to 32.2%$_{HHV}$ (T2C2), 32.4%$_{HHV}$ (T2C3) and 32.7%$_{HHV}$ (T2C1P1). The last configuration resulted in 2.1%$_{HHV}$ point net efficiency improvement over the reference CaL with the supercritical steam cycle (30.6%$_{HHV}$). As the specific capital cost of the s-CO_2 cycle is up to 27% lower than that of the equivalent steam cycle, this study proves the viability of the recompression s-CO_2 cycle application in CaL. Since the steam cycles for a high-grade heat recovery and power generation are integrated with other high-temperature looping cycles, such as chemical looping combustion, it can be expected that these can also benefit from the s-CO_2 cycle implementation.

The analysis revealed also that the performance of the coal-fired power plant retrofitted with the CaL plant, in which the excess heat is recovered in the recompression s-CO_2 cycle, can be further improved by:

- higher level of heat integration in the CaL plant, alternative sources of O_2 for oxy-combustion of fuel or sources of heat for sorbent regeneration to minimise or avoid the power requirement associated with O_2 production;
- alternative processes and technologies to minimise the power requirement for CO_2 compression prior to transport;
- higher efficiency of the secondary cycle, which for the recompression s-CO_2 cycle can be achieved through alternative configurations allowing increasing the turbine inlet temperature.

Nomenclature

a_1	sorbent average conversion model fitting parameter (−)
a_2	sorbent average conversion model fitting parameter (−)
b	sorbent average conversion model fitting parameter (−)
F_0	fresh limestone make up rate (kmol/s)
f_1	Sorbent average conversion model fitting parameter (−)
f_2	sorbent average conversion model fitting parameter (−)
E_{CO_2}	CO_2 capture level in the carbonator (−)
F_{CO_2}	CO_2 flow rate entering the carbonator (kmol/s)
F_R	CaO looping rate (kmol/s)
f_{calc}	calcination reaction extent (−)
f_{carb}	carbonation reaction extent (−)
X_{ave}	average sorbent conversion (−)
ΔX_{carb}	carbonation conversion (−)

Abbreviations

ASU	air separation unit
CaL	calcium looping
CCS	carbon capture and storage
CCU	CO_2 compression unit
HRSG	heat-recovery steam generator
HTR	high-temperature recuperator
LTR	low-temperature recuperator
s-CO_2	supercritical CO_2 cycle

References

[1] IPCC. Climate change 2007: the physical science basis: contribution of working group i to the fourth assessment report of the intergovernmental panel on climate change. Cambridge, UK and New York, NY, USA: Cambridge University Press; 2007.
[2] IPCC. Climate change 2013. the physical science basic. Working group I contribution to the fifth assessment report of the Intergovernmental panel on climate change. Cambridge, UK and New York, NY, USA: Cambridge Unviersity Press; 2013.
[3] European Commission. Communication from the commission to the European parliament, the council, the european economic and social committee and the committee of the regions - a roadmap for moving to a competitive low carbon economy in 2050. Brussels, Belgium: European Commission; 2011.
[4] IEA. Tracking clean energy progress 2013. IEA Input to the clean energy ministerial. Paris, France: IEA Publications; 2013.
[5] IEA. Tracking clean energy progress 2015. energy technology perspectives 2015 excerpt. IEA input to the clean energy ministerial. Paris, France: IEA Publications; 2015.
[6] EIA. Annual energy outlook 2015 with projections to 2040. Washington, DC, USA: U.S. Energy Information Administration; 2015.
[7] Edenhofer O. King coal and the queen of subsidies. Science 2015;349(6254):1286–7.
[8] IEA. Technology roadmap: carbon capture and storage. Paris, France: IEA Publications; 2013.
[9] Stanger R, Wall T, Spörl R, Paneru M, Grathwohl S, Weidmann M, et al. Oxyfuel combustion for CO_2 capture in power plants. Int J Greenh Gas Control 2015;40:55–125.
[10] Liang Z, Rongwong W, Liu H, Fu K, Gao H, Cao F, et al. Recent progress and new developments in post-combustion carbon-capture technology with amine based solvents. Int J Greenh Gas Control 2015;40:26–54.
[11] Xu G, Jin HG, Yang YP, Xu YJ, Lin H, Duan L. A comprehensive techno-economic analysis method for power generation systems with CO_2 capture. Int J Energy Res 2010;34(4):321–32.
[12] Hanak DP, Biliyok C, Yeung H, Białecki R. Heat integration and exergy analysis for a high ash supercritical coal-fired power plant integrated with a post-combustion carbon capture process. Fuel 2014;134:126–39.

[13] Kvamsdal HM, Romano MC, van der Ham L, Bonalumi D, van Os P, Goetheer E. Energetic evaluation of a power plant integrated with apiperazine-based CO_2 capture process. Int J Greenh Gas Control 2014;28(1):343–55.

[14] Van Wagener DH, Liebenthal U, Plaza JM, Kather A, Rochelle GT. Maximizing coal-fired power plant efficiency with integration of amine-based CO_2 capture in greenfield and retrofit scenarios. Energy 2014;72:824–31.

[15] Boot-Handford ME, Abanades JC, Anthony EJ, Blunt MJ, Brandani S, Mac Dowell N, et al. Carbon capture and storage update. Energy Environ Sci 2014;7:130–89.

[16] Hu Y, Li X, Li H, Yan J. Peak and off-peak operations of the air separation unit in oxy-coal combustion power generation systems. Appl Energy 2013;112: 747–54.

[17] Bhown AS, Freeman BC. Analysis and status of post-combustion carbon dioxide capture technologies. Environ Sci Technol 2011;45(20):8624–32.

[18] Kheshgi HS, Thomann H, Bhore NA, Hirsch RB, Parker ME, Teletzke GF. Perspectives on CCS cost and economics. SPE Econ Manag 2012;4(1): 24–31.

[19] Renner M. Carbon prices and CCS investment: a comparative study between the European Union and China. Energy Policy 2014;75:327–40.

[20] CSIRO. Assessing post-combustion capture for coal-fired power stations in Asia-Pacific Partnership countries. Newcastle, NW, USA: CSIRO Advanced Coal Technology; 2012.

[21] Abanades JC, Arias B, Lyngfelt A, Mattisson T, Wiley DE, Li H, et al. Emerging CO_2 capture systems. Int J Greenh Gas Control 2015;40:126–66.

[22] Shimizu T, Hirama T, Hosoda H, Kitano K, Inagaki M, Tejima K. A twin fluid-bed reactor for removal of CO_2 from combustion processes. Chem Eng Res Des 1999;77(1):62–8.

[23] Hanak DP, Anthony EJ, Manovic V. A review of developments in pilot plant testing and modelling of calcium looping process for CO_2 capture from power generation systems. Energy Environ Sci 2015;8:2199–249.

[24] Martínez I, Murillo R, Grasa G, Carlos Abanades J. Integration of a Ca looping system for CO_2 capture in existing power plants. AIChE J 2011;57(9): 2599–607.

[25] Hanak DP, Biliyok C, Manovic V. Rate-based model development, validation and analysis of chilled ammonia process as an alternative CO_2 capture technology for coal-fired power plants. Int J Greenh Gas Control 2015;34: 52–62.

[26] Yu S-C, Chen L, Zhao Y, Li H-X, Zhang X-R. A brief review study of various thermodynamic cycles for high temperature power generation systems. Energy Convers Manag 2015;94:68–83.

[27] Herranz LE, Linares JI, Moratilla BY. Power cycle assessment of nuclear high temperature gas-cooled reactors. Appl Therm Eng 2009;29(no. 8–9): 1759–65.

[28] Floyd J, Alpy N, Moisseytsev A, Haubensack D, Rodriguez G, Sienicki J, et al. A numerical investigation of the sCO_2 recompression cycle off-design behaviour, coupled to a sodium cooled fast reactor, for seasonal variation in the heat sink temperature. Nucl Eng Des 2013;260: 78–92.

[29] Moisseytsev A, Sienicki JJ. Investigation of alternative layouts for the supercritical carbon dioxide Brayton cycle for a sodium-cooled fast reactor. Nucl Eng Des 2009;239(no. 7):1362–71.

[30] Linares JI, Herranz LE, Fernández I, Cantizano A, Moratilla BY. Supercritical CO_2 Brayton power cycles for DEMO fusion reactor based on Helium Cooled Lithium Lead blanket. Appl Therm Eng 2015;76:123–33.

[31] Padilla RV, Soo Too YC, Benito R, Stein W. Exergetic analysis of supercritical CO_2 Brayton cycles integrated with solar central receivers. Appl Energy 2015;148:348–65.

[32] Turchi CS, Ma Z, Neises TW, Wagner MJ. Thermodynamic Study of Advanced supercritical carbon dioxide power cycles for concentrating solar power systems. J Sol Energy Eng 2013;135(no. 4):041007.

[33] Wright S, Vernon ME, Pickard PS. Concept design for a high temperature helium brayton cycle with interstage heating and cooling. Albuquerque, New Mexico and Livermore, California: Sandia National Laboratories; 2006.

[34] Dostal V, Driscoll MJ, Hejzlar P. A supercritical carbon dioxide cycle for next generation nuclear reactors. Cambridge, MA, USA: Massachusetts Institute of Technology; 2004.

[35] Pham HS, Alpy N, Ferrasse JH, Boutin O, Quenaut J, Tothill M, et al. Mapping of the thermodynamic performance of the supercritical CO_2 cycle and optimisation for a small modular reactor and a sodium-cooled fast reactor. Energy 2015;87:412–24.

[36] Feher EG. "The supercritical thermodynamic power cycle. Energy Convers 1968;8(no. 2):85–90.

[37] Angelino G. Carbon dioxide condensation cycles for power production. ASME J Eng Power 1968;90(no. 3):287–96.

[38] Kim YM, Kim CG, Favrat D. Transcritical or supercritical CO_2 cycles using both low- and high-temperature heat sources. Energy 2012;43(no. 1): 402–15.

[39] Sanchez D, Chacartegui R, Jimenez-Espadafor F, Sanchez T. A new concept for high temperature fuel cell hybrid systems using supercritical carbon dioxide. J Fuel Cell Sci Technol 2009;6(no. 2):021306.

[40] Song Y, Wang J, Dai Y, Zhou E. Thermodynamic analysis of a transcritical CO_2 power cycle driven by solar energy with liquified natural gas as its heat sink. Appl Energy 2012;92:194–203.

[41] Liu M, Lior N, Zhang N, Han W. Thermoeconomic analysis of a novel zero-CO_2-emission high-efficiency power cycle using LNG coldness. Energy Convers Manag 2009;50(no. 11):2768–81.

[42] Iverson BD, Conboy TM, Pasch JJ, Kruizenga AM. Supercritical CO_2 Brayton cycles for solar-thermal energy. Appl Energy 2013;111:957–70.

[43] Sarkar J, Bhattacharyya S. Optimization of recompression s-CO_2 power cycle with reheating. Energy Convers Manag 2009;50(no. 8):1939–45.

[44] Le Moullec Y. Conceptual study of a high efficiency coal-fired power plant with CO_2 capture using a supercritical CO_2 Brayton cycle. Energy 2013;49(no. 1):32–46.

[45] Hanak DP, Biliyok C, Anthony EJ, Manovic V. Modelling and comparison of calcium looping and chemical solvent scrubbing retrofits for CO_2 capture from coal-fired power plant. Int J Greenh Gas Control 2015;42: 226–36.

[46] Abanades JC, Anthony EJ, Wang J, Oakey JE. Fluidized bed combustion systems integrating CO_2 capture with CaO. Environ Sci Technol 2005;39(no. 8): 2861–6.

[47] Romeo LM, Abanades JC, Escosa JM, Paño J, Giménez A, Sánchez-Biezma A, et al. Oxyfuel carbonation/calcination cycle for low cost CO_2 capture in existing power plants. Energy Convers Manag 2008;49(no. 10):2809–14.

[48] Vorrias I, Atsonios K, Nikolopoulos A, Nikolopoulos N, Grammelis P, Kakaras E. Calcium looping for CO_2 capture from a lignite fired power plant. Fuel 2013;113:826–36.

[49] Ströhle J, Lasheras A, Galloy A, Epple B. Simulation of the carbonate looping process for post-combustion CO_2 capture from a coal-fired power plant. Chem Eng Technol 2009;32(no. 3):435–42.

[50] Lasheras A, Ströhle J, Galloy A, Epple B. Carbonate looping process simulation using a 1D fluidized bed model for the carbonator. Int J Greenh Gas Control 2011;5(no. 4):686–93.

[51] Lara Y, Lisbona P, Martínez A, Romeo LM. Design and analysis of heat exchanger networks for integrated Ca-looping systems. Appl Energy 2013;111:690–700.

[52] Berstad D, Anantharaman R, Jordal K. Post-combustion CO_2 capture from a natural gas combined cycle by CaO/$CaCO_3$ looping. Int J Greenh Gas Control 2012;11:25–33.

[53] Wang W, Ramkumar S, Fan L. Energy penalty of CO_2 capture for the Carbonation–calcination reaction (ccr) process: parametric effects and comparisons with alternative processes. Fuel 2013;104:561–74.

[54] Hanak DP, Biliyok C, Manovic V. Efficiency improvements for the coal-fired power plant retrofit with CO_2 capture plant using chilled ammonia process. Appl Energy 2015;151:258–72.

[55] Black J. Cost and performance baseline for fossil energy plants volume 1: bituminous coal and natural gas to electricity. National Energy Technology Laboratory; 2013.

[56] AspenTech. Aspen Plus: getting started modeling processes with solids. Burlington, MA, USA: Aspen Technology Inc; 2013.

[57] Sánchez-Biezma A, Paniagua J, Diaz L, Lorenzo M, Alvarez J, Martínez D, et al. Testing postcombustion CO_2 capture with CaO in a 1.7 MW_t pilot facility. Energy Procedia 2013;37:1–8.

[58] Sánchez-Biezma A, Ballesteros JC, Diaz L, de Zárraga E, Álvarez FJ, López J, et al. Postcombustion CO_2 capture with CaO. Status of the technology and next steps towards large scale demonstration. Energy Procedia 2011;4: 852–9.

[59] Arias B, Diego ME, Abanades JC, Lorenzo M, Diaz L, Martínez D, et al. Demonstration of steady state CO_2 capture in a 1.7MW_{th} calcium looping pilot. Int J Greenh Gas Control 2013;18:237–45.

[60] Charitos A, Rodriguez N, Hawthorne C, Alonso M, Zieba M, Arias B, et al. Experimental validation of the calcium looping CO_2 capture process with two circulating fluidized bed carbonator reactors. Industrial Eng Chem Res 2011;50(no. 16):9685–95.

[61] Rodríguez N, Alonso M, Abanades JC. Average activity of CaO particles in a calcium looping system. Chem Eng J 2010;156(no. 2):388–94.

[62] Baker EH. The calcium oxide-carbon dioxide system in the pressure range 1-300 atmospheres. J Chem Soc 1962:464–70.

[63] Sanpasertparnich T, Idem R, Bolea I, de Montigny D, Tontiwachwuthikul P. Integration of post-combustion capture and storage into a pulverized coal-fired power plant. Int J Greenh Gas Control 2010;4(no. 3):499–510.

[64] Pfaff I, Oexmann J, Kather A. Optimised integration of post-combustion CO_2 capture process in greenfield power plants. Energy 2010;35(no. 10): 4030–41.

[65] Posch S, Haider M. Optimization of CO_2 compression and purification units (CO_2CPU) for CCS power plants. Fuel 2012;101:254–63.

[66] AspenTech. Aspen Plus IGCC model. Burlington, MA, USA: Aspen Technology Inc.; 2011.

[67] Wright SA, Radel RF, Vernon ME, Rochau GE, Pickard PS. Operation and analysis of a supercritical CO_2 Brayton cycle. Albuquerque, New Mexico and Livermore, California: Sandia National Laboratories; 2010.

[68] Utamura M. "Thermodynamic analysis of part-flow cycle supercritical CO_2 gas turbines. J Eng Gas Turbines Power 2010;132(no. 11). pp. 111701(1–7).

[69] Cha JE, Lee THO, Eoh JH, Seong SH, Kim SO, Kim DE, et al. Development of a supercritical CO_2 brayton energy conversion system coupled with a sodium cooled fast reactor. Nucl Eng Technol 2009;41(no. 8):1025–44.

[70] Anantharaman R, Bollard O, Booth N, van Dorst E, Ekstrom C, Sanchez Fernandes E, et al. CArbon-free Electricity by SEWGS: advanced materials, reactor-, and process design. D 4.9 European best practice guidelines for assessment of CO_2 capture technologies. Alstom UK: Politecnico di Milano; 2011.
[71] Manovic V, Anthony EJ. Integration of calcium and chemical looping combustion using composite CaO/CuO-based materials. Environ Sci Technol 2011;45(no. 24):10750–6.
[72] Chen W, van der Ham L, Nijmeijer A, Winnubst L. Membrane-integrated oxy-fuel combustion of coal: process design and simulation. J Membr Sci 2015;492:461–70.
[73] Puig-Arnavat M, Søgaard M, Hjuler K, Ahrenfeldt J, Henriksen UB, Hendriksen PV. Integration of oxygen membranes for oxygen production in cement plants. Energy 2015;91:852–65.

8 EVALUATION AND MODELLING OF PART-LOAD PERFORMANCE OF COAL-FIRED POWER PLANT WITH POST-COMBUSTION CO_2 CAPTURE

Dawid P. Hanak, Chechet Biliyok and Vasilije Manovic

Published: Energy and Fuels, 2015, 29 (6), 3833–3844[i]

Statement of contributions of joint authorship

Dawid P. Hanak conducted the literature review, performed process analysis via process modelling and simulation, drafted and critically revised the manuscript, as well as prepared tables and figures. Chechet Biliyok and Vasilije Manovic proof-read and critically commented on the manuscript prior to its submission to Energy and Fuels (Journal Impact Factor 2016: 2.790).

Dawid P. Hanak, PhD Candidate

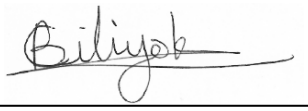

Chechet Biliyok, Associate supervisor

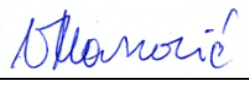

Vasilije Manovic, Principal supervisor

[i] Reprinted with permission from Hanak, D.P., Biliyok, C., and Manovic, V. (2015), "Evaluation and modelling of part-load performance of coal-fired power plant with post-combustion CO_2 capture", *Energy and Fuels*, 29 (6), 3833–3844, doi: 10.1021/acs.energyfuels.5b00591, American Chemical Society 2015.

energy&fuels

Article

pubs.acs.org/EF

Evaluation and Modeling of Part-Load Performance of Coal-Fired Power Plant with Postcombustion CO_2 Capture

Dawid P. Hanak, Chechet Biliyok, and Vasilije Manovic*

Combustion and CCS Centre, Cranfield University, Cranfield, Bedfordshire MK43 0AL, U.K.

Supporting Information

ABSTRACT: The share of the fossil-fuel power systems in the European Union energy portfolio has recently increased, even with new environmental incentives aimed at the reduction of CO_2 emissions from the power sector. Implementation of carbon capture technologies has been identified as a critical step toward reduction of CO_2 emissions. As the power plants usually operate with changing loads to meet the electricity demand, it is important to evaluate the process performance under different operating loads. Therefore, this study provides a methodology for modeling of part-load operation of coal-fired power plants in a process simulator, such as Aspen Plus. The part-load power plant model is validated using data from the literature, and it was demonstrated that a maximum discrepancy of 5% was obtained for the live steam pressure prediction at 40% load, while the discrepancy for all other compared parameters at other loads did not exceed 3%. Furthermore, the part-load model is used to evaluate the performance of the retrofitted power plant with the CO_2 capture plant at different loads, with monoethanolamine as a solvent, revealing that the net efficiency varied between 28.2%$_{HHV}$ and 21.1%$_{HHV}$. Moreover, the analysis showed that neglecting the off-design conditions due to steam extraction would result in overestimating the net thermal efficiency by up to 1.3%$_{HHV}$ points at 100% load operation and steam extracted at 11.9 bar.

1. INTRODUCTION

Concern about the impact of greenhouse gas emissions from human activity prompted the European Union to set an emissions reduction target of 80−95% below the 1990 levels by the year 2050.[1] As the power sector contributes more than a third of anthropogenic greenhouse gas emissions, it is targeted for decarbonisation by 2050 mainly through implementation of clean fossil-fuel technologies and the wider use of renewable energy sources. In 2011, coal-fired power plants accounted for 25% of the power generation capacity in the United Kingdom.[2] Moreover, due to the recent emergence of shale gas in North America, which has caused an oversupply of coal, the price of coal has dropped significantly. This is mirrored by the changes in the European energy market as coal-based electricity generation has increased by 8% in Germany, 35% in the United Kingdom, and 65% in Spain.[3] If in the following years the coal utilization rate follows the current trend, the actual coal demand in 2017 will be 17% higher than predicted under IEA's 2 °C Scenario (2DS).[4] If the current market trend continues, coal would continue to be used to meet an ample proportion of European power generation capacity.

The existing global coal-fired power plant fleet has an average net efficiency of 33%$_{LHV}$,[4] which corresponds to 30−31%$_{HHV}$, depending on the coal composition,[5] and substitution of subcritical units with more efficient supercritical units of the same power rating would result in approximately 15% reduction in CO_2 emissions.[6] However, operating the power plants at higher efficiencies is not sufficient to meet the emissions reduction targets. Therefore, the implementation of carbon capture and storage (CCS) technologies, along with the substitution of the fossil-fuel power generation systems with renewables have been identified as critical in order to reduce greenhouse gas emissions.[7]

In spite of the undeniable environmental benefit, implementation of clean energy technologies would introduce challenges in the operation of conventional thermal power systems. CCS technologies impose energy penalties on power plants. For example, postcombustion capture technologies, such as amine scrubbing, require a considerable amount of heat for solvent regeneration. This is usually satisfied by steam extraction from the power plant steam cycle, resulting in an efficiency penalty of 9.5−12.5% points.[8,9]

Computational models are widely employed in analysis of the performance of fossil-fuel power plants under different operating modes, as they are a lower cost alternative to pilot and demonstration studies. A number of commercial software programmes such as EBSILON Professional, GateCycle, and Cycle Tempo are used to explore the performance of power cycles. A major drawback of these is the fact that they are not suitable for the analysis of power plants retrofitted with CO_2 capture systems. Hence, it has become common practice to model the CO_2 capture plant in process simulators, such as Aspen Plus and the outputs are then used in the original power plant model.[10−14] Although power cycles have been successfully modeled in Aspen Plus,[15−18] model predictions are usually limited to base-load cases, making them unsuitable for analysis of multiple off-design or part-load cases due to the requirement for many specifications to ensure credible performance predictions. An attempt at part-load modeling in Aspen Plus and Aspen Plus Dynamics was undertaken by Alobaid et al.,[19] who developed a dynamic model of the steam cycle and showed that its prediction was in good agreement with measured data. However, such a

Received: March 20, 2015
Revised: May 1, 2015
Published: May 11, 2015

DOI: 10.1021/acs.energyfuels.5b00591
Energy Fuels 2015, 29, 3833−3844

model does not include the boiler model, as coal combustion modeling capability in Aspen Plus Dynamics is limited, and thus, it cannot be used to predict the effect of flue gas variations in CO_2 capture plant integration. It is worth pointing out that evaluation of the dynamic performance of the retrofitted system requires development of rigorous models,[20] the output of which must be validated with dynamic data to ensure a reliable and accurate prediction of the process performance.[21] The same should apply to the part-load predictions of the steady-state models.

The part-load analyses of the implementation of the postcombustion CO_2 capture plant have been performed for natural gas combined cycle power plants,[22] with both plants, however, being modeled separately in the Aspen HYSYS/ProTreat and GT PRO/GT Master, respectively.[23,24] In a study by Stępczyńska-Drygas et al.,[25] in which the part-load performance of a coal-fired power plant retrofitted with a CO_2 capture plant has been analyzed, the regeneration temperature and the specific heat requirement for solvent regeneration were kept constant at different loads, and the assumptions behind the part-load modeling of the CO_2 capture plant were not specified. This was also the case in a study by Jordal et al.,[24] who investigated the retrofit of a natural gas combined cycle power plant.

Therefore, this study is undertaken to provide a framework for building power cycle models in the Aspen Plus process simulator capable of reliably predicting plant performance under part-load operation and for different CO_2 capture retrofit scenarios. The part-load performance of the retrofitted system is also evaluated at different steam extraction pressures. Finally, the overestimation in the predicted net thermal efficiency, resulting from neglecting the off-design conditions due to steam extraction, is quantified for the first time in this study.

2. POWER PLANT MODELING

2.1. Process Description. The power plant selected as a benchmark in this study is a supercritical pulverized-coal-fired power plant, delivering a gross power output of 660 MW_{el}, with a net efficiency of 38.9%$_{HHV}$. The power plant is located in India, where high ambient temperatures have a negative impact on the electricity generation performance, and it uses the reference air and coal with characteristics presented in Table 1. The power plant configuration is presented in Figure 1 and consists of a once-through steam boiler with the flue gas treatment plant and a supercritical steam cycle with a single steam reheating stage.

Table 1. Coal and Combustion Air Characteristics

low-ash hard coal[26]		combustion air[27]	
component	as received ($\%_{wt}$)	component	volume fraction ($\%_{vol}$)
proximate analysis		air composition	
fixed carbon	59.00	carbon dioxide	0.03
volatile matter	22.29	water	3.12
ash	16.27	oxygen	20.30
moisture	2.44	nitrogen	75.62
ultimate analysis		sulfur dioxide	0.01
carbon	68.10	others	0.92
hydrogen	3.49	reference environment	
oxygen	7.47	ambient temperature (°C)	33.0
nitrogen	1.69	ambient pressure (bar)	1.013
sulfur	0.54		
higher heating value (MJ/kg)	26.83		
lower heating value (MJ/kg)	26.60		

At base load, the live steam at 537 °C and 242.2 bar is sent to a high-pressure (HP) turbine cylinder, where it is expanded to 44.3 bar. Steam is then returned to the boiler where it is reheated to 565 °C, before it is sent to an intermediate-pressure (IP) turbine and subsequently to the two low-pressure (LP) turbines. To enhance the overall power cycle efficiency, steam is extracted from the turbines for feedwater heating so that water is introduced to the boiler at 280 °C. A feedwater heating train consists of five LP feedwater heaters, the last one of which is called a deaerator and is a mixed feedwater heater, and three HP feedwater heaters. All feedwater heaters are modeled as surface heat exchangers with the terminal temperature difference of 3 °C. Moreover, the 3 °C temperature difference between hot-outlet and cold-inlet streams is maintained in all feedwater heaters with the exception of the first LP feedwater heater.

2.2. Modeling of Base-Load Power Plant Performance. A steady-state model of the 660 MW_{el} coal-fired power plant is developed in Aspen Plus and validated with the data provided in a study by Suresh et al.[27] The three main sections: the supercritical boiler, the steam cycle, and flue gas treatment train are modeled as separate submodels. The isentropic efficiencies of compressors and pumps in the system are assumed to be 80% and 85%, respectively, while the electrical efficiency of the generator is assumed to be 98.7%.

In the boiler model, solid fuel milling and combustion are modeled using Aspen Plus solids handling features.[28] The coal milling, its decomposition, and combustion are modeled using the grinder, RYield reactor and RGibbs reactor models, respectively. Operation of the coal mill, which is included to account for the milling power requirement, is characterized with a specific power of 0.187 MJ_{el}/kg, determined based on the data provided by Frankland et al.[29] Furthermore, the RGibbs reactor is used as it requires only a pressure specification to minimize the Gibbs free energy in the system to arrive at equilibrium for the provided products of coal combustion. Yet, to account for its composition, coal is modeled as a nonconventional component for which Gibbs free energy cannot be calculated. As a result, the coal is first decomposed into its constituents in the RYield reactor, before it is combusted in the RGibbs reactor model, and then both reactors are connected by the heat stream to account for the heat of coal decomposition.[28] The coal heating value is determined using Dulong's formula, and its consumption rate is adjusted to achieve the required base load. Moreover, to ensure complete combustion, the air flow rate is controlled to operate the boiler with 20% excess air at base-load operation. During part-load operation, the excess air is increased to meet the desired reheater outlet temperature. Desired excess air is controlled using eq 1[30] as a design specification to determine the desired O_2 content in the flue gas. This equation was used to take into account the products of incomplete combustion.

$$EA = \frac{y_{O_2,fg} - 0.5y_{CO,fg}}{\frac{y_{O_2,air}}{y_{N_2,air}} \cdot y_{N_2,fg} - y_{O_2,fg} + 0.5y_{CO,fg}} \times 100 \quad (1)$$

Furthermore, it is assumed that the bottom and fly ash distribution are 20%$_{wt}$ and 80%$_{wt}$, respectively,[31] and that the coal and ash handling equipment power requirement is directly dependent upon the coal consumption rate.[29]

DOI: 10.1021/acs.energyfuels.5b00591
Energy Fuels 2015, 29, 3833−3844

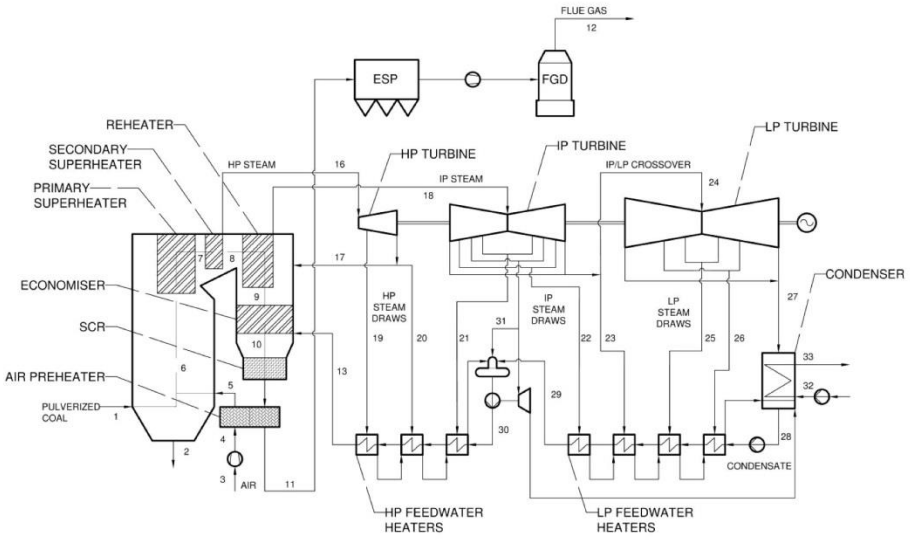

Figure 1. Process flow diagram of 660 MW_{el} supercritical coal-fired power plant.

There are four heat exchange sections considered in the supercritical boiler submodel: an economizer, a primary superheater, a secondary superheater, and a reheat superheater. At this stage of model development, the steam pressure drops and temperatures are fixed to simulate steam generator performance at the base load. Steam produced in the boiler is used to drive the steam turbines, which are characterized by design isentropic efficiencies of 89.6%, 91.7%, and 85.7% for the HP, IP, and LP cylinders, respectively. A difference in isentropic efficiency of the HP and IP cylinders stems from higher pressure drop, friction loss, and steam leakage in the HP cylinder.[32−34] Conversely, isentropic efficiency of the last cylinder is lower than that for the other cylinders due to the moisture present in the last stages.[35] The steam extraction from the turbines to feed the feedwater heaters cannot be directly modeled in Aspen Plus; therefore, each steam turbine cylinder is divided into stages with extraction points in between. The five LP and three HP feedwater heaters in the feedwater heating train are modeled as heat exchangers, while the deaerator is modeled as a flash heater.

Finally, the emissions control system includes NO_x, SO_x, and fly ash removal equipment. The selective catalytic reduction unit is modeled using a REquil reactor model, the flue gas desulfurization is conducted in an absorption column,[36] while the fly ash is removed in the electrostatic precipitator. The efficiencies of these units are set according to information given by Gerdes et al.[31]

2.3. Part-Load Modeling of Power Plant Performance. Using the base-load operating data in the power plant, the areas for the heat-exchange sections in the steam generator are sized and fixed for the part-load analysis. The coal-fired power plant can be operated in a sliding pressure mode, in which the steam pressure in the supercritical boiler follows the turbine load, or in a throttling control mode, in which a throttle valve is used to reduce the live steam pressure. In this study, the sliding pressure mode is used because it leads to net thermal efficiencies higher by up to 1.2%$_{HHV}$ points over the throttle control mode. This is mainly caused by reduced power consumption of the boiler feedwater pump.[27] Therefore, analysis of the part-load performance of the power plant requires the determination of new pressure distributions in the system as well as new efficiencies in the steam turbines. In the model, the live steam generation rate is controlled by the design specification to ensure that a constant temperature is always achieved within 40% to 100% load operating range. A Stodola's ellipse law, presented in eq 2, which is widely used for determination of the off-design performance in power plants,[37−39] is then implemented.

$$\frac{\dot{m}_{in}}{\dot{m}_{in}^{0}} = \frac{\mu}{\mu^{0}} \times \frac{p_{in}}{p_{in}^{0}} \times \sqrt{\frac{p_{in}^{0} \cdot v_{in}^{0}}{p_{in} \cdot v_{in}}} \times \sqrt{\frac{1 - \left(\frac{p_{out}}{p_{in}}\right)^{n+1/n}}{1 - \left(\frac{p_{out}^{0}}{p_{in}^{0}}\right)^{n+1/n}}} \tag{2}$$

Due to its complex structure, implementation of eq 2 results in convergence problems for a number of the steam turbine sections. Therefore, part-load performance of the steam cycle of the coal-fired power plant was conducted in an iterative manner using an MS Excel spreadsheet via the Aspen Simulation Workbook Add-on. As a result, the inlet pressures to each turbine section were calculated using the Stodola's ellipse law equation in a back-to-front manner, using the fixed condenser inlet pressure to determine the inlet pressure to the last low-pressure turbine section in a sequential series of calculations that end when the live steam inlet pressure is determined.

Additionally, pressure drops across the heat exchange sections in the steam generator are estimated, under the assumption the flow is homogeneous, by eq 3.[38]

$$\Delta p = 2f \times \frac{LV_{avg}^{2}\rho}{d} \tag{3}$$

The pressure loss estimates are updated at part-load operations using the average fluid velocity for the off-design and design modes and the design pressure drop as expressed by eq 4.

DOI: 10.1021/acs.energyfuels.5b00591
Energy Fuels 2015, 29, 3833−3844

Table 2. Validation of the Base-Load and Part-Load Prediction of the Coal-Fired Power Plant Model[b]

percent of base load	40%			60%			80%			100%		
	literature	model	deviation	literature	model	deviation	literature	model	deviation	literature	model	deviation
key parameters												
gross power output (MW_{el})	264.00	263.97	−0.01%	396.00	396.02	0.01%	528.00	528.02	0.00%	660.00	660.00	0.00%
net efficiency ($\%_{HHV}$)	34.80	34.51	−0.83%	37.10	37.08	−0.05%	38.20	38.39	0.50%	38.90	38.76	−0.36%
coal rate (kg/s)	25.70	26.44	2.88%	36.60	37.43	2.27%	47.60	48.53	1.95%	58.61	60.31	2.90%
final feedwater temperature (°C)	234.50	229.80	−2.00%	253.20	249.80	−1.34%	268.10	266.00	−0.78%	279.60	279.70	0.04%
LP turbine discharge steam quality (−)	0.99	0.97	−2.02%	0.97	0.95	−2.06%	0.95	0.94	−1.05%	0.93	0.93	0.00%
HP turbine inlet												
pressure (bar)	104.50	98.97	−5.29%	149.60	144.08	−3.69%	195.70	191.71	−2.04%	242.20	242.20	0.00%
temperature (°C)	537.00	537.00	0.00%	537.00	537.00	0.00%	537.00	537.00	0.00%	537.00	537.00	0.00%
mass flow rate (kg/s)	223.10	223.09	0.00%	325.90	325.89	0.00%	435.10	435.14	0.01%	550.70	550.67	−0.01%
IP turbine inlet												
pressure (bar)	17.80	17.72	−0.45%	25.70	25.71	0.04%	33.80	33.86	0.18%	42.00	42.00	0.00%
temperature (°C)	542.80	542.80	0.00%	556.90	556.90	0.00%	563.80	563.80	0.00%	565.00	565.00	0.00%
mass flow rate (kg/s)	197.70	198.96	0.64%	284.20	285.82	0.57%	373.40	375.14	0.47%	466.20	466.31	0.02%
LP turbine inlet												
pressure (bar)	1.40	1.38	−1.43%	1.90	1.94	2.11%	2.50	2.48	−0.80%	2.98	2.98	0.00%
temperature (°C)	211.90	207.30	−2.17%	217.40	212.80	−2.12%	218.40	213.40	−2.29%	215.60	210.10	−2.55%
mass flow rate (kg/s)	158.80	159.52	0.45%	222.20	222.28	0.04%	284.40	283.64	−0.27%	346.00	342.63	−0.97%

[b]The detailed stream data are available in Table S-2 of the Supporting Information.

$$\Delta p^{\text{off-design}} = \frac{\left(\frac{V_{\text{in}}^{\text{off-design}} + V_{\text{out}}^{\text{off-design}}}{2}\right)^2}{\left(\frac{V_{\text{in}}^{\text{design}} + V_{\text{out}}^{\text{design}}}{2}\right)^2} \Delta p^{\text{design}} \tag{4}$$

Finally, the values for the efficiencies of the steam turbines need to be updated in the off-design conditions. Knopf[38] proposed that the isentropic efficiency of the turbine section can be estimated using the approximate approach developed by Salisbury.[40] As the shaft speed remains constant at different loads, it is assumed that each turbine section is optimally designed and consists of 50% of reaction blading ($a = 0.7071$). Therefore, the ratio of the isentropic efficiency in off-design and design conditions is represented by eq 5.

$$\frac{\eta_i^{\text{off-design}}}{\eta_i^{\text{design}}} \cong 2\frac{a}{\frac{V_{\text{in}}^{\text{design}}}{V_{\text{in}}^{\text{off-design}}}} \times \left[\left(a - \frac{a}{\frac{V_{\text{in}}^{\text{design}}}{V_{\text{in}}^{\text{off-design}}}}\right) + \sqrt{\left(a - \frac{a}{\frac{V_{\text{in}}^{\text{design}}}{V_{\text{in}}^{\text{off-design}}}}\right)^2 + 1 - a^2}\right] \tag{5}$$

2.4. Model Validation and Discussion. An assessment of the model prediction accuracy should not only focus on the global performance indicators, such as the gross power output or the net thermal efficiency, but it also needs to address the model capability of predicting the local parameters like pressures, temperatures, and flow rates. Therefore, both the global and the local model parameters are compared with data available in the open literature to assess the overall reliability of the coal-fired power plant model.

As the coal consumption rate was controlled to reach the desired gross power output of 660 MW_{el} during base-load operation, the net thermal efficiency can be seen as the most important global indicator of coal-fired power plant performance, among the others reported in Table 2. Under base-load conditions, the net thermal efficiency of 38.8%$_{HHV}$ was estimated, which is only 0.1%$_{HHV}$ point lower than the reference value.[27] Moreover, the deviations of the local parameters for the key streams in the coal-power plant, which were identified in Figure 1, are benchmarked against the reference values in Figure 2. It is

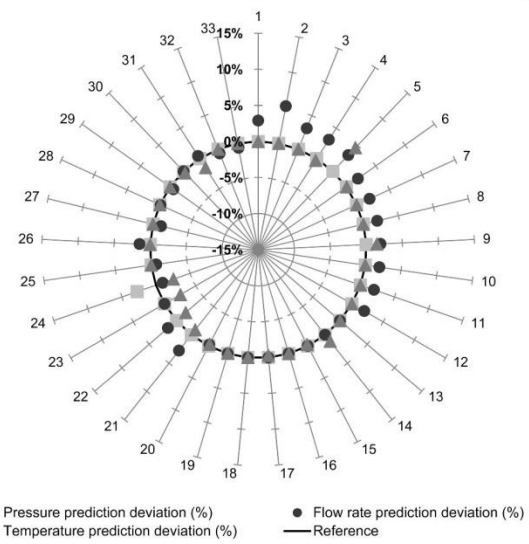

Figure 2. Validation of the base-load prediction of coal-fired power plant model developed in Aspen Plus. Numbers on the chart's perimeter refer to particular streams in the power plant model as depicted in Figure 1. Detailed information used for validation is available in Table S-1 of the Supporting Information.

DOI: 10.1021/acs.energyfuels.5b00591
Energy Fuels 2015, 29, 3833−3844

observed that the prediction of the stream pressures, temperatures, and flow rates is close to the reference data, with the majority of parameters having a deviation of less than ±3%. There are, however, a few exceptions, namely combustion air temperature, coal consumption rate and air flow rate, for which the deviation is still considerably less than 15%, which is an accepted design margin in industrial applications.[41] The combustion air temperature was found to be 4.5% higher than the reference value. This was a result of the exothermal reaction in the selective catalytic reactor for NO_x emissions control that is implemented between the economizer and the air heater in the model. The deviations in the coal consumption and air flow rates were incurred through consideration of the coal thermal decomposition and the moisture content in the fuel in the model developed in this work, while these were not accounted for in the reference study. Therefore, the coal consumption rate estimated was higher by 2.9%, leading to 5.3% more air required for combustion.

As mentioned above, prediction of the power plant models has mostly been validated at base-load operating condition, from which the part-load prediction was then estimated. It is pertinent, therefore, to benchmark the accuracy of the model prediction of the power plant operating under different loads. The coal-fired power plant modeled in this study is designed to operate within a 40−100% load envelope; as for loads below 40% of the base load, supplementary oil firing is required to meet the minimum heat rate in the boiler. With part-load performance data available at 40%, 60%, and 80% of the base load, the accuracy of the off-design performance prediction is validated. Table 2 reveals that the part-load prediction estimated using the coal-fired power plant model is in good agreement with the literature data for all analyzed loads, within a ± 3% deviation and with particularly close values for mass flow rates and temperatures of steam throughout the steam cycle. It was found that use of the Stodola's ellipse law resulted in accurate predictions of the steam inlet pressures for the IP and LP turbines; the live steam pressure at different part loads was underestimated by up to 5.3% at 40% of the base load. This may be due to the fact that, at reference conditions from which the part-load steam pressures are estimated, the live steam is in a supercritical state. Hence, the Stodola's ellipse law used in this region may have difficulty in providing close estimates of off-design conditions. Moreover, the assumption of constant temperature differences in the feedwater heaters is found to be reasonable as the resulting error in the final feedwater temperature does not exceed 2% at 40% load. Overall, the model provides close prediction of the part-load operation, and none of the estimated parameters differed from the reference data by more than ±6%, well within the accepted design margin of ±15%. This result implies that the approach described in Section 2.3 can be used to provide credible prediction of the part-load performance of a power plant, even in the absence of data for validation.

3. CO_2 CAPTURE SYSTEM MODELING

3.1. Monoethanolamine CO_2 Capture Plant. A rate-based modeling approach involving multicomponent mass transfer, heat transfer, kinetic reactions, and chemical equilibrium reactions is selected to model the CO_2 capture plant using $30\%_{wt}$ monoethanolamine (MEA) solvent. This approach has been used to develop a pilot-plant-scale model that is available in the Aspen Plus database. An extensive validation of this model with the experimental data from a testing facility for Separations Research Program at the University of Texas at Austin[42] was conducted by AspenTech[43] and Canepa et al.[44] In these studies, the model was found to well-represent the experimental facility performance under different liquid-to-gas ratios. Therefore, with the equipment in the CO_2 capture plant sized for operation under 100% load, the model is expected to predict the process performance under various loads with a reasonable accuracy.

In a previous study, Hanak et al.[45] have identified that decarbonization of the considered power plant required three absorbers and one stripper, all being cylindrical columns. However, recent experience from the Boundary Dam project in Saskatchewan, Canada[46] showed that application of rectangular or square columns for absorbers allowed for a simpler and less expensive design, without loss in column performance. Moreover an absorber design based on a rectangular or square concrete structure lined with anticorrosive material and structural packing negates the requirement for multiple absorption trains, as the column diameter no longer poses a structural constraint. However, considering the capabilities of the RadFrac model in Aspen Plus, only cylindrical columns can be modeled, and an alternative modeling approach that utilizes the definition of the hydraulic diameter, eq 6, needs to be implemented.

$$D_h = 4\frac{A}{P} \tag{6}$$

The square-column absorber would provide the same performance as a cylindrical one if their hydraulic diameters were equal. This assumption would be met if and only if the diameter (D) of the cylindrical column were equal to the side length (L) of the square column since:

$$D_{h,\mathrm{circ}} = 4\frac{\frac{\pi D^2}{4}}{\pi D} = D \tag{7}$$

$$D_{h,sq} = 4\frac{L^2}{4L} = L \tag{8}$$

Hence, the square column needs a $4/\pi$ times larger cross-section area to achieve the performance of the cylindrical column. However, assuming the same volume of the packing in the square and cylindrical column, larger cross-section area of the square column would require shorter columns. Also, in contrast to a steel vessel for the cylindrical columns, the square columns are erected as concrete structures for which the structural limitations are not as restrictive. Therefore, the capital cost of this kind of column would be lower regardless of the higher cross-section area required.

The initial guess for the sizes of the stripper and the absorber, which achieve $90\%_{wt}$ CO_2 capture level, is determined based on input from the power plant model at base-load conditions. Moreover, a design liquid/gas ratio (mass basis) in the absorber of 5, with a lean loading close to 0.3, is assumed (Table 3). The preliminary design calculations using the generalized pressure drop correlation revealed that the required cross-section area is 323.4 m^2 and 168.2 m^2, corresponding to the hydraulic diameter of 20.3 and 14.6 m, for the absorber and the stripper, respectively. When implemented in Aspen Plus, however, flooding higher than 75% was observed in the absorber and the stripper. Therefore, the hydraulic diameter for both columns is increased to 22 and 15 m, leading to an increase of the cross-sectional area to 380.1 m^2 and 176.7 m^2, respectively. As the square column absorber is considered, its actual area and packing height are estimated to be 484 m^2 and 23.6 m, respectively, based on the

DOI: 10.1021/acs.energyfuels.5b00591
Energy Fuels 2015, 29, 3833−3844

Table 3. Monoethanolamine CO_2 Capture Plant Equipment Design and Operating Conditions

design parameters		operating parameters	
column height (m)	30.0	flue gas flow rate (kg/s)	691.8
absorber cross-section area (m^2)	484.0	mass fraction of CO_2 ($\%_{wt}$)	21.3
absorber square length (m)	22.0	volume fraction of CO_2 ($\%_{vol}$)	14.5
number of absorbers	1	CO_2 capture efficiency ($\%_{wt}$)	90.0
stripper cross-section area (m^2)	176.7	reboiler temperature (°C)	122.4
stripper diameter (m)	15.0	condenser temperature (°C)	40.0
number of strippers	1	flue gas inlet temperature (°C)	40.0
packing type	Mellapack 350X	stripper pressure (bar)	1.7
lean-rich cross heat exchanger area (m^2)	13500	absorber pressure (bar)	1.0

derivation made above. The final design and operating parameters of the MEA CO_2 capture plant are summarized in Table 3.

Another important unit in the CO_2 capture plant is the lean-rich cross heat exchanger, as its performance would have an impact on the heat requirement for solvent regeneration. Therefore, assuming a minimum temperature approach between the cold rich and hot lean solution of 10 °C, and an overall heat transfer coefficient for amine−amine systems of 5000 W/m^2K,[47] a heat exchange area of 13500 m^2 was estimated. The off-design performance of the cross heat exchanger is computed using the correction to the overall heat transfer coefficient that depends on the actual solvent flow rate.[23,48]

$$\frac{U_{actual}}{U_{design}} = \left(\frac{\dot{m}_{actual}}{\dot{m}_{design}}\right)^{0.6} \quad (9)$$

3.2. CO_2 Compression Unit. A CO_2 compression unit is comprised of eight compression stages, each consisting of a centrifugal compressor, stage intercooler, and scrubber, working at 40 °C. Each compressor is modeled using the polytrophic compression model with efficiencies of 78−80%.[10,49] The number of compression stages was determined based on the assumptions that due to equipment restrictions the pressure ratio and the polytrophic head should not exceed 3 and 3050 m, respectively.[50] In the compression unit, CO_2 is first compressed to the critical pressure of 74 bar and then cooled to 30 °C so that it is present in the dense phase. For this reason, a final compression stage is conducted in a CO_2 pump, the operation of which is characterized by the discharge pressure of 110 bar and the isentropic efficiency of 80%. The power requirement of such configuration will be minimized, as it takes more effort to compress CO_2 in the gaseous phase, than to pump it in the dense phase.

4. ANALYSIS OF THE RETROFITTED SYSTEM

4.1. Considerations. Retrofit of the coal-fired power plant with the MEA CO_2 capture plant (Figure 3) requires identification of the proper steam extraction and condensate return locations that would maximize the net thermal efficiency.

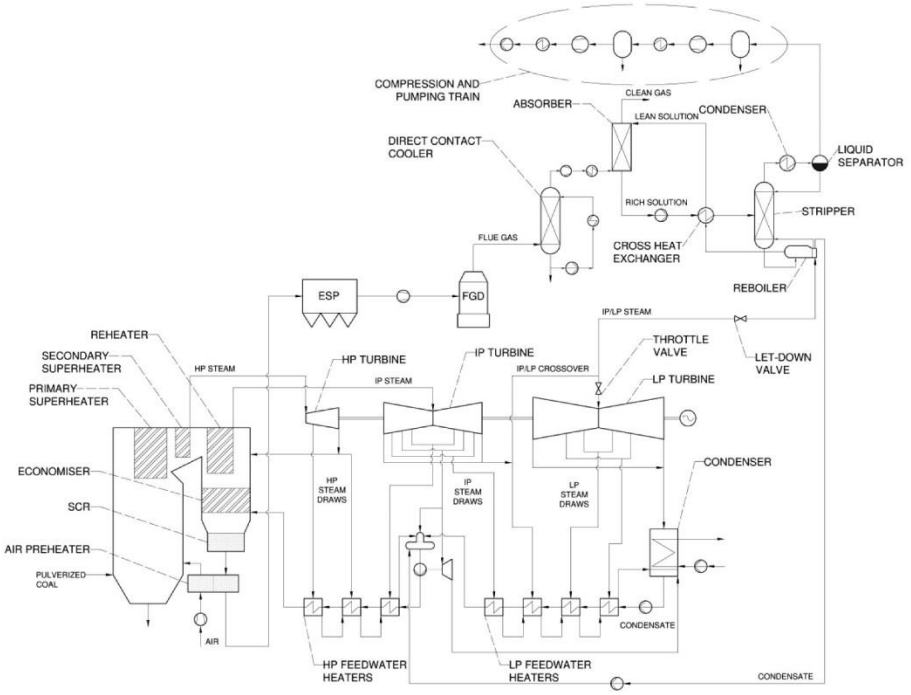

Figure 3. Process flow diagram of 660 MW_{el} supercritical coal-fired power plant retrofitted with monoethanolamine CO_2 capture plant (case 1). Detailed performance information is available in Table S-3 of the Supporting Information.

DOI: 10.1021/acs.energyfuels.5b00591
Energy Fuels 2015, 29, 3833−3844

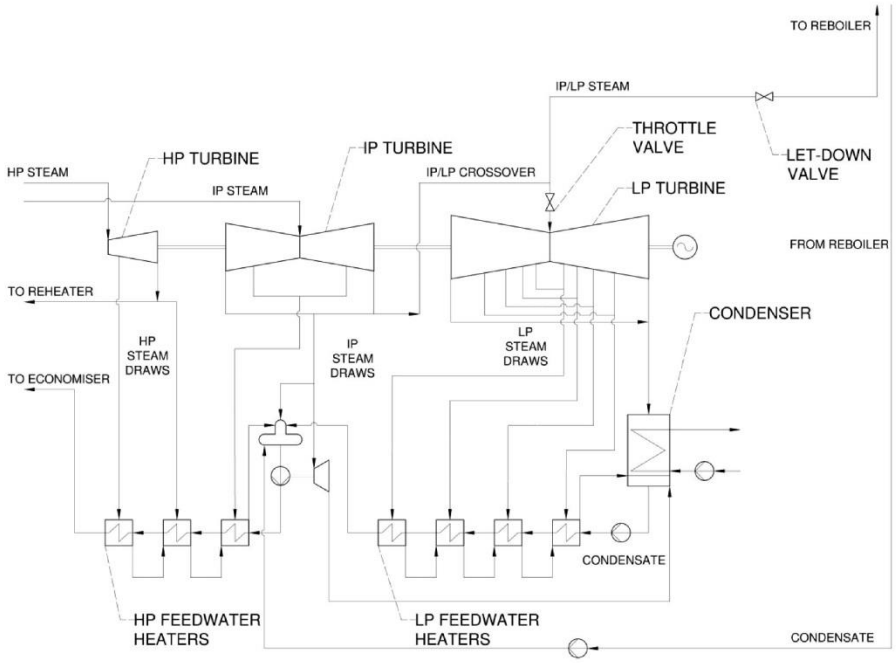

Figure 4. Process flow diagram of the retrofitted steam cycle in case 2. Detailed performance information is available in Table S-4 of the Supporting Information.

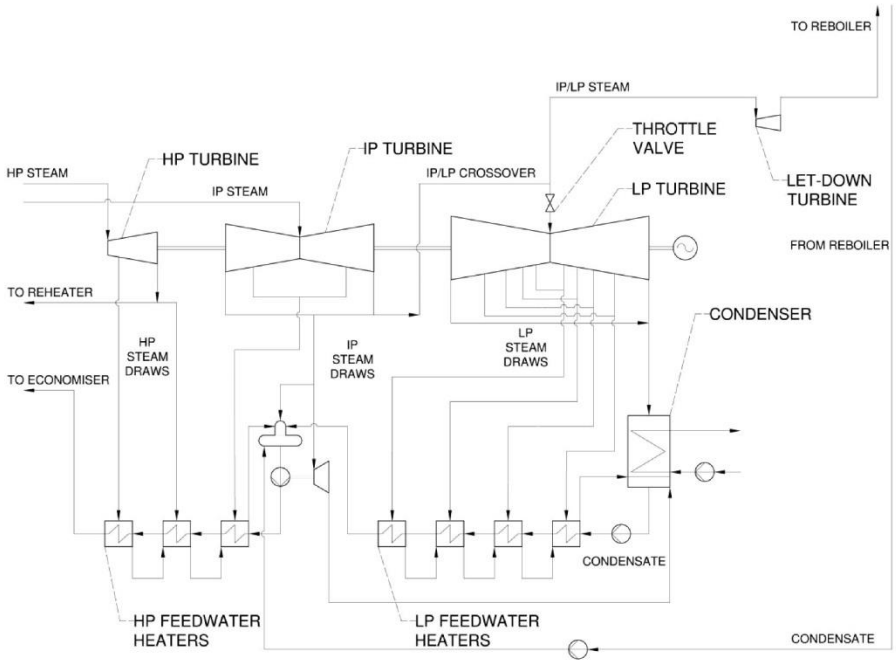

Figure 5. Process flow diagram of the retrofitted steam cycle in case 3. Detailed performance information is available in Table S-5 of the Supporting Information.

The optimum locations for these integration aspects were identified to be the IP/LP crossover pipe[51] and the last LP feedwater heater or deaerator,[45] respectively.

Although the base-load IP/LP crossover steam pressure in the considered power plant (2.98 bar) is suitable for meeting the 10 °C temperature pinch in the reboiler without the need for

DOI: 10.1021/acs.energyfuels.5b00591
Energy Fuels 2015, 29, 3833−3844

substantial throttling to 2.9 bar (case 1), it is much lower than the values of the 9−13 bar encountered in most existing coal-fired power plants.[27,36,51,52] The model developed in this study, which comprises multiple steam turbine sections, allows investigating different IP/LP crossover steam pressures without the need of changing its structure. Therefore, two additional scenarios shown in Figures 4 and 5, respectively, in which either a throttle valve (case 2) or a let-down turbine (case 3) is used to adjust the steam pressure, are considered in which the IP/LP crossover steam pressure is 11.9 bar at the base load. Moreover, it is common engineering practice to oversize the equipment to ensure its proper operation under variable loads during the life span of the system. Therefore, the part-load control strategy of the CO_2 capture plant assumes that the capture efficiency is maintained at 90%, which is achieved by varying the solvent circulation rate while maintaining the lean loading of 0.29 in all of the investigated cases. This approach has been proposed by Jordal et al.[24]

Furthermore, as the power plant usually operates under different loads, the net thermal efficiency of the retrofitted system is estimated for the scenarios identified above, with the assumption that the coal consumption rate remains constant for a particular power plant load in each of the investigated cases. However, as identified in Section 2.4, the IP/LP pressure drops with reduction of the coal-fired power plant load and thus it could become infeasible to meet the reboiler specification (case 1). A practical measure to resolve this issue is throttling the low-pressure turbine to keep the IP/LP pressure at the desired level. As such solution would affect the pressure distribution in the steam cycle, it is quantified and compared with cases 2 and 3 in which the drop of the IP/LP pressure at part-load operation is not restricted.

A considerable amount of steam would need to be extracted for solvent regeneration affecting the pressure distribution in the steam cycle.[45] Therefore, the impact on the net thermal efficiency prediction needs to be evaluated. As the power plant model developed in this study is capable of predicting steam cycle performance under various conditions, the effect of steam extraction is rigorously quantified and analyzed.

4.2. Performance Analysis. A reduction in the power plant load from 100% to 40% was found to have a significant effect on the heat and power requirements of the CO_2 capture system (Figure 6). Process analysis revealed that the reduction of the reboiler duty is not linear and for subsequent load changes from 100% to 40% (with 20% steps), it amounts to 17.6% (113.4 MW_{th}), 22.3% (118.4 MW_{th}), and 28.9% (119.2 MW_{th}), respectively. It is important to point out that the nonlinear correlation between the reboiler duty and the coal-fired power plant load is a result of the applied strategy for excess air at part-load operation, which assumes that the excess air is increased to meet the desired reheater outlet temperature. Such increase leads to higher O_2 concentration and thus, a corresponding drop in the CO_2 concentration in the flue gas from 14.5%$_{vol}$ at 100% to 8.0%$_{vol}$ at 40% load, making the CO_2 capture less efficient. Moreover, a gradual reduction in the CO_2 capture system power requirement with subsequent reduction of the coal-fired power plant load was observed from 7.5 to 7.0 MW_{el}. Integration of the CO_2 capture system imposed a considerable parasitic load requirement on the coal-fired power plant, leading to a drop in the net thermal efficiency (Figure 7).

Considering all three scenarios, the highest base-load net thermal efficiency of 28.2%$_{HHV}$, corresponding to an efficiency penalty of 10.5%$_{HHV}$ points, was achieved in case 1, while change

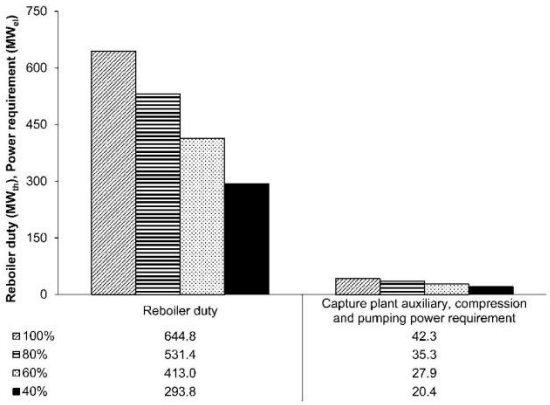

Figure 6. Part-load heat and power requirements for the CO_2 capture system.

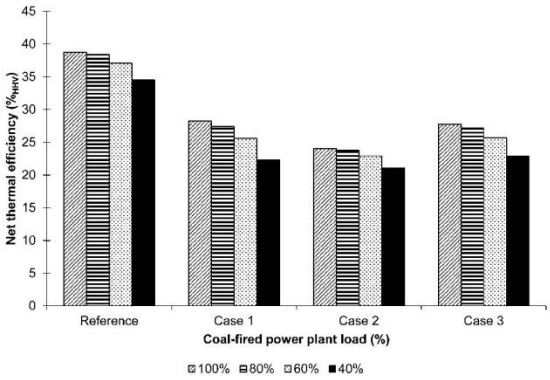

Figure 7. Base-load and part-load net thermal efficiencies under different scenarios.

of the IP/LP crossover location to increase the IP/LP steam pressure from 2.9 to 11.9 bar (case 2) caused a substantial drop in the net thermal efficiency to 24.1%$_{HHV}$. Although additional capital cost would be incurred in case 3, it is substantiated as the net thermal efficiency of the retrofitted system has increased to 27.8%$_{HHV}$, which is lower by only 0.4% points than that estimated in case 1. Such reductions in the retrofitted system performance stem from the steam extraction at higher pressure and throttling of the low-pressure turbine to maintain the desired pressure downstream of the steam extraction tie-in.

It is important to point out that the net thermal efficiency of the reference power plant reduces at part-load operation, mostly due to increased excess air ratio and drop in the electric generator efficiency. Figure 7 reveals that a similar trend occurred among all investigated integration scenarios. Interestingly, the estimated part-load performance of case 3 was better than that of case 1 at 60% and 40% of the base load, as the net thermal efficiency was higher by 0.1% points and 0.6% points, respectively. This is not only the result of an additional amount of power generated in the let-down turbine in case 3, but it is mostly because the IP/LP steam pressure becomes insufficient to meet the reboiler specification below 80% of the base load in case 1. In such case, the low-pressure turbine needs to be throttled to maintain the required steam pressure of 2.9 bar, affecting the pressure

DOI: 10.1021/acs.energyfuels.5b00591
Energy Fuels 2015, 29, 3833−3844

distribution downstream of the steam extraction point, leading to further drop in the power output.

Further analysis of data presented in Figure 7 indicated that the net thermal efficiency gain achieved in case 3 over case 2 reduces along with a decrease in the power plant load. This can be associated with the part-load reboiler requirements and the steam cycle performance, as the amount of extracted steam and the pressure drop across the let-down turbine reduce along with the coal-fired power plant load (Figure 8). For this reason, a shift

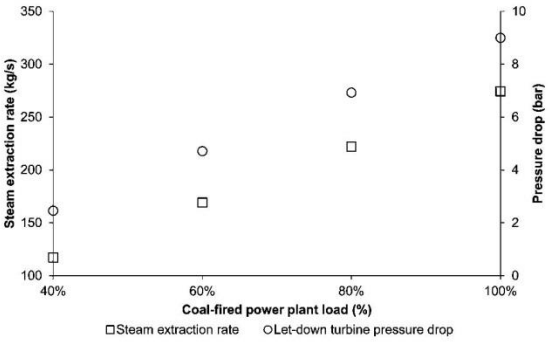

Figure 8. Changes of the steam extraction rate and the let-down turbine pressure drop with coal-fired power plant load for case 3.

in the balance of additional power generated by the let-down turbine and the total auxiliary power consumption of the retrofitted system is observed at loads lower than 80% (Figure 9).

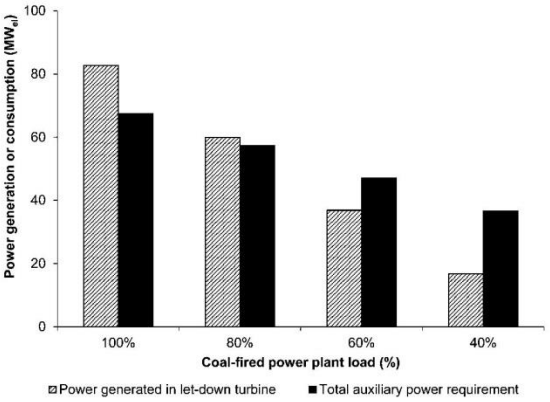

Figure 9. Balance between power generated in let-down turbine and consumed by the retrofitted system under different operating loads for case 3.

Such a shift can be associated with a higher drop in the additional power generated in the let-down turbine due to reduction in the reboiler heat requirement compared to reduction in the overall auxiliary power requirement.

Overall, the analysis reveals that, although the IP/LP steam pressure has an impact on the overall process performance at part load, implementation of the let-down turbine in cases of high IP/LP pressures (case 3) would provide comparable process benefits to the capture-ready systems with the IP/LP pressures designed for CO_2 capture plant integration (case 1). Regardless of the fact that the performance of case 3 was marginally lower than that of case 1 at 100% and 80% load, this configuration is the least adversely impacted by part-load operation, offering considerable advantages for plants to be operated under a load-following regime.

4.3. Impact of Pressure Drop on Performance Prediction. A considerable fraction of steam needs to be extracted from the IP/LP crossover pipe to meet the reboiler heat requirement, reducing the amount of steam used for power generation in the low-pressure steam turbine. However, a detailed analysis of the process performance prediction showed that the drop in the turbine throughput is not solely the responsible factor. This is because less steam passes through a fixed IP/LP pipe cross-section, leading to a drop of the pressure of steam entering the LP turbine.

Figure 10 revealed that variation in the relative change of the steam flow rate to the LP turbine is relatively small when

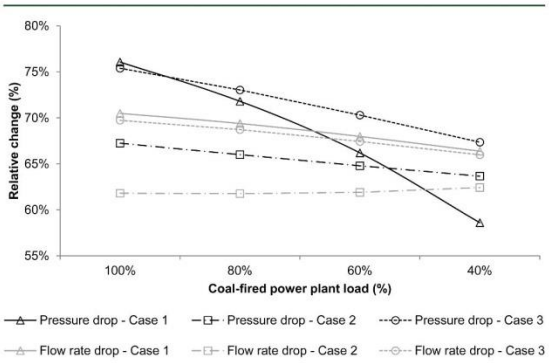

Figure 10. Dependence between the low-pressure steam flow rate due to steam extraction and the pressure drop under different operating loads.

reducing the power plant load, which is a result of a fixed lean loading during part-load operation. It was also found that nearly the same amount of steam was extracted in case 3 as was in case 1, while the amount of IP/LP steam extracted in case 2 was considerably smaller. This can be associated with the differences between the expansion process in the throttle valve and the steam turbine, leading to the higher temperature at the throttle valve outlet. Moreover, it needs to be highlighted that with reduction of the power plant load, the relative change of the steam extraction rate decreased in case 1 and case 3, while it increased in case 2. Figure 11 reveals that this is because in case 2, the variation in the steam temperature at the inlet to the reboiler attemperator is small due to the fact that its pressure is maintained at 2.9 bar through throttling of the LP turbine. On the contrary, a considerable increase of the steam temperature is observed on reduction of the power plant load in cases 1 and 3, leading to a decrease in the relative change in the steam requirement.

In addition, the analysis revealed that the relative change of the drop in the LP inlet pressure with the power plant load followed the same trend for case 2 and 3, while a considerable reduction in the relative change of the pressure drop was observed for case 1. As mentioned in Section 4.2, the IP/LP pressure becomes insufficient to meet the reboiler requirements at power plant loads below 80%. A reason for this is the reduced amount of IP/LP steam discharged from the IP turbine under part-load operation, causing a drop in the IP/LP steam pressure according to the Stodola's ellipse law. Therefore, not only does the relative

DOI: 10.1021/acs.energyfuels.5b00591
Energy Fuels 2015, 29, 3833−3844

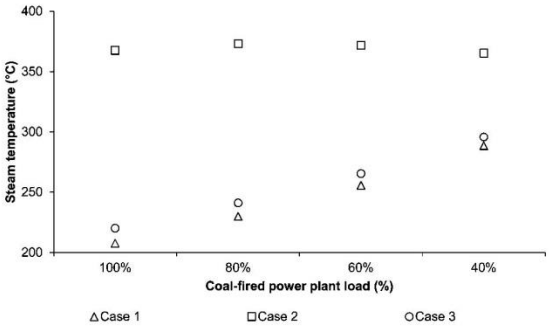

Figure 11. Changes in the IP/LP steam temperature at the inlet to the reboiler attemperator under different operating loads.

change in the pressure drop decrease due to reduction in the IP/LP steam flow rate, it is further decreased by the IP/LP pressure kept at a desired reboiler level through LP turbine throttling. On the contrary, the IP/LP steam pressures in cases 2 and 3 are higher than the steam pressure required in the reboiler and the relative change in the pressure drop depends on the change in the IP/LP steam flow rate only, which is the result of load reductions. Hence, the effect of reduced steam flow has a minor effect on the relative change in the pressure drop.

Finally, the shift of the relative change curves between the pressure drop, and the flow rate drop is a function of the temperature of steam, hence the specific volume as shown in the relationship between the mass flow rate and the pressure of steam, as described in the Stodola's ellipse law (eq 2).

As the pressure drop was found to be of a comparable magnitude to the drop in the IP/LP steam flow rate, it is important to quantify its impact on the process performance prediction. For this reason, the scenarios analyzed above were recalculated with the assumption that no pressure drop occurs due to IP/LP steam extraction. Comparing the net thermal efficiency values with the ones obtained in Section 4.2, it is concluded that if the pressure drop caused by steam extraction is neglected in the analysis, the overall performance of the retrofitted system would be overestimated by up to 1.3%$_{HHV}$ points, with an average of 1.1%$_{HHV}$ points (Figure 12). As the net efficiency penalty is underestimated by up to 11.4%, the error incurred by not considering the steam extraction-induced pressure drop is considerable. This, in turn, can lead to misleading conclusions regarding the performance of the retrofitted system, especially under part-load operation. For this reason, if steam extraction is one of the integration points, its effect on the pressure distribution in the steam cycle and on the power generation must be considered to accurately assess the retrofitted system performance.

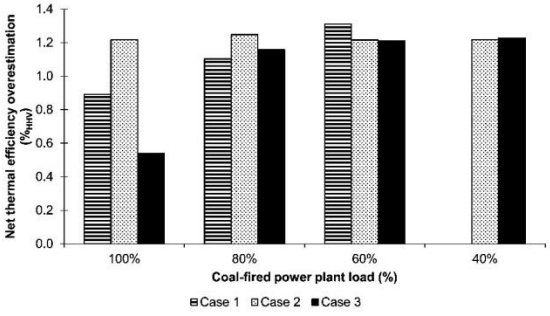

Figure 12. Estimation of the error in the net efficiency penalty prediction if the steam extraction-induced pressure drop is not considered. Case 1 could not have been computed at a 40% load since the inlet pressure to the last IP turbine dropped below 2.9 bar.

5. CONCLUSIONS AND RECOMMENDATION

The framework for part-load modeling of the coal-fired power plant retrofitted with the CO_2 capture plant in a process simulator such as Aspen Plus is developed in this work. A 660 MW_{el} coal-fired power plant is modeled and validated first at base load then at three different part-load conditions. The overall prediction of the model was in good agreement with the available data, although the live pressure steam was underestimated at part-load operation, up to a maximum of 5.3% deviation. Also, the assumption of constant temperature differences characterizing the operation of the feedwater heaters was proven to be valid as the maximum deviation of 2% in the final feedwater temperature was observed at 40% load.

Retrofitting of the CO_2 capture plant, which uses MEA as a solvent and comprises one square-column absorber, was found to impose an efficiency penalty ranging between 10.5%$_{HHV}$ points and 14.7%$_{HHV}$ points, depending on the operating conditions and integration scenario (case 1 in which steam is extracted at 2.9 bar at 100% load and case 2 where steam is extracted at 11.9 bar and its pressure adjusted in the throttle valve at 100% load, respectively). The performance analysis revealed that the heat requirement for the solvent regeneration drops nonlinearly with reduction of the power plant load. It was concluded that this could be a result of the implemented power plant and CO_2 capture plant control strategies, which assume variable excess air ratio to control the reheater temperature and constant liquid–gas ratio. It was also found that the lowest efficiency penalty occurred in case 1 for the 100% and 80% load, and case 3, in which steam is extracted at 11.9 bar and its pressure adjusted in a let-down turbine, for the 60% and 40% load. Finally, the effect of considering the pressure drop due to steam extraction was quantified and the analysis showed that if it is not taken into account, the efficiency penalty could be underestimated by up to 1.3%$_{HHV}$ points.

In conclusion, the part-load modeling framework developed in this study for coal-fired power plant retrofits was found to be an effective tool for the detailed part-load analysis resulting from changes in the power demands and/or modifications due to CO_2 capture plant integration. Also, analysis of the part-load performance of the coal-fired power plant retrofitted with the CO_2 capture plant using MEA solvent revealed that the configuration that achieves the best performance at base-load operation is not necessarily the best option for the part-load operation. Therefore, the proposed framework should lead to a more profound insight into operation of the retrofitted system and, thus, assessing the process performance in a more reliable fashion. Furthermore, the results generated by the model can be used to improve the prediction of a techno-economic analysis of various retrofit scenarios through a detailed assessment of the process performance under part-load operation. These results can also serve as a basis for future studies to assess the process reliability and operability. Finally, the proposed framework can be used as guidance in developing similar models for assessing the part-load operation of the precombustion and oxy-combustion CO_2 capture systems.

DOI: 10.1021/acs.energyfuels.5b00591
Energy Fuels 2015, 29, 3833−3844

■ ASSOCIATED CONTENT

Supporting Information

The Supporting Information is available free of charge on the ACS Publications website at DOI: 10.1021/acs.energyfuels.5b00591.

■ AUTHOR INFORMATION

Corresponding Author

*E-mail: v.manovic@cranfield.ac.uk. Tel: +44(0)1234 754649. Fax: +44 1234751671.

Notes

The authors declare no competing financial interest.

■ NOMENCLATURE

Parameters

A	Column cross-section area (m^2)
D_h	Hydraulic diameter (m)
EA	Excess air (% vol)
f	Friction coefficient
L	Pipe length (m)
$\dot{m}$	Mass flow rate (kg/s)
n	Adiabatic index
P	Column perimeter (m)
p_{in}	Steam pressure at stage inlet (bar)
U	Overall heat transfer coefficient (W/m^2K)
V	Velocity (m/s)
$y_{i,j}$	Mole fraction of species i in stream j (kmol/kmol)
ρ	Density (kg/m^3)
μ	Kinematic viscosity (m^2/s)
v_{in}	Specific volume (m^3/kg)
η_i	Isentropic efficiency

Superscripts

0 Parameter at design conditions

Subscripts

actual	Actual conditions
circ	Cylindrical column
design	Design conditions
in	Stream parameter at inlet to the unit operation
out	Stream parameter at outlet from the unit operation
sq	Square column

■ REFERENCES

(1) *Energy Roadmap 2050*; Publications Office of the European Union: Luxemburg, 2012.

(2) DECC, *UK Energy Sector Indicators 2012*; URN 12D/193; Department of Energy and Climate Change: London, 2012, available at: http://bit.ly/1jnBWjR.

(3) *Medium-Term Coal Market Report 2012*, IEA Publications: Paris, 2012.

(4) *Tracking Clean Energy Progress 2013. IEA Input to the Clean Energy Ministerial*; IEA Publications: Paris, 2013.

(5) *Technology Roadmap: High-Efficiency, Low-Emissions Coal-Fired Power Generation*; IEA Publications: Paris, France, 2012.

(6) Beér, J. M. High efficiency electric power generation: The environmental role. *Prog. Energy Combust. Sci.* **2007**, *33* (2), 107−134.

(7) *Technology Roadmap: Carbon Capture and Storage*; International Energy Agency: Paris, France, 2013.

(8) Yang, Y.; Zhai, R.; Duan, L.; Kavosh, M.; Patchigolla, K.; Oakey, J. Integration and evaluation of a power plant with a CaO-based CO_2 capture system. *Int. J. Greenhouse Gas Control* **2010**, *4* (4), 603−612.

(9) Xu, G.; Jin, H. G.; Yang, Y. P.; Xu, Y. J.; Lin, H.; Duan, L. A comprehensive techno-economic analysis method for power generation systems with CO_2 capture. *Int. J. Energy Res.* **2010**, *34* (4), 321−332.

(10) Pfaff, I.; Oexmann, J.; Kather, A. Optimised integration of post-combustion CO_2 capture process in greenfield power plants. *Energy* **2010**, *35* (10), 4030−4041.

(11) Cau, G.; Tola, V.; Deiana, P. Comparative performance assessment of USC and IGCC power plants integrated with CO_2 capture systems. *Fuel* **2014**, *116*, 820−833.

(12) Cau, G.; Tola, V.; Bassano, C. Performance evaluation of high-sulphur coal-fired USC plant integrated with SNO_X and CO_2 capture sections. *Appl. Therm. Eng.* **2014**, *74*, 136−145.

(13) Tola, V.; Pettinau, A. Power generation plants with carbon capture and storage: A techno-economic comparison between coal combustion and gasification technologies. *Appl. Energy* **2014**, *113*, 1461−1474.

(14) Karmakar, S.; Kolar, A. K. Thermodynamic analysis of high-ash coal-fired power plant with carbon dioxide capture. *Int. J. Energy Res.* **2013**, *37* (6), 522−534.

(15) Seltzer, A., Fan, Z. and Robertson, A. *Conceptual Design of Supercritical O_2-Based PC Boiler*; DE-FC26−04NT2207; Foster Wheeler Power Group, Inc: Livingston, NJ, USA, 2006.

(16) Yan, L.; He, B.; Pei, X.; Li, X.; Wang, C. Energy and exergy analyses of a Zero emission coal system. *Energy* **2013**, *55*, 1094−1103.

(17) Pei, X.; He, B.; Yan, L.; Wang, C.; Song, W.; Song, J. Process simulation of oxy-fuel combustion for a 300 MW pulverized coal-fired power plant using Aspen Plus. *Energy Convers. Manage.* **2013**, *76*, 581−587.

(18) Han, D.; Duan, L.; Duan, Y.; Hu, H.; Pan, X. Simulation and optimization of pressurized oxy-fuel combustion system. *Zhongguo Dianji Gongcheng Xuebao/Proceedings of the Chinese Society of Electrical Engineering* **2014**, *34* (5), 756−762.

(19) Alobaid, F.; Karner, K.; Belz, J.; Epple, B.; Kim, H. Numerical and experimental study of a heat recovery steam generator during start-up procedure. *Energy* **2014**, *64*, 1057−1070.

(20) Garoarsdóttir, S. Ó; Normann, F.; Andersson, K.; Prölß, K.; Emilsdóttir, S.; Johnsson, F. Post-combustion CO_2 capture applied to a state-of-the-art coal-fired power plant-The influence of dynamic process conditions. *Int. J. Greenhouse Gas Control* **2015**, *33*, 51−62.

(21) Biliyok, C.; Lawal, A.; Wang, M.; Seibert, F. Dynamic modelling, validation and analysis of post-combustion chemical absorption CO_2 capture plant. *Int. J. Greenhouse Gas Control* **2012**, *9*, 428−445.

(22) Möller, B. F.; Genrup, M.; Assadi, M. On the off-design of a natural gas-fired combined cycle with CO_2 capture. *Energy* **2007**, *32* (4), 353−359.

(23) Nord, L. O.; Anantharaman, R.; Bolland, O. Design and off-design analyses of a pre-combustion CO_2 capture process in a natural gas combined cycle power plant. *Int. J. Greenhouse Gas Control* **2009**, *3* (4), 385−392.

(24) Jordal, K.; Ystad, P. A. M.; Anantharaman, R.; Chikukwa, A.; Bolland, O. Design-point and part-load considerations for natural gas combined cycle plants with post combustion capture. *Int. J. Greenhouse Gas Control* **2012**, *11*, 271−282.

(25) Stępczyńska-Drygas, K.; Łukowicz, H.; Dykas, S. Calculation of an advanced ultra-supercritical power unit with CO_2 capture installation. *Energy Convers. Manage.* **2013**, *74*, 201−208.

(26) Barroso, J.; Ballester, J.; Ferrer, L. M.; Jiménez, S. Study of coal ash deposition in an entrained flow reactor: Influence of coal type, blend composition and operating conditions. *Fuel Process. Technol.* **2006**, *87* (8), 737−752.

(27) Suresh, M.; Reddy, K.; Kolar, A. K. 3-E analysis of advanced power plants based on high ash coal. *Int. J. Energy Res.* **2010**, *34* (8), 716−735.

(28) *Aspen Plus: Getting Started Modeling Processes with Solids*; Aspen Technology, Inc.: Burlington, MA, 2013.

(29) Frankland, S. C.; Johnar, J. M. S. *Technical and Economic Feasibility of Low Ash Power Station Fuel in India*, COAL R254 DTI/Pub URN 04/822; The Department of Trade and Industry: London, U.K., 2004.

(30) *Method 3. Gas analysis for carbon dioxide, oxygen, excess air and dry molecular weight*; Air Resources Board: Sacremento, CA, 1999, http://bit.ly/QyGfjG (accessed Mar 30, 2014).

(31) Gerdes, K., Haslbeck, J. L., Kuehn, N. J., Lewis, E. G., Pinkerton, L. L., Simpson, J., Turner, M. J., Varghese, E., Woods, M. C. *Cost and*

DOI: 10.1021/acs.energyfuels.5b00591
Energy Fuels 2015, 29, 3833−3844

Performance Baseline for Fossil Energy Plants: Vol. 1: Bituminous Coal and Natural Gas to Electricity; 2010/1397; DOE/NETL: Pittsburgh, PA, 2010.
(32) Reinker, J. K., Mason, P. B. *Steam Turbines for Large Power Applications*; GER-3646D; GE Power Systems: Schenectady, NY, 1999.
(33) Albert, P. *Steam Turbine Thermal Evaluation and Assessment*, GER-4190, GE Power Systems: Schenectady, NY, 2000.
(34) Beebe, R. Condition monitoring of steam turbines by performance analysis. *Journal of Quality in Maintenance Engineering* **2003**, *9* (2), 102−112.
(35) Bolland, O. Comparative evaluation of advanced combined cycle alternatives. *International Gas Turbine and Aeroengine Congress and Exposition*, Brussels, Belgium, June 11−14, 1990; ASME: New York, NY, 1990.
(36) Black, J. *Cost and Performance Baseline for Fossil Energy Plants Vol. 1: Bituminous Coal and Natural Gas to Electricity*; DOE/2010/1397 Revision 2a; National Energy Technology Laboratory: Morgantown, WV, 2013.
(37) Cooke, D. H. *Modelling of off-Design Multistage Turbine Pressures by Stodola's Ellipse*; Bechtel Power Corporation: Houston, TX, 1983.
(38) Knopf, F. C. *Modeling, Analysis and Optimization of Process and Energy Systems*; Wiley: Hoboken, NJ, 2012.
(39) Rusinowski, H. *Diagnostyka Cieplna Eksploatacji w Energetyce (Thermal Identification in Power Engineering)*; Polska Akademia Nauk: Katowice, Poland, 2010.
(40) Salisbury, J. K. *Steam Turbines and Their Cycles*; Robert E. Krieger Publishing: Huntington, NY, 1950.
(41) *Power Generation. Energy Efficient Design of Auxiliary Systems in Fossil-Fuel Power Plants*; ABB: Zurich, Switzerland and Wickliffe, OH, 2009.
(42) Dugas, R. E. *Pilot Plant Study of Carbon Dioxide Capture by Aqueous Monoethanolamine*. MSc Thesis, The University of Texas, 2006.
(43) *Rate-Based Model of the CO2 Capture Process by MEA Using Aspen Plus*; Aspen Technology, Inc.: Cambridge, MA, 2008.
(44) Canepa, R.; Wang, M.; Biliyok, C.; Satta, A. Thermodynamic analysis of combined cycle gas turbine power plant with post-combustion CO_2 capture and exhaust gas recirculation. *Proceedings of the Institution of Mechanical Engineers, Part E: Journal of Process Mechanical Engineering* **2013**, *227* (2), 89−105.
(45) Hanak, D. P.; Biliyok, C.; Yeung, H.; Białecki, R. Heat integration and exergy analysis for a high ash supercritical coal-fired power plant integrated with a post-combustion carbon capture process. *Fuel* **2014**, *134*, 126−139.
(46) Shaw, D. Cansolv: Capturing attention at Boundary Dam. *Carbon Capture Journal* [Online] **2012**.http://bit.ly/1BoPFCe (accessed Jan 18, 2015).
(47) *Perry's Chemical Engineers' Handbook*, 7th ed; Perry, R. H., Green, D. W. Maloney, J. O., Eds.; McGraw-Hill: New York, 2007.
(48) Haag, J.-Ch., Hildebrandt, A., Hönen, H., Assadi, M., Kneer, R. Turbomachinery simulation in design point and part-load operation for advanced CO_2 capture power plant cycles; *2007 ASME Turbo Expo*, Montreal, Quebec, May 14−17, 2007, pp 239; Vol. 3, 2007.
(49) Posch, S.; Haider, M. Optimization of CO_2 compression and purification units (CO2CPU) for CCS power plants. *Fuel* **2012**, *101*, 254−263.
(50) Sanpasertparnich, T.; Idem, R.; Bolea, I.; de Montigny, D.; Tontiwachwuthikul, P. Integration of post-combustion capture and storage into a pulverized coal-fired power plant. *Int. J. Greenhouse Gas Control* **2010**, *4* (3), 499−510.
(51) Lucquiaud, M.; Gibbins, J. On the integration of CO_2 capture with coal-fired power plants: A methodology to assess and optimize solvent-based post-combustion capture systems. *Chem. Eng. Res. Des.* **2011**, *89* (9), 1553−1571.
(52) Ahn, H.; Luberti, M.; Liu, Z.; Brandani, S. Process configuration studies of the amine capture process for coal-fired power plants. *Int. J. Greenhouse Gas Control* **2013**, *16*, 29−40.

DOI: 10.1021/acs.energyfuels.5b00591
Energy Fuels 2015, 29, 3833−3844

This page intentionally left blank.

9 CALCIUM LOOPING WITH INHERENT ENERGY STORAGE FOR DECARBONISATION OF COAL-FIRED POWER PLANT

Dawid P. Hanak, Chechet Biliyok, and Vasilije Manovic

Published: Energy and Environmental Science, 2016, 9, 971–983[j]

Statement of contributions of joint authorship

Dawid P. Hanak conducted the literature review, performed process analysis via process modelling and simulation, drafted and critically revised the manuscript, as well as prepared tables and figures. Chechet Biliyok and Vasilije Manovic proof-read and critically commented on the manuscript prior to its submission to Energy and Environmental Science (Journal Impact Factor 2016: 20.523).

Dawid P. Hanak, PhD Candidate

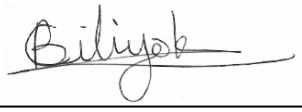

Chechet Biliyok, Associate supervisor

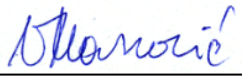

Vasilije Manovic, Principal supervisor

[j] Reprinted with permission from Hanak, D.P., Biliyok, C., and Manovic, V. (2016), "Calcium looping with inherent energy storage for decarbonisation of coal-fired power plant", *Energy and Environmental Science*, 9, 971–983, doi: 10.1039/C5EE02950C, Royal Society of Chemistry 2016.

Energy & Environmental Science

PAPER

View Article Online
View Journal

Cite this: DOI: 10.1039/c5ee02950c

Calcium looping with inherent energy storage for decarbonisation of coal-fired power plant†

Dawid P. Hanak,* Chechet Biliyok and Vasilije Manovic*

Received 25th September 2015,
Accepted 5th January 2016

DOI: 10.1039/c5ee02950c

www.rsc.org/ees

Implementation of carbon capture and storage, nuclear power stations and wide utilisation of renewable energy sources have been identified as capable of reducing around 42% of the energy sector's cumulative CO_2 emissions between 2009 and 2050. In scenarios assuming high shares of renewable energy sources in the energy portfolio, energy storage technologies and the remaining power generating assets would be required to flexibly balance energy supply and demand. With nuclear power plants operating at base load, this task would be handled by flexible fossil fuel power plants with CO_2 capture. However, mature CO_2 capture systems were shown to impose high efficiency penalties (8–12.5% points) and are better suited for base-load operation. An emerging calcium looping process, which has also been considered for energy storage, has been found to offer lower efficiency penalties (5–8% points). This study presents a concept of the calcium looping process with inherent energy storage for decarbonisation of the coal-fired power plant. Analysis has revealed that the possible routes for energy storage in this process include $CaO/CaCO_3$ solids storage, $CaO/Ca(OH)_2$ solids storage and cryogenic O_2 storage systems. Comparison of the $CaO/CaCO_3$ storage and cryogenic O_2 storage systems revealed that implementation of the latter would result in higher turndown of the entire system and would offer higher energy density. Also, the hydration reaction was found to improve the energy density of the $CaO/CaCO_3$ energy storage system by 57.4%, from 307.2 kW_{th} h m^{-3} to 483.6 kW_{th} h m^{-3}. Economic evaluation of the proposed concepts revealed that application of the cryogenic O_2 storage system in the calcium looping CO_2 capture process has the potential to increase the profitability of the integrated system, even over the reference coal-fired power plant without CO_2 capture.

Broader context

Fossil fuel power plants with CO_2 capture, nuclear power stations and renewable energy sources have been identified as capable of reducing around 42% of the energy sector's cumulative CO_2 emissions between 2009 and 2050. However, the increasing share of intermittent renewable energy sources in the energy portfolio will be a challenge for the balance of the energy network. Therefore, the fossil fuel power plants are expected to be decarbonised and to flexibly balance energy supply and demand to avoid energy wastage and shortages. Implementation of energy storage is seen as an alternative option to counterbalance the intermittent nature of renewables. In this study we present a concept of CO_2 capture systems based on calcium looping with inherent energy storage. We demonstrated that such systems, in addition to decarbonisation of power plants, can increase the degree of energy utilisation at very small additional capital costs. In the realistic future energy portfolio/policy scenarios, the fossil fuel energy systems based on the proposed concept can generate higher profit than current fossil fuel power plants without CO_2 capture. In other words, integration of carbon capture and storage with energy storage can enable decarbonisation of power and other carbon-intensive industries with no economic penalties.

1. Introduction

The International Energy Agency[1,2] has predicted that to limit the global mean temperature increase to 2 °C, around 42% of the cumulative CO_2 emission from the energy sector, between 2009 and 2050, can be mitigated through implementation of carbon capture and storage (CCS), nuclear power stations and utilisation of renewable energy sources. The greatest challenge of such a scenario is the intermittence of the renewable energy sources,[3] which would affect operation of the existing energy network,[4,5] especially in cases when their share in the energy portfolio exceeds 50%.[1] As the nuclear power plants operate at base load, fossil fuel power plants would need to flexibly balance energy supply and demand, so that neither energy produced from

Combustion and CCS Centre, Cranfield University, Bedford, Bedfordshire, MK43 0AL, UK. E-mail: d.p.hanak@cranfield.ac.uk, v.manovic@cranfield.ac.uk

† Electronic supplementary information (ESI) available. See DOI: 10.1039/c5ee02950c

renewable energy sources is wasted (high renewables generation period) nor energy shortages occur (low renewables generation period). Such periods of variable load operation or no operation would impose energy and economic penalties on the fossil fuel power systems, especially for plants with CCS that are better suited for base-load operation.[6]

Due to their capacity of decoupling energy supply and demand,[7] energy storage technologies can increase the degree of energy utilisation and should thus be widely deployed along with low-emission technologies. However, the energy storage could contribute to CO_2 emission reduction only in the scenario of wide renewables penetration.[8,9] Otherwise, energy storage may increase CO_2 emissions by an extent that depends on carbon prices and the share of coal-based power generation in the energy portfolio.[1,8] For this reason, a synergy between renewable energy sources, fossil fuel power generation and energy storage needs to be reached.

Presently about 145.8 GW of energy is stored globally, most of which as mechanical energy in pumped hydro storage plants (97.5%), and compressed air and flywheel energy storage techniques (1.0%). Interestingly, the share of thermal energy storage technologies surpassed electro-mechanical storage in 2013, and now accounts for 1.2% of the global energy storage capacity.[10] These technologies utilise media capable of storing thermal energy at low or high temperature, which can be recovered in the form of heat depending on the process demand.[11,12] Moreover, thermal energy storage systems are claimed to have the potential of improving the flexibility of the electricity grid, increasing the degree of the energy utilisation,[13,14] and balancing the mismatch between energy supply and demand.[15] These technologies do not have the disadvantages of pumped hydro storage and compressed air storage, such as requirements of specific site topology, and relatively high capital cost, which could have a negative environmental footprint.[11,12]

Thermal energy storage systems can be classified as sensible heat, latent heat, and thermochemical energy systems.[13,16,17] The last mechanism, in which heat is used to sustain an endothermic chemical reaction and is released in the reverse reaction, is claimed to offer high energy densities,[13,18] especially if one of the regeneration stage products is in the vapour phase.[19] Despite being proposed for energy storage in the mid-1970s,[19,20] the process involving either hydration or carbonation of CaO is still considered among the best candidates for energy storage.[18] A novel process design based on the reversible CaO hydration reaction for storing heat from a concentrated solar field has been recently analysed by Criado *et al.*[21] The proposed configuration comprises a single atmospheric pressure circulating fluidised bed, which can operate as hydrator and regenerator, and two silos for CaO and $Ca(OH)_2$ storage. This study revealed that, at maximum thermal output of 100 MW_{th}, the system offered an energy storage density of 260 kW h_{th} m^{-3} and a round-trip efficiency of 63%. Edwards and Materić[22] proposed a process based on reversible carbonation of CaO in the calcium looping process (CaL) that comprised two independent reactors – atmospheric pressure calciner (solar tower receiver) and pressurised fluidised bed carbonator – and three reservoirs for CaO, $CaCO_3$ and CO_2 storage. In addition, air leaving the carbonator was fed to a gas expander for power generation. The plant net thermal efficiency was found to be between 40–46%. Finally, Vandersickel *et al.*[23] proposed to integrate a similar process to the integrated gasification combined cycle power plant, with the difference being that only CaO and $CaCO_3$ are stored, and the heat for calcination is provided through oxy-combustion of syngas diverted from the gas turbine. In this system, the existing Selexol unit is by-passed and the carbonator is used to capture CO_2 from the syngas during the peak-demand period. Nevertheless, the primary function of this system is energy storage and unloading the existing CO_2 capture system. Such configuration was found to operate with a round-trip efficiency of 61%, and allowed for changing the power output by +25% (peak-load) and −20% (off-peak) with respect to a nominal 550 MW_{el}. However, this study did not consider variability of the power generation system during part-load operation, which would lead to a further reduction of the power output during the calcination step.

Although the carbonation reaction offers nearly 50% higher theoretical energy density (1222 kW h m^{-3}) compared to that of hydration (833 kW h m^{-3}),[13] there are some concerns that need to be resolved prior to large-scale deployment. These include capability for electrical energy storage,[12] reduction of sorbent activity,[19] and requirement for temporary CO_2 storage.[18] Also, the CaL process was proposed by Shimizu *et al.*[24] for CO_2 capture from fossil fuel power plants. Not only has this process been proven to impose lower net efficiency penalty (5–8% points)[25–28] compared to more mature CO_2 capture technologies (8–12.5% points),[29–32] it also has the ability to increase the net power output of the integrated system by more than 50%.[28,33,34] More importantly, this system can accept an excess amount of electricity produced in the renewable energy sources to drive the air (for O_2 production) and CO_2 compressors and has a permanent source of CO_2 from the fossil fuel power plant. Finally, it can operate with higher carbonation conversions (higher energy density) when a hydration stage is employed.[35]

The CaL process can, therefore, be seen as a promising technology for decarbonisation of the power sector as it has the ability to both decarbonise the fossil fuel power plant in an efficient manner and increase power generation flexibility. Hence, the fossil fuel power plant would not only meet its emission reduction targets, but also operate efficiently even in the energy portfolio containing large shares of intermittent renewable energy sources. In this study, the concept of CaL with inherent energy storage for CO_2 capture from coal-fired power plants is proposed and possible routes for energy storage in the proposed concept are identified. Finally, techno-economic performance of the selected routes is evaluated to analyse their degree of energy utilisation and profitability compared to the system without energy storage.

2 Concept process description

2.1 Calcium looping process

A core of the proposed concept is the CaL process proposed by Shimizu *et al.*[24] for CO_2 capture, which comprises two interconnected fluidised bed reactors operating at atmospheric pressure.

In the first reactor, a carbonator, CO_2 is removed from the flue gas stream *via* calcium-based sorbent. In the second reactor, a calciner, the sorbent is regenerated at a high temperature, provided through oxy-combustion of fuel. High-temperature operation of the CaL process allows for recovery of high-grade heat from the carbonator and the process streams. As a result high-pressure steam can be generated and utilised for power generation in a secondary steam cycle.

Yet, due to the decay of maximum sorbent conversion with the number of carbonation/calcination cycles,[36] which can drop to around 5–14% after 30 cycles depending on sulphur content in the flue gas and the fuel used in the calciner,[37,38] part of the sorbent needs to be replenished in the system. To achieve a higher conversion in the carbonator, the sorbent can be reactivated through hydration (CaL-HYD).[35,39,40] As a result of 60% sorbent hydration, the maximum sorbent conversion in the carbonator is about 55% after 15 cycles.[41] In the concept process proposed here, the low-pressure steam required for hydration can be extracted from the secondary steam cycle. Hydrated sorbent can be directed to either the carbonator or the calciner (Fig. 1). However, the latter route increases the calciner heat load, and although that heat can be regenerated, the need for a larger air separation unit and CO_2 compression unit incurs higher capital costs, making this route less attractive. In addition, around 4–10% of sorbent[42] could be elutriated due to attrition. As a result, a higher fresh limestone make-up rate would be required, leading to higher maximum sorbent conversions, at the expense of higher heat requirement in the calciner. Yet, a higher fresh limestone make-up rate would lead to higher average sorbent conversions in the carbonator, reducing the sorbent looping rate required for 90% capture and thus, the heat requirement in the calciner.

2.2 Routes for energy storage and CO_2 capture

Having analysed the process flow diagrams of the CaL process for CO_2 capture, three viable options for energy storage have been identified (Fig. 1):

- cryogenic O_2 storage,
- $CaO/CaCO_3$ solids storage,
- $CaO/Ca(OH)_2$ solids storage.

During the off-peak period, any of the identified energy storage systems can operate in the charging mode, which means that liquid O_2 is produced and/or the sorbent is regenerated in the calciner (in the CaL-HYD scenario reactivated sorbent is first fed to the carbonator). Under such operating mode, the air separation unit, the CO_2 compression unit and the calciner operate at their

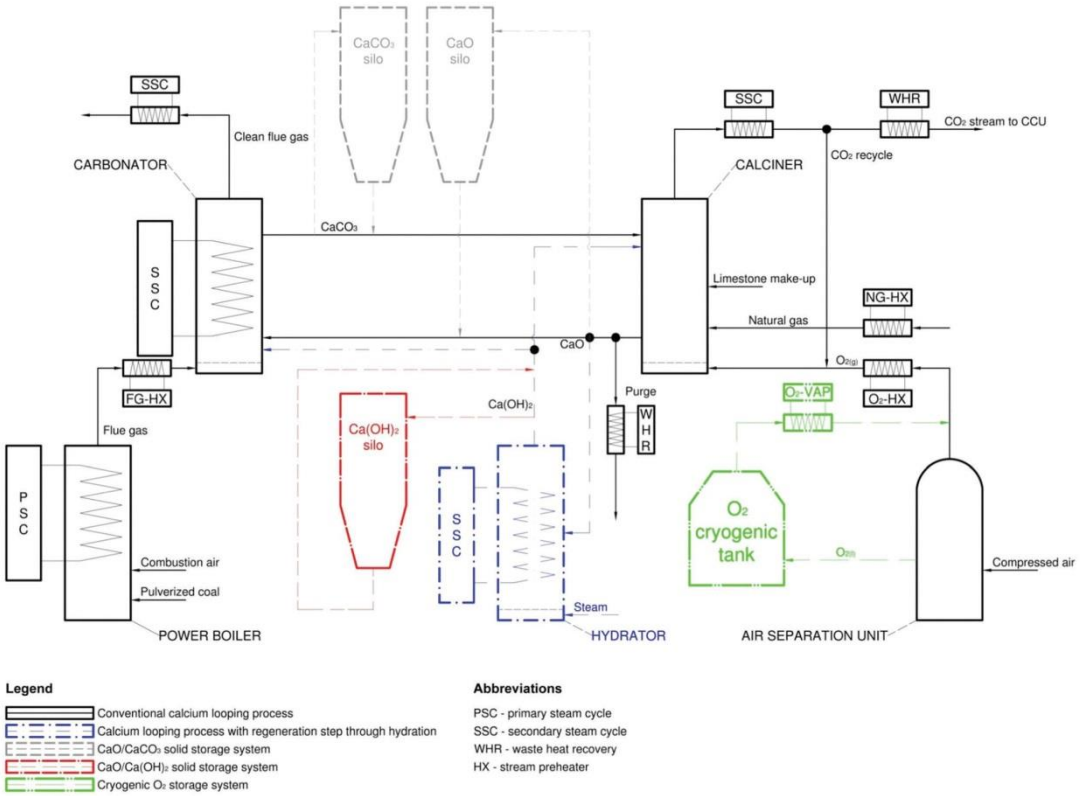

Fig. 1 Schematic of coal-fired power plant retrofitted with calcium looping process for CO_2 capture and energy storage.

nominal capacity, while the power plant operates at its minimum load of 40%. This will lead to higher fuel consumption and higher power consumption for air separation and CO_2 compression compared to the system operating at 40% load without the energy storage. During the peak-demand period, the coal-fired power plant operates at its nominal capacity, while the stored O_2 and/or regenerated sorbent is utilised to unload the air separation unit and the CO_2 compression unit, reducing their power requirements, and to reduce the heat requirement of the calciner. Therefore, the proposed concept would benefit from using more fuel during off-peak periods, storing its chemical energy when the electricity price is low, and using this energy to reduce the fuel consumption and/or the system's power requirement during the peak periods characterised by higher market prices for electricity. Such operation is expected to increase the flexibility and the profitability of the integrated system.

It needs to be highlighted that the carbonator is assumed to follow the power plant load changes, maintaining 90% CO_2 capture. Also, the air separation unit compressors can operate with a minimum load of 75% without recycling or venting, while the cold box operates at a minimum load of 50%.[45] This implies the need for three compression trains and two air separation unit trains to reach the minimum load of around 40% for the entire system. Due to the same minimum constraint, three compression trains are required in the CO_2 compression unit. The calciner, on the other hand, can operate with a minimum load of 25%.[46,47] It is also assumed that liquid O_2 is stored in the cryogenic tank at 1.2 bar at around −182 °C, which is maintained by the waste N_2 leaving the air separation unit,[43] while the sorbent is stored at high temperature in the solid storage tanks. As claimed by Arias *et al.*,[6] the heat losses in the solid storage tanks, characterised by a low surface-to-volume ratio, are negligible. Ma *et al.*[44] showed that storing energy using solid materials, such as ash or sand, in the insulated tanks can reach thermal efficiencies exceeding 99%. Such low heat losses (<1%) are a result of combined effects of highly effective thermal insulation and self-insulation of the particles. Assuming short-term $CaO/CaCO_3$ solids storage (<12 h) in the tanks insulated with concrete walls and refractory lining, which was also considered by Ma *et al.*,[44] heat losses are not expected to affect the process performance by much and thus they are neglected in this concept study. Nevertheless, at the process design stage and for long-term storage (days to weeks), the effect of heat loss on process performance needs to be taken into account.

3 Proof of concept

3.1 Considerations

After identifying possible routes for energy storage in the CaL plant integrated to the coal-fired power plant for CO_2 capture (Fig. 1), the performance of the following scenarios is evaluated:

- CaL (Case 1) and CaL-HYD (Case 4) systems without energy storage;
- CaL (Case 2) and CaL-HYD (Case 5) systems with cryogenic O_2 storage;
- CaL (Case 3) and CaL-HYD (Case 6) systems with $CaO/CaCO_3$ solids storage.

Although other routes for energy storage based on permutations of the identified systems could be analysed, these are unlikely to offer any practical benefit over the selected cases. This is because, in all possible cases for energy storage, the minimum operating load of the calciner is limited by the minimum operating load of the air separation unit and the CO_2 compression unit. Therefore, further reduction in the minimum load of these systems would require additional compressors, leading to higher capital costs. Nevertheless, implementation of the energy storage system utilising the $CaO/Ca(OH)_2$ reaction for energy storage has lower energy density compared to that based on $CaO/CaCO_3$,[13] and thus the heat storage capacity of the system would be lower.

To evaluate performance of the proposed concept, a model of the entire process has been developed in Aspen Plus™[32] with the key assumptions presented in Table 1. In addition to modelling of the CaL or CaL-HYD system, the air separation unit and the CO_2 compression unit were modelled in detail, to reliably assess process performance. The CO_2 capture system was scaled to remove 90% of the flue gas from the reference 660 MW_{el} coal-fired power plant, the process model of which has been described in detail elsewhere.[48] As opposed to the study by Vandersickel *et al.*,[23] the part-load performance of the coal-fired power plant and the secondary steam cycle was evaluated in detail using the framework for part-load modelling presented in Hanak *et al.*[48]

The capacity of energy storage technologies is usually characterised with energy density (D_v) or a specific energy (D_m)

Table 1 Key process model assumptions

Parameter		Value
Carbonator	Temperature (°C)	625
	Carbonation extent (−)	0.70
	Stoichiometric reactor. Average conversion model by Rodríguez *et al.*[49] with deactivation curves derived from experimental data from Sánchez-Biezma *et al.*[50] (non-hydrated sorbent) and Grasa *et al.*[41] (hydrated sorbent)	
Calciner	Temperature (°C)	900
	Calcination extent (−)	0.95
	Relative make up (fresh limestone/sorbent circulation rate) (−)	0.04
	O_2 concentration in the calciner fluidising gas ($\%_{vo,wet}$)	40.0
	O_2 excess ($\%_{vol,dry}$)	2.5
	Gibbs reactor. Gibbs free energy minimisation model	
Hydrator	Temperature (°C)	500
	Steam-to-calcium ratio (molar basis)	1.3
	Stoichiometric reactor. Complete sorbent conversion.	
Secondary steam cycle	Design live/reheat steam temperature (°C)	593.3/593.3
	Design live/reheat steam pressure (bar)	242.3/49.0

defined in eqn (1) and (2) as the ratio of the energy stored (E_{stored}) and the amount of storage media stored ($m_{storage\ media}$), while performance of the power generation systems is characterised with net power output (W_{net}) and net thermal efficiency (η_{th}), which is defined in eqn (3) as the ratio of the net power output and the heat input from fuel combustion (Q_{fuel}). Environmental performance is represented as the specific CO_2 emissions (e_{CO_2}) defined in eqn (4) as the ratio of CO_2 emission rate (m_{CO_2}) and the net power output.

$$D_V = \frac{\dot{E}_{stored}}{3.6 \times \dot{m}_{storage\ media}} \rho_{storage\ media} \quad (1)$$

$$D_m = 1000 \times \frac{\dot{E}_{stored}}{\dot{m}_{storage\ media}} \quad (2)$$

$$\eta_{th} = \frac{\dot{W}_{net}}{\dot{Q}_{fuel}} \quad (3)$$

$$e_{CO_2} = \frac{\dot{m}_{CO_2}}{\dot{W}_{net}} \quad (4)$$

Because energy can be stored in thermal ($CaO/CaCO_3$ solids) and electrical (cryogenic O_2 storage) forms in the proposed concept, the above metrics cannot fully represent the performance of the integrated system. Therefore, the degree of energy utilisation (η_u), which is defined in eqn (5) as the ratio of useful energy and total energy input, is used as a measure of overall process performance. In eqn (5), the useful energy term comprises net power output (W_{net}), electricity stored through cryogenic O_2 storage ($W_{storage,out}$), and heat stored through $CaO/CaCO_3$ solids storage ($Q_{storage,out}$), while the total energy input comprises the chemical energy input from fuel combustion (Q_{fuel}), electricity input through utilisation of stored liquid O_2 ($W_{storage,in}$), and heat input through utilisation of stored $CaO/CaCO_3$ solids ($Q_{storage,in}$). Although the considered forms of energy differ in quality, similar metrics, called degree of fuel utilisation, have been widely applied to assess performance of combined heat and power generation systems.[51]

$$\eta_u = \frac{\dot{W}_{net} + \dot{Q}_{storage,out} + \dot{W}_{storage,out}}{\dot{Q}_{fuel} + \dot{Q}_{storage,in} + \dot{W}_{storage,in}} \quad (5)$$

To assess the profitability of the proposed concepts with respect to the reference coal-fired power plant without CO_2 capture, the levelised cost of electricity (LCOE) and the cost of CO_2 avoided (AC) are calculated according to eqn (6) and (7)[52–54] respectively.

$$LCOE = \frac{TCR \times FCF + FOM}{\dot{W}_{net} \times CF \times 8760} + VOM + \frac{SFC}{\eta} \quad (6)$$

$$AC = \frac{LCOE_{capture} - LCOE_{ref}}{e_{CO_2,ref} - e_{CO_2,capture}} \quad (7)$$

These parameters allow assessing the economic viability of the proposed concept through correlating thermodynamic performance indicators, such as net power output, net thermal efficiency (η), capacity factor (CF) and specific emissions (E_{CO_2}), with economic performance, such as total capital requirement (TCR), variable (VOM) and fixed (FOM) operating costs, specific fuel cost (SFC), and the fixed charge factor (FCF), which considers the system's lifetime and project interest rate.

In addition, considering the average electricity prices in December 2014,[55] the daily profit is calculated. Using the approach employed by Mac Dowell and Shah,[56] eqn (8) allows calculating the daily short-run profit (SRP) as the difference between the daily revenue from electricity sales (R) and daily operating costs associated with fuel consumption (FC), sorbent make-up (SC), CO_2 transport and storage (CTS), and CO_2 emissions (CE).

$$SRP = R - (FC + SC + CTS + CE) \quad (8)$$

The capital cost of the coal-fired power plant and storage equipment is determined using the exponential method function[64] with economic data presented in Table 2. Taking the capital cost for an oxy-fuel circulating-fluidised bed system (C_0) as ref. 58, eqn (9) is employed to estimate the total capital cost of the CaL and CaL-HYD plants (C), considering the volume of the reactors (V) and the heat input to the calciner (Q_{calc}) with the scaling factors of 0.67 and 0.9, respectively. Moreover, the parameter representing the fraction of the total cost of a circulating fluidised bed reactor associated with the heat transfer surfaces (α) is assumed to be 0.85. It needs to be highlighted that in the CaL cases, this equation reduces to the exponential function used by Romano *et al.*[59]

$$C = C_0 \left[\alpha \left(\frac{\dot{Q}_{calc}}{\dot{Q}_0} \right)^{SF,Q} + (1-\alpha) \left(\frac{V_{calc}}{V_0} \right)^{SF,V} + (1-\alpha) \left(\frac{V_{carb}}{V_0} \right)^{SF,V} + (1-\alpha) \left(\frac{V_{hyd}}{V_0} \right)^{SF,V} \right] \quad (9)$$

Fixed and variable operating and maintenance costs are calculated as fractions of total capital cost, while operating costs associated with fuel and sorbent consumption, and CO_2 storage, transport and emission are determined based on process simulation outputs using economic data from Table 2.

Finally, performance of the selected cases for the proposed concept is assessed in the following operating modes:

- Charging mode in which the power plant operates at 40% load, while the considered energy storage system operates at 100% load,
- Discharging mode in which the power plant operates at 100% load, while the considered energy storage system operates at 40% load,
- Daily variable load operation in which the system operates in the charging mode during the off-peak period (11.00 pm – 5.30 am), discharging mode during the morning and evening peak periods (6.00 am – 9.30 am and 4.30 pm – 7.30 pm), and CO_2 capture only mode (no energy storage) in the remaining periods (10:00 am – 4:00 pm and 8:00 pm – 10:30 pm).‡

‡ A hypothetical daily energy demand was adapted from Mac Dowell and Shah.[56]

Table 2 Economic model assumptions

Parameter		Value
Coal-fired power plant	Reference equipment capital cost (€ per kW_{el})[42,52,54,57]	1100
	Reference power output (MW_{el})[42]	575
Calcium looping plant	Reference equipment capital cost (€ per kW_{el})[58]	1252.3
	Reference heat input (MW_{th})[58]	534.0
	Reference reactor volume (m^3)[58]	1150.5
Cryogenic O_2 storage tank	Reference equipment capital cost (€ per m^3)[43]	800 000
	Reference volume (m^3)[43]	2500
Solid storage tank	Reference equipment capital cost (€ per $MW_{th,sensible}$)[44]	8.0
Other economic parameters	Variable cost as a fraction of total capital cost (%)[54,60]	2.0
	Fixed cost as a fraction of total capital cost (%)[54,60]	1.0
	Carbon tax (€ per tCO_2)[54,60]	0.0
	Raw sorbent cost (€ per t)[54,60]	6.0
	CO_2 transport and storage cost (€ per tCO_2)[61]	7.0
	Coal price (€ per t)[60,62]	40.6
	Natural gas price (€ per t)[63]	157.1
	Expected lifetime (years)[54,60]	25
	Project interest rate (%)[54,60]	8.78
	Capacity factor (%)[54,60]	80

3.2 Thermodynamic performance evaluation

A performance analysis conducted for the selected cases (Table 3) revealed that the turndown of the reference coal-fired power plant, which is a ratio of the maximum and minimum net power output reached by the system, was 2.56. Interestingly, similar turndown values were estimated for Case 1 (2.62) and Case 4 (2.60), in which the power plant was retrofitted with the CaL and the CaL-HYD systems for CO_2 capture only, respectively. This is because integration of these systems resulted not only in increase of the maximum net power output by 51.7% and 33.7%, respectively, but it also caused increases in the minimum net power output of 48.3% and 32.0%, respectively. Results presented in Table 3 show also that turndown of the integrated system with cryogenic O_2 storage increased to 3.30 (Case 2) and 3.15 (Case 5), while for the integrated system with $CaO/CaCO_3$ solids storage it reduced to 2.54 (Case 3) and 2.44 (Case 6). It should be noted that in the discharge mode, a reduction in the calciner load to 40% led to reductions in fuel and O_2 requirements, and thus, less high-grade heat was available for recovery from the process streams. This, in turn, resulted in less high-pressure steam generation and a drop in its pressure, which has been estimated according to the Stodola ellipse law;[65] hence lower maximum net power output. Cryogenic O_2 energy storage, therefore, appears to be better suited to balance rapid changes of the energy demand, allowing for immediate increases of net power output by utilising O_2 produced in the air separation unit and stored in the cryogenic tank during the off-peak period. Importantly, a noticeable difference in net power output between the CaL and the CaL-HYD systems arose from differences in the amount of the high-grade heat available for recovery in these systems. Namely, the increase in the average sorbent conversion in the carbonator from 15.8% in the CaL system to 37.8% in the CaL-HYD system resulted in a lower solid looping rate required to achieve 90% CO_2 capture in the carbonator of the latter system. This, in turn, resulted in a

Table 3 Performance indicators for the considered energy storage and CO_2 capture routes[a] for the proposed process

	Reference power plant		Case 1		Case 2		Case 3		Case 4		Case 5		Case 6	
Charging (C)/Discharging (D) performance indicators	C	D	C	D	C	D	C	D	C	D	C	D	C	D
Net power output (MW_{el})	247.0	633.0	366.4	960.0	307.5	1019.5	370.3	941.5	326.1	846.6	282.4	890.8	338.3	824.8
Net thermal efficiency ($\%_{HHV}$)	34.5	38.8	25.7	30.1	21.6	32.0	16.3	40.2	26.2	30.4	22.7	32.0	18.1	38.2
Energy utilisation degree (%)	34.5	38.8	25.7	30.1	25.7	31.4	37.7	33.6	26.2	30.4	26.2	31.5	39.1	32.4
Net efficiency penalty ($\%_{HHV}$)	—		8.8	8.7	12.9	6.8	18.2	−1.5	8.3	8.4	11.8	6.8	16.4	0.6
Energy utilisation degree penalty (%)	—		8.8	8.7	8.8	7.4	−3.2	5.1	8.3	8.4	8.3	7.3	−4.6	6.3
CO_2 intensity factor (gCO_2 per kW_{el} h)	969.0	835.0	65.3	55.0	77.8	51.8	64.6	56.1	73.4	62.4	84.8	59.3	70.7	64.1
Instantaneous performance indicators														
Net power generation turndown (−)	2.56		2.62		3.30		2.54		2.60		3.15		2.44	
Energy density[b] (kW h m^{-3})	—		—		312.0		307.2		—		309.8		483.6	
Specific energy (kJ kg^{-1})	—		—		900		700		—		900		1200	
Daily average performance indicators														
Average daily net thermal efficiency ($\%_{HHV}$)	38.1		29.4		29.5		29.4		29.7		29.8		29.7	
Average daily degree of energy utilisation (%)	38.1		29.4		29.9		33.0		29.7		30.1		33.0	
Average daily CO_2 intensity factor (gCO_2 per kW_{el} h)	853.6		56.4		56.3		56.8		63.9		63.8		64.2	
Economic performance indicators														
Levelised cost of electricity (€ per MW_{el} h)	37.2		82.7		82.7		82.7		74.2		74.2		74.2	
Cost of CO_2 avoided (€ per tCO_2)	—		58.2		58.3		58.3		47.8		47.8		47.8	

[a] Case 1 – CaL with no ES, Case 2 – CaL with cryogenic O_2 storage, Case 3 – CaL with $CaO/CaCO_3$ solids storage, Case 4 – CaL-HYD with no ES, Case 5 – CaL-HYD with cryogenic O_2 storage, Case 6 – CaL-HYD with $CaO/CaCO_3$ solids storage. [b] The unit is kW_{el} h $m^{-3}{}_{O_2}$ in Case 2 and Case 5, and kW_{th} h m^{-3} $CaCO_3$ in Case 3 and Case 6.

reduction of the heat requirement for sorbent regeneration in the calciner, reducing the amount of recoverable heat from the carbonator and the process streams; hence less high-pressure steam was generated and used for power generation in the secondary steam cycle. The results obtained for the integrated system without energy storage were found to be consistent with the predictions by Wang *et al.*,[66] who compared performance of the CaL and the CaL-HYD systems.

Further analysis of process performance revealed that the $CaO/CaCO_3$ solid storage system would yield higher net thermal efficiencies in the discharging mode (40.2%$_{HHV}$ in Case 3 and 38.2%$_{HHV}$ in Case 6), compared to cryogenic O_2 storage (32.0%$_{HHV}$ in both Case 2 and Case 5) and even compared to the reference power plant (38.8%$_{HHV}$). Yet, this is achieved at the expense of much lower net thermal efficiencies in the charging mode (16.3%$_{HHV}$ in Case 3 and 18.1%$_{HHV}$ in Case 6), when the solids converted in the carbonator need to be regenerated. Net thermal efficiency for the cryogenic O_2 storage system operating in the charging mode would result in an even lower efficiency penalty.

Yet, it is important to highlight that in estimation of net thermal efficiency, the net power output was considered as the only source of useful work in the system, while energy stored in the form of heat or electricity has not been taken into account. This can also be seen as the main reason for high net thermal efficiencies estimated for the discharging mode, since the energy input from the energy storage system was not considered. Performance analysis of the proposed concept routes revealed that the system with $CaO/CaCO_3$ storage has 12–13% points higher degree of energy utilisation than the cryogenic O_2 storage system. Yet, this did not directly correlate to system storage capacity. Estimation of energy density for both systems did not give a clear answer as to which system has higher energy storage capacity; for the former it was estimated to be 307.2 and 483.6 kW_{th} h m^{-3} in Case 3 and Case 6, respectively, while for the latter it was 312.0 and 309.8 kW_{el} h m^{-3} in Case 2 and Case 5, respectively. However, direct comparison of these values cannot be used to determine which system has higher energy storage capacity, due to different forms of energy used in the energy density estimation. For cases with the cryogenic O_2 storage system, operation in the charging and discharging mode was found not to affect performance of the secondary steam cycle, compared to the system without energy storage. It can be claimed that changes in net power output in these operating modes were directly related to the amount of thermal energy input in the boiler. By using the gross thermal efficiency of the system operating in the discharging (38.4%$_{HHV}$) and charging mode (34.5%$_{HHV}$), the energy density of cryogenic O_2 storage is recalculated to be 812.4–897.9 kW_{th} h m^{-3}, which is higher than estimated values for the CaL and CaL-HYD with $CaO/CaCO_3$ storage. This implies that to store the same amount of fuel energy, cryogenic O_2 storage would require smaller volume than the $CaO/CaCO_3$ solids storage system, hence lower capital costs.

Incorporation of the sorbent regeneration step through hydration was found to result in a 57.4% increase in energy density and 71.4% increase in specific energy. This can be associated with the increase of average sorbent conversion in the carbonator from 15.8% to 37.8%, resulting in a reduction of unconverted CaO in the stored solids. As a result, the fraction of total thermal energy stored in the form of sensible heat reduced from 39.0% (Case 3) to 24.9% (Case 6), revealing that increased sorbent conversion promotes energy storage through chemical reaction. Also, it was estimated here that, for each percent of sorbent conversion improvement, energy density and the specific energy can be increased by 8 kW_{th} h m^{-3} and 21.6 kJ_{th} kg^{-1}, respectively. Therefore, not only would the systems including reactivation steps, such as the investigated CaL-HYD system with $CaO/CaCO_3$ solids storage, or using more efficient sorbents,[67,68] require smaller reactors (hence lower capital cost), these would also achieve a higher degree of energy utilisation. Moreover, the $CaO/Ca(OH)_2$ step in the proposed concept was used to increase the energy storage capacity of the $CaO/CaCO_3$ system by increasing the average conversion of the sorbent, hence increasing the fraction of $CaCO_3$ in the stored solids. This approach differs from the system investigated by Criado *et al.*,[21] who proposed to use the $CaO/Ca(OH)_2$ system as the primary energy storage system. This approach was found to increase the energy density of the $CaO/CaCO_3$ system to 483.6 kW_{th} h m^{-3}; that is 57% higher than the energy density of the $CaO/CaCO_3$ system without sorbent reactivation (307.2 kW_{th} h m^{-3}) and 86% higher compared to the $CaO/Ca(OH)_2$ system (260 kW_{th} h m^{-3}) evaluated by Criado *et al.*[21] As a result, storage of the same amount of heat would require smaller volume in the $CaO/CaCO_3$ system with sorbent reactivation through hydration compared to the $CaO/Ca(OH)_2$ system, leading to lower capital cost of the entire CO_2 capture system with energy storage, which is proven in the economic analysis presented below. The only downside of using the CaL-HYD instead of the CaL system is marginally higher values for CO_2 intensity factor in most of the cases investigated (Table 3). This is a result of lower net power output for the regenerated system, caused by less high-grade heat available for recovery from the process streams.

Analysis of the hypothetical daily energy demand curve adapted from Mac Dowell and Shah[56] revealed that the daily average degree of energy utilisation in the systems containing $CaO/CaCO_3$ storage (around 33%) and cryogenic O_2 storage (around 30%) was higher than in systems without energy storage (29.4% for Case 1 and 29.7% for Case 4). This implies that the systems with energy storage capability would result in higher degrees of energy utilisation. More importantly, as the periods of charging and discharging were equal in the hypothetical operating schedule, the average daily net thermal efficiency and the average daily CO_2 intensity factor were not affected much compared to the system without energy storage. Finally, the process evaluated in this study can conceptually be integrated with a solar power plant or wind turbine farm to utilise excess energy for sorbent regeneration or for liquid O_2 production, which can be utilised later to increase net thermal efficiency and the degree of energy utilisation.

3.3 Economic performance evaluation

The specific capital costs of the reference coal-fired power plant, the CaL system (Case 1) and the CaL-HYD system (Case 4) have

been estimated to be 1206.5 € per $kW_{el,gross}$, 2981.6 € per $kW_{el,gross}$ and 2776.4 € per $kW_{el,gross}$, respectively. This is in agreement with other studies, which assumed the specific capital costs for coal-fired power plants of 1200 € per $kW_{el,gross}$ and for the CaL system of 2500–3000 € per $kW_{el,gross}$.[25,52–54] Moreover, specific capital cost of the integrated CaL and CaL-HYD systems was estimated to be 2023.4 € per $kW_{el,gross}$ and 1799.1 € per $kW_{el,gross}$, respectively, which is close to the range 1250–1740 € per $kW_{el,gross}$ estimated in other studies.[42,52,54] A slightly higher specific capital cost obtained in this study is caused by the assumption of maximising heat recovery for power generation in the CaL and CaL-HYD plants. Also, the higher energy density due to sorbent regeneration in Case 6, compared to Case 3, reduces the specific capital cost of the entire system. An additional capital cost associated with cryogenic O_2 storage and $CaO/CaCO_3$ solid storage increases the specific capital cost of the integrated CaL system only by 0.6 € per $kW_{el,gross}$ (Case 2) and 2.3 € per $kW_{el,gross}$ (Case 3), and of the CaL-HYD by 0.6 € per $kW_{el,gross}$ (Case 5) and 1.4 € per $kW_{el,gross}$ (Case 6). Hence, addition of energy storage capability does not change the levelised cost of electricity, the value of which is in agreement with results from Romano *et al.*[59] and Yang *et al.*,[54] and has a negligible effect on the cost of CO_2 avoided (Table 3). Therefore, the inherent energy storage ability of the CaL and CaL-HYD systems is available at a very low additional capital cost to the CO_2 capture system.

Implementation of the CaL (Case 1) and the CaL-HYD (Case 4) plants for CO_2 capture will reduce the daily short run profit by 15.0% and 17.2% (Fig. 2), respectively, regardless of the better thermodynamic performance of Case 4 identified previously. This is due to 7.2% lower net power output in Case 4 with respect to Case 1 and thus lower expected revenue from electricity sales. Furthermore, addition of the cryogenic O_2 storage was found to increase the daily short-run profit of the CaL (Case 2) and CaL-HYD (Case 5) plants by 2.3% and 2.2%, respectively. Conversely, addition of the $CaO/CaCO_3$ solid storage system was found to slightly reduce the daily short-run profit of the CaL (Case 3) and CaL-HYD (Case 6) by 0.1% and 0.2%, respectively; yet it will increase the plant flexibility. Therefore, it appears as if the cryogenic O_2 storage system was more economically substantiated. Yet, with the secondary steam cycle designed for normal operating mode without energy storage, part-load operation of the calciner in discharging mode reduces the amount of recoverable heat that results in reduction of net power output in Case 3 and Case 6 by 0.2% and 0.3%, respectively.

As electricity prices are subject to annual fluctuations and to seasonal changes, the effect of the price difference, which is defined as change of the electricity price with respect to the reference value over the considered period, on the daily short-run profit, is evaluated. On increasing the daily price difference (Fig. 3a), it was found that the concepts proposed in Case 2 and Case 3 would generate the same daily short-run profit as the reference coal-fired power plant without CO_2 capture if the daily price of electricity increases by 12.5 € per MW_{el} h and 14.8 € per MW_{el} h, respectively, while the CaL plant without energy storage will break even at the 14.4 € per MW_{el} h increase in price difference. For the cases with sorbent regeneration through hydration, higher daily short-run profit would be achieved on increased price difference of 22.6–26.0 € per MW_{el} h, with the lowest increase associated to Case 5. Moreover, increased peak price difference (Fig. 3b) of more than 27.4 € per MW_{el} h and 49.2 € per MW_{el} h, would make the CaL (Case 2) and the CaL-HYD (Case 5) more economical than the reference coal-fired power plant. In addition, it was found that reduction of off-peak prices (Fig. 3c) will not bring any additional benefit, as the loss of profit in the charging mode during low electricity price periods outweighs the benefits of discharging mode operated at peak times with higher prices. Nevertheless, this analysis revealed that the proposed concept, in particular the CaL plant with cryogenic O_2 storage system (Case 2), could generate daily short-run profit higher than the reference coal-fired power plant depending on the daily spot prices of electricity. Further increase of the profit can be achieved on determination of the optimal charging and discharging times, using optimisation methodology developed by Barbour *et al.*[69]

Finally, economic performance of the proposed concepts is highly dependent upon the economic climate, as it is predicted that the carbon tax may vary between 10–150 € per tCO_2.[70,71] Moreover, economic performance will vary depending on whether the produced CO_2 is transported and stored (the costs for which vary between 2.5–36 € per tCO_2[62,72] depending on the CO_2 transport

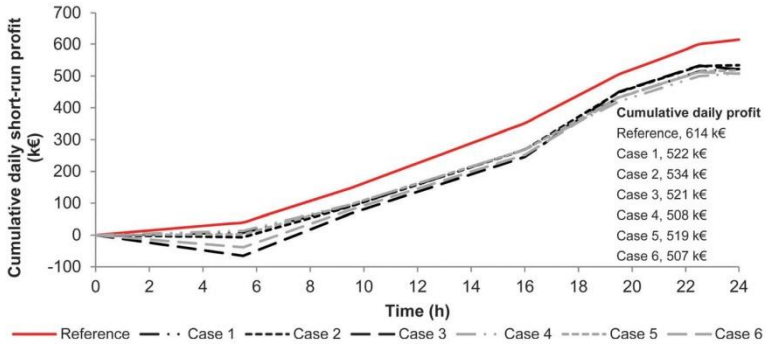

Fig. 2 Comparison of the daily short-run profit.

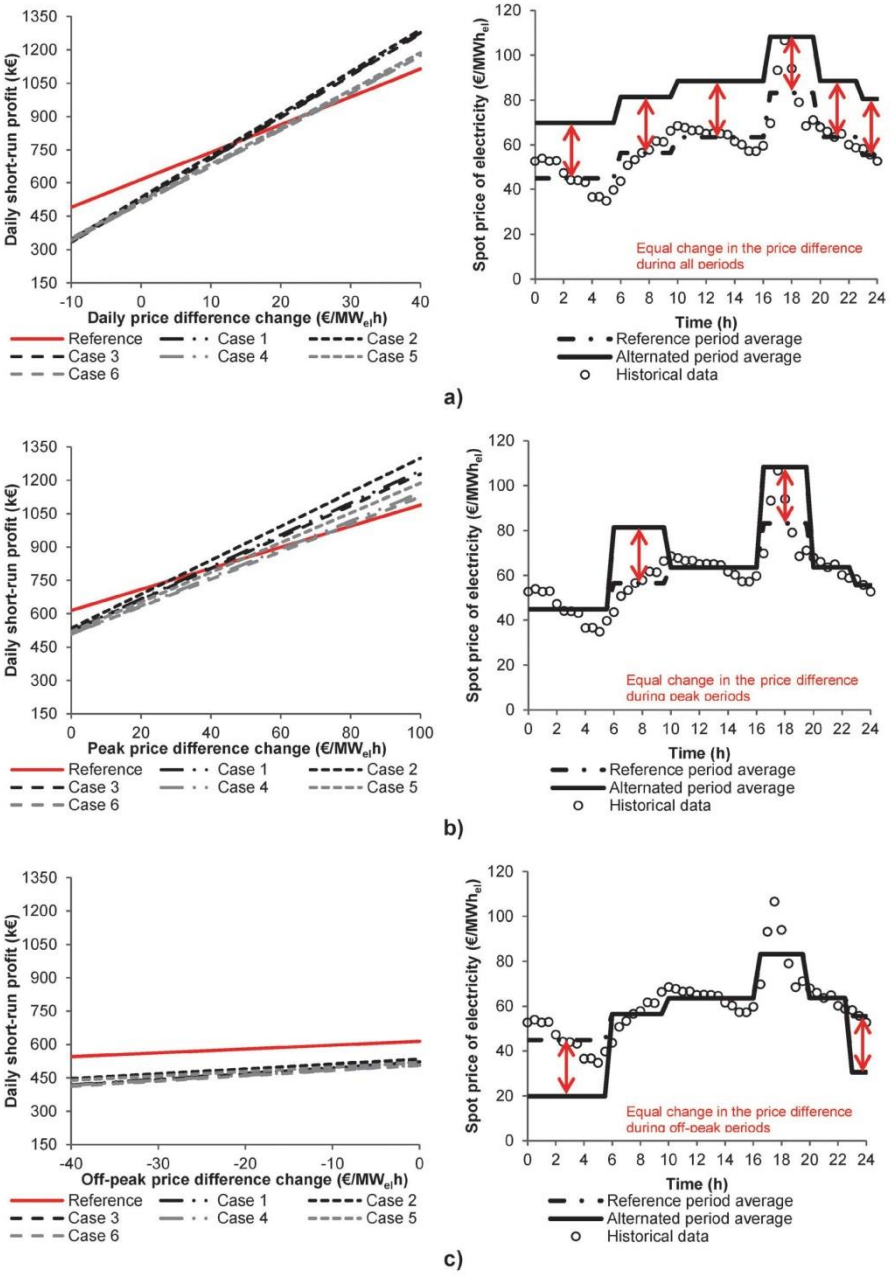

Fig. 3 Effect of a change in the (a) daily (b) peak and (c) off-peak price difference on daily short-run profit.

method and storage location), or used, for example, for enhanced oil recovery at a supply price of 12–15 € per tCO_2.[73,74] Fig. 4a reveals that the daily short-run profit of the reference coal-fired power plant is highly affected by increases in the carbon tax, while it is hardly affected in the remaining cases with 90% CO_2 capture. Importantly, when the carbon tax exceeds 8.3 € per tCO_2 for Case 2 (which is lower than the average price of 8.5 € per tCO_2 for the European emission allowances in November 2015[75]), and 11.1 € per tCO_2 for Case 6, the proposed concepts become more profitable than the reference coal-fired

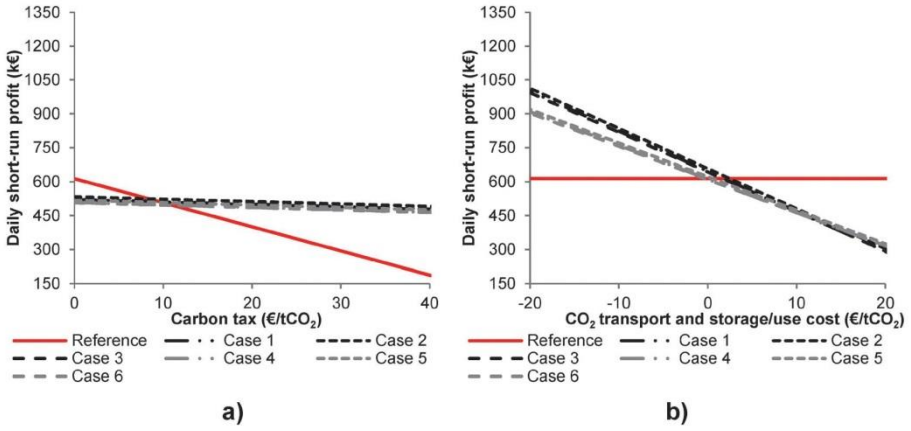

Fig. 4 Effect of (a) carbon tax and (b) cost of CO_2 transport and storage/use on daily short-run profit.

power plant. This implies that the proposed concept (Case 2) is already more profitable than the reference coal-fired power plant without CO_2 capture.

Furthermore, it can be seen in Fig. 4b that for the specific cost for CO_2 capture and transport of 2.5 € per tCO_2, the daily short-run profit for Case 2 is equal to that generated by the reference coal-fired power plant. On the other hand, for Case 6 to become more profitable than the reference coal-fired power plant, CO_2 would need to be sold for industrial use at prices higher than 0.3 € per tCO_2, which corresponds to negative values in Fig. 4b. This shows that the profitability of the proposed concepts could greatly exceed that of the reference coal-fired power plant, if pure CO_2 produced in the proposed concepts is industrially utilised, even at low price.

4. Conclusions

In this study, a concept for the CO_2 capture plant based on CaL with inherent energy storage is proposed and evaluated in the coal-fired power plant retrofit scenario. The CaL was previously proposed for energy storage from solar power plants; however, challenges such as the requirement for temporary CO_2 storage and sorbent deactivation were identified. These were resolved in the proposed system as the power plant acts as a permanent source of CO_2 and hydration was used as a means for sorbent regeneration.

Analysis of the process revealed that possible routes for energy storage include $CaO/CaCO_3$ solids storage, $CaO/Ca(OH)_2$ solids storage and cryogenic O_2 storage systems. The comparison of $CaO/CaCO_3$ and cryogenic O_2 storage systems revealed that implementation of the latter would result in higher turndown of the entire system and offer higher energy density, hence requiring lower capital cost. Although performance of the integrated system with energy storage through a $CaO/Ca(OH)_2$ loop was not evaluated here due to the lower energy density of such system, the reactivation step was found critical in improving the performance of the $CaO/CaCO_3$ energy storage system. Not only did it increase net thermal efficiency, it increased the energy density by 57.4% and specific energy by 71.4% leading to a higher degree of energy utilisation. Importantly, the proposed CaL-HYD system with $CaO/CaCO_3$ energy storage was found to offer 86% higher energy density than the conventional $CaO/Ca(OH)_2$ energy storage system. An increase in the energy density was found to be important from the economic perspective, as storing the same amount of heat in a lower volume would result in the specific capital cost of the CaL-HYD system lower by 6.8% compared to the CaL system.

The economic performance evaluation conducted revealed that the addition of energy storage capability to the CaL and the CaL-HYD plants for CO_2 capture from the coal-fired power plant has a low impact on the total capital cost and thus on the levelised cost of electricity and the cost of CO_2 avoided. Moreover, analysis of the daily short-run profit revealed that Case 2, in which the CaL plant was equipped with the cryogenic O_2 storage system, will reduce the daily short-run profit of the coal-fired power plant by 15.0%. This case was found to have the lowest impact on system profitability. Yet, the proposed concept (Case 2) can generate higher profit when the carbon tax exceeds 8.3 € per tCO_2. As the price of the European emission allowances in November 2015 was 8.5 € per tCO_2, the proposed concept is already more profitable than the reference coal-fired power plant without CO_2 capture.

Further studies will aim to provide a detailed design of the proposed concepts of CO_2 capture with inherent energy storage for decarbonisation and to optimise the charging and discharging times to maximise the daily short-run profit. Also, the applicability of the proposed concepts in natural gas combined cycle power plants will be assessed. Finally, the inherent energy storage capability of other clean power technologies, such as chemical looping combustion and oxy-combustion, will be assessed.

Nomenclature

AC	Cost of CO_2 avoided, € per tCO_2
C	Capital cost of calcium looping system, € per kW_{el}

C_0	Reference capital cost of oxy-fuel circulating fluidised bed system, € per kW_{el}
CE	CO_2 emission cost, €
CF	Capacity factor, —
CTS	CO_2 transport and storage cost, €
D_V	Energy density, kW h m^{-3}
D_m	Specific energy, kJ kg^{-1}
e_{CO_2}	Specific CO_2 emission, gCO_2 per kW_{el} h
$\dot{E}_{stored}$	Rate of energy to storage, MW
FC	Fuel cost, €
FCF	Fixed charge factor, —
FOM	Fixed operating and maintenance cost, €
LCOE	Levelised cost of electricity, € per MW h
$\dot{m}_{CO_2}$	Rate of CO_2 emission, kg s^{-1}
$\dot{m}_{storage\ media}$	Rate of media to storage, kg s^{-1}
R	Revenue from electricity sales, €
SC	Sorbent make-up cost, €
SCF	Specific fuel cost, € per MW h
SF,q	Scaling factor for reactor heat input, —
SF,v	Scaling factor for reactor volume, —
SRP	Daily short run profit, €
TCR	Total capital requirement, €
$\dot{Q}_0$	Reference heat input, MW_{th}
$\dot{Q}_{calc}$	Heat input to the calciner, MW_{th}
$\dot{Q}_{fuel}$	Chemical energy input from fuel combustion, MW
$\dot{Q}_{storage,in}$	Heat input from $CaO/CaCO_3$ solids storage, MW
$\dot{Q}_{storage,out}$	Heat stored through $CaO/CaCO_3$ solids storage, MW
V	Volume of reactors, m^3
V_0	Reference volume of reactor, m^3
VOM	Variable operating and maintenance cost, € per MW h
$\dot{W}_{net}$	Net power output of the integrated system, MW
$\dot{W}_{storage,in}$	Electricity input from cryogenic O_2 storage, MW
$\dot{W}_{storage,out}$	Electricity stored through cryogenic O_2 storage, MW
α	Fraction of the total cost of a circulating fluidised bed reactor associated with the heat transfer surfaces, —
η_{th}	Net thermal efficiency, —
η_u	Degree of energy utilisation, —

Abbreviations

CaL	Calcium looping process
CaL-HYD	Calcium looping process with sorbent reactivation step through hydration
CCS	Carbon capture and storage

References

1 IEA, *Energy technology perspectives 2012: pathways to a clean energy system*, IEA Publications, Paris, France, 2012.
2 IEA, *Technology Roadmap: carbon capture and storage*, IEA Publications, Paris, France, 2013.
3 J. Twidell and A. D. Weir, *Renewable energy resources*, Taylor & Francis, London, UK and New York, USA, 2006, vol. 2.
4 R. Jiang, J. Wang and Y. Guan, Robust unit commitment with wind power and pumped storage hydro, *IEEE Trans. Power Appar. Syst.*, 2012, **27**, 800–810.
5 M. Singh, V. Khadkikar, A. Chandra and R. K. Varma, Grid interconnection of renewable energy sources at the distribution level with power-quality improvement features, *IEEE Trans. Power Delivery*, 2011, **26**, 307–315.
6 B. Arias, Y. A. Criado, A. Sanchez-Biezma and J. C. Abanades, Oxy-fired fluidized bed combustors with a flexible power output using circulating solids for thermal energy storage, *Appl. Energy*, 2014, **132**, 127–136.
7 IEA, *Technology Roadmap: Energy Storage*, IEA Publications, Paris, France, 2014.
8 B. C. Ummels, E. Pelgrum and W. L. Kling, Integration of large-scale wind power and use of energy storage in the Netherlands' electricity supply, *IET Renew. Power Gener.*, 2008, **2**, 34–46.
9 A. Tuohy and M. O'Malley, Pumped storage in systems with very high wind penetration, *Energy Policy*, 2011, **39**, 1965–1974.
10 DOE, *DOE Global Energy Storage Database*, 2015, available at: www.energystorageexchange.org.
11 H. Chen, T. N. Cong, W. Yang, C. Tan, Y. Li and Y. Ding, Progress in electrical energy storage system: a critical review, *Prog. Nat. Sci.*, 2009, **19**, 291–312.
12 D. O. Akinyele and R. K. Rayudu, Review of energy storage technologies for sustainable power networks, *Sustain. Energy Technol. Assessments*, 2014, **8**, 74–91.
13 A. Gil, M. Medrano, I. Martorell, A. Lázaro, P. Dolado, B. Zalba and L. F. Cabeza, State of the art on high temperature thermal energy storage for power generation. Part 1-Concepts, materials and modellization, *Renewable Sustainable Energy Rev.*, 2010, **14**, 31–55.
14 T. M. I. Mahlia, T. J. Saktisahdan, A. Jannifar, M. H. Hasan and H. S. C. Matseelar, A review of available methods and development on energy storage: technology update, *Renewable Sustainable Energy Rev.*, 2014, **33**, 532–545.
15 P. Pardo, A. Deydier, Z. Anxionnaz-Minvielle, S. Rougé, M. Cabassud and P. Cognet, A review on high temperature thermochemical heat energy storage, *Renewable Sustainable Energy Rev.*, 2014, **32**, 591–610.
16 A. Sharma, V. V Tyagi, C. R. Chen and D. Buddhi, Review on thermal energy storage with phase change materials and applications, *Renewable Sustainable Energy Rev.*, 2009, **13**, 318–345.
17 Y. Hou, R. Vidu and P. Stroeve, Solar energy storage methods, *Ind. Eng. Chem. Res.*, 2011, **50**, 8954–8964.
18 T. Yan, R. Z. Wang, T. X. Li, L. W. Wang and I. T. Fred, A review of promising candidate reactions for chemical heat storage, *Renewable Sustainable Energy Rev.*, 2015, **43**, 13–31.
19 G. Ervin, Solar heat storage using chemical reactions, *J. Solid State Chem.*, 1977, **22**, 51–61.
20 R. Baker, The reversibility of the reaction $CaCO_3 \rightleftarrows CaO + CO_2$, *J. Appl. Chem. Biotechnol.*, 1973, **23**, 733–742.
21 Y. A. Criado, M. Alonso, J. C. Abanades and Z. Anxionnaz-Minvielle, Conceptual process design of a $CaO/Ca(OH)_2$

thermochemical energy storage system using fluidized bed reactors, *Appl. Therm. Eng.*, 2014, **73**, 1085–1092.
22 S. E. B. Edwards and V. Materic, Calcium looping in solar power generation plants, *Sol. Energy*, 2012, **86**, 2494–2503.
23 A. Vandersickel, R. P. Field, W. Chen, N. D. Mancini and A. Mitsos, CaO-based energy and CO_2 storage system for the flexibilization of an IGCC plant with carbon capture, *Ind. Eng. Chem. Res.*, 2014, **53**, 12032–12043.
24 T. Shimizu, T. Hirama, H. Hosoda, K. Kitano, M. Inagaki and K. Tejima, A Twin Fluid-Bed Reactor for Removal of CO_2 from Combustion Processes, *Chem. Eng. Res. Des.*, 1999, **77**, 62–68.
25 L. M. Romeo, J. C. Abanades, J. M. Escosa, J. Paño, A. Giménez, A. Sánchez-Biezma and J. C. Ballesteros, Oxyfuel carbonation/calcination cycle for low cost CO_2 capture in existing power plants, *Energy Convers. Manage.*, 2008, **49**, 2809–2814.
26 I. Martínez, R. Murillo, G. Grasa and J. Carlos Abanades, Integration of a Ca looping system for CO_2 capture in existing power plants, *AIChE J.*, 2011, **57**, 2599–2607.
27 J. C. Abanades, E. J. Anthony, J. Wang and J. E. Oakey, Fluidized Bed Combustion Systems Integrating CO_2 Capture with CaO, *Environ. Sci. Technol.*, 2005, **39**, 2861–2866.
28 I. Vorrias, K. Atsonios, A. Nikolopoulos, N. Nikolopoulos, P. Grammelis and E. Kakaras, Calcium looping for CO_2 capture from a lignite fired power plant, *Fuel*, 2013, **113**, 826–836.
29 M. E. Boot-Handford, J. C. Abanades, E. J. Anthony, M. J. Blunt, S. Brandani, N. Mac Dowell, J. R. Fernandez, M. C. Ferrari, R. Gross, J. P. Hallett, R. S. Haszeldine, P. Heptonstall, A. Lyngfelt, Z. Makuch, E. Mangano, R. T. J. Porter, M. Pourkashanian, G. T. Rochelle, N. Shah, J. G. Yao and P. S. Fennell, Carbon capture and storage update, *Energy Environ. Sci.*, 2014, **7**, 130–189.
30 H. M. Kvamsdal, M. C. Romano, L. van der Ham, D. Bonalumi, P. van Os and E. Goetheer, Energetic evaluation of a power plant integrated with a piperazine-based CO_2 capture process, *Int. J. Greenhouse Gas Control*, 2014, **28**, 343–355.
31 K. Goto, K. Yogo and T. Higashii, A review of efficiency penalty in a coal-fired power plant with post-combustion CO_2 capture, *Appl. Energy*, 2013, **111**, 710–720.
32 D. P. Hanak, C. Biliyok, E. J. Anthony and V. Manovic, Modelling and comparison of calcium looping and chemical solvent scrubbing retrofits for CO_2 capture from coal-fired power plant, *Int. J. Greenhouse Gas Control*, 2015, **42**, 226–236.
33 L. M. Romeo, Y. Lara, P. Lisbona and J. M. Escosa, Optimizing make-up flow in a CO_2 capture system using CaO, *Chem. Eng. J.*, 2009, **147**, 252–258.
34 J. Ströhle, A. Lasheras, A. Galloy and B. Epple, Simulation of the carbonate looping process for post-combustion CO_2 capture from a coal-fired power plant, *Chem. Eng. Technol.*, 2009, **32**, 435–442.
35 V. Manovic and E. J. Anthony, Steam reactivation of spent CaO-based sorbent for multiple CO_2 capture cycles, *Environ. Sci. Technol.*, 2007, **41**, 1420–1425.
36 J. C. Abanades, The maximum capture efficiency of CO_2 using a carbonation/calcination cycle of $CaO/CaCO_3$, *Chem. Eng. J.*, 2002, **90**, 303–306.
37 G. S. Grasa, J. C. Abanades, M. Alonso and B. González, Reactivity of highly cycled particles of CaO in a carbonation/calcination loop, *Chem. Eng. J.*, 2008, **137**, 561–567.
38 G. S. Grasa and J. C. Abanades, CO_2 capture capacity of CaO in long series of carbonation/calcination cycles, *Ind. Eng. Chem. Res.*, 2006, **45**, 8846–8851.
39 W. Wang, S. Ramkumar, S. Li, D. Wong, M. Iyer, B. B. Sakadjian, R. M. Statnick and L.-S. Fan, Subpilot demonstration of the carbonation-calcination reaction (CCR) process: high-temperature CO_2 and sulfur capture from coal-fired power plants, *Ind. Eng. Chem. Res.*, 2010, **49**, 5094–5101.
40 V. Materic, R. Symonds, D. Lu, R. Holt and V. Manovic, Performance of hydration reactivated Ca looping sorbents in a pilot-scale, oxy-fired dual fluid bed unit, *Energy Fuels*, 2014, **28**, 5363–5372.
41 G. Grasa, R. Murillo, M. Alonso, B. González, N. Rodríguez and J. C. Abanades, Steam reactivation of CaO-based natural sorbents applied to a carbonation/calcination loop for CO_2 capture, in 4th International Conference on Clean Coal Technologies, Dresden, Germany, 2009.
42 P. Lisbona, A. Martínez, Y. Lara and L. M. Romeo, Integration of carbonate CO_2 capture cycle and coal-fired power plants. A comparative study for different sorbents, *Energy Fuels*, 2010, **24**, 728–736.
43 Y. Hu, X. Li, H. Li and J. Yan, Peak and off-peak operations of the air separation unit in oxy-coal combustion power generation systems, *Appl. Energy*, 2013, **112**, 747–754.
44 Z. Ma, G. Glatzmaier and M. Mehos, Fluidized Bed Technology for Concentrating Solar Power With Thermal Energy Storage, *J. Sol. Energy Eng.*, 2014, **136**, 031014.
45 N. Perrin, R. Dubettier, F. Lockwood, J.-P. Tranier, C. Bourhy-Weber and P. Terrien, Oxycombustion for coal power plants: advantages, solutions and projects, *Appl. Therm. Eng.*, 2014, **74**, 75–82.
46 R. C. Brown and J. E. Foley, Method for improving load turndown in fluidised bed combustors, *Ind. Eng. Chem. Res.*, 1988, **27**, 24–30.
47 H. Kobro and C. Brereton, Control and fuel flexibility of circulating fluidised bed, Circ. Fluid. Bed Technol. Proc. First Int. Conf., 1986, p. 263.
48 D. P. Hanak, C. Biliyok and V. Manovic, Evaluation and Modeling of Part-Load Performance of Coal-Fired Power Plant with Postcombustion CO_2 Capture, *Energy Fuels*, 2015, **29**, 3833–3844.
49 N. Rodríguez, M. Alonso and J. C. Abanades, Average activity of CaO particles in a calcium looping system, *Chem. Eng. J.*, 2010, **156**, 388–394.
50 A. Sánchez-Biezma, J. Paniagua, L. Diaz, M. Lorenzo, J. Alvarez, D. Martínez, B. Arias, M.E. Diego and J.C. Abanades, Testing postcombustion CO_2 capture with CaO in a 1.7 MWt pilot facility, GHGT-11, 2013, vol. 37, pp. 1–8.
51 H. Rusinowski, *Diagnostyka cieplna eksploatacji w energetyce (thermal identification in power engineering)*, Polska Akademia Nauk, Katowice, Poland (in Polish), 2010.

52 J. C. Abanades, G. Grasa, M. Alonso, N. Rodriguez, E. J. Anthony and L. M. Romeo, Cost structure of a postcombustion CO_2 capture system using CaO, *Environ. Sci. Technol.*, 2007, **41**, 5523–5527.
53 M. Zhao, A. I. Minett and A. T. Harris, A review of techno-economic models for the retrofitting of conventional pulverised-coal power plants for post-combustion capture (PCC) of CO_2, *Energy Environ. Sci.*, 2013, **6**, 25–40.
54 Y. Yang, R. Zhai, L. Duan, M. Kavosh, K. Patchigolla and J. Oakey, Integration and evaluation of a power plant with a CaO-based CO_2 capture system, *Int. J. Greenhouse Gas Control*, 2010, **4**, 603–612.
55 APX, APX Power UK Auction, http://bit.ly/1RgNHui, 2015.
56 N. Mac Dowell and N. Shah, The multi-period optimisation of an amine-based CO_2 capture process integrated with a super-critical coal-fired power station for flexible operation, *Comput. Chem. Eng.*, 2015, **74**, 169–183.
57 E. S. Rubin, C. Chen and A. B. Rao, Cost and performance of fossil fuel power plants with CO_2 capture and storage, *Energy Policy*, 2007, **35**, 4444–4454.
58 J. Marion, N. Nsakala and R. McWhinnie, *Greenhouse Gas Emissions Control By Oxygen Firing In Circulating Fluidized Bed Boilers: Phase 1-A Preliminary Systems Evaluation*, 2003, vol. 2.
59 M. C. Romano, M. Spinelli, S. Campanari, S. Consonni, G. Cinti, M. Marchi and E. Borgarello, The Calcium Looping Process for Low CO_2 Emission Cement and Power, *Energy Procedia*, 2013, **37**, 7091–7099.
60 A. Martínez, Y. Lara, P. Lisbona and L. M. Romeo, Operation of a mixing seal valve in calcium looping for CO_2 capture, *Energy Fuels*, 2014, **28**, 2059–2068.
61 M. C. Romano, I. Martínez, R. Murillo, B. Arstad, R. Blom, D. C. Ozcan, H. Ahn and S. Brandani, Process simulation of Ca-looping processes: review and guidelines, in 11th International Conference on Greenhouse Gas Control Technologies, GHGT 2012, 2013, vol. 37, pp. 142–150.
62 H. C. Mantripragada and E. S. Rubin, Calcium looping cycle for CO_2 capture – performance, cost and feasibility analysis, *Energy Procedia*, 2013, **63**, 2199–2206.
63 EIA, *Annual energy outlook 2015 with projections to 2040*, U.S. Energy Information Administration, Washington, DC, USA, 2015.
64 R. H. Perry, D. W. Green and J. O. Maloney, *Perry's chemical engineers' handbook*, McGraw-Hill, New York, 2007, vol. 796.
65 D. H. Cooke, *Modelling of off-design multistage turbine pressures by Stodola's ellipse*, Bechtel Power Corporation, 1983.
66 W. Wang, S. Ramkumar and L. Fan, Energy penalty of CO_2 capture for the Carbonation–Calcination Reaction (CCR) Process: Parametric Effects and Comparisons with Alternative Processes, 10th Japan/China Symp. Coal C1 Chem., 2013, vol. 104, pp. 561–574.
67 J. Blamey, E. J. Anthony, J. Wang and P. S. Fennell, The calcium looping cycle for large-scale CO_2 capture, *Prog. Energy Combust. Sci.*, 2010, **36**, 260–279.
68 A. M. Kierzkowska, R. Pacciani and C. R. Müller, CaO-based CO_2 sorbents: from fundamentals to the development of new, highly effective materials, *ChemSusChem*, 2013, **6**, 1130–1148.
69 E. Barbour, I. a. G. Wilson, I. G. Bryden, P. G. McGregor, P. a. Mulheran and P. J. Hall, Towards an objective method to compare energy storage technologies: development and validation of a model to determine the upper boundary of revenue available from electrical price arbitrage, *Energy Environ. Sci.*, 2012, **5**, 5425.
70 DECC, *Updated energy and emissions projections 2014*, Department of Energy and Climate Change, London, UK, 2014.
71 EIA, *Energy market and economic impacts of the American Power Act of 2010*, U.S. Energy Information Administration, Washington, DC, USA, 2010.
72 ZEP, *The costs of CO_2 capture, transport and storage,* Zero Emission Platform, 2011.
73 R. Mendelevitch, The role of CO_2-EOR for the development of a CCTS infrastructure in the North Sea Region, *Int. J. Greenhouse Gas Control*, 2014, **20**, 132–159.
74 Gccsi, *Accelerating the uptake of CCS: industrial use of captured carbon dioxide*, Global Carbon Capture and Storage Institute, Parsons Brinckerhoff, Docklands, Australia, 2011.
75 EEX, *European Emission Allowances (EUA). Global Environmental Exchange*, European Energy Exchange, Leipzig, Germany, 2015.

10 PROBABILISTIC PERFORMANCE ASSESSMENT OF A COAL-FIRED POWER PLANT

Dawid P. Hanak, Athanasios J. Kolios, Chechet Biliyok and Vasilije Manovic

Published: Applied Energy, 2015, 139, 350–364[k]

Statement of contributions of joint authorship

Dawid P. Hanak conducted the literature review, performed process analysis via process modelling and simulation, and probabilistic analysis, drafted and critically revised the manuscript, as well as prepared tables and figures. Athanasios J. Kolios supported adaptation of the probabilistic analysis and critically commented on the manuscript. Chechet Biliyok and Vasilije Manovic proof-read and critically commented on the manuscript prior to its submission to Applied Energy (Journal Impact Factor 2016: 5.613).

Dawid P. Hanak, PhD Candidate

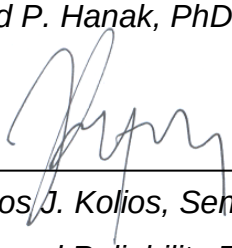

Athanasios J. Kolios, Senior lecturer in Risk and Reliability Engineering

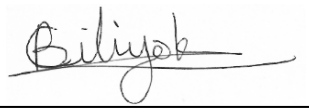

Chechet Biliyok, Associate supervisor

Vasilije Manovic, Principal supervisor

[k] Reprinted with permission from Hanak, D.P., Kolios, A.J., Biliyok, C., and Manovic, V. (2015), "Probabilistic performance assessment of a coal-fired power plant", *Applied Energy*, 139, 350–364, doi: 10.1016/j.apenergy.2014.10.079, Elsevier 2015.

Applied Energy 139 (2015) 350–364

Contents lists available at ScienceDirect

Applied Energy

journal homepage: www.elsevier.com/locate/apenergy

Probabilistic performance assessment of a coal-fired power plant

D.P. Hanak *, A.J. Kolios, C. Biliyok, V. Manovic

Energy and Power Engineering Division, School of Engineering, Cranfield University, Bedford, Bedfordshire MK43 0AL, UK

HIGHLIGHTS

- Power plant equipment is usually oversized to account for input uncertainties.
- Oversized equipment degrades its rated efficiency and increases capital cost.
- A stochastic methodology to assess probabilities of equipment failure was proposed.
- The methodology was proven applicable for design and analysis of the power plants.
- Estimated high reliability indices allow reducing power plant equipment oversizing.

ARTICLE INFO

Article history:
Received 30 June 2014
Received in revised form 14 October 2014
Accepted 26 October 2014
Available online 27 November 2014

Keywords:
Probabilistic performance assessment
Coal-fired power plant
Stochastic modelling
Stochastic response surface method
Monte Carlo simulation

ABSTRACT

Despite the low-carbon environmental policies, coal is expected to remain a main source of energy in the coming decades. Therefore, efficient and environmentally friendly power systems are required. A design process based on the deterministic models and application of the safety factors leads to the equipment oversizing, hence fall in the efficiency and increase in the capital and operating costs. In this work, applicability of a non-intrusive stochastic methodology to determine the probability of the power plant equipment failure was investigated. This alternative approach to the power plant performance assessment employs approximation methods for the deterministic prediction of the key performance indicators, which are used to estimate reliability indices based on the uncertainty of the input to a process model of the coal-fired power plant. This study revealed that high reliability indices obtained in the analysis would lead to reduced application of conservative safety factors on the plant equipment, which should result in lower capital and operating cost, through a more reliable assessment of its performance state over its service time, and lead to the optimisation of its inspection and maintenance interventions.

1. Introduction

Despite the environmental concern caused by greenhouse gas emissions from the power sector, coal remains a key primary energy resource globally [1,2] and its share in the energy mix has recently increased in countries such as Germany, Spain, China and the United Kingdom, mainly due to the emergence of shale gas [3–5]. Although this trend is inconsistent with the low-carbon scenarios, it is expected to continue as the global coal demand is predicted to increase from 155 EJ to 186 EJ between 2011 and 2018. Additionally, the coal demand in China alone is projected to increase by 24%, from 75 EJ to 93 EJ between 2011 and 2017 [3,6]. Nowadays, the global fleet of the coal-fired power plants operates with an average net thermal efficiency of 33%$_{LHV}$. For this reason, coal-based power generation is responsible for over 70% of the total CO_2 emissions from the power sector [3]. This makes the power sector one of the major contributors towards the global CO_2 emissions [7–11]. It is expected that the substitution of a subcritical unit with a supercritical unit of the same capacity, operating with the net thermal efficiencies of above 40%$_{LHV,}$ would result in a 15% reduction in CO_2 emission [12].

Application of the simulators has been identified as a powerful and cost-effective method in the design and analysis of the advanced power plant processes. Hence, assessment of both coal and gas power plant performance under different loads [13,14], combined power and heat plants configurations [15,16] and CO_2 capture plant retrofits [17,18] is widely conducted using computational process

Abbreviations: FORM, first order reliability method; SORM, second order reliability method; ULS, upper limit state; LLS, lower limit state; SRSM, stochastic response surface method; MPR, multivariate polynomial regression; LSM, least squares method; MCS, Monte Carlo simulation; KPI, key performance indicator.

* Corresponding author. Tel.: +44 (0) 1234 750111x5235.
E-mail address: d.p.hanak@cranfield.ac.uk (D.P. Hanak).

http://dx.doi.org/10.1016/j.apenergy.2014.10.079
0306-2619/

Nomenclature

Latin symbols

g	dependent variable
L	allowable (permitted limit) for a given variable
M_u	design matrix
$N_{failure}$	number of failures indicated in Monte Carlo simulation
N_{runs}	number of runs in Monte Carlo simulation
P_f	probability of failure
V	actual value for a given variable
x_k	independent variable in multi-variable system
X	multi-variable vector

Greek symbols

β	reliability index
ϕ^{-1}	inverse of the normal cumulative distribution

modelling tools. However, the deterministic nature of such models does not consider the randomness of the input variables [19], hence does not provide a definitive representation. Moreover, it is a common design practice to oversize the power plant equipment to account for uncertainties in process parameters that result mostly from the fluctuation of the power plant load to meet the market energy demand, but also due to integration of auxiliary systems to the power plant. This is usually achieved by applying the safety factors in design of rotating equipment, heat exchangers, and transformers. These units are typically selected according to sizing guidelines based mainly on field experience, so that material and operability limits are not exceeded. However, such an approach results in a considerable parasitic load on the system as the oversized and under-loaded equipment degrades its rated efficiency, leading not only to higher operating but also capital costs. Furthermore, this may trigger risks such as an increase in vibration stresses or unstable operation [20–22]. Also, some unit operations, such as pulverisers, may become bottlenecks of the process resulting in a limited load [23]. Equipment overheating and a fall in the power production could also be observed if the system is under-sized [20]. Ultimately, such poor design of the power plant equipment and an increased system complexity, among others, are identified as the main causes of failures [24].

In contrast to application of the safety factors, a probabilistic performance assessment approach provides a set of analytical tools which can be used to estimate the probability of failure for particular equipment and systems. These tools systematically consider the impact of the input parameter uncertainty. Frey and Rubin [25] have suggested that stochastic modelling provides a more profound insight into the process performance and may lead to different decisions compared to the deterministic analysis. Their study, where the performance and costs of an advanced technology for SO_2 and NO_x emission control from coal-fired power plant was stochastically analysed, revealed that uncertainties have a considerable effect on the system costs. In their pioneering work, Salmento and Rubin [26] have developed a stochastic modelling framework for the cost analysis of the environmental control systems which allows benchmarking novel technologies, such as integrated gasification combined cycle [27], carbon capture and sequestration [28] or abovementioned SO_2/NO_x emission control technologies with the existing technologies. According to Adhikary et al. [29], only a few studies have been conducted to investigate the reliability of individual pieces of equipment in the coal-fired power plants. In most of these studies, the reliability and availability indices for the power plant were estimated using equipment failure rates and mean times to failure [24,29ã32]. Guidelines for probabilistic modelling were proposed by Shayan [30] who developed a model that predicts the reliability of the coal milling system. Arora and Kumar [31] performed a stochastic analysis to calculate the availability of the ash handling system in a coal-fired power plant. Gupta and Tewari [32] used a probabilistic modelling in a Markov Birth-Dead process to represent the system operation and used the results obtained to optimise the process availability. These studies have shown that planned maintenance would increase the system availability, hence reliability, however at the expense of increased maintenance cost. Yet, the tools developed and the results obtained can be applied to design of new similar systems.

As no probabilistic assessment of the coal-fired power plant performance has been presented in literature yet, the aim of this work is to provide a systematic methodology that combines a finite number of deterministic numerical simulations of the power plant to approximation methods and Monte Carlo simulation (MCS). This is used to estimate the probabilities that specific thresholds in the system are exceeded in the presence of uncertain system inputs and boundaries. Similar methods have been successfully applied in safety-critical applications of other industries such as nuclear, aviation, manufacturing and offshore [33–36].

2. Coal-fired power plant modelling

2.1. Model description

This study analyses a performance of the supercritical coal-fired power plant located in India with a typical configuration (Fig. 1). The power plant follows the grid electricity demand and operates at its rated gross power output of 660 MW_{el} with a net efficiency of 38.8%$_{HHV}$ at a peak demand. The process model for this system has already been developed in Aspen Plus and its prediction, including the part-load operation, has been validated against the data available in the literature [14]. In general, the model of the power plant consists of three interconnected sub-systems: a supercritical steam boiler, a flue gas emission control system, and a steam cycle.

In the boiler sub-model, pulverized coal prepared in the mills is entrained by the primary air that is a part of the total air used in the coal combustion process. Feedwater enters the boiler via the economiser at nearly 309 bar at a base load and pressure losses are accounted for through a general pressure drop correlation. Live steam leaves the boiler at 537 °C and 242.2 bar and is expanded in the high-pressure turbine, and then returned to the boiler where it is reheated to 565 °C and subsequently expanded in intermediate- and low-pressure turbines, which are coupled to an electric generator. Waste heat from the flue gas leaving the boiler is recovered in an air preheater, before the flue gas enters the emission control system comprising the selective catalytic reduction reactor for NO_x, the electrostatic precipitator for particulate matter, and the flue gas desulphurisation unit for SO_x emission control.

A typical design of the coal-fired power plant includes several steam extractions to the high- and low-pressure feedwater heaters. This aims to increase the net thermal efficiency by increasing the average temperature of heat addition in the boiler. The pressure distribution in the system, which is dependent on the steam generation rate, is represented using the Stodola's ellipse law.

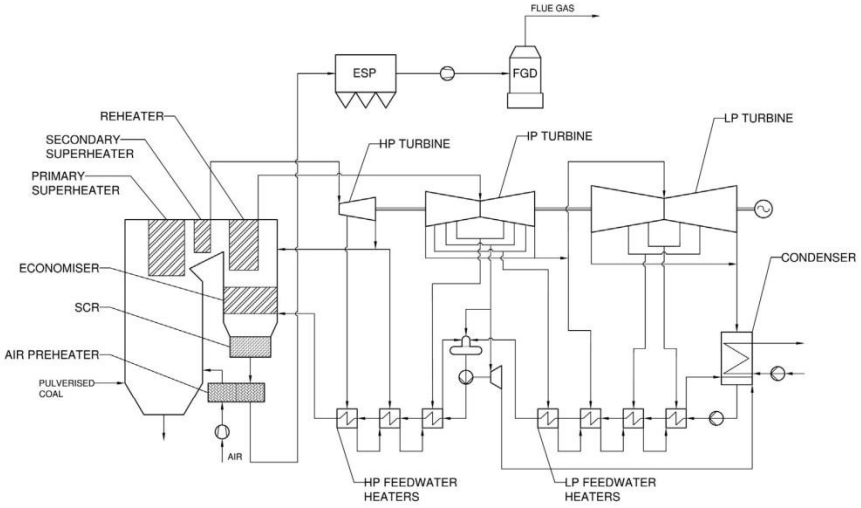

Fig. 1. Process flow diagram of 660 MW_{el} supercritical coal-fired power plant.

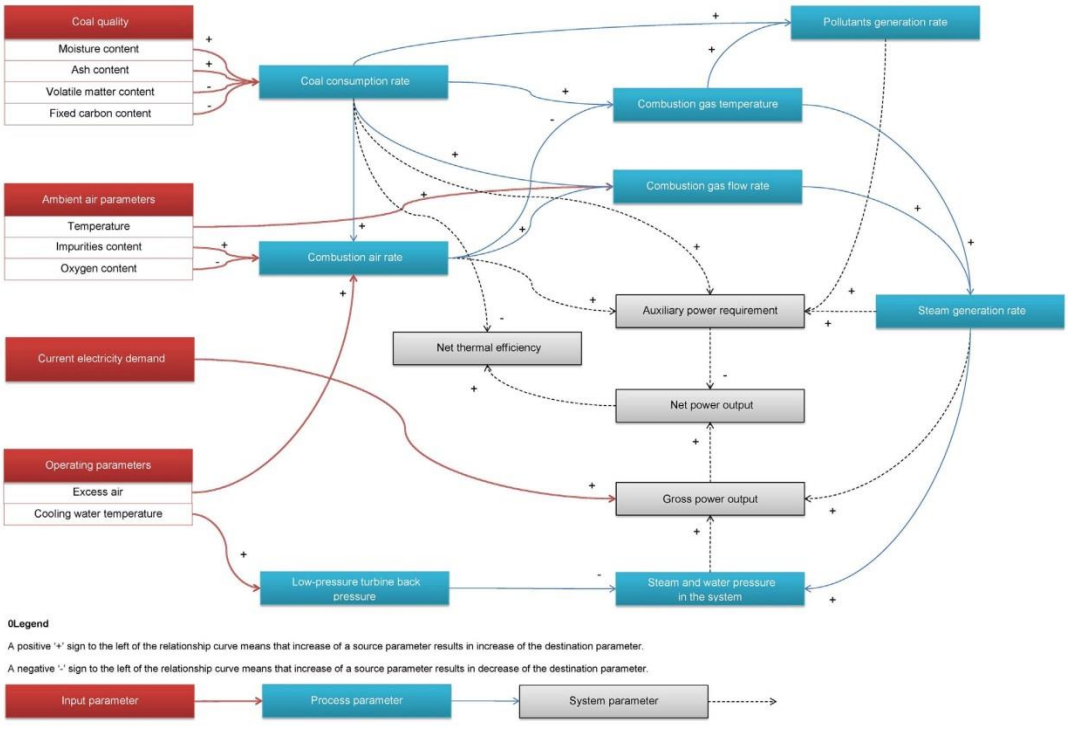

Fig. 2. A model of relationship between process parameters in the coal-fired power plant.

2.2. Key performance indicators

The key performance indicators (KPIs) of the coal-fired power plant are identified through analysis of the relationships among its operating parameters (Fig. 2). Main input data to the model comprise parameters related to the coal and air quality, environmental conditions reflected mainly in the cooling water temperature, as well as the required load to meet the market electricity demand. These input parameters affect the process performance that is observed in variation of both stream parameters and net power output.

On the process level, the coal quality, which is characterised in terms of moisture, ash, volatile matter and fixed carbon content, directly influences the coal consumption rate. For example, an increase in both the moisture and ash content (ballast) reduces the heating value of coal. Therefore, to introduce the same amount of energy into the system, the required coal consumption rate would increase with moisture and ash contents.

Furthermore, a minimum amount of oxygen is required to ensure a nearly complete combustion process of coal. Therefore, a variation in the coal consumption rate during the load following operation of the power plant would result in a subsequent variation of the air rate required for combustion. Additionally, the air requirement is affected by the air composition, which may differ in the vicinity of the power plant [37].

Although the increase in both coal and combustion air rates result in rise in combustion gas flow rate, they affect the combustion temperature differently. Since the air temperature is well below the adiabatic flame temperature of coal, the temperature at which the combustion process takes place would be reduced if the excess air is too high. Yet, both rise in the coal consumption rate and the combustion temperature result in increase in emission rate of the gaseous pollutants, such as CO_2 and NO_x.

Also, the combustion gas temperature and flow rate directly affects the amount of live steam that is generated in the boiler and the temperature of reheated steam. It is assumed that the power plant is operated in the sliding pressure mode. Therefore, variation in the steam rate affects the pressure distribution both in the boiler and the steam cycle. This pressure distribution is also influenced by the ambient cooling water temperature, which determines the operating pressure of the condenser, and hence the low-pressure turbine discharge pressure.

On a system level, the performance indicators are linked between the process level parameters and the market electricity demand. The gross power output is directly dependent upon the steam generation rate, as well as the live steam inlet pressure. However, due to the auxiliary power requirement of the power plant equipment, the net power output sent to the grid is less than gross output at a given load. As the market demand changes over the time, the required net power output would change as well. This is balanced by adjustment of the coal consumption rate. As the power plant output follows the market demand, all key parameters vary within the load operating envelope, of which the lowest operational load is 40%.

3. A framework for the probabilistic assessment of complex systems

3.1. Background of systems reliability

Reliability is defined as "the ability of a system to fulfil its design functions under designated operating and environmental conditions for a specified period of time" [38]. In analysing reliability, estimates of the joint probability of non-fulfilment for each individual functional requirement of the system are mathematically expressed through corresponding limit states, which indicate the safety margins between allowable and actual values of variables. For a multi-variable system $X = \{x_1, x_2, x_3, \ldots, x_k\}$ the limit state can be formulated as:

$$g(X) = L(X) - V(X) \tag{1}$$

where L stands for the allowable limit, often determined by design standards and practices, and V is the actual value of the corresponding variables. Examples of these variables in a power plant are coal firing rate and thermal efficiency. X is an n-dimensional vector representing the design variables, which individually have a known continuous joint distribution $f_g(X)$. Thus, each functional requirement must necessarily be expressed by $g_i(X)$, which is the limit-state function, and ascribes a negative value when the state identified by the variables results in failure region, a positive value for safe region and a null value for the critical limit condition. Therefore, the probability of failure can be mathematically defined as the probability for the limit state condition to be unsatisfied:

$$P_f = P[g(X) < 0] \tag{2}$$

Hence the probability of failure can be rewritten as:

$$P_f = \int_{-\infty}^{0} f_g dg = \int_{g(X)<0} f_g dg \tag{3}$$

For each limit state in the system, which is characterised by the correlation coefficient ρ_{LV} between the allowable and actual values, the mean and standard deviation can be determined using the elementary definition of the mean and the variance [39]:

$$\mu_g = \mu_L - \mu_V \tag{4}$$

$$\sigma_g = \sqrt{\sigma_L^2 + \sigma_V^2 - 2\rho_{LV}\sigma_L\sigma_V} \tag{5}$$

As illustrated in Fig. 3, the reliability index β represents the distance of the mean reliability margin from the limit-state surface and is defined as:

$$\beta = \frac{\mu_g}{\sigma_g} = \frac{\mu_L - \mu_V}{\sqrt{\sigma_L^2 + \sigma_V^2 - 2\rho_{LV}\sigma_L\sigma_V}} \tag{6}$$

In a special case in which the limit state function $g(X)$ is normally distributed, $g(X) = 0$, and in which the allowable limit and the actual value for the random variable are uncorrelated ($\rho_{LV} = 0$), the probability of failure can be expressed as a function of the reliability index:

$$P_f = \int_{-\infty}^{0} \frac{1}{\sigma_g\sqrt{2\pi}} \exp\left[-\frac{1}{2}\left(\frac{g-\mu_g}{\sigma_g}\right)^2\right] = \int_{-\infty}^{0} \frac{1}{\sigma_g\sqrt{2\pi}} \exp\left[-\frac{1}{2}\beta^2\right] = 1 - \Phi(\beta) \tag{7}$$

3.2. Solution techniques for reliability analysis

In most cases, an analytical solution of the integral presented in Eq. (3) is very difficult, if not impossible, to find; hence approximation or stochastic methods, characterised by different computational requirements and accuracy, are often employed.

Numerical approximation aims to linearise the limit-state $g(X) = 0$, usually using the Taylor series expansion. Two most commonly applied reliability methods, first-order reliability method

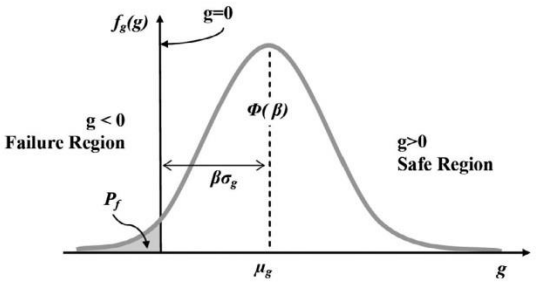

Fig. 3. Graphical interpretation of the reliability index [39].

(FORM) [40] and second-order reliability methods (SORM) [41,42], employ first and second order Taylor expansions, respectively, formulating easy to model algorithms for computation of the probability of failure. To achieve high accuracy and reliability of the prediction, application of the FORM is limited to linear responses and expected probabilities of failure $P_f > 10^{-5}$. For highly nonlinear responses, the SORM should be employed. In most cases, however, implementation of SORM results only in a slight improvement of the prediction accuracy, while significantly increasing the computational effort required [39]. Therefore, for systems of higher nonlinearity, other methods, such as radial basis functions [43], are employed, as the requirement of handling higher-order Taylor expansions significantly complicate the computational process, with no apparent benefit in accuracy, especially when there is a requirement for data extrapolation.

Stochastic methods, such as MCS, are widely used because they do not require much knowledge and statistical understanding of the problem. The MCS algorithm is easy to implement and involves evaluating a deterministic model a number of times utilising different inputs, and then checking each output to assess if one or more thresholds are exceeded or not. The main drawback of the method is that it is not suitable for low probabilities of failure as it becomes computationally demanding [44]. Further description of the methods and their mathematical formulation is available in Choi and Grandi [39].

3.3. Approximation methods for complex systems

Uncertainty in input variables results in randomness of the output quantities like the net thermal efficiency. The output is often limited by the equipment constraints and exceeding it could result in various failure modes. Analytical representation of limit state functions of complex systems for a systematic probabilistic assessment is not always feasible and often demands reduction of system through appropriate approximations, formulating expressions that implicitly or explicitly represent the relationship between inputs and outputs. The problem can be treated in a more mathematically intensive way through intrusive formulation, for example by embedding the stochastic variability of the system in the analysis codes, as done using Stochastic Galerkin or Spectral Stochastic Final Element Methods. Alternatively, the problem can be approached in a simpler, non-intrusive formulation, by keeping codes as black boxes and dealing with system response surfaces, as done using the Stochastic Response Surface Method (SRSM) [45]. Available methods can vary from simple interpolation, using least squares method analysis for polynomial regression, to more computationally intensive surrogate models that can capture extensive nonlinearities and complexities of the response surface [46].

The SRSM may be easily employed in order to provide an effective and precise estimate of the reliability of a limit state function. First, an approximated limit-state function is obtained by using some designated sample points, where the response surface is suited to the limit-state to construct a simpler mathematical function, such as a quadratic polynomial. This is then used as an estimate of the real limit-state function. Therefore, the SRSM is considered to be the link between input and output of a process, since it plays an important role in the construction of functions and variables that are simulated. A drawback of this method is the lack of accuracy in cases with strongly nonlinear limit-state functions to be approximated. In this work, quadratic functions are employed to express the limit-state function as a function of all design variables stochastically modelled, due to the fact that they can match the tail curvature of the response surface with good approximation and also restrict the number of required simulations [47].

A generic quadratic polynomial form can be denoted as [48]:

$$\tilde{g}(X) = a + \sum_{i=1}^{n} b_i \cdot X_i + \sum_{i=1}^{n} c_i \cdot X_i^2 \tag{8}$$

In order to calculate the $(2n + 1)$ coefficients a, b_i and c_i, an equal or greater number of sample points is required in order to apply multivariate polynomial regression (MPR). Determination of sampling points should be done in such a way that the measured response is 'mapped' in the most comprehensive way. Whichever method is used, the number of samples can be from $(2n + 1)$ to 3^n, corresponding to different numbers of simulations. Regression can be performed by application of the least square method [49], denoting that for a quadratic approximation with p sampling points, the design matrix M_u of the independent variables and the vector $\bar{g}$ with values of the response (dependent variables) are:

$$M_u = \begin{bmatrix} 1 & u_{11} & \cdot & u_{n1} & u_{11}^2 & \cdot & u_{n1}^2 & u_{i1} & \cdot & u_{j1} \\ \cdot & \cdot & \cdot & \cdot & \cdot & \cdot & \cdot & \cdot & & \\ 1 & u_{1p} & \cdot & u_{np} & u_{1p}^2 & \cdot & u_{np}^2 & u_{ip} & \cdot & u_{jp} \end{bmatrix} \tag{9}$$

$$\bar{g} = [g_1 \cdot g_p]^T \tag{10}$$

Calculation of coefficients vector $\bar{a}$, based on normal regression, is obtained by solving the following linear system:

$$\bar{a} = (M_U^T M_U)^{-1} M_U^T \bar{g} \tag{11}$$

3.4. Monte Carlo simulations in complex systems analysis

The MCS is often employed in random value generation for random variables X_i according to their statistical distribution, and then in estimating the probability of failure as the frequency with which $g(X_i) < 0$, for example, compared with the limit. Repeating this procedure for a large number of runs and summing up the number of times that the limit has been exceeded, the probability of failure can be estimated [39]:

$$P_f = \frac{N_{failure}}{N_{runs}} \tag{12}$$

Having determined the failure probability for a considered limit state, it is possible to assess the reliability index using Eq. (13) and then to benchmark it with the allowable value.

$$\beta = \phi^{-1}(1 - P_f) \tag{13}$$

Random input sets can be generated through relevant algorithms using the inverse function method where a random number in the range [0, 1] is first generated, and then knowing the shape of the density function the successive variable values can be found. If the variables are correlated, their covariance is first estimated, and the sampling is biased using a multivariate random number generation algorithm.

It is common practice to set the minimum number of runs as the inverse of two orders of magnitude of the expected order of the failure probability [39]. This makes the direct MCS implementation computationally demanding for values of low failure probabilities. Furthermore, in MCS, the design point is not calculated. This is the reason why the method is not always suitable for optimisation problems.

3.5. Probabilistic analysis algorithm

The methodology for a probabilistic performance analysis of a complex engineering system includes a set of fundamental discrete steps of analysis as presented in Fig. 4.

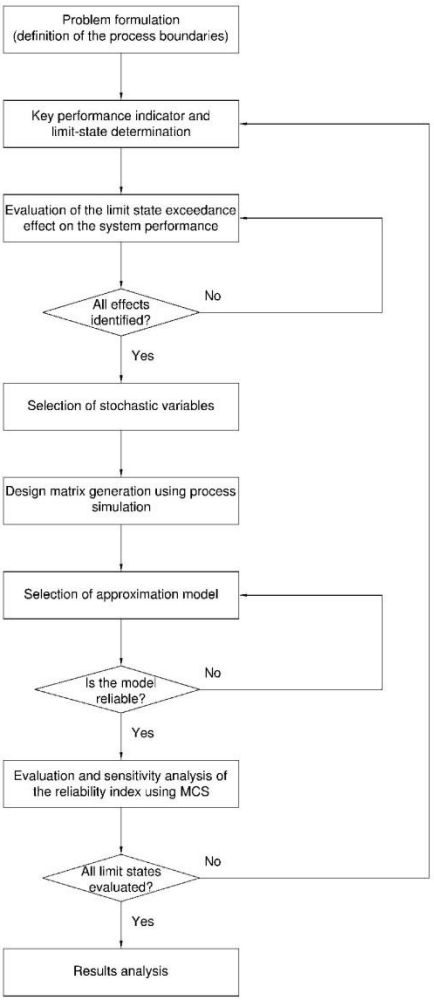

Fig. 4. Algorithm of probabilistic analysis.

In the first step, the system or process boundaries and variables considered in the analysis are identified and characterised. Next, based on the process analysis, the key performance indicators are identified, along with their upper and lower limit states that are used as the failure criteria in the reliability analysis. Moreover, the effect of the limit state exceedance on the system performance is determined.

The second step is the identification of the stochastic variables considered in the analysis along with their statistical representation. Furthermore, a series of deterministic simulations using the process model are conducted to generate the design matrix that is an input to a numerical approximation of the analysed limit state. A design matrix should consider an appropriate number of design points so that the response surface is adequately represented in the design space. A major advantage of employing non-intrusive methods is the ability to use specialized tools for each step. Selection of the most appropriate approximation method is a decision of great importance as this can introduce or minimise the effect of extra uncertainties on the calculation. Therefore, the approximation model accuracy and reliability is assessed before it is implemented in the MCS code.

Having the stochastic variables efficiently modelled, the MCS is used to estimate the probability that given limit state is exceeded. Finally, the reliability index is computed. A process design procedure should involve an iterative process in which the equipment design is amended based on the reliability index value. In addition, it is pertinent to analyse the effect of the key statistic parameters of the input data on the reliability index as they could considerably affect the equipment sizing. To achieve this, the mean and standard deviation are varied by 20% for all identified limit states and the changes of the reliability index are benchmarked with the initial estimates. The degree by which the statistic parameters are varied should be selected based on the past experience of a designer. Such an approach allows the designer to fully account for the uncertainty that may affect the system design.

4. Case study on power plant performance

4.1. Problem formulation

An analysis of the performance of the coal-fired power plant under different operating conditions gives a set of data that can be used to establish the operability envelope of the system. However, due to deterministic nature of such analysis, it does not account for the uncertainty corresponding to the input data. Therefore, introduction of the probabilistic analysis of the process performance would reveal the actual operating envelope of the system and probabilities of possible failure events and would aid the designer in sizing the equipment properly, without the need for excessive oversizing for safety margins. With the probability of events accounted for, along with their potential consequences, a risk-based approach to design and operation of the power plant is introduced.

4.2. Limit states formulation

Analysis of the relationships among the process variables in the coal-fired power plant presented in Section 2.2 revealed several KPIs which affect the system design. These can be used in the probabilistic performance assessment to analyse impact of the input uncertainty.

The process model developed in Aspen Plus was used to determine the limits of the KPIs, which correspond to the power plant operated at 40% and 100% load. These, together with the parameter impact on the equipment design, are presented in Table 1.

A number of KPIs is chosen (Table 2) to represent the operating envelope of the power plant in the developed process model and then used to predict the probability that the design limits would not be met via process simulation. The limit states are divided in two groups: upper limit state (ULS) for which failure occurs when the actual value of the key performance indicator is above the limit, and lower limit state (LLS) for which failure occurs when the actual value of the key performance indicator is below the limit.

4.3. Selection of stochastic variables

As the performance of the analysed system mainly depends on the coal quality, which is a function of the coal composition [50], and the current grid electricity demand, these input parameters are treated as stochastic. As the main aim of this study is to evaluate the applicability of the framework for the probabilistic performance assessment of the complex systems developed, it is assumed that the variables are uncorrelated. Although the selected

Table 1
Key performance indicators and their operating limits based on deterministic simulation.

Key performance indicator	Prediction at 40% load	Prediction at 100% load	Impact on the power plant equipment
Coal consumption rate (kg/s)	26.42	60.36	1. Capacity of coal and ash handling system 2. Size and number of mills
Air consumption rate (kg/s)	537.01	655.08	1. Size of forced draft and primary air fans 2. Size of air pre-heater 3. Piping size
Combustion gas flow rate (kg/s)	560.25	715.91	1. Capacity of emission control equipment 2. Size of induced draft fan 3. Boiler heat exchange sections size
CO_2 emission rate (kg/s)	66.44	146.96	1. Capacity of capture plant
Steam generation rate (kg/s)	222.92	551.24	1. Piping size 2. Steam turbine swallowing capacity 3. Condenser and feedwater heaters size 4. Boiler heat exchange sections size 5. Generator size 6. Boiler feedwater pump size
Cooling water rate (kg/s)	8998.38	18893.70	1. Cooling water pump size 2. Cooling tower size 3. Condenser size
Condensate rate (kg/s)	185.77	429.30	1. Condensate pump size 2. Feedwater heaters size
Boiler feedwater pump outlet pressure (bar)	155.96	309.67	1. Feedwater pump material 2. Boiler heat exchange sections, piping, turbine and feedwater heaters material
Reheated steam temperature (°C)	542.70	565.20	1. Turbine and piping material
Net thermal efficiency ($\%_{HHV}$)	34.54	38.73	–

Table 2
Interpretation of limit states.

What if?	Limit state	Result
Coal consumption rate	Is below lower limit	Possible requirement for supplementary oil firing
	Is above up limit	Mills, coal and ash handling equipment not capable of processing the required coal rate
Steam generation rate	Is below lower limit	A drop in pump and turbine efficiencies
	Is above upper limit	Swallowing capacity of the steam turbine is exceeded, the capacity of generator and transformer exceeded
Net thermal efficiency	Is below lower limit	Inefficient coal utilisation leading to increased cost of electricity and specific emissions
	Is above upper limit	Higher coal utilisation efficiency leading to reduced cost of electricity and specific emissions

stochastic data are well represented by the normal distribution, the presented framework can easily accommodate data of any statistical distribution.

It has been shown that the coal composition varies significantly, even that from the same coal field [51]. Therefore, the coal proximate analysis is chosen as a first set of stochastic variables (Table 3). Since the random value of each variable of the coal proximate analysis is generated separately, the coal composition is normalised, so that the sum of all components is always equal to 100 wt%. As no statistical data were available for the coal composition used in the development of the coal-fired power plant model, the composition of coal from the Carbondale coal field was used in this study, since the composition of coal originally used was found to be within the standard deviation of the coal from the Carbondale field [52].

Furthermore, as some coal-fired power plants are operated in a demand-following mode, their equipment is loaded in a variable manner. For the system under consideration, the expected annual load changes (Fig. 5) were estimated based on the data provided by Indian Energy Exchange [53]. As the variation was found to be considerable, the gross power plant output was used as a stochastic variable in the probabilistic performance analysis (Table 3).

Table 3
Statistical parameters of stochastic variables.

Stochastic variable	Mean value	Standard deviation
Gross power output (MW_{el})	388.92	85.47
Moisture content in coal (as received, wt%)	1.4	1.0
Ash content in coal (as received, wt%)	7.0	2.1
Fixed carbon content in coal (as received, wt%)	63.7	6.5
Volatile matter content in coal (as received, wt%)	27.9	5.5

4.4. Stochastic response surface approximation model development

Although the process model developed in Aspen Plus provides a flexible response to input variables within a reasonable time, it cannot be used directly in the probabilistic assessment of the coal-fired power plant performance. This is because a large number of iterations, which can be in excess of a million, is required for a reliable prediction of the event probabilities through conventional MCS. For this reason, the process model is used to generate the design matrix that is a base for an approximation method employment.

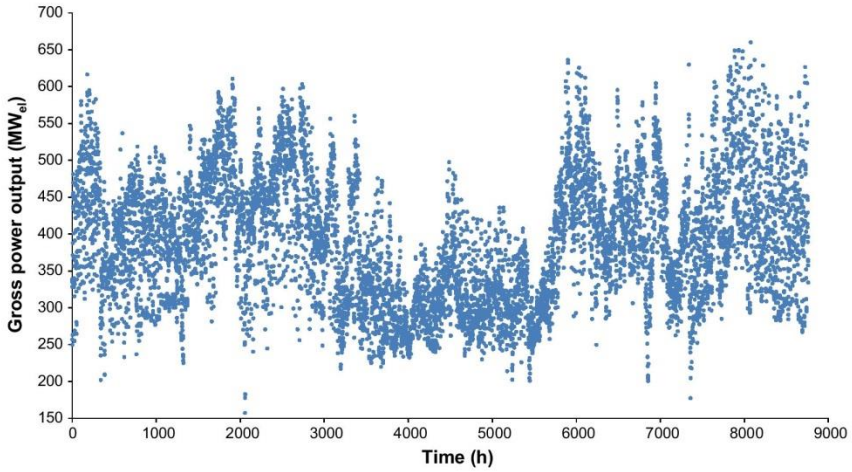

Fig. 5. Annual gross power output profile of the analysed coal-fired power plant.

The design matrix, which comprises the key performance indicators for the analysed system, was generated by changing the identified input variables to the model in the following manner:

- the gross power output was varied between 260 MW_{el} and 660 MW_{el} with a step of 8 MW_{el};
- the coal proximate analysis was varied based on 55 coal compositions from the ECN fossil fuel characteristics database [54].

The representative subset of the design matrix generated in deterministic simulations, which were run in automated series for each variable separately with each simulation requiring approximately 5 min to converge, is available as a supplementary material to this paper. The full design matrix containing the results of 266 deterministic results was used to create the approximation model in which the predicted value of the particular KPI is a function of the coal composition and the gross power output. In the first approximation attempt, a multivariable polynomial regression using a quadratic function was used and the estimated approximation coefficients are presented in Table 4.

Analysis of the average deviation (Table 4), which was defined as a difference between the process model and the approximation model prediction, revealed that the approximation model based on the polynomial regression provided a reasonably reliable prediction of the KPIs and analysis robustness. In different cases of highly nonlinear systems, which are currently under investigation by the authors, more complex investigation methods can be applied such as surrogate modelling methods using radial basis functions.

5. Results and discussion

A key output of the probabilistic performance assessment is a set of failure probabilities and the reliability indices for the analysed limit states. As presented in Fig. 6, the higher this index is, the lower the failure probability, and thus a smaller safety margin can be applied at the design stage. The evaluated reliability indices for the ULS and the LLS for selected key performance indicators are further discussed in this section.

5.1. Reliability index for coal consumption rate

5.1.1. Probabilistic performance analysis

The process analysis, along with the stochastic treatment of the input data, revealed that there are two failure modes that can affect the coal and ash handling systems reliability. On one hand, as the power plant is operated at various loads while following the market demand, it is possible that the load would need to be

Table 4
Assessment of the approximation model prediction.

Variable	Model parameter	Coal consumption rate (kg/s)	Steam generation rate (kg/s)	Net thermal efficiency ($\%_{HHV}$)
Moisture content	a_1	9.82E−03	−3.98E−04	−1.28E−04
	b_1	5.96E−01	−4.34E−03	−4.49E−01
FC content	a_2	−4.80E−04	1.66E−05	1.02E−05
	b_2	−1.16E−01	−1.98E−02	2.59E−03
VM content	a_3	6.27E−04	−9.47E−05	−1.30E−05
	b_3	−2.02E−01	−8.40E−03	4.33E−03
Ash content	a_4	1.14E−02	3.08E−04	−2.40E−04
	b_4	2.29E−01	−2.93E−02	−2.52E−03
Power output	a_5	1.59E−05	2.08E−04	−3.22E−05
	b_5	7.04E−02	6.34E−01	4.04E−02
	c	1.15E+01	4.40E+01	2.70E+01
Average deviation		1.27E−03	1.72E−04	3.23E−04

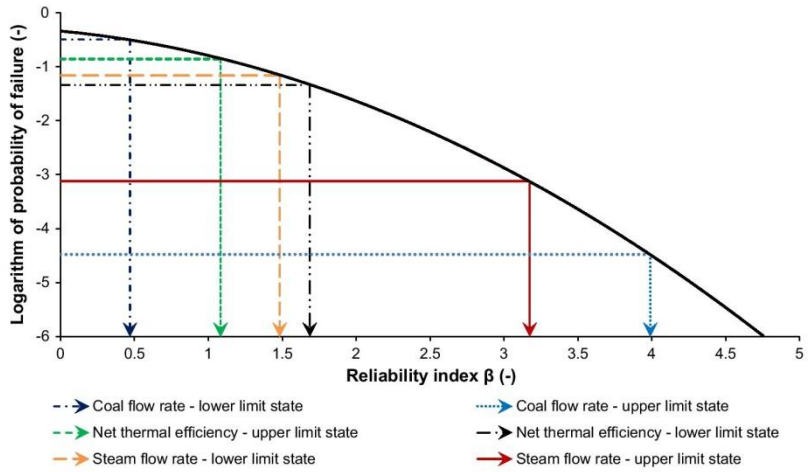

Fig. 6. Probability of failure and reliability index dependence.

below 40%. In such operating mode, the auxiliary oil firing would be required to reach required heat rate in the boiler. On the other hand, the variability of the coal composition affects the coal heating value and thus the coal consumption rate needs to be adjusted accordingly to reach the desired gross power output. Therefore, if not properly sized, the power plant may not be able to meet the desired gross power output due to the limitations imposed by the coal and ash handling system capacity, if the required coal consumption rate is too high, or due to limited oil availability in case of low load operation.

The probabilistic performance analysis has revealed that it is more likely that the coal consumption rate will be below the lower limit ($P_{f,LLS} = 0.3192$, $\beta_{LLS} = 0.45$) than above the upper limit ($P_{f,ULS} = 0.00003$, $\beta_{ULS} = 3.99$). This indicates that in terms of system reliability, more attention needs to be paid to the design of the auxiliary oil firing system rather than the coal and ash handling systems. Fig. 7 clearly shows that the coal consumption rate is normally distributed with a mean of 35 kg/s, which is closer to the LLS. Moreover, the cumulative probability curve indicates that for more than 90% of the operating time the coal consumption rate would be lower than 40 kg/s. This implies that the coal and ash handling equipment would be under-utilised for most of the time. Hence, it can be concluded that the equipment would not operate with its nominal performance and the net thermal efficiency of the power plant would be affected. It is also observed that the coal consumption rate would be lower than 30 kg/s for more than 50% of the operating time. Therefore, auxiliary oil firing would be often required to meet the boiler heat demand.

5.1.2. Sensitivity analysis

A sensitivity study has revealed that the coal consumption rate is most sensitive to changes in the fixed carbon content and load mean values, as well as the load standard deviation (Fig. 8).

An increase in the mean value of fixed carbon content reduces the probability that the coal and ash handling system capacity would be exceeded. This is reflected in nearly 5.5% increase in the reliability index for the ULS. Also, such a change in the coal composition results in a reduction of the reliability index for the LLS by 55% compared to the benchmark scenario. This, however, does not necessarily mean that oil firing would be required when the LLS is not met as the increase of the fixed carbon increases the heating value of coal. Conversely, an increase in the mean value

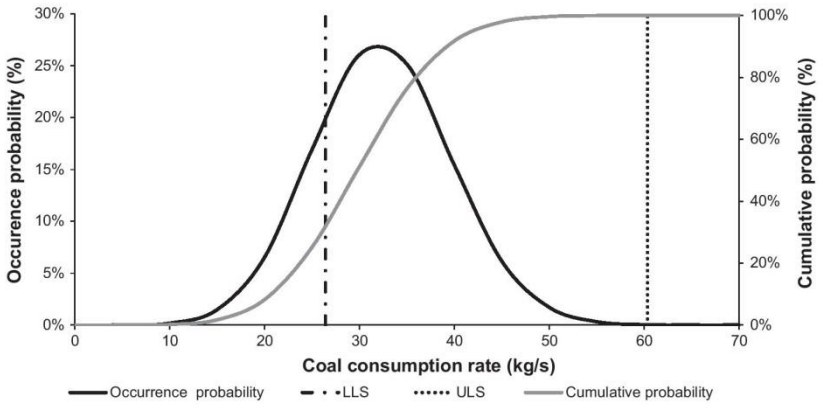

Fig. 7. Occurrence and cumulative probability for coal consumption rate.

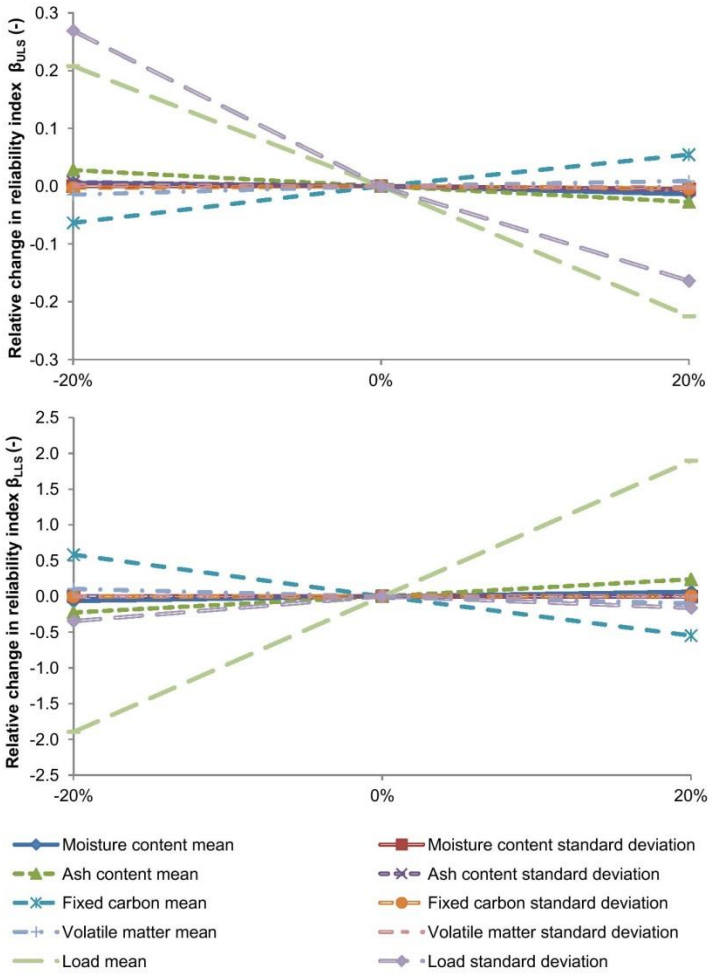

Fig. 8. Analysis of the key statistic parameters on the reliability index sensitivity for the coal consumption rate.

of ash content in coal results in a lower probability that the LLS is not achieved. In general, increase of ballast content in the coal has a negative effect on its heating value and thus, more fuel is required for the power plant to reach the desired load. Nevertheless, variations of the remaining constituents of coal were found to have a negligible impact on the coal consumption rate.

The highest variations in the reliability index were observed when either the mean value or the standard deviation of the desired power plant load was varied. It was found that the increase in both parameters resulted in the increase in the coal consumption rate, reducing the reliability indices. For this reason, it is more likely that the ULS will be exceeded. Due to the coal and ash handling equipment limitations, the system would not be capable to process the required amount of coal and thus not enough energy would be provided to the boiler. In turn, less steam would be generated and the desired load would not be met. In addition, an increase in the mean value of the load results in the doubling of the reliability index for the LLS and thus, reduces oil consumption requirement in the power plant as confirmed by the lower probability of the oil firing due to higher annual mean loads. The reverse is observed if the load mean and standard deviation values are reduced.

5.2. Reliability index for steam generation rate

5.2.1. Probabilistic performance analysis

As indicated in Fig. 2, steam generation rate and coal consumption rate, and hence its composition, are directly correlated. The 'what if' analysis of the power plant revealed that if the LLS for the steam generation rate is not met, energy will be wasted in the system due to inefficient performance of the steam turbines at the off-design operation. On the other hand, if the steam generation rate exceeds the ULS, the swallowing capacity of the turbine or the transformer capacity will be exceeded. This could cause the damage to the steam turbine, as well as loss of the power plant's ability to meet the current electricity demand.

Fig. 9 shows that the steam generation rate is nearly normally distributed with the mean of 350 kg/s. Similarly to the coal consumption rate, this value is closer to the LLS rather than ULS. Therefore, a similar trend in the reliability indices ($P_{f,LLS} = 0.0692$, $\beta_{LLS} = 1.48$ and $P_{f,ULS} = 0.0008$, $\beta_{ULS} = 3.17$) for the steam generation rate is observed. It should be stressed that the reliability index of the steam generation rate being above the desired value at 100% load is double the reliability index of the desired amount of steam

generated being less than what is specified at 40% load. This indicates that it is less likely that the steam turbine will need to operate above its rated capacity. Furthermore, for more than 95% of the operating time, the steam generation rate would be below 450 kg/s, corresponding to 81.5% of the nominal value. This implies that, if not properly sized, the steam cycle would be under-utilised for most of its operating time and thus, its efficiency would be affected.

5.2.2. Sensitivity analysis

The sensitivity analysis of the key statistic parameters revealed that the changes in the coal composition have no effect on the steam generation rate as the reliability indices remained unchanged when the coal composition was varied (Fig. 10). This is because the coal consumption rate is controlled to meet the load demand irrespective of the coal composition.

Conversely, variation in the mean value and standard deviation of the gross power output were found to influence the steam generation rate significantly. This is caused by direct correlation between the steam generation rate and the gross power output as described in Section 2.2. Fig. 10 reveals that a 20% increase in the mean load caused a 28.6% fall and a 61.5% rise in the reliability index for the ULS and LLS, respectively. This indicates that on average the system would operate at higher load and it would be possible that the required steam generation would be greater than designed value leading to exceedance of the steam turbine swallowing capacity or highly off-design operation of the electric generator. In contrast, reduction of the mean load would result in a 61.5% drop in the reliability index for the LLS, which would affect the machinery efficiencies due to off-design operation and thus, the net thermal efficiency of the coal-fired power plant.

Interestingly, a trend where the increase in the standard deviation results in reduction of the reliability index was observed for both ULS and LLS. This means that variability of the market demand has a significant impact on the equipment performance and should also be considered at the design stage to maximise the net thermal efficiency of the power plant.

5.3. Reliability index for net thermal efficiency

5.3.1. Probabilistic performance analysis

In contrast to previous cases, exceedance of either the LLS or the ULS for the net thermal efficiency would not cause any physical damage to the power plant equipment. Importantly, the net thermal efficiency is directly correlated to the cost of electricity since the higher it is, the less coal is consumed per unit amount of electricity produced. Therefore, the system design should aim to maximise the net thermal efficiency and minimise the operating costs.

The stochastic analysis (Fig. 11) has revealed that the net thermal efficiency is nearly normally distributed with the mean value of 38%. This value is close to the ULS and, based on analysis of the remaining KPIs, it can be inferred that it is a result of variation in the coal composition and thus coal heating value. In such a case, less coal would need to be transported and pulverised per unit amount of electricity produced leading to less electricity required for coal and ash handling, hence to higher net thermal efficiency. The evaluated reliability indices revealed that it is more likely that the ULS ($P_{f,ULS} = 0.1397$, $\beta_{ULS} = 1.08$) will be exceeded rather than the LLS ($P_{f,LLS} = 0.0456$, $\beta_{LLS} = 1.69$). However, the net thermal efficiencies above the ULS may not be achievable in practice due to physical limitations of the power plant equipment; for example, if the steam generation rate exceeds the steam turbine swallowing capacity. Although less probable, the net thermal efficiency can be below the LLS which could be caused either by high ballast content in coal or the power plant operation at a load lower than 40%. Moreover, it was found that the power plant would operate with the net thermal efficiency below LLS for approximately 7% of its operating time; that would result in higher operating costs.

5.3.2. Sensitivity analysis

The sensitivity analysis revealed a clear relationship between the net thermal efficiency and the mean load of the power plant (Fig. 12). This is because a 20% increase in the mean load would increase the probability that the ULS would be exceeded. This is reflected in a 71.6% reduction of the reliability index for the ULS. On the other hand, a 52.9% increase in the reliability index for the LLS was observed. Therefore, it is less probable that the LLS would be exceeded. Although such state does not necessarily lead to the physical damage to the power plant equipment, it indicates that on average the net thermal efficiency of the system is higher than the designed value. Although in some cases this could not be reached due to the equipment capacity limitations, it would lead to more efficient coal utilisation, a lower cost of electricity and reduced specific emissions compared to the designed conditions. As was the case previously, the increase in the standard deviation of the load results in reduction of the reliability index for both ULS and LLS. Therefore, it can be concluded that a reduction

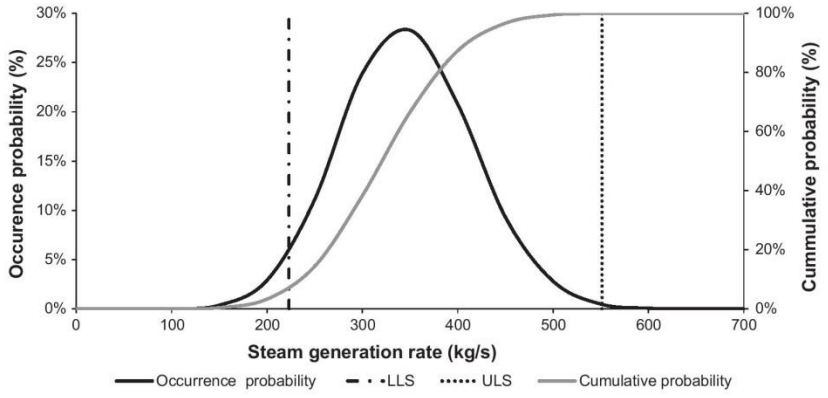

Fig. 9. Occurrence and cumulative probability for steam generation rate.

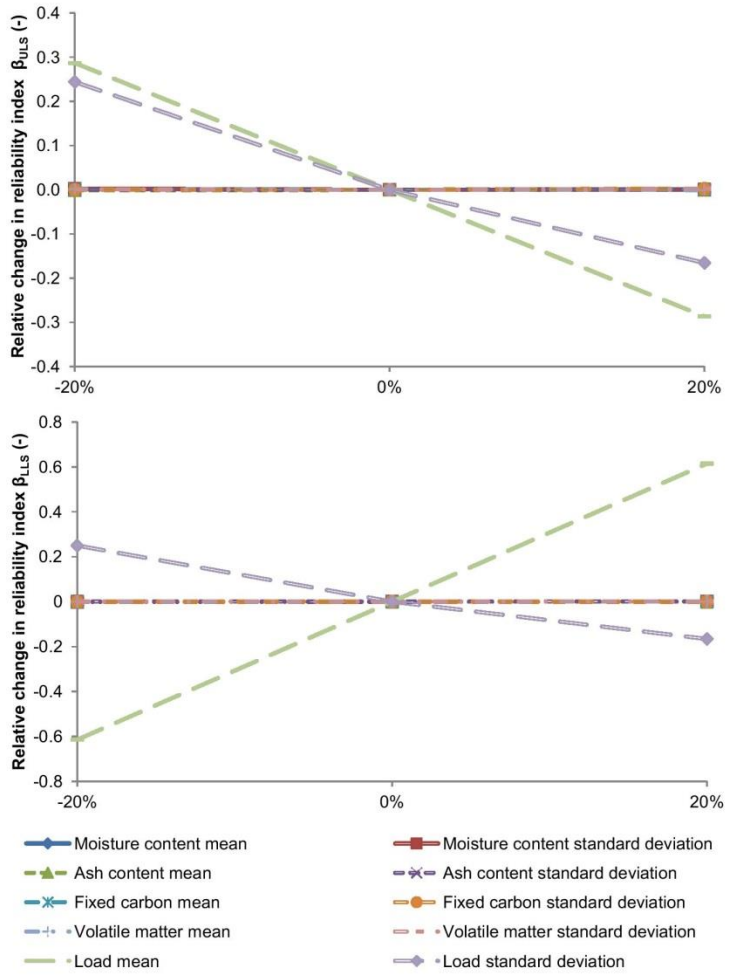

Fig. 10. Analysis of the key statistic parameters on the reliability index sensitivity for steam generation rate.

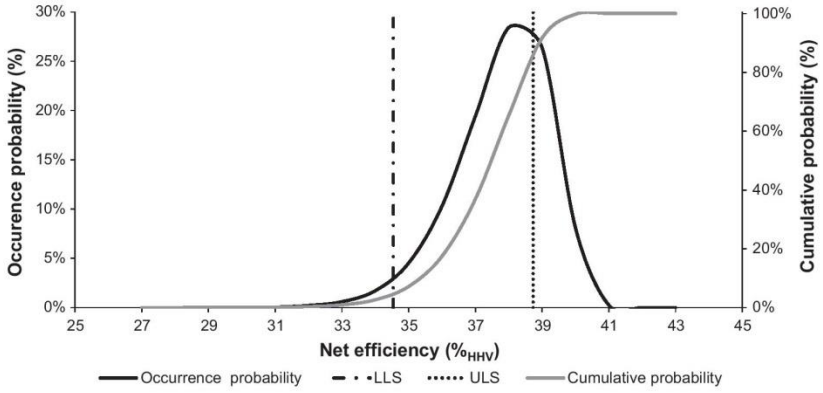

Fig. 11. Occurrence and cumulative probability for net thermal efficiency.

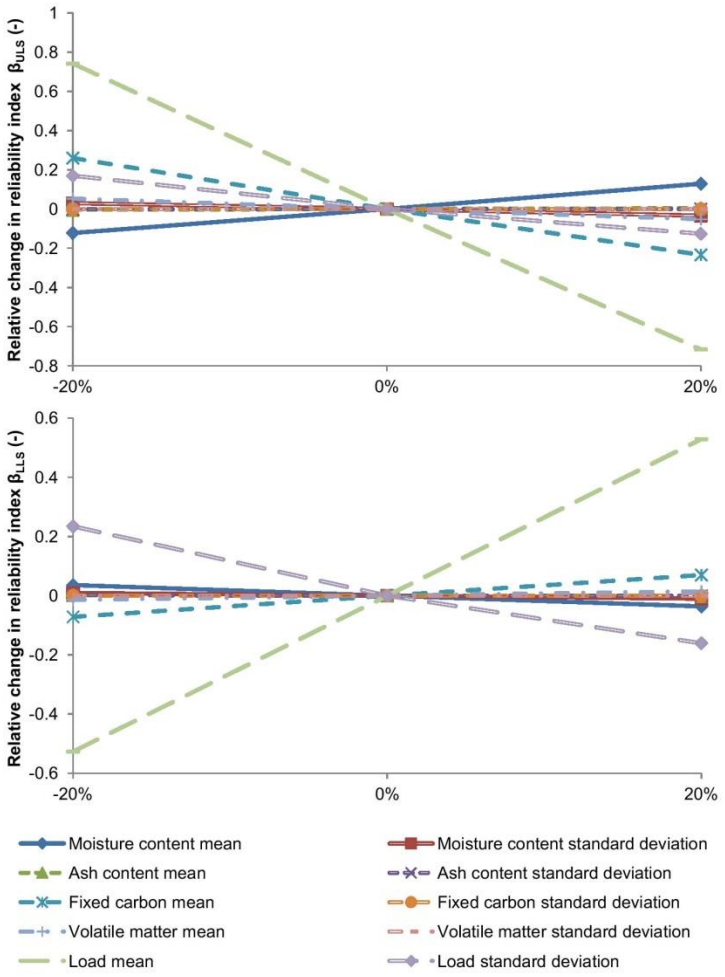

Fig. 12. Analysis of the key statistic parameters on the reliability index sensitivity for net thermal efficiency.

in the load variability reduces the failure probability and allows the designer to size the equipment more accurately.

Furthermore, it was found that the net thermal efficiency of the coal-fired power plant is considerably affected by the coal composition. Although the effect of variation in the standard deviations for the coal constituents was found to be of minor significance, there are several parameters that affect the overall performance. Namely, the increase in the mean value of moisture and fixed carbon contents resulted in a 12.9% increase and 23.4% decrease of the reliability index for the ULS, respectively. Hence, it can be concluded that it is more likely that the net thermal efficiency of the power plant would exceed the ULS for high fixed carbon contents and low moisture contents. Additionally, the sensitivity analysis revealed that 20% increase of the mean moisture content causes a slight reduction in the LLS reliability index (3.6%), while the effect of its reduction is negligible. Also, a 7.0% increase and a 7.2% drop in the LLS reliability index were observed for a 20% increase and a 20% decrease in the mean fixed carbon content, respectively.

5.4. Design implications

The reliability index provides a valuable insight in the process design, as it determines how likely the equipment is bound to fail to meet its design specification when subjected to the uncertain operating conditions. This would help the designer to assess whether considerable safety factors on the process equipment design are required. In general, the designer would need to determine the allowable failure probability that corresponds either to the serviceability limit state, in terms of the equipment design, or the ultimate limit state, in terms of the process performance.

Moreover, as risk should be kept as low as reasonably possible, the designer should decide on the minimal acceptable reliability index for the equipment failure or serviceability limit to optimise both the performance and the economy of the process. This would allow the designer to reduce the safety margin on the equipment design while keeping the probabilities of failure at a low level. Such an approach to the equipment design would result in reduced

equipment capital and operating cost, and possibly in increase of the equipment efficiency.

Although the capital and operating cost are out of the scope of this study, the framework for the reliability analysis described in this paper can be further extended to determine the economic value of the failure risk. At the design stage, oversizing of the equipment based on the design guidelines would increase the capital investment and could result in a drop of the equipment performance under off-design conditions. Therefore, if the equipment is sized based on the probabilistic performance data, which reveal the operating envelope of acceptable probability of failure, which is in example assumed to be 0.01, the capital cost could be reduced. Also, the equipment could be designed to operate at its optimal performance within this envelope leading to the operating cost optimisation. In addition, if the equipment degradation is considered, the maintenance and the equipment service scheduling can be integrated in the analysis with the assumption that these activities will take place if the reliability index of the equipment will drop below the serviceability level.

5.4.1. Coal, ash and oil handling systems

Based on the stochastic analysis presented in Section 5.1 it can be concluded that the coal and ash handling system design is determined by the ULS. This analysis revealed that, considering the uncertainty in the statistical data, the maximum coal consumption rate was 75.8 kg/s. It was also revealed that the lowest ULS reliability index (3.10) was obtained if the mean load was increased by 20%. However, such value of the reliability index indicates that the probability that the coal and ash handling system is overloaded is less than 0.001. Yet, the analysis also showed that for the initial statistical data it is most likely that the power plant would require 30.0 kg/s of coal to meet the market demand. This is reduced to approximately 23.6 kg/s on 20% decrease and increased to approximately 36.4 kg/s on a 20% increase of the mean load. Hence, it is advisable that the equipment would be designed in such a way that it operates with the highest efficiency within this range to maximise the overall process performance. However, the system design needs to allow for operation close to the maximum coal consumption rate to avoid excessive system overloading.

Furthermore, the design of the auxiliary oil system is determined by the LLS. For a minimal coal consumption rate in the system found to be 0.7 kg/s, with a negligible probability of 0.00001, the LLS reliability index was found to be 0.47, which dropped to −0.42 on a 20% reduction, and increased to 1.36 on a 20% increase of the mean load. Although a low value of the LLS reliability index could be a result of greater heating value of coal, which would cause a reduction in the coal requirement, the design of the auxiliary oil firing system is critical in terms of the reliability as reduction of the mean load could cause the LLS reliability index to drop below zero. Therefore, to assure that enough energy could be fed to the boiler at low load operation (below 40%), the oil handling and firing system would need to be sized in such a way, that even a 20% reduction in the mean load would not cause the LLS reliability index to drop below the desired serviceability limit.

5.4.2. Steam cycle and electricity generator

From the results presented in Section 5.2, it can be concluded that the machinery capacity, heat transfer areas for the feedwater heaters and condenser, as well as the electric generator size should be selected based on the ULS reliability index. The analysis revealed that, considering 20% deviation in the statistical data, the maximum steam generation rate that would need to be handled by the system is 714 kg/s. This corresponds to the moderate value of the ULS reliability index (2.26) and a probability of 0.0119. Also, the analysis showed that for the initial statistical data it is most likely that 350 kg/s of live steam will be generated in the boiler. This varies from 261.1 kg/s to 385.1 kg/s when the mean load is varied by ±20%. As was the case for the coal and ash handling system, the steam cycle equipment needs to be designed to reach its optimal operating performance within this range, as well as sized to reasonably minimise the under-utilisation and overloading probability and to maximise the system efficiency. This would reduce the capital cost as the sizing based on the predictive data rather than rigid safety factors will show the actual size required.

5.4.3. Net thermal efficiency of the power plant

The net thermal efficiency of the coal-fired power plant is the key parameter describing the overall performance of the process design. For this reason, if the desired efficiency is not met due to uncertainty present in the operating conditions, not only would the operating cost increase, but also the environmental impact of the system. Using the probabilistic performance assessment at the design stage makes it possible to assess whether the net thermal efficiency of the current design is within the desired range and evaluate the probability that the design specification is not met.

Based on the results presented in Section 5.3, it can be concluded that the net thermal efficiency will meet the specification for more than 80% of the operating time. It was also identified that the power plant will operate with efficiency exceeding the ULS with the probability of 0.1396, and below the LLS with the probability of 0.0459. Moreover, this indicates that to improve the performance and economy of the electricity generation, each of the power plant subsystems needs to be designed in such a way that it achieves its optimal performance within the operating envelope determined using the stochastic analysis.

6. Conclusions

The design and optimisation of state-of-the-art coal-fired power plants are usually conducted using deterministic models and reliability is handled using safety factors that are selected based on guidelines or industrial experiences. Not only does such approach affect the process efficiency, which is the result of the plant equipment not operated at optimal conditions, there is also a considerable increase in capital cost due to equipment oversizing. A different approach to performance assessment is proposed and is based on probabilistic analysis, where the impact of the process input uncertainty is systematically considered. This can be used to determine the reliability indices based on the analysis of the probability of failure of particular equipment.

The main aim of this work was to assess applicability of the probabilistic assessment methodology to analyse the coal-fired power plant performance. A process model developed and validated previously by the authors was analysed to identify key performance indicators. Sources of uncertainty, such as coal composition or the load at which the power plant is operated, were identified along with the operability limits. Information generated from 266 deterministic simulations of the coal-fired power plant model was used to create an approximation model. It was found that a polynomial regression provided a reasonably reliable prediction of the process performance, simultaneously assuring the simulation robustness. In the probabilistic assessment of the power plant performance several key performance indicators, such as the coal consumption rate, the steam generation rate and the net thermal efficiency, were analysed stochastically. It was shown that the reliability indices were positive for both ULS and LLS for all analysed parameters. This means that although the uncertainty included in the coal composition and the market demand result in considerable fluctuations of the system parameters, there is no need to apply conservative safety factors during the equipment design.

Moreover, the sensitivity analysis of the key statistical parameters revealed that the mean and standard deviation of the expected

power plant load have the highest impact on the reliability indices for all analysed key performance indicators. In addition, the effect of variation of the key statistical parameters of the coal composition on the value of the reliability index was found to be significant for the net thermal efficiency of the power plant (all components) and coal consumption rate (ash and fixed carbon content only). Therefore, a sensitivity study must follow the probabilistic performance analysis to reliably assess and apply the safety indices at the design stage.

Based on the obtained results, the methodology proposed for probabilistic assessment was proven applicable for the design and analysis of the coal-fired power plants. The estimated reliability indices provide a quantitative measure to assess whether the equipment needs to be oversized based on the uncertainty of the input.

Appendix A. Supplementary material

Supplementary data associated with this article can be found, in the online version, at http://dx.doi.org/10.1016/j.apenergy.2014.10.079.

References

[1] Goto K, Yogo K, Higashii T. A review of efficiency penalty in a coal-fired power plant with post-combustion CO_2 capture. Appl Energy 2013;111:710–20.
[2] Dai C, Cai XH, Cai YP, Huang GH. A simulation-based fuzzy possibilistic programming model for coal blending management with consideration of human health risk under uncertainty. Appl Energy 2014;133:1–13.
[3] IEA. Tracking clean energy progress 2013. IEA input to the clean energy ministerial. Paris, France: IEA Publications; 2013.
[4] Cong R, Wei Y. Potential impact of (CET) carbon emissions trading on China's power sector: a perspective from different allowance allocation options. Energy 2010;35(9):3921–31.
[5] Wang X, Cong R. Electric power supply chain management addressing climate change. Proc Eng 2012;29:749–53.
[6] IEA. Tracking clean energy progress 2014. Energy technology perspectives 2014 excerpt. IEA input to the clean energy ministerial. Paris, France: IEA Publications; 2014.
[7] IEA. CO_2 emissions from fuel combustion – highlights. 2012th ed. Paris, France: OECD/IEA; 2012.
[8] Li Z, Xu Z, Zhang D, West L, Forbes SM, Li L. Guidelines for carbon capture and storage in China. Beijing: Tsinghua University Press; 2010.
[9] Yu S, Wei Y, Guo H, Ding L. Carbon emission coefficient measurement of the coal-to-power energy chain in China. Appl Energy 2014;114:290–300.
[10] Jianfei S, Song X, Ming Z, Yi W, Yuejin W, Xiaoli L, et al. Low-carbon development strategies for the top five power generation groups during China's 12th five-year plan period. Renew Sustain Energy Rev 2014;34:350–60.
[11] Karampinis E, Nikolopoulos N, Nikolopoulos A, Grammelis P, Kakaras E. Numerical investigation Greek lignite/cardoon co-firing in a tangentially fired furnace. Appl Energy 2012;97:514–24.
[12] Beér JM. High efficiency electric power generation: the environmental role. Progr Energy Combust Sci 2007;33(2):107–34.
[13] Biliyok C, Yeung H. Evaluation of natural gas combined cycle power plant for post-combustion CO_2 capture integration. Int J Greenhouse Gas Control 2013;19:396–405.
[14] Hanak DP, Biliyok C, Manovic V. Hybrid modelling of a coal-fired power plant operating under load following mode, in preparation.
[15] Delattin F, De Ruyck J, Bram S. Detailed study of the impact of co-utilization of biomass in a natural gas combined cycle power plant through perturbation analysis. Appl Energy 2009;86(5):622–9.
[16] Rao AD, Francuz DJ. An evaluation of advanced combined cycles. Appl Energy 2013;102:1178–86.
[17] Hanak DP, Biliyok C, Yeung H, Białecki R. Heat integration and exergy analysis for a high ash supercritical coal-fired power plant integrated with a post-combustion carbon capture process. Fuel 2014;134:126–39.
[18] Seltzer A, Fan Z, Robertson A. Conceptual design of supercritical O_2-based PC boiler, DE-FC26-04NT2207. Livingston, NJ, USA: Foster Wheeler Power Group Inc.; 2006.
[19] Hu M, Cho H. A probability constrained multi-objective optimization model for CCHP system operation decision support. Appl Energy 2014;116:230–42.
[20] ABB, Power Generation. Energy Efficient Design of Auxiliary Systems in Fossil-Fuel Power Plants, ABB, Zurich, Switzerland; Wickliffe, OH, USA; 2009.
[21] Drbal L, Westra K, Boston P, editors. Power plant engineering. New York, NY, USA: Springer; 1996.
[22] Liptak BG, editor. Instrument engineers' handbook: process control and optimization, 2nd ed.. London, UK; New York, NY, USA; Washington, DC, USA: CRC-Press; 2005.
[23] Kitto JB, Stultz SC, editors. Steam – its generation and use, 41st ed.. Barberton, Ohio, USA: The Babcock & Wilcox Company; 2005.
[24] Kumar R, Sharma A, Tewari P. Markov approach to evaluate the availability simulation model for power generation system in a thermal power plant. Int J Indust Eng Computations 2012;3(5):743–50.
[25] Frey HC, Rubin ES. Probabilistic evaluation of advanced SO_2/NO_x control technology. J Air Waste Manage Assoc 1991;41(12):1585–93.
[26] Salmento JS, Rubin ES. Probabilistic framework for environmental control cost estimation, preprint – American Society of Mechanical Engineers, 25 September 1988 through 29 September 1988. Philadelphia, PA, USA, New York, NY, United States: American Soc of Mechanical Engineers (ASME); 1988.
[27] Rubin ES, Kalagnanam JR, Frey HC, Berkenpas MB. Integrated environmental control modeling of coal-fired power systems. J Air Waste Manage Assoc 1997;47(11):1180–8.
[28] Rubin ES, Rao AB. Uncertainties in CO_2 capture and sequestration costs. In: Kaya JG, editor. Greenhouse gas control technologies – 6th international conference. Oxford: Pergamon; 2003. p. 1119–24.
[29] Adhikary DD, Bose GK, Chattopadhyay S, Bose D, Mitra S. RAM investigation of coal-fired thermal power plants: a case study. Int J Indust Eng Comput 2012;3(3):423–34.
[30] Shayan ME. Probabilistic model of a coal-burning power plant. IEEE Trans Reliab 1986;R-35(5):488–93.
[31] Arora N, Kumar D. Stochastic analysis and maintenance planning of the ash handling system in the thermal power plant. Microelectron Reliab 1997;37(5):819–24.
[32] Gupta S, Tewari PC. Simulation, modeling and analysis of a complex system of a thermal power plant. J Indust Eng Manage 2009;2(2):387–406.
[33] Ellingwood BR. Issues related to structural aging in probabilistic risk assessment of nuclear power plants. Reliab Eng Syst Safety 1998;62(3):171–83.
[34] Micic TV, Chryssanthopoulos MK, Baker MJ. Reliability analysis for highway bridge deck assessment. Struct Safety 1995;17(3):135–50.
[35] Das PC. Application of reliability analysis in bridge management. Eng Struct 1998;20(11):957–9.
[36] Salonitis K, Kolios A. Reliability assessment of cutting tool life based on surrogate approximation methods. Int J Adv Manuf Technol 2014;71(5–8):1197–208.
[37] MacIntosh DL, Spengler JD, Staudt JE, Bachmann J. Emission of hazardous air pollutants from coal-fired power plants, EH&E Report 17505. Needham, MA, USA: Environmental Health & Engineering Inc.; 2011.
[38] International Standardization Organization. General principles on reliability for structures, 2394; 2008.
[39] Choi SK, Grandi RV. Reliability-based structural design. London, UK: Springer-Verlag; 2007.
[40] Hasofer AM, Lind NC. Exact and invariant second-moment code format. J Eng Mech Div 1974;100(1):111–21.
[41] Breitung K. Asymptotic approximations for multinormal integrals. J Eng Mech Div 1984;110(3):357–66.
[42] Tvedt L. Distribution of quadratic forms in normal space applications to structural reliability. J Eng Mech Div 1990;116(6):1183–97.
[43] Rajaguru P, Stoyanov S, Lu H, Baile C. Application of kriging and radial basis function for reliability optimization in power modules. J Electronic Packag 2013;135(2).
[44] Breitung K, Hohenbichler M. Asymptotic approximations for multivariate integrals with an application to multinormal probabilities. J Multivar Anal 1989;30(1):80–97.
[45] Choi SK, Grandhi RV, Canfield RA. Structural reliability under non-Gaussian stochastic behavior. Comput Struct 2004;82(13–14):1113–21.
[46] Kolios AJ, Casali D. Uncertainty quantification of pipe flow systems. Proceedings of the 10th International Probabilistic Workshop, November 2012, Stuttgart, Gernabt; 2012.
[47] Kolios AJ, Quinio A, Anoniadis A, Brennan F. An approach of stochastic expansions for the reliability assessment of complex structures. In: van Gelder P, Gucma L, Proske D. editors. Proceedings of the 8th international probabilistic workshop, Szczecin; 2010. p. 223.
[48] Gavin HP, Yau SC. High-order limit state functions in the response surface method for structural reliability analysis. Struct Safety 2008;30(2):162–79.
[49] Sudret B, der Kiureghian A. A stochastic finite element methods and reliability. State of the art report. UCB/SEMM-2000/08. Barkeley, CA, USA: University of California; 2000.
[50] Schweinfurth SS. Chapter C: an introduction to coal quality. In: Pierce BS, Dennen KO, editors. The national coal resource assessment overview. U.S. Geological Survey; 2009. p. 16.
[51] Affolter RH, Hatch JR. Chapter E: characterisation of the quality of coals from the Illinois basin. In: Affolter RH, Hatch JR, editors. Resource assessment of the springfield, herrin, danville, and baker coals in the illinois basin. U.S. Geological Survey; 2002. p. E1–E230.
[52] Affolter RH. Quality characterization of cretaceous coal from the Colorado Plateau coal assessment area. In: Krischbaum MA, Roberts LNR, Biewick LRH, editors. Geologic assessment of coal in the Colorado Plateau: Arizona, Colorado, New Mexico, and Utah, 1st ed., U.S. Geological Survey, <http://on.doi.gov/1iETfxA>, p. G1–G136 (accessed 22.04.14).
[53] IEX. Indian Energy Market Snapshot between 1st and 7th January 2014. <http://bit.ly/OZVIH8>; 2014 (accessed 14.04.14).
[54] ECN. ECN Phyllis classification, <http://bit.ly/1hrh1cu>; 2012 (accessed 05.05.14).

11 COMPARISON OF PROBABILISTIC PERFORMANCE OF CALCIUM LOOPING AND CHEMICAL SOLVENT SCRUBBING RETROFITS FOR CO_2 CAPTURE FROM COAL-FIRED POWER PLANT

Dawid P. Hanak, Athanasios J. Kolios, and Vasilije Manovic

Published: Applied Energy, 2016, 172, 323–336[I]

Statement of contributions of joint authorship

Dawid P. Hanak conducted the literature review, performed process analysis via process modelling and simulation, and probabilistic analysis, drafted and critically revised the manuscript, as well as prepared tables and figures. Athanasios J. Kolios supported adaptation of the probabilistic analysis and critically commented on the manuscript. Vasilije Manovic proof-read and critically commented on the manuscript prior to its submission to Applied Energy (Journal Impact Factor 2016: 5.613).

Dawid Piotr Hanak, PhD Candidate

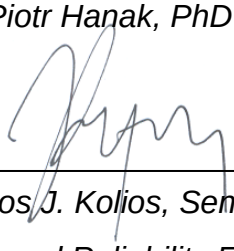

Athanasios J. Kolios, Senior lecturer in Risk and Reliability Engineering

Vasilije Manovic, Primary supervisor

[I] Reprinted with permission from Hanak, D.P., Kolios, A.J., and Manovic, V. (2016), "Comparison of probabilistic performance of calcium looping and chemical solvent scrubbing retrofits for CO_2 capture from coal-fired power plant", *Applied Energy*, 172, 323–336, doi: 10.1016/j.apenergy.2016.03.102, Elsevier 2016.

Applied Energy 172 (2016) 323–336

Contents lists available at ScienceDirect

Applied Energy

journal homepage: www.elsevier.com/locate/apenergy

Comparison of probabilistic performance of calcium looping and chemical solvent scrubbing retrofits for CO_2 capture from coal-fired power plant

Dawid P. Hanak *, Athanasios J. Kolios, Vasilije Manovic

Combustion and CCS Centre, Cranfield University, Bedford, Bedfordshire MK43 0AL, UK

HIGHLIGHTS

- Engineering equipment is usually oversized to account for input uncertainties.
- Probabilistic framework was employed to compare CO_2 capture retrofit scenarios.
- Effect of uncertainties on process performance and equipment design was evaluated.
- Most probable efficiency penalties were 9.5 and 11.5% points for CaL and MEA retrofits.
- Lower limit state was found crucial in design of the CO_2 capture systems.

ARTICLE INFO

Article history:
Received 3 February 2016
Received in revised form 8 March 2016
Accepted 28 March 2016
Available online 7 April 2016

Keywords:
Probabilistic performance assessment
Post-combustion capture
Calcium looping
Amine scrubbing
Stochastic modelling
Monte Carlo simulation

ABSTRACT

Carbon capture and storage technologies are seen as crucial for decarbonisation of the power sector because large-scale deployment of these technologies is expected to reduce wholesale electricity prices and decarbonisation costs significantly. An emerging calcium looping process (CaL) was found to be a promising alternative to the amine scrubbing process, as its retrofit has the potential to reduce the efficiency penalty and increase the net power output of the integrated system. Process modelling is often utilised in the development of novel low-carbon power generation systems, but the deterministic nature of the process models does not provide a definitive representation of the actual system's performance. This study provides a framework for comparison of the probabilistic performance of a coal-fired power plant (CFPP) in CO_2 capture retrofit scenarios. Having compared the probabilistic performance of the CFPP retrofitted with the mature MEA scrubbing process and emerging CaL process, it was found that the most probable values for the efficiency penalties are 9.5% and 11.5% points in the CaL and MEA retrofit scenarios, respectively. Also, the net power output in the CaL retrofit scenario was found to be 40% higher than that of the reference CFPP and two times higher than that in the case of the MEA retrofit scenario, even considering higher uncertainty in the operating conditions of the CaL process. Finally, the probabilistic approach was found to be capable of producing valuable information on the equipment operating envelope that would help designers assessing the number of equipment trains and their operating limits. Therefore, the probabilistic framework for comparison of CO_2 capture retrofit scenarios would provide valuable input to the investment decision-making process, as by considering the impact of uncertainty on the process performance, it generates information that could serve as valuable input to the probabilistic economic analysis and process design.

1. Introduction

It has recently been suggested through the Paris Agreement reached at the 21st Conference of the Parties held in Paris that to significantly reduce the risks and impacts of climate change, the mean temperature increase needs to be held well below 2 °C and efforts to limit it to 1.5 °C above pre-industrial levels need to be

Abbreviations: CaL, calcium looping; CFPP, coal-fired power plant; CCS, carbon capture and storage; CCU, CO_2 compression unit; KPI, key performance indicator; LLS, lower limit state; MDEA, methyldiethanolamine; MEA, monoethanolamine; PZ, piperazine; ULS, upper limit state.

* Corresponding author.
E-mail address: d.p.hanak@cranfield.ac.uk (D.P. Hanak).

http://dx.doi.org/10.1016/j.apenergy.2016.03.102
0306-2619/

Nomenclature

Latin symbols

a	approximation model parameter
b_i	approximation model parameters
c_i	approximation model parameters
F_0	fresh sorbent make-up rate (kmol/s)
F_R	sorbent looping rate (kmol/s)
$\tilde{g}$	dependent variable
L	allowable (permitted limit) for a given variable
Mo	mode of stochastic variable
M_u	design matrix
n	number of samples
$N_{failure}$	number of failures indicated in Monte Carlo simulation
N_{runs}	number of runs in Monte Carlo simulation
p	steam pressure (bar)
P_f	probability of failure
Q_{calc}	calciner heat duty (MW_{th})
Q_{reb}	reboiler duty (MW_{th})
X	multi-variable vector
X_i	stochastic variable

Greek symbols

β	reliability index
ϕ^{-1}	inverse of the normal cumulative distribution
μ	mean value of stochastic variable

pursued [1]. The power sector is one of the major global emitters of CO_2 [2–4], which is a result of a large share (42%) of coal-fired power plants (CFPP) in the global electricity generating capacity [5,6] accounting for over 70% of the sector's CO_2 emissions [7]. Carbon capture and storage (CCS) is seen as crucial for decarbonisation of this sector [8,9], as it is expected to account for 13% cumulative reduction of greenhouse gas emissions between 2012 and 2050 [10,11]. It is important to highlight that deployment of CCS in the power sector is often regarded as a precursor for decarbonisation of other sectors [12]. Moreover, large-scale deployment of CCS is seen as the least cost option for reduction of CO_2 emissions, primarily due to higher capital cost associated with alternative technologies, such as offshore wind farms and geothermal power plants, required to reach desired emission reduction levels [13]. Hence, implementation of CCS is predicted to reduce wholesale electricity prices in the UK by up to 15% by 2030 compared to a no-CCS scenario [13]. Also, if CCS is not implemented in the power sector, the capital cost required to achieve more than 50% reduction of the global energy-related CO_2 emissions by 2050 relative to 2009 (IEA 2 °C scenario) is expected to be 40% higher [14].

Implementation of post-combustion CO_2 capture is perceived as the most important CO_2 capture technology for reducing the environmental impact of the power sector [15]. Chemical solvent scrubbing using amine-based solvents, such as monoethanolamine (MEA), piperazine (PZ) or methyldiethanolamine (MDEA), is currently perceived as the most mature CO_2 capture technology that will probably be a first choice technology for decarbonisation of fossil fuel power plants [16–18]. However mature the amine scrubbing process is, retrofit of this technology to CFPPs was found to reduce their net efficiency by around 7.0–12.5% points [19–25]. Such efficiency penalties, which were estimated using process models, stem mainly from steam extraction from the steam cycle to provide heat for solvent regeneration, which leads to a reduction in the gross power output of the retrofitted system. This de-rating of the power plant efficiency and power output is expected to contribute towards an increase in the cost of electricity, which is estimated to be around 60–125% [26–28]. Therefore, novel technologies for decarbonisation of the CFPPs that will result in lower efficiency penalties are currently under development [29]. A calcium looping process (CaL) was found to be a promising alternative to the amine scrubbing process, as not only is it expected to result in lower efficiency penalties of around 3–8% points [30–37], but also has the ability to increase the net power output of the retrofitted system by around 50–80% compared to the reference coal-fired power plant [33–35,38,39]. This is due to availability of a large amount of high-grade heat in CaL that can be used to raise high-pressure steam for a secondary steam cycle. As a result, the CFPP retrofitted with CaL for 90% capture was found to bring higher daily profit than the reference CFPP if the price of CO_2 emission allowance exceeds 8.5 €/tCO_2 [40], which is equal to the average price of the European emission allowances in November 2015 [41]. Other advantages of CaL over amine scrubbing are the use of globally available and inexpensive sorbent (natural limestone or dolomite) that is characterised by high CO_2 carrying capacity [42], as well as low health and environmental footprints [43]. Yet, the CaL process for coal-fired power plants has only been successfully demonstrated at pilot-scale units up to 1–2 MW_{th} [36,37], while the amine scrubbing process has already been demonstrated at commercial scale at the Boundary Dam 139 MW_{el} coal-fired power plant [44]. Therefore, before the benefits of CaL will be utilised in the existing energy market, rapid demonstration of this technology at commercial scale is required.

Process modelling is often utilised in the development of novel low-carbon power generation systems, such as zero-emission coal gasification technologies [45,46] and integrated gasification combined cycle power plants [46–50], as well as the evaluation of CO_2 capture retrofits to existing systems [30,31,33–35,51–54]. Although such approach can provide reliable prediction of the system's performance under any operating conditions, these models do not consider the stochasticity of the input variables; hence, their deterministic nature does not provide a definitive representation of the actual system's performance that is usually subjected to random fluctuations in the external and internal operating conditions [55]. To account for uncertainties in the operating conditions, which result mostly from fluctuation of the load factors to meet market demand and integration of auxiliary systems, it is a common design practice to oversize equipment in engineering systems. This is usually achieved by applying safety factors to the equipment design, which are selected according to sizing guidelines derived from field experience, to ensure safe operation within material and operability limits. However, such a design approach results in a considerable parasitic load on the system as the oversized and under-loaded equipment degrades its rated efficiency and may operate in an unstable manner, as well as leads to higher operating and capital costs [56–58]. In addition, equipment overheating and a fall in electricity production or product yield could also be observed if the system is under-sized [56]. It is important to highlight that poor design and high system complexity, among others, have been identified as the main causes of failures [59].

Application of an alternative approach that utilises a probabilistic analysis to estimate the equipment failure probabilities was found to provide a more profound insight into operation, performance and economics of the engineering systems, such as integrated gasification combined cycle [60], CO_2 capture and sequestration [61],

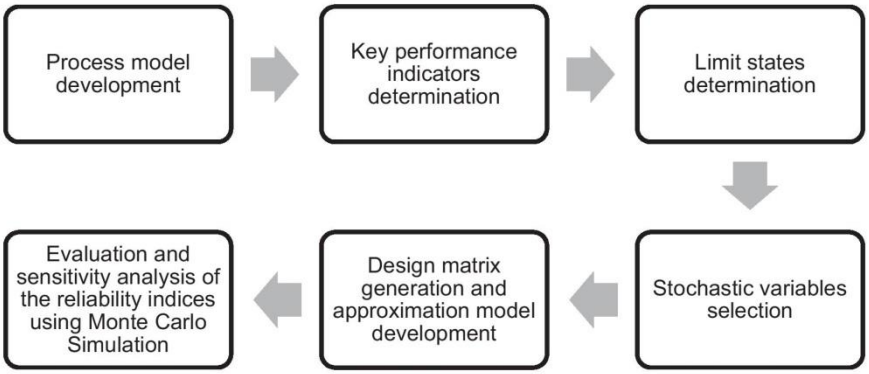

Fig. 1. Overview of the probabilistic performance assessment framework.

SO_2/NO_x emission control technology [62] and CFPP [63]. Yet, the literature search revealed that the CO_2 capture retrofit scenarios of the coal-fired power plant have been assessed and compared using only a deterministic approach [33,35,64], which does not provide a definitive representation of the system's performance. As opposed to previous studies, this study employs the probabilistic performance framework reported by Hanak et al. [63] (Fig. 1), which combines a finite number of deterministic simulations to approximation methods and Monte Carlo simulation, to compare the thermodynamic performance of the CFPP in two retrofit scenarios – with the emerging CaL process and mature MEA scrubbing process. As such approach considers the effect of uncertainties on the performance prediction, it is expected that the estimation of net efficiency penalties and variation in the net power output would be more realistic. Additionally, application of the probabilistic approach to analyse the CO_2 capture retrofit scenarios would reveal the system operating envelope, bringing a more profound insight into the process operation, and thus its design. Furthermore, an implication of uncertainty and expected operating envelope on the CO_2 capture design is analysed through estimation of the probabilities that critical system thresholds are exceeded due to uncertainty in the system's operating conditions. Such information would provide a valuable insight into design of the CO_2 capture retrofit scenarios.

2. Process models description

2.1. Supercritical coal-fired power plant

A conventional 660 MW_{el} supercritical CFPP, which at the base load operates with a net thermal efficiency of 38.8%$_{HHV}$, was selected as a benchmark power plant for this study. A high-fidelity process model of this unit, which consists of a once-through steam boiler with the flue gas treatment train, for NO_x, SO_x and fly ash removal, and a supercritical reheat steam cycle (242.2 bar/537 °C/565 °C), has been developed in Aspen Plus™ by Hanak et al. [51] based on data provided by Suresh et al. [65]. The prediction capabilities of the Aspen Plus process model were extended to off-design conditions through implementing a Stodola's ellipse law [66] to account for variability of the steam pressure in the steam cycle, Salisbury's equation [67] to account for variability of the isentropic efficiency of the steam turbine sections, and the general pressure drop correlation [68] for determining the off-design pressure drop in the heat exchanger sections of the boiler. The accuracy of the 660 MW_{el} CFPP process model prediction was found to be in good agreement with the data reported by Suresh et al. [65] at different operating loads (40–100%), proving the validity of the modelling approach even at off-design conditions [51].

2.2. Amine scrubbing post-combustion CO_2 capture plant

A chemical scrubbing CO_2 capture plant using 30%$_{wt}$ MEA as a solvent has been selected in this study as a reference CO_2 capture technology. A high-fidelity rate-based model for this unit has been developed by adapting the model developed by AspenTech [69], as described in detail by Hanak et al. [51,70]. The MEA plant model comprises a single absorber, modelled as a square column following the recent experience from the Boundary Dam project [71], and a single cylindrical stripper. The process model was adapted to capture 90% of CO_2 from the supercritical CFPP described in Section 2.1. For the off-design operation, it is assumed that the CO_2 capture plant operates with fixed CO_2 capture level of 90%, which is achieved by varying the solvent circulation rate while maintaining the lean loading of 0.29, as proposed by Jordal et al. [72]. Extensive validation of the selected modelling approach was conducted by AspenTech [69] and Canepa et al. [73] revealing that the model was capable of well-representing the experimental facility performance under different liquid-to-gas ratios. Therefore, with the equipment in the CO_2 capture plant sized for operation under 100% load, the model is expected to predict the process performance under various loads with reasonable accuracy.

2.3. Calcium looping post-combustion CO_2 capture plant

A CaL process, which is based on the reversible reaction between lime and CO_2 at high temperature, is considered in this study as an emerging CO_2 capture technology. A process model for this unit has been developed by Hanak et al. [35] and based on the semi-empirical model derived by Rodríguez et al. [74] with the sorbent deactivation curve derived from experimental tests at the 1.7 MW_{th} la Pereda pilot plant [75]. The CaL plant comprises a carbonator, which is modelled as a stoichiometric reactor, and a calciner, which is modelled as a Gibbs reactor and in which an additional amount of coal is combusted in an O_2/CO_2 environment to sustain the endothermic calcination reaction and ensure the high purity of CO_2 leaving the calciner. The model was found to show good agreement with the experimental data at different flue gas loads and, as in the case of the MEA plant model, it is expected to predict the process performance under various loads with reasonable accuracy. In this study, it is assumed that the overall CO_2 capture level, which comprises CO_2 capture from the power plant flue gas and coal oxy-combustion in the calciner, is 90%. This is

Table 1
Summary of the key process model assumptions.

Parameter		Value
Coal-fired power plant		
Combustor	Excess air ratio ($\%_{vol,dry}$)	20.0
Primary steam cycle	Design live/reheat steam temperature (°C)	537.0/565
	Design live/reheat steam pressure (bar)	242.2/44.3
	Final feedwater temperature (°C)	280.0
	Feedwater heater terminal temperature difference (°C)	3.0
	Feedwater heater minimum temperature approach (°C)	3.0
	Isentropic efficiency of compressors (%)	80.0
	Isentropic efficiency of high-pressure steam turbine (%)	89.6
	Isentropic efficiency of intermediate-pressure steam turbine (%)	91.7
	Isentropic efficiency of low-pressure steam turbine (%)	85.7
	Isentropic efficiency of pumps (%)	85.0
	Electrical efficiency of generator (%)	98.7
Flue gas treatment	SO_2 removal efficiency (%)	98.0
	Fly ash removal efficiency (%)	99.8
	NO_x removal efficiency (%)	86.0
Amine scrubbing CO_2 capture plant		
Absorber	Operating pressure (bar)	1.0
	Flue gas inlet temperature (°C)	40.0
	Lean solvent inlet temperature (°C)	40.0
	CO_2 capture level (%)	90.0
Stripper	Operating pressure (bar)	1.7
	Reboiler temperature (°C)	122.4
	Condenser temperature (°C)	40.0
Cross heat exchanger	Minimum temperature approach (°C)	10.0
Calcium looping CO_2 capture plant		
Carbonator	Temperature (°C)	650
	Carbonation extent (–)	0.70
Calciner	Temperature (°C)	900
	Calcination extent (–)	0.95
	Relative make up (fresh limestone/sorbent circulation rate) (–)	0.04
	O_2 concentration in fluidising gas entering the calciner ($\%_{vol,wet}$)	40.0
	O_2 excess ($\%_{vol,dry}$)	2.5
Secondary steam cycle	Design live/reheat steam temperature (°C)	593.3/593.3
	Design live/reheat steam pressure (bar)	242.3/49.0
Auxiliary equipment		
CO_2 compression unit	Polytrophic efficiency of CO_2 compressors (%)	78.0–80.0
	Isentropic efficiency of CO_2 pump (%)	80.0
	Intercooling temperature (°C)	40.0
	CO_2 final pressure (bar)	110.0
	CO_2 final temperature (°C)	30.0
Air separation unit	O_2 purity ($\%_{vol}$)	95.0
	Polytrophic efficiency of air compressors (%)	79.0–80.0
	Intercooling temperature (°C)	40.0
	Final air pressure (bar)	5.8

achieved by varying the sorbent looping rate while maintaining the relative limestone make-up rate at 0.04. The high-grade heat available in CaL is utilised to raise high-pressure steam for the secondary steam cycle.

2.4. Key model assumptions and performance indicators

A summary of the input parameters to the CFPP, MEA plant and CaL plant process models used to generate the deterministic design matrix in this study is presented in Table 1. Main input data to these models comprise design parameters, such as turbomachinery efficiencies, desired operating temperatures and pressures, pollutant removal efficiencies, and compositions of coal, limestone and air [63,76,77].

As indicated in Sections 2.1–2.3, the process models used in this study are capable of predicting the off-design performance reliably. Therefore, any change in the input data, which can be compared to the fluctuations in the real systems' parameters resulting from uncertainty in the operating load of the CFPP, compositions of coal, limestone and air, and the control system measurements, will influence the predictions of the operating conditions throughout the entire system. This would lead to subsequent variations in the process stream flow rates, temperatures and pressures that can fall outside of the design operating envelope of the system's equipment, leading to operation with a degraded efficiency or even a failure.

The key performance indicators characterising retrofit of the CO_2 capture plant to the CFPP are loss in the electricity generation efficiency, which can be defined as the difference between the net efficiency of the reference and the retrofitted CFPP under the same operating conditions, and the power plant de-rating, which can be defined as reduction of the net power output of the retrofitted system with respect to the reference value. However, the latter parameter will not be valid for evaluating the CaL retrofit scenarios, as this technology was found to be capable of increasing the net power output due to its high-temperature operation [33–35,38,39]. For this reason, the change in the net power output, rather than power plant de-rating, can serve as an additional performance indicator for comparison of the retrofitted systems.

3. Probabilistic performance assessment

3.1. Limit state determination

The process models of the reference CFPP [51], CFPP retrofitted with the MEA plant [51], and CFPP retrofitted with the CaL plant [35] were used to determine the operating envelopes for the key performance indicators, which correspond to these models operated at 40% and 100% load (Table 2). In this study, two groups of limit states are used. On the one hand, a first group comprises the key system performance indicators, such as net thermal efficiency and net power output. If any of these performance indicators is outside the design envelope, a physical failure does not necessarily occur in the system, but the design thermodynamic or economic performance targets will not be met. On the other hand, a second group includes the key system equipment performance indicators that are mainly related to the equipment throughput, operating pressure and temperature. In this case, exceedance of the upper limit state (ULS[1]) may lead to a physical failure of the equipment, while operating the equipment below the lower limit state (LLS) may lead to degraded efficiency and unstable operation of the equipment. A number of the key performance indicators have been selected for assessment using the probabilistic approach and are summarised in Table 3. Additionally, the effect of not meeting the limit states is identified.

3.2. Selection of stochastic variables

Selection of the stochastic variables, which are assumed to be uncorrelated and normally distributed with the statistic parameters presented in Table 4, has been conducted based on the analysis of the key model assumptions and the process model.

[1] Although ULS in reliability terminology normally stands for ultimate limit state, this paper considers it as upper limit state for consistency with the framework proposed by Hanak et al. [63].

Table 2
Key performance indicators and their operating limits based on deterministic simulation.

Key performance indicator	Reference CFPP		CFPP retrofitted with MEA plant		CFPP retrofitted with CaL plant	
	Minimum	Maximum	Minimum	Maximum	Minimum	Maximum
System performance indices						
Net thermal efficiency ($\%_{HHV}$)	34.5	38.8	22.3	28.2	25.1	29.8
Net power output (MW_{el})	247.0	633.0	159.8	461.1	338.6	899.8
Specific coal consumption (g/kW_{el} h)	385.3	343.0	595.6	470.9	530.4	445.7
Specific CO_2 emissions (g/kW_{el} h)	969.0	835.0	149.8	114.6	187.9	118.4
Equipment operating conditions						
Condenser total cooling water rate (kg/s)	9007.5	18874.2	3680.7	6661.0	14989.5	33147.2
High-pressure steam generation rate[a] (kg/s)	223.1	550.7	223.3	550.6	223.1	550.7
High-pressure steam pressure[a] (bar)	99.0	242.2	99.2	242.2	99.0	242.2
Intermediate-pressure steam pressure[a] (bar)	17.7	42.0	18.2	41.8	17.7	42.0
Low-pressure steam pressure[a] (bar)	1.4	3.0	0.6	0.7	1.4	3.0
High-pressure steam generation rate[b] (kg/s)					147.1	332.7
High-pressure steam pressure[b] (bar)					111.1	242.3
Intermediate-pressure steam pressure[b] (bar)					18.7	45.2
Low-pressure steam pressure[b] (bar)					4.3	9.5
Low-pressure steam extraction rate[a] (kg/s)			118.0	277.4		
Reboiler duty (MW_{th})			293.8	644.8		
Additional coal consumption (kg/s)					23.4	51.1
Calciner heat input (MW_{th})					634.8	1383.6
CO_2 flow rate to compression unit (kg/s)			60.9	134.4	134.4	295.2

[a] Parameter related to primary steam cycle in the reference coal-fired power plant.
[b] Parameter related to the secondary steam cycle in the CaL plant.

The performance of the reference CFPP, the MEA plant and the CaL plant is mainly dependent upon the current grid electricity demand, which determines the operating load of the system. Therefore, the systems modelled in this study are considered to operate in a demand-following mode with the CFPP load considered as a stochastic variable that is normally distributed. The stochastic parameters for the operating load were estimated based on expected annual load changes reported by the Indian Energy Exchange [78]. Moreover, it is important to consider variation in the fuel composition that determines the amount of chemical energy input per unit amount of fuel. As the moisture content can impact the coal consumption in the investigated systems, it is selected as the stochastic parameter with the normal distribution determined based on the coal composition from the Carbondale field [79]. Finally, the performance of the considered CO_2 capture plants is dependent upon different variables. Namely, it has been reported that the CaL plant is mainly dependent upon the relative make-up rate of fresh sorbent, which affects the average conversion in the carbonator and varies between 0.025 [80] and 0.06 [81]. However, a 20% error associated with measurement of the solid looping rates, and thus estimation of the average conversion, was reported by Charitos et al. [82] and Rodríguez et al. [83]. Therefore, the relative fresh sorbent make-up rate (F_0/F_R) is selected as a stochastic variable for the CaL retrofit scenario and is characterised by the coefficient of variation of ±20%. The average sorbent conversion in the carbonator and the calciner can be seen as equivalent to rich and lean loadings in the solvent scrubbing technologies [80]. As it has been proposed by Jordal et al. [72] to control the off-design performance of the MEA plant using lean loading, it is selected as a stochastic variable for the MEA retrofit scenario. Although the measurement of the lean loading in the sour gas treatment plant was reported to vary by ±2% [84], a more conservative coefficient of variation (3.4%) was used in this study.

It needs to be highlighted that although the moisture content in coal and the CFPP load can be well represented by the normal distribution [63,79], there are not enough data available to determine the statistical distribution of the lean loading and relative make-up rate of fresh sorbent. Although this study assumes these to be normally distributed, the probabilistic framework can easily accommodate any statistical distribution once the relevant data become available.

3.3. Stochastic response surface approximation model development for Monte Carlo simulation

The probabilistic analysis cannot be directly conducted using the process models developed in Aspen Plus, as the number of iterations required for reliable results of the Monte Carlo simulations can be higher than a million, and thus such approach would be extremely computationally demanding. For this reason, the process models described in Section 2 are used to generate the design matrix that is, in turn, used to develop the robust approximation model, which in this study is a generic quadratic polynomial model presented in Eq. (1) [85].

$$\tilde{g}(X) = a + \sum_{i=1}^{n} b_i \cdot X_i + \sum_{i=1}^{n} c_i \cdot X_i^2 \quad (1)$$

To achieve a reliable representation of the process performance and to calculate $(2n + 1)$ coefficients a, b_i and c_i, the number of samples in the design matrix needs to be at least $(2n + 1)$ to 3^n. The design matrix[2] generated for the purpose of this study comprises 32 entries of the key performance indicators resulting from the following variation of the stochastic parameters:

- The CFPP load was varied from 40% to 100% with 20% step for all investigated scenarios.
- The moisture content in coal was varied from 1.22% to 3.66% with 0.61% step (25% of the initial moisture content of 2.44%) for all investigated scenarios.
- The lean loading was varied from 0.26 to 0.30 with 0.01 step for the CFPP retrofitted with the MEA plant scenario.

[2] A full design matrix comprising a total of 32 entries is provided in Supplementary Information. These entries break down to 8 entries for the reference coal-fired power plant (5–9 required) and 24 entries for the retrofit scenarios (12 for MEA retrofit and 12 for CaL retrofit, 7–27 required for each).

Table 3
Interpretation of limit states.

What if?	Limit state	Result
Thermodynamic limit states		
Net thermal efficiency	Is below lower limit	Inefficient coal utilisation leading to increased cost of electricity and specific emissions
	Is above upper limit	Higher coal utilisation efficiency leading to reduced cost of electricity and specific emissions
Net power output	Is below lower limit	The contracted amount of power output may not be delivered to the grid leading to loss in profit
	Is above upper limit	Higher amount of power than contracted may increase the profit if it can be utilised in the grid
Specific coal consumption	Is below lower limit	Inefficient coal utilisation leading to increased cost of electricity and specific emissions
	Is above upper limit	Higher coal utilisation efficiency leading to reduced cost of electricity and specific emissions
Equipment limit states		
CO_2 flow rate to compression unit	Is below lower limit	Possible compressor stall or compressor surge, leading to reduced efficiency
	Is above upper limit	CO_2 compressors not capable of processing the required CO_2 rate. Increased amount of CO_2 to storage leading to faster utilisation of the reservoir
Low-pressure steam pressure in primary steam cycle	Is below lower limit	A drop in low-pressure turbine efficiency and power output
	Is above upper limit	Possible material deterioration and failures due to loads exceeding allowable material strength
High-pressure steam pressure in secondary steam cycle	Is below lower limit	A drop in high-pressure steam turbine efficiency and power output
	Is above upper limit	Possible material deterioration and failures due to loads exceeding allowable material strength
Reboiler duty	Is below lower limit	Not sufficient solvent regeneration leading to decreased CO_2 capture efficiency
	Is above upper limit	An increase in the heat requirement for solvent regeneration leading to increased parasitic load
Calciner heat duty	Is below lower limit	Not sufficient sorbent regeneration leading to decreased CO_2 capture efficiency. Possible requirement for supplementary gas firing to keep desired temperature in the calciner. Desired O_2 purity from ASU cannot be achieved
	Is above upper limit	An increase in the heat requirement for solvent regeneration leading to increased parasitic load. Coal and ash handling equipment not capable of processing the required solids rate. Air separation unit not capable of providing required O_2 rate

Table 4
Statistical parameters of stochastic variables.

Stochastic variable	Mean value	Standard deviation
Moisture content in coal (as received, $\%_{wt}$)	1.4	1.0
Coal-fired power plant load (%)	58.9	13.0
Lean loading (mol basis)	0.29	0.01
Relative sorbent make-up rate (mol basis)	0.04	0.008

- The relative limestone make-up rate was varied from 0.02 to 0.06 with 0.01 step for the CFPP retrofitted with the CaL plant scenario.

Prediction accuracy of the approximation model can be assessed by quantifying the average deviation, which is defined as the difference in parameter value predicted by the process model and the approximation model under the same input conditions. For the key performance indicators considered in this study, the average deviation was within 0.01–0.4%, with an average of 0.13%, indicating that application of the generic quadratic polynomial model can be expected to provide a reasonably reliable prediction. Further improvement in the prediction accuracy can be achieved through employing more complex approximation methods, such as Kriging, that are well-suited for capturing the non-linear limit states [86].

The Monte Carlo simulation, employed to randomly generate the values of the stochastic variables according to their statistical distribution, which are then used in the approximation models, can be used to estimate the probability that the key performance indicators fall outside the desired operating envelope, which occurs when $\tilde{g}(X) < 0$. By considering a large number of runs (N_{runs}), which should be at least the inverse of two orders of magnitude of the expected failure probability order, and counting the number of incidents that the failure condition is met ($N_{failues}$), probability of failure can be estimated using Eq. (2) [87,88].

If the limit state function $\tilde{g}(X)$ is normally distributed, $\tilde{g}(X) = 0$ and the actual values of the random variables are uncorrelated, estimated failure probability for each considered limit state can be used in Eq. (3) to estimate the reliability index (β), which can be benchmarked with the allowable value.

$$P_f = \frac{N_{failures}}{N_{runs}} \tag{2}$$

$$\beta = \phi^{-1}(1 - P_f) \tag{3}$$

4. Results and discussion

4.1. Thermodynamic performance comparison

The probabilistic approach employed in the analysis of the engineering systems allows predicting the operating envelopes of the systems' parameters under uncertain input conditions. When used to compare CO_2 capture retrofit scenarios, such approach provides valuable input to the investment decision-making process, as it can be used to compare the impact of uncertainty on the thermodynamic performance of the considered scenarios that can be further used as input to the probabilistic economic analysis and process design.

Comparing the thermodynamic performance of the considered scenarios, Fig. 2a has revealed that the net thermal efficiency of the reference CFPP is always higher than in any CO_2 capture retrofit scenario considered in this study, and reaches a maximum value of $39.8\%_{HHV}$ at a very low moisture content (0.2%) and high operating load (94.6%). This is reflected in the mean value (μ) of the efficiency penalty of 9.6% and 11.7% points estimated for the CaL retrofit and the MEA retrofit scenario, respectively. However, it needs to be highlighted that although the stochastic variables were assumed to be normally distributed, the statistical distribution of the net thermal efficiency is a negatively-skewed normal distribution that is a result of the nonlinear correlation between net thermal efficiency and the stochastic parameters. Therefore, the mode (Mo) of the efficiency penalty, which represents its value occurring with the highest probability, yields more accurate results compared to the mean value and is estimated to be 9.5% and 11.5%

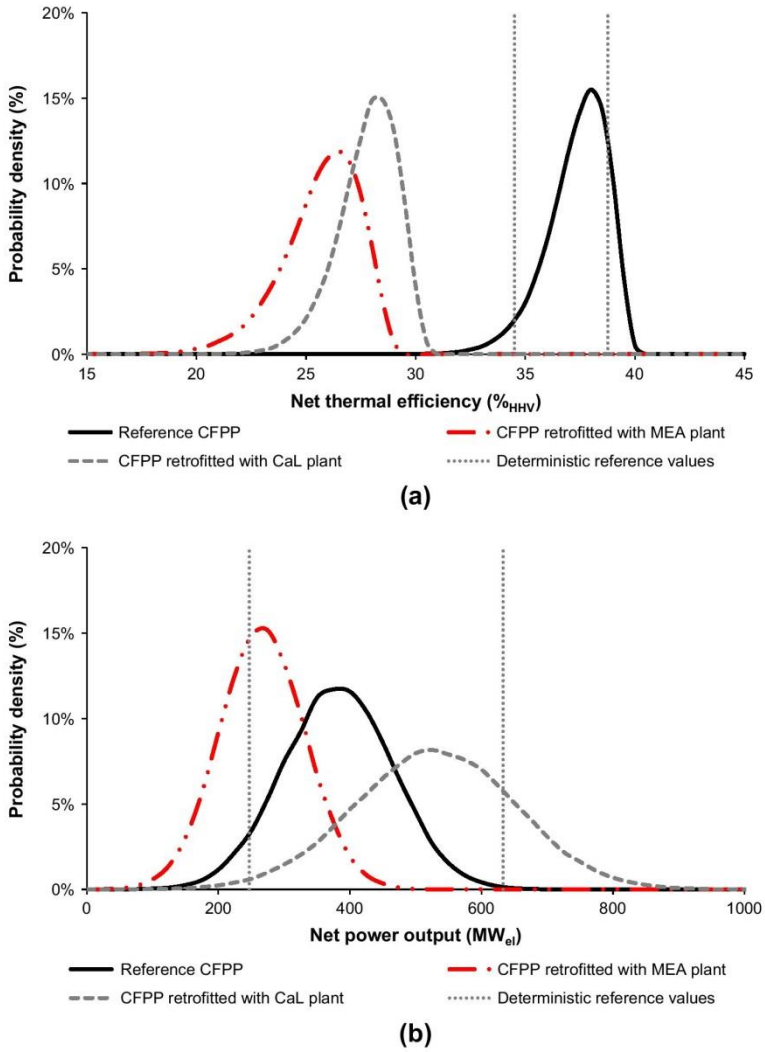

Fig. 2. Probabilistic comparison of thermodynamic performance.

points for the CaL retrofit and the MEA retrofit scenario, respectively. Importantly, the net thermal efficiency of the CaL retrofit scenario is higher than that of the MEA retrofit scenario as the mode and the mean values are 2% and 2.1% points, respectively, proving that the CaL plant has a potential to reduce the impact of CO_2 capture on the power generation efficiency. In addition, the probabilistic analysis has revealed that the influence of input uncertainty on the net thermal efficiency is lower for the CaL retrofit scenario, as the span of the operating envelope, which is defined as the difference between the maximum and minimum value identified in the probabilistic analysis, is 25% lower than in the MEA retrofit scenario. Yet, the minimum net efficiency penalty, with respect to the maximum net thermal efficiency of the reference coal-fired power plant of 39.8%$_{HHV}$, for the CaL and MEA retrofit scenario was found to be 9.3% points[3] and 10.6% points,[4] respectively.

In contrast to the net thermal efficiency, the statistical distribution of the net power output is found to be close to the normal distribution (Fig. 2b) that is a result of the nearly linear correlation of the net power output and the stochastic parameters. The probabilistic analysis has revealed that the CaL retrofit scenario (μ_{CaL} = 516.6 MW$_{el}$, Mo_{CaL} = 525.0 MW$_{el}$) is expected to deliver 40% higher net power output than the reference CFPP

[3] At randomly generated values for moisture content of 6.7%, load of 101.5%, and relative make-up rate of 0.039.

[4] At randomly generated values for moisture content of 0.5%, load of 99.3%, and lean loading of 0.299.

(μ_{CFPP} = 369.2 MW_{el}, Mo_{CFPP} = 375.0 MW_{el}) and double that of the MEA retrofit scenario (μ_{MEA} = 254.5 MW_{el}, Mo_{MEA} = 275.0 MW_{el}). Therefore, it is expected that in the CaL retrofit scenario the negative effect of the efficiency penalty will be outweighed by the increase in the net power output and in favourable economic conditions will increase the profit from electricity sales over the reference CFPP [40]. In addition, the operating envelope of the net power output in the CaL retrofit scenario is wider compared to the remaining scenarios, implying higher flexibility of this scenario.

It is important to highlight that by considering the statistical distribution of the stochastic variables, the results obtained in the probabilistic analysis can be considered as more realistic compared to previous deterministic studies analysing CaL retrofit scenarios that reported 50–80% increase in net power output over the reference CFPP [33–35,38,39] and net efficiency penalty of around 3–8% points [30–36]. However, the scenarios considered in this study are based on the CFPP operating under severe environmental conditions with high average ambient temperatures. As a result of limited steam cycle cooling capacity, the net thermal efficiency of the considered scenarios is, on average 1% point lower compared to the corresponding scenarios operated under European conditions.

Nevertheless, the results discussed in this section indicate that application of the probabilistic approach to analyse the CO_2 capture retrofit scenarios could bring a more profound insight into the process operation. This would allow the designer to consider the effect of uncertainty on the process performance and operating envelope, and thus to design the process that would operate in an efficient and reliable manner. Additionally, data presented in this section can be used as input to the probabilistic economic assessment that would help investors to make more accurate decisions on which CO_2 capture technology would be the most cost-effective for a given application.

4.2. CO_2 capture system design implications

4.2.1. Amine scrubbing

The reduction in the net thermal efficiency and de-rating of the net power output in the MEA retrofit scenario are caused primarily by the heat requirement for solvent regeneration that is provided in the most efficient way by extracting part of the low-pressure steam from the primary steam cycle [89]. Yet, the parasitic load imposed by the low-pressure steam extraction is not only a result of a reduction of the low-pressure turbine throughput, but also due to significant drop in the low-pressure steam pressure downstream of the extraction point [51]. The probabilistic analysis reveals that in the MEA retrofit scenario this pressure will be lower than in the reference CFPP (Fig. 3), which is true even under ±20% variation of the statistic parameters.

The energy intensity of the MEA plant is mainly determined by the amount of heat required for solvent regeneration, which, in turn, determines the amount of steam to be extracted from the steam cycle. The probabilistic analysis (Fig. 4a) indicates that the reboiler duty is nearly normally distributed (μ_{Qreb} = 407.9 MW_{th}, Mo_{Qreb} = 420.0 MW_{th}) and is more likely to be below the lower limit ($P_{f,LLS}$ = 0.0727, β_{LLS} = 1.46) rather than above the upper limit ($P_{f,ULS}$ = 0.0014, β_{ULS} = 2.99). This indicates that the design of the MEA scrubbing unit should be determined by the LLS, as more attention needs to be paid to ensure that enough heat is available for solvent regeneration. This is particularly important for the design of the steam extraction system, as operation below the lower limit state could induce an additional loss in the steam quality that can lead to reduced operating temperature of the reboiler, and thus the loss in the CO_2 capture efficiency.

The sensitivity analysis (Fig. 4b) reveals that the mean lean loading, mean power plant load and standard deviation of power plant load are the main variables that influence the reboiler duty. Having varied the mean value of the lean loading by −20% and 20%, it is observed that the reliability index for the ULS is reduced by 1.08 and 0.4 times, respectively, and for the LLS is increased by a factor of 1.6 and 0.5, respectively. Therefore, it can be concluded that the lean loading of 0.29 is an optimum value for the considered MEA plant, and any deviation would lead to increased reboiler duty and thus the probability of higher parasitic load imposed on the net power output. Additionally, 20% increase in mean value and standard deviation of the power plant load is found to reduce the reliability index for the ULS by 29% and 15%, respectively. Such increase in standard deviation of the operating load of the CFPP results also in a reduction of the reliability index for LLS by 16%, implying that deviation in the operating load negatively affects the reliability of the system by increasing the failure probability. Finally, reduction in the mean value of the operating load reduces the reliability index for the LLS by 61%, increasing the risk that the deteriorated steam quality will not allow achieving the design CO_2 capture level of 90%.

4.2.2. Calcium looping

In the CaL retrofit scenario, the drop in the net thermal efficiency is primarily associated with the production of pure O_2 in the ASU and consumption of an additional amount of fuel [35], the requirements for which are determined by the heat required to sustain the endothermic calcination process. The probabilistic analysis (Fig. 5a) reveals that the calciner heat duty is represented by a slightly skewed normal distribution (μ_{Qcalc} = 864.0 MW_{th}, Mo_{Qcalc} = 900.0 MW_{th}) and the design of the CaL retrofit scenario should be determined by the LLS. This is because the calciner heat duty is more likely to be below the lower limit ($P_{f,LLS}$ = 0.0859, β_{LLS} = 1.37) than above the upper limit ($P_{f,ULS}$ = 0.0006, β_{ULS} = 3.24), implying that failure of the auxiliary equipment is unlikely to happen if the capacity of the coal and ash handling equipment, as well as the ASU, are designed at the ULS without oversizing. Conversely, it is more likely that due to reduced temperature in the calciner the desired overall CO_2 capture rate of 90% may not be achieved. Additionally, attention needs to be paid to the design of the ASU at lower loads, due to compressors and cold box operating constraints [90], the latter of which is particularly important to the O_2 purity.

The sensitivity analysis of the key statistic parameters reveals that the reliability index for the calciner heat duty is mostly affected by the mean value and standard deviation of the operating load of the CFPP, and to a lesser extent, by mean value of the relative sorbent make-up. Fig. 5b indicates that the reliability index for the ULS will be reduced by 28% and 16% on 20% increase in the mean value and standard deviation of the power plant load, respectively, and by 9% on 20% reduction in the mean value of the relative sorbent make-up. Conversely, the reliability index for the LLS will be reduced by 66% on 20% reduction in the mean value of the operating load, as well as by 17% and 10% on 20% increase of standard deviation of the operating load and mean value of the relative sorbent make-up, respectively. As opposed to the lean loading in the MEA retrofit scenario, change in the mean value of the relative sorbent make-up rate was found to be followed by a subsequent change the calciner heat duty in the same direction; for example, an increase of the relative sorbent make-up rate increased the calciner heat duty. This implies that the heat requirement in the CaL plant would be minimised at low relative make-up rates which, unfortunately, require high solid looping rates and larger equipment. Therefore, optimisation of this key performance indicator requires techno-economic analysis, which is out of this study's scope.

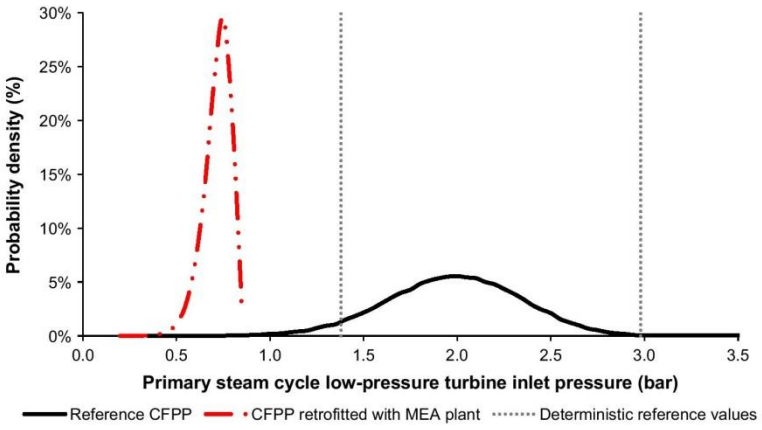

Fig. 3. Effect of uncertainty on probabilistic prediction of low-pressure turbine inlet pressure.

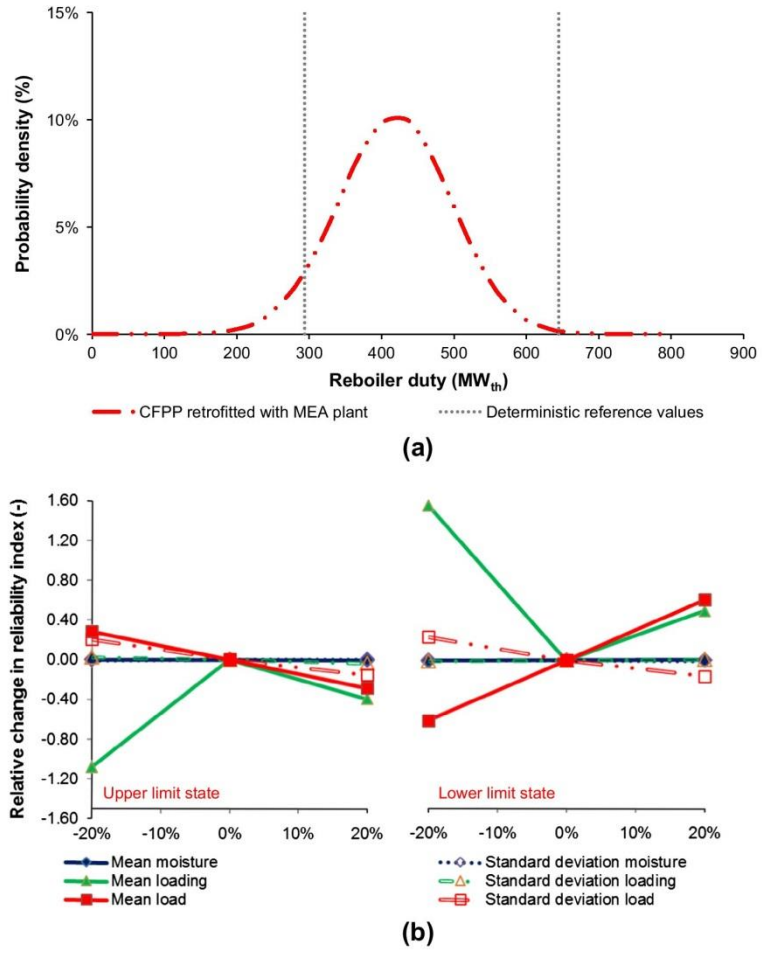

Fig. 4. Effect of (a) uncertainty and (b) key statistic parameters sensitivity on probabilistic prediction of reboiler duty.

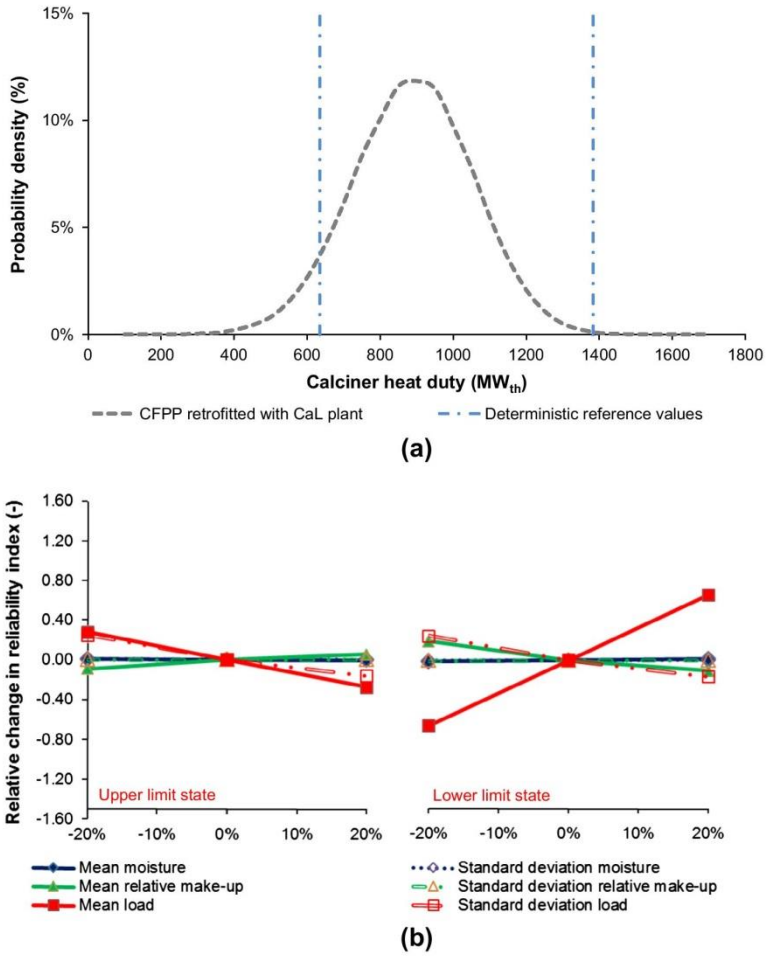

Fig. 5. Effect of (a) uncertainty and (b) key statistic parameters sensitivity on probabilistic prediction of calciner heat duty.

As has been pointed out above, the high-temperature operation of the CaL plant allows raising high-pressure steam that can be utilised in the secondary steam cycle to generate additional power. The probabilistic analysis (Fig. 6a) shows that the live steam pressure is nearly normally distributed (μ_p = 153.6 bar, Mo_p = 160.0 bar) and that it is considerably less likely to exceed the upper limit ($P_{f,ULS}$ = 0.0008, β_{ULS} = 3.15) than fall below the lower limit ($P_{f,LLS}$ = 0.0722, β_{ULS} = 1.46). It needs to be highlighted that reliability indices obtained for the live steam pressure are similar to the ones for the calciner heat duty. This is also observed in the results of the sensitivity analysis (Fig. 6b) that show similar trends in variations of the reliability index for the live steam pressure on changes of the key statistic parameters as observed for the calciner heat input. This implies that the design of the entire CaL plant would be determined by the calciner heat duty that is directly dependent on the amount of sorbent required to maintain the desired overall CO_2 capture level of 90%.

4.2.3. CO_2 compression

After being removed from the flue gas stream, CO_2 needs to be conditioned and compressed prior to transport and storage. The requirement associated with this process is the second most important parasitic load in both the MEA and CaL retrofit scenarios.

The results of the probabilistic analysis (Fig. 7) indicate that the throughput of the CO_2 compression unit is nearly normally distributed in both the MEA retrofit ($\mu_{CCU,MEA}$ = 84.6 kg/s, $Mo_{CCU,MEA}$ = 85.0 kg/s) and the CaL retrofit ($\mu_{CCU,CaL}$ = 186.3 kg/s, $Mo_{CCU,CaL}$ = 195.0 kg/s) scenarios, with the latter being slightly skewed. The higher operating range presented in Fig. 7 also implies that the CO_2 compression unit in the CaL retrofit scenario needs to be designed to operate with nearly two times higher turndown compared to the one in the MEA retrofit scenario, which can be achieved by considering a multiple-compression train design. Nevertheless, the design of the CO_2 compression train should be determined by the LLS that is more likely not to be meet ($P_{f,LLS}$ = 0.074, β_{LLS} = 1.45) compared to the ULS ($P_{f,ULS}$ = 0.008, β_{ULS} = 3.17) in both

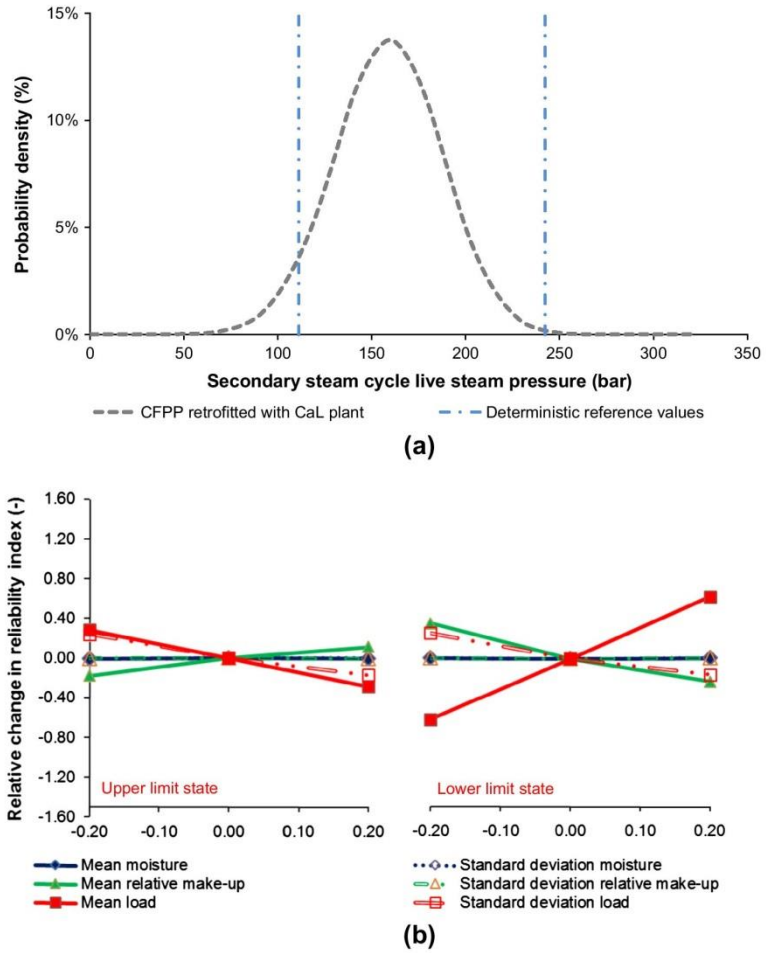

Fig. 6. Effect of (a) uncertainty and (b) key statistic parameters sensitivity on probabilistic prediction of live steam pressure in secondary steam cycle.

scenarios. These values of the reliability indices are comparable to the ones obtained for the reboiler duty (MEA retrofit scenario) and the calciner heat duty (CaL retrofit scenario), and are found to experience the same trends on variation of the key statistic parameters with regard to mean value and standard deviation of the CFPP load, while no effect of either lean loading or relative sorbent make-up rate was reported. Importantly, the same reliability indices for the CO_2 compression unit throughput obtained in the MEA retrofit and the CaL retrofit scenarios indicate that the design of this unit is independent of the CO_2 capture technology and is proportional to the required CO_2 processing rate.

4.3. Implication of the reference coal-fired power plant operation mode

The results analysed above would support the process design stage by indicating the most probable operating envelope for the equipment in the considered system. Such a prediction would allow the designer to properly size the equipment without the need for applying excessive sizing factors. As these are primarily based on previous experience in other industries, their application in CO_2 capture plants for coal-fired plants, which may operate in a demand-following or base-load mode, may lead to over- or under-sizing of the equipment, deteriorating its performance.

The probabilistic analysis has indicated that the energy requirement in both MEA and CaL retrofit scenarios is highly sensitive to variation in the CFPP load and, to a lesser extent, to changes in the lean loading (MEA retrofit scenario) or relative make-up rate (CaL retrofit scenario). This implies that if the reference coal-fired power plant is operated in the demand-following mode, the entire system needs to be designed to flexibly meet the market demand. Moreover, the results of the probabilistic analysis indicated that the retrofitted coal-fired power plant should be able to flexibly deliver high performance under a wide operating envelope. Alternatively, the small impact of variation in the moisture content and moderate influence of the CO_2 capture specific parameters imply that if the retrofitted coal-fired power plant is operated only at base-load capacity, the operating envelope would be considerably narrower, making the process design step less challenging. Yet, operation in the base-load mode only would result in all prob-

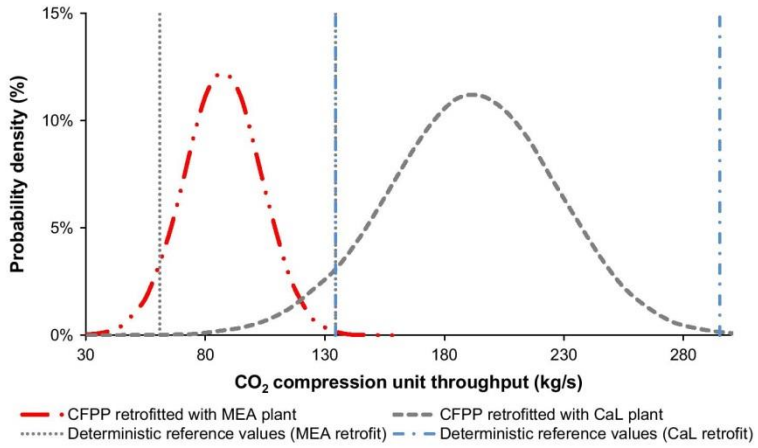

Fig. 7. Comparison of uncertainty effect on probabilistic prediction of CO_2 flow rate to storage in MEA and CaL retrofit scenarios,

abilistic curves being shifted near the ULS. It can be expected that the probability of failure associated with the exceedance of the ULS, which is induced via variation in the coal quality and CO_2 capture operating parameters, would be higher for the base-load mode compared to the load-following mode. Although this would result in negligible probability that the LLS will not be met, the system operating at the base-load will need to be slightly oversized, compared to the load-following system.

5. Conclusions

This study employed the probabilistic approach to compare the performance of MEA and CaL retrofit scenarios and to benchmark them with the performance of the reference CFPP, providing a framework for future studies in this field. It was found that the most probable values for the efficiency penalties are 9.5% and 11.5% points in the CaL and MEA retrofit scenarios, respectively. This also indicated that, considering higher uncertainty in the operating conditions of the CaL process, retrofit of the emerging CaL technology can be expected to yield net efficiencies that will be 2% higher than those in the retrofit with the mature MEA scrubbing technology. In addition, the CaL retrofit scenario was found to increase the net power output of the integrated system by 40%, which can be considered as a more realistic value compared to 50–80% identified in previous deterministic studies considering the base-load operation. Also, the net power output in the CaL retrofit scenario was found to be nearly double that in the MEA retrofit scenario, and thus it could outweigh the imposed net efficiency penalty leading to exceeding the profit of the reference CFPP from electricity sales in favourable economic conditions.

The probabilistic analysis of the particular process equipment revealed that the CO_2 capture plants and their auxiliary equipment need to be designed for the LLS and no excessive oversizing is required. It was found that the analysed key performance indicators were mostly affected by the variability in the power plant operating load, lean loading (MEA retrofit scenario) and relative sorbent make-up rate (CaL retrofit scenario), while no effect of uncertainty in the moisture content in coal was observed. Furthermore, the probabilistic approach helped determine if the optimum values of the design parameters (lean loading, relative sorbent make-up rate) were selected.

Finally, the probabilistic approach was found to be capable of producing valuable information on the equipment operating envelope that would help designers to assess the number of equipment trains and their operating limits. Therefore, the probabilistic framework for comparison of the CO_2 capture retrofit scenarios should be used in addition to the conventional thermodynamic analyses in future studies as, by considering the impact of uncertainty on process performance, it generates valuable information that could serve as input not only to the probabilistic economic analysis and the process design, but also to the investment decision-making process.

Appendix A. Supplementary material

Supplementary data associated with this article can be found, in the online version, at http://dx.doi.org/10.1016/j.apenergy.2016.03.102.

References

[1] UN. Adoption of the Paris agreement. Paris, France: United Nations Framework Convection on Climate Change; 2015.
[2] IEA. CO_2 emissions from fuel combustion - highlights. Paris, France: IEA Publications; 2012.
[3] Yu S, Wei YM, Guo H, Ding L. Carbon emission coefficient measurement of the coal-to-power energy chain in China. Appl Energy 2014;114:290–300.
[4] Karampinis E, Nikolopoulos N, Nikolopoulos A, Grammelis P, Kakaras E. Numerical investigation Greek lignite/cardoon co-firing in a tangentially fired furnace. Appl Energy 2012;97:514–24.
[5] IEA. Power generation from coal: measuring and reporting efficiency performance and CO_2 emissions. Paris, France: IEA Publications; 2010.
[6] Dai C, Cai XH, Cai YP, Huang GH. A simulation-based fuzzy possibilistic programming model for coal blending management with consideration of human health risk under uncertainty. Appl Energy 2014;133:1–13.
[7] IEA. Tracking clean energy progress 2013. IEA input to the clean energy ministerial. Paris, France: IEA Publications; 2013.
[8] IEA. Tracking clean energy progress 2015. Energy technology perspectives 2015 excerpt. IEA input to the clean energy ministerial. Paris, France: IEA Publications; 2015.
[9] IPCC. Climate change 2014: mitigation of climate change. Cambridge, UK and New York, NY, USA: Cambridge University Press; 2014.
[10] IEA. Carbon capture and storage: the solution for deep emissions reductions. Paris, France: IEA Publications; 2015.
[11] IEA. Energy technology perspectives 2015. Paris, France: IEA Publications; 2015.
[12] Benton D. Decarbonising British industry. London, UK: Green Alliance; 2015.
[13] Orion Innovations. A UK vision for carbon capture and storage. London, UK: Orion Innovations (UK) Ltd; 2013.

[14] IEA. Technology roadmap: carbon capture and storage. Paris, France: IEA Publications; 2013.
[15] Abdul Manaf N, Qadir A, Abbas A. Temporal multiscalar decision support framework for flexible operation of carbon capture plants targeting low-carbon management of power plant emissions. Appl Energy 2016;169:912–26.
[16] Blamey J, Anthony EJ, Wang J, Fennell PS. The calcium looping cycle for large-scale CO_2 capture. Prog Energy Combust Sci 2010;36(2):260–79.
[17] Boot-Handford ME, Abanades JC, Anthony EJ, Blunt MJ, Brandani S, Mac Dowell N, et al. Carbon capture and storage update. Energy Environ Sci 2014;7:130–89.
[18] Pires JCM, Martins FG, Alvim-Ferraz MCM, Simões M. Recent developments on carbon capture and storage: an overview. Chem Eng Res Des 2011;89(9):1446–60.
[19] Xu G, Jin HG, Yang YP, Xu YJ, Lin H, Duan L. A comprehensive techno-economic analysis method for power generation systems with CO_2 capture. Int J Energy Res 2010;34(4):321–32.
[20] Goto K, Yogo K, Higashii T. A review of efficiency penalty in a coal-fired power plant with post-combustion CO_2 capture. Appl Energy 2013;111:710–20.
[21] Hanak DP, Biliyok C, Yeung H, Białecki R. Heat integration and exergy analysis for a supercritical high-ash coal-fired power plant integrated with a post-combustion carbon capture process. Fuel 2014;134:126–39.
[22] Kvamsdal HM, Romano MC, van der Ham L, Bonalumi D, van Os P, Goetheer E. Energetic evaluation of a power plant integrated with a piperazine-based CO_2 capture process. Int J Greenhouse Gas Control 2014;28(1):343–55.
[23] Van Wagener DH, Liebenthal U, Plaza JM, Kather A, Rochelle GT. Maximizing coal-fired power plant efficiency with integration of amine-based CO_2 capture in greenfield and retrofit scenarios. Energy 2014;72:824–31.
[24] Li K, Leigh W, Feron P, Yu H, Tade M. Systematic study of aqueous monoethanolamine (MEA)-based CO2 capture process: techno-economic assessment of the MEA process and its improvements. Appl Energy 2016;165:648–59.
[25] Sharifzadeh M, Bumb P, Shah N. Carbon capture from pulverized coal power plant (PCPP): solvent performance comparison at an industrial scale. Appl Energy 2016;163:423–35.
[26] Kheshgi HS, Thomann H, Bhore NA, Hirsch RB, Parker ME, Teletzke GF. Perspectives on CCS cost and economics. SPE Econ Manage 2012;4(1):24–31.
[27] Renner M. Carbon prices and CCS investment: a comparative study between the European Union and China. Energy Policy 2014;75:327–40.
[28] CSIRO. Assessing post-combustion capture for coal-fired power stations in Asia-Pacific partnership countries. Newcastle, NW, USA: CSIRO Advanced Coal Technology; 2012.
[29] Abanades JC, Arias B, Lyngfelt A, Mattisson T, Wiley DE, Li H, et al. Emerging CO2 capture systems. Int J Greenhouse Gas Control 2015;40:126–66.
[30] Romeo LM, Abanades JC, Escosa JM, Paño J, Giménez A, Sánchez-Biezma A, et al. Oxyfuel carbonation/calcination cycle for low cost CO_2 capture in existing power plants. Energy Convers Manage 2008;49(10):2809–14.
[31] Martínez I, Murillo R, Grasa G, Carlos Abanades J. Integration of a Ca looping system for CO_2 capture in existing power plants. AIChE J 2011;57(9):2599–607.
[32] Abanades JC, Anthony EJ, Wang J, Oakey JE. Fluidized bed combustion systems integrating CO_2 capture with CaO. Environ Sci Technol 2005;39(8):2861–6.
[33] Vorrias I, Atsonios K, Nikolopoulos A, Nikolopoulos N, Grammelis P, Kakaras E. Calcium looping for CO_2 capture from a lignite fired power plant. Fuel 2013;113:826–36.
[34] Ströhle J, Lasheras A, Galloy A, Epple B. Simulation of the carbonate looping process for post-combustion CO_2 capture from a coal-fired power plant. Chem Eng Technol 2009;32(3):435–42.
[35] Hanak DP, Biliyok C, Anthony EJ, Manovic V. Modelling and comparison of calcium looping and chemical solvent scrubbing retrofits for CO_2 capture from coal-fired power plant. Int J Greenhouse Gas Control 2015;42:226–36.
[36] Hanak DP, Anthony EJ, Manovic V. A review of developments in pilot plant testing and modelling of calcium looping process for CO_2 capture from power generation systems. Energy Environ Sci 2015;8:2199–249.
[37] Perejón A, Romeo LM, Lara Y, Lisbona P, Martínez A, Valverde JM. The Calcium-Looping technology for CO2 capture: an the important roles of energy integration and sorbent behavior. Appl Energy 2016;162(January):787–807.
[38] Romeo LM, Lara Y, Lisbona P, Escosa JM. Optimizing make-up flow in a CO_2 capture system using CaO. Chem Eng J 2009;147(2–3):252–8.
[39] Li ZS, Cai NS, Croiset E. Process analysis of CO_2 capture from flue gas using carbonation/calcination cycles. AIChE J 2008;54(7):1912–25.
[40] Hanak DP, Biliyok C, Manovic V. Calcium looping with inherent energy storage for decarbonisation of coal-fired power plant. Energy Environ Sci 2016;9:971–83.
[41] EEX. European emission allowances (EUA). Global environmental exchange. Leipzig, Germany: European Energy Exchange; 2015.
[42] Lasheras A, Ströhle J, Galloy A, Epple B. Carbonate looping process simulation using a 1D fluidized bed model for the carbonator. Int J Greenhouse Gas Control 2011;5(4):686–93.
[43] Dean CC, Blamey J, Florin NH, Al-Jeboori MJ, Fennell PS. The calcium looping cycle for CO_2 capture from power generation, cement manufacture and hydrogen production. Chem Eng Res Des 2011;89:836–55.
[44] Stéphenne K. Start-up of world's first commercial post-combustion coal fired CCS project: contribution of Shell Cansolv to Saskpower boundary dam ICCS project. Energy Procedia 2014;63:6106–10.
[45] Romano MC, Lozza GG. Long-term coal gasification-based power plants with near-zero emissions. Part A: Zecomix cycle. Int J Greenhouse Gas Control 2010;4(3):459–68.
[46] Romano MC, Lozza GG. Long-term coal gasification-based power with near-zero emissions. Part B: Zecomag and oxy-fuel IGCC cycles. Int J Greenhouse Gas Control 2010;4(3):469–77.
[47] Cormos CC, Cormos AM. Assessment of calcium-based chemical looping options for gasification power plants. Int J Hydrogen Energy 2013;38(5):2306–17.
[48] Connell DP, Lewandowski DA, Ramkumar S, Phalak N, Statnick RM, Fan LS. Process simulation and economic analysis of the calcium looping process (CLP) for hydrogen and electricity production from coal and natural gas. Fuel 2013;105:383–96.
[49] Wang D, Chen S, Xu C, Xiang W. Energy and exergy analysis of a new hydrogen-fueled power plant based on calcium looping process. Int J Hydrogen Energy 2013;38(13):5389–400.
[50] Kunze C, De S, Spliethoff H. A novel IGCC plant with membrane oxygen separation and carbon capture by carbonation-calcinations loop. Int J Greenhouse Gas Control 2011;5(5):1176–83.
[51] Hanak DP, Biliyok C, Manovic V. Evaluation and modeling of part-load performance of coal-fired power plant with postcombustion CO_2 capture. Energy Fuels 2015;29(6):3833–44.
[52] Cau G, Tola V, Deiana P. Comparative performance assessment of USC and IGCC power plants integrated with CO_2 capture systems. Fuel 2014;116:820–33.
[53] Tola V, Pettinau A. Power generation plants with carbon capture and storage: a techno-economic comparison between coal combustion and gasification technologies. Appl Energy 2014;113:1461–74.
[54] Karmakar S, Kolar AK. Thermodynamic analysis of high-ash coal-fired power plant with carbon dioxide capture. Int J Energy Res 2013;37(6):522–34.
[55] Hu M, Cho H. A probability constrained multi-objective optimization model for CCHP system operation decision support. Appl Energy 2014;116:230–42.
[56] ABB. Power generation. Energy efficient design of auxiliary systems in fossil-fuel power plants. Zurich, Switzerland; Wickliffe, OH, USA: ABB; 2009.
[57] Drbal L, Westra K, Boston P. Power plant engineering. New York, NY, USA: Springer; 1996.
[58] Liptak BG. Instrument engineers' handbook: process control and optimization, 2. London, UK; New York, NY, USA; Washington, DC, USA: CRC-Press; 2005.
[59] Kumar R, Sharma A, Tewari P. Markov approach to evaluate the availability simulation model for power generation system in a thermal power plant. Int J Ind Eng Comput 2012;3(5):743–50.
[60] Rubin ES, Kalagnanam JR, Frey HC, Berkenpas MB. Integrated environmental control modeling of coal-fired power systems. J Air Waste Manage Assoc 1997;47(11):1180–8.
[61] Rubin ES, Rao AB. Uncertainties in CO2 capture and sequestration costs. In: Proceedings of the 6th international conference on greenhouse gas control technologies, Pergamon, vol. 2; 2003. p. 1119–24.
[62] Frey HC, Rubin ES. Probabilistic evaluation of advanced SO_2/NO_x control technology. J Air Waste Manage Assoc 1991;41(12):1585–93.
[63] Hanak DP, Kolios AJ, Biliyok C, Manovic V. Probabilistic performance assessment of a coal-fired power plant. Appl Energy 2015;139:350–64.
[64] Zhao M, Minett AI, Harris AT. A review of techno-economic models for the retrofitting of conventional pulverised-coal power plants for post-combustion capture (PCC) of CO_2. Energy Environ Sci 2013;6(1):25–40.
[65] Suresh M, Reddy KS, Kolar AK. 3-E analysis of advanced power plants based on high ash coal. Int J Energy Res 2010;34(8):716–35.
[66] Cooke DH. Modelling of off-design multistage turbine pressures by Stodola's ellipse. Richmond, VA, USA: Bechtel Power Corporation; 1983.
[67] Salisbury JK. Steam turbines and their cycles. NY, USA: Robert E. Krieger Publishing Huntington; 1950.
[68] Knopf FC. Modeling, analysis and optimization of process and energy systems. NJ, USA: Wiley Hoboken; 2012.
[69] AspenTech. Rate-based model of the CO2 capture process by MEA using aspen plus. Cambridge, MA, USA: Aspen Technology Inc.; 2008.
[70] Hanak DP, Biliyok C, Yeung H, Białecki R. Heat integration and exergy analysis for a high ash supercritical coal-fired power plant integrated with a post-combustion carbon capture process. Fuel 2014;134:126–39.
[71] Shaw D. Cansolv: capturing attention at Boundary Dam. Carbon Capture J 2012;27.
[72] Jordal K, Ystad PAM, Anantharaman R, Chikukwa A, Bolland O. Design-point and part-load considerations for natural gas combined cycle plants with post combustion capture. Int J Greenhouse Gas Control 2012;11:271–82.
[73] Canepa R, Wang M, Biliyok C, Satta A. Thermodynamic analysis of combined cycle gas turbine power plant with post-combustion CO_2 capture and exhaust gas recirculation. Proc Inst Mech Eng Part E J Process Mech Eng 2013;227(2):89–105.
[74] Rodríguez N, Alonso M, Abanades JC. Average activity of CaO particles in a calcium looping system. Chem Eng J 2010;156(2):388–94.
[75] Sánchez-Biezma A, Paniagua J, Diaz L, Lorenzo M, Alvarez J, Martínez D, et al. Testing postcombustion CO_2 capture with CaO in a 1.7 MW_t pilot facility. Energy Procedia 2013;37:1–8.
[76] MacIntosh DL, Spengler JD, Staudt JE, Bachmann J. Emission of hazardous air pollutants from coal-fired power plants. Needham, MA, USA: Environmental Health & Engineering Inc; 2011.
[77] Manovic V, Anthony EJ, Grasa G, Abanades JC. CO_2 looping cycle performance of a high-purity limestone after thermal activation/doping. Energy Fuels 2008;22(5):3258–64.

[78] IEX. Indian energy market snapshot between 1st and 7th January 2014, Indian energy exchange; 2014. <http://bit.ly/OZVIH8>.
[79] Affolter RH. Quality characterization of cretaceous coal from the Colorado Plateau coal assessment area. In: Krischbaum MA, Roberts LNR, Biewick LRH, editors. Geologic assessment of coal in the Colorado plateau: Arizona, Colorado, New Mexico, and Utah, 1. U.S. Geological Survey; 2000. p. G1–G136. http://on.doi.gov/1iETfxA.
[80] Mantripragada HC, Rubin ES. Calcium looping cycle for CO_2 capture - performance, cost and feasibility analysis. Energy Procedia 2013;63:2199–206.
[81] Berstad D, Anantharaman R, Jordal K. Post-combustion CO_2 capture from a natural gas combined cycle by CaO/$CaCO_3$ looping. Int J Greenhouse Gas Control 2012;11:25–33.
[82] Charitos A, Rodríguez N, Hawthorne C, Alonso M, Zieba M, Arias B, et al. Experimental validation of the calcium looping CO_2 capture process with two circulating fluidized bed carbonator reactors. Ind Eng Chem Res 2011;50 (16):9685–95.
[83] Rodríguez N, Alonso M, Abanades JC. Experimental investigation of a circulating fluidized-bed reactor to capture CO_2 with CaO. AIChE J 2011;57 (5):1356–66.
[84] Applied analytics. Lean amine/rich amine analysis applied analytics application note no. AN-025, applied analytics, Burlington, MA, USA; 2013.
[85] Gavin HP, Yau SC. High-order limit state functions in the response surface method for structural reliability analysis. Struct Saf 2008;30(2):162–79.
[86] Salonitis K, Kolios A. Reliability assessment of cutting tool life based on surrogate approximation methods. Int J Adv Manuf Technol 2014;71(5–8):1197–208.
[87] Choi SK, Grandhi RV, Canfield RA. Reliability-based structural design. London, UK: Springer-Verlag; 2007.
[88] Rutherford R, Moulitsas I, Snow BJ, Kolios AJ, De Dominicis M. CranSLIK v2.0: improving the stochastic prediction of oil spill transport and fate using approximation methods. Geosci Model Dev 2015;8(10):3365–77.
[89] Lucquiaud M, Gibbins J. On the integration of CO_2 capture with coal-fired power plants: a methodology to assess and optimise solvent-based post-combustion capture systems. Spec Issue Carbon Capture Storage 2011;89 (9):1553–71.
[90] Perrin N, Dubettier R, Lockwood F, Tranier J-P, Bourhy-Weber C, Terrien P. Oxycombustion for coal power plants: advantages, solutions and projects. Appl Therm Eng 2014;74:75–82.

This page intentionally left blank.

12 GENERAL DISCUSSION

Decarbonisation of the power sector has been recognised as a critical step towards reduction of global greenhouse gas emissions that would help to mitigate drastic climate change. Yet, it is projected that fossil fuels, especially coal, will remain an important energy source in the power sector (EIA, 2013, 2015). Importantly, the attempts undertaken to raise the net thermal efficiency of coal-fired power plants have been recognised as not sufficient to meet the desired reduction of around 90% of the power sector's CO_2 emissions, implying the need for a wide deployment of CCS to achieve this target (IEA, 2014; VGB, 2013). Implementation of CCS, along with nuclear power stations and renewable energy sources, has been identified as capable of reducing around 51% of the energy sector's cumulative CO_2 emissions between 2012 and 2050 (IEA, 2015a, 2015b). However, the intermittent nature of renewable energy sources and base-load operation of nuclear power stations would impose the requirement of flexible operation on the coal-fired power plants to balance energy supply and demand (IEA, 2012; Jiang et al., 2012; Singh et al., 2011; Twidell and Weir, 2006). Therefore, the CO_2 capture retrofit scenarios of the coal-fired power plant operating under both base-load (Chapter 4 to Chapter 7) and demand-following mode (Chapter 8 to Chapter 11) have been investigated.

Process modelling and simulation is regarded as a powerful and cost-effective tool for design and analysis of the advanced power plant processes. To meet the objectives of this research project, a number of process models were developed in Aspen Plus®. The basic model description, applicability and key limitation are summarised in Table 12-1. To ensure reliability and accuracy of the performance predictions, the process models of the coal-fired power plants and CO_2 capture plants have been validated, or at least verified, against data available in the open literature. As it has been observed in Chapter 4 and Chapter 8, the maximum deviation between the predictions of the coal-fired power plant models and data reported in the literature reached 5–6%, considering both base- and part-load operation. Considering the fact that Aspen

Plus® is not primarily designed for modelling power cycles, especially at part-load or under off-design conditions, the conclusions drawn in this PhD project were in no way affected by such deviation. Moreover, the performance estimated by the process models of the CAP and CaL CO_2 capture plants were found to be in good agreement with the experimental data under different flue gas loads. Such results implied that the modelling framework employed in this project was valid and led to generation of reliable results, and thus reliable conclusions.

Table 12-1: Applicability and limitations of developed process models

Model	Key limitations	Applicability*				
		BA	PA	NC	ES	PPA
580 MW_{el} supercritical coal-fired power plant (Chapter 4 and Chapter 5)	Validated for European climatic conditions at base-load only. No part-load performance data available.	✓	×	✓	×	×
660 MW_{el} supercritical coal-fired power plant (Chapter 8)	Validated for Indian climatic conditions at base- and part-load.	✓	✓	✓	✓	✓
Monoethanolamine scrubbing CO_2 capture plant (Chapter 8 and Hanak et al. (2014))	Validated at pilot-plant scale.	✓	✓	✓	✓	✓
Chilled ammonia process CO_2 capture plant (Chapter 4)	Validated at pilot-plant scale for aqueous ammonia process. No data for chilled ammonia process available.	✓	✓	✓	✓	✓
Calcium looping process CO_2 capture plant (Chapter 6)	Equilibrium-based model. Verified with pilot-plant operating data. No data for complete validation available.	✓	✓	✓	✓	✓
CO_2 compression unit	Part-load operation of compressors limited to 70% due to lack of performance data.	✓	✓	✓	✓	✓
Air separation unit	Part-load operation of compressors limited to 70% due to lack of performance data; part-load operation of cold box limited to 50%.	✓	✓	✓	✓	✓

*BA – base-load analysis; PA – part-load analysis; NC – novel concepts development; ES – energy storage; PPA – probabilistic performance analysis

Although chemical solvent scrubbing using amine-based solvents is regarded as a mature CO_2 capture technology (Blamey et al., 2010; Padurean et al., 2011; Pfaff et al., 2010) and has already been demonstrated at commercial scale (Stéphenne, 2014), its significant energy intensity would impose net efficiency penalties on the retrofitted system of up to 12.5% points that would increase the cost of electricity by at least 60% (Bhown and Freeman, 2011; CSIRO, 2012; Kheshgi et al., 2012; Renner, 2014). Therefore, a number of measures aiming at reducing the energy-intensity of the CO_2 capture plant have been identified in Section 2.5. These have been classified in four groups:

- Material improvements aimed at improving the cycling capacity and reducing the regeneration energy requirement.
- Heat integration aimed at improving waste heat utilisation in the system for reduced parasitic load.
- Alternative process configurations aiming at reducing the energy intensity of the CO_2 capture plant.
- Process intensification using rotating packed beds or vortex reactors to enhance mass and heat transfer for reduced equipment size and reduced parasitic load.

Analysis of the retrofit of the CAP process, which uses ammonia as an alternative chemical solvent to amines, to the 580 MW_{el} supercritical coal-fired power plant (Chapter 5) was found to impose net efficiency penalties between 10.4–10.9% points. Such performance is similar to that reported for the reference MEA scrubbing process, for which the net efficiency penalty was reported to fall within 9.5–12.5% points (Goto et al., 2013; Hanak et al., 2014; Xu et al., 2010; Yang et al., 2010). Evaluation of alternative configurations for the retrofit of the CAP plant to the coal-fired power plant revealed that by applying a dual IP/LP crossover pressure system with heat integration proposed by Lacquiaud and Gibbins (2011) would result in reduction of the net efficiency penalty to 9% points. This has been shown to be 0.5% points lower than the net efficiency penalty imposed in the MEA retrofit scenario to the 580 MW_{el} supercritical coal-fired power plant using the same retrofit configuration

(Chapter 6). Further reduction in the net efficiency penalty to 8.7–8.8% points was achieved through an advanced configuration that considers coupling of a new two-stage or a single-stage auxiliary steam turbine with the boiler feedwater pump and a back-pressure turbine for maintaining the desired intermediate-pressure turbine discharge pressure. Regardless of substantial improvement in the net efficiency of the retrofitted system, the predicted efficiency penalties are still higher than minimum net efficiency penalties reported in Section 2.4 for the dry sodium carbonate process (7.1–9.9% points) (Nelson et al., 2009), cryogenic separation (7.1–10.7% points) (Clodic et al., 2005; Schach et al., 2011) and CaL (3–8% points) (Abanades et al., 2005; Martínez et al., 2011; Romeo et al., 2008; Ströhle et al., 2009; Vorrias et al., 2013; Yang et al., 2010). It is also important to highlight that regardless of the reduction in energy intensity of the chemical solvent scrubbing technology, the net power output in the CAP retrofit scenario was reduced by around 23–25% compared to the reference the 580 MW_{el} supercritical coal-fired power plant. It was predicted that even with reductions in energy intensity of the chemical solvent scrubbing CO_2 capture plant, the net power output will be derated by 20–30% due to steam requirement for solvent regeneration (Rochelle, 2009), considerably degrading the economic performance of the retrofitted system. This issue of the chemical solvent scrubbing process can be resolved by application of emerging CO_2 capture technologies. It has been shown (Chapter 6 and Chapter 7) that retrofitting CaL to the 580 MW_{el} supercritical coal-fired power plant would not only result in lower efficiency penalties (5.8–7.9% points), but would also have potential to increase net power output of the retrofitted system by 45–54% over the reference coal-fired power plant (Figure 12-1). Although application of the s-CO_2 cycle in place of the conventional steam cycle was found to reduce the net efficiency penalty in the CaL retrofit scenario by up to 2.1% points (Chapter 7), further improvements can be achieved through a more efficient secondary cycle, use of low-ash fuel such as natural gas (depending on the economic climate), higher level of heat integration in the CaL plant to minimise fuel and O_2 consumption, and alternative O_2 sources for oxy-combustion of fuel such as the combined calcium

and chemical looping process, or heat sources, such as indirect heat transfer, to sustain sorbent regeneration.

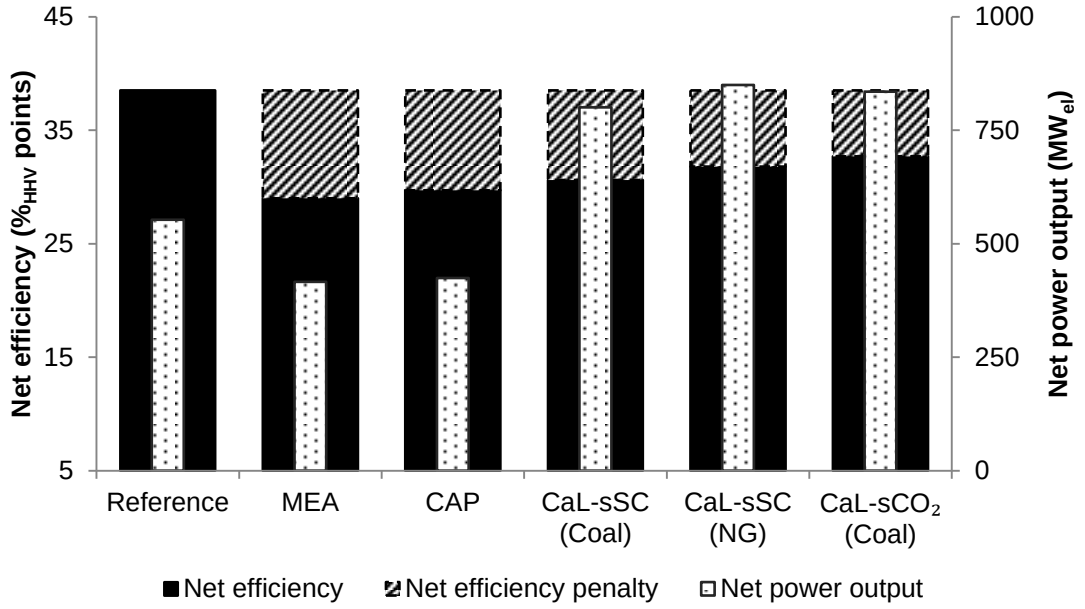

Figure 12-1: Performance summary of the considered retrofit scenarios

Importantly, part-load analysis of CO_2 capture retrofits to the 660 MW_{el} supercritical coal-fired power plant exposed considerable differences in the performance of the investigated CO_2 capture technologies. It has been shown that the net efficiency penalty in the MEA retrofit scenario increases from 10.6–11.0% points at 100% load to 11.6–12.2% points at 40% load (Chapter 8 and Chapter 11) while in the CaL retrofit scenario it increased slightly from 8.7% points to 8.8% points (Chapter 9) and from 8.9% points to 9.4% points (Chapter 11) for the calciner fired with natural gas and coal, respectively. Comparing the performance of the same retrofit scenarios for the 580 MW_{el} supercritical coal-fired power plant (Chapter 6), it was observed that the net efficiency penalties at base load for the 660 MW_{el} supercritical coal-fired power plant are roughly 1% point higher. This is because of the severe environmental conditions with high average ambient temperatures that limit the cooling capacity in the 660 MW_{el} supercritical coal-fired power plant. Furthermore, considering the uncertainties in the model input, the most probable efficiency penalties associated with the MEA and CaL retrofit scenarios were estimated to be 11.5% and 9.5% points, respectively (Chapter 11), proving the superior performance of

the latter technology. The most probable net power output in the CaL retrofit scenario would be 40% higher compared to the reference coal-fired power plant and double that of the MEA retrofit scenario. Such performance of the CaL retrofit scenario is slightly worse than reported 50–80% increase in net power output over the reference coal-fired power plant (Hanak et al., 2015a; Li et al., 2008; Romeo et al., 2009; Ströhle et al., 2009; Vorrias et al., 2013) and net efficiency penalty of around 3–8% points (Abanades et al., 2005; Hanak et al., 2015b, 2015b; Martínez et al., 2011; Romeo et al., 2008; Ströhle et al., 2009; Vorrias et al., 2013). Yet, it is expected that incorporation of the statistical analysis into the process analysis would not only indicate the probable operating envelope of the system, but would also result in more reliable results compared to those estimated using deterministic analysis.

Regardless of slightly higher net efficiency penalty under Indian conditions, increased net power output in the CaL retrofit scenario to 660 MW_{el} supercritical coal-fired power plant (Chapter 9) was proven to bring higher short-run daily profit compared to the reference coal-fired power plant without CO_2 capture for levied carbon tax above 9.6 €/tCO_2. The economic performance of this scenario was found to be improved by utilising the inherent energy storage capacity of CaL. By generating O_2 and storing it during off-peak periods and utilising it during peak periods to offset the higher efficiency penalty to the off-peak periods, at which the price of electricity is considerably lower than at peak periods, the CaL retrofit scenario was found to bring higher daily short-run profit compared to the reference coal-fired power plant when the carbon tax exceeded 8.3 €/tCO_2, which is below the average price of 8.5 €/tCO_2 for the European emission allowances in November 2015 (EEX, 2015). This implies that the CaL retrofit scenario with energy storage can not only become more profitable than the existing coal-fired power plant in the current economic climate, but it can also act as a link between fossil fuels and renewable energy sources in the future energy portfolio, as well as alleviating the implications of renewable energy sources intermittency on the reliability of the electricity grid. Finally, it needs to be highlighted that incorporation of sorbent reactivation through hydration can reduce the net efficiency penalty associated with the CaL

retrofit scenario from 8.7–8.8% points to 8.3–8.4% points, which arised from an increase of average sorbent conversion in the carbonator by a factor of 1.4 and is in line with findings presented in Section 2.5.1.2. However, implementation of a hydrator would only become more profitable than the reference coal-fired power plant without CO_2 capture for the carbon tax above 11.0 €/tCO_2. This can be associated to reduction in the solid looping rate due to higher average sorbent conversion that leads to less heat being available for steam generation, hence leading to lower net power output. For this reason, economic assessment of novel concepts must be carried out to substantiate their commercial applicability. Nevertheless, promising results obtained in this project indicate that CaL is a technically and economically favourable option for decarbonisation of coal-fired power plants. Considering the fact that the power sector is regarded as a precursor for other industries (Benton, 2015), the concepts evaluated in this study could be applied for decarbonisation of cement, lime, chemicals, hydrocarbon, and even steel plants.

References

Abanades, J.C., Anthony, E.J., Wang, J., and Oakey, J.E. (2005), "Fluidized bed combustion systems integrating CO_2 capture with CaO", *Environmental Science and Technology*, 39, 2861–2866.

Benton, D. (2015), *Decarbonising British industry*, Green Alliance, London, UK.

Bhown, A.S. and Freeman, B.C. (2011), "Analysis and status of post-combustion carbon dioxide capture technologies", *Environmental Science and Technology*, 45, 8624–8632.

Blamey, J., Anthony, E.J., Wang, J., and Fennell, P.S. (2010), "The calcium looping cycle for large-scale CO_2 capture", *Progress in Energy and Combustion Science*, 36, 260–279.

Clodic, D., El Hitti, R., Younes, M., Bill, A., and Casier, F. (2005), "CO_2 capture by anti-sublimation—thermo-economic process evaluation", *Proceedings of 4th Annual Conference on Carbon Capture and Sequestration*, Alexandria, VA, USA.

CSIRO (2012), *Assessing post-combustion capture for coal-fired power stations in Asia-Pacific partnership countries*, CSIRO Advanced Coal Technology, Newcastle, NSW, Australia.

EEX (2015), *European Emission Allowances (EUA), Global Environmental Exchange*, European Energy Exchange, Leipzig, Germany, available online: http://bit.ly/1LDgpWu (last accessed: 22/03/2016).

EIA (2015), *Annual energy outlook 2015 with projections to 2040*, U.S. Energy Information Administration, Washington, DC, USA.

EIA (2013), *International Energy Outlook 2013*, U.S. Energy Information Administration, Washington, DC, USA.

Goto, K., Yogo, K., and Higashii, T. (2013), "A review of efficiency penalty in a coal-fired power plant with post-combustion CO_2 capture", *Applied Energy*, 111, 710–720.

Hanak, D.P., Biliyok, C., Anthony, E.J., and Manovic, V. (2015a), "Modelling and comparison of calcium looping and chemical solvent scrubbing retrofits

for CO_2 capture from coal-fired power plant", *International Journal of Greenhouse Gas Control*, 42, 226–236.

Hanak, D.P., Anthony, E.J., and Manovic, V. (2015b), "A review of developments in pilot plant testing and modelling of calcium looping process for CO_2 capture from power generation systems", *Energy and Environmental Science*, 8, 2199–2249.

Hanak, D.P., Biliyok, C., Yeung, H., and Białecki, R. (2014), "Heat integration and exergy analysis for a supercritical high-ash coal-fired power plant integrated with a post-combustion carbon capture process", *Fuel*, 134, 126–139.

IEA (2015a), *Energy technology perspectives 2015: Executive summary*, IEA Publications, Paris, France.

IEA (2015b), *Carbon capture and storage: The solution for deep emissions reductions*, IEA Publications, Paris, France.

IEA (2014), *Emission reduction through upgrade of coal-fired power plants: Learning from Chinese experience*, IEA Publications, Paris, France.

IEA (2012), *Energy technology perspectives 2012: Pathways to a clean energy system*, IEA Publications, Paris, France.

Jiang, R., Wang, J., and Guan, Y. (2012), "Robust unit commitment with wind power and pumped storage hydro", *IEEE Transactions on Power Systems*, 27, 800–810.

Kheshgi, H.S., Thomann, H., Bhore, N.A., Hirsch, R.B., Parker, M.E., and Teletzke, G.F. (2012), "Perspectives on CCS cost and economics", *SPE Economics and Management*, 4, 24–31.

Li, Z.S., Cai, N.S., Croiset, E., Zhen-Shan, L., and Ning-Sheng, C. (2008), "Process analysis of CO_2 capture from flue gas using carbonation/calcination cycles", *AIChE Journal*, 54, 1912–1925.

Lucquiaud, M. and Gibbins, J. (2011), "Effective retrofitting of post-combustion CO_2 capture to coal-fired power plants and insensitivity of CO_2 abatement

costs to base plant efficiency", *International Journal of Greenhouse Gas Control*, 5, 427–438.

Martínez, I., Murillo, R., Grasa, G., and Abanades, J.C. (2011), "Integration of a Ca looping system for CO_2 capture in existing power plants", *AIChE Journal*, 57, 2599–2607. doi:10.1002/aic.12461

Nelson, T.O., Green, D.A., Box, P., Gupta, R.P., Henningsen, G., and Turk, B.S. (2009), *Carbon dioxide capture from flue gas using dry regenerable sorbents*, RTI International, Durham, NC, USA.

Padurean, A., Cormos, C.C., Cormos, A.M., and Agachi, P.S. (2011), "Multicriterial analysis of post-combustion carbon dioxide capture using alkanolamines", *International Journal of Greenhouse Gas Control*, 5, 676–685.

Pfaff, I., Oexmann, J., and Kather, A. (2010), "Optimised integration of post-combustion CO_2 capture process in greenfield power plants", *Energy*, 35, 4030–4041.

Renner, M. (2014), "Carbon prices and CCS investment: A comparative study between the European Union and China", *Energy Policy* 75, 327–340.

Rochelle, G.T. (2009), "Amine scrubbing for CO_2 capture", *Science*, 325, 1652–1654.

Romeo, L.M., Abanades, J.C., Escosa, J.M., Paño, J., Giménez, A., Sánchez-Biezma, A., and Ballesteros, J.C. (2008), "Oxyfuel carbonation/calcination cycle for low cost CO_2 capture in existing power plants", *Energy Conversion and Management*, 49, 2809–2814.

Romeo, L.M., Lara, Y., Lisbona, P., and Escosa, J.M. (2009), "Optimizing make-up flow in a CO_2 capture system using CaO", *Chemical Engineering Journal*, 147, 252–258.

Schach, M.O., Oyarzún, B., Schramm, H., Schneider, R., and Repke, J.U. (2011), "Feasibility study of CO_2 capture by anti-sublimation", *Energy Procedia*, 4, 1403–1410.

Singh, M., Khadkikar, V., Chandra, A., Varma, R.K. (2011), "Grid interconnection of renewable energy sources at the distribution level with

power-quality improvement features", *IEEE Transactions on Power Delivery*, 26, 307–315.

Stéphenne, K. (2014), "Start-up of world's first commercial post-combustion coal fired CCS project: Contribution of Shell Cansolv to Saskpower Boundary Dam ICCS project", *Energy Procedia*, 63, 6106–6110.

Ströhle, J., Lasheras, A., Galloy, A., and Epple, B. (2009), "Simulation of the carbonate looping process for post-combustion CO_2 capture from a coal-fired power plant", *Chemical Engineering and Technology*, 32, 435–442.

Twidell, J. and Weir, A.D. (2006), *Renewable energy resources*, Taylor & Francis, London, UK and New York, USA.

VGB (2013), *Electricity generation: Facts and figures 2012/2013*, VGB PowerTech e.V., Essen, Germany, available online: http://bit.ly/1o3DjLb (last accessed: 22/03/2016).

Vorrias, I., Atsonios, K., Nikolopoulos, A., Nikolopoulos, N., Grammelis, P., and Kakaras, E. (2013), "Calcium looping for CO_2 capture from a lignite fired power plant", *Fuel*, 113, 826–836.

Xu, G., Jin, H.G., Yang, Y.P., Xu, Y.J., Lin, H., and Duan, L. (2010), "A comprehensive techno-economic analysis method for power generation systems with CO_2 capture", *International Journal of Energy Research*, 34, 321–332.

Yang, Y., Zhai, R., Duan, L., Kavosh, M., Patchigolla, K., and Oakey, J. (2010), "Integration and evaluation of a power plant with a CaO-based CO_2 capture system", *International Journal of Greenhouse Gas Control*, 4, 603–612.

This page intentionally left blank.

13 GENERAL CONCLUSION AND RECOMMENDATION

13.1 General conclusion

This PhD project aimed at identification, quantification and analysis of the efficiency improvements and alternate operating modes of the coal-fired power plant retrofitted with post-combustion CO_2 capture process. This aim was achieved by meeting the objectives set in Section 1.3:

1. Conduct a general review on the efficiency improvement methods applicable to post-combustion CO_2 capture plants.
2. Conduct a detailed review of developments in the pilot-plant testing and modelling of the calcium looping process.
3. Develop base- and part-load models of the coal-fired power plant and validate them against data available in the public domain.
4. Develop and validate models of calcium looping and chilled ammonia post-combustion CO_2 capture plants.
5. Investigate alternative CO_2 capture technologies and integration configurations for reduction of the net efficiency penalty resulting from the CO_2 capture plant retrofit to the coal-fired power plants.
6. Evaluate performance of the developed configurations under off-design and alternative operating modes.
7. Adapt a methodology for a probabilistic performance assessment to analyse the impact of the post-combustion CO_2 capture plant integration to the coal-fired power plant.

To meet the established aim and objectives, this PhD project employed a number of engineering methods that ranged from process modelling and simulation using commercial software (Aspen Plus®), deterministic methods for process techno-economic analysis, and surface response approximation models coupled with the probabilistic framework based on statistical methods for probabilistic performance analysis. The main conclusion drawn from this PhD project is that the emerging high-temperature solid looping technologies, such as CaL, for decarbonisation of coal-fired power plants have the potential to significantly reduce the economic and net efficiency penalties associated with

mature CO_2 capture technologies, such as chemical solvent scrubbing. Importantly, the net power output in the CaL retrofit scenario was found to be around 40% higher than that of the reference coal-fired power plant and double that of the MEA retrofit scenario. Such performance of CaL was determined to have a positive impact on the daily short-run profit of the retrofitted system, as the CaL retrofit scenario could become more profitable than the reference coal-fired power plant without CO_2 capture under the current economic climate, especially if its inherent energy storage capability is utilised. It has also been identified that further improvements in thermodynamic and economic performance of the CaL retrofit scenario can be achieved mainly by considering alternative thermodynamic cycles such as the supercritical CO_2 cycle, enhanced heat integration, and alternative sources of heat or O_2 for oxy-combustion of fuel to drive the endothermic calcination process.

13.1.1 Developments in CO_2 capture for power generation systems

The major challenges for CCS to become cost-effective are the energy-intensity of the mature CO_2 capture technologies and considerable capital costs, both affecting the cost of electricity. Therefore, the literature was reviewed to classify the possible measures for reduction of the energy requirement associated with post-combustion CO_2 capture (Objective 1), which is expected to make a significant contribution towards decarbonisation of the power sector. It was identified that application of alternative CO_2 capture technologies, such as cryogenic separation, the dry carbonate process or CaL can significantly reduce the net efficiency penalty to 3–7% points, from up to 12.5% points reported for the mature chemical solvent scrubbing. It was also indicated that further reduction of the energy intensity of both CaL and chemical solvent scrubbing, which are regarded as the most promising post-combustion CO_2 capture technologies for fossil fuel power plants, can be achieved via enhancements of the CO_2 capture material performance, heat integration, alternative process configurations, and process intensification.

As CaL has been identified as one of the most promising technologies for CO_2 capture from fossil fuel power plants, a detailed review of both experimental and

computational research activities was conducted (Objective 2) to provide an update on development of CaL since the last major review in 2010. Until recently, the technical viability and performance of the CaL process has been evaluated worldwide using bench- and pilot-scale facilities the size of which varies between 1 kW_{th} and 1.9 MW_{th}. Regardless of rapid progress in testing of this emerging CO_2 capture technology at the pilot scale, it is still in the early stages of development compared to chemical solvent scrubbing using amines that was demonstrated at commercial scale in 2014.

The detailed review indicated that the literature provides data that give a valuable insight into the operation and operating conditions of the CaL process. Although it was found that these data are not detailed enough to allow complete process model validation, the CaL process has been widely modelled to assess the implication of its retrofit to fossil fuel power plants. Using process models, which were classified under five complexity levels ranging from simple thermodynamic models to complex predictive models, it was indicated that the mean net efficiency penalty associated with the retrofit of CaL to the coal-fired power plant is 6–7% points with only 2.5–3% points being associated with the CaL process itself. This value is considerably lower than the 9–12.5% points estimated for the mature amine scrubbing technology. However, integration of CaL to a natural gas combined cycle power plant was found to result in similar efficiency penalties to the mature CO_2 capture systems. Therefore, the CaL plant may not be the preferred option for natural gas combined cycle power plants, which can be attributed to the low CO_2 concentration in flue gas that results in lower driving force for the carbonation reaction. On the other hand, a novel coal-fired power generation system based on the CaL process were found to have the net thermal efficiency of 46.69%$_{LHV}$, which is higher than that of supercritical and even ultra-supercritical coal-fired power plants without CO_2 capture. This implies that CaL can serve as a base system for development of state-of-the-art power generation systems that could be implemented on a large scale in place of current technologies.

13.1.2 Process modelling and validation

As coal-fired power plants are expected to flexibly balance the energy demand and supply in the future energy portfolio, both base- and part-load models of the supercritical coal-fired power plants were developed in Aspen Plus® (Objective 3). Although Aspen Plus® is not primarily designed for modelling of power cycles, especially under part-load or off-design conditions, its prediction capabilities were extended to off-design conditions through implementing a Stodola's ellipse law to account for variability of the steam pressure in the steam cycle, Salisbury's equation to account for variability of the isentropic efficiency of the steam turbine sections, and the general pressure drop correlation for determining the off-design pressure drop in the heat exchanger sections of the boiler. The base-load studies conducted in this project (Chapter 4 to Chapter 7) utilised the process model of the 580 MW_{el} supercritical coal-fired power plant, which operates under European environmental conditions and is characterised with a net thermal efficiency of 38.5%$_{HHV}$, as a reference. Conversely, due to lack of detailed part-load data for the same coal-fired power plant in the literature, the part-load studies conducted in this project (Chapter 8 to Chapter 11) utilised the process model of the 660 MW_{el} supercritical coal-fired power plant, which operates under Indian environmental conditions and is characterised with a net thermal efficiency of 38.8%$_{HHV}$, as a reference. The predictions of the developed models were found to be in good agreement with the reported data both at base- and part-load conditions with a maximum relative error of 5–6%. This proved the validity of the modelling framework developed, and thus the conclusions drawn in this PhD project.

As this PhD project evaluated efficiency improvements and performance of the CO_2 capture retrofit scenarios, including chemical solvent scrubbing using MEA, and ammonia, as well as CaL, process models for these CO_2 capture processes were developed and the reliability of their predictions were assessed (Objective 4). First, a process model of chemical solvent scrubbing using MEA was adapted from another study to process the flue gas from the 660 MW_{el} supercritical coal-fired power plant. This rate-based model had been extensively validated in the literature under different flue gas loads, which proved its ability

to reliably predict process performance under part-load conditions. Unlike other studies analysing retrofits of chemical solvent scrubbing plants, however, this study used a square-column absorber, following recent experience from the Boundary Dam project in Saskatchewan, Canada. For this reason, to extend the capabilities of the RadFrac model in Aspen Plus®, an alternative approach utilising the definition of the hydraulic diameter was proposed. Second, as the rate-based approach to modelling the chemical solvent scrubbing process is regarded as superior to the equilibrium-based approach, the rate-based approach was employed to model the CAP, as opposed to the majority of studies in the literature. Due to the lack of the pilot-plant operating data for the CAP process, however, this model was scaled up from the developed rate-based model of the AAP process, which was successfully validated against the Munmorah pilot plant operating data (lean and rich loading of solvent, lean solvent flow rate, CO_2 capture level, stripper bottom liquid temperature, reboiler duty) under different flue gas loads and then tuned to CAP conditions to remove 90% of CO_2 from the 580 MW_{el} supercritical coal-fired power plant. Third, a process model of CaL was developed based on the operating data of the 1.7 MW_{th} la Pereda pilot plant using a semi-empirical model with correction factor to represent the sorbent performance. As opposed to other studies analysing CaL retrofit scenarios, the model prediction was compared with the pilot-plant operating data under different flue gas loads. As the model predictions were found to be in good agreement with experimental data, the energy requirement of CaL was expected to be reliably estimated. Therefore, the process model was then scaled up to process the flue gas from both the 660 MW_{el} supercritical coal-fired power plant and the 580 MW_{el} supercritical coal-fired power plant using the findings from the detailed literature review on CaL development. Finally, to reliably assess the overall parasitic load in the considered CO_2 capture retrofit scenarios, the auxiliary equipment, such as CO_2 compression unit and air separation unit, was modelled in detail, instead of using specific power requirements to factor their contribution in the total parasitic load.

13.1.3 Deterministic performance analysis

Retrofit of the CAP plant, for which the lowest parasitic load was estimated at lean loading of 0.29 and NH_3 concentration of 12.5%$_{wt}$, to the 580 MW_{el} supercritical coal-fired power plant led to a net efficiency penalty of 10.9% points for the initial stripper pressure of 10 bar, which is similar to the other studies on CAP and MEA retrofit scenarios. However, the actual parasitic load was found to be 24.7 MW_{el} higher than the estimated theoretical work requirement. This indicated a limitation of the previous studies that utilised thermodynamic estimates and did not account for pressure drops and corresponding temperature variations throughout the steam cycle due to extraction of large amount of steam for solvent regeneration. Application of the advanced process configurations was found to considerably reduce the net efficiency penalty. In particular, the novel configuration, which involves coupling of a new two-stage or a single-stage auxiliary steam turbine with the boiler feedwater pump for extracted steam pressure control and a back-pressure turbine for maintaining the desired intermediate-pressure turbine discharge pressure, was found to impose the net efficiency penalty of 8.7–8.8%$_{HHV}$ points. This was 2.1–2.2%$_{HHV}$ points lower than in the base case for the CAP retrofit scenario (Objective 5).

As the efficiency penalty of the CAP retrofit scenario was still close to that of chemical solvent scrubbing using the reference MEA solvent, the CaL retrofit scenario was considered for the same reference coal-fired power plant. With the assumption to capture 90% of CO_2 from the flue gas, the net efficiency penalty of the CaL retrofit scenario was 8.6%$_{HHV}$ points, which is close values from other studies analysing retrofits of CaL to the coal-fired power plants. Although this was only slightly better than to the best case CAP retrofit scenario, it needs to be highlighted that, considering fuel combustion in the calciner, the overall CO_2 capture level was 95.7%. The sensitivity analysis revealed that the net thermal efficiency of the retrofitted system and the net power output are most affected by the sorbent make-up rate, CO_2 capture efficiency, and O_2 content in the calciner fluidising gas. On optimisation of these parameters, it was shown that the net thermal efficiency can be reduced to

6.7–7.9%$_{HHV}$ points for a calciner fired with natural gas and coal, respectively, with an overall CO_2 capture of 90% (Objective 5). Moreover, it was found that the net power output in the CaL retrofit scenario will increase by 39.0–53.7% over the reference coal-fired power plant without CO_2 capture, which was in agreement with other studies. Yet, the performance of the CaL retrofit scenario has never been compared to chemical solvent scrubbing technologies using the same reference coal-fired power plant. Therefore, having conducted such comparison for the first time, the performance of the CaL retrofit scenario was found to be superior to the reference amine scrubbing technology, for which the net efficiency penalty was 9.5%, leading to 24.7% drop in the net power output. Not only was retrofit of the CaL process to the coal-fired power plant found to be less complex compared to chemical solvent scrubbing, it would also generate nearly double revenue from electricity sales to the power plant operators.

The state-of-the-art CaL retrofit scenario assumed that the high-grade heat available for recovery was utilised to raise high-pressure steam for the conventional steam cycle. As CaL operates within the temperature envelope that is similar to high-temperature gas-cooled nuclear reactors, sodium-cooled fast nuclear reactors, and concentrating solar power plants, it was proposed for the first time to apply the recompression s-CO_2 cycle in place of the conventional steam cycle for high-grade heat utilisation (Objective 5). The net efficiency penalty in the CaL with s-CO_2 retrofit scenario was found to be 6.9%$_{HHV}$ points, which was 1%$_{HHV}$ point lower than the corresponding case of CaL with a coal-fired calciner and with the supercritical steam cycle under the same turbine inlet conditions. Increase of the turbine inlet conditions to 300 bar/620°C/620°C from 242.3 bar/593.3°C/593.3°C resulted in a 0.6%$_{HHV}$ point reduction in the net efficiency penalty, indicating further room for net thermal efficiency improvement that is dependent only on availability of material that would be capable of maintaining its properties under such conditions. Moreover, the hardware analysis revealed that further improvement in the net thermal efficiency of the retrofitted system can be obtained by increasing the number of reheating and/or intercooling stages, as well as by replacing

the first stage of the main compressor with a CO_2 pump. The latter solution was found to further improve the net thermal efficiency by 0.5%$_{HHV}$ points; hence the minimum net efficiency penalty of 5.8%$_{HHV}$ points is estimated for CaL with a coal-fired calciner. Finally, further improvements in the performance of the coal-fired power plant retrofitted with the CaL plant can be achieved through using natural gas in the calciner, higher level of heat integration, alternative sources of O_2 for oxy-combustion of fuel or sources of heat for sorbent regeneration to minimise or avoid the power requirement associated with O_2 production, alternative processes and technologies to minimise the power requirement for CO_2 compression, and higher efficiency of the secondary cycle.

The part-load analysis of the MEA retrofit scenario (Objective 6) indicated that, depending on the integration scenario and operating conditions, it would result in net efficiency penalties of 10.5–14.7%$_{HHV}$ points. More importantly, the study revealed that the reboiler duty drops nonlinearly with reduction of the coal-fired power plant load. This indicated that the approach employed by other studies that used fixed specific reboiler duty to estimate the system's part-load performance would lead to underestimation of the reboiler duty, and thus the net efficiency penalty. Furthermore, it was estimated that if the pressure drop due to steam extraction for solvent regeneration was not considered, the net efficiency penalty can be underestimated by up to 1.3%$_{HHV}$ points. These results reinforce the need for detailed modelling of both the coal-fired power plant and the CO_2 capture plant to reliably assess the performance of the retrofitted system under off-design and part-load operating conditions. As the proposed part-load modelling framework was found to be an effective tool for detailed part-load analysis, it can be utilised for feasibility and techno-economic studies of CO_2 capture retrofit scenarios. Therefore, it was employed to assess the part-load performance and inherent energy storage capability of the CaL retrofit scenario (Objective 6). As opposed to the MEA retrofit scenario, the net efficiency penalty in the CaL retrofit scenario was not considerably affected under part-load operation as it varied between 8.7–8.8%$_{HHV}$ points and 8.9–9.4%$_{HHV}$ points for a calciner fired with natural gas and coal, respectively. When sorbent reactivation via hydration was considered,

the net efficiency penalty reduced to 8.3–8.4%$_{HHV}$ for the natural gas fired calciner, yet the net power output of the retrofitted system dropped by 11–12% compared to the CaL retrofit scenario without sorbent reactivation. The economic analysis revealed that regardless of the improved net thermal efficiency, such drop in the net power output will have significant implications on the economic performance, as in all cases with sorbent regeneration through hydration, the daily short-run profit was lower compared to the cases without sorbent reactivation. Furthermore, the techno-economic analysis of the CaL with inherent energy storage indicated that application of liquid-O_2 energy storage would result in higher turndown of the entire system and offer higher energy density, hence lower capital cost, compared to the other identified routes for energy storage. It would also offer the highest daily short-run profit, even higher than that of the reference coal-fired power plant without CO_2 capture at 8.3 €/tCO_2. As the average price of European emission allowances in November 2015 was 8.5 €/tCO_2, it is concluded that implementation of the CaL retrofit scenario with a liquid-O_2 energy storage system is beneficial in the current economic climate. It is expected that utilisation of the inherent energy storage capability of chemical looping combustion and oxy-combustion can yield similar economic benefits.

13.1.4 Probabilistic performance analysis

Process modelling and simulation tools are widely utilised in design and optimisation of advanced clean power generation systems. Yet, their deterministic nature implies the need to apply safety factors to ensure reliable operation of the system under uncertain operating conditions. As this could lead to equipment oversizing, affecting process efficiency and increasing capital cost, a probabilistic approach to performance assessment is adapted to systematically account for input uncertainty in power generation systems (Objective 7). By considering the variability in the fuel composition and the market energy demand, the probability that the limit states of the 660 MW_{el} supercritical coal-fired power plant were exceeded was found to be small. The probabilistic analysis also indicated that fluctuations in the market energy

demand had the highest impact on the process reliability. Nevertheless, it was observed that there is no need to apply conservative safety factors during the equipment design.

Having applied probabilistic approach to compare the CaL and MEA retrofit scenarios, it was shown that the most probable values for the net efficiency penalties are 9.5% and 11.5% points in the CaL and MEA retrofit scenarios, respectively, regardless of higher uncertainty in the operating conditions of CaL. These values are in the higher-end of the net efficiency penalties reported in the literature. Moreover, the CaL retrofit scenario was found to increase the net power output of the integrated system by 40%, which can be considered as a more realistic value compared to 50–80% identified in previous deterministic studies considering only base-load operation. Also, the net power output in the CaL retrofit scenario was found to be nearly double that in the MEA retrofit scenario, and thus it could outweigh the imposed net efficiency penalty leading to exceeding the profit of the reference CFPP from electricity sales in favourable economic conditions. Probabilistic analysis of particular process equipment revealed that CO_2 capture plants and their auxiliary equipment need to be designed for the lower limit state and no excessive oversizing is required. It was found that the analysed key performance indicators were mostly affected by variability in the power plant operating load, lean loading (MEA retrofit scenario) and relative sorbent make-up rate (CaL retrofit scenario), while no effect of uncertainty in the moisture content in coal was observed. Finally, the probabilistic approach was found to be capable of producing valuable information on the equipment operating envelope that would help designers to assess the number of equipment trains and their operating limits.

It is concluded that the probabilistic framework should be used in addition to conventional thermodynamic analyses in future studies aiming at development of novel clean power generation systems and CO_2 capture processes. Importantly, by considering the impact of uncertainty on process performance, it valuable information is generated that could serve as an input not only to

the probabilistic economic analysis and process design, but also to the investment decision-making process.

13.2 Recommendations for future research

The work conducted within this PhD project has not only significantly contributed to the scientific body of knowledge in the fields of CO_2 capture and power engineering, which is proven via project outputs published in nine high-impact-factor peer-reviewed journal papers, but also has identified further knowledge gaps and indicated research directions. Therefore, the following recommendations for future research are made in relation to process modelling, process analysis, and development of clean power generation and industrial systems:

- Process modelling
  - Kinetics and hydrodynamics correlations should be implemented in the carbonator and the calciner models to enhance the credibility of the process model prediction.
  - A detailed validation of the CaL and CAP process models with experimental operating data should be conducted to identify differences in prediction of the process models of different complexity level once relevant data become available.
  - A database comprising the baseline models for fossil fuel power plants, such as supercritical, ultra-supercritical and advanced ultra-supercritical coal-fired power plants, natural gas fired and integrated gasification combined cycle power plants, and CO_2 capture plants, such as chemical solvent scrubbing and CaL, should be established and made freely available to the academic and industrial community to make direct comparisons across different studies viable and reliable.
- Process analysis of the developed concepts
  - Applicability of the CAP and CaL concepts developed in this project to other power generation systems, such as natural gas fired and

integrated gasification combined cycle power plants, should be assessed and their techno-economic viability determined.

- Once the CaL process model is improved, a further techno-economic analysis of the developed concepts should be carried out to prove their technical and economic viability. Additionally, deterministic data generated using a high-fidelity CaL model will serve as a design matrix for detailed probabilistic techno-economic analyses that would provide reliable data to support the design study.
- Applicability of other thermodynamic cycles, such as Kalina cycle or humid air turbine cycle, and combined cycles, such as supercritical CO_2 cycle (topping cycle) with conventional steam cycle (bottoming cycle), for high-grade heat recovery from CaL should be evaluated.
- Further studies on the inherent storage capability of CaL to maximise the daily short-run profit via optimising the charging and discharging times should be conducted.
- The inherent energy storage capability of other clean power technologies, such as chemical looping combustion and oxy-combustion, should be assessed.

- Advancement of clean power generation and industrial systems
  - A detailed design study of the proposed concepts of CaL, including cases with conventional steam cycle, supercritical CO_2 cycle and inherent energy storage capability, should be undertaken to advance large-scale implementation of this technology.
  - A techno-economic analysis of CaL with supercritical CO_2 cycle and/or inherent energy storage for decarbonisation of other industries, such as cement, lime, chemicals, hydrocarbon, and steel, should be conducted.
  - A techno-economic analysis of CaL retrofit to a combined heat and power plant should be conducted and the performance compared with the power plant of the same rated power output.
  - The effect of using alternative sorbents, such as lithium silicate, synthetic sorbents, pre-treated sorbents and sorbent reactivation

strategies on the techno-economic performance of the high-temperature solid looping cycle for CO_2 capture from fossil fuel power plants should be estimated.

- Implementation of the process intensification in CO_2 capture plants via considering rotating packed beds or vortex reactors should be evaluated from techno-economic standpoint.
- Development of novel power generation systems based on high-temperature looping cycles and high-efficiency thermodynamic cycles should be pursued and their techno-economic performance quantified.

This page intentionally left blank.

Appendix A SUPPLEMENTARY INFORMATION FOR PRESENTED PUBLICATIONS

A.1 Modelling and comparison of calcium looping and chemical solvent scrubbing retrofits for CO_2 capture from coal-fired power plant

Calciner fuel characteristic

Table A-1: Coal characteristics (Black, 2013)

Illinois No 6 Bituminous coal	As received ($\%_{wt}$)
Proximate analysis	
Fixed carbon	44.2
Volatile matter	35.0
Ash	9.7
Moisture	11.1
Ultimate analysis	
Carbon	63.8
Hydrogen	4.5
Oxygen	6.9
Nitrogen	1.3
Sulphur	2.5
Higher heating value (MJ/kg)	27.1
Lower heating value (MJ/kg)	26.2

Table A-2: Biomass characteristics (Ciferno and Marano, 2002)

Beech wood (Short rotation woody crops)	As received ($\%_{wt}$)
Proximate analysis	
Fixed carbon	11.3
Volatile matter	68.9
Ash	0.8
Moisture	19.0
Ultimate analysis	
Carbon	50.4
Hydrogen	7.2
Oxygen	41.0
Nitrogen	0.3
Sulphur	0.0
Higher heating value (MJ/kg)	18.4
Lower heating value (MJ/kg)	N/A

Table A-3: Natural gas characteristics (Black, 2013)

Natural gas	As received ($\%_{vol}$)
Methane	93.1
Ethane	3.2
Propane	0.7
n-Butane	0.4
Carbon dioxide	1.0
Nitrogen	1.6
Higher heating value (MJ/kg)	52.6
Lower heating value (MJ/kg)	47.5

A.2 Evaluation and modelling of part-load performance of coal-fired power plant with post-combustion CO_2 capture

Table A-4: Validation of the base load prediction of the coal-fired power plant model developed in Aspen Plus

Stream number	Pressure (bar)			Temperature (°C)			Mass flow rate (kg/s)		
	Literature	Model	Deviation	Literature	Model	Deviation	Literature	Model	Deviation
Coal/bottom ash									
1	1.030	1.030	0.0%	33.0	33.0	0.0%	58.6	60.3	2.9%
2	1.013	1.013	0.0%	1050.0	1050.0	0.0%	1.9	2.0	3.3%
Air/flue gas									
3	1.013	1.013	0.0%	33.0	33.0	0.0%	634.5	654.3	3.1%
4	1.040	1.040	0.0%	35.9	35.8	0.3%	634.5	654.3	3.1%
5	1.030	1.030	0.0%	258.5	270.2	4.5%	634.5	654.3	3.1%
6	1.010	1.010	0.0%	1921.4	1922.4	0.1%	691.1	704.8	2.0%
7	1.010	1.010	0.0%	1070.8	1070.8	0.0%	691.1	704.8	2.0%
8	1.005	1.005	0.0%	921.8	921.8	0.0%	691.1	704.8	2.0%
9	1.005	1.005	0.0%	547.6	555.7	1.5%	691.1	704.8	2.0%
10	1.000	1.000	0.0%	319.0	319.0	0.0%	691.1	704.8	2.0%
11	1.000	1.000	0.0%	122.4	122.4	0.0%	691.1	704.8	2.0%
12	1.060	1.060	0.0%	130.0	130.0	0.0%	691.1	704.8	2.0%
Water/steam									
13	308.70	308.70	0.0%	279.6	279.7	0.0%	550.7	550.7	0.0%
14	294.70	294.70	0.0%	341.0	344.9	1.1%	550.7	550.7	0.0%
15	263.20	263.20	0.0%	480.0	478.9	0.2%	550.7	550.7	0.0%
16	242.20	242.20	0.0%	537.0	537.0	0.0%	550.7	550.7	0.0%
17	44.30	44.30	0.0%	288.7	287.9	0.3%	466.2	466.3	0.0%
18	42.00	42.00	0.0%	565.0	565.0	0.0%	466.2	466.3	0.0%
19	66.80	66.80	0.0%	340.0	339.8	0.1%	36.2	36.2	0.1%
20	44.30	44.30	0.0%	288.7	287.9	0.3%	48.3	48.2	0.3%
21	21.00	21.00	0.0%	459.9	455.9	0.9%	14.4	14.8	2.5%
22	6.10	6.10	0.0%	295.4	290.4	1.7%	19.2	19.5	1.3%
23	2.98	2.98	0.0%	215.6	210.1	2.6%	31.4	31.4	0.1%
24	2.90	2.98	2.8%	215.6	210.1	2.6%	346	342.6	1.0%
25	0.64	0.64	0.0%	87.6	87.6	0.0%	14.1	14.0	0.7%
26	0.27	0.27	0.0%	66.7	66.7	0.0%	13.5	13.7	1.8%
27	0.10	0.10	0.0%	46.4	46.4	0.0%	318.5	314.9	1.1%
28	0.10	0.10	0.0%	46.4	46.4	0.0%	429.5	429.0	0.1%
29	11.90	11.90	0.0%	46.5	46.5	0.1%	429.5	427.1	0.6%
30	308.70	308.70	0.0%	193.9	193.3	0.3%	550.7	550.7	0.0%
31	11.90	11.90	0.0%	381.1	375.4	1.5%	22.4	22.5	0.6%
32	2.03	2.03	0.0%	33.0	33.0	0.0%	18992.8	18874.2	0.6%
33	1.03	1.03	0.0%	43.0	43.0	0.0%	18992.8	18874.2	0.6%

A.3 Calcium looping with inherent energy storage for decarbonisation of coal-fired power plant

Evaluation of the heat loss from the storage tank in Case 3

The rate and the amount of heat loss over time from the solid storage tank (Figure A-1) can be defined as (Ma et al., 2014a):

$$\dot{Q}_{loss} = \dot{Q}_{foundation} + \dot{Q}_{wall} + \dot{Q}_{top} \quad \text{(A-1)}$$

$$\Delta Q_{loss} = \int_{t_0}^{t_f} \dot{Q}_{loss}\, dt \quad \text{(A-2)}$$

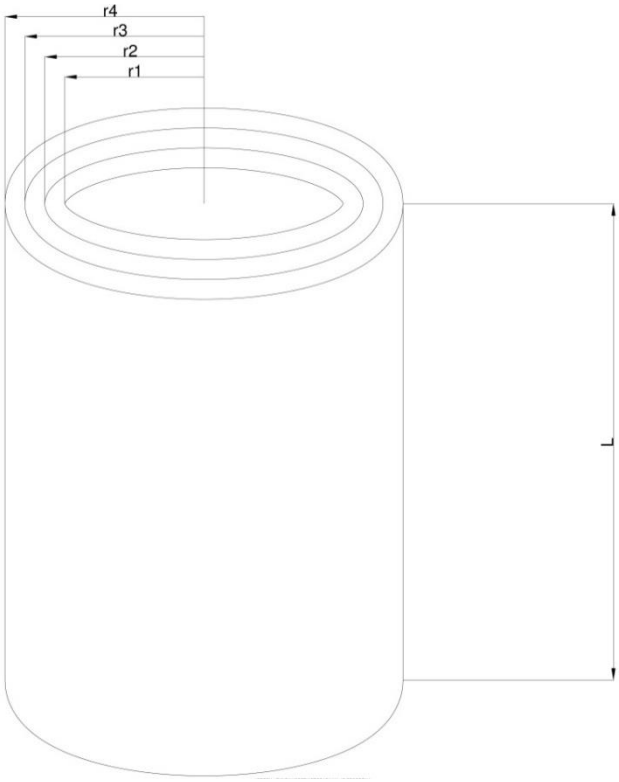

Figure A-1: Drawing of insulated solid storage tank for heat loss calculation

It is expected that a particle self-insulation layer will develop near the walls of the storage tank and provide additional resistance to conductive heat loss. Hence, for the cylindrical tank lined with refractory insulation and surrounded with a concrete wall, the rate of heat transfer through the wall, top and foundation under steady state can be expressed using Eq. (A-3)–(A-5), respectively. The heat loss through the top of the tank will be due to conduction

through the insulation consisting of refractory lining and cement, and due to convection to the environment. Alternatively, heat loss through the foundation will be a result of conduction only.

$$\dot{Q}_{wall} = \frac{T_{storage} - T_{ambient}}{\frac{ln\left(\frac{r_2}{r_1}\right)}{2\pi k_{p,eff} L} + \frac{ln\left(\frac{r_3}{r_2}\right)}{2\pi k_r L} + \frac{ln\left(\frac{r_4}{r_3}\right)}{2\pi k_c L} + \frac{1}{2\pi r_4 L h_{ambient}}} \quad \text{(A-3)}$$

$$\dot{Q}_{top} = \frac{T_{storage} - T_{ambient}}{\frac{t_c}{\pi r_2 k_r} + \frac{t_r}{\pi r_2 k_c} + \frac{1}{\pi r_2 h_{ambient}}} \quad \text{(A-4)}$$

$$\dot{Q}_{foundation} = \frac{T_{storage} - T_{ambient}}{\frac{t_c}{\pi r_2 k_r} + \frac{t_r}{\pi r_2 k_c}} \quad \text{(A-5)}$$

The effective thermal conductivity for the particles in the solid storage tank ($k_{p,eff}$) was obtained from the Okazaki et al. (1981) model, which was found to reasonably represent the experimental data by Abou-Sena et al. (2007).

Table A-5: Parameters for heat loss calculation

Parameter	Unit	Value
Thermal conductivity of refractory-insulating lining, k_r (Ma et al., 2014b)	W/mK	0.5
Thermal conductivity of cement wall, k_c (Ma et al., 2014b)	W/mK	1.0
Thermal conductivity of sorbent, k_p (Robertson, 1988)	W/mK	1.5
Convective heat transfer coefficient, h_{amb} (Koschenz and Dorer, 1999)	W/K	2.0
Porosity, ε	-	0.5
Storage tank height, L	m	30
Radius of tank without insulation, r_1 ($CaO/CaCO_3$ tank)	m	13.1/14.2
Self-insulation layer thickness, t_p (Ma et al., 2014b)	m	0.5
Refractory lining thickness, t_r	m	0.25
Cement wall thickness,t_c	m	1.0
Sensible heat stored, Q_{sens} ($CaO/CaCO_3$ tank)	MW_{th}	190.4/165.6

Using the parameters from Table A-1, it was estimated that the heat loss in the CaO and $CaCO_3$ tanks will be 0.7 and 1.3 MW_{th}, respectively. This accounts for 0.4% and 0.8% of the total sensible heat stored in these tanks, which is in line with the results obtained for thermal storage by Ma et al. (2014a).

In addition, sensitivity analyses on the thermal conductivities, convective heat transfer coefficient and insulation thicknesses have been performed and are presented in the following figures. These revealed that the heat loss is not higher than 1.5%, indicating that heat storage efficiency is more than 98.5%. As the analysis revealed that the heat loss will be very low and thus will not affect the performance of the system significantly, it can be assumed that there is no heat loss in the tanks at the concept development stage.

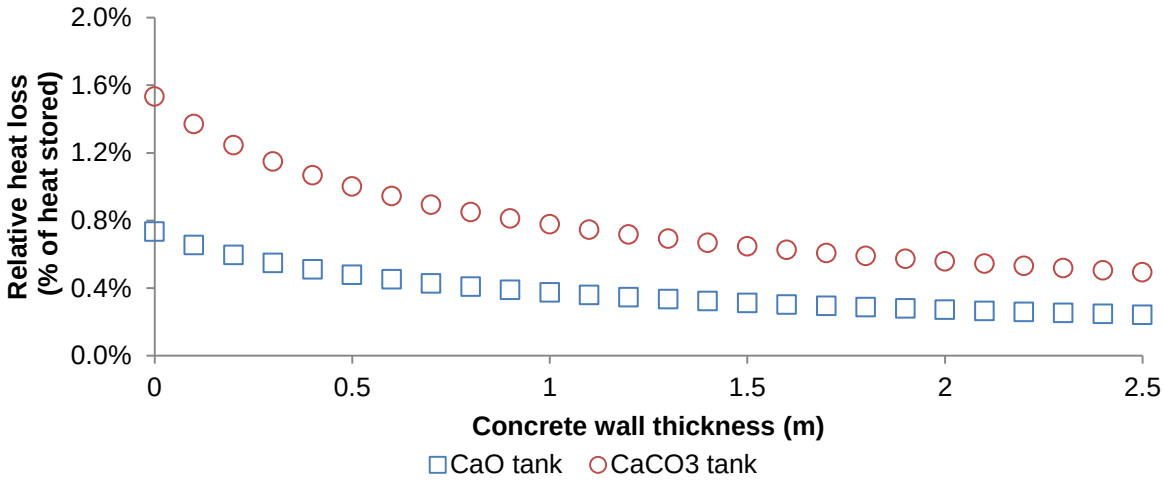

Figure A-2: Effect of the concrete wall thickness on the relative heat loss in the solid storage tank

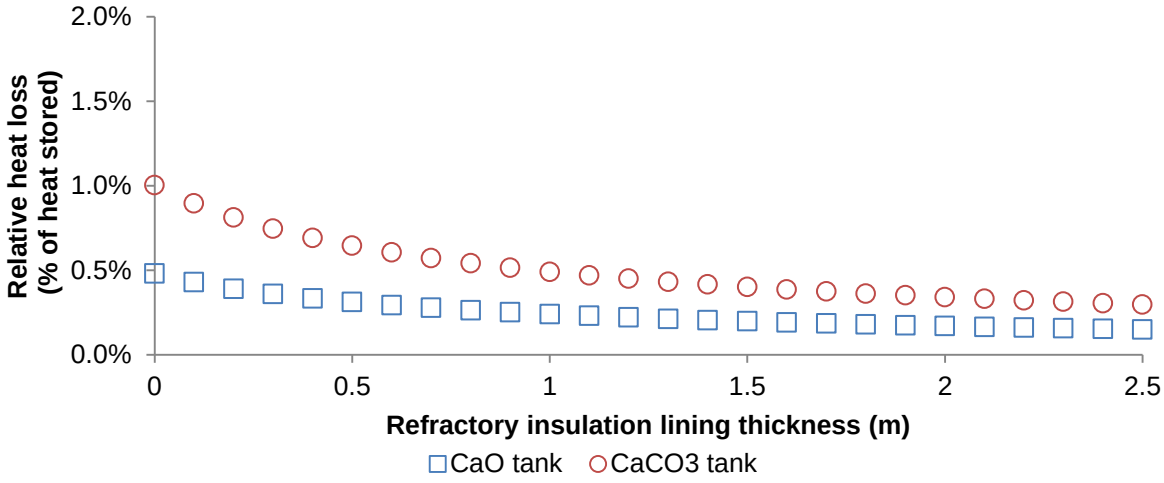

Figure A-3: Effect of the refractory insulation lining thickness on the relative heat loss in the solid storage tank

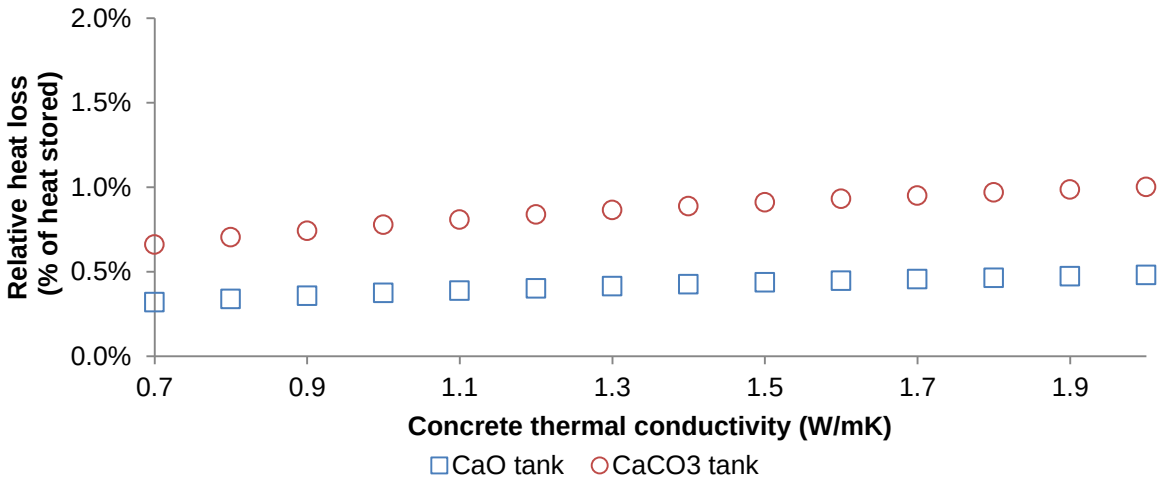

Figure A-4: Effect of concrete thermal conductivity on the relative heat loss in the solid storage tank

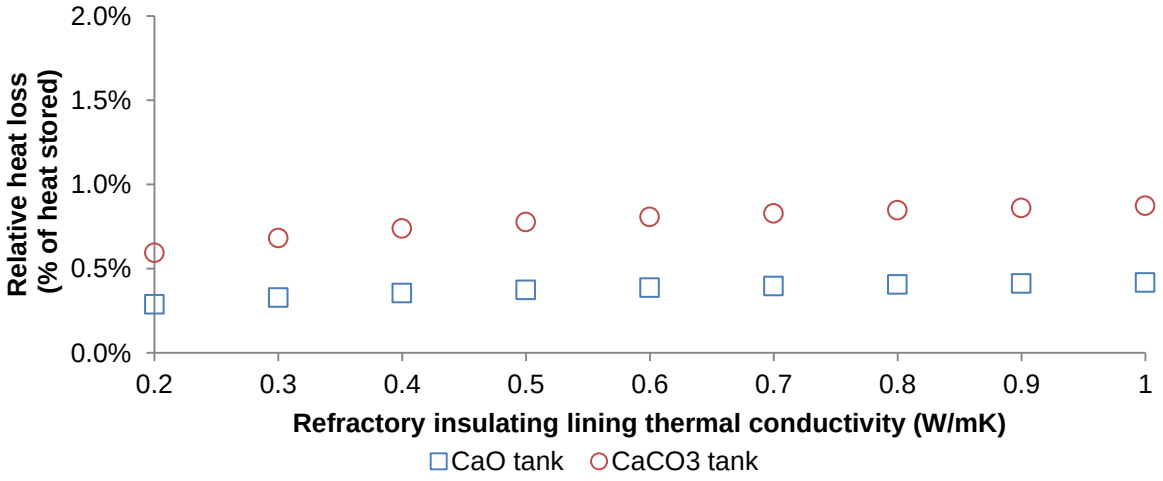

Figure A-5: Effect of refractory insulating lining thermal conductivity on the relative heat loss in the solid storage tank

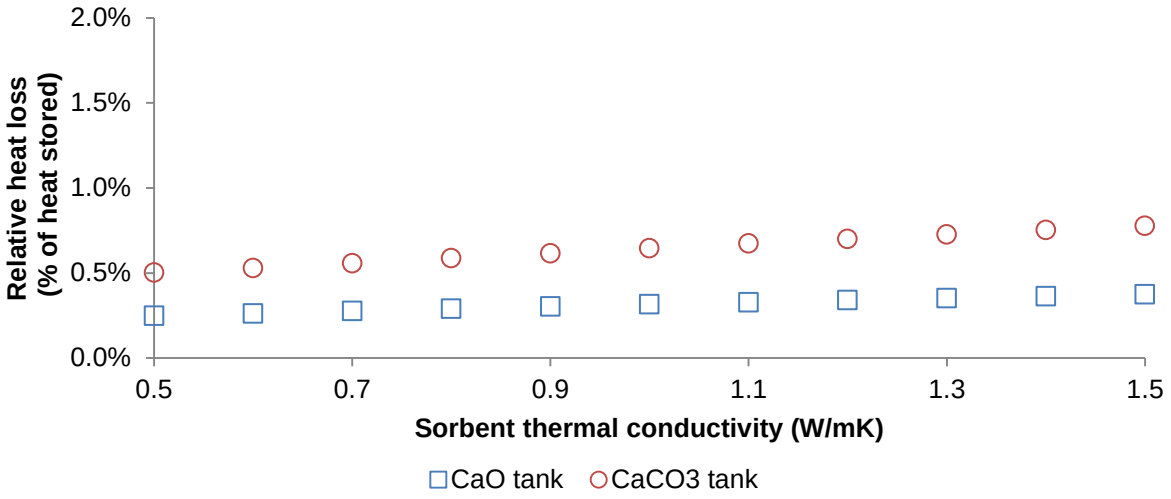

Figure A-6: Effect of sorbent thermal conductivity on the relative heat loss in the solid storage tank

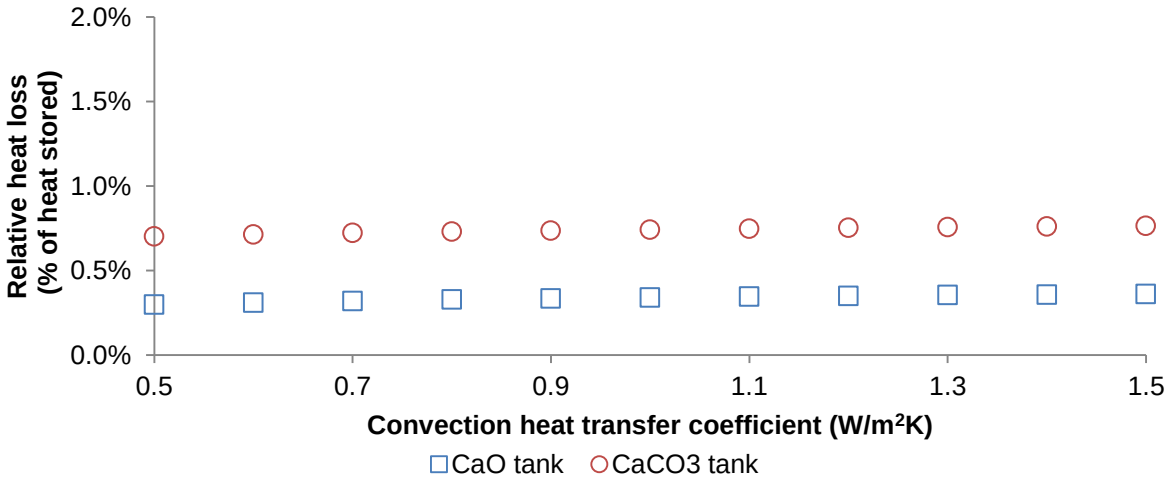

Figure A-7: Effect of convection heat transfer coefficient on the relative heat loss in the solid storage tank

A.4 Probabilistic performance assessment of a coal-fired power plant

Table A-6: Representative subset of the design matrix

Moisture content ($\%_{wt}$)	Fixed carbon content ($\%_{wt}$)	Volatile matter content ($\%_{wt}$)	Ash content ($\%_{wt}$)	Gross power output (MW_{el})	Steam generation rate (kg/s)	Net efficiency ($\%_{HHV}$)	Coal consumption rate (kg/s)
0.32	60.28	22.78	16.63	660	551.242	39.681	58.936
1.90	59.32	22.42	16.36	660	551.242	38.968	59.997
3.77	58.19	21.99	16.05	660	551.226	38.127	61.297
5.86	56.93	21.51	15.70	660	551.235	37.182	62.827
11.00	53.82	20.34	14.85	660	551.228	34.856	66.944
17.00	50.19	18.97	13.84	660	551.245	32.130	72.512
2.44	**18.53**	45.68	33.35	660	551.251	38.427	76.652
2.44	**45.01**	30.38	22.18	660	551.231	38.643	65.142
2.44	**51.71**	26.51	19.35	660	551.240	38.687	62.759
2.44	**53.17**	25.66	18.73	660	551.230	38.691	62.270
2.44	**58.15**	22.78	16.63	660	551.234	38.722	60.633
2.44	**87.22**	5.98	4.36	660	551.233	38.866	52.578
2.44	70.69	**7.37**	19.50	660	551.224	38.676	62.896
2.44	54.05	**28.59**	14.91	660	551.223	38.747	59.353
2.44	52.28	**30.86**	14.42	660	551.235	38.754	59.000
2.44	50.80	**32.74**	14.01	660	551.231	38.760	58.709
2.44	47.88	**36.47**	13.21	660	551.241	38.770	58.143
2.44	35.08	**52.81**	9.68	660	551.231	38.811	55.783
2.44	69.27	26.18	**2.11**	660	551.240	38.892	51.323
2.44	66.41	25.10	**6.05**	660	551.237	38.854	53.550
2.44	64.65	24.43	**8.48**	660	551.231	38.823	55.028
2.44	63.01	23.81	**10.74**	660	551.242	38.799	56.472
2.44	61.46	23.22	**12.88**	660	551.237	38.771	57.921
2.44	46.59	17.60	**33.37**	660	551.238	38.423	76.682
2.44	58.99	22.29	16.27	**660**	551.235	38.729	60.361
2.44	58.99	22.29	16.27	**580**	479.030	38.739	52.928
2.44	58.99	22.29	16.27	**492**	404.270	38.174	45.413
2.44	58.99	22.29	16.27	**404**	332.886	37.129	38.148
2.44	58.99	22.29	16.27	**316**	263.504	35.652	30.836
2.44	58.99	22.29	16.27	**260**	219.809	34.445	26.069

A.5 Comparison of probabilistic performance of calcium looping and chemical solvent scrubbing retrofits for CO_2 capture from coal-fired power plant

A supplementary information to Hanak, D.P., Kolios, A.J., and Manovic, V. (2016), "Comparison of probabilistic performance of calcium looping and chemical solvent scrubbing retrofits for CO_2 capture from coal-fired power plant", *Applied Energy*, 172, 323–336, which comprises a detailed design matrix for the probabilistic analysis and assessment of the approximation models, is available online at http://bit.ly/1qe7KQm.

Appendix references

Abou-Sena, A., Ying, A., and Abdou, M. (2007), “Experimental measurements of the effective thermal conductivity of a lithium titanate (Li_2TiO_3) pebbles-packed bed”, *Journal of Materials Processing Technology*, 181, 206–212.

Black, J. (2013), *Cost and performance baseline for fossil energy plants Volume 1: Bituminous coal and natural gas to electricity*, Report no.: DOE20101397, Revision 2a, National Energy Technology Laboratory, Pittsburgh, PA, USA.

Ciferno, J.P. and Marano, J.J. (2002), *Benchmarking biomass gasification technologies for fuels, chemicals and hydrogen production*, U.S. Department of Energy National Energy Technology Laboratory, Washington, DC, USA.

Koschenz, M. and Dorer, V. (1999), “Interaction of an air system with concrete core conditioning”, *Energy and Buildings*, 30, 139–145.

Ma, Z., Glatzmaier, G., and Mehos, M. (2014a), “Fluidized bed technology for concentrating solar power with thermal energy storage”, *Journal of Solar Energy Engineering*, 136, 031014.

Ma, Z., Glatzmaier, G., and Mehos, M. (2014b), “Development of solid particle thermal energy storage for concentrating solar power plants that use fluidized bed technology”, *Energy Procedia*, 49, 898–907.

Okazaki, M., Yamasaki, T., Gotoh, S., and Toei, R. (1981), “Effective thermal conductivity for granular beds of various binary mixtures”, *Journal of Chemical Engineering of Japan*, 14, 183–189.

Robertson, E.C. (1988), *Thermal properties of rocks*, US Department of the Interior Geological Survey, Reston, VA, USA.